frontiers | Research Topics

Antarctic krill and interactions in the East Antarctic ecosystem

Edited by
So Kawaguchi, Sophie Bestley, Martin Cox,
Kerrie M. Swadling and Elanor Bell

Published in
Frontiers in Marine Science



FRONTIERS EBOOK COPYRIGHT STATEMENT

The copyright in the text of individual articles in this ebook is the property of their respective authors or their respective institutions or funders. The copyright in graphics and images within each article may be subject to copyright of other parties. In both cases this is subject to a license granted to Frontiers.

The compilation of articles constituting this ebook is the property of Frontiers.

Each article within this ebook, and the ebook itself, are published under the most recent version of the Creative Commons CC-BY licence. The version current at the date of publication of this ebook is CC-BY 4.0. If the CC-BY licence is updated, the licence granted by Frontiers is automatically updated to the new version.

When exercising any right under the CC-BY licence, Frontiers must be attributed as the original publisher of the article or ebook, as applicable.

Authors have the responsibility of ensuring that any graphics or other materials which are the property of others may be included in the CC-BY licence, but this should be checked before relying on the CC-BY licence to reproduce those materials. Any copyright notices relating to those materials must be complied with.

Copyright and source acknowledgement notices may not be removed and must be displayed in any copy, derivative work or partial copy which includes the elements in question.

All copyright, and all rights therein, are protected by national and international copyright laws. The above represents a summary only. For further information please read Frontiers' Conditions for Website Use and Copyright Statement, and the applicable CC-BY licence.

ISSN 1664-8714
ISBN 978-2-8325-6611-4
DOI 10.3389/978-2-8325-6611-4

Generative AI statement
Any alternative text (Alt text) provided alongside figures in the articles in this ebook has been generated by Frontiers with the support of artificial intelligence and reasonable efforts have been made to ensure accuracy, including review by the authors wherever possible. If you identify any issues, please contact us.

About Frontiers

Frontiers is more than just an open access publisher of scholarly articles: it is a pioneering approach to the world of academia, radically improving the way scholarly research is managed. The grand vision of Frontiers is a world where all people have an equal opportunity to seek, share and generate knowledge. Frontiers provides immediate and permanent online open access to all its publications, but this alone is not enough to realize our grand goals.

Frontiers journal series

The Frontiers journal series is a multi-tier and interdisciplinary set of open-access, online journals, promising a paradigm shift from the current review, selection and dissemination processes in academic publishing. All Frontiers journals are driven by researchers for researchers; therefore, they constitute a service to the scholarly community. At the same time, the *Frontiers journal series* operates on a revolutionary invention, the tiered publishing system, initially addressing specific communities of scholars, and gradually climbing up to broader public understanding, thus serving the interests of the lay society, too.

Dedication to quality

Each Frontiers article is a landmark of the highest quality, thanks to genuinely collaborative interactions between authors and review editors, who include some of the world's best academicians. Research must be certified by peers before entering a stream of knowledge that may eventually reach the public - and shape society; therefore, Frontiers only applies the most rigorous and unbiased reviews. Frontiers revolutionizes research publishing by freely delivering the most outstanding research, evaluated with no bias from both the academic and social point of view. By applying the most advanced information technologies, Frontiers is catapulting scholarly publishing into a new generation.

What are Frontiers Research Topics?

Frontiers Research Topics are very popular trademarks of the *Frontiers journals series*: they are collections of at least ten articles, all centered on a particular subject. With their unique mix of varied contributions from Original Research to Review Articles, Frontiers Research Topics unify the most influential researchers, the latest key findings and historical advances in a hot research area.

Find out more on how to host your own Frontiers Research Topic or contribute to one as an author by contacting the Frontiers editorial office: frontiersin.org/about/contact

Antarctic krill and interactions in the East Antarctic ecosystem

Topic editors

So Kawaguchi — Australian Antarctic Division, Australia
Sophie Bestley — University of Tasmania, Australia
Martin Cox — Australian Antarctic Division, Australia
Kerrie M. Swadling — University of Tasmania, Australia
Elanor Bell — Australian Antarctic Division, Australia

Citation

Kawaguchi, S., Bestley, S., Cox, M., Swadling, K. M., Bell, E., eds. (2025). *Antarctic krill and interactions in the East Antarctic ecosystem*. Lausanne: Frontiers Media SA.
doi: 10.3389/978-2-8325-6611-4

Table of contents

05 Editorial: Antarctic krill and interactions in the East Antarctic ecosystem
So Kawaguchi, Elanor Bell, Sophie Bestley, Martin J. Cox and Kerrie M. Swadling

08 Surfacing rates, swim speeds, and patterns of movement of Antarctic blue whales
Susannah V. Calderan, Russell Leaper, Virginia Andrews-Goff, Brian S. Miller, Paula A. Olson, M. V. Reyes Reyes, Elanor Bell and Michael C. Double

21 Spatial link between Adélie penguin foraging effort and krill swarm abundance and distribution
Javed Riaz, Sophie Bestley, Simon Wotherspoon, Martin J. Cox and Louise Emmerson

36 Per-length biomass estimates of Antarctic krill (*Euphausia superba*)
Abigail J. R. Smith, Simon J. Wotherspoon and Martin J. Cox

44 KRILLPODYM: a mechanistic, spatially resolved model of Antarctic krill distribution and abundance
David B. Green, Olivier Titaud, Sophie Bestley, Stuart P. Corney, Mark A. Hindell, Rowan Trebilco, Anna Conchon and Patrick Lehodey

62 Marine distribution and habitat use by Snow Petrels *Pagodroma nivea* in East Antarctica throughout the non-breeding period
Benjamin Viola, Barbara Wienecke, Cara-Paige Green, Stuart Corney, Ben Raymond, Colin Southwell, Michael D. Sumner, Patti Virtue, Simon Wotherspoon and Louise Emmerson

78 Antarctic sonobuoy surveys for blue whales from 2006-2021 reveal contemporary distribution, changes over time, and paths to further our understanding of their distribution and biology
Brian S. Miller, Virginia Andrews-Goff, Jay Barlow, Elanor Bell, Susannah Calderan, Michael C. Double, Jason Gedamke, Nat Kelly, Sarah Laverick, Russell Leaper, Elanor J. Miller, Kym Reeve, Ana Širović and Kathleen M. Stafford

93 The energy content and demographic composition of Antarctic krill (*Euphausia superba*) swarms in East Antarctica
Camila Cataldo-Mendez, So Kawaguchi, Martin J. Cox, Jessica Melvin, Victor Rae and Kerrie M. Swadling

103 Demography of Antarctic krill (*Euphausia superba*) from the KY1804 austral summer survey in the eastern Indian sector of the Southern Ocean (80 to 150°E), including specific investigations of the upper surface waters
Fokje L. Schaafsma, Ryan Driscoll, Kohei Matsuno, Rikuto Sugioka, Sara Driscoll, Marin van Regteren, Hiroko Sasaki, Ryuichi Matsukura, Jan Andries van Franeker and Hiroto Murase

118 Beyond counting calls: estimating detection probability for Antarctic blue whales reveals biological trends in seasonal calling
Franciele R. de Castro, Danielle V. Harris, Susannah J. Buchan, Naysa Balcazar and Brian S. Miller

132 Ship-based RPA operations for cetacean research in Antarctica: progress, opportunities and challenges
Virginia Andrews-Goff, Joshua N. Smith, Lyn G. Irvine and Michael C. Double

146 Observed water-mass characteristics and circulation off Prydz Bay, East Antarctica
Annie Foppert, Sophie Bestley, Elizabeth H. Shadwick, Andreas Klocker, Clara R. Vives, Guillaume Liniger and Karen J. Westwood

165 Drivers of phytoplankton distribution, abundance and community composition off East Antarctica, from 55-80°E (CCAMLR Division 58.4.2 East)
Asta C. Heidemann, Karen J. Westwood, Annie Foppert, Simon W. Wright, Andreas Klocker, Clara R. Vives, Simon Wotherspoon and Sophie Bestley

186 Zooplankton abundance and distribution along the Mawson coast, East Antarctica
Christine K. Weldrick, Madeleine J. Brasier, Alicia Burns, Olivia J. Johnson and Dale Maschette

202 Observed upper-ocean structure and seasonal production in the southern Kerguelen Plateau region, 1994-2021
Man Liang, Annie Foppert, Karen J. Westwood and Sophie Bestley

220 Antarctic krill habitat suitability variation in the Southern Ocean over 20 years
Yiyang Tan and Yan Bai

240 Resource potential and maturity estimates of *Euphausia superba* in East Antarctica
Dale Maschette, Simon Wotherspoon, Hiroto Murase, Nat Kelly, Philippe Ziegler, Kerrie M. Swadling and So Kawaguchi

256 Monitoring Antarctic krill (*Euphausia superba*) distribution in the Southern Ocean: environmental DNA (eDNA) adds to the toolbox
Leonie Suter, Alicia Burns, Sophie Bestley, Jez Bird, Madeleine J. Brasier, Martin Cox, Derek Hamer, Olivia J. Johnson, So Kawaguchi, Rob King, Andreas Klocker, Jessica Melvin, Christine K. Weldrick, Simon Wotherspoon and Ben Raymond

frontiers | Frontiers in Marine Science

TYPE Editorial
PUBLISHED 01 July 2025
DOI 10.3389/fmars.2025.1642870

Check for updates

OPEN ACCESS

EDITED AND REVIEWED BY
Stelios Katsanevakis,
University of the Aegean, Greece

*CORRESPONDENCE
So Kawaguchi
So.Kawaguchi@aad.gov.au

RECEIVED 07 June 2025
ACCEPTED 19 June 2025
PUBLISHED 01 July 2025

CITATION
Kawaguchi S, Bell E, Bestley S, Cox MJ and Swadling KM (2025) Editorial: Antarctic krill and interactions in the East Antarctic ecosystem.
Front. Mar. Sci. 12:1642870.
doi: 10.3389/fmars.2025.1642870

COPYRIGHT
© 2025 Kawaguchi, Bell, Bestley, Cox and Swadling. This is an open-access article distributed under the terms of the Creative Commons Attribution License (CC BY). The use, distribution or reproduction in other forums is permitted, provided the original author(s) and the copyright owner(s) are credited and that the original publication in this journal is cited, in accordance with accepted academic practice. No use, distribution or reproduction is permitted which does not comply with these terms.

Editorial: Antarctic krill and interactions in the East Antarctic ecosystem

So Kawaguchi[1,2]*, Elanor Bell[1], Sophie Bestley[2,3], Martin J. Cox[1,2] and Kerrie M. Swadling[2,3]

[1]Australian Antarctic Division, Department of Climate Change, Energy, the Environment and Water, Kingston, TAS, Australia, [2]Australian Antarctic Program Partnership, Institute for Marine and Antarctic Studies, University of Tasmania, Hobart, TAS, Australia, [3]Institute for Marine and Antarctic Studies, University of Tasmania, Hobart, TAS, Australia

KEYWORDS

marine ecology, Southern Ocean ecosystem, TEMPO voyage, ENRICH voyage, CCAMLR

Editorial on the Research Topic
Antarctic krill and interactions in the East Antarctic ecosystem

Collectively, the seventeen articles comprising this Research Topic represent a significant advancement in understanding the ecological role, spatial variability, and trophic significance of Antarctic krill (*Euphausia superba*) across East Antarctica and the broader Southern Ocean. Eight papers in this multidisciplinary research initiative were based on data collected between February and March 2021, within 62°S to 68°S and 55°E to 80°E during the TEMPO (Trends in Euphausiids off Mawson, Predators, and Oceanography) voyage. Data from two more contemporary voyages were also used: Japan's 2018/19 (KY1804; 80°E to 150°E) and Australia's 2018/19 ENRICH (Euphausiids and Nutrient Recycling in Cetacean Hotspots). Other articles used historical data (Liang et al., Tan and Bai), and data collected using a variety of sampling platforms, from ship-based surveys (Schaafsma et al.; Abe et al., 2023) to autonomous moorings (de Castro et al.; Smith et al., 2025), remotely sensed satellite observations (Foppert et al.; Tan and Bai), animal trackers (Riaz et al.), and remotely piloted aircraft (Andrews-Goff et al.).

The datasets compiled encompass physical oceanography, passive and active acoustic measurements, biogeochemical analyses, and environmental DNA (eDNA) sampling (Suter et al.), necessitating the development of novel technologies and analytical methods (Bairstow et al., 2021, 2022; Smith et al.). These comprehensive efforts have unveiled rapid changes in krill habitats, leading to a possible redistribution of krill populations throughout East Antarctica, as evidenced by variations in krill density and distribution observed from fine (Cox et al., 2022) to basin scales (Green et al.). Beyond krill, the taxa studied span from phytoplankton (Heidemann et al.), to zooplankton (Weldrick et al.) to whales (de Castro et al.; Miller et al.), with investigations into physical processes ranging from surface sea observations to the characterization of entire water masses, discerned from Conductivity Temperature Depth (CTD) profiles (Foppert et al.). In sum, these fieldwork endeavors and analyses reflect a sustained commitment to krill research and is high-relevant to improving our understanding of marine ecosystem function and the management of krill.

The influence of environmental variability on krill habitats across the Southern Ocean was investigated. Habitat suitability modeling—employing satellite remote sensing data, sea-ice phenology, and phytoplankton bloom timing—has documented both long-term habitat degradation and spatial redistributions of krill populations in response to climate forcing (Foppert et al.; Heidemann et al.; Liang et al.; Tan and Bai). These studies are particularly valuable in projecting how krill may shift their range under changing sea-ice dynamics and altered primary production regimes. Importantly, they provide a bridge between physical forcing and krill availability to higher predators, creating synergies with both biomass modeling and predator-prey interaction studies.

In parallel, physical oceanography and biogeochemistry studies have provided context for interpreting habitat models. However, the picture is complex, with many potential explanatory variables, operating at a variety of spatial scales influencing krill behaviour and distribution. For example, a slight deepening of the mixed layer depth was found towards the northern limits of the TEMPO survey area (Foppert et al.), along with changes in the number and structure of krill swarms (Cox et al., 2022). However, spatial heterogeneity of phytoplankton communities, partly shaped by regional light availability (Vives et al., 2022), may also influence krill distribution.

The ecological importance of Antarctic krill is further underscored by its role in structuring the behavior and distribution of higher predators. Studies on Adélie penguins (*Pygoscelis adeliae*), Snow Petrels (*Pagodroma nivea*), and baleen whales have demonstrated that predator foraging activity is closely aligned with krill swarm frequency, structure, and vertical accessibility, rather than simple measures of biomass (Cox et al., 2023; Miller et al.; Riaz et al.; Viola et al.). These relationships highlight the value of integrating multiple scales of predator movement data with concurrent acoustic and environmental observations.

Recent advances in technology and modeling frameworks have expanded our capacity to monitor Antarctic krill and their interactions with the environment. Mechanistic models like KRILLPODYM simulate krill life-cycle stages in response to oceanographic conditions and fisheries pressure (Green et al.). Meanwhile, shipborne drones, and multi-frequency acoustics have greatly enhanced spatial and vertical resolution of swarm structure (Andrews-Goff et al.; Cox et al., 2023). These tools not only improve biomass estimation but also enable direct comparisons with predator movement data and carbon flux models and should be coupled with time-series observations from fixed locations (Smith et al., 2025) enabling observation of seasonal variability in krill distribution.

The long-term sustainable management of krill requires estimates of the standing stock of krill (biomass) calculated from acoustic-trawl surveys (Abe et al., 2023), recruitment, demographics and the requirements of krill-dependent predators, such as Adélie penguin (Riaz et al.). Balancing the competing needs of fishers and krill-dependent predators is a focus of several studies and is a driver of Commission for the Conservation of Antarctic Marine Living Resources (CCAMLR's) precautionary approach to krill fisheries. Maschette et al., based on information from the recent surveys (Cox et al., 2022; Murase, 2025) updates estimates of precautionary catch limits across longitudinal range between 50 to 140 degrees east in East Antarctica. Krill swarms become sparse away from the continent, and the bioenergetic content of krill varies by swarm composition (swarms of gravid females containing the most energy) (Cataldo-Mendez et al.). This illustrates the importance of considering both recruitment (Maschette et al.) and stage-specific maturity representations of krill (Green et al.; Schaafsma et al.).

The collective insights from recent Antarctic krill research have direct relevance for ecosystem-based fisheries management strategies employed by CCAMLR. Improved demographic and energetic characterization of krill enhances the precision of yield models and supports spatially differentiated catch limits (Cataldo-Mendez et al.; Maschette et al.). Furthermore, simulation frameworks like KRILLPODYM enable scenario testing under varying environmental and harvest regimes (Green et al.), and they rely heavily on empirical observations of habitat use and predator interaction.

Crucially, the use of predator foraging metrics and spatial fidelity as monitoring proxies offers a practical means to assess krill availability across trophic levels (Calderan et al.; Viola et al.). These integrative approaches support CCAMLR's precautionary harvest framework by emphasizing ecological roles and the importance of krill for dependent species. Recent studies collectively encourage a shift toward adaptive, spatial management informed by feedback from coupled ecological indicators and biomass models.

Several knowledge gaps remain that are critical for advancing the science and stewardship of Antarctic krill dominated ecosystems. High priorities include empirical studies of under-ice and winter ecology, energy-based metrics in trophic models, and improved seasonal resolution in predator-prey data collection (Cataldo-Mendez et al.; Weldrick et al.). The incorporation of autonomous platforms—such as gliders, drones, and moored acoustic arrays—can provide continuous, high-resolution coverage of krill habitats (Andrews-Goff et al.; Miller et al.).

Additionally, modeling efforts should further integrate machine learning techniques and coupled physical-biogeochemical frameworks to improve predictions of krill dynamics under future climate and fishery scenarios (Green et al.; Tan and Bai). Cross-study synergies, such as integrating habitat models with predator telemetry (Riaz et al.) and biomass estimates (Cox et al., 2022, represent a fertile area for synthesis and inter-disciplinary collaboration. Long-term, multinational research collaborations will be indispensable in filling observational gaps and ensuring robust, dynamic, and ecologically coherent management strategies for krill-based ecosystems.

Author contributions

SK: Writing – review & editing, Conceptualization, Project administration. EB: Writing – review & editing. SB: Writing –

review & editing. MC: Conceptualization, Writing – original draft. KS: Writing – review & editing.

Acknowledgments

Thank you to all the editors, authors, and reviewers that contributed to this Research Topic.

Conflict of interest

The authors declare that the research was conducted in the absence of any commercial or financial relationships that could be construed as a potential conflict of interest.

Generative AI statement

The author(s) declare that no Generative AI was used in the creation of this manuscript.

Publisher's note

All claims expressed in this article are solely those of the authors and do not necessarily represent those of their affiliated organizations, or those of the publisher, the editors and the reviewers. Any product that may be evaluated in this article, or claim that may be made by its manufacturer, is not guaranteed or endorsed by the publisher.

References

Abe, K., Matsukura, R., Yamamoto, N., Amakasu, K., Nagata, R., and Murase, H. (2023). Biomass of Antarctic krill (Euphausia superba) in the eastern Indian sector of the Southern Ocean (80–150°E) in the 2018–19 austral summer. *Prog. Oceanography* 218, 103107. doi: 10.1016/j.pocean.2023.103107

Bairstow, F., Gastauer, S., Finley, L., Edwards, T., Brown, C. T. A., Kawaguchi, S., et al. (2021). Improving the accuracy of krill target strength using a shape catalog. *Front. Mar. Sci.* 8. doi: 10.3389/fmars.2021.658384

Bairstow, F., Gastauer, S., Wotherspoon, S., Brown, C. T. A., Kawaguchi, S., Edwards, T., et al. (2022). Krill biomass estimation: Sampling and measurement variability. *Front. Mar. Sci.* 9, 903035. doi: 10.3389/fmars.2022.903035

Cox, M. J., Macaulay, G., Brasier, M. J., Burns, A., Johnson, O. J., King, R., et al. (2022). Two scales of distribution and biomass of Antarctic krill (Euphausia superba) in the eastern sector of the CCAMLR Division 58.4.2 (55°E to 80°E). *PloS One* 17, e0271078. doi: 10.1371/journal.pone.0271078

Cox, M., Smith, A., Brierley, A., Potts, J., Wotherspoon, S., and Terauds, A. (2023). Scientific echosounder data provide a predator's view of Antarctic krill (Euphausia superba). *Sci. Data* 10, 284. doi: 10.1038/s41597-023-02187-y

Murase, H. (2025). Overview of the multidisciplinary ecosystem survey in the eastern Indian sector of the Southern Ocean (80–150°E) by the Japanese research vessel Kaiyo-maru in the 2018–19 austral summer (KY1804 survey). *Prog. Oceanography* 233, 103456. doi: 10.1016/j.pocean.2025.103456

Smith, A. J. R., Wotherspoon, S., Ratnarajah, L., Cutter, G. R., Macaulay, G. J., Hutton, B., et al. (2025). Antarctic krill vertical migrations modulate seasonal carbon export. *Sci. (New York N.Y.)* 387, eadq5564. doi: 10.1126/science.adq5564

Vives, C. R., Schallenberg, C., Strutton, P. G., and Westwood, K. J. (2022). Iron and light limitation of phytoplankton growth off East Antarctica. *J. Mar. Syst.* 234, 103774. doi: 10.1016/j.jmarsys.2022.103774

frontiers | Frontiers in Marine Science

TYPE Original Research
PUBLISHED 26 January 2023
DOI 10.3389/fmars.2023.1087967

Check for updates

OPEN ACCESS

EDITED BY
Stefano Aliani,
National Research Council (CNR), Italy

REVIEWED BY
Russel D. Andrews,
Marine Ecology and Telemetry Research (MarEcoTel), United States
Salvatore Siciliano,
Fundação Oswaldo Cruz (Fiocruz), Brazil
Holly Crystal Raudino,
Department of Biodiversity, Conservation and Attractions (DBCA), Australia

*CORRESPONDENCE
Susannah V. Calderan
susannah.calderan@sams.ac.uk

SPECIALTY SECTION
This article was submitted to Marine Ecosystem Ecology, a section of the journal Frontiers in Marine Science

RECEIVED 02 November 2022
ACCEPTED 11 January 2023
PUBLISHED 26 January 2023

CITATION
Calderan SV, Leaper R, Andrews-Goff V, Miller BS, Olson PA, Reyes MVR, Bell E and Double MC (2023) Surfacing rates, swim speeds, and patterns of movement of Antarctic blue whales. *Front. Mar. Sci.* 10:1087967. doi: 10.3389/fmars.2023.1087967

COPYRIGHT
© 2023 Calderan, Leaper, Andrews-Goff, Miller, Olson, Reyes, Bell and Double. This is an open-access article distributed under the terms of the Creative Commons Attribution License (CC BY). The use, distribution or reproduction in other forums is permitted, provided the original author(s) and the copyright owner(s) are credited and that the original publication in this journal is cited, in accordance with accepted academic practice. No use, distribution or reproduction is permitted which does not comply with these terms.

Surfacing rates, swim speeds, and patterns of movement of Antarctic blue whales

Susannah V. Calderan[1,2]*, Russell Leaper[1,3], Virginia Andrews-Goff[1], Brian S. Miller[1], Paula A. Olson[1,4], M. V. Reyes Reyes[1,5,6], Elanor Bell[1] and Michael C. Double[1]

[1]Australian Antarctic Division, Department of Climate Change, Energy, the Environment and Water, Kingston, TAS, Australia, [2]Scottish Association for Marine Science (SAMS), Argyll, Scotland, United Kingdom, [3]International Fund for Animal Welfare, London, United Kingdom, [4]Southwest Fisheries Science Center, National Marine Fisheries Service, National Oceanic and Atmospheric Administration, La Jolla, CA, United States, [5]Whale and Dolphin Conservation, Wiltshire, United Kingdom, [6]Fundación Cethus, Buenos Aires, Argentina

During three surveys in the austral summers of 2013, 2015, 2019, data on Antarctic blue whale blow rates, dive times, swim speeds, and broadscale movements were collected using video photogrammetric tracking and intra-voyage photo-identification. A total of 24.4 hours of video observations were suitable for blow interval or movement analysis. Similar to other blue whale populations, Antarctic blue whale dive behaviour comprised a sequence of short dives followed by a long dive with a mean dive time for short dives of 17.6 s, and a mean long dive time of 189.3 s. Two separate methods were used to estimate the average blow rate for Antarctic blue whales, giving estimates of 59.7 and 63.2 blows per hour. The overall mean swim speed over the course of all suitable video track segments was 1.59 ms^{-1}, but there were significant differences between years in the mean of the overall movement rate for each track; average movement rates were lower in 2015 compared to 2013 and 2019 (0.90 ms^{-1}, 1.84 and 1.55 ms^{-1} respectively), with higher rates of turning in 2015. In 2019, there was faster overall movement through the study area in a consistent direction. The total number of photo-identified blue whales re-sighted intra-season in 2013 was nine (out of 50 identified individuals); in 2015 it was seven (out of 46); in 2019 two (out of 25). Whales remained for several days with little overall movement within the 2015 study area, whereas they were moving through the study area in 2019, which would explain the low number of intra-season resights. The predominant heading in 2019 was towards the area of Antarctic blue whale concentrations at the entrance to the Ross Sea observed in previous years. The photo-identification data also show a high proportion of resighted whales with coherent movements. This suggests that Antarctic blue whales might travel together, at least over periods of several days or sometimes up to a month. The differences between behaviours in 2015 and 2019 in particular may be related to differences in the characteristics of krill swarms between the study areas.

KEYWORDS

blue whales, Antarctic, photogrammetry, photo-identification, behaviour

1. Introduction

Following heavy depletion by 20th century industrial whaling, Antarctic blue whales *Balaenoptera musculus intermedia* remain critically endangered (Cooke, 2018). Their small population size and distribution over areas which are often difficult to access means they are challenging to study, and their ecology, movements and behaviour are poorly understood. Some data from satellite telemetry are available (Andrews-Goff et al, 2022), but otherwise little is known about their surfacing behaviours or movement, particularly over fine spatial and temporal scales.

Knowledge of Antarctic blue whale fine-scale movements and behaviour is important for informing studies which involve approaching and/or surveying whales, and also for a variety of long-term or multidisciplinary studies. Metrics of Antarctic blue whale behavioural parameters may assist in the interpretation of a range of datasets. Blow (cue) rates are important in visual survey data analysis for estimating g(0) (the probability of detecting an animal directly on the survey trackline) for single platform surveys, or if cue counting methods are used (Hiby, 1992). For example Leaper et al. (2015) used a simulation approach to estimate g(0) based on previous work which classified blue whale dives as either short or long dives (Lagerquist et al., 2000; de Vos et al., 2013). Information on movements and surfacing behaviour can potentially add value to passive acoustic studies when behaviours can be linked to vocalisations (Oleson et al., 2007; Schall et al., 2020). Movements and vocalisations have also been hypothesised to be related to behavioural state, and thus may be indicative of prey availability and characteristics (Miller et al., 2019). Additionally, this information may be useful when investigating hypotheses on the role of whales in the ecosystem, for which overall movements through an area might be compared with phytoplankton, bacteria, and biogeochemistry e.g. iron concentrations (Smith et al., 2021). Natural behaviours and movements may also inform assessment of anthropogenic impacts, for example, by providing baseline data against which impacts can be evaluated (Lomac-MacNair and Smultea, 2016). Similarly, this information provides direct parameters which are required by individual-based energetic models for investigating population consequences of disturbance (Pirotta et al., 2022). Fine-scale movement data may also help to improve interpretation of longer-term telemetry studies where potentially large positional errors and small sample sizes in terms of both locations and tracks can limit understanding of behavioural states. For example, measurements of short-term swim speeds over minutes will inevitably be higher than longer-term movement rates over hours, making it difficult to compare fine-scale tracking with longer-term movement data. In such cases, relationships between measured speed and interval time may facilitate comparisons between different studies.

Information on whale movements comes from a small number of highly-specialised methods including large-scale and long-term satellite-telemetry tags (Andrews-Goff et al, 2022); mark-recapture during whaling (Branch et al., 2007), and visual and acoustic focal follows (Leaper and Gordon, 2001; Miller et al., 2014). These methods operate over temporal scales from decades to seconds, and over spatial scales from global to fine-scale. Information on Antarctic blue whale movements can also be obtained from photographic mark-recapture studies, particularly from the Antarctic Blue Whale Catalogue. The Catalogue was established in 2007 and currently holds 562 identified whales (represented by 421 left side and 413 right side photographs) from the years 1980-2022 (unpub. data). Over a dozen research organisations and independent scientists have contributed photographs to the Catalogue (Olson et al., 2020). Whilst most prior photographic mark-recapture studies have focused on large-scale movements between years, photographic identification (photo-ID) can also provide information on intra-seasonal movements for whales which are photographically captured more than once each year (e.g. recaptured later during the same voyage). These intra-seasonal recaptures can potentially help to relate the overall direction of travel throughout a voyage to other measures of movement e.g. obtained *via* satellite tags (described above), or focal follows (described below). Recently, inter-seasonal data have also been examined for movement patterns of Antarctic blue whales (Olson et al., 2022).

Focal follows of animals typically involve following groups of whales to record behaviours, understand behavioural contexts, including interactions and responses, and describe sequences of events (Oleson et al., 2007; Quick et al., 2008; Crance et al., 2017). This type of study is often conducted from a small boat, or from shore with instruments such as theodolites and hydrophone arrays (Dunlop et al., 2016). Video photogrammetric systems may also be used from research vessels in order to carry out and obtain a series of locations (Leaper and Gordon, 2001). Like theodolites, video photogrammetric systems enable the measurement of distances and bearings to provide locations with high precision and accuracy (Williams et al., 2007; Leaper et al., 2010), as well as recording sequences of behaviours as whales surface (Leaper and Gordon, 2001). Video photogrammetric tracking can provide information on blow (cue) rates and swimming speeds. However, estimation of swim speeds this way can be sensitive to errors in location. For example, locations for more distant groups are less accurate than those closer to the ship due to measurement error (Leaper and Gordon, 2001).

This study describes blow rates, movements, and swim speeds of Antarctic blue whales on their Antarctic feeding grounds using a combination of intra-voyage photographic recaptures, and photogrammetric analysis of video recordings (video range tracking). Comparisons between these swim speeds and those observed in the Antarctic using other methods and different spatial scales are made, as well as between these observations and those observed from other blue whale populations/sub-species.

2. Materials and methods

2.1. Data collection

Antarctic blue whales were studied on three Antarctic voyages during the austral summers of 2013, 2015 and 2019 on the 65 m *FV Amaltal Explorer*, the 70 m *RV Tangaroa*, and the 94 m *RV Investigator* respectively (Double et al., 2013; Double et al., 2015; Double et al., 2021). Whales were detected acoustically using

directional frequency analysis and recording (DIFAR) sonobuoys (which enable the detection of both whale vocalisations and the bearings to those vocalisations). Then individuals or groups of whales (referred to hereafter as 'groups') were tracked and approached using acoustic bearings, until they had been sighted by visual observers (see Miller et al. (2015) for description of acoustic methodology). Once a group was visually detected, the survey vessel slowed down or stood off, allowing focal follows using video photogrammetric tracking to take place whilst the group was largely undisturbed (Calderan et al., 2014; Calderan et al., 2017; Calderan et al., 2022). Following photogrammetric video tracking, the research team would then guide the ship for a closer approach to the group for photo-ID (if video-tracking was not undertaken, the ship would move directly to approach for photo-ID). Both sides of each whale were photographed whenever possible. Typically two photographers worked from the bow of the ship. In 2013, during optimal weather conditions, a RHIB was launched and one photographer worked on each vessel. DSLR cameras with image-stabilized zoom lenses were used to gather images for photo-ID.

Movement data were collected using the photogrammetric methods described in Leaper and Gordon (2001). Whale locations were measured at each surfacing, enabling focal follows of Antarctic blue whales as they were observed from the survey vessel. Groups which were first seen at distances of several km were observed and video tracked before the vessel moved to close-approach mode for photo-ID, allowing behavioural data to be gathered when the whales were first sighted, and before the research vessel was so close that behaviour was likely to be substantially affected. The aim was to gain as much understanding as possible about the behaviour of the group before making a close approach. Photogrammetric and photo-ID data were collected between sunrise and sunset (much of the study area remained almost-continuously in daylight due to the high latitude and time of year).

The video tracking system comprised a front-facing Panasonic HCV700 camcorder with a calibrated lens of known focal length, downward-facing Canon A40 stills camera (reference marks were made on the deck to enable angle measurement), and binoculars. These were mounted on a single frame and monopod. The observation platform heights were 10.2 m, 14.4 m and 16.9 m respectively on the 2013, 2015 and 2019 voyages. The system enabled a combination of locations and behavioural observations, including surfacing locations, blow rates, swimming speeds and changes in heading to be measured by a tracking observer. The tracker was assisted by another observer to ensure the consistent resighting and tracking of the focal animal if there was more than one whale in the group. The tracker also recorded a concurrent audio commentary to assist with disambiguating the video during post-processing and analysis. At the conclusion of video tracking, the vessel moved towards the whale group to allow photo-ID. The video and stills data were post-processed using the Video Range module in PAMGuard (www.pamguard.org) to derive distances and bearings, following methods in Leaper and Gordon (2001). Once a series of whale times and positions had been compiled into a track, these were analysed to estimate blow rates and movement parameters.

2.2. Data analysis

In order to analyse photogrammetric and photo-ID data, three types of velocity measurements (speed in ms^{-1} and heading in degrees) were used, representing different temporal scales:

(a) Swim speed: over the shortest period between surfacings that allowed for measurement of speed to meet the criteria for accuracy discussed in 2.2.1.3; close to actual speed through the water (not accounting for vertical movement);

(b) Movement rate: measured from the start to end of a track, representing an overall speed of travel in a particular direction over 10 minutes or longer;

(c) Broadscale movement rate: measured from the distance between locations over a day or longer apart.

2.2.1. Photogrammetry

2.2.1.1. Combining locations into tracks

The data used in analysis were selected to avoid some of the major sources of bias which can be associated with photogrammetric tracking data, resulting in only a proportion of tracks being included. These potential sources of bias are that individual blows or sequences of blows might be missed, resulting in potentially biased blow rates. Furthermore, in groups where there is more than one whale, the focal animal may be confused with another individual, which will bias surfacing and movement parameters. Measurement error will also cause bias in swim speeds measured over short time periods because apparent movement may in fact be the result of measurement error. Whales may also react to the approaching vessel. Therefore the tracks which were included in analysis were those where the group comprised a single animal, several animals surfacing and moving together, or where there was confidence that the focal animal in the group was followed throughout. In 2013 a small RHIB was sometimes deployed during approaches. All periods when the RHIB was in the water were excluded from the analysis because of the potential for disturbance. The use of hidden Markov models to characterise whale movements and diving behaviour (DeRuiter et al., 2017) was investigated, but the tracks were too short to reliably fit such models.

2.2.1.2. Overall movement across tracks (movement rate and heading)

To investigate any patterns in overall movements from the start to the end of a track, measurements to whales up to 6 km from the ship were included. In addition, a minimum tracking time of 600 s was applied. The end of the track was defined as the last observation before a group was lost, potentially confused with a different group, or came within 500 m of the vessel during a close approach. Distance travelled and heading were calculated using the 'traipse' package (Sumner, 2021), and the distribution of headings was analysed using the 'circular' package in R (Agostinelli and Lund, 2017); the Rayleigh test was used to determine whether the headings in each year showed any pattern in headings that was significantly different from a uniform distribution (R Core Team, 2021).

2.2.1.3. Fine-scale movement within track (swim speed and heading)

A maximum radial distance from the research vessel of 2 km was chosen for measurements of locations used to derive swim speeds, as a compromise between discarding data and an acceptable level of measurement error. The expected measurement error was based on estimates from Leaper and Gordon (2001), who found that from a platform height of 18 m, the RMS error in measured distances was around 3.5 % of the radial distance. RMS errors in bearing were 1.21° (angle errors were greater for situations where the ship turned frequently but improvements in GPS heading sensors probably mean this is less of an issue than when the calibration tests were conducted). Whilst video camera technology has also improved, with considerably higher resolution images than used for the estimates of accuracy in Leaper and Gordon (2001), the factor that most limited photogrammetric accuracy was swell, which not only introduced errors in the bearing and angle of dip from the horizon, but also errors in platform height, none of which would be fully resolved by improvement in image-resolution.

At 2 km, a 3.5 % error in distance corresponds to a location error of 70 m, and a 1.2° error in angle corresponds to a location error of 40 m. A simple simulation where radial distance error was drawn from a distribution with mean 0 and standard deviation of 70 m, and angle error was drawn from a distribution with mean 0 and standard deviation of 1.2° indicated that the combined effect of these errors for a whale initially at a radial distance of 2 km would be expected to introduce an RMS error in the estimated distance between two observations of 113 m. A minimum interval time of 150 s was then selected as approximately the minimum duration of a full sequence of a few short dives (submersions between breaths) and a long dive (submersion between a bout of breathing surfacings). For a typical swimming speed of 2 ms^{-1}, speed estimates at maximum range and minimum interval time would be subject to an RMS error of around 38%. Locations that were closer than 500 m to the vessel were also rejected because of the possibility of responsive movement. This distance was chosen based on qualitative observations during the voyages, on the analysis of Lesage et al. (2017), who noted behavioural changes in blue whales in the St. Lawrence estuary Canada when vessels were within 400 m, and research by Szesciorka et al. (2019) who reported a change in surfacing behaviour as a ship approached within 300m.

Whale locations for swim speed and heading measurements were therefore selected on the criterion that the radial distance was between 500 m and 2000 m. For each track, the first location which met this criterion was determined to be the start point for speed and heading measurements. Speed and heading were then measured along the segment of whale track to the next surfacing location that met the criterion and was >150 s later. This process was repeated until the end of the track (as defined in 2.2.1.2). The change in heading in degrees between each track segment was also calculated.

2.2.1.4. Blow rates

For this study, a bimodal distribution of short and long dives was assumed (but with potentially some overlap between the two), such that the observed frequency of intervals could be modelled as the sum of two distributions. These distributions would not be expected to be normally distributed because longer intervals occur less frequently in the same time period (e.g. there is potential for 10 intervals of 10s in a 100s time period, but only 5 intervals of 20 s). Thus data transformations were investigated, including fitting distribution functions to log(interval). The mixR package in R (Yu, 2022) was used to fit a two-component mixture model using maximum likelihood estimation (R Core Team, 2021).

In the dataset from tracks which were confidently assessed as including just a single individual, the minimum observed blow interval was 5 s. Thus any intervals less than this were excluded from the full data set on the assumption that they were probably a result of blows from different whales which were misidentified when more than one individual was present. Surfacing intervals of more than 900 s were also removed on the assumption that these represented situations where a surfacing had occurred, but had not been detected. The value of 900 s was taken from the maximum observed dive duration from telemetry studies by Croll et al. (2001), although longer dive times have also been observed on a few occasions (e.g. Lagerquist et al., 2000; Owen et al., 2016).

Where a log transformation was used, the mean blow interval for the untransformed data to compare with other studies was assumed to be

$$\exp\left(\mu + \frac{\sigma^2}{2}\right)$$

where μ and σ are the mean and standard deviation respectively of the transformed data.

In addition to estimating the mean blow interval of short and long dives, the ratio of the number of short intervals to each long interval (b) was also estimated, in order to model the overall blow rate.

2.2.2. Intra-season photo-ID recaptures (broadscale movement rate and heading)

Photographs of Antarctic blue whales were judged to meet minimum quality criteria based on distance to the subject (whale), focus, angle and lighting (Olson et al., 2021). Photographs meeting these criteria were considered suitable for identifying individual blue whales and were compared within each season and to the Antarctic Blue Whale Catalogue following methods outlined in Sears et al. (1990) and in Gendron and Ugalde de la Cruz (2012). Distances between intra-seasonal recapture locations were calculated using great circle estimates from the traipse package in R (Sumner, 2021; R Core Team, 2021).

3. Results

The voyage tracks of the three research vessels are shown in Figure 1, as well as the heading direction in the overall movements of whales across video tracks in each of the voyages (Table 1). A total of 24.4 hours of video observations were suitable for blow interval or movement analysis. This resulted in 577 surfacing locations at intervals of greater than 5 s. These were divided into 181 segments of track between locations which were more than 150 s apart and suitable for measurement of whale swim speeds and headings. The total track length of these segments was 137 km.

10.3389/fmars.2023.1087967

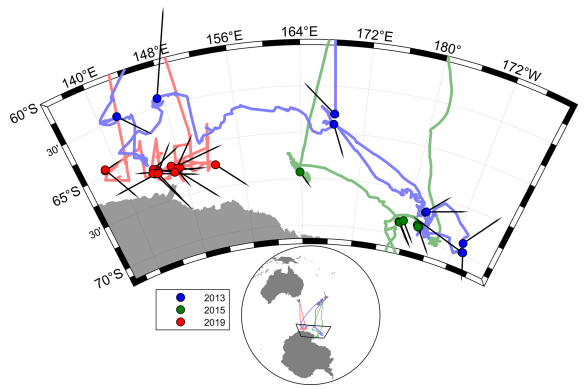


FIGURE 1
Map showing whole voyage tracks for all three voyages, with dots for positions of the video tracks used, and directions of overall whale movement in each video track (black pointers).

3.1. Photogrammetry

3.1.1. Overall movement across tracks (movement rate and heading)

In 2013 and 2015, headings showed no overall significant difference from a uniform distribution (Figures 2A, B), but in 2019 (Figure 2C), there was a significant departure from uniform headings, with a bias towards an east-southeast heading (Table 2).

The overall mean component of movement for all whales in 2019 along the median heading was 0.88 ms^{-1}. Two of the tracks in 2013 were also in the 2019 study area, and both had an easterly component (mean 78°).

3.1.2. Swim speeds

The mean distance between locations used to estimate speed was 1035 m with a mean interval of 480 s. For these mean values and a swim speed of 1 ms^{-1}, the RMS error in speed due to measurement error would be expected to be around 15 %.

TABLE 1 Video tracks and measurements of movement rate and heading across each track.

Year	Track ID	Start Time (UTC)	Start Latitude	Start Longitude	Distance travelled (m)	Duration (s)	Movement Rate (ms^{-1})	Heading (degrees)
2013	3	07/02/2013 21:04:14	-62.27	142.24	17494	10612	1.65	137
2013	9	14/02/2013 01:25:19	-62.03	147.32	6235	1664	3.75	20
2013	13	20/02/2013 01:04:19	-64.54	168.13	3942	2696	1.46	161
2013	19	25/02/2013 18:40:36	-68.44	-177.68	3857	3052	1.26	44
2013	20	25/02/2013 19:35:32	-68.41	-177.58	3468	2016	1.72	74
2013	22	01/03/2013 06:14:43	-69.38	-170.85	5225	2665	1.96	34
2013	23	01/03/2013 18:35:43	-69.85	-170.47	5325	2122	2.51	-76
2013	24	01/03/2013 22:27:16	-69.85	-170.35	2108	1808	1.17	160
2013	25	07/03/2013 21:55:12	-63.99	168.17	12888	7088	1.82	-47
2015	1	06/02/2015 04:21:43	-67.14	163.76	2350	2877	0.82	146
2015	2	09/02/2015 18:26:06	-69.29	178.82	2304	2211	1.04	146
2015	3	09/02/2015 19:33:47	-69.30	178.96	3102	2658	1.17	146
2015	4	10/02/2015 00:14:48	-69.18	179.45	5244	5054	1.04	146
2015	6	10/02/2015 19:56:38	-69.22	-178.36	7805	5836	1.34	146
2015	7	11/02/2015 01:29:08	-69.29	-178.05	1314	3769	0.35	146
2015	8	11/02/2015 18:10:02	-69.31	-178.20	3453	6237	0.55	146
2019	1	30/01/2019 01:23:05	-64.73	138.46	3261	3892	0.84	80
2019	2	30/01/2019 07:31:14	-64.68	138.51	1826	1000	1.83	154
2019	3	01/02/2019 21:33:37	-65.88	144.32	6559	3117	2.10	152
2019	5	03/02/2019 05:34:50	-65.81	144.61	665	724	0.92	-76
2019	7	03/02/2019 07:47:42	-65.66	144.61	1695	1252	1.35	118
2019	8	03/02/2019 09:36:22	-65.62	144.27	2187	1494	1.46	66
2019	10	04/02/2019 01:28:07	-65.79	144.83	8141	4022	2.02	104
2019	11	04/02/2019 19:18:44	-65.81	144.07	3862	1980	1.95	110

(Continued)

10.3389/fmars.2023.1087967

TABLE 1 Continued

Year	Track ID	Start Time (UTC)	Start Latitude	Start Longitude	Distance travelled (m)	Duration (s)	Movement Rate (ms^{-1})	Heading (degrees)
2019	12	08/02/2019 19:16:16	-65.86	146.87	8487	3829	2.22	81
2019	13	08/02/2019 23:38:00	-65.91	146.92	3183	1407	2.26	138
2019	17	17/02/2019 00:00:55	-66.25	152.41	5537	3355	1.65	134
2019	18	18/02/2019 01:52:36	-65.95	147.16	4072	4120	0.99	156
2019	19	18/02/2019 19:34:40	-65.95	147.70	3193	4555	0.70	115
2019	20	22/02/2019 01:28:18	-65.87	144.82	3466	1707	2.03	-100
2019	21	22/02/2019 03:50:06	-65.90	144.67	1567	1108	1.41	39
2019	22	23/02/2019 04:32:35	-65.74	146.65	3077	5926	0.52	144
2019	23	24/02/2019 02:32:22	-65.95	147.40	1253	4267	0.29	-44
2019	24	24/02/2019 08:26:36	-66.11	146.88	4444	2573	1.73	41

The overall mean swim speed over the course of all suitable track segments (total combined distance/total combined time) was 1.59 ms^{-1}, with the average duration of a track being 3924 s (65.4 minutes). For the tracks which also met the criteria for movement rate measurements, the mean swim speed and movement rate from the start to the end of the track are given in Table 3. Linear regression indicated mean movement rate was 83 % of mean swim speed (R^2 = 0.73). Tracks with slower swim speeds tended to be longer and have more speed measurements. Thus the mean of the swim speeds for each track was used in the regression analysis rather than the separate individual swim speed measurements. On average, movement rates measured over the course of around an hour were about 83 % of swim speeds measured over the course of 6-minute intervals.

There were significant differences between years in the mean of the movement rates for each track (Anova, p=0.01) and the mean heading change between segments for each track (Anova, p=0.007). The differences between the mean swim speeds followed a similar pattern but were not significantly different between years (Anova, p=0.06). The larger differences seen between years for the movement rates compared to the swim speeds could be explained by relatively consistent swim speeds through the water, but higher rates of turning when movement rates were lower. Swim speeds varied between 0.01 and 4.15 ms^{-1}. 2015 stands out for low movement rates and high rates of turning.

3.1.3. Blow rates

Excluding dives of longer than 900 s from the analysis (on the basis that they were likely due to a missed bout of surfacings) resulted in the removal of 11 dives (0.6% of the total).

Based on the fitted distributions to the log(interval) data (Figure 3), the mean short dive was 17.6 s (95% CI 7-42 s) and mean long dive was 189.3 s (95% CI 43-674s). The median for short dives was 18 s. The ratio from the fitted normal distributions gave *b*=3.37 short dives to each long dive. Thus an average of 4.37 dives would occur over an average time period of 248.6 s (3.37x17.6 + 189.3). Therefore mean dive time for all the observations would be 56.9 s (63.2 blows per hour) based on the fitted distributions. The minimum of the combined distributions of short and long blow intervals (Figure 3) occurred at an interval of 58.9 s. This was so close to one minute that an interval of greater than 60 s was chosen to define a long dive (which also matches the definition of Lagerquist et al. (2000)).

If a long dive is defined as more than 60 s, then for groups comprising only one animal in 2019, there were 64 occasions when, in

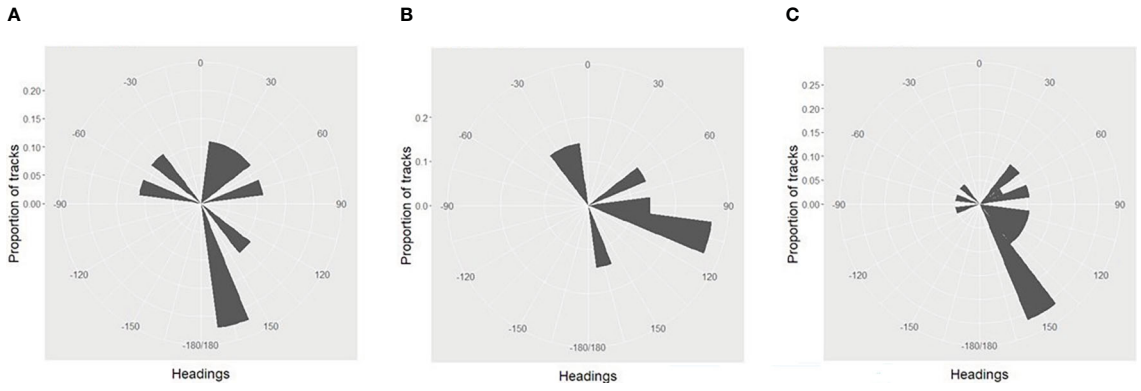


FIGURE 2
(A). Distribution of whale headings from video tracks, 2013 **(B)**. Distribution of whale headings from video tracks, 2015 **(C)**. Distribution of whale headings from video tracks, 2019.

10.3389/fmars.2023.1087967

TABLE 2 Tracks used to test for patterns in whale headings.

Year	n	Mean (+-95% CI)	Median	Rayleigh Test of Uniformity (p)
2013	9	n/a	n/a	0.522
2015	7	n/a	n/a	0.200
2019	18	115.7° +33°	118.5	0.004

TABLE 3 Summary of information from video tracking and photo-ID.

	2013	2015	2019
Video tracks			
Number of tracks used for movement rates	9	7	18
Annual mean of mean movement rate (ms^{-1})	1.84	0.90	1.55
Annual median of mean movement rate (ms^{-1})	1.72	1.04	1.65
Number of measured swim speeds	34	65	89
Annual mean of mean swim speed ms^{-1}	2.06	1.32	1.80
Annual median of mean swim speed ms^{-1}	2.02	1.10	2.10
Annual mean of mean heading change between segments (degrees)	44.9	57.4	35.3
Photo-ID			
Total number of photo-IDs	50	46	25
Number of photo-ID resights	9	7	2
Annual mean of broadscale movement rates from photo-ID resights ms^{-1}	0.68	0.16	0.55
Annual median of broadscale movement rates from photo-ID resights ms^{-1}	0.56	0.09	0.55

a bout of short dives followed by a long dive, all the blows could be accurately counted. The number of blows between long dives ranged from 1-13 (mean = 4.3, sd = 2.59). This mean number of blows for groups comprising one animal was very similar to the overall mean for all data from the fitted distributions of 4.37 blows per bout.

Long dives separated by a single surfacing were observed on several occasions. For example, out of 118 long dives by groups comprising only one animal, 22 (19%) were reported as separated by just a single blow, although it is possible that some blows were missed. For these successive pairs of long dives, the average total dive time for the two dives combined was 325 s (range of 123 – 714; sd = 84 s). Over the total period of time where groups comprising one animal were tracked (13 tracks, 5.86 hours), there were 350 blows, corresponding to a mean rate of 59.7 blows per hour. This resulted in an estimated mean blow interval of 60.3 s.

3.2. Movements based on intra-season photo-ID recaptures

The total number of photo-identified blue whales in 2013 was 50 individuals, in 2015 it was 46, and in 2019 it was 25. The potential for photo-ID recaptures within each voyage was dependent on the movements of the research vessel. There were nine individuals in intra-season matches in 2013, seven in 2015 and two in 2019 (Table 3). Of these, just one individual was sighted on more than two occasions, on three separate days (in 2015).

Based on the straight-line distances between capture and recapture locations, the fastest broadscale movement rate observed from photo-ID was 1.13 ms^{-1} over a distance of 77.4 km (Table 4). Amongst the 18 individuals resighted, three individuals (following similar trajectories) were seen at an average minimum distance of 1100 km from their first sightings and were recaptured together in the same group. These three individuals had a broadscale movement rate of 0.53 ms^{-1} (Figure 4) and all remained north of 65°S. In the recapture sighting, the three were part a group of five individuals. Another two individuals were resighted together three times over two days, eventually 78 km from their first sightings. Six further individuals remained within the same small area. This suggests that coherent movements of Antarctic blue whales on the feeding grounds may be common (i.e. 11 out of 18 individuals observed in this study showed coherent movements).

The same patterns of broadscale movement rates by year were apparent from the photo-ID resightings as from the movement rates from the video tracks. Four whales were resighted in 2015 within 15km of their original sighting locations between 39 and 72 hours later, with a broadscale movement rate of 0.05 ms^{-1}.

4. Discussion

This study presents data on fine-scale movements of Antarctic blue whales, including swim speeds and blow rates, and broadscale movements of identified whales within a season. The overall pattern

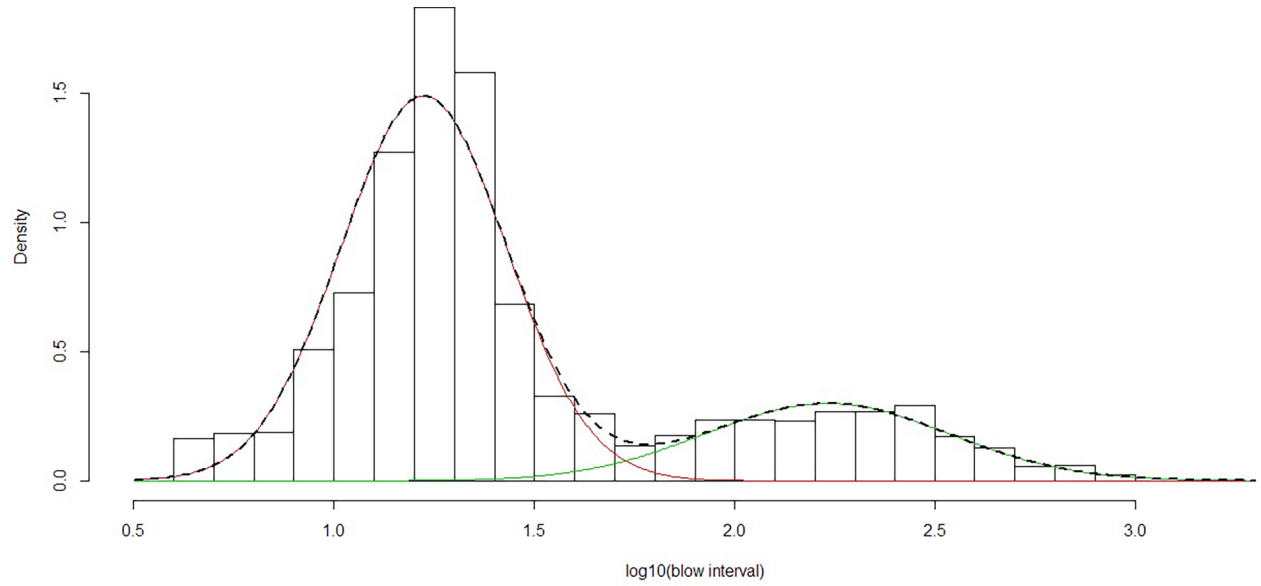


FIGURE 3
Mixed fit of normal distributions to log(10) of observed blow intervals using data from 2013, 2015 and 2019. The line indicates the fitted combination of two normal distributions representing 'short' (red) and 'long' (green) dives.

of all blue whale dives (not only of Antarctic blue whales) can be summarised by a sequence of short dives followed by a long dive. The length of short dives appears consistent over time and between areas, with a distinct peak in occurrence of intervals of around 18 s. For example, the observed values in this study for short dives are very similar to the equivalent dive times of blue whales observed off Sri Lanka (17.6 s) (de Vos et al., 2013). This may indicate a swimming gait associated with breathing that is common across blue whale subspecies and populations.

Long dives are much more variable and differ between activities and areas. For example, New Zealand blue whale long dives are relatively short (170s ± 16.2s SE) (Torres et al., 2020), compared to 640 s off Sri Lanka (de Vos et al., 2013). Studies of blue whale dives off California reported average long dives of 252 s to 432 s (Lagerquist et al., 2000). These differences are consistent with short dives being optimised for respiration and long dives being in response to the nature and location of prey, and support previous studies (Lagerquist et al., 2000) that a dive time of over 60 s is a useful definition of a long dive. That study found that 72% of blue whale dives off California were less than 60 s long. This is an equivalent ratio of 2.6 short dives to each long dive, which is a little lower than for Antarctic blue whales in this study (3.76). Unlike off Sri Lanka where long dives were never observed with just a single surfacing between them (de Vos et al., 2013), this was observed on several occasions in this study.

An estimate of average Antarctic blue whale surfacing rates has been calculated using two different methods (59.7 and 63.2 blows an hour). The model of patterns of short and long dives could be used with models to estimate g(0) for single platform or opportunistic visual surveys. The mean blow interval is rather lower than that estimated off Sri Lanka (84.7s sd 11.17) by de Vos et al. (2013), mainly due to the much shorter 'long' dives for Antarctic blue whales. de Vos et al (2013) used a Monte Carlo model-based method to adjust for the fact that most whales in their study were lost after a long dive (i.e. the last long dive of a sequence was not included). This was not the case for this study where the tracking usually ended when the vessel made a close approach for photo-ID, and it was likely that when a long dive occurred the whale would usually be resighted.

If blows were missed, particularly the first blow after a long dive, then the estimate of number of blows per hour would be negatively biased. This certainly did happen, but during focal follows there were usually several observers monitoring the full 360° around the vessel, so this was likely a rare occurrence for the tracks included in the analysis. For observational studies there may be occasions when a full bout of surfacings between long dives is missed. Thus the longest observed intervals may be due to observational error.

Estimates of blue whale swimming speeds from the video tracking dataset were highly variable. The maximum reliable video track-derived swimming speed estimate was 4.15 ms^{-1} over a period of 217 s, but blue whales are known to be capable of much faster speeds, upwards of 10 ms^{-1} (Sears and Perrin, 2009). In comparison, satellite tagged Antarctic blue whales swam at an overall movement rate of 1.2 ± 0.8 ms^{-1} (median speed: 1.0 ms^{-1}), with faster rates for transit-like movement (1.4 ± 0.9 ms^{-1}; median: 1.2 ms^{-1}) and slower rates during area restricted search (ARS)-like movement (0.8 ± 0.6 ms^{-1}; median: 0.7 ms^{-1}, which is often considered as a proxy for foraging, but also resting and nursing (Andrews-Goff et al, 2022). The maximum movement rate derived from the satellite tracking data was 5.1 ms^{-1}. Estimates of mean Antarctic blue whale swimming speeds and movement rates derived from both the video tracking dataset and satellite tag derived data are distinctly faster than comparable estimates for other blue whale populations (Table 5).

Whilst large-scale movements of Antarctic blue whales are not well-documented, there is assumed to be some annual migratory movement between austral summer Antarctic feeding grounds and mid-latitude locations in winter (Branch et al., 2007). To date, satellite tags have been deployed on just two Antarctic blue whales, in a study

TABLE 4 Intra-season resights of known individuals from photo-ID.

Track ID	First sighting time (UTC)	Latitude of first sighting	Longitude of first sighting	Distance to resighting (km)	Hours between sightings	Heading to resighting (degrees)	Broadscale movement rate (ms^{-1})
1	07/02/2013 21:30	-62.30	142.25	229.9	143.7	93.2	0.44
2	09/02/2013 08:24	-64.96	143.48	1190.4	642.6	96.5	0.51
3	13/02/2013 03:10	-62.34	147.72	75.0	28.5	62.9	0.73
4	12/02/2013 19:33	-62.45	147.21	29.9	25.6	-67.5	0.32
5	13/02/2013 03:55	-62.27	147.88	1030.7	547.3	109.2	0.52
6	13/02/2013 19:50	-62.43	146.82	1081.4	534.2	108.9	0.56
7	20/02/2013 03:49	-64.43	168.15	52.6	18.9	-84.0	0.77
8	25/02/2013 02:44	-68.01	-178.39	79.3	20.6	136.8	1.07
9	25/02/2013 04:02	-67.96	-178.30	77.4	19.0	141.6	1.13
10	09/02/2015 07:38	-69.27	178.38	136.4	66.4	89.8	0.57
11	09/02/2015 07:39	-69.27	178.38	138.5	64.1	90.1	0.60
12	11/02/2015 02:47	-69.28	-178.02	14.9	72.3	-151.5	0.06
13	12/02/2015 02:04	-69.23	-178.17	14.0	43.5	179.5	0.09
14	12/02/2015 05:01	-69.29	-178.21	7.8	40.6	168.5	0.05
15	12/02/2015 05:33	-69.33	-178.13	0.9	39.2	-125.2	0.01
16	09/02/2015 07:41	-69.27	178.39	269.9	469.0	110.5	0.16
17	23/02/2019 03:55	-65.70	146.52	48.3	28.1	162.8	0.48
18	23/02/2019 03:55	-65.70	146.52	49.9	22.4	125.6	0.62

by Andrews-Goff et al, (2022). These tag data demonstrate that it is possible for Antarctic blue whales to travel large distances when on their feeding grounds – 96 ± 43 km daily (mean ± SD) – a scale of movement greater than has been measured in other blue whale populations. The large tagging datasets of Eastern Indian Ocean stock (EIO) pygmy blue whales [n = 22; (Thums et al., 2022)] and the Northeast Pacific (NP) blue whale population (n = 128; (Bailey et al., 2009)), including movement on feeding and calving grounds, indicate movement rates of approximately 70 km per day for EIO pygmy blue whales and approximately 65 km per day for NP blue whales (Table 5).

Large-scale movements were also recorded in the intra-seasonal recaptures of the Discovery marking program which was conducted during Antarctic whaling operations in the early part of the 20th century (Branch et al., 2007). Marked metal tubes were fired into whales, and sometimes recovered by whaling operations. 54 marks were recovered in the same season in which the individual blue whales had been marked. Distances and time intervals between mark and recapture varied widely, from 32-3516 km and from 1-114 days (Appendix 4, Branch et al., 2007).

Satellite tag derived datasets are often analysed to distinguish transit-like movement, which may include travel between foraging patches or migratory pathways, and is associated with relatively straight movement paths and faster travel speeds, from ARS-like movement, where travel speed has slowed and turning angles have increased (Kareiva and Odell, 1987; Bailey et al., 2009; Möller et al., 2020; Thums et al., 2022). For the Antarctic blue whale satellite tracking data, mean transit and ARS movement rates fall within the range of transit and ARS movement rates seen across blue whale populations (Table 5). Video tracking data may provide additional insight into ARS movement detected *via* analysis of satellite tracking datasets. The video tracking data analysed here revealed that slower movement rates appeared to be related to tracks with more turns, suggesting that swim speed through the water is more consistent than overall travel rate, i.e. slower travel is a result of turning more frequently rather than swimming slower. Additionally, speeds measured over the course of around an hour were, on average, 83 % of speeds measured over the course of 6 minutes, suggesting that measures of speed over shorter intervals may be biased towards faster speeds. This can help inform comparisons of horizontal speed measurements from studies with different intervals between observation locations, such as telemetry studies which rely on satellite passes to generate an irregular time series.

The general movement or 'flux' of whales through an area is relevant to studies of prey consumption and other ecological impacts such as iron fertilisation. In addition, it can have a large influence on the resighting probability of individuals from photo-ID. The overall mean movement for all whales in 2019 of 0.88 ms^{-1} suggests a high net 'flux' of whales through the study area. In comparison the higher rate of heading changes observed in 2015, resulting in lower movement rates suggests a low net 'flux' of whales through the area. There are no concurrent krill data available for the 2013 voyage, but in 2015 and 2019 the core study areas differed from each other in the characteristics of the krill swarms (Miller et al., 2019; Double et al.,

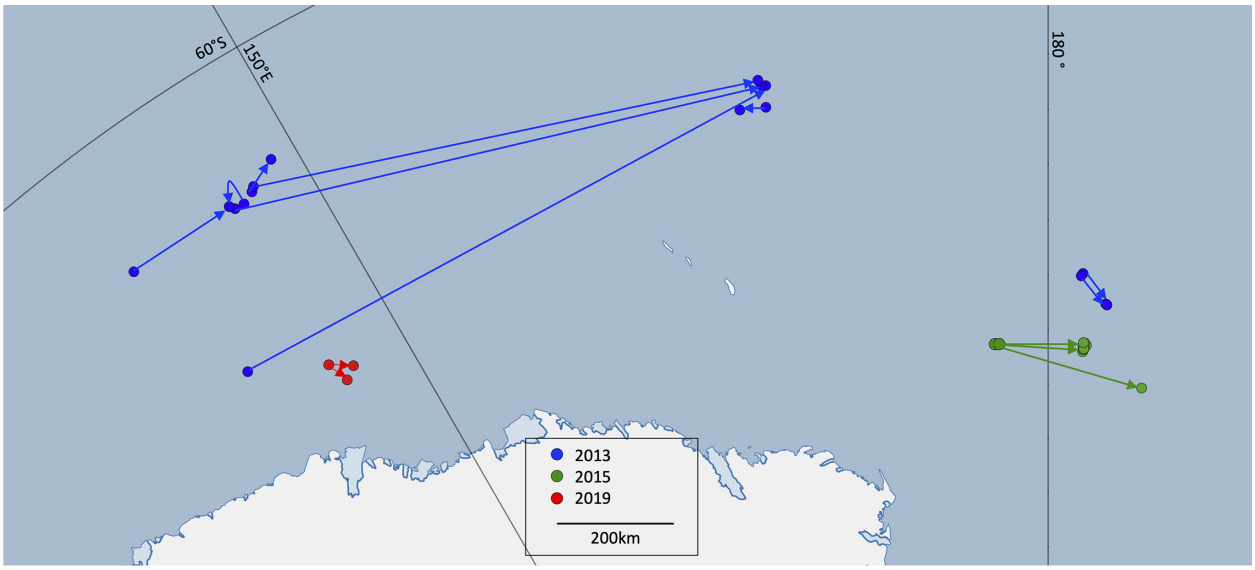


FIGURE 4
Capture and recapture locations of photo-identified whales in 2013 (blue), 2015 (green) and 2019 (red). In 2015 the capture and recapture locations of four whales appear clustered together due to the relatively short distances between locations. (Lines connect the locations and do not necessarily represent whale movement).

2021). The concentrated area of Antarctic blue whale distribution encountered at the entrance to the Ross Sea in 2013 (and also on the 2017 Antarctic Circumnavigation Expedition (Miller et al., 2017), for which there are neither krill nor photogrammetric data) may have had krill characteristics similar to those favoured by blue whales in that same area in 2015. Slower swim speeds and greater headings changes were observed in 2015 (e.g. ARS) compared to faster speeds and an overall movement through the 2019 study area. Photo-ID also

TABLE 5 Blue whale swim speeds and movement rates from satellite telemetry.

Population location	Year	n	Movement rate (ms^{-1})	Max. speed (ms^{-1})	Habitat	Behaviour-specific movement rate (ms^{-1}); mean ± SD)	Reference
Antarctica	2013	2	1.2 ± 0.8 (mean ± SD)	5.1	feeding grounds	1.4 ± 0.9 (transit); 0.8 ± 0.6 (ARS)	Andrews-Goff et al, (2022)
Eastern Indian Ocean	2009 2011	12	0.3 (calculated from distance travelled per day)	5.3	feeding, migration, nursery grounds		Double et al. (2014)
Eastern Indian Ocean	2015	13	0.9 ± 0.2 (mean ± SD)	4.4	feeding, migration, nursery grounds		Möller et al. (2020)
Eastern Indian Ocean	2019/20	6	0.7 (median)	3.9	feeding, migration, nursery grounds		Thums et al. (2022)
Eastern Indian Ocean	2021	6	0.6 (median)	3.3	feeding, migration, nursery grounds		Thums et al. (2022)
Eastern Indian Ocean	2014	1	0.8 ± 0.6 (mean ± SD)		migration		Owen et al. (2016)
Northeast Pacific	1993 to 2007	128	0.7 ± 0.3 (mean ± SD)	2.4	feeding, migration, nursery grounds		Bailey et al. (2009)
Chilean Northern Patagonia	2013, 2015, 2016	7		2.1	feeding grounds	1.2 ± 0.4 (transit); 0.2 ± 0.2 (ARS)	Hucke-Gaete et al. (2018)
North Atlantic	1999	1	0.8 ± 0.5 (mean ± SD)		migration		Heide-Jørgensen et al. (2001)
North Atlantic	2002, 2010-2015	23			feeding, migration, nursery grounds	1.6 ± 0.7 (transit); 0.3 ± 0.3 (ARS)	Lesage et al. (2017)
North Atlantic	2009 2011	3	~ 0.5 (GAM derived)		migration	1.8 ± 1 (transit); 1.2 ± 0.6 (ARS)	Silva et al. (2013)

showed whales remaining for several days with little overall movement within the 2015 study area. The direction of travel of the overall movement in 2019 was directly towards the area of Antarctic blue whale concentrations at the entrance to the Ross Sea observed in previous years. The bearing to these concentrations was 120° at a distance of 1600km compared to a median observed heading of 118.5°. The mean speed of 1.55 ms^{-1} from 2019 is at the top end of mean movement rates observed from satellite telemetry. Even allowing for higher speeds due to being averaged over a shorter time, the speeds of whales through the area would appear to be comparable to those assumed to in transit. The results from the video tracks show that the simple behavioural observations during this study can help understand blue whale movements and feeding ecology. The movement through the area rather than persistent concentrations of whales would be consistent with the lack of spatial relationship between whale presence and surface ocean iron concentrations observed in the 2019 survey area (Smith et al., 2021).

Although any inferences of movement from photo-ID matches are influenced by the track of the research vessel (i.e. the opportunities to resight whales only occur where the vessel is), the data do also indicate the same qualitative patterns, with slow overall movement speeds in 2015 compared to 2019. The movement of whales through the 2019 study area explains the low number of intra-season photo-ID matches. Most of the 2019 study area, and the western portion of the 2013 study area are located south of the eastern Indian Ocean (the eastern Indian Ocean defined by the longitudinal meridians of 70 °E and 146.49°E). When examining inter-seasonal recapture data, Olson et al. (2022) found that only 20 % of the whales marked in the eastern Indian Ocean sector were recaptured there, as opposed to the three other ocean basin sectors with recapture rates of 50-79 %. This suggests that the eastern Indian Ocean sector may be a region through which blue whales generally transit rather swiftly. In addition to the differences in overall movement between years demonstrated by both the photogrammetric and photo-ID data, with whales in 2019 heading directly towards the area of Antarctic blue whale concentrations at the entrance to the Ross Sea observed in previous years, data also show a high proportion of resighted whales with coherent movements. This suggests that Antarctic blue whales might travel together, at least over periods of several days or sometimes up to a month, with possible implications for group behaviour dynamics which are currently poorly understood.

5. Conclusions

This study estimated surfacing rates, swim speeds, and movement rates of Antarctic blue whales from photogrammetric and photo-ID measurements made over the course of three Antarctic voyages.

Estimates of surfacing intervals of short dives of Antarctic blue whales were consistent across all voyages and were similar to those measured from other blue whale populations, whilst estimates of long dives yielded intervals which were shorter than those estimated from other populations. These estimates of mean overall surfacing intervals of Antarctic blue whales on their feeding grounds provide cue rates for studies which employ cue-counting for estimating abundance; patterns of short and long dives could be used to estimate g(0) for single platform visual surveys.

Estimates of movement rates on their high-latitude feeding grounds demonstrate that Antarctic blue whales have the highest movement rate of all blue whale populations measured to date. These are consistent with movement rates estimated from satellite telemetry of two individual Antarctic blue whales in 2013 (Andrews-Goff et al, 2022). The broadscale movements indicated by photographic re-sightings also suggest some coordinated movements across multiple individuals.

In this study, significantly different mean movement rates and directions of travel were observed across the three different voyages. These differences may be indicative of different behavioural states, namely transit vs. area restricted search. Further, we hypothesise that these differences were driven by differences in environmental conditions, namely distribution of prey, and that future studies should aim to test this hypothesis.

Our findings increase our understanding of Antarctic blue whale fine-scale movements and behaviour, and may assist with the interpretation of datasets such as visual surveys, acoustic studies, ecosystem research, and assessments of human impacts. They may also inform how the different behavioural states of Antarctic blue whales may be driven by distribution of prey, and thus their role in the Antarctic ecosystem.

Data availability statement

The datasets presented in this study can be found in online repositories. The names of the repository/repositories and accession number(s) can be found below: SC, RL, BM and MD (2014) Photogrammetric video tracks of Antarctic blue whale movements recorded during the 2013 Antarctic Blue Whale Voyage, Ver. 1, Australian Antarctic Data Centre - doi:10.4225/15/59d6fd7185a29 SC, RL, BM and MD (2017) Photogrammetric video tracks of Antarctic blue whale movements recorded during the 2015 NZ Australia Antarctic Ecosystems Voyage, Ver. 1, Australian Antarctic Data Centre - doi:10.4225/15/59d2d94589980 SC, RL and BM (2022) Photogrammetric video tracks of whale movements recorded during the 2019 ENRICH Voyage, Ver. 1, Australian Antarctic Data Centre - doi:10.26179/tcbe-4h63.

Ethics statement

The animal study was reviewed and approved by the Australian Antarctic Ethics Committee (under Australian Antarctic Science Project 4102) and complied with all relevant permits including the Australian Government Environment Protection and Biodiversity Conservation Act Cetacean Permit (C12-0006, 2017-004).

Author contributions

All authors contributed to conception and design of the study. SC, RL, BM, VA-G, PO wrote specific sections of the manusript. SC, RL collected the photogrammetric data. SC, RL, BM, PO, MR performed the analysis. All authors contributed to the article and approved the submitted version.

Acknowledgments

It is a pleasure to acknowledge the input and assistance of the voyage leaders, scientists, support staff, vessel crew and management on the three voyages during which our data were collected: *Amaltal Explorer* (2013), *Tangaroa* (2015), and *RV Investigator* (2019; (*IN2019_V01*)). We thank the Australian Antarctic Division, CSIRO Marine National Facility, New Zealand's National Institute of Water & Atmospheric Research, Antarctica New Zealand, the New Zealand Ministry for Business, Innovation and Employment, and the International Whaling Commission Southern Ocean Research Partnership for funding and logistical support. Thank you to all those who have contributed photographs to the Antarctic Blue Whale Catalogue. We are grateful to Simon Wotherspoon for analytical advice. Thank you to Trevor Joyce and to the reviewers for their constructive comments.

Conflict of interest

The authors declare that the research was conducted in the absence of any commercial or financial relationships that could be construed as a potential conflict of interest.

Publisher's note

All claims expressed in this article are solely those of the authors and do not necessarily represent those of their affiliated organizations, or those of the publisher, the editors and the reviewers. Any product that may be evaluated in this article, or claim that may be made by its manufacturer, is not guaranteed or endorsed by the publisher.

References

Agostinelli, C., and Lund, U. (2017) *R package 'circular': Circular statistics*. Available at: https://r-forge.r-project.org/projects/circular/.

Andrews-Goff, V., Bell, E. M., Miller, B. S., Wotherspoon, S. J., and Double, M. C. (2022). Satellite tag derived data from two Antarctic blue whales (Balaenoptera musculus intermedia) tagged in the east Antarctic sector of the southern ocean. *Biodiversity Data J* 10, e94228. doi: 10.3897/BDJ.10.e94228

Bailey, H., Mate, B. R., Palacios, D. M., Irvine, L., Bograd, S. J., and Costa, D. P. (2009). Behavioural estimation of blue whale movements in the northeast pacific from state-space model analysis of satellite tracks. *Endangered Species Res.* 10, 93–106. doi: 10.3354/esr00239

Branch, T. A., Stafford, K. M., Palacios, D. M., Allison, C., Bannister, J. L., Burton, C. L. K., et al. (2007). Past and present distribution, densities and movements of blue whales in the southern hemisphere and northern Indian ocean. *Mammal Rev.* 37 (2), 116–175. doi: 10.1111/j.1365-2907.2007.00106.x

Calderan, S., Leaper, R. C., and Miller, B. S. (2022). *Photogrammetric video tracks of whale movements recorded during the 2019 ENRICH voyage* (AADC: Australian Antarctic Data Centre). doi: 10.26179/tcbe-4h63

Calderan, S., Leaper, R. C., Miller, B. S., and Double, M. (2014). *Photogrammetric video tracks of Antarctic blue whale movements recorded during the 2013 Antarctic blue whale voyage* (Australian Antarctic Data Centre). Available at: https://researchdata.edu.au/photogrammetric-video-tracks-whale-voyage. doi: 10.4225/15/59d6fd7185a29

Calderan, S., Leaper, R. C., Miller, B. S., and Double, M. (2017). *Photogrammetric video tracks of Antarctic blue whale movements recorded during the 2015 NZ Australia Antarctic ecosystems voyage* (Australian Antarctic Data Centre). Available at: https://researchdata.edu.au/photogrammetric-video-tracks-ecosystems-voyage. doi: 10.4225/15/59d2d94589980

Cooke, J. G. (2018). "Balaenoptera musculus ssp. intermedia," in *The IUCN red list of threatened species 2018*. Available at: https://www.iucnredlist.org/species/41713/50226962.

Crance, J. L., Berchok, C. L., and Keating, J. L. (2017). Gunshot call production by the north pacific right whale eubalaena japonica in the southeastern Bering Sea. *Endangered Species Res.* 34, 251–267. doi: 10.3354/esr00848

Croll, D. A., Acevedo-Gutierrez, A., Tershy, B. R., and Urban-Ramýrez, J. (2001). The diving behavior of blue and fin whales: is dive duration shorter than expected based on oxygen stores? *Comp. Biochem. Physiol. Part A* 129, 797–809. doi: 10.1016/S1095-6433(01)00348-8

DeRuiter, S. L., Langrock, R., Skirbutas, T., Goldbogen, J. A., Calambokidis, J., Friedlaender, A. S., et al. (2017). A multivariate mixed hidden Markov model for blue whale behaviour and responses to sound exposure. *Ann. Appl. Stat* 11 (1), 362–392. doi: 10.1214/16-AOAS1008

de Vos, A., Christiansen, F., Harcourt, R. G., and Pattiaratchi, C. B. (2013). Surfacing characteristics and diving behaviour of blue whales in Sri Lankan waters. *J. Exp. Mar. Biol. Ecol.* 449, 149–153. doi: 10.1016/j.jembe.2013.09.010

Double, M. C., Andrews-Goff, V., Jenner, K. C. S., Jenner, M. N., and Laverick, S. M. (2014). Migratory movements of pygmy blue whales (*Balaenoptera musculus brevicauda*) between Australia and Indonesia as revealed by satellite telemetry. *PloS One* 9 (4), e93578. doi: 10.1371/journal.pone.0093578

Double, M. C., Barlow, J., Miller, B. S., Olson, P., Andrews-Goff, V., Leaper, R., et al. (2013). Cruise report of the 2013 Antarctic blue whale voyage of the southern ocean research partnership. In *Paper SC/65a/SH/21 presented to IWC Scientific Committee*. Available from the International Whaling Commission (http://iwc.int).

Double, M. C., Bell, E., Miller, B., Kelly, N., Kawaguchi, S., Lawrence, J., et al. (2021). "ENRICH voyage report, IN2019_V01: The availability of Antarctic krill to large predators and their role in biogeochemical recycling in the southern ocean," in *Paper SC/68c/SH19 presented to IWC Scientific Committee*. Available from the International Whaling Commission (http://iwc.int).

Double, M. C., Miller, B. S., Leaper, R., Olson, P., Cox, M. J., Miller, E., et al. (2015). "Cruise report on blue whale research from the NZ/Aus Antarctic ecosystems voyage 2015 of the southern ocean research partnership," in *Paper SC/66a/SH07 presented to the IWC Scientific Committee*, San Diego, California. Available from the International Whaling Commission (http://iwc.int).

Dunlop, R. A., Noad, M. J., McCauley, R. D., Kniest, E., Slade, R., Paton, D., et al. (2016). Response of humpback whales (Megaptera novaeangliae) to ramp-up of a small experimental air gun array. *Mar. pollut. Bull.* 103 (1), 72–83. doi: 10.1016/j.marpolbul.2015.12.044

Gendron, D., and Ugalde de la Cruz, A. (2012). A new classification method to simplify blue whale photo-identification technique. *J. Cetacean Res. Manage* 12 (1), 79–84.

Heide-Jørgensen, M. P., Kleivane, L., Øien, N., Laidre, K. L., and Jensen, M. V. (2001). A new technique for deploying satellite transmitters on baleen whales: Tracking a blue whale (*Balaenoptera musculus*) in the north Atlantic. *Mar. Mammal Sci.* 17 (4), 949–954. doi: 10.1111/j.1748-7692.2001.tb01309.x

Hiby, A. R. (1992). *Fin whale surfacing rate as a calibration factor for cue-counting abundance estimates* Vol. 42 (Cambridge, UK: Reports of the International Whaling Commission), 707–709.

Hucke-Gaete, R., Bedriñana-Romano, L., Viddi, F. A., Ruiz, J. E., Torres-Florez, J. P., and Zerbini, A. N. (2018). From Chilean Patagonia to Galapagos, Ecuador: novel insights on blue whale migratory pathways along the Eastern south pacific. *PeerJ* 6, e4695. doi: 10.7717/peerj.4695

Kareiva, P., and Odell, G. (1987). Swarms of predators exhibit `prey taxis' if individual predators use area-restricted search. *Am. Nat.* 130 (2), 233–270. doi: 10.1086/284707

Lagerquist, B. A., Stafford, K. M., and Mate, B. R. (2000). Dive characteristics of satellite-monitored blue whales ({IBalaenoptera musculus}) off the central California coast. *Mar. Mammal Sci.* 16 (2), 375–391. doi: 10.1111/j.1748-7692.2000.tb00931.x

Leaper, R., Burt, L., Gillespie, D., and MacLeod, K. (2010). Comparisons of measured and estimated distances and angles from sighting surveys. *J. Cetacean Res. Manage.* 11 (3), 229–238.

Leaper, R., Calderan, S., and Cooke, J. (2015). A simulation framework to evaluate the efficiency of using visual observers to reduce the risk of injury from loud sound sources. *Aquat. Mammals* 41, 375–387. doi: 10.1578/AM.41.4.2015.375

Leaper, R., and Gordon, J. (2001). Application of photogrammetric methods for locating and tracking cetacean movements at sea. *J. Cetacean Res. Manage.* 3 (2), 131–141.

Lesage, V., Gavrilchuk, K., Andrews, R. D., and Sears, R. (2017). Foraging areas, migratory movements and winter destinations of blue whales from the western north Atlantic. *Endangered Species Res.* 34, 27–43. doi: 10.3354/esr00838

Lomac-MacNair, K., and Smultea, M. A. (2016). Blue whale (Balaenoptera musculus) behavior and group dynamics as observed from an aircraft off southern California. *Anim. Behav. Cogn.* 3 (1), 1–21. doi: 10.12966/abc.02.01.2016

Möller, L. M., Attard, C. R. M., Bilgmann, K., Andrews-Goff, V., Jonsen, I. D., Paton, D. A., et al. (2020). Movements and behaviour of blue whales satellite tagged in an Australian upwelling system. *Sci. Rep.* 10(1), 1–19. doi: 10.1038/s41598-020-78143-2

Miller, B. S., Barlow, J., Calderan, S., Collins, K., Leaper, R., Olson, P., et al. (2015). Validating the reliability of passive acoustic localisation: a novel method for encountering rare and remote Antarctic blue whales. *Endangered Species Res.* 26 (3), 257–269. doi: 10.3354/esr00642

Miller, B. S., Leaper, R., Calderan, S., and Gedamke, J. (2014). Red shift, blue shift: Investigating doppler shifts, blubber thickness, and migration as explanations of seasonal variation in the tonality of Antarctic blue whale song. *PloS One* 9 (9), e107740. doi: 10.1371/journal.pone.0107740

Miller, B. S., Miller, E., Calderan, S., Leaper, R., Stafford, K., Širović, A., et al. (2017). "Circumpolar acoustic mapping of endangered southern ocean whales: Voyage report and preliminary results for the 2016/17 Antarctic circumnavigation expedition," in *Paper SC/67a/SH/03 presented to the IWC Scientific Committee*, Bled, Slovenia. Available from the International Whaling Commission (http://iwc.int).

Miller, E. J., Potts, J. M., Cox, M. J., Miller, B. S., Calderan, S., Leaper, R., et al. (2019). The characteristics of krill swarms in relation to aggregating Antarctic blue whales. *Sci. Rep.* 9 (1), 16487. doi: 10.1038/s41598-019-52792-4

Oleson, E. M., Calambokidis, J., Burgess, W. C., McDonald, M. A., LeDuc, C. A., and Hildebrand, J. A. (2007). Behavioural context of call production by eastern north pacific blue whales. *Mar. Ecol. Prog. Ser.* 330, 269–284. doi: 10.3354/meps330269

Olson, P. A., Andrews-Goff, V., Double, M., Matsuoka, K., and Pastene, L. A. (2022). "Movements of Antarctic blue whales derived from discovery tag, photo-ID, and satellite tag data," in *Paper SC/68D/SH/09 presented to IWC Scientific Committee*. Available from the International Whaling Commission (http://iwc.int).

Olson, P. A., Double, M., Matsuoka, K., Pastene, L. A., and Findlay, K. (2020). "The Antarctic blue whale catalogue: new data from 2015-2019," in *Paper SC/68b/PH04 presented to IWC Scientific Committee*. Available from the International Whaling Commission (http://iwc.int).

Olson, P. A., Galletti Vernazzani, B., and Torres Florez, J. P. (2021). "Southern hemisphere blue whale catalogue photo quality coding guide," in *Paper SC/68C/PH02 presented to IWC Scientific Committee*. Available from the International Whaling Commission (http://iwc.int).

Owen, K., Jenner, C. S., Jenner, M.-N. M., and Andrews, R. D. (2016). A week in the life of a pygmy blue whale: migratory dive depth overlaps with large vessel drafts. *Anim. Biotelemetry* 4 (1), 17. doi: 10.1186/s40317-016-0109-4

Pirotta, E., Booth, C. G., Calambokidis, J., Costa, D. P., Fahlbusch, J. A., Friedlaender, A. S., et al. (2022). From individual responses to population effects: Integrating a decade of multidisciplinary research on blue whales and sonar. *Anim. Conserv* 25 (6), 796–810. doi: 10.1111/acv.12785

Quick, N. J., Rendell, L. E., and Janik, V. M. (2008). Note: A mobile acoustic localization system for the study of free-ranging dolphins during focal follows. *Mar. Mammal Sci.* 24 (4), 979–989. doi: 10.1111/j.1748-7692.2008.00231.x

R Core Team (2021). *R: A language and environment for statistical computing* (Vienna, Austria: R Foundation for Statistical Computing). Available at: https://www.R-project.org/.

Schall, E., Thomisch, K., Boebel, O., Gerlach, G., Spiesecke, S., and Van Opzeeland, I. (2020). Large-Scale spatial variabilities in the humpback whale acoustic presence in the Atlantic sector of the southern ocean. *R. Soc. Open Sci.* 7 (12), 201347. doi: 10.1098/rsos.201347

Sears, R., and Perrin, W. F. (2009) "Blue whale (Balaenoptera musculus)," in *Encyclopedia of marine mammals*, *2nd ed.*Eds. W. F. Perrin, B. Wursig and G. M. Thewissen (New York, US: Academic Press), 120–124.

Sears, R., Williamson, J. M., Wenzel, F. W., Bérubé, M., Gendron, D., and Jones, P. (1990). *Photographic identification of the blue whale (Balaenoptera musculus) in the gulf of st. Lawrence, Canada* Vol. 12 (New York, US: Reports of the International Whaling Commission), 335–342.

Silva, M. A., Prieto, R., Jonsen, I., Baumgartner, M. F., and Santos, R. S. (2013). North Atlantic blue and fin whales suspend their spring migration to forage in middle latitudes: Building up energy reserves for the journey? *PloS One* 8 (10), e76507. doi: 10.1371/journal.pone.0076507

Smith, A. J. R., Ratnarajah, L., Holmes, T. M., Wuttig, K., Townsend, A. T., Westwood, K., et al. (2021). Circumpolar deep water and shelf sediments support late summer microbial iron remineralization. *Global Biogeochemical Cycles* 35 (11), e2020GB006921. doi: 10.1029/2020GB006921

Sumner, M. (2021) *Traipse: Shared tools for tracking data*. Available at: https://CRAN.R-project.org/package=traipse.

Szesciorka, A. R., Allen, A. N., Calambokidis, J., Fahlbusch, J., McKenna, M. F., and Southall, B. (2019). A case study of a near vessel strike of a blue whale: Perceptual cues and fine-scale aspects of behavioral avoidance. *Front. Mar. Sci.* 6. doi: 10.3389/fmars.2019.00761

Thums, M., Ferreira, L. C., Jenner, C., Jenner, M., Harris, D., Davenport, A., et al. (2022). Pygmy blue whale movement, distribution and important areas in the Eastern Indian ocean. *Global Ecol. Conserv.* 35, e02054. doi: 10.1016/j.gecco.2022.e02054

Torres, L. G., Barlow, D. R., Chandler, T. E., and Burnett, J. D. (2020). Insight into the kinematics of blue whale surface foraging through drone observations and prey data. *PeerJ* 8, e8906. doi: 10.7717/peerj.8906

Williams, R., Leaper, R., Zerbini, A., and Hammond, P. S. (2007). Methods for investigating measurement error in cetacean line-transect surveys. *J. Mar. Biol. Assoc. U.K.* 87, 313–320. doi: 10.1017/S0025315407055154

Yu, Y. (2022). mixR: An R package for Finite Mixture Modeling for Both Raw and Binned Data. *J Open Source Softw.* 7 (69), 4031. doi: 10.21105/joss.04031

frontiers | Frontiers in Marine Science

TYPE Original Research
PUBLISHED 26 January 2023
DOI 10.3389/fmars.2023.1060984

Check for updates

OPEN ACCESS

EDITED BY
Bernardo Antonio Perez Da Gama,
Fluminense Federal University, Brazil

REVIEWED BY
Kristen B. Gorman,
University of Alaska Fairbanks,
United States
David Ainley,
H.T. Harvey &Associates,
United States

*CORRESPONDENCE
Javed Riaz
javed.riaz@utas.edu.au

SPECIALTY SECTION
This article was submitted to Marine Ecosystem Ecology, a section of the journal Frontiers in Marine Science

RECEIVED 04 October 2022
ACCEPTED 09 January 2023
PUBLISHED 26 January 2023

CITATION
Riaz J, Bestley S, Wotherspoon S, Cox MJ and Emmerson L (2023) Spatial link between Adélie penguin foraging effort and krill swarm abundance and distribution. *Front. Mar. Sci.* 10:1060984. doi: 10.3389/fmars.2023.1060984

COPYRIGHT
© 2023 Riaz, Bestley, Wotherspoon, Cox and Emmerson. This is an open-access article distributed under the terms of the Creative Commons Attribution License (CC BY). The use, distribution or reproduction in other forums is permitted, provided the original author(s) and the copyright owner(s) are credited and that the original publication in this journal is cited, in accordance with accepted academic practice. No use, distribution or reproduction is permitted which does not comply with these terms.

Spatial link between Adélie penguin foraging effort and krill swarm abundance and distribution

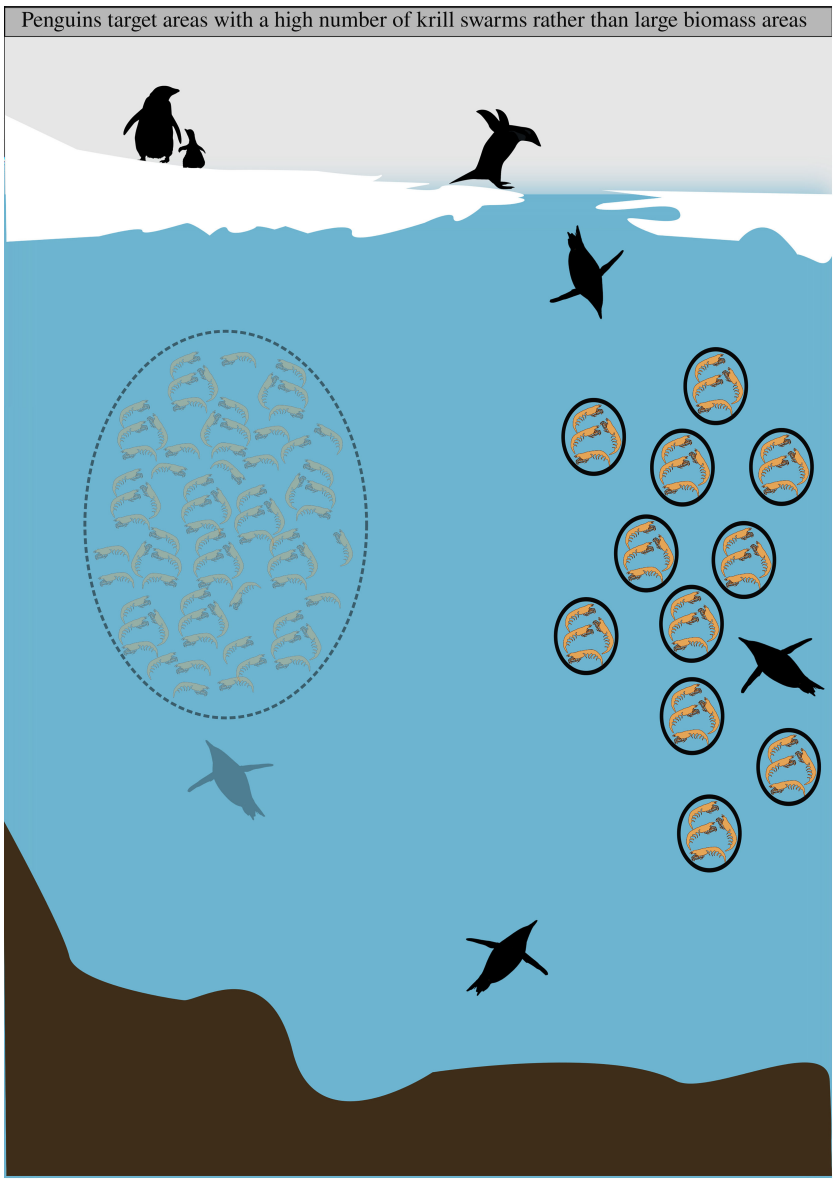
Javed Riaz[1,2*], Sophie Bestley[1], Simon Wotherspoon[2], Martin J. Cox[2] and Louise Emmerson[2]

[1]Institute for Marine and Antarctic Studies, University of Tasmania, Hobart, Tasmania, Australia, [2]Australian Antarctic Division, Kingston, Tasmania, Australia

Understanding how predator foraging behaviour is influenced by the distribution and abundance of prey is a fundamental challenge in marine foraging ecology. This is particularly relevant in Southern Ocean ecosystems where the relationships between select predator species and Antarctic krill (*Euphausia superba*) can inform ecosystem conservation and precautionary fisheries management. In this study, we examine the spatial associations between krill swarm characteristics and Adélie penguin (*Pygoscelis adeliae*) foraging effort at Béchervaise Island, a long-term monitoring site in East Antarctica. Spatially integrating two years of regional-scale krill acoustic data with contemporaneous horizontal and vertical movement information from chick-rearing adult Adélie penguins, we assessed how penguin foraging effort changed in relation to krill swarm abundance and distribution across the survey area. Our findings show that penguin diving effort was focused in areas with a high number of krill swarms, yet they did not focus their effort in areas with high krill biomass. These results suggest the spatial organisation of Adélie penguin foraging effort can provide an indication of krill presence (and/or availability) but may not reflect krill abundance. We discuss our results in the context of penguin foraging strategies, capturing single krill within the water column rather than the engulfment feeding strategy of larger marine mammals such as whales. Our work substantially improves understanding of penguin-krill dynamics in East Antarctica and provides a greater level of nuance regarding the utility of Adélie penguins as indicator species under CCAMLR's Ecosystem Monitoring Programme (CEMP). Understanding these predator-prey linkages will become increasingly important for managing any expanding krill fisheries in the region or changes in the prey field under future climate change scenarios. Thus, our results can be interpreted alongside other ecological indicators to support management of the East Antarctic sector of the Southern Ocean ecosystem.

KEYWORDS

foraging behaviour, *Pygoscelis adeliae*, *Euphausia superba*, krill swarm, dive behaviour, predator-prey



GRAPHICAL ABSTRACT

1 Introduction

Understanding how predator behaviour relates to the distribution and abundance of prey is a key objective in ecology (Hunsicker et al., 2011). This can be particularly challenging in marine environments, where predator-prey interactions occur in a dynamic three-dimensional environment (Bestley et al., 2015; Kuhn et al., 2015). Synchronous information on predator foraging behaviour and prey fields at spatiotemporal scales relevant to marine predators can be difficult to obtain. These survey efforts are both financially and logistically intensive, and are therefore, rarely undertaken (Grémillet et al., 2004; Bedford et al., 2015).

Studies investigating the fine-scale spatial overlap between marine predator foraging and prey fields have commonly coupled acoustic surveys with direct shipboard observations of predator density and feeding activity (Table 1). This can provide a snapshot of predator-prey spatial overlap in real time. However, these observational techniques have a very limited spatial coverage and only examine a small part of a predator's foraging range. This limits inferences about predator-prey interactions occurring over larger spatial scales (Kuhn et al., 2015; Yamamoto et al., 2015). Furthermore, visual observations are generally restricted to surface foraging behaviour (in fair weather), omitting critical information on underwater foraging activity (Enstipp et al., 2007; Hazen et al., 2009). Bio-logging and telemetry devices are increasingly being used to provide a more detailed understanding of predator-prey relationships at a broader spatial resolution (horizontally and vertically) (Hunsicker et al., 2011). Marine surveys incorporating telemetry have developed understanding of predator-prey relationships in various temperate and polar ecosystems for a range of predator taxa (See Table 1 for examples).

TABLE 1 Examples of studies on predator-prey relationship which couple prey field acoustic surveys with predator locations through biologging or shipboard observations.

Predator species	Predator metrics	Prey species	Prey units	Reference
Bio-logging				
Northern fur seal (*Callorhinus ursinus*)	Spatial binning: hours spent, average transit rate, total and per hour number of dives, bottom time, vertical distance, wiggles, dive duration.	Walleye pollock (*Gadus chalcogrammus*)	Biomass and density	(Kuhn et al., 2015)
Harbour porpoise (*Phocoena phocoena*); Mackerel (*Scomber scombrus*)	Spatial binning: number of fixes and density	Herring (*Clupea harengus*)	Density	(Sveegaard et al., 2012)
Adélie penguins (*Pygoscelis adeliae*)	Coarse scale breeding success and foraging trip parameters (duration and meal mass) and spatial location	Krill (*Euphausia superba*)	Biomass	(Nicol et al., 2008)
Antarctic fur seal (*Arctocephalus gazella)* and *Pygoscelis* spp.	Spatial binning: fixes and behavioural indices	Krill (*E. superba*)	Density	(Hinke et al., 2017)
Little penguin (*Eudyptula minor*)	Spatial location and dive information	Non-specific – acoustic backscatter	Density	(Phillips et al., 2022)
Adélie penguin	Spatial location and dive information	Krill and fish spp.	Density (derived from underwater glider)	(Ainley et al., 2015)
Shipboard observations				
Cape petrel (*Daption capense*); Chinstrap penguin (*P. antarctica*)	Spatial binning: abundance and behaviour (feeding, transit or resting)	Krill (swarms; principally, *E. superba*)	Nautical area scattering coefficient (NASC)	(Santora et al., 2009)
Humpback whale (*Megaptera novaeangliae)*; Fin whale (*Balaenoptera physalus*); Antarctic minke whale (*B. bonaerensis*)	Spatial binning: relative abundance	Krill (swarms; principally, *E. superba*)	Abundance	(Santora et al., 2010)
Humpback whale; Fin whale; Minke whale (*B. acutorostrata*); Sei whale (*B. borealis)*	Spatial binning: density	Capelin; Krill spp. (*Meganyctiphanes norvegica; Thysanoessa* sp.)	Biomass density	(Laidre et al., 2010)
Snow petrel (*Pagodroma nivea*); Antarctic petrel (*Thalassoica antarctica*); Adélie penguin; Crabeater seal (*Lobodon carcinophagus*)	Spatial binning: density	Krill (*E. superba*)	Biomass density	(Ribic et al., 2008)

Within the Southern Ocean, the area of interest in this study, regionally high abundances of Antarctic krill (*Euphausia superba*) support a diverse range of higher-order predators (Atkinson et al., 2009; Trathan and Hill, 2016). While the importance of krill-dominated energy pathways can vary over time and space, Antarctic krill (hereafter, krill) are an important forage resource for fish, squid, seabirds and marine mammals in Southern Ocean ecosystems (Croxall et al., 1999; Trathan et al., 2012). The substantial biomass of krill also supports a commercial fishery largely, concentrated around the Antarctic Peninsula (Watters et al., 2020).

A fundamental aspect of krill biology and ecology is their swarming behaviour resulting in their distribution being heterogenous and patchy (Tarling et al., 2009; Nicol and Brierley, 2010). In some regions, ~ 98% of krill biomass is contained in swarms (Fielding et al., 2014). Swarming plays an important role in krill reproduction (Watkins et al., 1992), foraging (Hamner and Hamner, 2000) and predator avoidance (Cox et al., 2009). Swarms can take a variety of shapes and can form large aggregations. Horizontal extent can span up to thousands of metres in length and can contain billions of krill in densities of several thousand individuals per cubic metre (Cox et al., 2010; Tarling and Fielding, 2016). The swarming behaviour of krill has a strong influence on the distribution and foraging strategies of Southern Ocean predators. Higher-order predators, such as seabirds and marine mammals, are reported to target and concentrate predation efforts in dense krill swarms (Veit et al., 1993; Santora et al., 2017).

In the Southern Ocean, krill harvesting is managed under the Commission for the Conservation of Marine Living Resources (CCAMLR). Through its ecosystem monitoring programme (CEMP), predator response parameters, such as breeding and foraging success, can be used to inform precautionary krill catch limits (Agnew, 1997; Constable et al., 2000). Adélie penguins (*Pygoscelis adeliae*) are a key indicator species under CEMP because they are important consumers of krill (Croxall et al., 2002). However, since the establishment of CEMP, there is increasing recognition Adélie penguin diets are more diverse than traditionally believed, with substantial spatial and temporal variability in the proportion of krill and fish consumed (Clarke et al., 2002; Ainley et al., 2003; Lynnes et al., 2004; Tierney et al., 2009; Gorman et al., 2021). The diet of Adélie penguin populations in the Scotia Sea, East Antarctic and regions of the Antarctic Peninsula are generally dominated by krill, while populations in the Ross Sea have a more varied diet and

consume a mixture of fish and euphausiid species (Ratcliffe and Trathan, 2012). Despite establishing a greater understanding of the specific prey consumed, there remains a limited understanding of how the distribution and foraging behaviours of this indicator species are related to the spatiotemporal variability of krill patches (Ainley et al., 2015; Ford et al., 2015). Understanding foraging behaviour responses of Southern Ocean predators to krill distribution and abundance may provide insight into ecological factors influencing predator population dynamics.

Given the variability in krill abundance and density around coastal Antarctic waters (Atkinson et al., 2004; Jarvis et al., 2010) and variation in key physical and environmental features (i.e. sea ice and proximity of land-based colonies to shelf break), it is likely krill-predators adopt different foraging strategies at the regional-scale (Ford et al., 2015; Cimino et al., 2016). In East Antarctica, Nicol et al. (2008) conducted fine-scale acoustic surveys during 2001 and 2003 to assess krill distribution and abundance using a standard two-dimensional grid-based approach, where the acoustic data are integrated to depths of 250 m and averaged over one nautical mile intervals. The simultaneous collection of Adélie penguin spatial [horizontal] movements *via* telemetry also enabled key predator foraging parameters to be interpreted in the context of krill data. Using horizontal information, Nicol et al. (2008) relied upon area-restricted search (ARS) assumptions to make broad spatial associations between penguin movements and krill distribution and abundance. Results showed that penguin breeding success, foraging trip duration and meal mass were broadly related to overall krill biomass estimates in those two years. In this same area of East Antarctica, Emmerson et al. (2015) considered the spatiotemporal variability of penguin response parameters in relation to the two years using krill biomass estimates and proposed that krill availability was a function of its abundance in the water column and its accessibility, primarily related to the presence of extensive fast-ice. However, neither of these studies were able to consider their results in the context of krill in the vertical dimension; how predator foraging effort and prey abundance are distributed in the underwater environment; and the extent of their three-dimensional spatial overlap.

Here, we further explore the concept of krill availability to penguins, specifically in relation to krill swarm distribution and abundance by reanalysing krill biomass estimates reported by Nicol et al. (2008) and integrating these estimates with the recent processing of extensive multi-year Adélie penguin dive data (Riaz et al., 2020) and quantitative integration of spatial location estimates from the same years (Riaz et al., 2021). Methods for swarm-based acoustic analyses (Tarling et al., 2009; Cox et al., 2010) offer an opportunity to re-examine acoustic prey-field data to characterise krill swarm structure (e.g., internal density, height, length) and location (depth) in the water column. Integrating this with penguin dive and location data provides an opportunity to examine where penguin underwater [vertical] foraging efforts are concentrated along horizontal movement trajectories in relation to krill swarm distribution and abundance. The benefits of examining krill abundance and distribution through a swarm-based analysis are twofold: (1) processing of acoustic information can be concentrated around the natural aggregation structures of krill swarms, reducing pre-processing, subjective noise removal and associated loss of acoustic information; (2) broad-scale summary information of the krill prey-field (e.g. swarm biomass and depth) are provided at a scale in which predator foraging decisions and prey encounters occur (Cox, 2017; Bestley et al., 2018). Combining horizontal-vertical predator movement with three-dimensional krill prey-field information can improve understanding of predator-prey spatial overlap and interactions (Ainley et al., 2015).

In this study, we investigated the spatial associations of krill swarm characteristics and Adélie penguin foraging effort by integrating predator-prey data streams collected simultaneously (in the same area and during the same seasons). We provide a novel reassessment of the krill acoustic data collected during surveys conducted in two years (2001 and 2003), using a swarm-based approach to estimate krill swarm distribution and physical structure. To understand how penguin foraging relates to krill swarm abundance and distribution we integrate contemporaneous horizontal and vertical movement information from chick-rearing Adélie penguins at Béchervaise Island, East Antarctica, which were dual-tagged with platform terminal transmitters (PTTs) and time-depth recorders (TDRs). We test whether foraging dive effort (summarised dive activity) changed in relation to krill swarm biomass and number across the gridded offshore survey domain. We expected all indices of underwater foraging effort would increase in areas with a greater krill abundance and number of swarms. Through this work, we provide an improved understanding of predator-prey interactions for this CEMP indicator species, and the prey-field characteristics critical to penguin foraging success at this colony.

2 Materials and methods

2.1 Prey-field data: Krill swarms

Shipboard acoustic surveys were performed off the coast of Béchervaise Island (67°35 S, 67°49 E) in East Antarctica in 2001 (KACTAS – Krill Availability, Community Trophodynamics and AMISOR Survey) and 2003 (KAOS – Krill Acoustics and Oceanography Survey). These surveys were conducted from 12 to 23 January, and from 16 January to 1 February, respectively. For both KACTAS and KAOS, the survey areas ranged from 66° to 67°S and 61.8° to 64.6°E, covering an estimated 11,921 km^2. Due to operational curtailment, only 75% of transects within the survey area were completed during KACTAS. Full details of the survey design and acoustic data collection can be found in Nicol et al. (2008).

The acoustic data processing was carried out using Echoview (v5.4 Myriax, Hobart, Australia). The swarm-based acoustic analysis used 38 and 120 kHz frequencies of calibrated Simrad (Horten, Norway) EK500 echosounder for the KACTAS survey and EK60 for the KAOS survey. Echosounder transducers were hull-mounted split-beam transducers with a 7° beam width. Krill swarms were identified up to a 250 m depth limit at a 2 Hz pulse repetition rate. The mean vessel speed was 7.8 knots with a mean inter-pin space of 2 m. Surface noise, seabed and false seabed returns were isolated and removed from acoustic observations. Calibrations parameters applied to acoustic data are provided in Table S1. Time varied gain noise correction was performed using the procedure described in De Robertis and Higginbottom (2007).

Individual krill swarms were isolated in Echoview using the schools detection algorithm of Barange (1994). School detection

was carried out on a 7 x 7 identity matrix convolution of the 120 kHz pre-processed data using the detection parameters established in Tarling et al. (2009) and a mean volume backscattering strength (S_v) threshold of -70 dB re 1 m^{-1}, equivalent to a krill wet mass density of 0.9 g m^{-3}. A description of acoustic terminology, symbols and units are provided by MacLennan et al. (2002). These aggregations are assigned a krill or non-krill status by applying a validated 'dB-difference' technique to the 7 x 7 convolution of 120 - 38 kHz pre-processed data falling within the detected aggregation boundaries (Madureira et al., 1993). As implemented here, the dB-difference technique is a binary classification, with aggregations falling within a dB difference range deemed to be krill. Outside of this range an aggregation is classified as coming from other species and excluded from further analysis. The dB-difference ranges were calculated using the distorted-wave Born approximation (DWBA) krill acoustic target strength model developed by McGehee et al. (1998), and extended by Conti and Demer (2006) to account for stochastic variation in the received signal phase. Consistent with CCAMLR recommendations, the Calise and Skaret (2011) krill target strength model was applied, using a tilt angle distribution, a wrapped normal distribution with mean -28° (head down) and standard deviation 20°. Stochastic DWBA krill target strength model parameters were set at their default values as given in Calise and Skaret (2011).

Once an aggregation was identified as krill, volume integrations were carried out on 120 kHz data falling within the boundary of individual krill swarms at a -80 dB re 1 m^{-1} threshold, equivalent to average (across length frequency clusters) krill wet mass density of 0.09 g m^{-3}, and swarm internal density (ρ) was calculated using $\rho=10^{(S_v-TS_{kg})/10}$, where TS_{kg} is the krill length cluster specific target strength of 1 kg (wet mass) of krill. Once krill swarms were identified, a range of physical properties were calculated within the Echoview software. For each individual swarm, this included the mean depth (m), cross-sectional area (m^2), length (m), height (m), internal density (g wet mass per m^3) and nautical area scattering coefficient (NASC) (m^2 n $mile^{-2}$). To calculate swarm biomass, we assumed swarms had a cylindrical shape an applied the following [Equation 1]:

$$\text{Swarm biomass} = \left(\Pi\left(\frac{\text{Swarm height}}{2}\right)^2 \times \text{Swarm length}\right) \times \text{Swarm internal density}$$

We note that in some instances, the cylindrical shape assumption may underestimate swarm biomass, since swarms can take complex 3D shapes and structures which have volumes larger than cylindrical or ellipsoid shapes (Brierley and Cox, 2010).

2.2 Predator data: Movement and diving

Béchervaise Island is an Adélie penguin nesting site located in East Antarctica home to over 2000 breeding pairs. It is a CEMP site which has been the focus of a long-term Adélie penguin monitoring program since 1990 (Kerry et al., 2000). During 2001 and 2003, spatial location and dive data were collected from adult chick-rearing Adélie penguins at the Béchervaise Island colony through dual-tagging of individuals with PTTs and TDRs. These data were comprised of 18 dual-tagged individuals over 19 foraging trips during the guard and crèche chick-rearing periods (one individual from the 2003 season recorded two foraging trips). Individuals tagged in the two years were different individuals. Penguin movement data ranged from 12 to 25 January in 2001, and 9 to 26 January in 2003. Full details of PTT and TDR deployments and data processing are provided by Riaz et al. (2020); Riaz et al. (2021).

Archived dive data were downloaded using Wildlife Computers software packages. A zero-offset correction and surface noise exclusion (< 3 m) were applied to dive profiles (Riaz et al., 2020). All subsequent processing and analyses of data was performed using R statistical software version 3.5.1 (R Core Team, 2018). A series of dive indices were calculated for each dive. This included the maximum dive depth (m); bottom duration of dives (s) (defined as the maximum time spent within 50% of maximum dive depth and where the rate of change in depth during descent or ascent did not exceed 50%); and wiggles (the number of undulations in a dive profile > 2 m in depth).

Raw Argos location estimates were subjected to several quality control measures. Location estimates were removed when they occurred within 120 s of each other (n = 200), and we ensured our dataset did not contain foraging trips with fewer than 10 location fixes or lasting less than 1 day in duration. After quality control processing, PTT location estimates were fit with a continuous-time correlated random walk state-space model (SSM) using the '*foieGras*' package (version 0.7.6; Jonsen and Patterson, 2021). This accounted for observation error in tracking data and provided location estimates at regular time intervals (Jonsen et al., 2013; Ropert-Coudert et al., 2020). Process models and equations are established in Jonsen et al. (2020). Spatial locations were regularised to 1-hour time steps, consistent with Riaz et al. (2021).

We binned diving activity into 1-hour periods corresponding to SSM location estimates. At each hourly location estimate along regularised tracks, we quantified underwater foraging effort by summing dive parameters (Pütz et al., 2006; Zimmer et al., 2008). The sum of the maximum dive depth (m), bottom duration (s), number of dives, and number of wiggles for each hour of an individual's foraging trip were calculated. Summed dive parameters over regular time-steps are commonly used to quantify marine predator foraging effort underwater (Pütz et al., 2006; Zimmer et al., 2010; Kuhn et al., 2015; Riaz et al., 2021).

2.3 Predator-prey statistical integration

To examine the spatial associations of krill swarm characteristics and penguin foraging effort, we integrated the horizontal-vertical movements of Adélie penguins with krill survey estimates. We summarised our prey and predator indices across the entire survey area at a 0.05° latitude x 0.38° longitude resolution (approximately 5.5 x 17 km). The size of our spatial grid was chosen for three reasons. First, krill swarm characteristics are expected to have a greater variability over latitudinal gradients (i.e. offshore-inshore), associated with oceanographic conditions and food availability (Klevjer et al., 2010); second, it generally captures survey estimates from two adjacent transect lines, which were longitudinally spaced at approximately 5 – 10 nautical mile intervals (Nicol et al., 2008); and third, it is sufficiently broad to cater for prey horizontal transport through time, accommodating the temporal mismatch between survey estimates and penguin location estimates, which is a common challenge of survey efforts linking predators and prey (Santora et al., 2010; Kuhn et al.,

2015; Hinke et al., 2017). The gridded approach adopted here is analogous to other studies examining prey-fields in the context of predator-prey relationships (Santora and Reiss, 2011; Sveegaard et al., 2012).

Using the raw acoustic transects, we calculated the geometric mean [hereafter referred to as 'mean'] swarm biomass within defined 0.05° x 0.38° grid cells. The geometric mean is demonstrated to be an effective parameter in describing skewed prey-field data, as is it less sensitive to large outlier values (Cade et al., 2021). We also calculated the total number of swarms per grid cell and standardised this metric by the total length of the survey transect in each spatial bin to account for survey effort.

Gridded krill indices were overlaid with the horizontal-vertical movements of chick-rearing Adélie penguins at Béchervaise Island. To quantify foraging effort in corresponding 0.05° x 0.38° bins, for each penguin we calculated (1) total dive depth, (2) total number of wiggles, (3) total bottom duration, and (4) total number of dives per grid cell. By gridding the predator-prey data, spatial autocorrelation present within the high-resolution along-transect and along-track datasets is reduced (Warwick-Evans et al., 2022).

With the integrated final predator-prey dataset, we make inferences about how penguin foraging effort is associated with krill metrics using generalised linear mixed effects models to ('glmmTMB' package; version 1.1.4; Brooks et al., 2017). For independent models of each of the four penguin diving response variables [depth, bottom duration, number of wiggles, and number of dives], we fitted as predictor variables the two krill swarm metrics [mean krill biomass and number of swarms]. Prior to analysis, predictor variables were assessed for any collinearity issues [Pearson correlation coefficient = -0.13] ('corrplot' package; version 0.92; Wei and Simko, 2021). All four models were configured with individual penguin ID nested within year (i.e. Year/Bird ID) to allow relationships to vary among individuals. The small sample size of penguin individuals from 2003 (due to logistical, financial, and field constraints) precluded us from examining the influence of year as a fixed effect. To account for overdispersion and right skew in data, number of wiggles and dives (count data) models were fitted with a negative binomial distribution, while depth and bottom duration were configured with a gamma distribution and log link function. Both krill predictor metrics were scaled and centred to aid model convergence. Model covariates were considered significant at p-values< 0.05.

3 Results

3.1 KACTAS characteristics

The KACTAS voyage performed eight north-south acoustic transects spanning a 9374 km^2 area (Figure 1). At a 0.05° latitude x

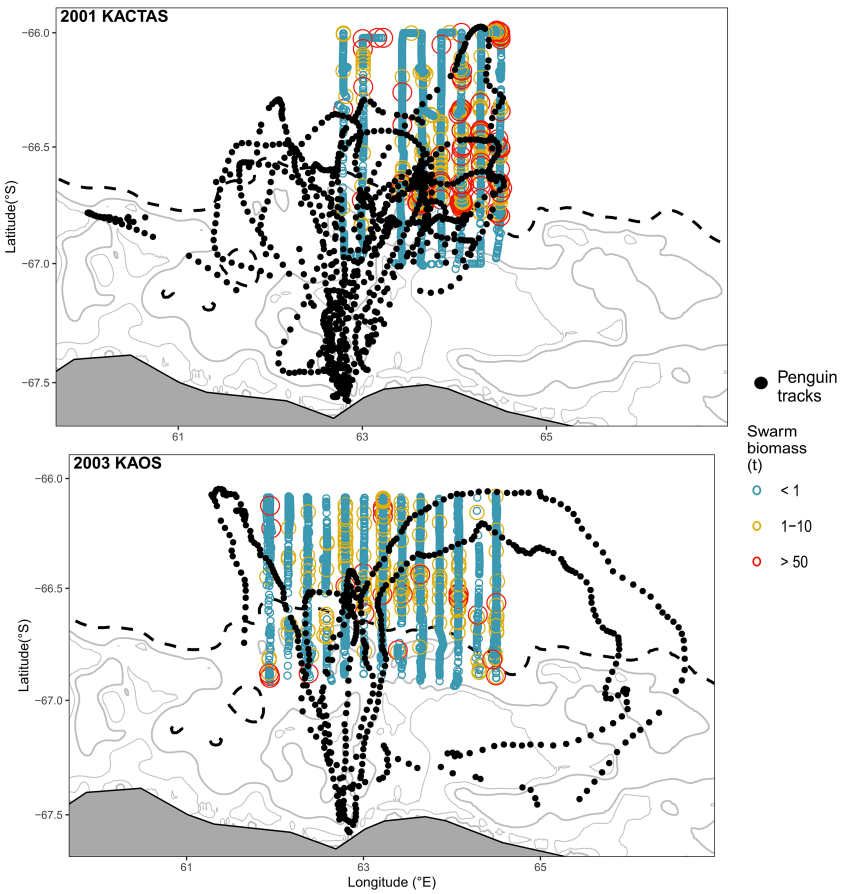


FIGURE 1
Distribution of krill swarm biomass in the waters off Béchervaise Island collected during KACTAS and KAOS. To aid visual presentation, krill swarms are grouped in discrete biomass categories. Swarms within transects are overlaid with SSM-filtered location estimates for chick-rearing Adélie penguins (n = 18 individuals on n = 19 foraging trips). Major land features are in grey and major bathymetric features (shelf break and other bathymetric features > 1000m) are illustrated by black dashed lines. Bathymetric contours are displayed at 100m intervals. Inset panel in (A) shows the study region (red circle) in East Antarctica.

0.38° longitude resolution, there were 106 grid cells across the survey area (Figure 2). A total of 5792 krill swarms were recorded with a total estimated biomass of 8123 t. The mean krill swarm biomass was 3.83 kg. On average, swarms were 124.7 m^2 in area (where area is the intersection between the acoustic beam and the swam) with an internal density of 5.87 g m^{-3}. The mean NASC was 53.4 m^2n $mile^{-2}$, with 1% of swarms exceeding 5000 m^2n $mile^{-2}$ (see Table 2 for means and 95% CI).

The mapped distribution shows mean swarm biomass was higher in grid cells located over the eastern part of the shelf break, with high biomass also patchily distributed further north (Figure 2 upper panels). The number of krill swarms across the survey area showed a different and more consistent pattern, largely concentrated in the middle of the survey area in waters over the shelf break and north (Figure 2).

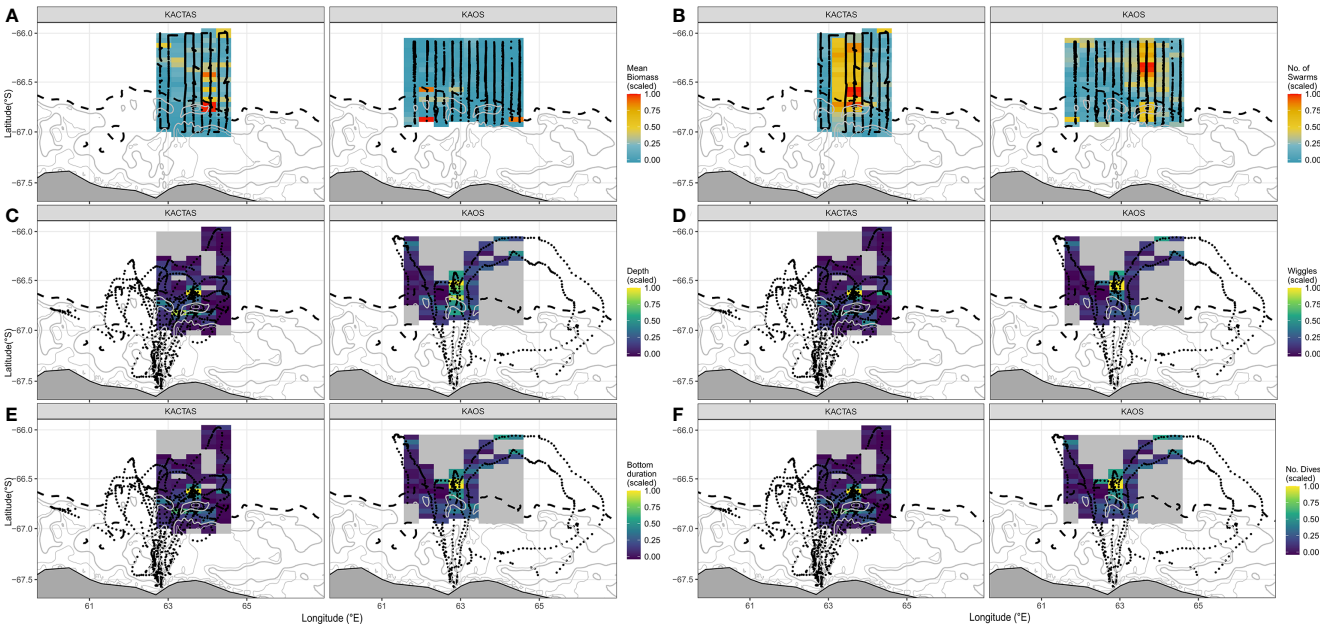


FIGURE 2
Maps displaying the distribution of krill metrics (mean biomass and number of swarms) and four penguin diving metrics (depth, wiggles, bottom duration and # of dives) over the KACTAS and KAOS survey area. Grid cell metrics are binned at a 0.05° latitude x 0.38° longitude spatial resolution. The black points represent krill transect **(A, B)** and penguin tracking observations for krill and penguin plots **(C–F)**, respectively. Maps displayed illustrate spatially grided predator-prey data, as inputed into models. Land and bathymetric features are displayed as per Figure 1.

TABLE 2 Summaries of physical properties of krill swarms and the depth-stratified total number of swarms and biomass recorded during KACTAS and KAOS voyages that occurred over the entire survey area.

	KACTAS (n swarms = 5792)		KAOS (n swarms = 7192)	
Survey Characteristics	Mean	Range	Mean	Range
Biomass (kg)	3.83 (3.55 – 4.14)	0.001 – 855,472	4.72 (4.45 – 5.01)	0.04 – 1,266,769
Density (g/m^3)	5.87 (5.70 – 6.04)	2 - 2156	11.41 (11.05 – 11.77)	2 – 4001
Area (m^2)	124.70 (120.19 – 129.37)	0.4 – 464,809	64.25 (62.63 – 65.91)	6 – 107,789
NASC	53.40 (51.36 – 55.51)	4 – 53,284	73.11 (70.20 – 76.13)	2 – 36,178
	No. swarms	Sum biomass (t)	No. swarms	Sum biomass (t)
Depth range				
0 - 25 m	2382	406.7	3082	278.5
25 - 50 m	1549	3387.7	1275	319.5
50 - 75 m	901	3164.6	1417	581.8
> 75 m	960	1164.0	1418	1729.2

Mean values represent the geometric mean and 95% CI. See Methods for definitions of krill swarm metrics.

In vertical space, KACTAS krill swarms were observed at depths in the water column ranging between 4 – 246 m, with an average depth of 42 m. Most swarms (68%) were located in the upper 50 m (Figure 3) but the sum of the krill biomass was mostly concentrated between 25 – 50 m depths (81%) (Table 2).

3.2 KAOS characteristics

The KAOS voyage covered a larger spatial extent compared to KACTAS. Active acoustics were recorded over 13 transects, covering approximately 11,921 km^2 (Figure 1). There were 144 grid cells when binned at a 0.05° latitude x 0.38° longitude spatial resolution (Figure 2). A greater number of swarms (n = 7192) were recorded compared to KACTAS, however total biomass (2909 t) was substantially lower. The mean biomass of krill swarms during KAOS was 4.80 kg. While the average internal density of krill swarms was also larger compared to KACTAS (11.41 g m^{-3}), the mean swarm area was around half the size (64.63 m^2). The mean NASC was 73.1 m^2n $mile^{-2}$ (see Table 2 for means and 95% CI). Similar to KACTAS, 1% of swarms exceeded 5000 m^2n $mile^{-2.}$

During KAOS, mean swarm biomass showed a relatively uniform distribution of low biomass across the survey area, with the majority of biomass concentrated across few grid cells. In comparison, the horizontal distribution of swarm frequency was patchily distributed along the eastern part of the shelf break and was most pronounced in grid cells located in more northern waters (Figure 2).

Over the KAOS survey area, swarms were observed within 6 – 248 m depths, but at 46 m on average. The distribution of swarms through the upper water column was relatively even, although 43% were recorded in waters shallower than 25 m. In contrast, most (66%) of the krill swarm biomass was in depths greater than 75 m (Figure 3).

3.3 Penguin activity in the survey area

Over the two breeding seasons, we recorded diving activity from 18 dual-tagged individuals on 19 foraging trips (Figure 1). Within the KACTAS and KAOS survey areas, we documented 12,278 dives spread across 787 at-sea locations. In 2001 (KACTAS), 14 individuals and 14 foraging trips were recorded. Within the KACTAS survey area, 8821 dives were logged over 500 spatial locations. This accounted for 48% of

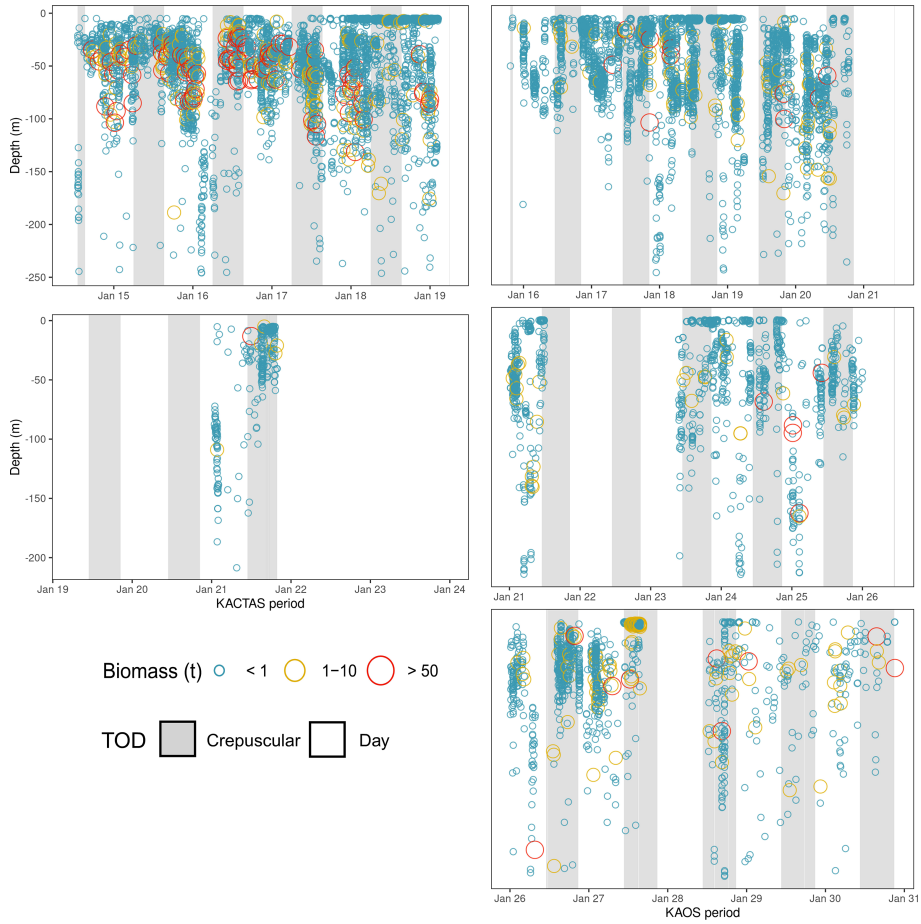


FIGURE 3
Time-series showing krill swarm distribution through time for KACTAS and KAOS (left and right panels, respectively). Each panel represents a vertical snapshot of the water column (0 – 250 m) over a specific period of time during survey efforts. Each circle represents a krill swarm observed and are sized and coloured in relation to their biomass values (see Methods for details). To aid visual presentation, biomass estimates are grouped into discrete categories. Shaded areas represent the diurnal period in which krill swarms were observed. Using the *'maptools'* package, we calculate the solar position values during survey effort period (Bivand and Lewin-Koh, 2016). Solar positions values > 12° were assigned as day and those between -12° and 12° were assigned as crepuscular; at this time of year there are no night (< -12°) values.

dives at 22% of locations over the entire foraging trip distribution. In 2003 (KAOS), 4 individuals and 5 foraging trips were recorded, and 3457 dives over 247 spatial locations occurred within the KAOS survey area (Figure 1). This comprised 40% and 31% of foraging trip dives and at-sea location, respectively.

At the trip level, mean dive effort (total depth travelled, bottom duration and number of wiggles and dives) across KACTAS and KAOS grid cells (n= 106 and n= 144 cells, respectively) were broadly similar but slightly higher during KACTAS (Table 3). Generally, higher values (i.e. greater dive effort, longer bottom duration, more wiggles and more dives) of all penguin dive metrics were centred in the vicinity of the shelf-break during both surveys (Figure 2).

3.4 Predator-prey relationships

The total depth and bottom duration travelled, and number of wiggles and dives performed were consistently greater in areas where there were a higher number of krill swarms. In contrast, penguin foraging effort was not significantly related to mean swarm biomass in any model (Table 4; Figure 4).

Within a given grid cell (covering approximately 100 km), a change of 0 to 3 krill swarms would correspond with a predicted average change in penguin behaviour from 33 to 89 dives, and 255 to 656 wiggles. Similarly, predicted summed vertical dive distance would increase from 810m to 2527 m, and bottom time would increase from 1331 s (~ 22 mins) to 3656 s (~ 61 mins) (Figure 4).

4 Discussion

By spatially integrating krill swarm data with location and dive data for Adélie penguins, this study advances our understanding of Southern Ocean predator-prey relationships and contributes to a longstanding objective in ecosystem monitoring efforts. Our findings show areas of increased penguin diving effort corresponded with high krill swarm numbers. In contrast, areas of increased mean krill biomass did not influence the spatial distribution of penguin foraging activity. These results indicate that while the spatial distribution of penguin underwater

TABLE 3 Summaries of chick-rearing Adélie penguin activity at Béchervaise Island that occurred over the KACTAS and KAOS survey areas.

	KACTAS (n individuals = 14)		KAOS (n individuals = 4)	
Trip Characteristics	Sum	Mean (CI)	Sum	Mean (CI)
Depth (km)	240	1.25 (1.12 – 1.37)	77	0.92 (0.85 – 0.99)
Bottom duration (h)	99	0.51 (0.46 – 3.44)	39	0.47 (0.43 – 2.61)
# Wiggles	66811	346.2 (310.2 – 382.2)	26349	317.5 (288.9 – 346.0)
# Dives	8821	45.70 (41.08 – 50.33)	3390	40.84 (37.62 – 44.07)

Mean values are calculated per individual and then averaged across individuals within each 0.05° latitude x 0.38° longitude grid cell; 95% confidence intervals are also displayed. See Methods for dive metric definitions.

TABLE 4 Results of the four generalised linear mixed effects models for each dive metrics in relation to krill swarm metrics (number of swarms and mean swarm biomass).

Response variable	Predictor variable	Coefficients			
		Est	SE	z-value	*p*-value
Depth	Intercept	6.70	0.13	50.3	<0.0001
	Number of swarms	0.38	0.09	4.2	< **0.001**
	Mean swarm biomass	0.01	0.08	0.01	0.98
# Wiggles	Intercept	5.52	0.13	41.2	<0.0001
	Number of swarms	0.31	0.09	3.5	< **0.001**
	Mean swarm biomass	0.06	0.09	0.80	0.42
Bottom duration	Intercept	7.18	0.14	52.5	<0.0001
	Number of swarms	0.34	0.09	4.0	< **0.001**
	Mean swarm biomass	0.04	0.07	0.6	0.56
# Dives	Intercept	3.49	0.14	24.91	<0.0001
	Number of swarms	0.33	0.08	3.93	< **0.001**
	Mean swarm biomass	0.02	0.07	0.33	0.74

Model data comprises 747 observations across 18 birds, summarised over n= 106 and n= 144 grid cells, respectively for KACTAS and KAOS Coefficient estimates ± SE are presented on the scale of the link function. Model terms with a significant *p*-value at the 0.05 level are highlighted in bold text.

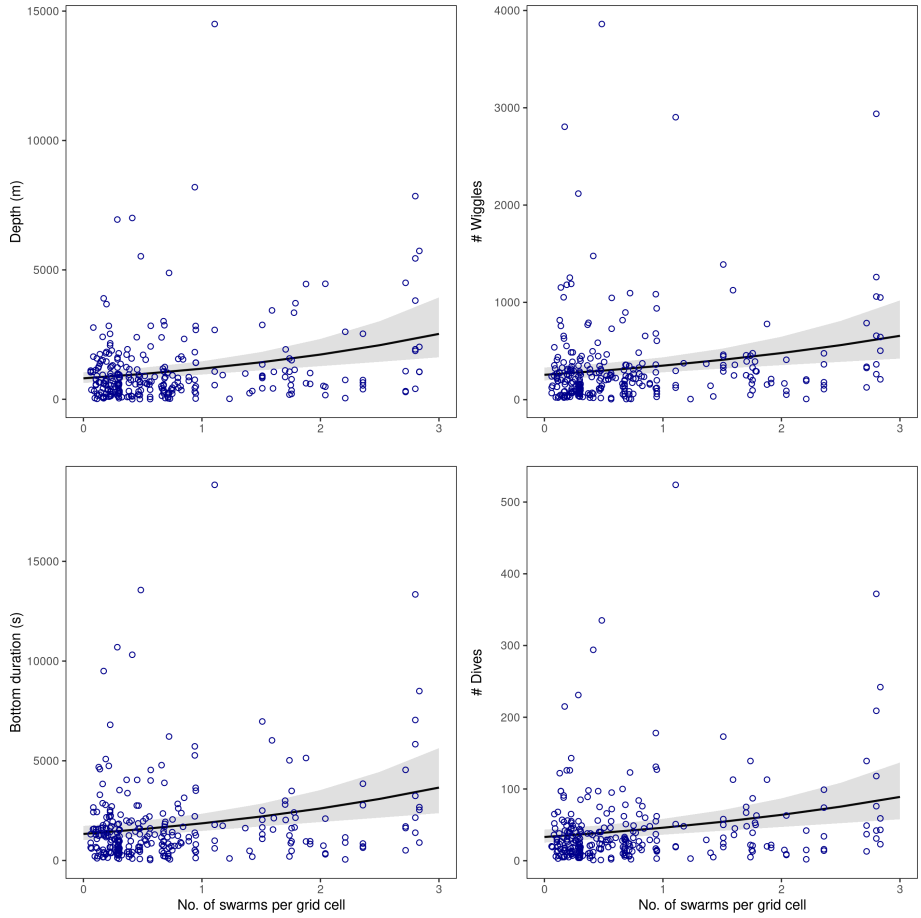


FIGURE 4
Results from the generalised linear mixed effects models showing the diving responses [summed depth, bottom duration, number of wiggles, and number of dives over each spatial grid; y-axes] modelled in relation to krill swarm number within spatial grid cells across the acoustic survey domain. Diving parameters showed no association with krill swarm biomass; full model results are given in Table 4.

foraging effort could be used as a proxy for krill presence (and/or availability), it may not necessarily indicate krill abundance. We discuss this in the context of Adélie penguin foraging ecology and how this information can be used to inform ecosystem assessment and management.

4.1 Acoustic prey field characteristics

Shipboard acoustic surveys provide a powerful means to record krill abundance and swarming characteristics over vast three-dimensional spatial scales (Cox et al., 2009; Cox et al., 2010). Our swarm-based analyses indicated substantial differences in krill biomass between the 2001 KACTAS and 2003 KAOS survey efforts. KACTAS recorded 8123 t of krill biomass within swarms, and KAOS recorded only 2909 t. While KAOS covered a spatial area that was 21% larger than KACTAS, it recorded only 36% of the biomass observed during KACTAS. Differences in biomass magnitude between survey years were consistent with previous grid-based analyses in Nicol et al. (2008), which characterised KACTAS and KAOS as krill rich and krill poor years, respectively.

For 2001 KACTAS, the biomass distribution was broadly similar to what was in reported in Nicol et al. (2008), occurring mostly over the eastern survey area. However, our analyses indicated the horizontal distribution of 2003 KAOS biomass to be aggregated in relatively small patches over the central and western area of the survey box, whereas previous analyses located biomass largely over the eastern survey area. These qualitative differences between swarm- and grid-based analyses were unexpected. Preliminary comparisons of the two approaches have yielded broadly similar density estimations (Cox, 2017), however comprehensive comparisons of krill distribution and abundance parameters are yet to be performed. Further work is needed to quantitatively assess the comparability in prey-field characteristics generated by swarm- and grid-based acoustic techniques; particularly if swarm-based approaches are likely to be the future of krill biomass mapping.

The swarm-based reanalysis showed that the greatest aggregations of swarm biomass generally occurred near the shelf break. Around the Antarctic coastline, this bathymetric feature is widely reported as an area where high krill biomass predictably occurs (Trathan et al., 2003; Jarvis et al., 2010; Silk et al., 2016; Bestley et al., 2018). These spatial patterns are driven by multiple factors, including krill food abundance and predictability, and oceanographic dynamics (Nicol et al., 2008; Silk et al., 2016). We found swarm biomass was highly patchy, with the majority of biomass concentrated in a small number of swarms (Lascara et al., 1999; Lawson et al., 2008; Klevjer et al., 2010). Hence the prey field in this region is largely comprised of an abundance of small, low-biomass

krill aggregations, consistent with observations from other surveys in East Antarctica (Pauly et al., 2000; Jarvis et al., 2010) and elsewhere in the Southern Ocean (Lascara et al., 1999; Lawson et al., 2008).

Comparisons of krill swarm parameters across studies can be challenging due to differences in techniques and reported metrics (Nicol et al., 2008; Klevjer et al., 2010). During krill surveys in 2001 and 2003, swarms were mostly recorded at ~ 40 m depth, but were also observed as deep as the 250 m acoustic detection limit. The mean and range of water column depths occupied by krill swarms were similar to reports in the Scotia Sea and East Antarctic (Tarling et al., 2009; Bestley et al., 2018). Similarly, surface area values were broadly similar to observations from other Antarctic regions (Cox et al., 2009; Cox et al., 2010; Klevjer et al., 2010). However, the internal density of swarms recorded during both surveys in this part of East Antarctica was higher than elsewhere in Antarctica with several krill swarms having an internal density greater than 1000 g m^{-3}, which is three times higher than previous swarm density observations in the region (Bestley et al., 2018). Further research is needed to understand the biophysical factors influencing krill swarm dynamics and aggregation structures in this region of East Antarctica.

4.2 Penguin foraging strategies

Examining the spatial links between prey distribution and abundance and predator foraging effort can provide critical insight into ecosystem-level trophodynamics and response to environmental change associated with harvesting and climate scenarios (Forcada and Trathan, 2009; Lynch et al., 2012). In this region, broad-scale predator foraging parameters (e.g. trip duration and meal mass) have been widely used to understand the role of krill in supporting penguin energetic needs during the breeding season (Clarke, 2001; Clarke et al., 2002; Nicol et al., 2008; Tierney et al., 2009; Emmerson et al., 2015; Southwell et al., 2015). Here, we extend these analyses by quantitatively integrating empirical data on penguin movement and krill abundance and distribution.

Our findings indicate the foraging effort of the Adélie penguin, one of the most abundant seabirds in East Antarctica, increases in areas where there are more krill swarms. All penguin dive metrics (total depth travelled, dive bottom time, number of wiggles and dives performed) were greater in areas corresponding with a higher number of swarms. This suggests chick-rearing penguins preferentially target and forage in areas where krill aggregations are more frequently encountered. This highlights the importance of krill availability (i.e., encounter frequency) to penguin foraging effort, and by association, foraging success. In contrast to our expectations, penguins did not increase their foraging activity in areas with a high mean swarm biomass. Through highlighting the spatial importance of krill swarm number, our results extend the concept of krill availability provided in Emmerson et al. (2015), which was centred on prey abundance and ice-driven access to foraging grounds.

Intercepting many small krill swarms likely represent a reliable prey-field feature which Adélie penguins can exploit. From the perspective of a penguin, a profitable krill prey field in this region appears to be dependent upon a high encounter rate with swarms rather than their specific biomass. We suggest this is likely due to opportunistic diving and prey-capture attempts in areas where krill patches are frequent and closely spaced, which maximises food intake and reduces energy loss associated with commuting between forage opportunities (Santora et al., 2009; Bernard and Steinberg, 2013; Ford et al., 2015). These behavioural results are consistent with Adélie penguins feeding continuously and opportunistically during foraging trips (Ford et al., 2015; Warwick-Evans et al., 2019; Riaz et al., 2021). Larger predators, such as baleen whales, must consume relatively high densities of krill to satisfy their high energetic requirements. For example, humpback whales are conservatively estimated to each consume 390 – 874 kg of krill per day (i.e. a substantial biomass) (Reilly et al., 2004). Adopting an engulfment-feeding strategy and consuming bulk quantities of krill during high velocity lunges (Goldbogen et al., 2013), baleen whales maximise efficiency by selectively targeting large/dense krill aggregations (Santora et al., 2010; Goldbogen et al., 2012; Miller et al., 2019; Harrison et al., 2020). In contrast, penguins forage on individual krill, even when foraging within a swarm (Watanabe et al., 2014), and require a much smaller energy load (total prey kg consumed). Bioenergetics models for breeding Adélie penguins at Béchervaise Island indicate that foraging success is achieved if daily per capita ingested energy is equivalent to 579 - 635 g of krill (Southwell et al., 2015). Our results suggest that penguins at this colony do not necessarily need to selectively target large krill aggregations to satisfy their energy requirements. Frequent prey encounters are likely to be an efficient way to meet the required energy intake. While penguins consume individual prey items at a time, they have been observed foraging together in flocks of varying size (Ainley et al., 2015). Smaller and more frequent krill swarm encounters may be conducive to penguin group foraging strategies. It is also plausible the foraging effort of whales disperses large biomass krill swarms, creating a krill prey-field more favourable to penguins. Further work is needed to assess how predation pressure exerted by penguins and other marine predators alter the physical structure, size and distribution of krill swarms in the region, and how this affects penguin foraging behaviour (Ainley et al., 2015).

Our findings provide valuable insight regarding how Adélie penguins respond to krill swarm distribution, abundance and biomass. These results provide insight for CEMP which assumes that foraging efforts of land-based predators, such as Adélie penguins, respond to krill availability, and can therefore assist in monitoring ecosystem change associated with climate change or harvesting (Nicol et al., 2008). Although our study only examined data from two seasons and may not reflect the full range of Adélie penguin response parameters (Emmerson et al., 2015), our results suggest Adélie penguin foraging effort may not reliably indicate total krill biomass. Instead, we provide evidence that the spatial distribution of foraging effort reflects krill distribution in terms of the number of swarms present. While studies in this area indicate that penguin foraging trip durations, meal mass and breeding success vary in relation to overall krill biomass (Clarke et al., 2003; Nicol et al., 2008; Emmerson et al., 2015; Southwell et al., 2017), our study extends understanding of predator-prey dynamics within the water column as a first step towards a mechanistic understanding of penguin response reflected in different demographic parameters. This is particularly relevant amidst potential changes in prey availability associated with climate change (Bestley et al., 2020; McBride et al., 2021), and renewed interests to expand krill fishing operations in the Mawson region (Kelly et al., 2018; Watters et al., 2020).

4.3 Spatiotemporal predator-prey linkages

When investigating the spatial overlap of marine predators and their prey, selection of appropriate spatiotemporal scales is critical (Fauchald et al., 2000). This can be challenging when trying to integrate predator and prey information that are derived from separate data streams and recorded at

different spatial and temporal resolutions. Inferences regarding predator-prey relationship can vary depending on the spatial scales selected to assess these interactions (Rose and Leggett, 1990; Reid et al., 2004; Bailey and Thompson, 2009; Kuhn et al., 2015). Addressing temporal disparities arising from predator-prey data *via* spatial design should be guided by an informed understanding of how prey dynamics shift over space and time (Hunsicker et al., 2011). In terms of krill distribution, horizontal displacements over time are poorly understood. A key driver of horizontal advection is obviously oceanographic currents (Bestley et al., 2018; McBride et al., 2021; Nocera et al., 2021). However, krill can also swim at high speeds for extended periods of time against local currents (Krafft et al., 2015). Clearly, understanding rates of advection and structural persistence of swarms in the Southern Ocean is a complex and challenging task (Tarling and Thorpe, 2014). Furthermore, it is unknown how krill swarm horizontal-vertical distribution, aggregation and structure may be altered by penguin foraging activity and predation pressure through time (Ainley et al., 2015).

Through our gridded approach to summarising penguin foraging effort and krill swarm information, we assume the large spatial area chosen to bin predator-prey information adequately captures the spatiotemporal krill displacements over the penguin foraging period (Sveegaard et al., 2012; Kuhn et al., 2015; Hinke et al., 2017). We also assume the entire prey field within grid cells are accessible and available to penguins during their foraging efforts, disregarding the swarm depths during surveys. While this enables us to make broad-scale conclusions regarding predator-prey spatial overlap, further research is needed to understand finer-scale spatiotemporal associations (real- or near-time representation). The complementary use of devices capable of recording contemporaneous three-dimensional predator-prey interactions, such as underwater gliders (Ainley et al., 2015; Reiss et al., 2021) or animal-borne echosounders (Goulet et al., 2019) may advance this field.

Data availability statement

The raw data supporting the conclusions of this article will be made available by the authors, without undue reservation.

Ethics statement

The animal study was reviewed and approved by Australian Antarctic Division Animal Ethics Committee.

Author contributions

SB, MC, LE and JR conceived the study. JR analysed the data and drafted the manuscript. SB, MC, SW and LE provided supervision and assistance during the analyses and results interpretation. All authors contributed to the article and approved the submitted version.

Funding

SB was supported under the Australian Research Council Discovery Early Career Research Award (DECRA) project DE180100828. This work is a contribution to Australian Antarctic Science project AAS # 4518 drawing on data from projects #2205 and 2722.

Acknowledgments

We thank the ship-based field teams and engineers during KACTAS and KAOS who assisted with data collection and led by Steve Nicol. Krill swarm analyses for the KACTAS and KAOS data were performed by St Andrews. We thank the penguin monitoring field staff, Knowles Kerry and Judy Clarke for instigating and overseeing the initial years of the penguin monitoring programme. We also thank Julien Freyer for his help synthesising and processing the penguin dive data, Natalie Kelly for her assistance unpacking the reprocessed krill acoustic data, and Colin Southwell and So Kawaguchi for providing their ecological wisdom. We thank the Australian Antarctic Division for logistics and financial support. All animal handling procedures and biologging devices attached to penguins were with approval from the Australian Antarctic Division Animal Ethics Committee to AAS projects # 2205 and 2722.

Conflict of interest

The authors declare that the research was conducted in the absence of any commercial or financial relationships that could be construed as a potential conflict of interest.

Publisher's note

All claims expressed in this article are solely those of the authors and do not necessarily represent those of their affiliated organizations, or those of the publisher, the editors and the reviewers. Any product that may be evaluated in this article, or claim that may be made by its manufacturer, is not guaranteed or endorsed by the publisher.

Supplementary material

The Supplementary Material for this article can be found online at: https://www.frontiersin.org/articles/10.3389/fmars.2023.1060984/full#supplementary-material

References

Agnew, D. J. (1997). The CCAMLR ecosystem monitoring programme. *Antarctic Sci.* 9 (3), 235–242. doi: 10.1017/S095410209700031X

Ainley, D. G., Ballard, G., Barton, K. J., Karl, B. J., Rau, G. H., Ribic, C. A., et al. (2003). Spatial and temporal variation of diet within a presumed metapopulation of Adélie penguins. *Condor* 105 (1), 95–106. doi: 10.1093/condor/105.1.95

Ainley, D. G., Ballard, G., Jones, R. M., Jongsomjit, D., Pierce, S. D., Smith, W. O.Jr., et al. (2015). Trophic cascades in the western Ross Sea, Antarctica: revisited. *Mar. Ecol. Prog. Ser.* 534, 1–16. doi: 10.3354/meps11394

Atkinson, A., Siegel, V., Pakhomov, E., Jessopp, M., and Loeb, V. (2009). A re-appraisal of the total biomass and annual production of Antarctic krill. *Deep Sea Res. Part I: Oceanographic Res. Papers* 56 (5), 727–740. doi: 10.1016/j.dsr.2008.12.007

Atkinson, A., Siegel, V., Pakhomov, E., and Rothery, P. (2004). Long-term decline in krill stock and increase in salps within the Southern Ocean. *Nature* 432 (7013), 100–103. doi: 10.1038/nature02996

Bailey, H., and Thompson, P. M. (2009). Using marine mammal habitat modelling to identify priority conservation zones within a marine protected area. *Mar. Ecol. Prog. Ser.* 378, 279–287. doi: 10.3354/meps07887

Barange, M. (1994). Acoustic identification, classification and structure of biological patchiness on the edge of the Agulhas Bank and its relation to frontal features. South African Journal of Marine Science. 14 (1), 333–47. doi: 10.2989/025776194784286969

Bedford, M., Melbourne-Thomas, J., Corney, S., Jarvis, T., Kelly, N., and Constable, A. (2015). Prey-field use by a Southern Ocean top predator: enhanced understanding using integrated datasets. *Mar. Ecol. Prog. Ser.* 526, 169–181. doi: 10.3354/meps11203

Bernard, K. S., and Steinberg, D. K. (2013). Krill biomass and aggregation structure in relation to tidal cycle in a penguin foraging region off the Western Antarctic peninsula. *ICES J. Mar. Sci.* 70 (4), 834–849. doi: 10.1093/icesjms/fst088

Bestley, S., Jonsen, I., Hindell, M., Harcourt, R., and Gales, N. (2015). Taking animal tracking to new depths: synthesizing horizontal–vertical movement relationships for four marine predators. *Ecology* 96 (2), 417–427. doi: 10.1890/14-0469.1

Bestley, S., Raymond, B., Gales, N. J., Harcourt, R. G., Hindell, M., Jonsen, I. D., et al. (2018). Predicting krill swarm characteristics important for marine predators foraging off East Antarctica. *Ecography* 41 (6), 996–1012. doi: 10.1111/ecog.03080

Bestley, S., Ropert-Coudert, Y., Bengtson Nash, S., Brooks, C. M., Cotté, C., Dewar, M., et al. (2020). Marine ecosystem assessment for the Southern Ocean: Birds and marine mammals in a changing climate. *Front. Ecol. Evol.* 8 (338). doi: 10.3389/fevo.2020.566936

Bivand, R., and Lewin-Koh, N. (2016). *Maptools: Tools for reading and handling spatial objects*, R package version 0.8-39. Available at: https://cran.r-project.org/web/packages/maptools/index.html

Brierley, A. S., and Cox, M. J. (2010). Shapes of krill swarms and fish schools emerge as aggregation members avoid predators and access oxygen. *Curr. Biol.* 20 (19), 1758–1762. doi: 10.1016/j.cub.2010.08.041

Brooks, M. E., Kristensen, K., Van Benthem, K. J., Magnusson, A., Berg, C. W., Nielsen, A., et al. (2017). glmmTMB balances speed and flexibility among packages for zero-inflated generalized linear mixed modeling. *R J.* 9 (2), 378–400. doi: 10.32614/RJ-2017-066

Cade, D. E., Seakamela, S. M., Findlay, K. P., Fukunaga, J., Kahane-Rapport, S. R., Warren, J. D., et al. (2021). Predator-scale spatial analysis of intra-patch prey distribution reveals the energetic drivers of rorqual whale super-group formation. *Funct. Ecol.* 35 (4), 894–908. doi: 10.1111/1365-2435.13763

Calise, L., and Skaret, G. (2011). Sensitivity investigation of the SDWBA Antarctic krill target strength model to fatness, material contrasts and orientation. *CCAMLR Sci* 18, 97–122

Conti, S.G., and Demer, D.A. (2006). Improved parameterization of the SDWBA for estimating krill target strength. *ICES Journal of Marine Science* 63 (5), 928–935. doi: 10.1016/j.icesjms.2006.02.007

Cimino, M. A., Moline, M. A., Fraser, W. R., Patterson-Fraser, D. L., and Oliver, M. J. (2016). Climate-driven sympatry may not lead to foraging competition between congeneric top-predators. *Sci. Rep.* 6, 18820. doi: 10.1038/srep18820

Clarke, J. (2001). Partitioning of foraging effort in Adélie penguins provisioning chicks at Béchervaise island, Antarctica. *Polar Biol.* 24 (1), 16–20. doi: 10.1007/s003000000168

Clarke, J., Emmerson, L., Townsend, A., and Kerry, K. (2003). Demographic characteristics of the Adélie penguin population on Béchervaise island after 12 years of study. *CCAMLR Sci.* 10, 53–74.

Clarke, J., Kerry, K., Irvine, L., and Phillips, B. (2002). Chick provisioning and breeding success of Adélie penguins at Béchervaise island over eight successive seasons. *Polar Biol.* 25 (1), 21–30. doi: 10.1007/s003000100307

Constable, A. J., de la Mare, W. K., Agnew, D. J., Everson, I., and Miller, D. (2000). Managing fisheries to conserve the Antarctic marine ecosystem: Practical implementation of the convention on the conservation of Antarctic marine living resources (CCAMLR). *ICES J. Mar. Sci.* 57 (3), 778–791. doi: 10.1006/jmsc.2000.0725

Cox, M. J. (2017). *Describing krill: swarms or integration intervals?* (Hobart, Tamania: CCAMLR).

Cox, M. J., Demer, D. A., Warren, J. D., Cutter, G. R., and Brierley, A. S. (2009). Multibeam echosounder observations reveal interactions between Antarctic krill and air-breathing predators. *Mar. Ecol. Prog. Ser.* 378, 199–209. doi: 10.3354/meps07795

Cox, M. J., Warren, J. D., Demer, D. A., Cutter, G. R., and Brierley, A. S. (2010). Three-dimensional observations of swarms of Antarctic krill (*Euphausia superba*) made using a multi-beam echosounder. *Deep Sea Res. Part II: Topical Stud. Oceanography* 57 (7), 508–518. doi: 10.1016/j.dsr2.2009.10.003

Croxall, J., Reid, K., and Prince, P. (1999). Diet, provisioning and productivity responses of marine predators to differences in availability of Antarctic krill. *Mar. Ecol. Prog. Ser.* 177, 115–131. doi: 10.3354/meps177115

Croxall, J. P., Trathan, P., and Murphy, E. (2002). Environmental change and Antarctic seabird populations. *Science* 297 (5586), 1510–1514. doi: 10.1126/science.1071987

De Robertis, A., and Higginbottom, I. (2007). A post-processing technique to estimate the signal-to-noise ratio and remove echosounder background noise. *ICES Journal of Marine Science* 64 (6), 1282–1291. doi: 10.1093/icesjms/fsm112

Emmerson, L., Southwell, C., Clarke, J., Tierney, M., and Kerry, K. (2015). Adélie penguin response parameters signal reduced prey accessibility: implications for predator–prey response curves. *Mar. Biol.* 162 (6), 1187–1200. doi: 10.1007/s00227-015-2661-5

Enstipp, M. R., Grémillet, D., and Jones, D. R. (2007). Investigating the functional link between prey abundance and seabird predatory performance. *Mar. Ecol. Prog. Ser.* 331, 267–279. doi: 10.3354/meps331267

Fauchald, P., Erikstad, K. E., and Skarsfjord, H. (2000). Scale-dependent predator–prey interactions: the hierarchical spatial distribution of seabirds and prey. *Ecology* 81 (3), 773–783. doi: 10.1890/0012-9658(2000)081[0773:SDPPIT]2.0.CO;2

Fielding, S., Watkins, J. L., Trathan, P. N., Enderlein, P., Waluda, C. M., Stowasser, G., et al. (2014). Interannual variability in Antarctic krill (*Euphausia superba*) density at south Georgia, Southern Ocean: 1997–2013. *ICES J. Mar. Sci.* 71 (9), 2578–2588. doi: 10.1093/icesjms/fsu104

Forcada, J., and Trathan, P. N. (2009). Penguin responses to climate change in the Southern Ocean. *Global Change Biol.* 15 (7), 1618–1630. doi: 10.1111/j.1365-2486.2009.01909.x

Ford, R. G., Ainley, D., Lescroël, A., Lyver, P. O. B., Toniolo, V., and Ballard, G. (2015). Testing assumptions of central place foraging theory: a study of Adélie penguins *Pygoscelis adeliae* in the Ross Sea. *J. Avian Biol.* 46 (2), 193–205. doi: 10.1111/jav.00491

Goldbogen, J. A., Calambokidis, J., Croll, D. A., McKenna, M. F., Oleson, E., Potvin, J., et al. (2012). Scaling of lunge-feeding performance in rorqual whales: mass-specific energy expenditure increases with body size and progressively limits diving capacity. *Funct. Ecol.* 26 (1), 216–226. doi: 10.1111/j.1365-2435.2011.01905.x

Goldbogen, J. A., Friedlaender, A. S., Calambokidis, J., McKenna, M. F., Simon, M., and Nowacek, D. P. (2013). Integrative approaches to the study of baleen whale diving behavior, feeding performance, and foraging ecology. *BioScience* 63 (2), 90–100. doi: 10.1525/bio.2013.63.2.5

Gorman, K. B., Ruck, K. E., Williams, T. D., and Fraser, W. R. (2021). Advancing the Sea ice hypothesis: Trophic interactions among breeding *pygoscelis* penguins with divergent population trends throughout the Western Antarctic peninsula. *Front. Mar. Sci.* 8. doi: 10.3389/fmars.2021.526092

Goulet, P., Guinet, C., Swift, R., Madsen, P. T., and Johnson, M. (2019). A miniature biomimetic sonar and movement tag to study the biotic environment and predator-prey interactions in aquatic animals. *Deep Sea Res. Part I: Oceanographic Res. Papers* 148, 1–11. doi: 10.1016/j.dsr.2019.04.007

Grémillet, D., Kuntz, G., Delbart, F., Mellet, M., Kato, A., Robin, J. P., et al. (2004). Linking the foraging performance of a marine predator to local prey abundance. *Funct. Ecol.* 18 (6), 793–801. doi: 10.1111/j.0269-8463.2004.00914.x

Hamner, W. M., and Hamner, P. P. (2000). Behavior of Antarctic krill (*Euphausia superba*): schooling, foraging, and antipredatory behavior. *Can. J. Fisheries Aquat. Sci.* 57, 192–202. doi: 10.1139/f00-195

Harrison, L.-M. K., Goetz, K., Cox, M. J., and Harcourt, R. (2020). A Southern Ocean archipelago enhances feeding opportunities for a krill predator. *Mar. Mammal Sci.* 36 (1), 260–275. doi: 10.1111/mms.12645

Hazen, E. L., Friedlaender, A. S., Thompson, M. A., Ware, C. R., Weinrich, M. T., Halpin, P. N., et al. (2009). Fine-scale prey aggregations and foraging ecology of humpback whales *Megaptera novaeangliae*. *Mar. Ecol. Prog. Ser.* 395, 75–89. doi: 10.3354/meps08108

Hinke, J. T., Cossio, A. M., Goebel, M. E., Reiss, C. S., Trivelpiece, W. Z., and Watters, G. M. (2017). Identifying risk: concurrent overlap of the Antarctic krill fishery with krill-dependent predators in the Scotia Sea. *PloS One* 12 (1), e0170132. doi: 10.1371/journal.pone.0170132

Hunsicker, M. E., Ciannelli, L., Bailey, K. M., Buckel, J. A., Wilson White, J., Link, J. S., et al. (2011). Functional responses and scaling in predator–prey interactions of marine fishes: contemporary issues and emerging concepts. *Ecol. Lett.* 14 (12), 1288–1299. doi: 10.1111/j.1461-0248.2011.01696.x

Jarvis, T., Kelly, N., Kawaguchi, S., van Wijk, E., and Nicol, S. (2010). Acoustic characterisation of the broad-scale distribution and abundance of Antarctic krill (*Euphausia superba*) off East Antarctica (30-80°E) in January-march 2006. *Deep Sea Res. Part II: Topical Stud. Oceanography* 57 (9), 916–933. doi: 10.1016/j.dsr2.2008.06.013

Jonsen, I., Basson, M., Bestley, S., Bravington, M., Patterson, T., Pedersen, M. W., et al. (2013). State-space models for bio-loggers: A methodological road map. *Deep Sea Res. Part II: Topical Stud. Oceanography* 88, 34–46. doi: 10.1016/j.dsr2.2012.07.008

Jonsen, I. D., and Patterson, T. A. (2021) *foieGras: Fit continuous-time state-space and latent variable models for filtering Argos satellite (and other) telemetry data and estimating movement behaviour*. Available at: https://CRAN.R-project.org/package=foieGras.

Jonsen, I. D., Patterson, T. A., Costa, D. P., Doherty, P. D., Godley, B. J., Grecian, W. J., et al. (2020). A continuous-time state-space model for rapid quality control of argos

locations from animal-borne tags. *Movement Ecol.* 8 (1), 1–13. doi: 10.1186/s40462-020-00217-7

Kelly, N., Emmerson, L., Kawaguchi, S., Southwell, C., and Welsford, D. (2018). *An ecological risk assessment of current conservation measures for krill fishing in East Antarctica (CCAMLR divisions 58.4.1 and 58.4.2)*, WG-EMM-18/37). Available online at: https://www.ccamlr.org/en/wg-emm-18/37.

Kerry, K., Meyer, L., Papps, W., Clarke, J., and Irvine, L. (2000). Béchervaise island, MacRobertson land, Antarctica–CCAMLR ecosystem monitoring program (CEMP) monitoring site: description, maps and colony photographs. CCAMLR Science Abstracts No. WG-EMM-00/32, p 9.

Klevjer, T., Tarling, G., and Fielding, S. (2010). Swarm characteristics of Antarctic krill *euphausia superba* relative to the proximity of land during summer in the Scotia Sea. *Mar. Ecol. Prog. Ser.* 409, 157–170. doi: 10.3354/meps08602

Krafft, B. A., Skaret, G., and Knutsen, T. (2015). An Antarctic krill (*Euphausia superba*) hotspot: population characteristics, abundance and vertical structure explored from a krill fishing vessel. *Polar Biol.* 38 (10), 1687–1700. doi: 10.1007/s00300-015-1735-7

Kuhn, C. E., Sterling, J. T., and Zeppelin, T. K. (2015). Linking northern fur seal behavior with prey distributions: the impact of temporal mismatch between predator studies and prey surveys. *Anim. Biotelemetry* 3 (1), 1–12. doi: 10.1186/s40317-015-0064-5

Laidre, K. L., Heide-Jørgensen, M. P., Heagerty, P., Cossio, A., Bergström, B., and Simon, M. (2010). Spatial associations between large baleen whales and their prey in West Greenland. *Mar. Ecol. Prog. Ser.* 402, 269–284. doi: 10.3354/meps08423

Lascara, C. M., Hofmann, E. E., Ross, R. M., and Quetin, L. B. (1999). Seasonal variability in the distribution of Antarctic krill, *Euphausia superba*, west of the Antarctic peninsula. *Deep Sea Res. Part I: Oceanographic Res. Papers* 46 (6), 951–984. doi: 10.1016/S0967-0637(98)00099-5

Lawson, G. L., Wiebe, P. H., Ashjian, C. J., and Stanton, T. K. (2008). Euphausiid distribution along the Western Antarctic peninsula–part b: distribution of euphausiid aggregations and biomass, and associations with environmental features. *Deep Sea Res. Part II: Topical Stud. Oceanography* 55 (3-4), 432–454. doi: 10.1016/j.dsr2.2007.11.014

Lynch, H. J., Naveen, R., Trathan, P. N., and Fagan, W. F. (2012). Spatially integrated assessment reveals widespread changes in penguin populations on the Antarctic peninsula. *Ecology* 93 (6), 1367–1377. doi: 10.1890/11-1588.1

Lynnes, A., Reid, K., and Croxall, J. (2004). Diet and reproductive success of Adélie and chinstrap penguins: linking response of predators to prey population dynamics. *Polar Biol.* 27 (9), 544–554. doi: 10.1007/s00300-004-0617-1

MacLennan, D.N., Fernandes, P.G., and Dalen, J.. (2002). A consistent approach to definitions and symbols in fisheries acoustics. *ICES Journal of Marine Science* 59 (2), 365–369. doi: 10.1006/jmsc.2001.1158

Madureira, L.S., Everson, I., and Murphy, E.J.. (1993). Interpretation of acoustic data at two frequencies to discriminate between Antarctic krill (Euphausia superba Dana) and other scatterers. *Journal of Plankton Research* 15 (7), 787–802. doi: 10.1093/plankt/15.7.787

McBride, M. M., Stokke, O. S., Renner, A. H., Krafft, B. A., Bergstad, O. A., Biuw, M., et al. (2021). Antarctic Krill *Euphausia superba*: spatial distribution, abundance, and management of fisheries in a changing climate. *Mar. Ecol. Prog. Ser.* 668, 185–214. doi: 10.3354/meps13705

McGehee, D., O'Driscoll, R.L., and Traykovski, L.M. (1998). Effects of orientation on acoustic scattering from Antarctic krill at 120 kHz. *Deep Sea Research Part II: Topical Studies in Oceanography* 45 (7), 1273–1294. doi: 10.1016/S0967-0645(98)00036-8

Miller, E. J., Potts, J. M., Cox, M. J., Miller, B. S., Calderan, S., Leaper, R., et al. (2019). The characteristics of krill swarms in relation to aggregating Antarctic blue whales. *Sci. Rep.* 9 (1), 16487. doi: 10.1038/s41598-019-52792-4

Nicol, S., and Brierley, A. S. (2010). Through a glass less darkly–new approaches for studying the distribution, abundance and biology of euphausiids. *Deep Sea Res. Part II: Topical Stud. Oceanography* 57 (7-8), 496–507. doi: 10.1016/j.dsr2.2009.10.002

Nicol, S., Clarke, J., Romaine, S., Kawaguchi, S., Williams, G., and Hosie, G. (2008). Krill (*Euphausia superba*) abundance and Adélie penguin (*Pygoscelis adeliae*) breeding performance in the waters off the Béchervaise island colony, East Antarctica in 2 years with contrasting ecological conditions. *Deep Sea Res. Part II: Topical Stud. Oceanography* 55 (3-4), 540–557. doi: 10.1016/j.dsr2.2007.11.013

Nocera, A. C., Giménez, E. M., Diez, M. J., Retana, M. V., and Winkler, G. (2021). Krill diel vertical migration in southern Patagonia. *J. Plankton Res.* 43 (4), 610–623. doi: 10.1093/plankt/fbab047

Pauly, T., Nicol, S., Higginbottom, I., Hosie, G., and Kitchener, J. (2000). Distribution and abundance of Antarctic krill (*Euphausia superba*) off East Antarctica (80–150 e) during the austral summer of 1995/1996. *Deep Sea Res. Part II: Topical Stud. Oceanography* 47 (12-13), 2465–2488. doi: 10.1016/S0967-0645(00)00032-1

Phillips, L. R., Carroll, G., Jonsen, I., Harcourt, R., Brierley, A. S., Wilkins, A., et al. (2022). Variability in prey field structure drives inter-annual differences in prey encounter by a marine predator, the little penguin. *R. Soc. Open Sci.* 9 (9), 220028. doi: 10.1098/rsos.220028

Pütz, K., Rey, A. R., Huin, N., Schiavini, A., Pütz, A., and Lüthi, B. H. (2006). Diving characteristics of southern rockhopper penguins (*Eudyptes c. chrysocome*) in the southwest Atlantic. *Mar. Biol.* 149 (2), 125–137. doi: 10.1007/s00227-005-0179-y

Ratcliffe, N., and Trathan, P. (2012). A review of the diet and at-sea distribution of penguins breeding within the CAMLR convention area. *CCAMLR Sci.* 19, 75–114.

R Core Team (2018). "R: a language and environment for statistical computing," in *R foundation for statistical computing*(Vienna).

Reid, K., Sims, M., White, R. W., and Gillon, K. W. (2004). Spatial distribution of predator/prey interactions in the Scotia Sea: implications for measuring predator/fisheries overlap. *Deep Sea Res. Part II: Topical Stud. Oceanography* 51 (12-13), 1383–1396. doi: 10.1016/j.dsr2.2004.06.007

Reilly, S., Hedley, S., Borberg, J., Hewitt, R., Thiele, D., Watkins, J., et al. (2004). Biomass and energy transfer to baleen whales in the south Atlantic sector of the Southern Ocean. *Deep Sea Res. Part II: Topical Stud. Oceanography* 51 (12), 1397–1409. doi: 10.1016/j.dsr2.2004.06.008

Reiss, C. S., Cossio, A. M., Walsh, J., Cutter, G. R., and Watters, G. M. (2021). Glider-based estimates of meso-zooplankton biomass density: a fisheries case study on Antarctic krill (*Euphausia superba*) around the northern Antarctic peninsula. *Front. Mar. Sci.* 8, 256. doi: 10.3389/fmars.2021.604043

Riaz, J., Bestley, S., Wotherspoon, S., and Emmerson, L. (2021). Horizontal-vertical movement relationships: Adélie penguins forage continuously throughout provisioning trips. *Movement Ecol.* 9 (1), 43. doi: 10.1186/s40462-021-00280-8

Riaz, J., Bestley, S., Wotherspoon, S., Freyer, J., and Emmerson, L. (2020). From trips to bouts to dives: temporal patterns in the diving behaviour of chick-rearing Adélie penguins, East Antarctica. *Mar. Ecol. Prog. Ser.* 654, 177–194. doi: 10.3354/meps13519

Ribic, C. A., Chapman, E., Fraser, W. R., Lawson, G. L., and Wiebe, P. H. (2008). Top predators in relation to bathymetry, ice and krill during austral winter in Marguerite bay, Antarctica. *Deep Sea Res. Part II: Topical Stud. Oceanography* 55 (3-4), 485–499. doi: 10.1016/j.dsr2.2007.11.006

Ropert-Coudert, Y., Van de Putte, A. P., Reisinger, R. R., Bornemann, H., Charrassin, J.-B., Costa, D. P., et al. (2020). The retrospective analysis of Antarctic tracking data project. *Sci. Data* 7 (1), 1–11. doi: 10.1038/s41597-020-0406-x

Rose, G. A., and Leggett, W. C. (1990). The importance of scale to predator-prey spatial correlations: An example of Atlantic fishes. *Ecology* 71 (1), 33–43. doi: 10.2307/1940245

Santora, J. A., Dorman, J. G., and Sydeman, W. J. (2017). Modeling spatiotemporal dynamics of krill aggregations: size, intensity, persistence, and coherence with seabirds. *Ecography* 40 (11), 1300–1314. doi: 10.1111/ecog.02250

Santora, J. A., and Reiss, C. S. (2011). Geospatial variability of krill and top predators within an Antarctic submarine canyon system. *Mar. Biol.* 158 (11), 2527–2540. doi: 10.1007/s00227-011-1753-0

Santora, J. A., Reiss, C. S., Cossio, A. M., and Veit, R. R. (2009). Interannual spatial variability of krill (*Euphausia superba*) influences seabird foraging behavior near elephant island, Antarctica. *Fisheries Oceanography* 18 (1), 20–35. doi: 10.1111/j.1365-2419.2008.00490.x

Santora, J. A., Reiss, C. S., Loeb, V. J., and Veit, R. R. (2010). Spatial association between hotspots of baleen whales and demographic patterns of Antarctic krill *Euphausia superba* suggests size-dependent predation. *Mar. Ecol. Prog. Ser.* 405, 255–269. doi: 10.3354/meps08513

Silk, J. R., Thorpe, S. E., Fielding, S., Murphy, E. J., Trathan, P. N., Watkins, J. L., et al. (2016). Environmental correlates of Antarctic krill distribution in the Scotia Sea and southern drake passage. *ICES J. Mar. Sci.* 73 (9), 2288–2301. doi: 10.1093/icesjms/fsw097

Southwell, D., Emmerson, L., Forcada, J., and Southwell, C. (2015). A bioenergetics model for estimating prey consumption by an Adélie penguin population in East Antarctica. *Mar. Ecol. Prog. Ser.* 526, 183–197. doi: 10.3354/meps11182

Southwell, C., Emmerson, L., Takahashi, A., Barbraud, C., Delord, K., and Weimerskirch, H. (2017). Large-Scale population assessment informs conservation management for seabirds in Antarctica and the Southern Ocean: A case study of Adélie penguins. *Global Ecol. Conserv.* 9, 104–115. doi: 10.1016/j.gecco.2016.12.004

Sveegaard, S., Nabe-Nielsen, J., Stæhr, K.-J., Jensen, T. F., Mouritsen, K. N., and Teilmann, J. (2012). Spatial interactions between marine predators and their prey: herring abundance as a driver for the distributions of mackerel and harbour porpoise. *Mar. Ecol. Prog. Ser.* 468, 245–253. doi: 10.3354/meps09959

Tarling, G. A., and Fielding, S. (2016). "Swarming and behaviour in Antarctic krill," in *Biology and ecology of Antarctic krill* (Springer), 279–319. doi: 10.1007/978-3-319-29279-3_8

Tarling, G. A., Klevjer, T., Fielding, S., Watkins, J., Atkinson, A., Murphy, E., et al. (2009). Variability and predictability of Antarctic krill swarm structure. *Deep Sea Res. Part I: Oceanographic Res. Papers* 56 (11), 1994–2012. doi: 10.1016/j.dsr.2009.07.004

Tarling, G. A., and Thorpe, S. E. (2014). Instantaneous movement of krill swarms in the Antarctic circumpolar current. *Limnology Oceanography* 59 (3), 872–886. doi: 10.4319/lo.2014.59.3.0872

Tierney, M., Emmerson, L., and Hindell, M. (2009). Temporal variation in Adélie penguin diet at Béchervaise island, east Antarctica and its relationship to reproductive performance. *Mar. Biol.* 156 (8), 1633–1645. doi: 10.1007/s00227-009-1199-9

Trathan, P., Brierley, A., Brandon, M., Bone, D., Goss, C., Grant, S., et al. (2003). Oceanographic variability and changes in Antarctic krill (*Euphausia superba*) abundance at south Georgia. *Fisheries oceanography* 12 (6), 569–583. doi: 10.1046/j.1365-2419.2003.00268.x

Trathan, P. N., and Hill, S. L. (2016). "The importance of krill predation in the Southern Ocean," in *Biology and ecology of Antarctic krill* (Springer), 321–350. doi: 10.1007/978-3-319-29279-3_9

Trathan, P., Ratcliffe, N., and Masden, E. (2012). Ecological drivers of change at south Georgia: the krill surplus, or climate variability. *Ecography* 35 (11), 983–993. doi: 10.1111/j.1600-0587.2012.07330.x

Veit, R. R., Silverman, E. D., and Everson, I. (1993). Aggregation patterns of pelagic predators and their principal prey, Antarctic krill, near south Georgia. *J. Anim. Ecol.* 62 (3), 551–564. doi: 10.2307/5204

Warwick-Evans, V., Downie, R., Santos, M., and Trathan, P. N. (2019). Habitat preferences of Adélie *Pygoscelis adeliae* and chinstrap penguins *Pygoscelis antarctica* during pre-moult in the weddell Sea (Southern Ocean). *Polar Biol.* 42 (4), 703–714. doi: 10.1007/s00300-019-02465-9

Warwick-Evans, V., Fielding, S., Reiss, C., Watters, G., and Trathan, P. N. (2022). Estimating the average distribution of Antarctic krill *Euphausia superba* at the northern Antarctic peninsula during austral summer and winter. *Polar Biol.* 45 (5), 857–871. doi: 10.1007/s00300-022-03039-y

Watanabe, Y. Y., Ito, M., and Takahashi, A. (2014). Testing optimal foraging theory in a penguin–krill system. *Proc. R. Soc. B: Biol. Sci.* 281 (1779), 20132376. doi: 10.1098/rspb.2013.2376

Watkins, J. L., Buccholz, F., Priddle, J., Morris, D., and Ricketts, C. (1992). Variation in reproductive status of Antarctic krill swarms; evidence for a size-related sorting mechanism? *Mar. Ecol. Prog. Ser.* 82, 163–174. doi: 10.3354/meps082163

Watters, G. M., Hinke, J. T., and Reiss, C. S. (2020). Long-term observations from Antarctica demonstrate that mismatched scales of fisheries management and predator-prey interaction lead to erroneous conclusions about precaution. *Sci. Rep.* 10 (1), 1–9. doi: 10.1038/s41598-020-59223-9

Wei, T., and Simko, V. (2021). *R package 'corrplot': Visualization of a correlation matrix; version 0.92*. Available at: https://cran.r-project.org/web/packages/corrplot/index.html.

Yamamoto, T., Watanuki, Y., Hazen, E. L., Nishizawa, B., Sasaki, H., and Takahashi, A. (2015). Statistical integration of tracking and vessel survey data to incorporate life history differences in habitat models. *Ecol. Appl.* 25 (8), 2394–2406. doi: 10.1890/15-0142.1

Zimmer, I., Wilson, R. P., Beaulieu, M., Ropert-Coudert, Y., Kato, A., Ancel, A., et al. (2010). Dive efficiency versus depth in foraging emperor penguins. *Aquat. Biol.* 8 (3), 269–277. doi: 10.3354/ab00213

Zimmer, I., Wilson, R. P., Gilbert, C., Beaulieu, M., Ancel, A., and Plötz, J. (2008). Foraging movements of emperor penguins at pointe géologie, Antarctica. *Polar Biol.* 31 (2), 229–243. doi: 10.1007/s00300-007-0352-5

frontiers | Frontiers in Marine Science

TYPE Original Research
PUBLISHED 31 May 2023
DOI 10.3389/fmars.2023.1107567

Check for updates

OPEN ACCESS

EDITED BY
Kerrie M. Swadling,
University of Tasmania, Australia

REVIEWED BY
Robert McCauley,
Curtin University, Australia
Doug Kinzey,
National Oceanic and Atmospheric Administration, United States

*CORRESPONDENCE
Abigail J. R. Smith
Abigail.Smith@utas.edu.au

RECEIVED 25 November 2022
ACCEPTED 16 May 2023
PUBLISHED 31 May 2023

CITATION
Smith AJR, Wotherspoon SJ and Cox MJ (2023) Per-length biomass estimates of Antarctic krill (*Euphausia superba*). *Front. Mar. Sci.* 10:1107567. doi: 10.3389/fmars.2023.1107567

COPYRIGHT
© 2023 Smith, Wotherspoon and Cox. This is an open-access article distributed under the terms of the Creative Commons Attribution License (CC BY). The use, distribution or reproduction in other forums is permitted, provided the original author(s) and the copyright owner(s) are credited and that the original publication in this journal is cited, in accordance with accepted academic practice. No use, distribution or reproduction is permitted which does not comply with these terms.

Per-length biomass estimates of Antarctic krill (*Euphausia superba*)

Abigail J. R. Smith[1]*, Simon J. Wotherspoon[2] and Martin J. Cox[2,3]

[1]Australian Antarctic Program Partnership, Institute for Marine and Antarctic Studies, University of Tasmania, nipaluna/Hobart, TAS, Australia, [2]Southern Ocean Ecosystems Program, Australian Antarctic Division, Kingston, TAS, Australia, [3]Integrated Digital East Antarctica (IDEA), Australian Antarctic Division, Kingston, TAS, Australia

Total biomass and areal biomass density are often necessary to establish ecological relationships and enable informed management decisions, in particular setting fisheries catch limits. Further refining these estimates to sub-population biomass based on length informs ecological models of predator-prey dynamics, ecosystem energy transfer and biogeochemical cycles; however, measures of uncertainty in these per-length biomass estimates are needed. We present a statistical method to calculate the per-length biomass of Antarctic krill (*Euphausia superba*) from conversion factors using acoustic and net sample data. Variability in krill length-frequency, and wetmass introduced by net sampling is also explored through non-parametric bootstrapping. We applied this method on a 1 mm length window to active acoustic and net sample data collected during an Antarctic krill biomass survey in CCAMLR Division 58.4.2 (62 – 67°S; 55 – 80°E, with a survey area of 775,732 km^2) performed between February – March 2021. We found that 77% of the total estimated biomass was attributable to krill of length 14 – 49 mm. The largest biomass of krill in a single length bin was estimated as 340,000 t (95% CI: 148,000 - 408,000 t) and was found in the 49 mm length bin (i.e., 48.5 to 49.5 mm). This method will allow future surveys (with sufficient data) to estimate biomass of krill on a per-length basis along with associated uncertainty (confidence intervals) derived from net sampling and so may be used to provision size-based ecosystem models with krill biomass.

KEYWORDS

conversion factor, length-wetmass relationship, length-frequency, size distribution, net sampling

1 Introduction

Antarctic krill (*Euphausia superba*) are a keystone species in Southern Ocean ecosystems, preyed on by whales, seals, seabirds and fish. With a circumpolar biomass of more than 300 million tons (Atkinson et al., 2009), Antarctic krill have a strong influence

on biogeochemical cycles (Cavan et al., 2019, Ratnarajah, 2021, Smith et al., submitted) and contribute to the largest fishery in the Southern Ocean (Meyer et al., 2020). Environmental pressures as a result of climate change, including rising sea surface temperatures, sea ice melt and ocean acidification negatively impact Antarctic krill reproduction and recruitment (Moline et al., 2004, Veytia et al., 2021, Kawaguchi et al., 2011; Kawaguchi et al., 2013). This, in combination with an expanding fishery (CCAMLR, 2019), is expected to influence future Antarctic krill populations. Due to the significant role Antarctic krill (hereafter krill) play in Southern Ocean ecosystems, understanding the long-term trajectories for their populations and distributions is critical to sustainable management (Constable and de la Mare, 1996; Meyer et al., 2020).

Predators tend to be larger than their prey and the body size of an organism typically decreases with increasing abundance (Blanchard et al., 2017). Krill total length is proportional to the energy available to predators (Reid and Croxall, 2001) and the amount of biogenic and inorganic carbon retained or released by the animal (Wilson et al., 2009, Cavan et al., 2019, Clarke and Morris, 1983). Therefore, size-specific biomass may be used to inform trophodynamic and biogeochemical models. In fisheries, length and stock size is used to classify juvenile or spawning populations, estimate recruitment, and protect key reproductive areas (Larkin, 1978; Galaiduk et al., 2018). Furthermore, accurate estimates of juvenile krill abundance are required to map transport pathways from spawning grounds with oceanographic currents (Veytia et al., 2021; Bhattacharya, 1967). Measures of uncertainty in biomass estimates are needed to capture the sensitivity of models, particularly when considering impacts to ecosystems under changing climate conditions (Bryndum-Buchholz et al., 2019; Lotze et al., 2019).

Antarctic krill biomass is typically estimated from ship-based acoustic-trawl surveys (e.g., Krafft et al., 2021 and Bairstow et al., 2022, but see Cutter et al., 2022 for alternative sampling platforms). Currently, a single biomass estimate for the survey area is determined from the fisheries (active) acoustic and net sample data. The acoustic data is sampled along line transects and is used to sample krill in space, whereas the net data is used to sample krill demographics, length distribution and the length to wetmass relationship. The acoustic data do not sample krill density directly, so the net data are used to scale the acoustic data using a single survey-specific conversion factor.

The conversion factor C transforms a linear form of reflected acoustic energy (Nautical Area Scattering Coefficient, (s_A [m^2 nmi^{-2}]; Maclennan et al., 2002) arising from krill into an areal biomass density ρ_A [g m^{-2}]. In addition to the krill length frequency distribution and krill length to wetmass relationship, a length dependent target strength (spherical scattering cross-section, σ_{sp}) is also required to calculate the conversion factor (Calise and Skaret, 2011; Han et al., 2020; Bairstow et al., 2021). For a single survey, it is possible to use s_A data to map the distribution of relative krill densities, but for repeat or interannual surveys the krill demographic parameters will change making the use of s_A tenuous. This is because the same value of s_A may be generated by different areal densities of krill with different length-frequency distributions (Figure 1).

There are potential sources of uncertainty in the conversion factor. Krill swarms have demonstrated size sorting mechanisms in

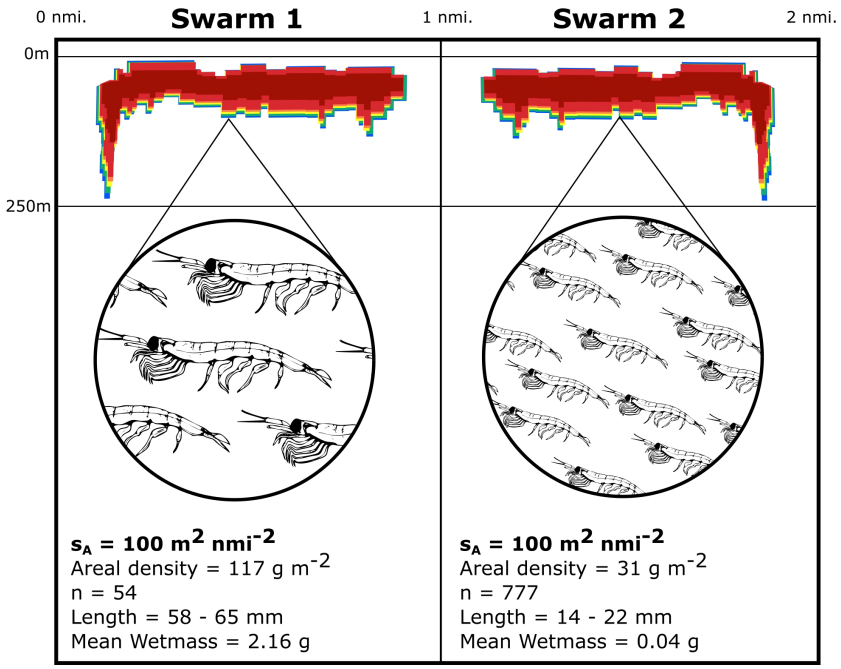


FIGURE 1
Two near-identical swarms may have a Nautical Area Scattering Coefficient (s_A) value of 100 m^2 nmi^{-2}, yet comprise krill of different mean areal densities, length frequency distributions and wetmass demonstrating the importance of net samples to obtain information of krill demographics.

the field, meaning net sampling strategy may influence the length frequency distribution of krill measured from net samples (Watkins et al., 1992; Watkins, 1986) particularly when insufficient trawls are performed. Additionally, while total length measurements may be straightforward at sea, measuring krill wetmass on a moving vessel is challenging. As a result, many biomass surveys use established length-wetmass relationships, such as those described by Hewitt et al. (2004) and Morris et al. (1988), see for example Krafft et al. (2021). Such relationships assume a standard growth rate for all krill, i.e., a single regression line is fitted, and are often based on data from krill collected in West Antarctic (e.g. Morris et al., 1998; Hewitt et al., 2004), therefore may not be representative of krill collected in other locations. Variability in both krill length to wetmass relationships and length frequency distributions should be accounted for in calculation of conversion factors and associated confidence intervals.

The objective of this research is to develop methods enabling estimation of per-length krill biomass and variability attributed to net sampling. We apply the method to data from a recent (2021) acoustic-trawl survey of krill conducted in the East Antarctic in CCAMLR Division 58.4.2 (775,732 km^2, Cox et al., 2022). Our method estimates biomass of krill in 1 mm length bins and associated measures of reliability using conversion factors with data derived from net samples.

2 Methods

2.1 Calculating the conversion factor

The conversion factor for a traditional krill biomass survey is calculated using:

$$C = \frac{\sum f_i \; W(L_i)}{\sum f_i \sigma_{sp}(L_i)} \times \frac{1}{1852^{2}} \tag{1}$$

where L_i denotes the mid-length of the ith length bin, f_i is the frequency of occurrence of krill in the ith length bin, $W(L_i)$ is the estimated wetmass of an individual at length i and σ_{sp} (L_i) is the spherical cross-section scattering coefficient of krill at L_i. The second term is applied to convert areal biomass density from nautical miles^{-2} to m^{-2}.

Krill wetmass (g) was modelled as a power law in a standard measure of body length (L, mm)

$$W \; = \; aL^{b} \tag{2}$$

where a and b are coefficients to be estimated. This relation was fitted to the net sample data by (nonlinear) generalized least squares (Pinheiro and Bates, 2023), assuming the error variance is proportional to the power of the predicted weight to allow for any heteroscedasticity in the data. A self-starting routine was implemented to establish suitable starting parameters for the power law and avoid convergence failures (Pinheiro and Bates, 2000).

The biomass density, B, for a survey is calculated by:

$$B = \; C \; \times \; \overline{s_A} \tag{3}$$

where $\overline{s_A}$ is the mean s_A for the survey area.

The per-length conversion factor for the jth length interval were calculated by the ratio:

$$C_j = \frac{f_j \; W(L_j)}{\sum_{i=1}^{n} f_i \sigma_{sp}(L_i)} \times \frac{1}{1852^{2}} \tag{4}$$

where n is the number of length bins. And C_j can be written as:

$$C_j = \frac{f_j W(L_j)}{K} \tag{5}$$

where K is the normalizing factor:

$$K \; = \; 1852^{2} \times \sum_{i=1}^{n} f_i \sigma_{sp}(L_i) \tag{6}$$

Per-length conversion factors (C_j) were calculated and applied to $\overline{s_A}$ to produce per-length biomass (B_i),

$$B_i = C_j \times \overline{s_A} \tag{7}$$

Where the sum of C_j is equal to C for the total survey and the sum of B_i equals the survey biomass.

2.2 Estimating uncertainty

The uncertainty in both the length specific and total conversion factors is estimated by non-parametric bootstrap (Tibshirani and Efron, 1993) over net hauls (see Supplementary Materials). Bootstrap samples are drawn by resampling (n = 2000) with replacement hauls from the net sample data. For each bootstrap sample, the length frequency distribution and length-wetmass relationship are re-estimated and used to determine new length specific and total conversion factors. The percentiles of the conversion factors derived from the bootstrap samples provide approximate confidence intervals for the conversion factors derived from the actual sample.

2.3 Data description

Acoustic and net sample data used in this study are described in Cox et al. (2022). Briefly acoustic data was collected along six latitudinal transects (62 - 68°S, 55 - 80°E), using a cold-water calibrated EK80 scientific echosounder (Simrad, Horten, Norway). All acoustic data processing was performed on the 120 kHz frequency using the 'swarms-based' method (CCAMLR, 2017; Krafft et al., 2021), however this method of calculating per-length biomass could also be applied to other target classification methods such as 'dB-differencing'.

Net samples were taken using a rectangular mid-water trawl (RMT8 + 1, mesh size 4.5 mm, Roe and Shale, 1979). Both routine and target trawls were performed throughout the survey. Routine trawls were performed at regular intervals along transects in< 200 m depth, with the net open for an average of 20 minutes (n = 18). Target trawls were performed spontaneously in response to detection of an acoustic target (n = 41). Up to 250 krill were

measured for total length (using S1 method, Mauchline et al., 1980) from each station. From 16 stations, a further 10 - 60 krill were subsampled for wetmass measurements using onboard motion-compensated balances (Ohaus AX224, Parsippany, USA). For a complete description of acoustic methods and total survey biomass determination see Cox et al. (2022).

All data were accessed at: https://data.aad.gov.au/metadata/AAS_4512_TEMPO_bioacoustics.

Spherical cross-section scattering coefficients (target strengths, TS) were taken from the 120 kHz target strength values ($TS = 10log_{10}(4\pi\sigma_{sp})$) calculated by the 2019 CCAMLR Area 48 Survey (Krafft et al., 2021). The effect of target strength variability on biomass estimates has been explored by Bairstow et al. (2022), and will therefore not be considered at length in this study.

3 Results

3.1 Krill length frequency distribution

Krill total length ranged from 14.4 - 60.0 mm. Length frequency distributions from all trawls had a platykurtic distribution (Figure 2) and showed no apparent trend between stations (Bairstow et al., 2022; Cox et al., 2022). The mean length of krill caught by target trawls was 40.6 ± 7.1 mm compared to a marginally greater mean of 41.4 ± 7.8 mm caught by routine trawls. An asymptotic two-sample Kolmogorov-Smirnov test (KS-test) revealed significant variability in the length frequency distributions achieved by the two net haul methods (D = 0.087, p-value = 4.01 x 10^{-6}), but it is unclear if this distribution difference is due to inherent sampling variability, rather than the trawling strategy used, i.e., routine or target trawling. Indeed, when the routine trawls were randomly assigned into two groups by trawl number (n = 7 trawls in each group), the KS-test result was (D = 0.1714, p-value = 1 x 10^{-7}) and for target trawls (n = 10 in each group; D = 0.2505, p-value< 2.2 x 10^{-16}), suggesting that sampling variability is of a similar magnitude to net sampling method.

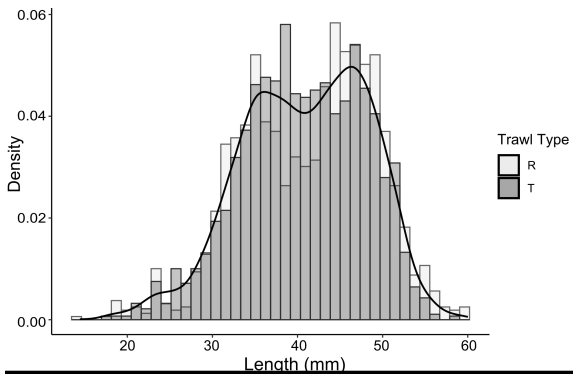


FIGURE 2
Histogram of observed krill length frequencies at 1 mm intervals from routine trawls (light grey) and target trawls (dark grey) with frequency polygon for the distribution of all net samples based on densities overlaid (solid black line).

3.2 Krill length-wetmass relationship

Krill length to wetmass data followed a power law (Figure 3) and were modeled as such (Equ. 2) producing a mean coefficient (a, $\times 10^{-6}$) of 4.4 (CV = 14.5%) and exponent (b) of 3.16 (CV = 1.26%). Increasing variability with length could be observed in the length-wetmass data, therefore a variance proportional to a 0.91 power of weight was used to normalize the data. Use of generalized nonlinear least squares to fit the length-wetmass relationship allowed for this heteroscedasticity to be captured in the model, where a nonlinear least squares fit would not (Supplementary Materials, Figure S1). Overlap in length and wetmass was observed between, male, female, and juvenile krill (Figure 3 box plots). Sex and stage may influence the variance observed in length to wetmass relationships. However, as the overlap makes it difficult to differentiate subpopulations, the effect of sex and stage on the length to wetmass relationship is not considered further.

3.3 Per-length conversion factors, biomass and uncertainty

With a survey-specific length-wetmass relationship (calculated here using generalized least squares) and length-target strength relationship provided by Krafft et al. (2021), conversion factors and biomass could be calculated for each 1 mm integer length of krill weighted by the frequency of occurrence at each length (from 10 – 65 mm, Figure 4).

Per-length conversion factors represent a fraction of the total survey conversion factor, ranging from 2.81 × 10^{-6} to 0.025. When applied to $\overline{s_A}$ the largest B_i was observed for 49 mm krill at 346,847 t (95%: 217,638 – 490,742 t). The minimum B_i was 38.8 t (95%: 0 – 145.6 t) for 14 mm krill. Krill with lengths 14 – 49 mm contributed 77.1% of total biomass (Supplementary Figure S2). Length classes where conversion factors are equal to zero represent unobserved

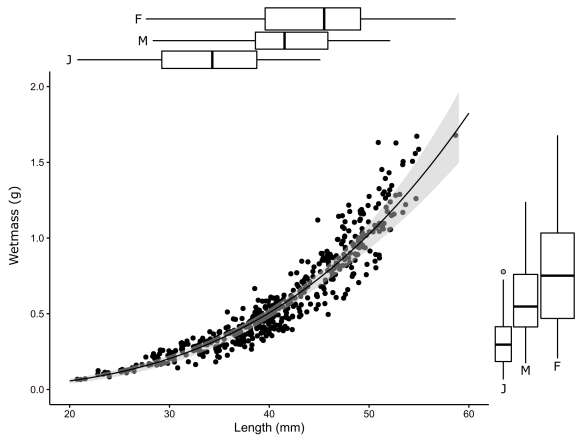


FIGURE 3
Length-wetmass relationship with 95% confidence intervals from bootstrapping (Section 2.2) overlayed in grey. Marginal boxplot quantiles for krill length (top) and weight (right) by sex are displayed for juveniles (J), adult and subadult males (M) and females (F).

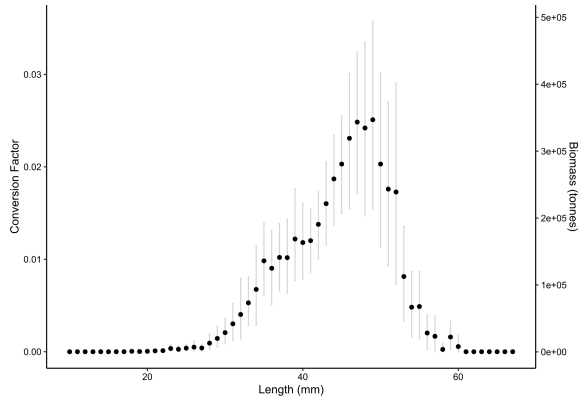


FIGURE 4
Mean per-length conversion factors (left axis) and biomass (right axis) with 95% confidence intervals (grey lines) determined from non-parametric bootstrap simulations.

lengths from this dataset; here one may elect Bayesian bootstrapping approaches to weight the missing observations (see Section 4.1 for further detail).

By summing per-length conversion factors, the total survey conversion factor was 0.346 with 95% confidence intervals of 0.301 and 0.389 (Figure 5). This gave a total survey biomass estimate of 4.78 million t (95%: 4.12 – 5.31 million t). It should be noted that biomass variance presented here is derived from the krill length-frequency distribution and length-wetmass relationships. Whilst bootstrapping over trawl stations incorporates some element of spatial variability, the spatial coverage of net samples is low compared to the active acoustic transect effort; therefore, biomass confidence intervals presented here do not account for variability in s_A from transects across the survey area (Jolly and Hampton, 1990).

Discrepancies in the length-frequency distribution collected by differing trawl methods resulted in total survey biomass estimates of 4.68 million t (95%: 3.90 – 5.45 million t) from target trawls and 4.78 million t (95%: 3.95 – 5.53 million t) from routine trawls. Although length-frequency distributions varied, the final total survey biomass was not significantly different between the two net sampling methods (Kolmogorov-Smirnov test, D = 0.103, p-value = 0.883).

Using all net samples, the total survey conversion factors and biomass estimates calculated here were marginally smaller than those given by Cox et al. (2022) using traditional methods (Figure 5, C = 0.348, B = 4.8 million t). Although similar, differences between the two methods of estimating biomass are likely the result of applying generalized least squares fit to the length-wetmass relationship.

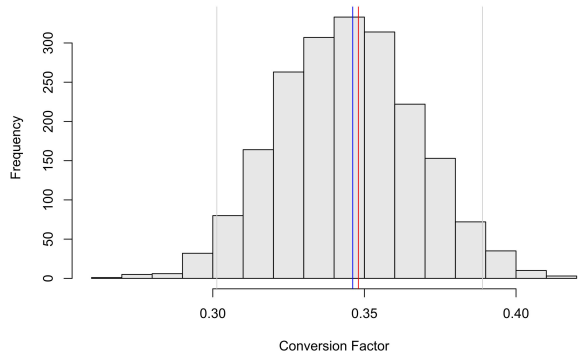


FIGURE 5
Histogram of bootstrapped conversion factors (n = 2000 replicates) for 1 mm krill length bins. Each realization was simply the sum of the length-specific conversion factors with the point sum of conversion factors (blue line), 95% confidence intervals (grey lines) and conversion factor for Cox et al. (2022, red line) displayed.

4 Discussion

Here we have successfully calculated per-length biomass estimates for Antarctic krill and their associated uncertainty due to net sampling. These methods are useful for models which require empirical data to incorporate krill size as a parameter of ecosystem processes. The uncertainty estimates enable researchers to assess the utility of the per-length biomass estimates for their particular purpose. Whilst we have provided biomass in 1 mm length bins, the bin width can be tailored to suit the question or data in hand. For example, length bins can be split into biologically relevant ranges to suit the study species, e.g., age class 0 (furcilia and juveniles): 8 – 24 mm (Siegel, 1987; Schaafsma et al., 2016; Schaafsma et al., 2022). Further, should a paucity of data lead to biomass confidence intervals too wide for the purpose in hand, larger length bins may reduce the confidence interval width.

4.1 Modeling length to wetmass relationships

Equality of variance is a key assumption of nonlinear least squares. Increasing variability if wetmass with length indicates standard nonlinear least squares may not be entirely appropriate for this data. Such variability at larger lengths may be due to spatial and temporal conditions or physiological behavior (Nahdi et al., 2016). The generalized least squares fit accounted for this heteroscedasticity and captured the nonlinear relationship between length and wetmass measurements. This explains the small deviations between the fit reported here and that of Cox et al. (2022).

Fitting linear mixed effects models to the log transformed data offers an alternative technique to determining a survey-specific power law length-wetmass relationships on a broad spatial scale. Trawl stations incorporated as a random effect would represent the trawl variability and spatial heterogeneity in length-wetmass relationships across the survey area. Noting also that linear mixed effects models will require manual correction of biases associated with log transforming data (Brodziak, 2012).

Nonparametric bootstraps are less robust when data contain a small number of strongly influential observations, which may be under- or over-represented in individual bootstrap samples (Efron, 2012). For net sample data containing trawls with highly variable total krill counts, Bayesian bootstrap procedures (Rubin, 1981) may be considered. The Bayesian bootstrap draws bootstrap samples by

up-weighting or down-weighting observations, but no observation is ever entirely excluded from the sample and is therefore more robust to strongly influential observations.

4.2 Sampling variability on conversion factors

Because conversion factors are weighted by the length-frequency distribution, net sampling techniques which bias krill size will influence subsequent biomass calculations (Krag et al., 2014). Heterogeneity and sorting mechanisms in krill length, sex and stage have been observed amongst swarms, wherein swarms comprise a narrow array of total lengths (Watkins et al., 1992; Watkins, 1986; Watkins et al., 1990; Ricketts et al., 1992). While systematic sampling of pre-defined routine trawl stations reduces bias associated with swarm-sorting behaviors, net samples for biomass estimates are often collected from target trawls, especially when considering non-scientific surveys performed by fisheries vessels. Responsive target trawls sample densely aggregating swarms, whereas routine trawls may sample dispersed individuals or scattering layers. Such variability is akin to target classification methods using image cluster analysis such as the SHAPES algorithm (Coetzee, 2000) which identify schooling or swarming targets, compared to more generalized 'dB-differencing' techniques (Korneliussen, 2018). Although the two net sampling strategies produced variable length frequency distributions, differences were not apparent in conversion factors and mean biomass estimates from routine and target trawling in this study. However, the variability of krill biomass introduced by differing trawl methods and target classification techniques should be assessed across a wider collection of surveys in the future.

Measurements from approximately 100 krill across 3 – 80 sampling events (net hauls) have been suggested to represent the local population, with emphasis on maintaining a synoptic acoustic survey (Watkins et al., 1990). Additionally, seasonal variability may influence length-wetmass relationships. For example, gravid females in summer have been observed as smaller in total length than spent females (Watkins et al., 1992), which will bias a power law length-wetmass relationship that does not explicitly account for gravid krill. The application of this method is therefore dependent on collection of spatially and seasonally representative length-frequency datasets.

Uncertainty in per-length biomass estimates here are derived from variability in the length-wetmass relationship and length frequency distribution of krill collected through net sampling, yet other sources of variability may also influence biomass estimates. Krill total length is a key parameter in krill target strength models (Greene et al., 1991), however acoustic material properties, shape and orientation within the acoustic beam influence these estimates (Demer and Conti, 2005, Lawson et al., 2006; Bairstow et al., 2021). Conversion factors have demonstrated sensitivity to variability in target strength, specifically from orientation (Bairstow et al., 2021; Bairstow et al., 2022). Furthermore, net sampling has reduced spatial coverage compared to acoustic data. Geostatistical conditional simulations, whereby s_A mean and standard deviation is determined through kriging, offer an opportunity to incorporate the spatial distribution of krill at the scale of an echo integration interval (Gastauer et al., 2017; Bairstow et al., 2022). Combining both the spatial variability of krill and variability in conversion factors (through target strength and net sampling) will further refine measures of uncertainty in per-length biomass estimates.

4.3 Applications and limitations

To our knowledge this is the first time krill biomass has been presented as estimates on a per-length class basis with associated estimates of uncertainty. Estimating biomass by length represents a valuable opportunity to model size-specific processes and how these relationships are expected to change under future environmental pressures. Importantly, this statistical approach provides a means of constraining size spectra model outputs by incorporating uncertainty from net sampling into biomass estimates. At the spatial scale of the krill biomass surveys this method could refine ecosystem model outputs to the same scale e.g., 100,000 km^2 - >1 million km^2 (Meyer et al., 2020; Krafft et al., 2021; Cox et al., 2022).

Biomass by size also allows valuable predictions of biogeochemical mechanisms such as carbon export and micronutrient recycling through krill life cycles and movement due to lateral advection (Veytia et al., 2021) and vertical migration (Schmidt et al., 2011). For example, the volume of nutrient-rich sinking fecal pellets (Pauli et al., 2021, Smith et al., submitted) and size of exoskeletal moults (Cavan et al., 2019) is dependent on krill size, therefore driving the concentration of nutrients and carbon released into seawater. The approaches used in this study, may provide population-level data towards models which explore the influence of krill on their environment.

The prevalence of small krill lengths may indicate the presence of juvenile krill (Fielding et al., 2014); this data is often used to infer krill recruitment success, fisheries stock dynamics and to identify key reproductive grounds (Kinzey et al., 2013, De la Mare, 1994; Hill et al., 2016). Although, caution should be exercised when differentiating sex and stage using size (as demonstrated by overlap in Figure 2), as metabolic processes such as regression or starvation may lead adults to shrink (Tarling et al., 2016).

Future surveys wishing to apply this technique should ensure their data is sufficient to represent length-frequency distributions across the entire survey area and minimize bias introduced by spatial variability and swarm size-sorting. Wetmass may be estimated from length data following relationships described by Morris et al. (1998) or Hewitt et al. (2004). However, where possible, studies should strive to obtain *in situ* measurements of wetmass and derive their own survey-specific relationships. Under these conditions, per-length biomass estimates, and associated reliability may be determined for past and future acoustic surveys.

5 Conclusion

This research presents a method to calculate conversion factors (and therefore biomass) for krill on a per-length basis with 95%

confidence based on non-parametric bootstrapping and predictions of wetmass from net samples. The technique uses nonlinear generalized least squares to fit a length-wetmass relationship, from which a conversion factor may be estimated for each length. The methods presented here may be used on existing or future acoustic surveys with net data to quantify the reliability of sub-populations biomass estimates, providing empirical data to ecosystem/size spectrum models and helping inform management of the krill fishery.

Data availability statement

Publicly available datasets were analyzed in this study. This data can be found here: https://data.aad.gov.au/metadata/AAS_4512_TEMPO_bioacoustics.

Author contributions

AS, SW, and MC contributed to the conception and design of the study. SW performed statistical analysis. AS drafted the original manuscript. All authors contributed to the article and approved the submitted version.

Funding

Australian Antarctic Program Partnership (AAPP) ASCI000002, The Pew Charitable Trust (ID 00034287), Antarctic Science Foundation (ASF) T1F:115595.

Acknowledgments

We are grateful to the captain and crew of the RV Investigator and the Marine National Facility for making this research possible. We thank TEMPO voyage Chief Scientists So Kawaguchi and Rob King, and scientists Jess Melvin, Maddie Brasier, Olivia Johnson, Christine Weldrick, Alicia Burns, Dale Maschette and Gavin Macaulay for collecting this data.

This project received grant funding from the Australian Government as part of the Antarctic Science Collaboration Initiative program.

Conflict of interest

The authors declare that the research was conducted in the absence of any commercial or financial relationships that could be construed as a potential conflict of interest.

Publisher's note

All claims expressed in this article are solely those of the authors and do not necessarily represent those of their affiliated organizations, or those of the publisher, the editors and the reviewers. Any product that may be evaluated in this article, or claim that may be made by its manufacturer, is not guaranteed or endorsed by the publisher.

Supplementary material

The Supplementary Material for this article can be found online at: https://www.frontiersin.org/articles/10.3389/fmars.2023.1107567/full#supplementary-material

References

Atkinson, A., Siegel, V., Pakhomov, E. A., Jessopp, M. J., and Loeb, V. (2009). A re-appraisal of the total biomass and annual production of Antarctic krill. *Deep Sea Res. Part I: Oceanographic Res. Papers* 56, 727–740. doi: 10.1016/j.dsr.2008.12.007

Bairstow, F., Gastauer, S., Finley, L., Edwards, T., Brown, C. T. A., Kawaguchi, S., et al. (2021). Improving the accuracy of krill target strength using a shape catalog. *Front. Mar. Sci.* 290. doi: 10.3389/fmars.2021.658384

Bairstow, F., Wotherspoon, S., Brown, C. T. A., Kawaguchi, S., Edwards, T., and Cox, M. J. (2022). Krill biomass estimation: sampling and measurement variability. *Front. Mar. Sci.* 9. doi: 10.3389/fmars.2022.903035

Bhattacharya, C. G. (1967). A simple method of resolution of a distribution into Gaussian components. *Biometrics* 23, 115–135. doi: 10.2307/2528285

Blanchard, J. L., Heneghan, R. F., Everett, J. D., Trebilco, R., and Richardson, A. J. (2017). From bacteria to whales: using functional size spectra to model marine ecosystems. *Trends Ecol. Evol.* 32, 174–186. doi: 10.1016/j.tree.2016.12.003

Brodziak, J. K. T. (2012). Fitting length-weight relationships with linear regression using the log-transformed allometric model with bias-correction. *Pacific Islands Fish. Sci.* 12-03, 1–4. Available at: https://repository.library.noaa.gov/view/noaa/4222

Bryndum-Buchholz, A., Tittensor, D. P., Blanchard, J. L., Cheung, W. W. L., Coll, M., Galbraith, E. D., et al. (2019). Twenty-first-century climate change impacts on marine animal biomass and ecosystem structure across ocean basins. *Global Change Biol.* 25, 459–472. doi: 10.1111/gcb.14512

Calise, L., and Skaret, G. (2011). Sensitivity investigation of the SDWBA Antarctic krill target strength model to fatness, material contrasts and orientation. *CCAMLR Sci.* 18, 97–122.

Cavan, E. L., Belcher, A., Atkinson, A., Hill, S. L., Kawaguchi, S., McCormack, S., et al. (2019). The importance of antarctic krill in biogeochemical cycles. *Nat. Commun.* 10, 4742. doi: 10.1038/s41467-019-12668-7

CCAMLR (2017). *Report of the thirty-sixth meeting of the scientific committee (SC-CAMLR-XXXVI). report no.: SC-CAMLR-XXXVI/06* (Hobart, Australia: CCAMLR). Available at: https://www.ccamlr.org/en/sc-camlrxxxvi.

CCAMLR (2019). *Report of the thirty-eighth meeting of the scientific committee (SC-CAMLR-38)* (Hobart, Australia: CCAMLR).

Clarke, A., and Morris, D. J. (1983). Towards an energy budget for krill: The physiology and biochemistry of euphausia superba dana. *Polar Biol.* 2, 69–86. doi: 10.1007/BF00303172

Coetzee, J. (2000). Use of a shoal analysis and patch estimation system (SHAPES) to characterise sardine schools. *Aquat. Living Resour.* 13, 1–10. doi: 10.1016/S0990-7440(00)00139-X

Constable, A., and de la Mare, W. (1996). A generalised model for evaluating yield and the long-term status of fish stocks under conditions of uncertainty. *CCAMLR Sci.* 3, 31–54.

Cox, M. J., Macaulay, G., Brasier, M. J., Burns, A., Johnson, O. J., King, R., et al. (2022). Two scales of distribution and biomass of Antarctic krill (*Euphausia superba*) in the eastern sector of the CCAMLR division 58.4.2 (55°E to 80°E). *PloS One* 17, e0271078. doi: 10.1371/journal.pone.0271078

Cutter, G. R., Reiss, C. S., Nylund, S., and Watters, G. M. (2022). Antarctic Krill biomass and flux measured using wideband echosounders and acoustic Doppler current profilers on submerged moorings. *Front. Mar. Sci.* 9. doi: 10.3389/fmars.2022.784469

Demer, D. A., and Conti, S. G. (2005). New target-strength model indicates more krill in the southern ocean. *ICES J. Mar. Sci.* 62, 25–32. doi: 10.1016/j.icesjms.2004.07.027

De la Mare, W. (1994). Estimating krill recruitment and its variability. *CCAMLR Sci.* 1, 55–69.

Efron, B. (2012). Bayesian Inference and the parametric bootstrap. *Ann. Appl. Stat* 6, 1971. doi: 10.1214/12-AOAS571

Fielding, S., Watkins, J. L., Trathan, P. N., Enderlein, P., Waluda, C. M., Stowasser, G., et al. (2014). Interannual variability in antarctic krill (Euphausia superba) density at south georgia, southern ocean: 1997–2013. *ICES J. Mar. Sci.* 71, 2578–2588. doi: 10.1093/icesjms/fsu104

Galaiduk, R., Radford, B. T., and Harvey, E. S. (2018). Utilizing individual fish biomass and relative abundance models to map environmental niche associations of adult and juvenile targeted fishes. *Sci. Rep.* 8, 9457. doi: 10.1038/s41598-018-27774-7

Gastauer, S., Scoulding, B., and Parsons, M. (2017). Towards acoustic monitoring of a mixed demersal fishery based on commercial data: the case of the northern demersal scalefish fishery (Western Australia). *Fisheries Res.* 195, 91–104. doi: 10.1016/j.fishres.2017.07.008

Greene, C. H., Stanton, T. K., Wiebe, P. H., and McClatchie, S. A. M. (1991). Acoustic estimates of Antarctic krill. *Nature* 349, 110–110. doi: 10.1038/349110a0

Han, I., Oh, W., La, H. S., Choi, S.-G., Kang, S., Yoon, E., et al. (2020). Verification of the backscattering strength based on the swimming behavior of Antarctic krill. *Ocean Sci. J.* 55, 391–403. doi: 10.1007/s12601-020-0031-9

Hewitt, R. P., Watkins, J., Naganobu, M., Sushin, V., Brierley, A. S., Demer, D., et al. (2004). Biomass of Antarctic krill in the Scotia Sea in January/February 2000 and its use in revising an estimate of precautionary yield. *Deep Sea Res. Part II: Topical Stud. Oceanogr.* 51, 1215–1236. doi: 10.1016/S0967-0645(04)00076-1

Hill, S. L., Atkinson, A., Darby, C., Fielding, S., Krafft, B. A., Godø, O. R., et al. (2016). Is current management of the Antarctic krill fishery in the Atlantic sector of the southern ocean precautionary? *CCAMLR Sci.* 23, 31–51.

Jolly, G. M., and Hampton, I. (1990). A stratified random transect design for acoustic surveys of fish stocks. *Can. J. Fisheries Aquat. Sci.* 47, 1282–1291. doi: 10.1139/f90-147

Kawaguchi, S., Ishida, A., King, R., Raymond, B., Waller, N., Constable, A., et al. (2013). Risk maps for Antarctic krill under projected southern ocean acidification. *Nat. Climate Change* 3, 843–847. doi: 10.1038/nclimate1937

Kawaguchi, S., Kurihara, H., King, R., Hale, L., Berli, T., Robinson, J. P., et al. (2011). Will krill fare well under southern ocean acidification? *Biol. Lett.* 7, 288–291. doi: 10.1098/rsbl.2010.0777

Kinzey, D., and Watters, G. (2013). Effects of recruitment variability and natural mortality on generalised yield model projections and the CCAMLR decision rules for antarctic krill. *CCAMLR Sci.* 20, 81–96.

Krafft, B. A., Macaulay, G. J., Skaret, G., Knutsen, T., Bergstad, O. A., Lowther, A., et al. (2021). Standing stock of Antarctic krill (*Euphausia superba* Dana 1850) (Euphausiacea) in the southwest Atlantic sector of the southern ocean 2018–19. *J. Crustacean Biol.* 41, ruab046. doi: 10.1093/jcbiol/ruab071

Krag, L. A., Herrmann, B., Iversen, S. A., Engås, A., Nordrum, S., and Krafft, B. A. (2014). Size selection of Antarctic krill (*Euphausia superba*) in trawls. *PloS One* 9, e102168. doi: 10.1371/journal.pone.0102168

Korneliussen, R. J. (2018). "Acoustic target classification," in *ICES cooperative research report no. 344*, vol. 104. doi: 10.17895/ices.pub.4567

Larkin, P. A. (1978). Fisheries management - an essay for ecologists. *Annu. Rev. Ecol. systematics* 9, 57–73. doi: 10.1146/annurev.es.09.110178.000421

Lawson, G. L., Wiebe, P. H., Ashjian, C. J., Chu, D., and Stanton, T. K. (2006). Improved parametrization of Antarctic krill target strength models. *J. Acoustical Soc. America* 119, 232–242. doi: 10.1121/1.2141229

Lotze, H. K., Tittensor, D. P., Bryndum-Buchholz, A., Eddy, T. D., Cheung, W. W. L., Galbraith, E. D., et al. (2019). Global ensemble projections reveal trophic amplification of ocean biomass declines with climate change. *Proc. Natl. Acad. Sci.* 116, 12907–12912. doi: 10.1073/pnas.1900194116

Maclennan, D. N., Fernandes, P. G., and Dalen, J. (2002). A consistent approach to definitions and symbols in fisheries acoustics. *ICES J. Mar. Sci.* 59, 365–369. doi: 10.1006/jmsc.2001.1158

Mauchline, J. (1980). *Measurements of body length of euphausia superba dana. BIOMASS handbook no. 6.*

Meyer, B., Atkinson, A., Bernard, K. S., Brierley, A. S., Driscoll, R., Hill, S. L., et al. (2020). Successful ecosystem-based management of Antarctic krill should address uncertainties in krill recruitment, behaviour and ecological adaptation. *Commun. Earth Environ.* 1, 28. doi: 10.1038/s43247-020-00026-1

Moline, M. A., Claustre, H., Frazer, T. K., Schofield, O., and Vernet, M. (2004). Alteration of the food web along the Antarctic peninsula in response to a regional warming trend. *Global Change Biol.* 10, 1973–1980. doi: 10.1111/j.1365-2486.2004.00825.x

Morris, D., Watkins, J. L., Ricketts, C., Buchholz, F., and Priddle, J. (1988). An assessment of the merits of length and weight measurements of antarctic krill euphausia superba. *Br. Antarctic Survey Bull.*, 27–50.

Nahdi, A. A. L., Garcia de Leaniz, C., and King, A. J. (2016). Spatio-temporal variation in length-weight relationships and condition of the ribbonfish *Trichiurus lepturus* (Linnaeus 1758): implications for fisheries management. *PloS One* 11, e0161989. doi: 10.1371/journal.pone.0161989

Pauli, N.-C., Flintrop, C. M., Konrad, C., Pakhomov, E. A., Swoboda, S., Koch, F., et al. (2021). Krill and salp fecal pellets contribute equally to the carbon flux at the Antarctic peninsula. *Nat. Commun.* 12, 7168. doi: 10.1038/s41467-021-27436-9

Pinheiro, J., and Bates, D. (2000). *Mixed-Effects Models in S and S-PLUS* (New York: Springer). doi: 10.1007/b98882

Pinheiro, J., and Bates, D. (2023). *Nlme: linear and nonlinear mixed effects models*. R package version 3.1-162, https://CRAN.R-project.org/package=nlme

Ratnarajah, L. (2021). Regenerated iron: how important are different zooplankton groups to oceanic productivity? *Curr. Biol.* 31, R848–R850. doi: 10.1016/j.cub.2021.05.016

Reid, K., and Croxall, J. P. (2001). Environmental response of upper trophic-level predators reveals a system change in an Antarctic marine ecosystem. *Proc. R. Soc. London. Ser. B: Biol. Sci.* 268, 377–384. doi: 10.1098/rspb.2000.1371

Ricketts, C., Watkins, J. L., Priddle, J., Morris, D. J., and Buchholz, F. (1992). An assessment of the biological and acoustic characteristics of swarms of Antarctic krill. *Deep Sea Res. Part A. Oceanographic Res. Papers* 39, 359–371. doi: 10.1016/0198-0149(92)90113-8

Roe, H. S. J., and Shale, D. M. (1979). A new multiple rectangular midwater trawl (RMT 1 + 8M) and some modifications to the institute of oceanographic sciences' RMT 1 + 8. *Mar. Biol.* 50, 283–288. doi: 10.1007/BF00394210

Rubin, D. B. (1981). The bayesian bootstrap. *Ann. Stat* 9 (1), 130–134. doi: 10.1214/aos/1176345338

Schaafsma, F. L., David, C. L., Kohlbach, D., Ehrlich, J., Castellani, G., Lange, B. A., et al. (2022). Allometric relationships of ecologically important Antarctic and Arctic zooplankton and fish species. *Polar Biol.* 45, 203–224. doi: 10.1007/s00300-021-02984-4

Schaafsma, F. L., David, C., Pakhomov, E. A., Hunt, B. P. V., Lange, B. A., Flores, H., et al. (2016). Size and stage composition of age class 0 Antarctic krill (*Euphausia superba*) in the ice–water interface layer during winter/early spring. *Polar Biol.* 39, 1515–1526. doi: 10.1007/s00300-015-1877-7

Schmidt, K., Atkinson, A., Steigenberger, S., Fielding, S., Lindsay, M. C., Pond, D. W., et al. (2011). Seabed foraging by Antarctic krill: implications for stock assessment, bentho-pelagic coupling, and the vertical transfer of iron. *Limnology Oceanogr.* 56, 1411–1428. doi: 10.4319/lo.2011.56.4.1411

Siegel, V. (1987). Age and growth of Antarctic euphausiacea (Crustacea) under natural conditions. *Mar. Biol.* 96, 483–495. doi: 10.1007/BF00397966

Tarling, G. A., Hill, S., Peat, H., Fielding, S., Reiss, C., and Atkinson, A. (2016). Growth and shrinkage in Antarctic krill *Euphausia superba* is sex-dependent. *Mar. Ecol. Prog. Ser.* 547, 61–78. doi: 10.3354/meps11634

Tibshirani, R. J., and Efron, B. (1993). An introduction to the bootstrap. *Monogr. Stat Appl. probability* 57, 1–436. doi: 10.1201/9780429246593

Veytia, D., Bestley, S., Kawaguchi, S., Meiners, K. M., Murphy, E. J., Fraser, A. D., et al. (2021). Overwinter sea-ice characteristics important for antarctic krill recruitment in the southwest atlantic. *Ecol. Indic.* 129, 107934. doi: 10.1016/j.ecolind.2021.107934

Watkins, J. L. (1986). Variations in the size of antarctic krill, euphausia superba dana, in small swarms. *Mar. Ecol. Prog. Ser.* 31, 67–73. doi: 10.3354/meps031067

Watkins, J. L., Buccholz, F., Priddle, J., Morris, D. J., and Ricketts, C. (1992). Variation in reproductive status of Antarctic krill swarms; evidence for a size-related sorting mechanism? *Mar. Ecol. Prog. Ser.* 82, 163–174. doi: 10.3354/meps082163

Watkins, J. L., Morris, D. J., Ricketts, C., and Murray, A. W. A. (1990). Sampling biological characteristics of krill: effect of heterogeneous nature of swarms. *Mar. Biol.* 107, 409–415. doi: 10.1007/BF01313422

Wilson, R. W., Millero, F. J., Taylor, J. R., Walsh, P. J., Christensen, V., Jennings, S., et al. (2009). Contribution of fish to the marine inorganic carbon cycle. *Science* 323, 359–362. doi: 10.1126/science.1157972

frontiers | Frontiers in Marine Science

TYPE Original Research
PUBLISHED 25 July 2023
DOI 10.3389/fmars.2023.1218003

Check for updates

OPEN ACCESS

EDITED BY
Christian Reiss,
Southwest Fisheries Science Center (NOAA), United States

REVIEWED BY
David Ainley,
H.T. Harvey & Associates, United States
Brian Wells,
National Oceanic and Atmospheric Administration (NOAA), United States

*CORRESPONDENCE
David B. Green
david.green@utas.edu.au

RECEIVED 06 May 2023
ACCEPTED 22 June 2023
PUBLISHED 25 July 2023

CITATION
Green DB, Titaud O, Bestley S, Corney SP, Hindell MA, Trebilco R, Conchon A and Lehodey P (2023) KRILLPODYM: a mechanistic, spatially resolved model of Antarctic krill distribution and abundance. *Front. Mar. Sci.* 10:1218003. doi: 10.3389/fmars.2023.1218003

COPYRIGHT
© 2023 Green, Titaud, Bestley, Corney, Hindell, Trebilco, Conchon and Lehodey. This is an open-access article distributed under the terms of the Creative Commons Attribution License (CC BY). The use, distribution or reproduction in other forums is permitted, provided the original author(s) and the copyright owner(s) are credited and that the original publication in this journal is cited, in accordance with accepted academic practice. No use, distribution or reproduction is permitted which does not comply with these terms.

KRILLPODYM: a mechanistic, spatially resolved model of Antarctic krill distribution and abundance

David B. Green[1,2*], Olivier Titaud[3], Sophie Bestley[1,2,4], Stuart P. Corney[1,4,5], Mark A. Hindell[1], Rowan Trebilco[5,6], Anna Conchon[3] and Patrick Lehodey[7]

[1]Institute for Marine and Antarctic Studies, University of Tasmania, Hobart, TAS, Australia, [2]Australian Centre for Excellence in Antarctic Science (ACEAS), University of Tasmania, Hobart, TAS, Australia, [3]Collecte Localisation Satellites, Ramonville St Agne, France, [4]Australian Antarctic Program Partnership, University of Tasmania, Hobart, TAS, Australia, [5]Centre for Marine Socioecology, University of Tasmania, Hobart, TAS, Australia, [6]CSIRO Environment, Hobart, TAS, Australia, [7]Oceanic Fisheries Programme, Pacific Community, Noumea, New Caledonia

Robust prediction of population responses to changing environments requires the integration of factors controlling population dynamics with processes affecting distribution. This is true everywhere but especially in polar pelagic environments. Biological cycles for many polar species are synchronised to extreme seasonality, while their distributions may be influenced by both the prevailing oceanic circulation and sea-ice distribution. Antarctic krill (krill, *Euphausia superba*) is one such species exhibiting a complex life history that is finely tuned to the extreme seasonality of the Southern Ocean. Dependencies on the timing of optimal seasonal conditions have led to concerns over the effects of future climate on krill's population status, particularly given the species' important role within Southern Ocean ecosystems. Under a changing climate, established correlations between environment and species may breakdown. Developing the capacity for predicting krill responses to climate change therefore requires methods that can explicitly consider the interplay between life history, biological conditions, and transport. The Spatial Ecosystem And Population Dynamics Model (SEAPODYM) is one such framework that integrates population and general circulation modelling to simulate the spatial dynamics of key organisms. Here, we describe a modification to SEAPODYM, creating a novel model – KRILLPODYM – that generates spatially resolved estimates of krill biomass and demographics. This new model consists of three major components: (1) an age-structured population consisting of five key life stages, each with multiple age classes, which undergo age-dependent growth and mortality, (2) six key habitats that mediate the production of larvae and life stage survival, and (3) spatial dynamics driven by both the underlying circulation of ocean currents and advection of sea-ice. We present the first results of KRILLPODYM, using published deterministic functions of population processes and habitat suitability rules. Initialising from a non-informative uniform density across the Southern Ocean our model independently develops a circumpolar

population distribution of krill that approximates observations. The model framework lends itself to applied experiments aimed at resolving key population parameters, life-stage specific habitat requirements, and dominant transport regimes, ultimately informing sustainable fishery management.

KEYWORDS

Southern Ocean, ecosystem modelling, earth systems, population connectivity, fisheries, mid-trophic prey, spatial processes

1 Introduction

The interplay between species life history and environmental spatio-temporal processes is fundamental in determining population connectivity (Levin, 1992). This plays a crucial role in informing effective species management (Treml et al., 2008; Rassweiler et al., 2020), particularly in the face of global change (Carr et al., 2017). Prediction of how populations might respond to environmental change requires the interfacing of factors controlling individual growth, survival, and reproduction, with processes affecting distribution. This is especially true for polar marine species, such as Antarctic krill *Euphausia superba*, which are strongly influenced by the extreme seasonality of environmental conditions (Hagen and Auel, 2001; Kawaguchi et al., 2007).

Antarctic krill (hereafter krill) have a complex life history with numerous developmental stages that each depend on a unique suite of biophysical conditions to grow and survive (Thorpe et al., 2019). This complex history leads to a strong bottom-up control of the population (Hofmann and Hüsrevoğlu, 2003; Loeb et al., 2009). For example, primary productivity over spring and summer determines the timing and magnitude of spawning, and the growth of recently spawned larvae (Ross and Quetin, 1989), while recruitment is dependent on the spatial extent of winter sea-ice (Kawaguchi and Satake, 1994; Wiedenmann et al., 2009). These dependencies make krill potentially susceptible to changing biophysical conditions. Indeed, in recent decades krill's range has contracted southwards in the face of warming and reductions in sea-ice extent, with concomitant increases in population mean length (population aging) arising from poor recruitment (Atkinson et al., 2019, but see also Cox et al., 2018; Candy, 2021). These changes are particularly concerning both because of its importance within Southern Ocean food webs (Murphy et al., 2007; Saunders et al., 2019; McCormack et al., 2020), and because it is commercially harvested. Currently, krill fishing occurs only within the Southwest Atlantic, but while landings remain well below the total annual catch limit (8.6 million tons; Nicol et al., 2012) set by the Commission for the Conservation of Antarctic Marine Living Resources (CCAMLR), there are growing concerns over the increasingly localised nature of this fishery and its impacts on dependent ecosystems (Lowther et al., 2020; Krüger et al., 2021). Under these combined pressures there is increasing need for spatio-temporally resolved frameworks that capture the dynamics and environmental underpinnings of the krill population, building capacity for fine-scale management of the species (*e.g.* Constable and Nicol, 2002).

While there is growing understanding of the relationships between biophysical conditions and krill life history requirements (*e.g.* Siegel and Watkins, 2016), there remains limited representation of the transport processes that control krill's distribution within these environments (Meyer et al., 2020). Yet, to project krill responses to change, spatial population processes need to be modelled across multiple generations and with a circumpolar range. To date, much of the work considering krill transport has used particle tracking (Lagrangian) techniques (*e.g.* Fach and Klinck, 2006; Mori et al., 2019; Veytia et al., 2021), which become very computationally expensive (Jones et al., 2016) when considering a full life cycle and large spatial scales. Eulerian approaches offer a computationally efficient alternative, by computing spatial dynamics on a gridded density field using advection-diffusion-reaction equations. This is already commonplace in ocean circulation modelling, but efforts in recent decades to integrate this methodology with population modelling have generated capacity for extending the approach to pelagic organisms (Lehodey et al., 2008; Maury, 2010).

The Spatial Ecosystem And Population Dynamics Model (SEAPODYM) is one such framework. SEAPODYM couples general circulation and biogeochemical forcings with mechanistic bioenergetic functions to simulate the spatial and temporal fluxes of pelagic ocean biomass across multiple trophic levels (Lehodey et al., 2008; Senina et al., 2008; Lehodey et al., 2010; Lehodey et al., 2015; Senina et al., 2020). To achieve this, the model makes use of two component sub-models. The first sub-model uses bioenergetics to simulate the spatial dynamics of mid-trophic level organisms (micronekton), represented as 6 functional groups occurring across three broad pelagic depth zones (epipelagic, upper mesopelagic and lower mesopelagic, with the width of each being defined as multiples of euphotic depth; Lehodey et al., 2015). The second sub-model extends the first by incorporating a population model to represent the spatial dynamics of key predatory (fish) species feeding on mid-trophics. Initially, this population model focused on tuna species (Lehodey, 2004) but has since been generalised to other tuna-like predators (Abecassis et al., 2011; Dragon et al., 2018) as well as small pelagic fish (Hernandez et al., 2014). The approach allows SEAPODYM to jointly consider life history, as well as transport processes acting to reshape distribution and interactions with the biophysical environment. This gives the

model considerable flexibility to be adapted for other pelagic species with complex life histories, such as krill.

Here, we present a framework and first implementation adapting the predator sub-model of SEAPODYM to create a new model – KRILLPODYM. This model is specifically modified to simulate the spatio-temporal dynamics of krill within the circumpolar Southern Ocean. Below, we detail the new model in terms of the three major structural components required to achieve a krill-centred version of SEAPODYM, namely:

1. an age-structured population reflecting the life history of krill, together with population-level processes including age-dependent growth and survival
2. key habitat requirements affecting spawning and modulating krill survival at different ages
3. major transport processes acting to redistribute krill biomass depending on its vertical position within the water column

Following this, we provide output from the initialisation and first simulation of KRILLPODYM and discuss potential applications, noting that fisheries and fishing impact are to be included at a later stage of development.

2 Methods

2.1 Framework for the three integrated structural components of KRILLPODYM

2.1.1 Component 1: considering an age-structured population with growth, survival, and reproduction

2.1.1.1 Age structure

Antarctic krill have a complex life-history in which they transition through 13 larval stages, and a juvenile stage (Ikeda, 1984; Kawaguchi, 2016), before reaching maturity (adult). For modelling purposes, these 15 developmental stages can be allocated amongst five broader life stages, based on unique physiological requirements and how they interact with the environment.

Model stage 1 – The first life stage (young larvae; Figure 1) occurs during the descent/ascent cycle and lasts about one month (Ikeda, 1984; Hofmann et al., 1992). Krill eggs sink to depths of 500-1000 m (Hofmann et al., 1992) before hatching as yolk-dependent larvae and subsequently returning to the surface. Over this period, krill likely experience different transport conditions from later stages, which are later largely associated with the upper 200m of the water column (*e.g.* Godlewska and Klusek, 1987; Bestley et al., 2018).

Model stage 2 – Upon reaching the surface, larvae transition into the next life stage (stage 2 – free larvae; Figure 1). Free larvae (calyptopes) have generally exhausted their yolk reserves, and have limited fasting capacity, so must begin feeding immediately (Ross and Quetin, 1989). Feeding during this stage requires access to ice-free waters and phytoplankton as these krill lack thoracic appendages necessary for feeding on ice algae (Jia et al., 2014).

Model stage 3 – After approximately three months (Ikeda, 1984; Hofmann et al., 1992), coinciding with the autumn advance of sea ice, summer-spawned krill transition into furcilia IV or higher larval stages (stage 3 – late larvae; Figure 1), which, like post-larval krill, are able to swarm and have fully developed feeding baskets for grazing on ice algae (Jia et al., 2014). Larval krill that successfully recruit into the juvenile population likely overwinter at this developmental stage (Daly, 2004), during which they are thought to feed on sea ice algae as a dominant food source.

Model stage 4 – Recruitment into the juvenile (stage 4; Figure 1) population occurs in the spring a year after spawning.

Model stage 5 – Half of the juvenile population later mature as adult (stage 5; Figure 1) female krill (age at 50% maturity) at the end of their second winter (Siegel and Loeb, 1994), while the remaining juveniles recruit as adult males a year later. For female krill spawned in January – the prevalent month of spawning (Hosie et al., 1988; Spiridonov, 1995; Siegel, 2012; Kawaguchi, 2016) – this would coincide with an age of approximately 88 weeks. Male krill subsequently mature after the third winter (Siegel and Loeb, 1994)

Following the same structural approach as SEAPODYM, we formalise these generalised life history requirements into an age-structured population that comprises a total of 291 age classes, each lasting one week, and covering the full life span (~ 6 years) (Table 1). Age classes are allocated amongst the five broad life stages described above and each has its own unique length, weight, and survival (as determined by age; see below Age-dependent growth and Age-dependent mortality for details) (Figure 1). The last age class (week 291) also contains any remaining krill that are older than this (Table 1). At any time, each age class has a given density of individuals allocated to it, the magnitude of which depends on recruitment from the previous (younger) age class.

2.1.1.2 Age-dependent growth

Based on the age-structured population outlined above, growth between age classes is predetermined and dependent on time (Lehodey et al., 2008). To assign lengths to individual age classes we use a seasonal, stepwise von Bertalanffy growth curve (Figure 2) following methods used in Rosenberg et al. (1986), and which assumes an asymptotic maximum length of 60 mm, such that:

$$\begin{cases} I_t = L_{inf}(1 - e^{-k(t-n(1-g))}) & n < t \leq n+g \\ I_t = I_{t+g} & n+g < t < n+1 \end{cases} \quad (1)$$

Where I_t is length at time t And L_{inf} is asymptotic maximum length (mm). Seasonal growth is determined by a growth constant (k), proportion of the year when krill grow (g) and the number of winters survived (n).

While this model does not explicitly consider shrinkage (Candy and Kawaguchi, 2006; Constable and Kawaguchi, 2018), it provides a simple approximation of length-at-age by allowing for rapid growth in spring and summer, and zero growth over winter. Cohorts older than 6 years are all assigned to an adult+ age/size class which represents the maximum size and age of individual krill. Thereafter, we then assign a basic estimate of mass for each age-class based on its exponential relationship with length, following methods outlined in Ju and Harvey (2004), such that:

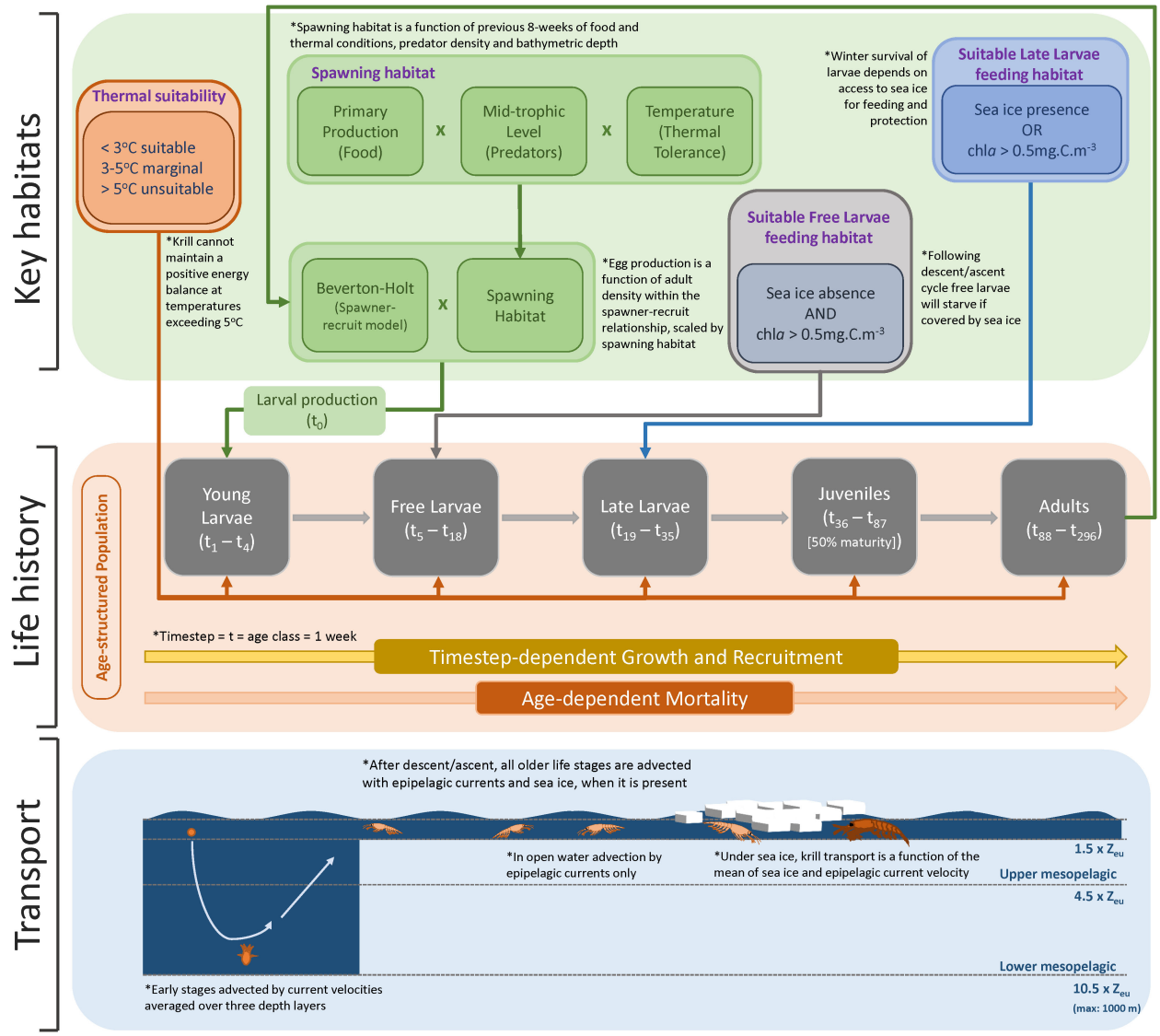


FIGURE 1
Conceptualisation of KRILLPODYM highlighting the three major structural components within the model, namely: 1) age-structured population with distinct life stages, each consisting of multiple age classes lasting the time step of the model (1 week); 2) key habitat requirements, including thermal requirements across all life stages, spawning habitat which, together with a stock-recruit model, modulates the number of larvae introduced into the system by mature adults, open water requirements for free larvae, and sea ice presence for late larvae that must survive winter in order to recruit; and 3) transport of krill based on associated life stage, including transport with average current velocities across the full mesopelagic water column for young larvae undergoing the descent/ascent cycle, and current or current and ice driven transport, based on the presence of sea ice for all older life stages.

TABLE 1 Key life stages and their duration as defined by age classes, each lasting a week.

	Life stage	Age classes	Year	Typical stage timing	Total age classes (weeks)	Reason for separation	Reference
1	Young larvae	1–4	1	Jan	4	Transport requirements	Hofmann et al. (1992); Ikeda (1984)
2	Free larvae	5–18	1	Feb – mid-May	14	Feeding requirements	Ross and Quetin (1989); Lancelot et al. (1993)
3	Late larvae	19–35	1	mid-May – Aug	17	Winter habitat requirements	Meyer et al. (2002); Meyer et al. (2017); Daly (2004)
4	Juvenile	36–87	2	Sep – Aug	52	Relaxation of developmental requirements	
5	Adult	88–291	3-6	Sep – Aug	204	Reproduction	

Duration of life stages, and timing of transitions between stages are based on a typical cohort that is spawned during the peak spawning season (1 Jan).

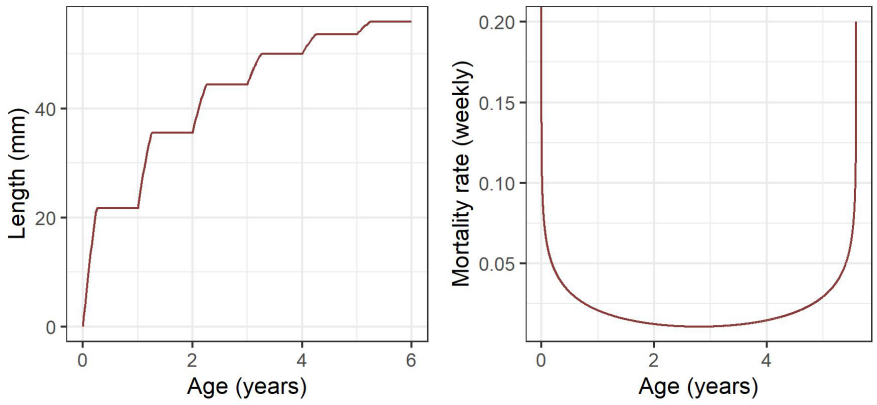


FIGURE 2
Seasonal, stepwise von Bertalanffy growth curve following Rosenberg et al. (1986) (left) and weekly age-dependent mortality following Pakhomov (1995a) (right) represented as a modified quadratic function with high mortality rates in early life and as krill approach 6 years old.

$$WW = (0.1 \cdot 10^{-6}) \cdot TL^{3.478} \quad (2)$$

Where WW is wet weight (g) and TL denotes total length (length from anterior margin of the eye to the tip of the telson; mm).

2.1.1.3 Age-dependent mortality

Krill mortality is highly variable depending on age. Both empirical and model-based studies indicate that mortality is highest for the first and last years, declining at intermediate ages towards a minimum in adult krill of approximately three years age (Pakhomov, 1995b). High mortality in early life is likely driven by predation and starvation (Ryabov et al., 2017), with senescence playing a larger role in older individuals. We represent age-dependent mortality using the following equation (Figure 2) with parameter values taken from Pakhomov (1995a) such that:

$$m(t) = \frac{(-1 \cdot log(1 - (a \cdot t^2 + b \cdot t + c)))}{52} \quad (3)$$

Where t is age, while a and b denote the quadratic slope coefficients and c the intercept of the estimated annual extinction rate respectively. The quadratic slope function is parameterised such that the extinction rate remains ≤ 1, to ensure that the log in equation 3 remains defined for all age classes. The numerator represents annual mortality rates (Pakhomov, 1995b), and has been divided by 52 to give mortality rates at the weekly time step of this model.

2.1.2 Component 2: representing key habitat requirements modulating spawning and survival of different life stages

Numerous environmental variables control krill populations through their effects on spawning (Schmidt et al., 2012), growth (Murphy et al., 2017), and survival (Perry et al., 2020; Tarling, 2020). For example, studies addressing winter survival of larvae, make use of a combination of sea-ice variables (*e.g.* sea ice concentration, thickness and ridging rate) to provide better estimates of the 3-dimensional structure of under ice habitat (Melbourne-Thomas et al., 2016; Veytia et al., 2021) than simple metrics of areal ice coverage. However, for the whole-of-life-cycle approach adopted by this study, we follow a similar approach to Thorpe et al. (2019) and make use of relatively simple habitat rules based on variables known to have the strongest influence on krill throughout their life. In particular, ocean temperature, primary production, and the presence or absence of sea ice (see ESM Table S1 for specific variables used in habitat calculation, along with associated sources).

To do so, we define two habitat categories: one that considers the suitability of habitat for spawning, which scales the production of larvae, while a second modulates survival of the five life stages based on their specific physiological requirements.

2.1.2.1 Habitat category 1: spawning habitat and larval production

The magnitude of larval production is strongly influenced by the quality of the underlying environment (Marrari et al., 2008; Conroy et al., 2020), as well as the density of adult krill (Ryabov et al., 2017). We compute larval production as the product of spawning habitat quality and a stock-recruitment model representing the density ratio between adults and larvae. Spawning habitat quality is calculated as the product of biological suitability functions considering adult thermal and feeding conditions over the 8 weeks before spawning, as well as the density of micronekton (predators) at the time of spawning. Here, we provide an overview how spawning habitat is calculated, but the detailed implementation of this model can be found in Green et al. (2021).

We represent habitat quality as the product of suitability scores (scaled 0-1) for key biophysical variables that affect egg production and survival. This approach uses three key variables: (i) temperature; (ii) net primary productivity (PP); and (iii) predator density. Spawning habitat quality (Hs) can be defined as:

$$H_s = f_1(T) \cdot f_2(PP) \cdot f_3(Pred) \quad (4)$$

where $f_1(T)$ denotes a sigmoid function (Eq.5.) representing metabolic tolerance of adult krill to variations in temperature, $f_2(P$ $P)$ gives a Holling type III functional response (Eq.6.) representing

the suitability of the feeding environment (*PP*) for egg production, and $f_3(Pred)$ is a modified lognormal function (Eq.7.) representing survival of eggs and larvae under predation.

$$f_1(T) = \frac{1}{1 + \ exp^{\lambda(T-\theta)}} \tag{5}$$

$$f_2(PP) = \frac{PP^2}{\alpha + \ PP^2} \tag{6}$$

$$f_3(Pred) = \frac{e^{\mu - 0.5\cdot\sigma^2 - \frac{(\log(Pred+1)-\mu)^2}{2\cdot\sigma^2}}}{Pred + 1} \tag{7}$$

Estimated spawning habitat quality is computed for each timestep and is combined with a Beverton-Holt model (Figure 3), to modify the stock-recruit relationship between adult density at a given location and the number of young larvae produced in the following timestep. The Beverton-Holt model is represented by equation 8 below, where *Adults* denotes adult krill density R represents the maximum reproductive rate, H_s inputs spawning habitat quality as calculated in eq. 4, and β is a slope coefficient that modulates density dependence (see also Figure 4. Initial parameter 201 values are given in Table 2. Krill spawn predominantly over austral summer (Kawaguchi, 2016). To represent this, we constrain krill spawning activity to occur only between 1 Dec and 28 Feb.

$$f(Adults) = \frac{R \cdot Adults \cdot H_s}{1.0 + \beta \cdot Adults} \tag{8}$$

2.1.2.2 Habitat category 2: habitats modifying survival of life stages

Biophysical conditions are known to have a strong influence on krill survival. Furthermore, as krill transition through different developmental stages, each with unique morphological and physiological characteristics, their specific environmental requirements for survival change. This is particularly true for larval krill, which have limited capacity for dealing with reduced food availability (Ross and Quetin, 1989). To represent these specific requirements, we compute five separate habitats to modify survival of each life stage (*i.e.* habitats for young larvae, free larvae, late larvae, juveniles, and adults; Figure 4).

These habitats incorporate three key criteria, namely: thermal suitability (affecting survival of all life stages of krill), and sea ice conditions affecting free larvae survival, and late larvae survival. For each of these criteria we classify suitability as one of three scores: suitable (1), marginal (0.5) or unsuitable (0).

Criterion 1: Thermal suitability – Throughout their life cycle, krill remain highly stenothermic (survival restricted to a narrow temperature range), growing best in temperature < 2°C (Atkinson et al., 2006). At higher temperatures, heightened aerobic activity (Tarling, 2020) and a shortened inter-moult period (Kawaguchi et al., 2007) place stress on the capacity for individuals to maintain a positive energy balance. At temperatures > 5°C, metabolic constraints likely exceed capabilities for ingesting and assimilating sufficient food supplies to maintain energy balance (Atkinson et al., 2006; Tarling, 2020). Similarly, reduced hatching success and increased deformity rates in Young Larvae are associated with temperatures exceeding 3°C (Perry et al., 2020). We represent these requirements by using the 3°C isotherm as a threshold between suitable and unsuitable thermal conditions for Young Larvae, and in older life stages define thermal habitat as suitable up to 3°C, marginal from 3-5°C, and unsuitable in waters warmer than 5°C (see Figure 4).

In calculating thermal habitat for Young Larvae we consider average temperature across the three depth layers represented by SEAPODYM (epipelagic, upper mesopelagic and lower

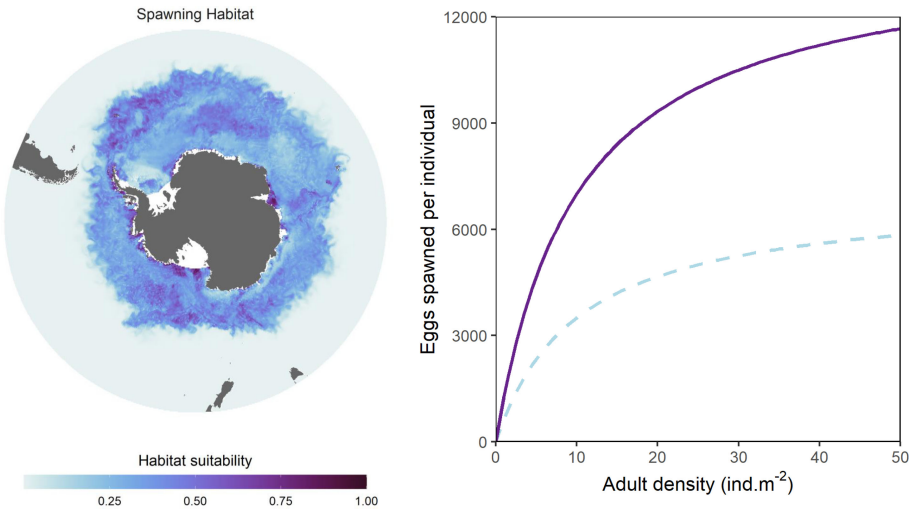


FIGURE 3
Illustration of modelled spawning habitat quality (left) and the Beverton-Holt stock-recruitment function used to modulate larval production (right). Spawning habitat quality is given for the first week of January (*i.e.* during peak spawning season) and follows Green et al. (2021). The two curves representing the Beverton-Holt function (right) denote the relationship between adult density and number of spawned eggs for spawning habitat values of 1 (high quality; solid purple line) and 0.5 (moderate quality; dashed blue line).

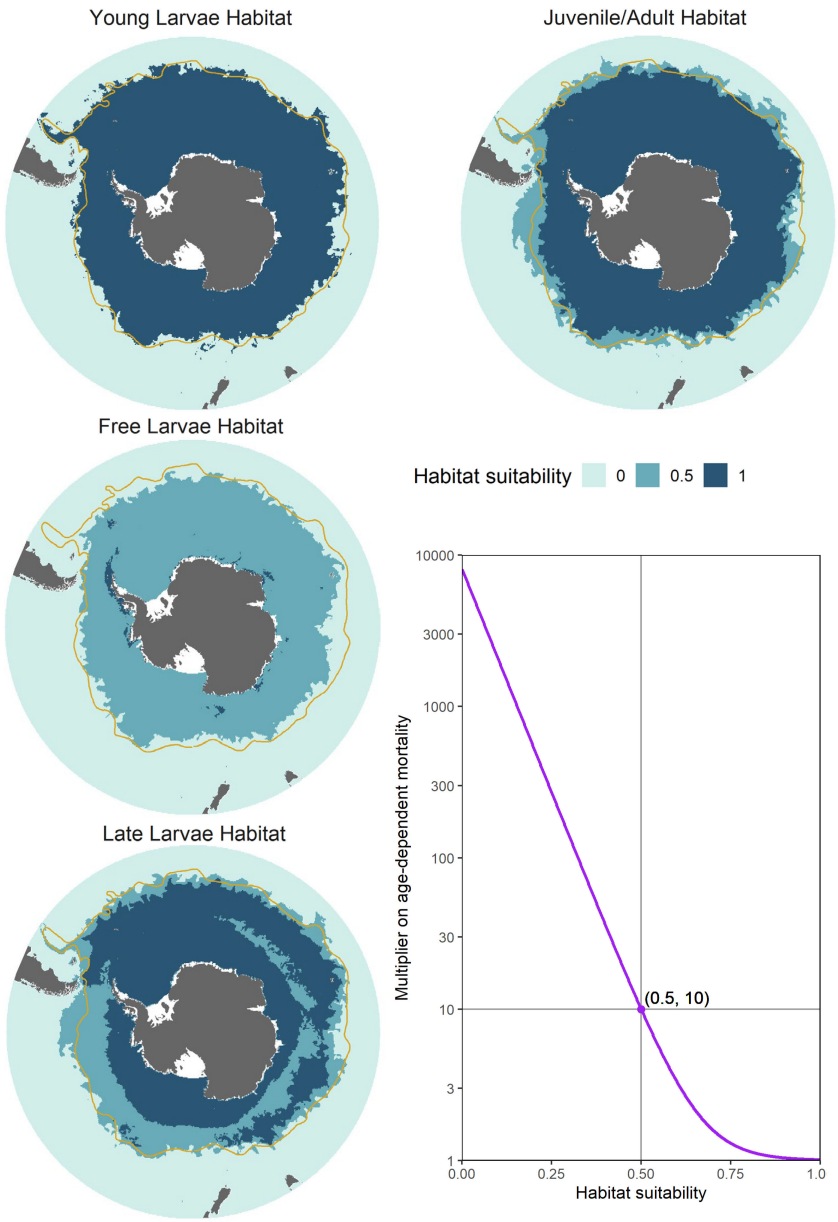


FIGURE 4
Illustration of computed habitat suitabilities for the five different life stages (left and top panels), along with the exponential function used to scale habitat-dependent mortality (bottom right panel). Each plotted habitat shows input for a single model timestep, representative of the period in which each life stage is in high relative abundance. In order of life stage, these habitats represent the first week of January, April, July and October. In the figure denoting the exponential mortality function (bottom right), habitat values of 1, 0.5, and 0 generate, respectively, mortality rate multipliers of 1, 10, and a value approaching 10000, which effectively enforces complete mortality. The orange line denotes the approximate climatological location of the Subantarctic Front (Orsi et al., 1995).

mesopelagic). These layers define the vertical distribution of young larvae during the descent/ascent cycle. For older life stages, which generally occur closer to the surface, we use epipelagic temperatures to calculate thermal habitat. Here, thermal suitability alone encompasses habitat conditions for young larvae, juveniles, and adults, but is combined with additional habitats for the free larvae and late larvae stages, which require specific feeding conditions to survive (detailed below).

Criterion 2: Feeding conditions affecting free larvae survival – Following the descent/ascent cycle, larval krill (calyptopes) transition into the free larvae stage and must immediately begin feeding (Ross and Quetin, 1989). However, unlike older life stages (Furcilia IV-) they lack fully developed thoracic appendages for grazing on sea ice algae (Jia et al., 2014). Survival of free larvae krill is therefore restricted to regions where there is sufficient available food in the water column (predominantly phytoplankton). Based

10.3389/fmars.2023.1218003

TABLE 2 Descriptions and initial values for parameters used in each KRILLPODYM model component.

Parameter	Parameter description	Value	Units	Reference section/ equation
	Growth			
L_{inf}	Asymptotic maximum length (mm)	60		Equation 1
k	Seasonal growth constant	0.45		Equation 1
g	Proportion of year when krill grow	0.25		Equation 1
	Age-dependent Mortality			
a	Slope coefficient for modified quadratic mortality function	0.073		Equation 3
b	Slope coefficient for modified quadratic mortality function	-0.408		Equation 3
c	Intercept for modified quadratic mortality function	1		Equation 3
	Spawning			
T_{spawn}	Threshold temperature for maturation and spawning	3.03		Equation 5
θ	Slope coefficient of thermal suitability function for maturation and spawning	2.2		Equation 5
α	Holling III slope of food availability for maturation and spawning	196.3		Equation 6
μ	Modified log-normal function mean denoting micronekton predation on spawned eggs	4.59		Equation 7
σ	Modified log-normal function sd denoting micronekton predation on spawned eggs	2.16		Equation 7
R	Beverton Holt proliferation rate	1400		Equation 9
β	Beverton Holt density dependent spawning saturation	0.01		Equation 9
S_{start}	Spawning start date	01-Dec		Component 2; Habitat category 1
S_{end}	Spawning end date	28-Feb		Component 2; Habitat category 1
	Habitat Suitability			
T_{YL}	Temperature threshold for Young Larvae	3	°C	Component 2; Criterion 1
TS_{OL}	Suitable habitat temperature maximum threshold for older life stages	3	°C	Component 2; Criterion 1
TM_{OL}	Marginal habitat temperature maximum threshold for older life stages	5	°C	Component 2; Criterion 1
Chl_{FL}	Suitable habitat chla minimum threshold for Free Larvae	0.5	mg.chl$a$.m^{-3}	Component 2; Criterion 2
SI_{FL}	Suitable habitat maximum sea ice fraction threshold Free Larvae	0.4		Component 2; Criterion 2
Chl_{LL}	Suitable habitat chla minimum threshold for Late Larvae	0.2	mg.chl$a$.m^{-3}	Component 2; Criterion 3
SI_{LL}	Suitable habitat minimum sea ice fraction threshold Late Larvae	0.15		Component 2; Criterion 3
	Habitat Scaled Mortality			
d	Slope coefficient for exponential function scaling mortality	13.6		Equation 9
e	Slope coefficient for exponential function scaling mortality	4.6		Equation 9
	Transport			
D	Diffusion parameter	0.1	m^2.s^{-1}	Component 3
P_{UVL1}	Proportional contribution of epipelagic current advection in ice covered water (sea ice fraction ≥ 0.15)	0.75		Component 3
P_{UVSI}	Proportional contribution of sea ice advection in ice covered water (sea ice fraction ≥ 0.15)	0.25		Component 3

on literature, we define suitable Free Larvae feeding habitat as the co-occurrence of chlorophyll *a* concentrations ≥ 0.5 mg.chl*a*.m^{-3} (Ross and Quetin, 1989; Piñones and Fedorov, 2016; Trebilco et al., 2019) and sea ice concentrations < 40% (Thorpe et al., 2019).

Realised Free Larvae habitat (values of 1) is then computed as the combination of thermal habitat and feeding conditions. Suitable habitat coincides with the co-occurrence of suitable thermal and feedings conditions, marginal habitat occurs in association with suitable or marginal thermal conditions (< 5°C) but poor feeding conditions, and unsuitable habitat occurs where temperatures are > 5°C, irrespective of feeding conditions (Figure 4).

Criterion 3: Feeding conditions affecting late larvae survival – During winter, primary production across much of the Southern Ocean is greatly reduced. Larval krill (late larvae) do not have sufficient energy reserves to fast over extended periods (Meyer and Oettl, 2005). Where sea ice is present, late larvae (furcilia IV-) can increase food intake through grazing on sea ice communities (Frazer, 2002). Recent work has also shown that overwintering larvae can survive in ice-free waters provided there is sufficient primary production (Walsh et al., 2020; Veytia et al., 2022). In some cases, small size classes are capable of maintaining positive growth in chl*a* concentrations as low as 0.2 mg.C.m^{-3} (Tarling et al., 2006).

Consequently, we assume that suitable Late Larvae habitat (values of 1) occurs under sea ice (sea ice fraction of ≥ 15 %; *e.g.* Worby, 2004), or in open waters < 3°C with chl *a* concentrations of ≥ 0.2 mg.C.m^{-3}. Marginal habitat (values of 0.5) consists of waters of 3-5°C, or waters < 3°C and chl *a* concentrations < 0.2 mg.C.m^{-3}. As with the other life stages, waters > 5°C are considered unsuitable for survival (values of 0).

2.1.2.3 Enforcing habitat driven mortality

Habitat suitability scores, as computed above, are then used to scale age-dependent mortality such that suitable habitat has no effect on baseline (Eq. 3.) mortality rates, but forces an exponential decrease in survival as habitat suitability approaches zero. We implement this by incorporating our habitat suitability within the following exponential function (Eq. 9),

$$f(H) = 1 + e^{(d\cdot(1-H)-e)} \quad (9)$$

where H represents habitat suitability, while coefficients d and e modulate the slope of the function. In this first implementation, we have parameterised this function such that age-dependent mortality increases by an order of magnitude in marginal habitat (values of 0.5), and approaches total mortality in unsuitable habitat (values of 0; see Figure 4).

2.1.3 Component 3: enacting transport across life stages

Spatial redistribution of biomass for each age class and timestep is calculated based on the prevailing circulation of ocean currents and seasonal sea ice. To enact these spatial dynamics, implementation of this model will use methods already implemented and published in SEAPODYM. Age classes are redistributed by the underlying circulation using advection-diffusion-reaction equations, which are numerically solved across a regular grid and timestep (Lehodey et al., 2008; Senina et al., 2020), to generate spatially dynamic density fields. This approach considers both directed advection by currents (and sea ice) as well as random animal movements related to density within a given cell (diffusion). This method is well suited to describing dynamics over large spatial and temporal scales. Variables, and associated sources, used to represent these circulation patterns are detailed in ESM Table S1.

In this model, we compute two separate forms of transport, which are related to the vertical distribution and behaviour of krill at different developmental stages. The first form considers transport of young larvae (model stage 1), while the second encompasses transport of all older life stages.

Transport of young larvae (model stage 1) – Following spawning, eggs and nauplii undergo a descent/ascent cycle lasting approximately one month (Hofmann et al., 1992). During this time, they cover a range of depths spanning 0 and ~ 1000 m (Hofmann et al., 1992), and their transport is a function of currents occurring throughout this depth range. To apply this, we assume young larvae are redistributed by the average current velocities across all three depth layers (epipelagic, upper mesopelagic and lower mesopelagic; Figure 1) represented in SEAPODYM. In doing so, we compute eastward and northward current velocity fields across all three depth layers represented within SEAPODYM, with values weighted by the relative thickness of each layer. It is worth noting that while this simple metric would likely produce low advection rates, it may still over represent time spent within the upper 200m of the water column (Hofmann et al., 1992), where advection rates are highest.

Transport of free larvae, late larvae, juveniles, and adults (model stages 2 – 5) – Once krill return to surface waters as free larvae, they generally occur within the upper 200 m of the water column (*e.g.* Godlewska and Klusek, 1987; Bestley et al., 2018). From this point, we consider their movement to be driven by epipelagic currents in ice-free regions and by a combination of epipelagic currents and sea-ice dynamics when associated with ice (Thorpe et al., 2007; Veytia et al., 2021). To represent this, for cells within the sea ice zone (> 15% sea ice concentration) we compute a weighted mean such that epipelagic current contribute 75% and sea-ice velocities 25% to the composite advection field (equivalent to 18h in water column and 6h with ice). We note here that previous work has used a 12h split between ocean current and sea ice advection (e.g. Meyer et al., 2017; Veytia et al., 2021). However, we found here that a higher weighting (*e.g.* 12h/12h) of sea ice advection led to krill being advected further northwards, beyond their observed distribution (see ESM Figure S2).

2.2 KRILLPODYM simulation spin up

In this first implementation of KRILLPODYM we initialise the model using a 12-year spin up (approximately two full krill generation cycles), repeating forcings for the year 2010. The spatial domain of this implementation covers the circumpolar Southern Ocean and extends northwards from the Antarctic coast to 40° S at a horizontal grid resolution of 0.25°x 0.25°. As initial conditions we assume a uniform density (1 ind.m^{-2} per age class;

Figure S1) across the full spatial domain. The model advances with a weekly time step, and at each step generates spatially resolved density fields for all age classes, which are subsequently aggregated by life stage (as in Table 1).

3 Results

3.1 Spatial patterns in computed habitats

3.1.1 Habitat category 1: spawning Habitat

The spatial distribution of high quality spawning habitat was the same as that outlined in Green et al., 2021 for austral summer. Briefly, the highest quality spawning habitat in Dec-Feb, occurred along the Antarctic continent, particularly around Prydz Bay, and the region from the Ross Sea eastwards to the northern Antarctic Peninsula, extending offshore past South Georgia to the Scotia Arc (as shown in Figure 3 and also described in Green et al., 2021, Figure 2). Moderate quality spawning habitat was supported by oceanic waters further north.

3.1.2 Habitat category 2: habitats modifying survival of life stages

This initial model utilised relatively simple habitat rules for classifying suitability and modulating age-dependent survival of cohorts. Thermal constraints were the most important driver of mortality, rendering habitats north of the Subantarctic Front (~ 5°C) largely unsuitable for all krill life stages (Figure 4). Within the suitable thermal range, habitats had fairly uniform suitability for Young Larvae, Juveniles, and Adults. The strictest controls on habitat-influenced survival and distribution occurred during the Free Larvae stage, where suitable feeding conditions were primarily restricted to the Antarctic coast, as well as waters around South Georgia (as shown in Figure 4). At the Late Larvae stage, slightly more relaxed controls on survival and distribution effectively only limited survival in low productivity waters north of the Antarctic convergence spanning the Indian and Pacific Sectors of the Southern Ocean.

3.2 Model spin-up and evolution of krill spatial distribution and dynamics

3.2.1 Modelled krill distribution

During model spin-up, it took approximately 2-6 iterations for the distribution and dynamics of all life stages to stabilise, linked with the timing of adult recruitment (2 years) and maximum lifespan (6 years) (see spin up animation in ESM). Initially, uniform krill density was assumed across the entire spatial domain; however, high temperature-linked mortality rates in the north rapidly constrained the latitudinal distribution of all life stages to waters south of the Subantarctic Front (Figure 5). Spatial patterns in krill biomass developed mainly from areas of cold water and high primary production, supporting both large summer pulses of spawning activity and subsequent survival of Free Larvae. Transport by ocean currents and sea ice advection served to progressively broaden cohort distributions as they aged through later life stages. High biomasses of juveniles and younger life stages were largely contained within the maximum winter ice extent, with high densities also occurring around South Georgia. Adult krill exhibited the broadest distribution, extending well downstream of South Georgia, into the Indian Sector of the Southern Ocean (Figure 5). The model predicted the highest biomasses of krill along the Antarctic coastal band stretching eastwards from the eastern edge of the Ross Sea to South Georgia across all life stages. Approximately 65% of all post-larval krill biomass (juveniles and adults combined) occurred within the Atlantic sector stretching between CCAMLR Subareas 88.3 and 48.6 (Table 3). However, high post-larval krill abundances were also evident for other locations along the Antarctic coast; particularly the Amundsen and western Ross seas, as well as moderate biomasses across coastal East Antarctica and the Cosmonauts Sea (Figure 5).

3.2.2 Spatial dynamics of krill biomass

Particularly noticeable from the model spin up was the significant influence of ocean currents and sea ice advection on krill biomass redistribution. Krill biomass downstream of South Georgia was advected progressively eastward with increasing age, while there was a contrasting westward and, in some cases, northward propagation of biomass from areas of high larval production along the Antarctic coast stretching from the Weddell Sea to East Antarctica. For instance, high larval biomasses spawned in Prydz Bay were transported westwards, reaching the margin between the Cooperation and Cosmonauts Seas as Late Larvae, whereafter some were advected further west, while others were entrained in the northward sea ice advance (see spin up animation in ESM). Ultimately these larvae recruited into the juvenile population across a band stretching from the Cosmonauts Seas to the southern Kerguelen Plateau (Figure 5).

Spatial mismatches between spawned larvae and recruitment into the post larval population were not evident everywhere. Most notably, the distribution of life stages was relatively uniform in the high biomass region between the eastern edge of the Ross Sea and northern Antarctic Peninsula, with a high proportion of spawned larvae seemingly retained within these systems as they aged.

3.3 Modelled versus observed krill distributions

The modelled distribution of post-larval krill (juveniles and adults combined) showed broad similarities with observed krill distributions estimated from KRILLBASE (the most comprehensive observation database available; Atkinson et al., 2017). Both modelled and observed distributions indicated that the bulk of biomass was located within the southwest Atlantic, particularly around the Antarctic Peninsula and Scotia Sea (Figures 5, 6), and that moderate to low krill densities occurred within Indian and western Pacific sectors. Differences in modelled and observed densities were however apparent in the eastern Pacific sector, where our model predicted high krill densities in coastal

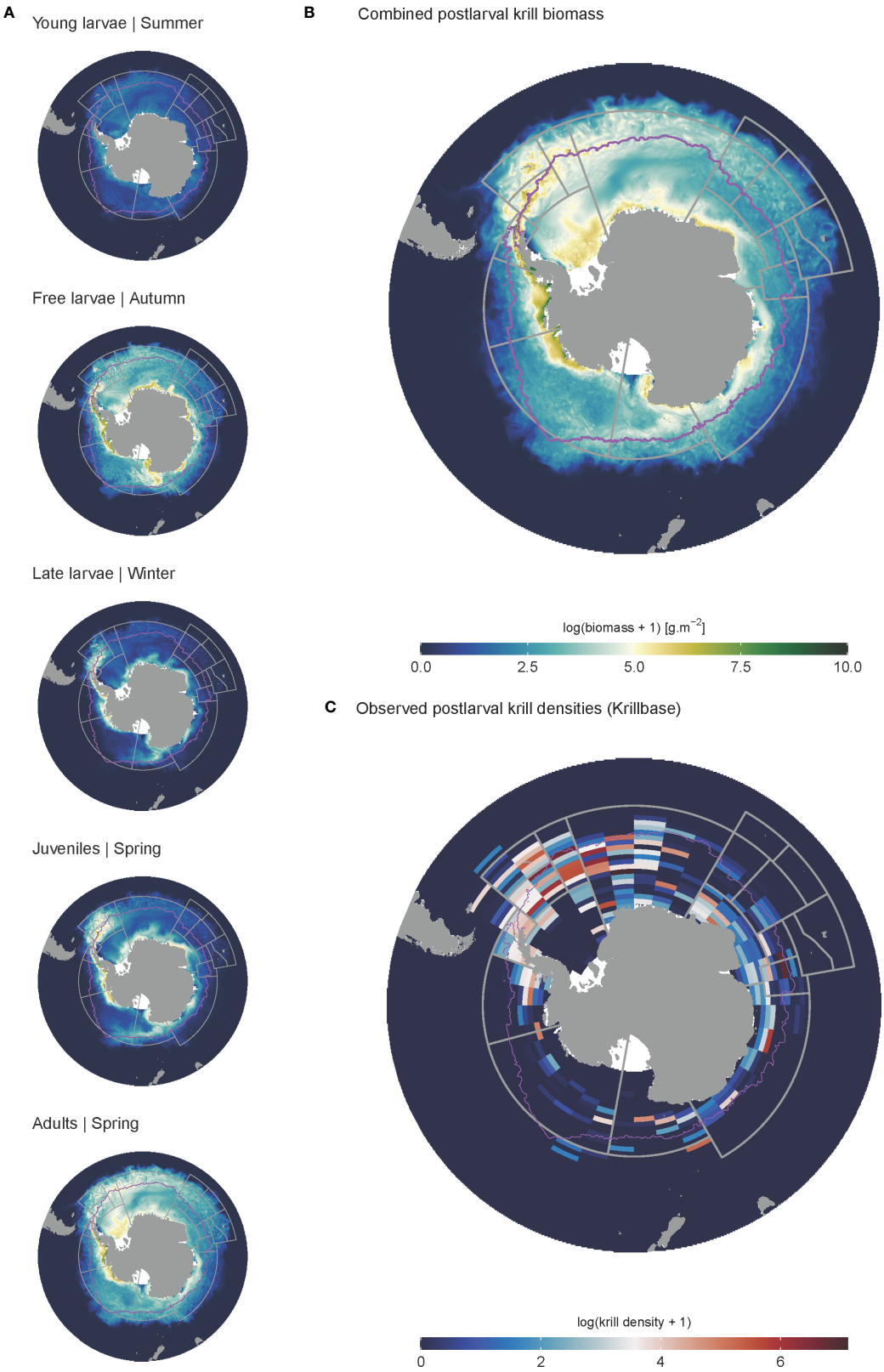


FIGURE 5
Modelled and observed distributions of krill. **(A)** denotes the biomass distributions of the different life stages in the final iteration of the model spin up. Each represents a mean biomass associated with the season in which each life stage is in highest relative abundance. **(B)** denotes the biomass distribution of all post-larval krill, representing the combined biomass of juveniles and adults. **(C)** gives observed post-larval krill densities obtained from KRILLBASE Atkinson et al. (2017). Maximum sea ice extent is given by the pink line.

TABLE 3 Mean biomass density and relative summed biomass of post-larval krill for CCAMLR Subarea/Division.

Subarea/ Division	Mean biomass density ($g.m^{-2}$)	Proportional summed biomass
88.3	81.62	8%
48.1	147.19	4%
48.2	179.90	7%
48.3	105.67	5%
48.4	116.40	5%
48.5	150.30	14%
48.6	71.30	21%
	Total	**65%**
58.4.2	79.68	6%
58.4.3a	16.59	< 1%
58.4.3b	13.17	< 1%
58.4.4a	28.34	1%
58.4.4b	17.78	1%
58.5.1	4.52	< 1%
58.5.2	8.52	< 1%
58.6	6.61	< 1%
58.7	7.08	< 1%
	Total	**10%**
58.4.1	34.33	7%
88.1	58.15	7%
88.2	50.91	11%
	Total	**25%**

Mean biomass density is calculated as the mean biomass ($g.m^{-2}$) across all cells within a Subarea/Division. Relative summed biomass represents the sum of biomass across all cells within a Subarea/Division, relative to the total summed biomass across all Subareas/Divisions. Note, prior to calculation of the below relative mean densities and summed biomass, we capped the maximum biomass values for cells at the 99^{th} percentile.

Antarctic waters of the Ross, Amundsen and Bellingshausen Seas, whereas observations suggest that krill are largely absent from these areas (Figure 5).

4 Discussion

Our key aim here was to provide a "proof-of-concept" for our novel krill model configuration, KRILLPODYM, that allows joint consideration of life history, habitat, and transport processes. Seeded with a uniform initial density, and using only a basic parameterisation based predominantly on simple thresholds, we have illustrated the model's capacity to reproduce Antarctic krill's circumpolar distribution and spatial dynamics. This represents a foundational step in generating highly resolved distribution and abundance estimates for a relatively data poor species (outside of the south Atlantic). The model framework also provides flexibility for future work to develop simulation experiments testing key biological processes including population processes such as growth, mortality, and reproduction, and environmental influences through exploring specific habitat requirements and advective processes.

4.1 Contrasting modelled vs observed circumpolar krill distribution

Output from this implementation indicated that the model could reasonably represent krill distribution, and regional abundances as they are currently understood. Particularly noticeable was the dominance (65%; Table 3) of modelled biomass in the south Atlantic, which aligns well with previous work that found 70% of krill biomass was concentrated between 0-90°W (Atkinson et al., 2009). Also interesting were regions that our model predicted to support high biomasses of krill, but for which observations indicate much lower densities. In the south Atlantic, such discrepancies may partly be explained by fisheries (*e.g.* Subarea 48.1 where much of the fishery is concentrated; see Figure 6 and Meyer et al., 2020) and consumption by predators (*e.g.* mesopelagics, baleen whales, seals and penguins; Saunders et al., 2019; Savoca et al., 2021; Hoffman et al., 2022; Warwick-Evans et al., 2022) remaining unaccounted for in our current model setup. Future work should consider the role of fishery catch and consumption by predators in shaping the dynamics of krill within the region. Beyond the south Atlantic, many regions of the Southern Ocean remain relatively poorly sampled for krill. As such, the discrepancy in abundance within these regions could highlight regions of relatively low sampling effort, where krill have gone largely undetected. For example, there are few KRILLBASE observations for the western Ross Sea, where our model predicts moderate to high densities of krill, which matches with independent surveys of the region (Davis et al., 2017). Further, while there is a regional paucity of directed krill sampling, it is known that the Ross Sea region has historically been an important foraging area for krill-eating whales (Branch et al., 2007). Over the course of the 1920s several thousand blue whales (Balaenoptera musculus) were taken from continental slope waters of the Ross Sea, indicating an abundant population of this species, until its extirpation in the 1930s (Branch et al., 2007; Ainley, 2010). Such large numbers of blue whales would almost certainly have required a much greater regional biomass of krill than apparent in the observed krill densities denoted in Figure 5. Indeed, the aggregations of whales along the Ross Sea continental slope suggest that our model may in fact be underestimating krill biomass here (Branch et al., 2007; Murase et al., 2013). Such findings highlight the potential value in considering indicator species distributions during model parameterisation and evaluation, particularly within regions that have received relatively little directed sampling.

In other regions, such as the Amundsen and Weddell Seas, it is unclear whether the high simulated krill biomasses here are a true reflection of the environment. Indeed, while both seas remain relatively poorly observed, the few dedicated sampling efforts within these regions have indicated that their zooplankton

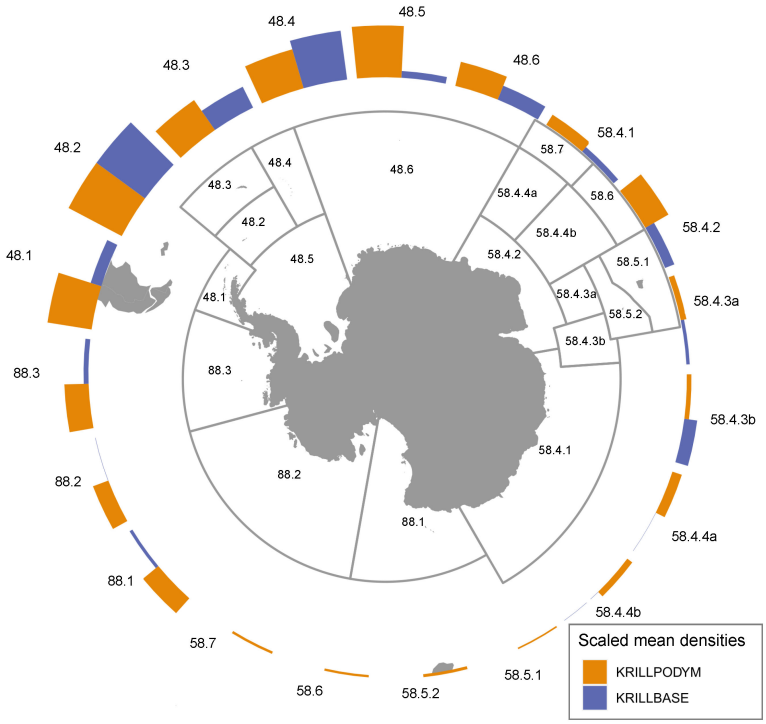


FIGURE 6
Modelled and observed relative (scaled 0-1) mean densities of krill, aggregated by CCAMLR Subarea/Division. Observed post-larval krill densities are derived from KRILLBASE Atkinson et al. (2017). Relative krill densities are computed by first computing mean densities at a 50km resolution, and subsequently taking the mean of all 50km cells occurring within each Subarea/Division. Relative densities are then computed by dividing each by the maximum mean density across all Subareas/Divisions. Note, prior to calculation of the below relative mean densities and summed biomass, we capped the maximum biomass values for cells at the 99th percentile.

communities are dominated by ice krill (La et al., 2015; *E. crystallorophias*), rather than Antarctic krill (Wilson et al., 2015). One reason for this might be that there are competition effects between the two species, which are not accounted for within the model. Alternatively, our model habitats may not have adequately captured underlying environmental conditions modifying krill survival. Both the Amundsen and Weddell Seas are known to maintain exceptionally thick and persistent sea ice (Kurtz and Markus, 2012; Stammerjohn et al., 2015). These ice regimes could limit primary production both in the water column and within the sea ice itself, restricting feeding opportunities for krill, particularly during the Free and Late Larvae stages (Meyer et al., 2017). While the current model implementation does consider sea ice presence, it does not yet consider how sea ice characteristics, such as thickness or rugosity (Veytia et al., 2021), could modify the suitability of under ice habitat for krill survival. The role of sea ice characteristics in influencing krill survival, growth and recruitment has been highlighted as a key knowledge gap, and is one that the KRILLPODYM framework is well placed to address in future iterations.

Also notable was the broader northward distribution of modelled vs observed krill in the Atlantic and Indian sectors, particularly for the adult life stage. This highlights the role advective processes play in shaping krill's distribution. Most obvious, was the progressive ACC-driven eastward transport of krill spawned in the southwest Atlantic as they age. However, our findings during model initialisation also indicated that sea ice advection had an important, but counter-intuitive influence on northward krill transport. Along coastal Antarctica, spawned krill appeared to be entrained in the advancing sea ice, and advected northwards, but were thereafter released into the open waters as sea ice retreated. This effectively served to push krill northward beyond ice-dominated systems, increasing its relative densities in open ocean habitats outside the maximum ice extent. Indeed, early model initialisations indicated that transport schemes of 12h/12h epipelagic currents and sea ice transport (following previous work; *e.g.* Meyer et al., 2017; Veytia et al., 2021) led to a much more northerly distribution of krill, while a transport regime driven entirely by epipelagic currents served to aggregate krill biomass over the Antarctic shelf, leading to much higher densities in Antarctic waters (especially the western Ross Sea; see ESM Figures S2, S3). These initial results emphasise the sensitivity of krill's distribution to different transport mechanisms.

A notable feature of krill's known distribution is that high biomasses are supported in the vicinity of South Georgia (Atkinson et al., 2008), but not at similar latitudes in the Indian sector, despite similar temperature regimes (see Figure 4). In this implementation, we have only considered the role of temperature in shaping suitable habitat for post-larval krill. However, previous work modelling krill growth rates has demonstrated a strong link between temperature-linked metabolism and food requirements in krill (Atkinson et al., 2006; Murphy et al., 2017; Veytia et al., 2020). For example, under

temperature stress krill must feed at higher rates to maintain a positive energy balance (Atkinson et al., 2006; Hill et al., 2013). Indeed, while post-larval krill within suitable thermal habitat are able to maintain positive energy balances during periods of low food availability, at higher temperatures increased metabolic demands means that this is less feasible (Constable and Kawaguchi, 2018). Persistence of the South Georgia krill stock at its thermal limits (Tarling, 2020) is therefore likely because of the persistence of elevated primary production for much of the year (Atkinson et al., 2001). Eastwards of this, between the Scotia Arc and the Kerguelen Plateau, annual primary production within this latitudinal band is much lower (Arrigo et al., 2008). This suggests a potentially reduced capacity of these waters to maintain post-larval krill survival. Another mechanism which could be explored further is the role of heterotrophy (feeding on zooplankton such as copepods; Atkinson et al., 2002) in shaping feeding habitat quality for overwintering post-larval krill. The interplay between food availability and temperature on post-larval krill survival and subsequent distribution could be explored directly through modifying modelled juvenile and adult habitat suitability within future model iterations.

4.2 Future experiments addressing knowledge gaps in krill spatial ecology

As a first model implementation we have used published deterministic functions to represent krill life history, together with relatively simple habitat requirements and advection regimes. However, the model framework is highly flexible, allowing for parameter testing and interchangeability of the growth, mortality, and stock-recruitment functions. Likewise, because the habitats and advection fields are input as forcings, these can be recomputed offline to reflect more sophisticated relationships between krill life stages and their ocean-ice environment. This provides exciting scope for targeted experiments with the biological parameterisation, as well as testing theorised mechanisms dictating krill population processes and interactions with the biophysical environment. Future studies should use sensitivity analyses to identify how different configurations of key habitat forcings (including temperature as well as primary and secondary production) and ocean-ice advection mechanisms, influence the abundance, distribution and dynamics of krill.

Considering our model components, sensitivity analyses could focus on the following three priority areas:

1. **Sensitive population parameters** - Our model represents krill growth, mortality, and reproduction using deterministic functions and, wherever possible, parameter values derived from literature. While these functions and parameters are based on empirical data, most values are derived at a regional population level (*e.g.* Pakhomov, 1995b), and may not be fully generalisable across the full spatial domain. Sensitivity analyses considering a range of biologically feasible parameter values (and functions), would generate important understanding on how different representations of these key population processes could influence krill's spatio-temporal population dynamics and age structure. Foremost of these should be exploring population responses to changes in the stock-recruit relationship modulating larval production.
2. **Habitat suitability** – Habitat suitability plays an important role in shaping krill population processes and subsequent distribution. Indeed, changes in the distribution of suitable habitat can have profound effects on overall krill abundance and distribution. This is especially true for changes in larval krill habitat suitability (*e.g.* Free Larvae), which have the strictest requirements. However, these suitability scores are likely also important for post-larval krill given the interacting roles of temperature and food availability on growth, as discussed above. Future model experiments could consider the sensitivity of krill spatio-temporal dynamics to different habitat scores across life stages with the aim of identifying which habitats have the greatest impact on distribution and abundance. Key experiments should explore model sensitivity to increase resolution of: 1) under ice habitat suitability, and 2) thermal – feeding habitat suitability (including the role of heterotrophy) for all krill life stages older than Young Larvae.
3. **Transport processes** – The role of advective processes in shaping krill distribution and metapopulation dynamics continues to be an important knowledge gap. Here we have shown that applying different relative influences of ocean currents and sea ice transport can lead to very different krill distributions across the circumpolar Southern Ocean (Figure 4 and ESM Figures 2, 3). We have assumed that krill are partly advected by sea ice in waters of > 15% cover. However, krill's association with sea ice, and subsequent transport dynamics is certainly more complex than this. Following work on under-ice characteristics (above), future experiments should explore model sensitivity to the relative contribution of ocean currents and ice advection to krill transport.

4.3 KRILLPODYM potential applications

Here we have presented a model framework and implementation that reasonably captures the circumpolar distribution of Antarctic krill, while concurrently demonstrating the sensitivity of krill dynamics to different forcing mechanisms (*e.g.* transport). In so doing, we have highlighted the model's potential for testing key assumptions on krill biology and guiding formulation of new hypotheses for improved ecosystem understanding (Cury et al., 2008; Seidl, 2017). Additionally, KRILLPODYM's capacity to match observed spatial patterns in sampled regions suggests that it could provide a promising avenue for extending our understanding to systems sampled less frequently. Once fully parameterised, KRILLPODYM should provide a powerful operational tool for studies exploring sustainable krill fishery management, as well as broader ecological questions on ecosystem functioning. Given the

flexible model framework, future KRILLPODYM iterations could also incorporate forcings computed from climate projection models (*e.g.* CMIP; Eyring et al., 2016), to generate projections of krill population dynamics over the upcoming decades.

4.3.1 Source-sink dynamics and krill harvest scenarios

A key challenge in sustainable management of the krill fishery is characterising metapopulation dynamics and the sources of different regional krill populations. Through its highly resolved spatial processes the model could expand capacity for identifying source-sink dynamics between different krill stocks which could subsequently be applied to harvest scenarios to investigate consequences of krill harvesting (i.e. removal of biomass from selected grid cells) on local and downstream abundance. This would be an important step towards improving understanding of how krill harvesting could impact dependent ecosystem components, including krill-eating predators (Hinke et al., 2017; Lowther et al., 2020).

4.3.2 Evaluating predator foraging habitat in a changing Southern Ocean

Our capacity to represent bottom-up trophic linkages spanning environment – predators is central to understanding Southern Ocean ecosystem responses to a changing climate. Models representing highly resolved spatial estimates of mid-trophic levels are important tools for providing synoptic forage information for higher predators (*e.g.* Green et al., 2020; Romagosa et al., 2021; Green et al., 2023). As an operational product, KRILLPODYM would open opportunities for investigating the foraging habitat of krill-dependent marine predators (*e.g.* baleen whales, crabeater seals, Adelie and chinstrap penguins) based on direct spatio-temporal estimates of their prey. Using an implementation forced by climate projection models, established links between krill and predator foraging could then be projected into upcoming decades, generating valuable insights into potential future ecosystem structure. Furthermore, by reconciling model representations of krill with knowledge derived from both direct (active sampling, *e.g.* KRILLBASE; Atkinson et al., 2017) and indirect observations (*e.g.* through indicator species such as baleen whales; Alvarez and Orgeira, 2022), we can arrive at a more integrated representation of these remote and inaccessible ecosystems (Santora et al., 2013; Santora et al., 2021).

Data availability statement

The datasets presented in this study can be found in online repositories. Output from this first model initialisation can be found on the Institute for Marine and Antarctic Studies (IMAS) Data Portal (https://doi.org/10.25959/895K-K978).

Author contributions

All authors contributed towards model conceptualisation. DG coordinated the project, model initialisation, and wrote the initial manuscript, while OT adapted SEAPODYM model programming and structure for KRILLPODYM. All authors contributed biological and technical expertise, reviewed and commented on the manuscript. All authors contributed to the article and approved the submitted version.

Funding

This research was supported by the Australian Research Council Special Research Initiative, Australian Centre for Excellence in Antarctic Science (Project Number SR200100008). DG received funding through a Tasmania Graduate Research Scholarship. SB was supported by the Australian Research Council under DECRA award DE180100828. Further funding was provided through the European H2020 International Cooperation project Mesopelagic Southern Ocean Prey and Predators No 692173.

Acknowledgments

The authors thank Bettina Fach and Stephanie Brodie for useful comments on a previous version of this manuscript.

Conflict of interest

The authors declare that the research was conducted in the absence of any commercial or financial relationships that could be construed as a potential conflict of interest.

Publisher's note

All claims expressed in this article are solely those of the authors and do not necessarily represent those of their affiliated organizations, or those of the publisher, the editors and the reviewers. Any product that may be evaluated in this article, or claim that may be made by its manufacturer, is not guaranteed or endorsed by the publisher.

Supplementary material

The Supplementary Material for this article can be found online at: https://www.frontiersin.org/articles/10.3389/fmars.2023.1218003/full#supplementary-material

References

Abecassis, M., Lehodey, P., Senina, I., Polovina, J. J., Calmettes, B., and Williams, P. (2011). *Application of the SEAPODYM model to swordfish in the pacific ocean* (Pacific Islands Fisheries Science Center: US Department of Commerce, National Oceanic and Atmospheric Administration, National Marine Fisheries Service).

Ainley, D. G. (2010). A history of the exploitation of the ross sea, antarctica. *Polar Rec.* 46, 233–243. doi: 10.1017/S003224740999009X

Alvarez, F., and Orgeira, J. (2022). Krill finder: spatial distribution of sympatric fin (*Balaenoptera physalus*) and humpback (*Megaptera novaeangliae*) whales in the southern ocean. *Polar Biol.* 45, 1427–1440. doi: 10.1007/s00300-022-03080-x

Arrigo, K. R., Van Dijken, G. L., and Bushinsky, S. (2008). Primary production in the southern ocean, 1997–2006 *J. Geophys. Res* 113, C08004. doi: 10.1029/2007jc004551

Atkinson, A., Hill, S. L., Pakhomov, E. A., Siegel, V., Anadon, R., Chiba, S., et al. (2017). KRILLBASE: a circumpolar database of Antarctic krill and salp numerical densities 1926–2016. *Earth System Sci. Data* 9, 193–210. doi: 10.5194/essd-9-193-2017

Atkinson, A., Hill, S. L., Pakhomov, E. A., Siegel, V., Reiss, C. S., Loeb, V. J., et al. (2019). Krill (*Euphausia superba*) distribution contracts southward during rapid regional warming. *Nat. Climate Change* 9, 142–147. doi: 10.1038/s41558-018-0370-z

Atkinson, A., Meyer, B., Stuübing, D., Hagen, W., Schmidt, K., and Bathmann, U. V. (2002). Feeding and energy budgets of Antarctic krill *Euphausia superba* at the onset of winter-II. juveniles and adults. *Limnology Oceanography* 47, 953–966. doi: 10.4319/lo.2002.47.4.0953

Atkinson, A., Shreeve, R. S., Hirst, A. G., Rothery, P., Tarling, G. A., Pond, D. W., et al. (2006). Natural growth rates in Antarctic krill (*Euphausia superba*): II. predictive models based on food, temperature, body length, sex, and maturity stage. *Limnology Oceanography* 51, 973–987. doi: 10.4319/lo.2006.51.2.0973

Atkinson, A., Siegel, V., Pakhomov, E., Jessopp, M., and Loeb, V. (2009). A re-appraisal of the total biomass and annual production of antarctic krill. *Deep Sea Res. Part I: Oceanographic Res. Papers* 56, 727–740. doi: 10.1016/j.dsr.2008.12.007

Atkinson, A., Siegel, V., Pakhomov, E. A., Rothery, P., Loeb, V., Ross, R. M., et al. (2008). Oceanic circumpolar habitats of Antarctic krill. *Mar. Ecol. Prog. Ser.* 362, 1–23. doi: 10.3354/meps07498

Atkinson, A., Whitehouse, M., Priddle, J., Cripps, G., Ward, P., and Brandon, M. (2001). South georgia, antarctica: a productive, cold water, pelagic ecosystem. *Mar. Ecol. Prog. Ser.* 216, 279–308. doi: 10.3354/meps216279

Bestley, S., Raymond, B., Gales, N. J., Harcourt, R. G., Hindell, M. A., Jonsen, I. D., et al. (2018). Predicting krill swarm characteristics important for marine predators foraging off East Antarctica. *Ecography* 41, 996–1012. doi: 10.1111/ecog.03080

Branch, T. A., Stafford, K., Palacios, D., Allison, C., Bannister, J., Burton, C., et al. (2007). Past and present distribution, densities and movements of blue whales balaenoptera musculus in the southern hemisphere and northern indian ocean. *Mammal Rev.* 37, 116–175. doi: 10.1111/j.1365-2907.2007.00106.x

Candy, S. G. (2021). Long-term trend in mean density of Antarctic krill (*Euphausia superba*) uncertain. *Annu. Res. Rev. Biol.* 36, 27–43. doi: 10.9734/arrb/2021

Candy, S. G., and Kawaguchi, S. (2006). Modelling growth of Antarctic krill. II. novel approach to describing the growth trajectory. *Mar. Ecol. Prog. Ser.* 306, 17–30. doi: 10.3354/meps306017

Carr, M. H., Robinson, S. P., Wahle, C., Davis, G., Kroll, S., Murray, S., et al. (2017). The central importance of ecological spatial connectivity to effective coastal marine protected areas and to meeting the challenges of climate change in the marine environment. *Aquat. Conservation: Mar. Freshw. Ecosyst.* 27, 6–29. doi: 10.1002/aqc.2800

Conroy, J. A., Reiss, C. S., Gleiber, M. R., and Steinberg, D. K. (2020). Linking Antarctic krill larval supply and recruitment along the Antarctic peninsula. *Integr. Comp. Biol.* 60, 1386. doi: 10.1093/icb/icaa111

Constable, A. J., and Kawaguchi, S. (2018). Modelling growth and reproduction of Antarctic krill, *Euphausia superba*, based on temperature, food and resource allocation amongst life history functions. *ICES J. Mar. Sci.* 75, 738–750. doi: 10.1093/icesjms/fsx190

Constable, A., and Nicol, S. (2002). Defining smaller-scale management units to further develop the ecosystem approach in managing large-scale pelagic krill fisheries in antarctica. *Ccamlr Sci.* 9, 117–131.

Cox, M. J., Candy, S., de la Mare, W. K., Nicol, S., Kawaguchi, S., and Gales, N. (2018). No evidence for a decline in the density of Antarctic krill *Euphausia superba* Dana 1850, in the southwest Atlantic sector between 1976 and 2016. *J. Crustacean Biol.* 38, 656–661. doi: 10.1093/jcbiol/ruy072

Cury, P. M., Shin, Y.-J., Planque, B., Durant, J. M., Fromentin, J.-M., Kramer-Schadt, S., et al. (2008). Ecosystem oceanography for global change in fisheries. *Trends Ecol. Evol.* 23, 338–346. doi: 10.1016/j.tree.2008.02.005

Daly, K. L. (2004). Overwintering growth and development of larval *Euphausia superba*: an interannual comparison under varying environmental conditions west of the Antarctic peninsula. *Deep Sea Res. Part II: Topical Stud. Oceanography* 51, 2139–2168. doi: 10.1016/j.dsr2.2004.07.010

Davis, L. B., Hofmann, E. E., Klinck, J. M., Piñones, A., and Dinniman, M. S. (2017). Distributions of krill and antarctic silverfish and correlations with environmental variables in the western ross sea, antarctica. *Mar. Ecol. Prog. Ser.* 584, 45–65. doi: 10.3354/meps12347

Dragon, A.-C., Senina, I., Hintzen, N., and Lehodey, P. (2018). Modelling south pacific jack mackerel spatial population dynamics and fisheries. *Fisheries Oceanography* 27, 97–113. doi: 10.1111/fog.12234

Eyring, V., Bony, S., Meehl, G. A., Senior, C. A., Stevens, B., Stouffer, R. J., et al. (2016). Overview of the coupled model intercomparison project phase 6 (cmip6) experimental design and organization. *Geoscientific Model. Dev.* 9, 1937–1958. doi: 10.5194/gmd-9-1937-2016

Fach, B. A., and Klinck, J. M. (2006). Transport of Antarctic krill (*Euphausia superba*) across the Scotia sea. part I: circulation and particle tracking simulations. *Deep Sea Res. Part I: Oceanographic Res. Papers* 53, 987–1010. doi: 10.1016/j.dsr.2006.03.006

Frazer, T. K. (2002). Abundance, sizes and developmental stages of larval krill, *Euphausia superba*, during winter in ice-covered seas west of the Antarctic peninsula. *J. Plankton Res.* 24, 1067–1077. doi: 10.1093/plankt/24.10.1067

Godlewska, M., and Klusek, Z. (1987). Vertical distribution and diurnal migrations of krill ? *Euphausia superba* Dana ? from hydroacoustical observations, SIBEX, December 1983/January 1984. *Polar Biol.* 8, 17–22. doi: 10.1007/bf00297159

Green, D. B., Bestley, S., Corney, S. P., Trebilco, R., Lehodey, P., and Hindell, M. A. (2021). Modeling Antarctic krill circumpolar spawning habitat quality to identify regions with potential to support high larval production. *Geophysical Res. Lett.* 48, e2020GL091206. doi: 10.1029/2020GL091206

Green, D. B., Bestley, S., Corney, S. P., Trebilco, R., Makhado, A. B., Lehodey, P., et al. (2023). Modelled prey fields predict marine predator foraging success. *Ecol. Indic.* 147, 109943. doi: 10.1016/j.ecolind.2023.109943

Green, D. B., Bestley, S., Trebilco, R., Corney, S. P., Lehodey, P., McMahon, C. R., et al. (2020). Modelled mid-trophic pelagic prey fields improve understanding of marine predator foraging behaviour. *Ecography* 43, 1014–1026. doi: 10.1111/ecog.04939

Hagen, W., and Auel, H. (2001). Seasonal adaptations and the role of lipids in oceanic zooplankton. presented at the 94th annual meeting of the deutsche zoologische gesellschaft in osnabrück, June 4–8, 2001. *Zoology* 104, 313–326. doi: 10.1078/0944-2006-00037

Hernandez, O., Lehodey, P., Senina, I., Echevin, V., Ayón, P., Bertrand, A., et al. (2014). Understanding mechanisms that control fish spawning and larval recruitment: parameter optimization of an eulerian model (SEAPODYM-SP) with Peruvian anchovy and sardine eggs and larvae data. *Prog. Oceanogr.* 123, 105–122. doi: 10.1016/j.pocean.2014.03.001

Hill, S. L., Phillips, T., and Atkinson, A. (2013). Potential climate change effects on the habitat of Antarctic krill in the weddell quadrant of the southern ocean. *PloS One* 8, e72246. doi: 10.1371/journal.pone.0072246

Hinke, J. T., Cossio, A. M., Goebel, M. E., Reiss, C. S., Trivelpiece, W. Z., and Watters, G. M. (2017). Identifying risk: concurrent overlap of the Antarctic krill fishery with krill-dependent predators in the Scotia Sea. *PloS One* 12, e0170132. doi: 10.1371/journal.pone.0170132

Hoffman, J. I., Chen, R. S., Vendrami, D. L., Paijmans, A. J., Dasmahapatra, K. K., and Forcada, J. (2022). Demographic reconstruction of antarctic fur seals supports the krill surplus hypothesis. *Genes* 13, 541. doi: 10.3390/genes13030541

Hofmann, E. E., Capella, J. E., Ross, R. M., and Quetin, L. B. (1992). Models of the early life history of *Euphausia superba*–part i. time and temperature dependence during the descent-ascent cycle. *Deep Sea Res. Part I. Oceanographic Res. Papers* 39, 1177–1200. doi: 10.1016/0198-0149(92)90063-Y

Hofmann, E. E., and Hüsrevoğlu, Y. S. (2003). A circumpolar modeling study of habitat control of Antarctic krill (*Euphausia superba*) reproductive success. *Deep Sea Res. Part II: Topical Stud. Oceanography* 50, 3121–3142. doi: 10.1016/j.dsr2.2003.07.012

Hosie, G. W., Ikeda, T., and Stolp, M. (1988). Distribution, abundance and population structure of the Antarctic krill (*Euphausia superba* Dana) in the prydz bay region, Antarctica. *Polar Biol.* 8, 213–224. doi: 10.1007/bf00443453

Ikeda, T. (1984). Development of the larvae of the Antarctic krill (*Euphausia superba* Dana) observed in the laboratory. *J. Exp. Mar. Biol. Ecol.* 75, 107–117. doi: 10.1016/0022-0981(84)90175-8

Jia, Z., Virtue, P., Swadling, K. M., and Kawaguchi, S. (2014). A photographic documentation of the development of Antarctic krill (*Euphausia superba*) from egg to early juvenile. *Polar Biol.* 37, 165–179. doi: 10.1007/s00300-013-1420-7

Jones, B. T., Solow, A., and Ji, R. (2016). Resource allocation for lagrangian tracking. *J. Atmospheric Oceanic Technol.* 33, 1225–1235. doi: 10.1175/jtech-d-15-0115.1

Ju, S.-J., and Harvey, H. R. (2004). Lipids as markers of nutritional condition and diet in the Antarctic krill *Euphausia superba* and *Euphausia crystallorophias* during austral winter. *Deep Sea Res. Part II: Topical Stud. Oceanography* 51, 2199–2214. doi: 10.1016/j.dsr2.2004.08.004

Kawaguchi, S. (2016). "Reproduction and larval development in Antarctic krill (Euphausia superba)," in *Biology and ecology of Antarctic krill*. Ed. V. Siegel (Basel, Switzerland: Springer), 225–246. doi: 10.1007/978-3-319-29279-3_6

Kawaguchi, S., and Satake, M. (1994). Relationship between recruitment of the Antarctic krill and the degree of ice cover near the south Shetland islands. *Fisheries Sci.* 60, 123–124. doi: 10.2331/fishsci.60.123

Kawaguchi, S., Yoshida, T., Finley, L., Cramp, P., and Nicol, S. (2007). The krill maturity cycle: a conceptual model of the seasonal cycle in Antarctic krill. *Polar Biol.* 30, 689–698. doi: 10.1007/s00300-006-0226-2

Krüger, L., Huerta, M. F., Santa Cruz, F., and Cárdenas, C. A. (2021). Antarctic Krill fishery effects over penguin populations under adverse climate conditions: implications for the management of fishing practices. *Ambio* 50, 560–571. doi: 10.1007/s13280-020-01386-w

Kurtz, N. T., and Markus, T. (2012). Satellite observations of antarctic sea ice thickness and volume. *J. Geophysical Research: Oceans* 117. doi: 10.1029/2012JC008141

La, H. S., Lee, H., Fielding, S., Kang, D., Ha, H. K., Atkinson, A., et al. (2015). High density of ice krill (euphausia crystallorophias) in the amundsen sea coastal polynya, antarctica. *Deep Sea Res. Part I: Oceanographic Res. Papers* 95, 75–84. doi: 10.1016/j.dsr.2014.09.002

Lancelot, C., Mathot, S., Veth, C., and de Baar, H. (1993). Factors controlling phytoplankton ice-edge blooms in the marginal ice-zone of the northwestern Weddell Sea during sea ice retreat 1988: field observations and mathematical modelling. *Polar Biol.* 13, 377–387.

Lehodey, P. (2004). *A spatial ecosystem and populations dynamics model (SEAPODYM) for tuna and associated oceanic top-predator species: part I – lower and intermediate trophic components* (Noumea, New Caledonia: Oceanic Fisheries Programme, Secretariat of the Pacific Community).

Lehodey, P., Conchon, A., Senina, I., Domokos, R., Calmettes, B., Jouanno, J., et al. (2015). Optimization of a micronekton model with acoustic data. *ICES J. Mar. Sci.* 72, 1399–1412. doi: 10.1093/icesjms/fsu233

Lehodey, P., Murtugudde, R., and Senina, I. (2010). Bridging the gap from ocean models to population dynamics of large marine predators: a model of mid-trophic functional groups. *Prog. Oceanogr.* 84, 69–84. doi: 10.1016/j.pocean.2009.09.008

Lehodey, P., Senina, I., and Murtugudde, R. (2008). A spatial ecosystem and populations dynamics model (SEAPODYM)–modeling of tuna and tuna-like populations. *Prog. Oceanogr.* 78, 304–318. doi: 10.1016/j.pocean.2008.06.004

Levin, S. A. (1992). The problem of pattern and scale in ecology: the Robert h. MacArthur award lecture. *Ecology* 73, 1943–1967. doi: 10.2307/1941447

Loeb, V. J., Hofmann, E. E., Klinck, J. M., Holm-Hansen, O., and White, W. B. (2009). ENSO and variability of the Antarctic peninsula pelagic marine ecosystem. *Antarctic Sci.* 21, 135–148. doi: 10.1017/s0954102008001636

Lowther, A. D., Staniland, I., Lydersen, C., and Kovacs, K. M. (2020). Male Antarctic Fur seals: neglected food competitors of bioindicator species in the context of an increasing Antarctic krill fishery. *Sci. Rep.* 10, 1–12. doi: 10.1038/s41598-020-75148-9

Marrari, M., Daly, K. L., and Hu, C. (2008). Spatial and temporal variability of SeaWiFS chlorophyll a distributions west of the Antarctic peninsula: implications for krill production. *Deep Sea Res. Part II: Topical Stud. Oceanography* 55, 377–392. doi: 10.1016/j.dsr2.2007.11.011

Maury, O. (2010). An overview of APECOSM, a spatialized mass balanced "Apex predators ECOSystem model" to study physiologically structured tuna population dynamics in their ecosystem. *Prog. Oceanogr.* 84, 113–117. doi: 10.1016/j.pocean.2009.09.013

McCormack, S. A., Melbourne-Thomas, J., Trebilco, R., Blanchard, J. L., and Constable, A. (2020). Alternative energy pathways in southern ocean food webs: insights from a balanced model of prydz bay, antarctica. *Deep Sea Res. Part II: Topical Stud. Oceanography* 174, 104613. doi: 10.1016/j.dsr2.2019.07.001

Melbourne-Thomas, J., Corney, S. P., Trebilco, R., Meiners, K. M., Stevens, R. P., Kawaguchi, S., et al. (2016). Under ice habitats for Antarctic krill larvae: could less mean more under climate warming? *Geophys. Res. Lett.* 43, 10322–10327. doi: 10.1002/2016gl070846

Meyer, B., Atkinson, A., Bernard, K. S., Brierley, A. S., Driscoll, R., Hill, S. L., et al. (2020). Successful ecosystem-based management of Antarctic krill should address uncertainties in krill recruitment, behaviour and ecological adaptation. *Commun. Earth Environ.* 1, 1–12. doi: 10.1038/s43247-020-00026-1

Meyer, B., Atkinson, A., Stöbing, D., Oettl, B., Hagen, W., and Bathmann, U. V. (2002). Feeding and energy budgets of Ant arctic krill Euphausia superba at the onset of winter. I.Furcilia III larvae. *Limnol. Oceanogr.* 47, 943–952.

Meyer, B., Freier, U., Grimm, V., Groeneveld, J., Hunt, B. P. V., Kerwath, S., et al. (2017). The winter pack-ice zone provides a sheltered but food-poor habitat for larval Antarctic krill. *Nat. Ecol. Evol.* 1, 1853–1861. doi: 10.1038/s41559-017-0368-3

Meyer, B., and Oettl, B. (2005). Effects of short-term starvation on composition and metabolism of larval Antarctic krill euphausia superba. *Mar. Ecol. Prog. Ser.* 292, 263–270. doi: 10.3354/meps292263

Mori, M., Corney, S. P., Melbourne-Thomas, J., Klocker, A., Kawaguchi, S., Constable, A., et al. (2019). Modelling dispersal of juvenile krill released from the Antarctic ice edge: ecosystem implications of ocean movement. *J. Mar. Syst.* 189, 50–61. doi: 10.1016/j.jmarsys.2018.09.005

Murase, H., Kitakado, T., Hakamada, T., Matsuoka, K., Nishiwaki, S., and Naganobu, M. (2013). Spatial distribution of antarctic minke whales (b alaenoptera bonaerensis) in relation to spatial distributions of krill in the ross sea, antarctica. *Fisheries Oceanography* 22, 154–173. doi: 10.1111/fog.12011

Murphy, E. J., Thorpe, S. E., Tarling, G. A., Watkins, J. L., Fielding, S., and Underwood, P. (2017). Restricted regions of enhanced growth of Antarctic krill in the circumpolar southern ocean. *Sci. Rep.* 7, 6963. doi: 10.1038/s41598-017-07205-9

Murphy, E. J., Watkins, J. L., Trathan, P. N., Reid, K., Meredith, M. P., Thorpe, S. E., et al. (2007). Spatial and temporal operation of the Scotia Sea ecosystem: a review of large-scale links in a krill centred food web. *Philos. Trans. R. Soc. B: Biol. Sci.* 362, 113–148. doi: 10.1098/rstb.2006.1957

Nicol, S., Foster, J., and Kawaguchi, S. (2012). The fishery for Antarctic krill - recent developments. *Fish Fisheries* 13, 30–40. doi: 10.1111/j.1467-2979.2011.00406.x

Orsi, A. H., Whitworth, T., and Nowlin, W. D. (1995). On the meridional extent and fronts of the Antarctic circumpolar current. *Deep Sea Res. Part I: Oceanographic Res. Papers* 42, 641–673. doi: 10.1016/0967-0637(95)00021-w

Pakhomov, E. A. (1995a). Demographic studies of Antarctic krill *Euphausia superba* in the cooperation and cosmonaut seas (Indian sector of the southern ocean). *Mar. Ecol. Prog. Ser.* 119, 45–61. doi: 10.3354/meps119045

Pakhomov, E. A. (1995b). Natural age-dependent mortality rates of Antarctic krill *Euphausia superba* Dana in the Indian sector of the southern ocean. *Polar Biol.* 15, 69–71. doi: 10.1007/BF00236127

Perry, F. A., Kawaguchi, S., Atkinson, A., Sailley, S. F., Tarling, G. A., Mayor, D. J., et al. (2020). Temperature–induced hatch failure and nauplii malformation in Antarctic krill. *Front. Mar. Sci.* 7. doi: 10.3389/fmars.2020.00501

Piñones, A., and Fedorov, A. V. (2016). Projected changes of Antarctic krill habitat by the end of the 21st century. *Geophys. Res. Lett.* 43, 8580–8589. doi: 10.1002/2016GL069656

Rassweiler, A., Ojea, E., and Costello, C. (2020). Strategically designed marine reserve networks are robust to climate change driven shifts in population connectivity. *Environ. Res. Lett.* 15, 34030. doi: 10.1088/1748-9326/ab6a25

Romagosa, M., Pérez-Jorge, S., Cascão, I., Mouriño, H., Lehodey, P., Pereira, A., et al. (2021). Food talk: 40-Hz fin whale calls are associated with prey biomass. *Proc. R. Soc. B: Biol. Sci.* 288, 20211156. doi: 10.1098/rspb.2021.1156

Rosenberg, A. A., Beddington, J. R., and Basson, M. (1986). Growth and longevity of krill during the first decade of pelagic whaling. *Nature* 324, 152–154. doi: 10.1038/324152a0

Ross, R. M., and Quetin, L. B. (1989). Energetic cost to develop to the first feeding stage of *Euphausia superba* Dana and the effect of delays in food availability. *J. Exp. Mar. Biol. Ecol.* 133, 103–127. doi: 10.1016/0022-0981(89)90161-5

Ryabov, A. B., De Roos, A. M., Meyer, B., Kawaguchi, S., and Blasius, B. (2017). Competition-induced starvation drives large-scale population cycles in Antarctic krill. *Nat. Ecol. Evol.* 1, 1–8. doi: 10.1038/s41559-017-0177

Santora, J. A., Rogers, T. L., Cimino, M. A., Sakuma, K. M., Hanson, K. D., Dick, E., et al. (2021). Diverse integrated ecosystem approach overcomes pandemic-related fisheries monitoring challenges. *Nat. Commun.* 12, 6492. doi: 10.1038/s41467-021-26484-5

Santora, J. A., Sydeman, W. J., Messié, M., Chai, F., Chao, Y., Thompson, S. A., et al. (2013). Triple check: observations verify structural realism of an ocean ecosystem model. *Geophysical Res. Lett.* 40, 1367–1372. doi: 10.1002/grl.50312

Saunders, R. A., Hill, S. L., Tarling, G. A., and Murphy, E. J. (2019). Myctophid fish (family myctophidae) are central consumers in the food web of the Scotia Sea (Southern ocean). *Front. Mar. Sci.* 6. doi: 10.3389/fmars.2019.00530

Savoca, M. S., Czapanskiy, M. F., Kahane-Rapport, S. R., Gough, W. T., Fahlbusch, J. A., Bierlich, K., et al. (2021). Baleen whale prey consumption based on high-resolution foraging measurements. *Nature* 599, 85–90. doi: 10.1038/s41586-021-03991-5

Schmidt, K., Atkinson, A., Venables, H. J., and Pond, D. W. (2012). Early spawning of Antarctic krill in the Scotia Sea is fuelled by "superfluous" feeding on non-ice associated phytoplankton blooms. *Deep Sea Res. Part II: Topical Stud. Oceanography* 59, 159–172. doi: 10.1016/j.dsr2.2011.05.002

Seidl, R. (2017). To model or not to model, that is no longer the question for ecologists. *Ecosystems* 20, 222–228. doi: 10.1007/s10021-016-0068-x

Senina, I. N., Lehodey, P., Sibert, J., and Hampton, J. (2020). Integrating tagging and fisheries data into a spatial population dynamics model to improve its predictive skills. *Can. J. Fisheries Aquat. Sci.* 77 (3), 576–593. doi: 10.1139/cjfas-2018-0470

Senina, I. N., Sibert, J., and Lehodey, P. (2008). Parameter estimation for basin-scale ecosystem-linked population models of large pelagic predators: application to skipjack tuna. *Prog. Oceanogr.* 78, 319–335. doi: 10.1016/j.pocean.2008.06.003

Siegel, V. (2012). Krill stocks in high latitudes of the Antarctic lazarev Sea: seasonal and interannual variation in distribution, abundance and demography. *Polar Biol.* 35, 1151–1177. doi: 10.1007/s00300-012-1162-y

Siegel, V., and Loeb, V. (1994). Length and age at maturity of Antarctic krill. *Antarctic Sci.* 6, 479–482. doi: 10.1017/s0954102094000726

Siegel, V., and Watkins, J. L. (2016). "Distribution biomass and demography of Antarctic krill euphausia superba," in *Biology and ecology of Antarctic krill*. Ed. V. Siegel (Basel, Switzerland: Springer), 21–100.

Spiridonov, V. (1995). Spatial and temporal variability in reproductive timing of Antarctic krill (*Euphausia superba* Dana). *Polar Biol.* 15, 161–174. doi: 10.1007/bf00239056

Stammerjohn, S., Maksym, T., Massom, R., Lowry, K., Arrigo, K., Yuan, X., et al. (2015). Seasonal sea ice changes in the amundsen sea, antarctica, over the period of 1979–2014 seasonal sea ice changes in the amundsen sea. *Elementa: Sci. Anthropocene* 3. doi: 10.12952/journal.elementa.000055

Tarling, G. A. (2020). Routine metabolism of Antarctic krill (*Euphausia superba*) in south Georgia waters: absence of metabolic compensation at its range edge. *Mar. Biol.* 167, 1–15. doi: 10.1007/s00227-020-03714-w

Tarling, G. A., Shreeve, R. S., Hirst, A. G., Atkinson, A., Pond, D. W., Murphy, E. J., et al. (2006). Natural growth rates in Antarctic krill (*Euphausia superba*): i. improving methodology and predicting intermolt period. *Limnol. Oceanogr.* 51, 959–972. doi: 10.4319/lo.2006.51.2.0959

Thorpe, S. E., Murphy, E. J., and Watkins, J. L. (2007). Circumpolar connections between Antarctic krill (*Euphausia superba* Dana) populations: investigating the roles of ocean and sea ice transport. *Deep Sea Res. Part I: Oceanographic Res. Papers* 54, 792–810. doi: 10.1016/j.dsr.2007.01.008

Thorpe, S. E., Tarling, G. A., and Murphy, E. J. (2019). Circumpolar patterns in Antarctic krill larval recruitment: an environmentally driven model. *Mar. Ecol. Prog. Ser.* 613, 77–96. doi: 10.3354/meps12887

Trebilco, R., Melbourne-Thomas, J., Sumner, M., Wotherspoon, S., and Constable, A. (2019). Assessing status and trends of open ocean habitats: a regionally resolved approach and southern ocean application. *Ecol. Indic.* 107, 105616. doi: 10.1016/j.ecolind.2019.105616

Treml, E. A., Halpin, P. N., Urban, D. L., and Pratson, L. F. (2008). Modeling population connectivity by ocean currents, a graph-theoretic approach for marine conservation. *Landscape Ecol.* 23, 19–36. doi: 10.1007/s10980-007-9138-y

Veytia, D., Bestley, S., Kawaguchi, S., Meiners, K. M., Murphy, E. J., Fraser, A. D., et al. (2021). Overwinter sea-ice characteristics important for Antarctic krill recruitment in the southwest Atlantic. *Ecol. Indic.* 129, 107934. doi: 10.1016/j.ecolind.2021.107934

Veytia, D., Bestley, S., Meiners, K., Kawaguchi, S., Murphy, E., Kusahara, K., et al. (2022). Quality of sea-ice habitat traversed by Antarctic krill larvae influences recruitment success. *Res. Square*. doi: 10.21203/rs.3.rs-1255733/v1

Veytia, D., Corney, S., Meiners, K. M., Kawaguchi, S., Murphy, E. J., and Bestley, S. (2020). Circumpolar projections of Antarctic krill growth potential. *Nat. Climate Change* 10, 568–575. doi: 10.1038/s41558-020-0758-4

Walsh, J., Reiss, C., and Watters, G. (2020). Flexibility in Antarctic krill *Euphausia superba* decouples diet and recruitment from overwinter sea-ice conditions in the northern Antarctic peninsula. *Mar. Ecol. Prog. Ser.* 642, 1–19. doi: 10.3354/meps13325

Warwick-Evans, V., Kelly, N., Dalla Rosa, L., Friedlaender, A., Hinke, J., Kim, J., et al. (2022). Using seabird and whale distribution models to estimate spatial consumption of krill to inform fishery management. *Ecosphere* 13, e4083. doi: 10.1002/ecs2.4083

Wiedenmann, J., Cresswell, K. A., and Mangel, M. (2009). Connecting recruitment of Antarctic krill and sea ice. *Limnol. Oceanogr.* 54, 799–811. doi: 10.4319/lo.2009.54.3.0799

Wilson, S. E., Swalethorp, R., Kjellerup, S., Wolverton, M. A., Ducklow, H. W., and Yager, P. L. (2015). Meso-and macro-zooplankton community structure of the amundsen sea polynya, antarctica (summer 2010–2011) zooplankton community structure of the amundsen sea polynya, antarctica. *Elementa: Sci. Anthropocene* 3. doi: 10.12952/journal.elementa.000033

Worby, A. (2004). Studies of the Antarctic sea ice edge and ice extent from satellite and ship observations. *Remote Sens. Environ.* 92, 98–111. doi: 10.1016/j.rse.2004.05.007

frontiers | Frontiers in Marine Science

TYPE Original Research
PUBLISHED 23 October 2023
DOI 10.3389/fmars.2023.1278229

Check for updates

OPEN ACCESS

EDITED BY
Matt Rayner,
Auckland Museum, New Zealand

REVIEWED BY
Akinori Takahashi,
National Institute of Polar Research, Japan
David Ainley,
H.T. Harvey & Associates, United States

*CORRESPONDENCE
Benjamin Viola
benjamin.viola@utas.edu.au;
benjamin.viola@aad.gov.au

RECEIVED 16 August 2023
ACCEPTED 10 October 2023
PUBLISHED 23 October 2023

CITATION
Viola B, Wienecke B, Green C-P, Corney S, Raymond B, Southwell C, Sumner MD, Virtue P, Wotherspoon S and Emmerson L (2023) Marine distribution and habitat use by Snow Petrels *Pagodroma nivea* in East Antarctica throughout the non-breeding period.
Front. Mar. Sci. 10:1278229.
doi: 10.3389/fmars.2023.1278229

COPYRIGHT
© 2023 Viola, Wienecke, Green, Corney, Raymond, Southwell, Sumner, Virtue, Wotherspoon and Emmerson. This is an open-access article distributed under the terms of the Creative Commons Attribution License (CC BY). The use, distribution or reproduction in other forums is permitted, provided the original author(s) and the copyright owner(s) are credited and that the original publication in this journal is cited, in accordance with accepted academic practice. No use, distribution or reproduction is permitted which does not comply with these terms.

Marine distribution and habitat use by Snow Petrels *Pagodroma nivea* in East Antarctica throughout the non-breeding period

Benjamin Viola[1,2]*, Barbara Wienecke[2], Cara-Paige Green[1], Stuart Corney[1,3], Ben Raymond[1,2], Colin Southwell[2], Michael D. Sumner[1,2], Patti Virtue[1,2], Simon Wotherspoon[1,2] and Louise Emmerson[2]

[1]Institute for Marine and Antarctic Studies, University of Tasmania, Hobart, TAS, Australia, [2]Department of Climate Change, Energy, the Environment, and Water, Australian Antarctic Division, Kingston, TAS, Australia, [3]Australia Antarctic Program Partnership, University of Tasmania, Hobart, TAS, Australia

The relationships between flying Antarctic seabirds and their at-sea environments remain poorly understood, particularly outside of the breeding season. Improving our knowledge of how these marine predators use their habitat is a critical step towards conservation of these species. We tracked 27 adult Snow Petrels from two large breeding colonies in East Antarctica during the Austral winter (non-breeding period) – when they are primarily at sea away from their nesting sites. During this time, Snow Petrel habitat use was most associated with bathymetry (> 5000 m), low sea-surface height, relatively close distance to the southern boundary of the Antarctic Circumpolar Current, relatively close distance to the ice-edge, relatively high sea-ice concentration, and low sea-surface temperature. Individuals displayed various movement patterns: 20 birds occupied overlapping winter areas that ranged broadly (up to 2000 km) from their breeding sites. The remaining birds ventured far beyond their breeding sites – reaching a maximal distance from the colony of 5,268 km. One individual circumnavigated Antarctica. Daily activity patterns were related to day length, with peak activity occurring near dawn and dusk. Nocturnal activity increased from March until August/September. Key results reveal and depict Snow Petrel habitat maps for the non-breeding period in the East Antarctic region.

KEYWORDS

fulmarine petrels, GLS tracking, GLS tags, geolocation, seabirds, polar ecosystems, machine learning, boosting

1 Introduction

Understanding ecological interactions and habitat use are fundamental tenets in spatial ecology (Cox et al., 2018). Such an understanding is important for decision makers considering the use of resources in ecosystem-based management (Hawkes et al., 2011). However, gaining insights into ecosystem interactions can be difficult in marine settings, where most fauna are difficult to observe (Furness and Camphuysen, 1997; Roncon et al., 2018; Riaz et al., 2021). To overcome this obstacle, tracking devices that collect data *in situ* are often deployed on highly mobile marine predators (Bondavalli and Ulanowicz, 1999; Hazen et al., 2019; Hindell et al., 2020). Such predators are often active across large expanses of habitat, where they hunt prey from multiple trophic levels, and subsequently amplify trophic information across multiple spatiotemporal dimensions (Hazen et al., 2019).

In the Southern Ocean, seabirds are top-order predators, many of whom spend most of their life at sea, only returning to land (or in the case of Emperor Penguins (*Aptenodytes forsteri*), sea-ice) to breed (Brown, 1980; del Hoyo, 2020). This life strategy – shared with seals – makes seabirds more accessible to study, and *in situ* data collection more feasible, than other marine taxa. It also allows researchers to deploy and retrieve tracking devices from a reliable point of origin such as a breeding colony (Hipfner et al., 2020). Tracking devices can remotely collect large quantities of data over extended periods of time (Jaeger et al., 2017). This makes them particularly valuable in marine ecology, as synoptic, at-sea observations of marine species requires ship-time, and the capacity for this is generally limited (Viola et al., 2022). This limitation is amplified at high latitudes such as in the Southern Ocean where environmental conditions are harsh and extended marine-based field work is logistically difficult or hazardous (Poland et al., 2003).

Many seabirds travel distances of thousands, tens of thousands (MacLeod et al., 2008; Rayner et al., 2008; Pinet et al., 2011), or hundreds of thousands of kilometers every year (Weimerskirch et al., 2015). The at-sea distribution of seabirds varies seasonally (Menkhorst et al., 2017) with birds travelling to areas remote from their breeding sites during the non-breeding season (González-Solís et al., 2007; Hedd et al., 2012; Gilg et al., 2013). Variation in conditions encountered during the non-breeding season can affect important demographic parameters like breeding success and quality of parental care (Webster and Marra, 2005; Reudink et al., 2009; Puskic et al., 2019). And when considering species with high migratory connectivity — the degree to which migratory movements of an individual or a population are linked spatially and temporally between and within seasons — demographic parameters associated with gene flow and natal dispersal become important considerations (Steiner and Gaston, 2005). As seabirds may be susceptible to benefits and stressors not encountered in their terrestrial breeding territory (Davis et al., 2016), a thorough understanding of at-sea distribution is vital to their conservation. Resource managers (such as fisheries targeting the prey fields of important marine predators) need to remain cognisant of at-sea predator distributions throughout the year, and not just during the breeding season. Tracking seabirds throughout the non-breeding period is an important step in addressing these concerns.

Despite the advantages and importance of studying seabirds, and their global recognition as bio-indicators of ecosystem health (Burger and Gochfeld, 2004; Piatt et al., 2007; Hazen et al., 2019), there is a paucity of literature on Antarctic flying seabirds when compared to seabird species in temperate and equatorial regions, but also when compared to other Antarctic vertebrate fauna (i.e., pinnipeds, cetaceans, and penguins) (Ainley et al., 2012; Roncon et al., 2018). Antarctic ecosystems host a suite of flying and non-flying seabird species (Menkhorst et al., 2017; Harrison et al., 2021). Many of the flying seabirds belong to the family Procellariidae, of which the most diverse guild (in terms of body size) is the fulmarine petrels (Harrison et al., 2021).

The smallest fulmarine petrel is the Snow Petrel (*Pagodroma nivea*), whose body mass ranges from< 250 to nearly 500 g (Moe et al., 2007). Snow Petrels occupy a circumpolar breeding distribution (Croxall et al., 1995), and along with Antarctic Petrels (*Thalassoica antarctica*) and South Polar Skuas (*Catharacta maccormicki*), are the most southerly breeding birds (Weathers et al., 2000). Much of the recent work regarding Snow Petrels has focused on breeding ecology, breeding sites, or understanding historical conditions using paleo-ecological deposits (Amundsen, 1995; Barbraud and Chastel, 1999; Einoder et al., 2014; Younger et al., 2016; Berg et al., 2019; Carrea et al., 2019; McClymont et al., 2021). Snow Petrels breed during the austral summer, often in small colonies or loose aggregations, along the coast of Antarctica and surrounding islands (Olivier et al., 2004). However, some birds breed in mountain ranges deep inland, up to 440 km from the coast (Goldsworthy and Thomson, 2000; Thor and Low, 2011).

Whilst seemingly abundant, historical attempts to estimate the global population size for Snow Petrels have been inconclusive, and hence, a comprehensive measure of their abundance remains unknown (Croxall et al., 1995). A sound ecological understanding of Snow Petrels — and many other petrel species — remains elusive. Despite concerted efforts to gather data on these seabirds in the 1980s, 1990s and early 2000s, the number of published datasets that exist for petrels in the Antarctic regions is small (Olivier et al., 2004). Moreover, early records are usually anecdotal, making it difficult to identify changes in population size and patterns over time (Olivier et al., 2004). To date, much of what we understand about Snow Petrel marine habitat use is derived from shipboard surveys in the 1980's and 1990's (Ainley et al., 1993; Ribic et al., 2011). Shipboard data is extremely beneficial to our understanding of the pelagic distribution of seabirds, and many seabird communities have been described via this method (Ainley et al., 2012).

However, it is well established that integrating data from tracking studies with observational data substantially improves our understanding of the pelagic distribution of seabirds (Priddel et al., 2014). Occasional sightings near research stations in winter suggest that some individuals remain in Antarctica, either relatively close to their breeding sites, or inland, during the non-breeding period (AAD personnel, pers. comms.). Yet, the non-breeding distribution of these birds is still poorly documented. To date,

only one tracking study of birds breeding at Île des Pétrels, Pointe Géologie archipelago (66.67°S, 140.02°E), examined the movements of Snow Petrels during the non-breeding period (Delord et al., 2016). For all other colonies/breeding sites (> 195, based off estimates from Croxall et al., 1995), it remains unclear where important areas are during winter, or to what extent populations overlap and individuals share foraging habitat. Increasing our understanding of Snow Petrel habitat requirements will help create a baseline from which potentially threatening changes can be predicted and determined.

Hereby, to improve our understanding of how Snow Petrels use habitat during the non-breeding period, we deployed geolocators and concurrently tracked post-breeding Snow Petrels from two widely separated breeding sites in East Antarctica. Our aims were to determine their habitat use and foraging activity patterns throughout the non-breeding period, and to develop habitat suitability maps for the non-breeding period relevant to Snow Petrels in the East Antarctic region.

2 Methods

2.1 Study sites and field methods

Geolocator tracking devices (MK 18L geolocators (GLS), British Antarctic Survey) were fitted to incubating adult Snow Petrels at two widely separated breeding locations in East Antarctica: Béchervaise Island (67.59°S, 62.82°E), Mac. Robertson Land, and Filla Island (68.81°S, 77.83°E) in Prydz Bay, Princess Elizabeth Land (Figure 1). At Béchervaise Island, the birds were equipped with GLS

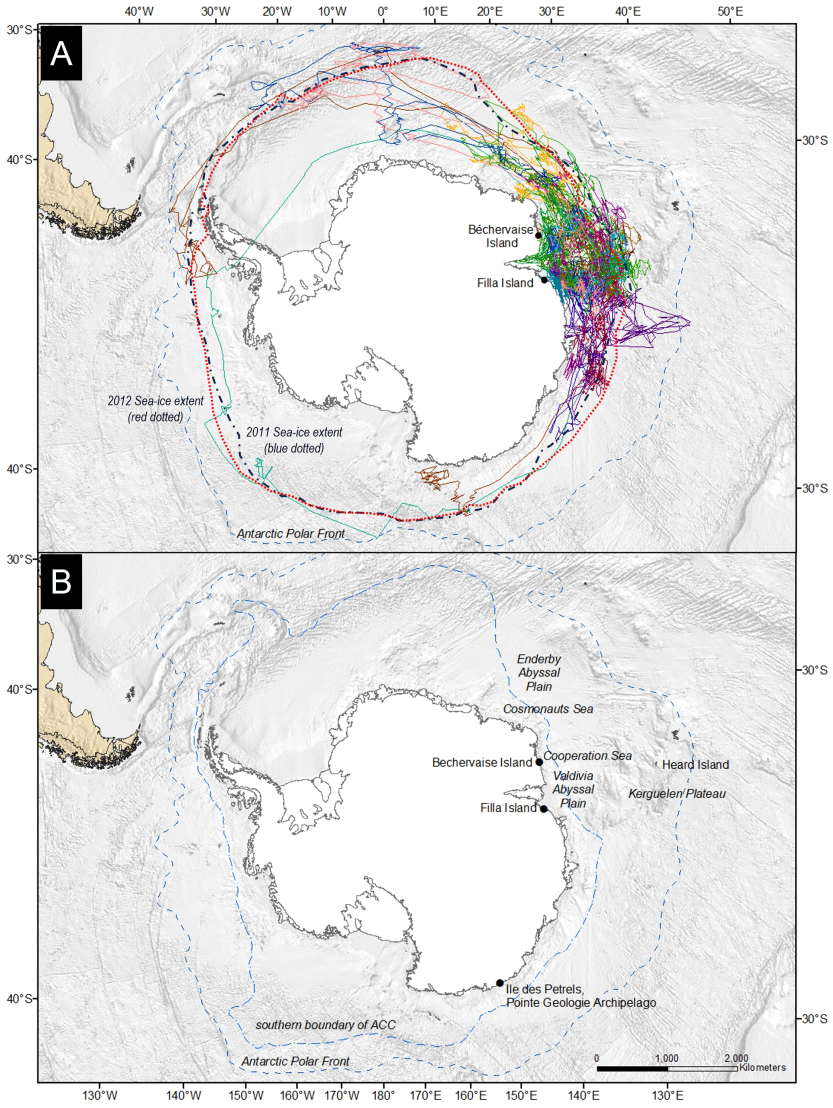


FIGURE 1
(A) Tracks of Snow Petrels *Pagodroma nivea* from Béchervaise and Filla islands in 2011 and 2012. Each colored solid line represents a tracked individual. The Antarctic Polar Front (or Antarctic Convergence) is shown as a dashed line. **(B)** Location of important sites and features mentioned within this manuscript. The southern boundary of the Antarctic Circumpolar Current (ACC) (light blue) and the Antarctic Polar Front (dark blue) are labelled and shown as dashed lines. The 2011 (blue) and 2012 (red) maximal sea-ice extents are added as dotted contours and labelled in **(A)**.

devices during the incubation stage from the 17th – 20th of January 2011 (n = 14), and from the 24th – 25th of January 2012 (n = 14). At Filla Island, devices were fitted from the 11th – 13th January 2011 (n = 10). Devices were attached with small cable ties to 12 mm wide, soft, double-sided Velcro©. The Velcro band was then wrapped around the birds' tarsi, and the end of the band was secured with an industrial strength superglue, Loctite 401. The combined weight of the device, cable ties, and Velcro was three grams, equivalent to ~1% of the birds' mean body mass. At Filla Island, eight of ten birds were recaptured in the following season and the devices retrieved. At Béchervaise Island, eight of 14 tags deployed in January 2011 were retrieved in December 2011, while two were recovered in December 2012. Nine of 14 birds equipped in January 2012 were recaptured in December 2012. All recovered tags delivered data.

2.2 Data analyses

Analyses were limited to data collected from the 1st of March — when a clear day-night cycle occurs at the latitudes under study, and all birds had left the colonies — until the 31st of October, just prior to the birds' return in early November (and subsequent tag retrieval). All data handling and processing occurred in Microsoft Excel (Microsoft Corporation 2018) and in the R statistical environment (R Core Team 2021) unless stated otherwise.

2.3 Tracking data

The geolocation tags recorded light levels every 10 minutes. The positions of individual birds were estimated using the light-level data twice daily (dawn and dusk) with the SGAT and BAStag packages (Sumner et al., 2009; Lisovski and Hahn, 2012). These packages apply a threshold method that determines twilight as the time at which the ambient light levels cross a predefined threshold (Sumner et al., 2009; Wotherspoon et al., 2013).

The GLS tags recorded saturation status (wet or dry) at three-second intervals and stored the data in five-minute bins. We assumed that the tags were always wet while a bird was feeding but dried quickly once a bird became airborne. Prolonged 'wet' activity was most likely associated with resting and/or preening on the ocean surface, but we acknowledge some feeding may have occurred when the sensor read wet over this time. 'Dry' activity included flying but also resting on a dry surface.

2.4 Distances travelled, at-sea movements, and activity patterns

To compare differences in distances travelled by Snow Petrels from the two deployment sites, Welch's t-tests were used. All means are given ± 1 SE, and the level of significance was set at p = 0.05 unless stated otherwise. The proportions of wet/dry activities were calculated per day per bird and summarised by month, as well as day. The loggers recorded time in UT (universal time). For the examination of cathemeral patterns, these data were adjusted to local times relative to the deployment location.

2.5 Habitat suitability, preference, and use

Throughout this manuscript, we use the following terms to describe subtly different, but related, conditions: 'Habitat' refers to the polar environment surrounding Snow Petrels; 'habitat use' refers to the environmental conditions in which tracked Snow Petrels were recorded (i.e. the habitats that they were observed to make use of); 'available habitat' refers to the environmental conditions that were accessible to (within flying distance of) the birds, and thus they could potentially have made use of; 'habitat preference' is a measure of habitat use relative to availability, whereby "preferred habitats" are environmental conditions that are used more often than would be expected according to their availability (the animals "prefer" to use these habitats). Note that habitat preference is based only on the environmental conditions of the area in question, and does not consider whether it is physically accessible to the animals. 'Habitat suitability' is a modified version of habitat preference that additionally accounts for the accessibility of the area in question. A given area might therefore have a high habitat preference value (indicating that it contains environmental conditions preferred by the animals), but a low habitat suitability if it is located far from the colony and therefore not readily accessible to the animals.

Tracks of geographic positions and expected flight activities (foraging/resting/travelling) were generated by a state-space model using the BSAM package (Jonsen et al., 2015). Once the track of each bird had been established, 50 random tracks were simulated for each observed track, using the availability package (Raymond et al., 2015; Reisinger et al., 2018). These simulated tracks provide an estimate of available geographic space from which available habitat (environmental conditions) can be inferred. By comparing the environmental conditions associated with simulated tracks to those of actual tracks, the model seeks to quantify preference. Explicitly, the model identifies Snow Petrel preference for environmental variables by comparing environmental conditions at known locations with a continuous array of points in space and time that reflect available habitat [see eqn. 1 below, Aarts et al. (2012)].

Equation 1:

$$f^u(X_i) = \frac{w(X_i)f^a(X_i)}{\int_{allX} w(X)f^a(X)dX} = K^{-1}w(X_i)f^a(X_i)$$

Here, habitat i denotes a unique point in environmental space X. Usage $f^u(X_i)$ and availability $f^a(X_i)$ are defined as two continuous probability density functions. Preference $w(X_i)$ is related to the ratio of habitat use over habitat availability $\left(w(X_i) \propto \frac{f^u(X_i)}{f^a(X_i)}\right)$. The denominator K is a normalizing constant ensuring that $f^u(X)$ integrates to 1 over all of X (Aarts et al., 2012). Put simply, the model compares simulated tracks to actual tracks and uses the environmental differences between them to infer habitat preference.

To ensure that simulated tracks remained in biologically plausible areas, a conservative limit of 40°S (Menkhorst et al., 2017) was set as the northern latitudinal boundary to the simulated tracks. A land mask was also used to constrain simulated tracks to remain over oceanic areas. Environmental variables were then sourced to match true and simulated tracks at values closest to the track date, time, latitude, and longitude. Variables included oceanic parameters such as sea-surface temperature, wind, eddy kinetic energy, and bathymetry that could be ecologically important (Hindell et al., 2020; Skov et al., 2021; Warwick-Evans et al., 2021), as well as Antarctic-specific variables such as sea-ice concentration, distance to open-water, distance to ice-edge, and ice category. Ice category information was based on Fraser et al. (2020) and allocates a value under the following classifications: 0 = pack ice or ocean; 1 = continent; 2 = islands; 3 = ice shelf; 4 = fast ice; 5 = manually derived fast ice edge; and 6 = automatically (i.e., reduced subjectivity) derived fast ice edge. Additionally, a suite of variables was acquired and used as a proxy for large environmental processes. These variables are described in detail in Table 1. Upon completing these steps, there were > 4.5 million data points with relevant environmental information for each point/simulated point.

Following Reisinger et al. (2018), we then used a case-control design that assigned location estimates from real tracks a value of 1, and those from simulated tracks (habitat available to any given individual Snow Petrel) a value of 0. Next, we used boosted regression trees (BRTs) to discriminate between real and simulated tracks based on their environmental covariates. Boosting is an iterative technique that adjusts the weight of an observation based on previous iterations (Boehmke and Greenwell, 2019). This approach vastly improves the predictive performance of a model (Boehmke and Greenwell, 2019), and works well for distribution modelling (Elith et al., 2008).

The output of this model ($w(X_i)$ from equation 1, above), is an estimate of the habitat preference of the environment X_i, associated with the i^{th} data point (Aarts et al., 2008). We used univariate and bivariate partial effects plots to understand the influence of each predictor variable on habitat preference. The birds were expected to vary their habitat preferences over the course of the winter season, but the standard method used for assessing variable importance in BRTs (the sum of the squared improvements over all internal nodes of the trees for which that variable was chosen as the split variable, see e.g. Friedman, 2001) does not easily allow changes in importance to be assessed over time. We therefore generated a bivariate interaction between day of year and each of the other predictor variables and, following the approach used by the vip package in R (Greenwell et al., 2022), calculated the standard deviation of each partial effect for each distinct day of year. This gives a time-varying measure of the importance of each predictor variable. At a time (day of year) when a predictor variable has no influence on the model output, its partial effect will be flat and standard deviation will be zero. The larger a variable's influence at other times, the greater the range of its partial effect and therefore the larger its standard deviation. Standard deviations were calculated on the response (probability) scale, and so these variable importance are comparable between predictor variables. The steps described above yield a model that statistically describes the difference between the habitats used by the animals and those available to them, thus giving an indication of habitat preference. We wanted to be able to predict from those models using a regional grid of environmental data to obtain a spatial depiction of suitable habitat in the region. To do so, it is also necessary to account for accessibility.

During the breeding period the birds are biologically constrained in terms of how far from their chick they can travel. A grid cell that is far from the colony is less likely to be suitable than one close to the colony, even if the cells contain identical environmental conditions. This distance constraint will likely change over time, becoming less pronounced as the non-breeding period progresses. However, the habitat preference models described above are fitted on training data from grid cells that are all available to the animals (i.e., all data came from cells that were visited by either a real or simulated track). The habitat preference models do not account for the fact that when predicting on new data, some of the cells in the new data might not be accessible to the animals. Accordingly, we fitted a second set of binomial models in a similar fashion to Reisinger et al. (2018), that assume accessibility to be a function solely of distance from the colony. A grid cell was deemed to be accessible if it contained any tracks (real or simulated), and inaccessible if it did not. Probability of accessibility was fitted as a non-increasing function of distance from colony, using the scam package in R (Pya, 2022).

A regional grid for each environmental variable was constructed by first acquiring data (on the native grid of the variable) over the circumpolar region south of 40°S, for the same variables used in fitting the models (Table 1). For time-varying variables, data were acquired for the relevant dates and averaged for each day over the winter period of each respective year. Each regional layer was resampled at a resolution of 0.1 degree to create a set of consistent, regional environmental layers.

Regional maps of suitable habitat were then produced by using the habitat preference models to infer habitat preference over the region using the regional environmental layers. The accessibility models were used to infer the accessibility of each grid cell in the regional grid, and the habitat suitability was calculated as the product of those two (Reisinger et al., 2018; Hindell et al., 2020):

Equation 2:

$$habitat\ \ suitability = H(X_i) \star p(accessible)$$

The habitat suitability values obtained by the procedure described above are not necessarily intuitive to interpret. The mean value of habitat preference is arbitrary and is controlled by the number of simulated tracks that were generated, because this controls the number of zeros in the training data (the number of simulated track points) relative to the number of ones (the number of real track points). To provide more intuitive plots, we rescaled the habitat suitability values following the percentile procedure of Raymond et al. (2015) and Hindell et al. (2020). Habitat suitability values above 80, for example, represent the top 20% (by area) of most suitable habitat.

TABLE 1 Environmental variables used for habitat modelling.

Variable	Spatial resolution	Temporal resolution	Source	Justification
Sea surface temperature (°C)	0.25°	Daily	NOAA OISST https://doi.org/10.1175/JCLI-D-20-0166.1	Considered an important driver of ecosystem dynamics that influences diversity, abundance, and richness of many species including those in prey fields (Tittensor et al., 2010; Hindell et al., 2020)
Sea surface temperature gradient	0.25°	Daily	Derived from SST as per http://australianantarcticdivision.github.io/raadtools/reference/index.html	Used to measure maximum rate of local change and is associated with frontal activity (Skov et al., 2021)
Sea surface height (m)	0.25°	Daily	SSALTO/DUACS experimental products distributed by AVISO+ with support from CNS https://tinyurl.com/yx997ksf	Associated with oceanic surface pressure, and other physical factors (Vivier et al., 1999; Talley et al., 2011)
Sea surface height anomaly (m)	0.25°	Daily	Derived from SSH as per http://australianantarcticdivision.github.io/raadtools/reference/index.html	Indicative of upwelling activity (Cropper et al., 2014)
Sea-ice concentration (%)	25 km grid	Daily	NSIDC Polar Stereographic Data https://tinyurl.com/bb3zr7r6	Known to affect marine and terrestrial ecosystem dynamics (Post et al., 2013), such as abundance and availability of prey (Emmerson et al., 2015)
Ice category	1000 m grid	15-day timestep	High-resolution mapping of circum-Antarctic sea-ice distribution, derived from polar stereographic grid by Fraser et al. https://essd.copernicus.org/articles/12/2987/2020/	Antarctic-specific variable that categorizes fine scale habitat type as described in text preceding this table
Wind (speed and direction) (m/s)	0.25° at 10 m	6-hourly	NOAA NCEP-DOE Reanalysis 2 https://psl.noaa.gov/data/gridded/data.ncep.reanalysis2.html https://tinyurl.com/2zn6zz24	Standard oceanographic parameter (Warwick-Evans et al., 2021) that also has ecological importance – particularly with relation to flying seabirds (Spear & Ainley, 2008)
Eddy Kinetic Energy (cm^2/s^2)	0.25°	Daily	Derived using link below. Data accessible via SSH source. http://knossos.eas.ualberta.ca/anha/data/EKE.pdf	Considered to be an important driver of ecosystem dynamics such as species diversity (Tittensor et al., 2010), correlated with ocean stratification and temperature (Cordero Quirós et al., 2022)
Bathymetry (m)	30 arc-second grid	N/A	GEBCO_08 gridded bathymetry data http://www.gebco.net/data_and_products/gridded_bathymetry_data/	Associated with oceanic properties and sea-ice dynamics (Sun et al., 2022)
Surface heat flux (W/m^2)	0.25°	Daily	Derived using AAD files http://australianantarcticdivision.github.io/raadtools/reference/index.html	Reveals areas where polynyas are present (Tamura et al., 2008; Malpress et al., 2017)
Distance to ice-edge (m)	12.5 km grid	Daily	Derived from sea-ice concentration as per http://australianantarcticdivision.github.io/raadtools/reference/index.html	Standard polar oceanic ecological parameter (Hindell et al., 2020). included to see if sea-ice drives presence during the winter months. The ice edge represents both the physical boundary between the sea ice and the open ocean, as well as an area of elevated primary and secondary productivity.
Distance to open water (m)	12.5 km grid	Daily	Derived from sea-ice concentration (code available on request)	Distance to nearest open water excluding any open-water pixel that is reachable from the open ocean (northern edge of the ice pack generally do not count, but holes in the pack margin do)
Distance to the southern boundary of the Antarctic Circumpolar Current (m)	0.125°	N/A (mean front position)	Derived from Park and Durand (2019) Altimetry-derived Antarctic Circumpolar Current fronts. https://doi.org/10.17882/59800. See reference list for full citations.	Many Antarctic marine fauna are bound by this feature (Clarke et al., 2005). This feature is known to have profound effects on Southern Ocean productivity (Sokolov & Rintoul, 2007)

N/A, Not applicable.

10.3389/fmars.2023.1278229

We assumed that the responses of birds to environmental features were the same regardless of colony or year, meaning that inter-annual or inter-colony differences in habitat usage are the result of differences in environmental conditions, rather than different responses to environmental conditions. We therefore fitted a single model to all data and present habitat suitability maps for these combined data. Notably, we also fitted separate models by year and colony, and present these outputs in the Supplementary Material. Encouragingly, the influence assigned to environmental variables on Snow Petrel presence by the boosted regression models did not show substantial differences between the inter-colony, inter-annual, or combined models.

3 Results

3.1 Deployment duration and distances travelled

Snow Petrels from Béchervaise Island were tracked for 330 ± 12 days. Two individuals were recaptured two years post-deployment after 695 and 701 days, respectively. At Filla Island, the petrels were recaptured after 361 ± 6 days. At both locations, all Snow Petrels had returned to their nests by the 10th of November. One individual performed a complete circumpolar navigation. Tracks are shown in Figure 1. The Snow Petrels from Béchervaise Island travelled on average 86,192 ± 2670 km and 106,077 ± 11,607 km in 2011 and 2012, respectively (Table 2). The difference was not statistically significant (Welch's t-test, $t_{11,916} = 2.17$, $p = 0.98$). The birds from Filla Island travelled 107,094 ± 16,735 km in 2011. This was not significantly different from the distances of Snow Petrels from Béchervaise Island in 2011 ($t_{7,840} = 10.32$, $p = 1.0$) (Table 2).

TABLE 2 Characteristics of winter movements of Snow Petrels *Pagodroma nivea* from two colonies in East Antarctica.

Variable	Béchervaise Island*	Filla Island
2011	(n = 9)	(n = 8)
Mean distance travelled per bird per year (km) ± standard error	86,192 ± 2670 (83,522–88,862)	107,094 ± 16,735 (90,360–123,829)
Maximal distance from colony (km)	~5500	~5900
Latitudinal range (°S)	55–72	49–72
Most westerly position (°W)	82.5	176.9
Most easterly position (°E)	174.5	178.2
2012	(n = 10)	
Mean distance travelled per bird per year (km) ± standard error	106,077 ± 11,607 (94,470–117,684)	–
Maximal distance from colony (km)	~3900	–
Latitudinal range (°S)	54–71	–
Most westerly position (°W)	35.0	–
Most easterly position (°E)	120.0	–

Differences between mean distance travelled per bird at Béchervaise Island and Filla Island (2011) were not significant ($p > 0.05$). Differences between mean distance travelled per bird at Béchervaise Island in 2011 and 2012 were not significant ($p > 0.05$).
*two birds carried tags for 2 years.

3.2 At-sea movements

In 2011, the main area used by Snow Petrels from Béchervaise in the non-breeding period covered waters near the southern Kerguelen Plateau and the Valdivia Abyssal Plain (Figure 1, but see also Supplementary Material). Generally, despite covering greater distance, and hosting the greatest vagrant within this study (Table 2), Snow Petrels from Filla Island remained closer to their breeding colony than birds from Béchervaise Island (Figure 2). For birds from both colonies in each year, the monthly distribution of individuals tended to remain within eastern longitudes, and at latitudes south of 54° (Figure 2).

3.3 Activity patterns

Tags remained dry for 55–73% of the time of deployment. Immersion/moisture sensor data alternating between wet and dry were attributed to feeding activity (herein: foraging), and accounted for 21–35% of recordings. The least time was spent with immersed sensors (wet) (7–18%), and such activity was attributed to rafting (resting on the water), preening, or extended feeding events. For all individuals, foraging times were shortest in March to May ranging from 21–27% for birds from Béchervaise Island, and from 22–39% for birds from Filla Island. In the remaining months, foraging status ranged from 30–32% and 31–35% at Béchervaise and Filla, respectively.

Foraging by birds from Filla occurred 43 ± 12% of the time during diurnal hours (57 ± 12% nocturnal). This was slightly lower (higher) than the foraging efforts observed for birds from Béchervaise 48 ± 12% diurnal (52 ± 12% nocturnal) (Figure 3). The diel differences between colony foraging were not statistically significant (ANOVA (day), $F = 0.791$, df =15, $p = 0.389$; ANOVA (night), $F = 0.856$, df =15, $p = 0.371$). However, throughout the tracking period, foraging activity changed for both colonies. From March until July, foraging activity was predominantly nocturnal (50–75%) and was highest in June and July. Petrels from Béchervaise switched to a diurnal pattern in August while the petrels from Filla did so in September (Figure 3).

3.4 Habitat suitability, preference, and use

The rank importance (ranked by relative importance of variable) of environmental predictors were similar between years and colonies. Bathymetry, sea-surface height, distance to the southern boundary of the Antarctic Circumpolar Current, distance to the ice-edge, sea-ice concentration, and sea-surface temperature were broadly found to be important predictors for single colony models, and the combined model (Table 3). Notably,

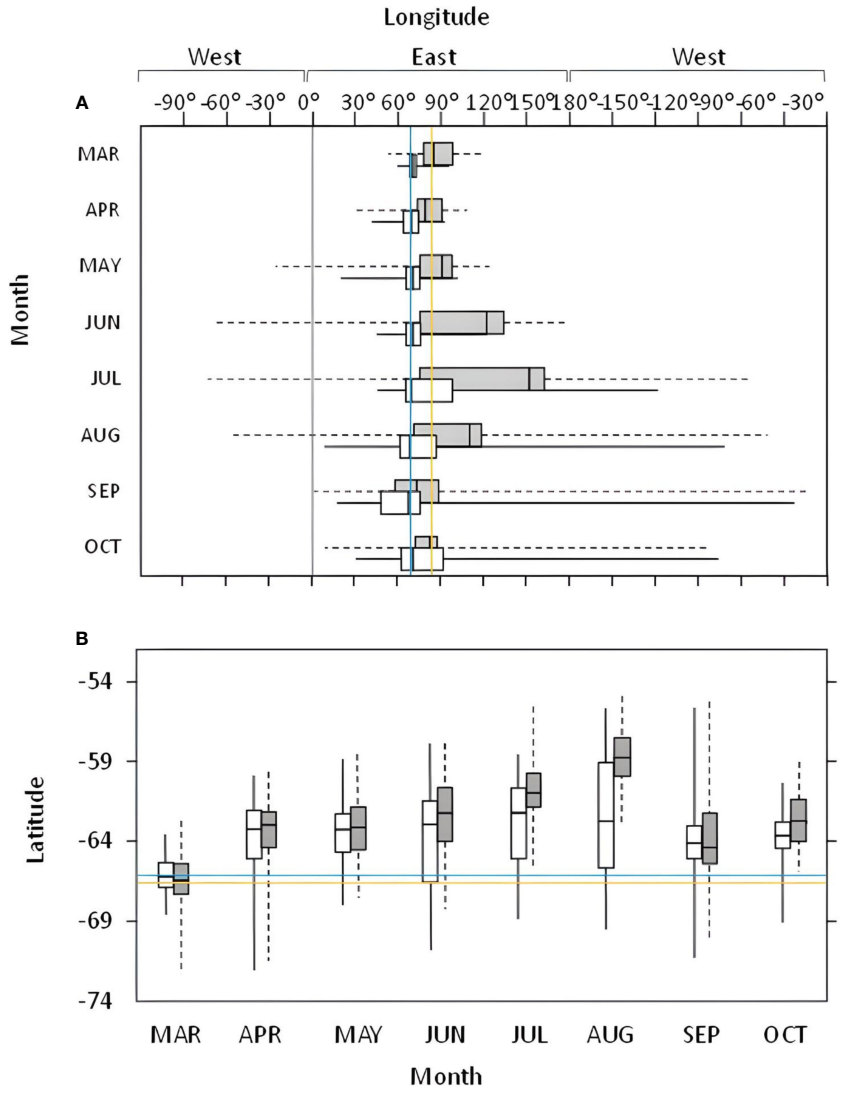


FIGURE 2
Box plots of monthly longitudinal **(A)** and latitudinal **(B)** distribution of Snow Petrels *Pagodroma nivea* from Béchervaise (grey), and Filla (white) islands in 2011. Colony locations are shown by the blue (Béchervaise), and yellow (Filla) lines. The 0-degree longitude line is shown in grey.

the partial plots for variable contribution (see Supplementary Material) show that bathymetric depths greater than 5000 meters were associated with more preferred habitat. Such deep features are not habitat features of direct relevance to a surface-feeding species, but rather are indicating the effect of depth on other environmental processes (such as circulation and subsequent sea-ice coverage, Sun et al., 2022).

The contribution of environmental variables changed temporally, and the importance of some variables, such as distance to the southern boundary of the Antarctic Circumpolar Current were found to be most important between April and May, before sharply dropping off in the later months (Figure 4). Other variables, such as distance to ice edge were consistently important during the non-breeding period (Figure 4).

Habitat suitability maps for Snow Petrels in the non-breeding period (Figure 5) show that suitable habitat was circumpolar, but with the higher values tending to be in areas closer to breeding sites. In June, suitable cells were observed further away from the coast, and continued to expand around west Antarctica until the end of the non-breeding cycle in October. The maps signify waters over the Kerguelen Plateau, and the Enderby and Valdivia Abyssal Plains as areas highly associated with Snow Petrel habitat suitability (a trend consistent with Figure 2). Highly suitable cells tend to be seen around the Cosmonaut Sea in earlier months, before shifting around to the Cooperation Sea in the later months. Maps and outputs for individual colonies are presented in the Supplementary Material.

4 Discussion

This work presents an important step in our understanding of Snow Petrel habitat suitability throughout the non-breeding period for two large colonies in East Antarctica. It provides habitat

10.3389/fmars.2023.1278229

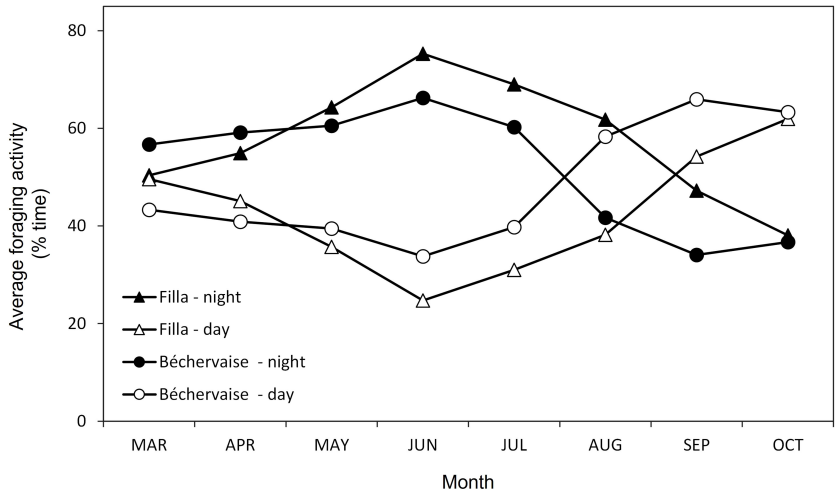


FIGURE 3
Monthly percentages of diurnal and nocturnal foraging activities of Snow Petrels *Pagodroma nivea* from Filla and Béchervaise islands in 2011.

suitability maps for Snow Petrels during the non-breeding period, and contributes to knowledge of their at-sea winter habitat requirements. The mean distances travelled by adult Snow Petrels were similar across years and between colonies, and in all cases, the mean distance travelled by individuals during the non-breeding period exceeded 80,000 km (Table 2). Individual tracks suggest a wide range of movement strategies throughout the winter – with four of 27 individuals reaching west Antarctica, and one individual performing a complete circumpolar navigation (Figure 1). To our knowledge, this is the first record of a Snow Petrel completing such a feat, though it is not uncommon for other, larger, Antarctic seabirds such as Wandering Albatross (*Diomedea exulans*) to perform single, double, or even triple circumnavigations over the course of a year (Weimerskirch et al., 2015).

Bathymetry, sea-surface height, distance to the southern boundary of the Antarctic Circumpolar Current, distance to the ice-edge, sea-ice concentration, and sea-surface temperature were important determinants of Snow Petrel habitat preference (Table 3,

TABLE 3 Influence of environmental variables on Snow Petrel (*Pagodroma nivea*) habitat preference as determined by boosted regression tree (BRT) analyses.

Variable	Béchervaise Island (2011)	Béchervaise Island (2012)	Filla Island (2011)	All
Sea surface temperature	3.43	13.95	15.26	8.91
Sea surface temperature gradient	0.88	0.69	0.19	0.53
Sea surface height	17.08	13.74	6.81	19.17
Sea surface height anomaly	2.05	0.81	0.77	1.03
Sea-ice concentration	5.39	9.55	6.65	9.34
Ice category	3.37	7.08	1.23	1.10
Wind	0.01	0.11	0.04	0.07
Eddy kinetic energy	2.19	0.61	1.50	1.05
Bathymetry	16.81	23.32	31.43	25.41
Surface heat flux	3.72	2.95	1.64	3.36
Distance to open water	0.87	1.05	1.94	0.36
Distance to ice-edge	14.35	3.15	8.31	9.70
Distance to southern boundary of the Antarctic Circumpolar Current	15.13	12.97	15.20	11.06
Day of Year	14.72	10.02	9.03	8.90

Red cells indicate preference associated with higher values (as per BRT partial plots; see Supplementary Material), and blue cells indicate preference associated with lower values. For ice category, red cells indicate preference associated with icier regions, and blue cells indicate preference associated with open water. White indicates neutral association with preference. Variables with a stronger influence are represented by larger values, and increasing opacity.

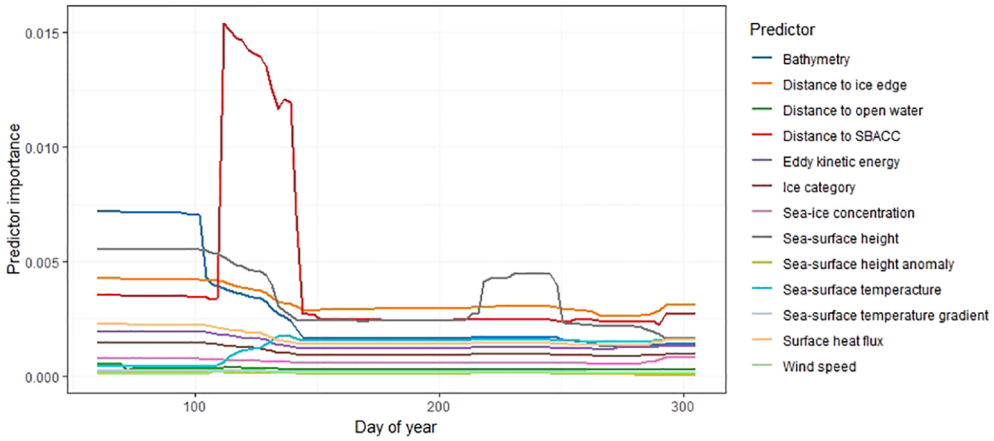


FIGURE 4
Relative importance of each environmental variable (habitat use) by day of year for all colonies. Environmental variables are shown in the legend on the right, where SBACC refers to distance to the southern boundary of the Antarctic Circumpolar Current. The y-axis values describe the standard deviation of the partial effect for each distinct value of day of year (where 1 would be the 1st of January, and 365 would be the 31st of December – note that dates are restricted from March to October).

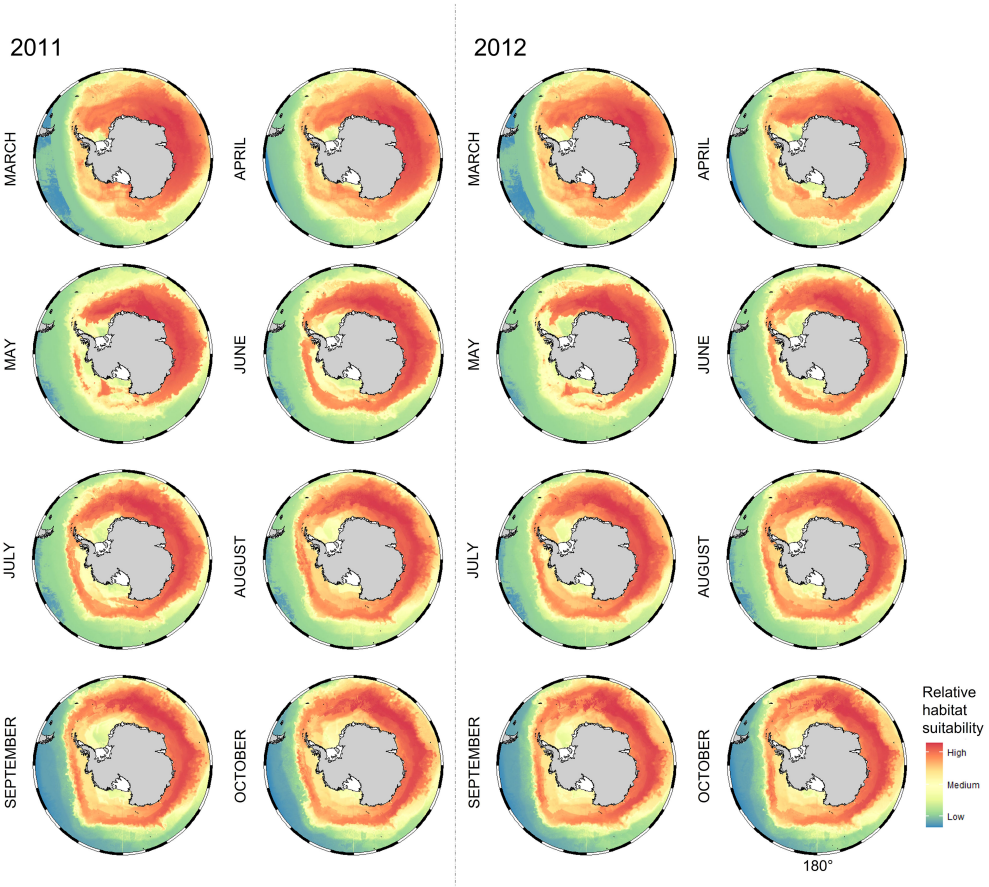


FIGURE 5
Monthly non-breeding habitat suitability maps for Snow Petrels (*Pagodroma nivea*) breeding at Béchervaise and Filla Islands in 2011 (left of dotted line) and 2012 (right of dotted line). Redder colors indicate higher habitat suitability. Preferred habitat (i.e. with appropriate environmental conditions) occurs elsewhere around Antarctica but is less likely to be suitable for Snow Petrels from Filla Island and Béchervaise Island given the distance to their respective breeding sites. The numerical values for the legend correspond as follows: High = 80%, Medium = 50%, and Low = 20%.

Figure 4). Areas between the breeding colonies, Cosmonauts Sea, Cooperation Sea, and the southern Kerguelen Plateau were particularly important regions. However, suitable habitat was observed around the entire continent (Figure 5). Given suitability was informed by presence data, this observation suggests Snow Petrels are highly mobile and have generalist habitat requirements throughout the winter, and likely contributes to their existence as the singular species within their genus with a circumpolar distribution [i.e., there has been a lack of environmental pressure to promote speciation. We note that there are two sub-species, but this is subject to debate (Carrea et al., 2019; Kim and Kim, 2020)].

The only other study to assess habitat use by Snow Petrels during the non-breeding period was conducted at Pointe Géologie, Adélie Land, East Antarctica – roughly 2,500 kilometers to the east of Filla Island (Figure 1). The Snow Petrels from Pointe Géologie remained in ice-associated waters, and moved towards similar geographic regions as those described in this paper throughout the non-breeding period (Delord et al., 2016). Notably, the previous study used immersion sensors to understand Snow Petrel activity patterns (Delord et al., 2016). Though our values differ slightly (due to differences in method), our findings on immersion and diurnal activity align with the French study (Figure 3). Snow Petrels from both colonies were predominantly active during nocturnal hours throughout the non-breeding period (Figure 3), and remained in ice-associated waters (Figure 1). Petrels from Béchervaise Island switched to a diurnal pattern in August, and petrels from Filla Island did so in September (Figure 3). This earlier change in cathemeral activity is possibly because birds from Béchervaise Island tended to be farther north than those from Filla Island (Figure 2). Snow Petrels are known to be particularly active during crepuscular hours. It is believed that such activity is associated with the vertical movement of prey (such as Antarctic Krill (*Euphausia superba*)) towards the sea surface during hours of darkness (Fraser et al., 1989; Delord et al., 2016). It is likely that the nocturnal activity observed in Snow Petrels from Béchervaise, and Filla Islands is also in response to this, though we expect greater foraging success during twilight as Snow Petrels are visual predators and it is slightly lighter at dawn/dusk than during the night.

The comparatively lower foraging activity of Snow Petrels during autumn (March/April, Figure 3) may be related to their complex and protracted annual moult that occurs in several phases. Their primary feathers are moulted in January; by March, all wing and tail feathers have been replaced; flight feathers are replaced continuously without impairing the ability to fly (allowing adults to feed their chicks); and the final phase is the post-breeding moult in late March/April when the body feathers are replaced (Maher, 1962). During this final phase, Snow Petrels may limit their exposure to water as body feathers are crucial for thermoregulation and, at least in some terrestrial birds, the disorder of plumage caused by moult can induce heat loss and increased energy demands (Schieltz and Murphy, 1997). Although the Snow Petrel plumage is very dense and heat loss may not be severe, a disruption to the integrity of the plumage is likely.

Given the foraging potential associated with the Kerguelen Axis (the area extending from the Kerguelen Plateau, over the BANZARE Bank south to east Antarctica) (Constable and Swadling, 2020), and its proximity to our study sites, it is unsurprising that most of the Snow Petrels in this study remained relatively close (< 1000 km) to their breeding area (and thus the Kerguelen region) throughout the non-breeding period (Figures 1, 2, 5). Throughout winter, chlorophyll-*a* levels are particularly low in the Southern Ocean (Sokolov and Rintoul, 2007). In summer studies, chlorophyll-*a* levels are routinely used as a proxy for primary productivity in the ocean – where planktivorous species (such as krill, zooplankton, and small fish) are present within their prey fields (Hammond et al., 2020; Hellessey et al., 2020). This is then used to infer biological activity within a region, and it is expected that tertiary consumers (such as Snow Petrels) will follow the secondary consumers (such as planktivores) to the prey fields (Santora et al., 2009). We did not include ocean color as a predictor in the habitat preference models, because satellite-derived chlorophyll-*a* concentration is not available during times of darkness, or in areas covered by sea ice or cloud, which constituted the majority of our study. Nevertheless, though reduced, phytoplankton production persists in areas where the Antarctic Circumpolar Current interacts with large topographic features such as the Kerguelen Islands (Sokolov and Rintoul, 2007). Thus, the Kerguelen Axis is one of the most important locations for primary production in the region (Arrigo et al., 2008). If chlorophyll-a levels in the Southern Ocean decrease during winter, while areas near the breeding colonies remain productive, it seems unnecessary for a bird to expend additional energy to reach a more distant foraging area. It is more practical for them to rely on a nearby and dependable food source. However, it should be noted that this theory may not apply uniformly to all Snow Petrel colonies, given the variations in conditions between breeding sites and the fact that the south-polar region is not homogeneous (Subramaniam et al., 2022).

The early peak (around April 10th/Day 100) in the importance of distance to the southern boundary of the Antarctic Circumpolar Current (SBACC, Figure 4) is driven by birds from Béchervaise Island in 2011 (see Supplementary Figure 1; herein Figure S1). Many of the environmental predictors deemed to be important for habitat preference are shared between the single colony models and the combined model (Table 3). However, there are temporal differences between colonies regarding the time of year in which each variable is most important (Figure S1). For birds from Béchervaise Island in 2011, SBACC was important throughout the non-breeding period, but most important in the earlier months (Figure S1). This may be associated with the biological productivity, and subsequent foraging potential, linked to the Antarctic Circumpolar Current (Ito et al., 2005; Ribic et al., 2011). We suspect the proximity to SBACC may be more important at the start of the non-breeding period as local (closer) foraging areas could be depleted by foraging effort related to the chick-rearing stages – where shorter flights and larger catches are required to maintain proximity to, and satiety of, newly hatched Snow Petrel chicks. Such localized prey depletion has been observed around breeding areas for other Antarctic seabirds such as the Macaroni Penguin (*Eudyptes chrysolophus*) (Bedford et al., 2015). However, the quantification of prey-fields is an emerging area of research, and not yet applicable to the areas described within this manuscript.

Bathymetry was overwhelmingly the most important environmental predictor throughout the year for birds from Filla Island in 2011(Figure S1). Bathymetry has previously been recognized as an important environmental feature for other groups of seabirds with variable foraging strategies, such as sulids (Young et al., 2015). It is thought that individual birds may seek out distinct bathymetric features known to increase productivity, or oceanographic features that harbor prey due to bathymetric variability (Young et al., 2015). The same may be true for Snow Petrels.

The temporal importance of environmental predictors was most variable when modelled for birds from Béchervaise Island in 2012 (Figure S1). Almost all variables were highly important at one point of the year, but bathymetry, distance to open water, and sea-surface height were the strongest predictors for habitat preference. These variables are associated with the Antarctic Circumpolar Current and are likely representing preference for biological productivity associated with the current (Sokolov and Rintoul, 2009).

Despite the increase in sea-ice concentrations from March to September, monthly activity remained relatively constant throughout the non-breeding period for birds from both colonies (Figure 3). This suggests that Snow Petrels remain to the north of the sea ice zone, utilize gaps in the sea-ice to forage, or do both. Our "distance to open water" predictor was based on gridded sea ice data (Table 1). The grid size (12.5 km) is sufficient to detect large gaps in the sea-ice, but too coarse to detect leads that are usable by highly mobile flying birds. Notably, we initially conducted analyses using daily leads data (Reiser et al., 2020), but we did not find a strong association between the presence of Snow Petrels and the presence of leads. Consequently, we excluded the leads data from the final results. However, we are confident that future studies, with improved tracking accuracy, will be able to incorporate leads data as an environmental variable. Although our model included a range of sea-ice variables, the mismatch between the spatial resolution of current satellite sensors and the tracking inaccuracies of GLS devices may explain the unexpectedly weak associations between sea-ice variables and the tracking data.

To clarify, the use of GLS tracking devices allowed us to monitor the birds continuously throughout the study period without being limited by battery capacity. However, these devices have relatively poor location accuracy (~186 ± 114 km for flying birds; Phillips et al., 2004). Nonetheless, the scale of our study far exceeded the scale of inaccuracy, and in conjunction with our quantitative approach (Elith et al., 2008; Reisinger et al., 2018; Hindell et al., 2020), the accuracy of GLS devices is unlikely to have significantly impacted the results. Therefore, our findings provide a broad indication of distribution and habitat suitability rather than a detailed account of fine-scale movement dynamics (Quillfeldt et al., 2017).

Future studies in the region will benefit from advancements in battery technology, enabling the use of smaller GPS tracking devices that offer higher accuracy compared to GLS devices (Bernard et al., 2021). These devices will allow researchers to track animals with GPS-scale resolution for extended periods, further enhancing the understanding of animal movements.

It is possible that Snow Petrels spend the majority of their sea-time in productive areas where they forage successfully, but this interpretation is limited to nesting birds (a common limitation in seabird tracking studies (Priddel et al., 2014), as those are the individuals accessible to researchers (i.e., juveniles, pre-breeders, and non-breeders are generally not constrained to a nest and are therefore extremely difficult to retrieve from the same location when attaching/detaching tracking devices). State-space modelling of GPS tracking data would allow researchers to identify specific "foraging only" regions [i.e., environmental features actively targeted by the birds; Halpin et al. (2022)]. Moreover, with the emergence of circumpolar databases that increasingly provide information on mesopelagic fish species (Woods et al., 2022), and krill (Atkinson et al., 2017), relevant seabird studies whose data overlap with prey data could gain valuable insight on which prey species are most commonly associated with seabird presence. Ideally, these foraging areas are regions that should be considered in conservation management planning (Thaxter et al., 2012; Veit and Harrison, 2017). Other species of seabird, such as penguins and shearwaters, associate with areas of subsurface productivity influenced by topographic features (Raymond et al., 2010; Kokubun et al., 2015; Riaz et al., 2021), and it is possible that Snow Petrels do the same. Subsurface productivity is not well detected by the satellite chlorophyll-*a* sensors currently available, but could also be considered in future works. Interestingly, the 'knots' observed in the flight paths of tracked Snow Petrels (Figure 1), may indicate the use of icebergs for roosting and temporary foraging mounts. Snow Petrels are well known to roost on icebergs (Brown, 1966), and increased primary productivity has been shown to occur around icebergs (Hopwood et al., 2019; Liniger et al., 2020; Smith et al., 2007). Such enhanced primary productivity could lead to hotspots of bountiful prey, distant from breeding locations.

Our study presents the first detailed analysis of environmental variables associated with Snow Petrel presence throughout the winter in East Antarctica using colonies near Mawson (Béchervaise) and Davis (Filla) stations. Congruent with other ecological studies in the region (Bestley et al., 2018; Hindell et al., 2020), our research demonstrates the great biological importance of the Kerguelen axis. The Kerguelen region is subject to both research and commercial fishing activity (Hill et al., 2017; Tixier et al., 2019; Subramaniam et al., 2022). Preliminary studies show little impact from commercial fishing activities on ecosystem interactions (Subramaniam et al., 2020). However, more research is needed to disentangle the influence of human activity and natural variation in the region on ecosystems and their inhabitants such as Snow Petrels (Subramaniam et al., 2022). The single most important habitat feature for fulmarine petrels (including Snow Petrels) to persist on Earth's coldest continent is an abundance of food (Weathers et al., 2000). Although Antarctic Petrels (*Thalassoica antarctica*) and Snow Petrels are better insulated than lower-latitude species, their best adaptation to dealing with cold environments is an increased metabolic rate (Weathers et al., 2000). When combined with plasticity in behavior, and variations between individuals regarding habitat use, Snow Petrels may be able to overcome challenges associated with anthropogenic climate change provided their prey fields remain plentiful. Once a more comprehensive understanding of Snow Petrel at-sea habitat use has been realized, we also recommend that future studies seek to explore how the

suitability of Snow Petrel habitat will change under different climate scenarios. In any case, to give the Snow Petrel the best possible chance of adapting to climate change, we must ensure it has time to do so. As with other wide-ranging species, protecting their prey availability and suitable nesting habitat will contribute to their conservation (Guixé and Arroyo, 2011).

Data availability statement

The datasets presented in this study can be found in online repositories. The names of the repository/repositories and accession number(s) can be found below: http://dx.doi.org/doi:10.4225/15/518831951455A Wienecke, B. (2013) GLS tag deployments on Snow petrels (Pagodroma nivea) in 2011 and 2012 from Bechervaise Island, Mawson Coast and Filla Island, Rauer Group, Ver. 1, Australian Antarctic Data Centre - ASAC_2722_SP_GLS.

Ethics statement

All applicable international, national, and/or institutional guidelines for the care and use of animals were followed. All animal handling and attachment of device procedures were approved by the Australian Government Antarctic Animal Ethics Committee through Australian Antarctic Science (AAS) projects # 2722 and 4087. The study was conducted in accordance with the local legislation and institutional requirements.

Author contributions

BV: Conceptualization, Data curation, Formal Analysis, Funding acquisition, Investigation, Methodology, Project administration, Resources, Software, Validation, Visualization, Writing – original draft, Writing – review & editing. BW: Conceptualization, Formal Analysis, Investigation, Project administration, Resources, Supervision, Validation, Visualization, Writing – review & editing. CG: Formal Analysis, Investigation, Methodology, Software, Validation, Writing – review & editing. SC: Funding acquisition, Investigation, Project administration, Resources, Supervision, Validation, Writing – review & editing. BR: Data curation, Formal Analysis, Investigation, Methodology, Resources, Software, Validation, Visualization, Writing – review & editing. CS: Conceptualization, Funding acquisition, Investigation, Project administration, Resources, Supervision, Validation, Writing – review & editing. MS: Data curation, Investigation, Resources, Software, Validation, Writing – review & editing. PV: Investigation, Supervision, Validation, Writing – review & editing. SW: Data curation, Formal Analysis, Investigation, Methodology, Software, Validation, Visualization, Writing – review & editing. LE: Conceptualization, Funding acquisition, Investigation, Project administration, Resources, Supervision, Validation, Writing – review & editing.

Funding

The author(s) declare financial support was received for the research, authorship, and/or publication of this article. This work was funded by the Australian Antarctic Division AAS projects # 2722 and 4087 and a post- graduate scholarship for BV from University of Tasmania.

Acknowledgments

We thank S. Doust, J. McInnes, H. Achurch, and L. Einoder for assistance in the field, and the ATAAMS team for early discussions surrounding this work. We extend thanks to N. Kelly, D. Fierro-Arcos, T. Travers, D. Green, A. Henderson, B. Woods, A. Fraser, J. Lieser, and J. Cleeland for fruitful discussions, and technical assistance with this work. We also thank S. Willmes for providing us with daily leads data for initial models that were not included in the final output. Finally, we thank the Australian Antarctic Division for funding and logistics support to deliver this work as a contribution to AAS projects # 2722, 4087, and 4518, and the Integrated Digital East Antarctica program. The work was carried out according to permits and conditions issued under the Australian Antarctic Treaty (Environmental Protection) Act 1980 (Permit numbers ATEP-4087-2011/12 and ATEP-4087-2012/13). This research was supported by use of the Nectar Research Cloud, a collaborative Australian research platform supported by the NCRIS-funded Australian Research Data Commons (ARDC).

Conflict of interest

The authors declare that the research was conducted in the absence of any commercial or financial relationships that could be construed as a potential conflict of interest.

Publisher's note

All claims expressed in this article are solely those of the authors and do not necessarily represent those of their affiliated organizations, or those of the publisher, the editors and the reviewers. Any product that may be evaluated in this article, or claim that may be made by its manufacturer, is not guaranteed or endorsed by the publisher.

Supplementary material

The Supplementary Material for this article can be found online at: https://www.frontiersin.org/articles/10.3389/fmars.2023.1278229/full#supplementary-material

References

Aarts, G., Fieberg, J., and Matthiopoulos, J. (2012). Comparative interpretation of count, presence–absence and point methods for species distribution models. *Methods Ecol. Evol.* 3 (1), 177–187. doi: 10.1111/j.2041-210X.2011.00141.x

Aarts, G., MacKenzie, M., McConnell, B., Fedak, M., and Matthiopoulos, J. (2008). Estimating space-use and habitat preference from wildlife telemetry data. *Ecography* 31, 140–160. doi: 10.1111/j.2007.0906-7590.05236.x

Ainley, D. G., Ribic, C. A., and Spear, L. B. (1993). Species-Habitat Relationships among Antarctic Seabirds: A Function of Physical or Biological Factors? *Condor* 95 (4), 806–816. doi: 10.2307/1369419

Ainley, D. G., Ribic, C. A., and Woehler, E. J. (2012). Adding the ocean to the study of seabirds: a brief history of at-sea seabird research. *Mar. Ecol. Prog. Ser.* 451, 231–243. doi: 10.3354/meps09524

Amundsen, T. (1995). Egg Size and Early Nestling Growth in the Snow Petrel. *Condor* 97 (2), 345–351. doi: 10.2307/1369020

Arrigo, K. R., van Dijken, G. L., and Bushinsky, S. (2008). Primary production in the Southern Ocean 1997–2006. *J. Geophysical Res.: Oceans* 113 (C8). doi: 10.1029/2007JC004551

Atkinson, A., Hill, S. L., Pakhomov, E. A., Anadon, R., Chiba, S., Daly, K. L., et al. (2017). KRILLBASE: a circumpolar database of Antarctic krill and salp numerical densities 1926-2016. 9 (1), 193–210. doi: 10.5194/essd-9-193-2017

Barbraud, C., and Chastel, O. (1999). Early body condition and hatching success in the snow petrel *Pagodroma nivea*. *Polar Biol.* 21 (1), 1–4. doi: 10.1007/s003000050326

Bedford, M., Melbourne-Thomas, J., Corney, S., Jarvis, T., Kelly, N., and & Constable, A. (2015). Prey-field use by a Southern Ocean top predator: enhanced understanding using integrated datasets. *Mar. Ecol. Prog. Ser.* 526, 169–181. doi: 10.3354/meps11203

Berg, S., White, D., Hermichen, W.-D., and Emmerson, L. (2019). Late Holocene colonisation of snow petrels (*Pagodroma nivea*) of the Prince Charles Mountains, Antarctica. *Polar Biol.* 42, 1167–1173. doi: 10.1007/s00300-019-02509-0

Bernard, A., Rodrigues, A. S. L., Cazalis, V., and Grémillet, D. (2021). Toward a global strategy for seabird tracking. *Conserv. Lett.* 14 (3), e12804. doi: 10.1111/conl.12804

Bestley, S., Raymond, B., Gales, N. J., Harcourt, R. G., Hindell, M. A., Jonsen, I. D., et al. (2018). Predicting krill swarm characteristics important for marine predators foraging off East Antarctica. *Ecography* 41 (6), 996–1012. doi: 10.1111/ecog.03080

Boehmke, B., and Greenwell, B. (2019). *Hands-on machine learning with R (1 ed.)* (New York, USA: Chapman and Hall/CRC).

Bondavalli, C., and Ulanowicz, R. E. (1999). Unexpected effects of predators upon their prey: the case of the American alligator. *Ecosystems* 2 (1), 49–63. doi: 10.1007/s100219900057

Brown, D. A. (1966). Breeding biology of the snow petrel pagodroma nivea (forster). *ANARE Sci. Rep.* 89, 1–63.

Brown, R. G. B. (1980). "Seabirds as Marine Animals," in *Behavior of Marine Animals: Current Perspectives in Research. Marine Birds*. Eds. J. Burger, B. L. Olla and H. E. Winn (US: Springer), 1–39.

Burger, J., and Gochfeld, M. (2004). Marine Birds as Sentinels of Environmental Pollution. *EcoHealth* 1 (3), 263–274. doi: 10.1007/s10393-004-0096-4

Carrea, C., Burridge, C. P., Wienecke, B., Emmerson, L. M., White, D., and Miller, K. J. (2019). High vagility facilitates population persistence and expansion prior to the Last Glacial Maximum in an antarctic top predator: The Snow petrel (Pagodroma nivea). *J. Biogeography* 46 (2), 442–453. doi: 10.1111/jbi.13513

Clarke, A., Barnes, D. K. A., and Hodgson, D. A. (2005). How isolated is Antarctica? *Trends Ecol. Evol.* 20 (1), 1–3. doi: 10.1016/j.tree.2004.10.004

Constable, A., and Swadling, K. M. (2020). Ecosystem drivers of food webs on the Kerguelen Axis of the Southern Ocean. *Deep Sea Res. Part II: Topical Stud. Oceanography* 174, e104790. doi: 10.1016/j.dsr2.2020.104790

Cordero Quirós, N., Jacox, M. G., Pozo Buli, M., and Bograd, S. J. (2022). Future Changes in Eddy Kinetic Energy in the California Current System From Dynamically Downscaled Climate Projections. *Geophysical Res. Lett.* 49 (21), e2022gl099042. doi: 10.1029/2022GL099042

Cox, S. L., Embling, C. B., Hosegood, P. J., Votier, S. C., and Ingram, S. N. (2018). Oceanographic drivers of marine mammal and seabird habitat-use across shelf-seas: A guide to key features and recommendations for future research and conservation management. *Estuarine Coast. Shelf Sci.* 212, 294–310. doi: 10.1016/j.ecss.2018.06.022

Cropper, T. E., Hanna, E., and Bigg, G. R. (2014). Spatial and temporal seasonal trends in coastal upwelling off Northwest Africa 1981–2012. *Deep Sea Res. Part I: Oceanographic Res. Papers* 86, 94–111. doi: 10.1016/j.dsr.2014.01.007

Croxall, J., Steele, W., McInnes, S., and Prince, P. (1995). Breeding distribution of the Snow Petrel Pagodroma nivea. *Mar. Ornithol.* 23, 69–100.

Davis, S. E., Maftei, M., and Mallory, M. L. (2016). Migratory Connectivity at High Latitudes: Sabine's Gulls (Xema sabini) from a Colony in the Canadian High Arctic Migrate to Different Oceans. *PloS One* 11 (12), e0166043. doi: 10.1371/journal.pone.0166043

del Hoyo, J. (2020). *All the Birds of the World*. Ed. J. del Hoyo (Barcelona, Spain: Lynx Edicions).

Delord, K., Pinet, P., Pinaud, D., Barbraud, C., De Grissac, S., Lewden, A., et al. (2016). Species-specific foraging strategies and segregation mechanisms of sympatric Antarctic fulmarine petrels throughout the annual cycle. *Ibis* 158 (3), 569–586. doi: 10.1111/ibi.12365

Einoder, L. D., Emmerson, L. M., Southwell, D. M., and Southwell, C. J. (2014). Cavity characteristics and ice accumulation affect nest selection and breeding in snow petrels Pagodroma nivea. *Mar. Ornithol.* 42, 175–182.

Elith, J., Leathwick, J. R., and Hastie, T. (2008). A working guide to boosted regression trees. *J. Anim. Ecol.* 77 (4), 802–813. doi: 10.1111/j.1365-2656.2008.01390.x

Emmerson, L., Southwell, C., Clarke, J., Tierney, M., and Kerry, K. (2015). Adélie penguin response parameters signal reduced prey accessibility: implications for predator–prey response curves. *Mar. Biol.* 162, 1187–1200. doi: 10.1007/s00227-015-2661-5

Fraser, A. D., Massom, R. A., Ohshima, K. I., Willmes, S., Kappes, P. J., Cartwright, J., et al. (2020). High-resolution mapping of circum-Antarctic landfast sea ice distribution 2000–2018. *Earth Syst. Sci. Data* 12 (4), 2987–2999. doi: 10.5194/essd-12-2987-2020

Fraser, W. R., Pitman, R. L., and Ainley, D. G. (1989). Seabird and fur seal responses to vertically migrating winter krill swarms in Antarctica. *Polar Biol.* 10 (1), 37–41. doi: 10.1007/BF00238288

Friedman, J. H. (2001). "Greedy Function Approximation: A Gradient Boosting Machine,". *Ann. Stat* 29 (5), 1189–1232. doi: 10.1214/aos/1013203451

Furness, R. W., and Camphuysen, K. (1997). Seabirds as monitors of the marine environment. *ICES J. Mar. Sci.* 54 (4), 726–737. doi: 10.1006/jmsc.1997.0243

Gilg, O., Moe, B., Hanssen, S. A., Schmidt, N. M., Sittler, B., Hansen, J., et al. (2013). Trans-Equatorial Migration Routes, Staging Sites and Wintering Areas of a High-Arctic Avian Predator: The Long-tailed Skua (Stercorarius longicaudus). *PloS One* 8 (5), e64614. doi: 10.1371/journal.pone.0064614

Goldsworthy, P., and Thomson, P. (2000). An extreme inland breeding locality of snow petrels (*Pagodroma nivea*) in the southern Prince Charles Mountains, Antarctica. *Polar Biol.* 23, 717–720. doi: 10.1007/s003000000146

González-Solís, J., Croxall, J. P., Oro, D., and Ruiz, X. (2007). Trans-equatorial migration and mixing in the wintering areas of a pelagic seabird. *Front. Ecol. Environ.* 5 (6), 297–301. doi: 10.1890/1540-9295(2007)5[297:TMAMIT]2.0.CO;2

Greenwell, B., Boehmke, B., and Gray, B. (2022). *Package 'vip'. R Package version 0.3.2* (Auckland, New Zealand: CRAN).

Guixé, D., and Arroyo, B. (2011). Appropriateness of Special Protection Areas for wide-ranging species: the importance of scale and protecting foraging, not just nesting habitats. *Anim. Conserv.* 14 (4), 391–399. doi: 10.1111/j.1469-1795.2011.00441.x

Halpin, L. R., Mott, R., Clay, T. A., Humphries, G. R. W., Chatwin, T. A., Carlile, N., et al. (2022). Predicting the Foraging Habitats of Sympatrically Breeding Gadfly Petrels in the South Pacific Ocean. *Front. Mar. Sci.* 9. doi: 10.3389/fmars.2022.853104

Hammond, M. L., Beaulieu, C., Henson, S. A., and Sahu, S. K. (2020). Regional surface chlorophyll trends and uncertainties in the global ocean. *Sci. Rep.* 10 (1), 15273. doi: 10.1038/s41598-020-72073-9

Harrison, P., Perrow, M., and Larsson, H. (2021). *Seabirds: The New Identification Guide* (Barcelona, Spain: Lynx Edicions).

Hawkes, L. A., Witt, M. J., Broderick, A. C., Coker, J. W., Coyne, M. S., Dodd, M., et al. (2011). Home on the range: spatial ecology of loggerhead turtles in Atlantic waters of the USA. *Diversity Distributions* 17 (4), 624–640. doi: 10.1111/j.1472-4642.2011.00768.x

Hazen, E. L., Abrahms, B., Brodie, S., Carroll, G., Jacox, M. G., Savoca, M. S., et al. (2019). Marine top predators as climate and ecosystem sentinels. *Front. Ecol. Environ.* 17 (10), 565–574. doi: 10.1002/fee.2125

Hedd, A., Montevecchi, W. A., Otley, H., Phillips, R. A., and Fifield, D. A. (2012). Trans-equatorial migration and habitat use by sooty shearwaters Puffinus griseus from the South Atlantic during the nonbreeding season. *Mar. Ecol. Prog. Ser.* 449, 277–290. doi: 10.3354/meps09538

Hellessey, N., Johnson, R., Ericson, J. A., Nichols, P. D., Kawaguchi, S., Nicol, S., et al. (2020). Antarctic krill lipid and fatty acid content variability is associated to satellite derived chlorophyll-a and sea surface temperatures. *Sci. Rep.* 10 (1), 1–11. doi: 10.1038/s41598-020-62800-7

Hill, N. A., Foster, S. D., Duhamel, G., Welsford, D., Koubbi, P., and Johnson, C. R. (2017). Model-based mapping of assemblages for ecology and conservation management: A case study of demersal fish on the Kerguelen Plateau. *Diversity Distributions* 23 (10), 1216–1230. doi: 10.1111/ddi.12613

Hindell, M. A., Reisinger, R. R., Ropert-Coudert, Y., Hückstädt, L. A., Trathan, P. N., Bornemann, H., et al. (2020). Tracking of marine predators to protect Southern Ocean ecosystems. *Nature* 580 (7801), 87–92. doi: 10.1038/s41586-020-2126-y

Hipfner, J. M., Prill, M. M., Studholme, K. R., Domalik, A. D., Tucker, S., Jardine, C., et al. (2020). Geolocator tagging links distributions in the non-breeding season to population genetic structure in a sentinel North Pacific seabird. *PloS One* 15 (11), e0240056. doi: 10.1371/journal.pone.0240056

Hopwood, M. J., Carroll, D., Höfer, J., Achterberg, E. P., Meire, L., Le Moigne, F. A. C., et al. (2019). Highly variable iron content modulates iceberg-ocean fertilisation and potential carbon export. *Nat. Commun.* 10, 5261. doi: 10.1038/s41467-019-13231-0

Ito, T., Parekh, P., Durkiewicz, S., and & Follows, M. J. (2005). The Antarctic Circumpolar Productivity Belt. *Geophysical Res. Lett.* 32 (13), L13604. doi: 10.1029/2005GL023021

Jaeger, A., Feare, C. J., Summers, R. W., Lebarbenchon, L., Larose, C. S., and Le Corre, M. (2017). Geolocation Reveals Year-Round at-Sea Distribution and Activity of a Superabundant Tropical Seabird, the Sooty Tern Onychoprion fuscatus. *Front. Mar. Sci.* 394 (4). doi: 10.3389/fmars.2017.00394

Jonsen, I., Bestley, S., Wotherspoon, S., Sumner, M., and Flemming, J. (2015). *bsam: Bayesian state-space models for animal movement. R package. R Foundation for Statistical Computing version 0.43, 1* (Auckland, New Zealand: CRAN).

Kim, J.-U., and Kim, J.-H. (2020). Complete mitochondrial genome of the snow petrel, Pagodroma nivea. *Mitochondrial DNA Part B.* 5 (3), 3337–3338. doi: 10.1080/23802359.2020.1820389

Kokubun, N., Lee, W. Y., Kim, J. H., and Takahashi, A. (2015). Chinstrap penguin foraging area associated with a seamount in Bransfield Strait, Antarctica. *Polar Sci.* 9 (4), 393–400. doi: 10.1016/j.polar.2015.10.001

Liniger, G., Strutton, P. G., Lannuzel, D., and Moreau, S. (2020). Calving event led to changes in phytoplankton bloom phenology in the Mertz Polynya, Antarctica. *J. Geophys. Res.: Oceans* 125 (11), e2020JC016387. doi: 10.1029/2020JC016387

Lisovski, S., and Hahn, S. (2012). GeoLight – processing and analysing light-based geolocator data in R. *Methods Ecol. Evol.* 3 (6), 1055–1059. doi: 10.1111/j.2041-210X.2012.00248.x

MacLeod, C., Adams, J., and Lyver, P. (2008). At-sea distribution of satellite-tracked Grey-faced Petrels, Pterodroma macroptera gouldi, captured on the Ruamaahua (Aldermen) Islands, New Zealand. *Papers Proc. R. Soc. Tasmania* 142 (1), 73–88. doi: 10.26749/rstpp.142.1.73

Maher, W. J. (1962). Breeding Biology of the Snow Petrel near Cape Hallett, Antarctica. *Condor* 64 (6), 488–499. doi: 10.2307/1365472

Malpress, V., Bestley, S., Corney, S., Welsford, D., Labrousse, S., Sumner, M., et al. (2017). Bio-physical characterisation of polynyas as a key foraging habitat for juvenile male southern elephant seals (*Mirounga leonina*) in Prydz Bay, East Antarctica. *PloS One* 12 (9), e0184536. doi: 10.1371/journal.pone.0184536

McClymont, E. L., Bentley, M. J., Hodgson, D. A., Spencer-Jones, C. L., Wardley, T., West, M. D., et al. (2021). Summer sea-ice variability on the Antarctic margin during the last glacial period reconstructed from snow petrel (*Pagodroma nivea*) stomach-oil deposits. *Clim. Past Discuss* 2021, 1–39. doi: 10.5194/cp-2021-134

Menkhorst, P., Rogers, D., Clarke, R., Davies, J., Marsack, P., and Franklin, K. (2017). *The Australian Bird Guide* (Clayton, Australia: CSIRO Publishing).

Moe, B., Angelier, F., Bech, C., and Chastel, O. (2007). Is basal metabolic rate influenced by age in a long-lived seabird, the snow petrel? *J. Exp. Biol.* 210 (19), 3407–3414. doi: 10.1242/jeb.005090

Olivier, F., Lee, A. V., and Woehler, E. J. (2004). Distribution and abundance of snow petrels Pagodroma nivea in the Windmill Islands, East Antarctica. *Polar Biol.* 27 (5), 257–265. doi: 10.1007/s00300-004-0595-3

Park, Y.-H., and Durand, I. (2019). *Altimetry-drived Antarctic Circumpolar Current fronts* (Plouzané, France: SEANOE).

Phillips, R. A., Silk, J. R. D., Croxall, J. P., Afanasyev, V., and Briggs, D. R. (2004). Accuracy of geolocation estimates for flying seabirds. *Mar. Ecol. Prog. Ser.* 266, 265–272. doi: 10.3354/meps266265

Piatt, J. F., Sydeman, W. J., and Wiese, F. (2007). Seabirds as indicators of marine ecosystems. *Mar. Ecol. Prog. Ser.* 352, 199–204. doi: 10.3354/meps07070

Pinet, P., Jaquemet, S., Pinaud, D., Weimerskirch, H., Phillips, R. A., and Le Corre, M. (2011). Migration, wintering distribution and habitat use of an endangered tropical seabird, Barau's petrel Pterodroma baraui. *Mar. Ecol. Prog. Ser.* 423, 291–302. doi: 10.3354/meps08971

Poland, J. S., Riddle, M. J., and Zeeb, B. A. (2003). Contaminants in the Arctic and the Antarctic: a comparison of sources, impacts, and remediation options. *Polar Rec.* 39 (4), 369–383. doi: 10.1017/S0032247403002985

Post, E., Bhatt, U. S., Bitz, C. M., Brodie, J. F., Fulton, T. L., Hebblewhite, M., et al. (2013). Ecological Consequences of Sea-Ice Decline. *Science* 341 (6145), 519–524. doi: 10.1126/science.1235225

Priddel, D., Carlile, N., Portelli, D., Kim, Y., O'Neill, L., Bretagnolle, V., et al. (2014). Pelagic distribution of Gould's Petrel (Pterodroma leucoptera): linking shipboard and onshore observations with remote-tracking data. *Emu* 114 (4), 360–370. doi: 10.1071/MU14021

Puskic, P., Lavers, J. L., Adams, L. R., Grünenwald, M., Hutton, I., and & Bond, A. L. (2019). Uncovering the sub-lethal impacts of plastic ingestion by shearwaters using fatty acid analysis. *Conserv. Physiol.* 7 (1), e107. doi: 10.1093/conphys/coz017

Pya, N. (2022). "Package 'scam'," in *R package version 1.2-13* (Auckland, New Zealand: CRAN).

Quillfeldt, P., Engler, J. O., Silk, J. R. D., and Phillips, R. A. (2017). Influence of device accuracy and choice of algorithm for species distribution modelling of seabirds: a case study using black-browed albatrosses. *J. Avian Biol.* 48 (12), 1549–1555. doi: 10.1111/jav.01238

Raymond, B., Lea, M. A., Patterson, T., Andrews-Goff, V., Sharples, R., Charrassin, J.-B., et al. (2015). Important marine habitat off East Antarctica revealed by two decades of multi-species predator tracking. *Ecography* 38 (2), 121–129. doi: 10.1111/ecog.01021

Raymond, B., Shaffer, S. A., Sokolov, S., Woehler, E. J., Costa, D. P., Einoder, L., et al. (2010). Shearwater Foraging in the Southern Ocean: The Roles of Prey Availability and Winss. *PloS One* 5 (6), e10960. doi: 10.1371/journal.pone.0010960

Rayner, M. J., Hauber, M. E., Clout, M. N., Seldon, D. S., Van Dijken, S., Bury, S., et al. (2008). Foraging ecology of the Cook's petrel Pterodroma cookii during the austral breeding season: a comparison of its two populations. *Mar. Ecol. Prog. Ser.* 370, 271–284. doi: 10.3354/meps07660

Reiser, F., Willmes, S., and Heinemann, G. (2020). A New Algorithm for Daily Sea Ice Lead Identification in the Arctic and Antarctic Winter from Thermal-Infrared Satellite Imagery. *Remote Sens.* 12 (12), 1957. doi: 10.3390/rs12121957

Reisinger, R. R., Raymond, B., Hindell, M. A., Bester, M. N., Crawford, R. J. M., Davies, D., et al. (2018). Habitat modelling of tracking data from multiple marine predators identifies important areas in the Southern Indian Ocean. *Diversity Distributions* 24 (4), 535–550. doi: 10.1111/ddi.12702

Reudink, M. W., Marra, P. P., Kyser, T. K., Boag, P. T., Langin, K. M., and Ratcliffe, L. M. (2009). Non-breeding season events influence sexual selection in a long-distance migratory bird. *Proc. R. Soc. B.: Biol. Sci.* 276 (1662), 1619–1626. doi: 10.1098/rspb.2008.1452

Riaz, J., Bestley, S., Wotherspoon, S., and Emmerson, L. (2021). Horizontal-vertical movement relationships: Adélie penguins forage continuously throughout provisioning trips. *Movement Ecol.* 9 (1), 43. doi: 10.1186/s40462-021-00280-8

Ribic, C. A., Ainley, D. G., Ford, R. G., Fraser, W. R., Tynan, C. T., and Woehler, E. J. (2011). Water masses, ocean fronts, and the structure of Antarctic seabird communities: Putting the eastern Bellingshausen Sea in perspective. *Deep Sea Res. Part II* 58 (13-16), 1695–1709. doi: 10.1016/j.dsr2.2009.09.017

Roncon, G., Bestley, S., McMahon, C. R., Wienecke, B., and Hindell, M. A. (2018). View From Below: Inferring Behavior and Physiology of Southern Ocean Marine Predators From Dive Telemetry [Review]. *Front. Mar. Sci.* 5 (464). doi: 10.3389/fmars.2018.00464

Santora, J. A., Reiss, C. S., Cossio, A. M., and Veit, R. R. (2009). Interannual spatial variability of krill (Euphausia superba) influences seabird foraging behavior near Elephant Island, Antarctica. *Fisheries Oceanography* 18 (1), 20–35. doi: 10.1111/j.1365-2419.2008.00490.x

Schieltz, P. C., and Murphy, M. E. (1997). The contribution of insulation changes to the energy cost of avian molt. *Can. J. Zool.* 75 (3), 396–400. doi: 10.1139/z97-049

Skov, H., Theophilus, T. Z. E., Heinänen, S., Fauchald, P., Madsen, M., Mortensen, J. B., et al. (2021). Real-time predictions of seabird distribution improve oil spill risk assessments. *Mar. pollut. Bull.* 170, 112625. doi: 10.1016/j.marpolbul.2021.112625

Smith, K., Robison, B. H., Helly, J. J., Kauffman, R. S., Ruhl, H. A., Shaw, T. J., et al. (2007). Free-drifting icebergs: hot spots of chemical and biological enrichment in the weddell sea. *Science.* 317(5837), 478–482. doi: 10.1126/science.1142834

Sokolov, S., and Rintoul, S. R. (2007). On the relationship between fronts of the Antarctic Circumpolar Current and surface chlorophyll concentrations in the Southern Ocean. *J. Geophysical Res.: Oceans* 112 (C7). doi: 10.1029/2006JC004072

Sokolov, S., and Rintoul, S. (2009). Circumpolar structure and distribution of the Antarctic Circumpolar Current fronts: 2. Variability and relationship to sea surface height. *J. Geophysical Res.: Oceans* 114 (C11). doi: 10.1029/2008JC005248

Spear, L. B., and Ainley, D. G. (2008). Flight speed of seabirds in relation to wind speed and direction. *Ibis* 139 (2), 234–251. doi: 10.1111/j.1474-919X.1997.tb04621.x

Steiner, U. K., and Gaston, A. J. (2005). Reproductive consequences of natal dispersal in a highly philopatric seabird. *Behav. Ecol.* 16 (3), 634–639. doi: 10.1093/beheco/ari035

Subramaniam, R. C., Corney, S. P., Melbourne-Thomas, J., Péron, C., Ziegler, P., and Swadling, K. M. (2022). Spatially explicit food web modelling to consider fisheries impacts and ecosystem representation within Marine Protected Areas on the Kerguelen Plateau. *ICES J. Mar. Sci.* 79 (4), 1327–1339. doi: 10.1093/icesjms/fsac056

Subramaniam, R. C., Melbourne-Thomas, J., Corney, S. P., Alexander, K. A., Péron, C., Ziegler, P., et al. (2020). Time-dynamic food web modelling to explore environmental drivers of ecosystem change on the Kerguelen Plateau. *Front. Mar. Sci.* 7, 1–20. doi: 10.3389/fmars.2020.00641

Sumner, M. D., Wotherspoon, S. J., and Hindell, M. A. (2009). Bayesian Estimation of Animal Movement from Archival and Satellite Tags. *PloS One* 4 (10), e7324. doi: 10.1371/journal.pone.0007324

Sun, C., Liu, C., Wang, Z., Yan, L., Tao, T., Qin, Q., et al. (2022).) On the influences of the continental shelf bathymetry correction in Prydz Bay, East Antarctica. *Front. Mar. Sci.* 9, e1641. doi: 10.3389/fmars.2022.957414

Talley, L., Pickard, G. L., Emery, W. J., and Swift, J. H. (2011). *Descriptive Physical Oceanography. Sixth Edition* (Oxford, UK: Elsevier Publishing).

Tamura, T., Ohshima, K. I., and Nihashi, S. (2008). Mapping of sea ice production for Antarctic coastal polynyas. *Geophysical Res. Lett.* 35 (7). doi: 10.1029/2007GL032903

Thaxter, C. B., Lascelles, B., Sugar, K., Cook, A. S. C. P., Roos, S., Bolton, M., et al. (2012). Seabird foraging ranges as a preliminary tool for identifying candidate Marine Protected Areas. *Biol. Conserv.* 156, 53–61. doi: 10.1016/j.biocon.2011.12.009

Thor, G., and Low, M. (2011). The persistence of the snow petrel (Pagodroma nivea) in Dronning Maud Land (Antarctica) for over 37,000 years. *Polar Biol.* 34 (4), 609–613. doi: 10.1007/s00300-010-0912-y

Tittensor, D., Mora, C., Jetz, W., Lotze, H. K., Ricard, D., Vanden Berghe, E., et al. (2010). Global patterns and predictors of marine biodiversity across taxa. *Nature* 466, 1098–1101. doi: 10.1038/nature09329

Tixier, P., Welsford, D., Lea, M.-A., Hindell, M. A., Guinet, C., Janc, A., et al. (2019). Fisheries interaction data suggest variations in the distribution of sperm whales on the Kerguelen Plateau. The Kerguelen Plateau: marine ecosystem and fisheries. *Proceedings of the Second Symposium*. Available at: https://figshare.utas.edu.au/articles/conference_contribution/Fisheries_interaction_data_suggest_variations_in_the_distribution_of_sperm_whales_on_the_Kerguelen_Plateau/23099726

Veit, R. R., and Harrison, N. M. (2017). Positive Interactions among Foraging Seabirds, Marine Mammals and Fishes and Implications for Their Conservation [Review]. *Front. Ecol. Evol.* 5. doi: 10.3389/fevo.2017.00121

Viola, B. M., Sorrell, K. J., Clarke, R. H., Corney, S. P., and Vaughan, P. M. (2022). Amateurs can be experts: A new perspective on collaborations with citizen scientists. *Biol. Conserv.* 274, e109739. doi: 10.1016/j.biocon.2022.109739

Vivier, F., Kelly, K. A., and Thompson, L. (1999). Contributions of wind forcing, waves, and surface heating to sea surface height observations in the Pacific Ocean. *J. Geophysical Res. Oceans* 104 (C9), 20767–20788. doi: 10.1029/1999JC900096

Warwick-Evans, V., Santora, A., Waggitt, J. J., and Trathan, P. N. (2021). Multi-scale assessment of distribution and density of procellariiform seabirds within the Northern Antarctic Peninsula marine ecosystem. *ICES J. Mar. Sci* 78 (4), 1324-1339. doi: 10.1093/icesjms/fsab020

Weathers, W., Gerhart, K., and Hodum, P. (2000). Thermoregulation in Antarctic fulmarine petrels. *J. Comp. Physiol. B.* 170 (8), 561–572. doi: 10.1007/s003600000134

Webster, M. S., and Marra, P. P. (2005). "The importance of understanding migratory connectivity and Seasonal Interactions," in *Birds of Two Worlds: The Ecology and Evolution of Migration*. Eds. R. S. Greenberg and P. P. Marra (Baltimore, USA: JHU Press), 199–209.

Weimerskirch, H., Delord, K., Guitteaud, A., Phillips, R. A., and Pinet, P. (2015). Extreme variation in migration strategies between and within wandering albatross populations during their sabbatical year, and their fitness consequences. *Sci. Rep.* 5, 8853–8853. doi: 10.1038/srep08853

Woods, B., Trebilco, R., Walters, A., Hindell, M., Duhamel, G., Flores, H., et al. (2022). Myctobase, a circumpolar database of mesopelagic fishes for new insights into deep pelagic prey fields. *Sci. Data* 9 (1), 404. doi: 10.1038/s41597-022-01496-y

Wotherspoon, S., Sumner, M., and Lisovski, S. (2013). *BAStag: Basic data processing for light based geolocation archival tags. R Package version 0.1-3* (Auckland, New Zealand: CRAN).

Young, H. S., Maxwell, S. M., Conners, M. G., and Shaffer, S. A. (2015). Pelagic marine protected areas protect foraging habitat for multiple breeding seabirds in the central Pacific. *Biol. Conserv.* 181, 226–235. doi: 10.1016/j.biocon.2014.10.027

Younger, J. L., Emmerson, L. M., and Miller, K. J. (2016). The influence of historical climate changes on Southern Ocean marine predator populations: a comparative analysis. *Global Change Biol.* 22 (2), 474–493. doi: 10.1111/gcb.13104

frontiers | Frontiers in Marine Science

TYPE Original Research
PUBLISHED 26 April 2024
DOI 10.3389/fmars.2024.1324816

Check for updates

OPEN ACCESS

EDITED BY
Todd Atwood,
U.S. Geological Survey, United States

REVIEWED BY
Holger Klinck,
Cornell University, United States
John P. Ryan,
Monterey Bay Aquarium Research Institute (MBARI), United States

*CORRESPONDENCE
Brian S. Miller
brian.miller@aad.gov.au

RECEIVED 24 October 2023
ACCEPTED 01 April 2024
PUBLISHED 26 April 2024

CITATION
Miller BS, Andrews-Goff V, Barlow J, Bell E, Calderan S, Double MC, Gedamke J, Kelly N, Laverick S, Leaper R, Miller EJ, Reeve K, Širović A and Stafford KM (2024) Antarctic sonobuoy surveys for blue whales from 2006-2021 reveal contemporary distribution, changes over time, and paths to further our understanding of their distribution and biology.
Front. Mar. Sci. 11:1324816.
doi: 10.3389/fmars.2024.1324816

COPYRIGHT
© 2024 Miller, Andrews-Goff, Barlow, Bell, Calderan, Double, Gedamke, Kelly, Laverick, Leaper, Miller, Reeve, Širović and Stafford. This is an open-access article distributed under the terms of the Creative Commons Attribution License (CC BY). The use, distribution or reproduction in other forums is permitted, provided the original author(s) and the copyright owner(s) are credited and that the original publication in this journal is cited, in accordance with accepted academic practice. No use, distribution or reproduction is permitted which does not comply with these terms.

Antarctic sonobuoy surveys for blue whales from 2006-2021 reveal contemporary distribution, changes over time, and paths to further our understanding of their distribution and biology

Brian S. Miller[1*], Virginia Andrews-Goff[1], Jay Barlow[2], Elanor Bell[1], Susannah Calderan[1,3], Michael C. Double[1], Jason Gedamke[1,4], Nat Kelly[1], Sarah Laverick[1,5], Russell Leaper[1,6], Elanor J. Miller[1,7], Kym Reeve[1,8], Ana Širović[9] and Kathleen M. Stafford[2]

[1]Australian Antarctic Division, Kingston, TAS, Australia, [2]Marine Mammal Institute, Oregon State University, Newport, OR, United States, [3]Scottish Association for Marine Science, Oban, United Kingdom, [4]Office of Science and Technology, National Oceanic and Atmospheric Administration (NOAA) Fisheries, Silver Spring, MD, United States, [5]Blue Planet Marine, Canberra, ACT, Australia, [6]International Fund for Animal Welfare, London, United Kingdom, [7]Independent Researcher, Hobart, TAS, Australia, [8]Independent Researcher, Nelson, New Zealand, [9]Trondhjem Biological Station, Department of Biology, Norwegian University of Science and Technology, (NTNU), Trondheim, Norway

Seven passive acoustic surveys for marine mammal sounds were conducted by deploying sonobuoys along ship tracks during Antarctic voyages spanning years 2006-2021. These surveys included nearly 330° of longitude throughout Antarctic (south of 60°S) and sub-Antarctic (between 50-60°S) latitudes. Here, we summarise the presence of calls from critically endangered Antarctic blue whales (*Balaenoptera musculus intermedia*) detected on all seven of these surveys. We describe and compare the spatial distribution of detections of three different types of Antarctic blue whale calls: unit-A, Z-calls, and D-calls. Three sets of voyages partially overlapped spatially but in different years, providing three regions (Indian Sector, Dumont d'Urville Sea, Ross Sea) to investigate differences over time for these three different call types. The proportion of sonobuoys with calls present was significantly higher in the more recent years for seven of the 15 combinations of years, regions, and call type. The proportion of sonobuoys with calls present was significantly lower only for one of the 15 combinations (unit A in the Ross Sea between 2015 vs 2017), and not significantly different for the remaining seven pairwise comparisons. We discuss possible explanations for these observations including: differences in probability of detection, whale behaviour, whale distribution, and abundance. These explanations are not mutually exclusive and cannot yet be resolved without application of complex analytical methods and collection of additional data. Lastly, we discuss future work that could help clarify the contributions of each of these potential drivers of acoustic detection. We propose continued acoustic data collection, application of new analytical methods, and collection of other synergistic data from Antarctic blue whales on their feeding grounds as a basis for

future work on this species. This could provide a cost effective and holistic means of monitoring their status after the effects of 20th century industrial whaling, as well as their responses to natural and anthropogenic changes to their main prey, Antarctic krill, and a changing climate.

KEYWORDS

Antarctic blue whale, passive acoustic monitoring, sonobuoy, ecology, marine biology, Antarctic, Southern Ocean

Introduction

Antarctic blue whales (*Balaenoptera musculus intermedia*; henceforth ABWs) are the largest animals on the planet and were nearly extirpated during 20th century industrial whaling (Rocha et al., 2015). In 1966 in the face of severe population decline, the International Whaling Commission (IWC) prohibited the take of blue whales, and in 1982 agreed a moratorium on commercial whaling for all whale species and populations, including ABWs, starting from the 1985/1986 season onwards. Presently, the IUCN conservation status of ABWs is 'critically endangered' (Cooke, 2018), and there remain large knowledge gaps surrounding their modern-day distribution and abundance. In the absence of human-driven mortality from hunting, some Antarctic cetacean populations, such as Eastern Australian and southwest Atlantic humpback whales (*Megaptera novaeangliae*), have recovered rapidly (Noad et al., 2019; Zerbini et al., 2019; Baines et al., 2021). However, studies of some other species, such as sperm whales (Branch and Butterworth, 2001; Carroll et al., 2014) have not detected evidence of recovery. The most recent circumpolar population abundance estimate for ABWs had a mid-point of 1997/98, so is now more than 25 years out of date. Moreover, there were large uncertainties around the population trend from these surveys; the 95% confidence intervals on the estimated annual population growth rate spanned 1.6-14.8% (Branch, 2007). Thus, contemporary knowledge of the recovery of this subspecies is required by management organisations such as the International Whaling Commission (IWC).

Like other Antarctic rorquals (humpback whales, Antarctic minke whales, *B. bonaerensis*, and fin whales, *B. physalus*), ABWs primarily feed on Antarctic krill, *Euphausia superba* (Mackintosh et al., 1929; Mackintosh, 1966; Gaskin, 1976; Kawamura, 1980). There is also a fishery for Antarctic krill, managed by the Commission for the Conservation of Antarctic Marine Living Resources (CCAMLR), a 27-member international body (CCAMLR, 1980). In order to manage the existing, and potentially expanding krill fishery (Kawaguchi and Nicol, 2020) in a sustainable manner, CCAMLR requires information about the distribution, abundance, and krill consumption rates of ABWs, all of which presently represent substantial gaps in our knowledge of their life history. Article II of CCAMLR states that any harvesting activities shall be conducted following conservation principles that include the maintenance of ecological relationships. This ecosystem-based management approach is designed to afford protection to populations of whales, seals, and seabirds who are dependent on harvested species, such as Antarctic krill, as their primary food source. Ecosystem-based management not only aims to protect against reduction of harvested and dependent populations, but also to protect against situations that might interfere with restoration of depleted populations, such as ABWs (CCAMLR, 1980 Article II.3.b).

Since the early 2000s, a substantial amount of data collection on ABWs has relied upon passive acoustics e.g (Ljungblad et al., 1998; Širović et al., 2004; Rankin et al., 2005; Sirovic et al., 2006; Širović et al., 2009; Širović and Hildebrand, 2011; Gavrilov et al., 2012; Balcazar et al., 2015; Miller et al., 2015; Tripovich et al., 2015; Leroy et al., 2016; Miller et al., 2017; Shabangu et al., 2017; Thomisch, 2017; Shabangu et al., 2019; Miller et al., 2019a; Shabangu et al., 2020; Miller et al., 2021c; Letsheleha et al., 2022). ABWs produce only a few different types of sound, but most of these are distinctive to the subspecies, and are very low in frequency (i.e. <100Hz), and detectable over very large areas (Širović et al., 2007; Samaran et al., 2010; Miller et al., 2015; Shabangu et al., 2020). ABW sounds can be classified as either song or non-song, with the former category consisting of highly stereotyped units and calls often repeated at regular intervals (Figure 1). The song of ABWs is typically described as a 3-unit vocalisation (Rankin et al., 2005), and in the literature these three components are often referred to as units A, B, and C, with the full call (comprising all three units) often referred to as a Z-call e.g. see Miller et al. (2021c). In many studies, often only the first song unit, unit-A, is detected, and this is sometimes treated as a separate category from full Z-calls, though more often no distinction is made. When detected without units B and C, unit-A has been found to be produced with lower mean source level than it is when detected within Z-calls (Miller et al., 2021a).

The bulk of passive acoustic studies of ABWs have focused predominantly on song calls, which are distinctive from the songs of other populations of blue whales. This distinction allows for a straightforward means to differentiate ABW song from nearby populations of pygmy blue whales (*B. m. brevicauda*) that may share sub-Antarctic feeding grounds (Samaran et al., 2013). In other populations song has been found to be produced only by male blue whales (Oleson et al., 2007b; Lewis et al., 2018), and it is widely assumed that ABW songs are also only produced by males.

Non-song calls (Figure 1; D-calls) are produced by all populations of blue whales globally, including ABWs. Furthermore, non-song calls

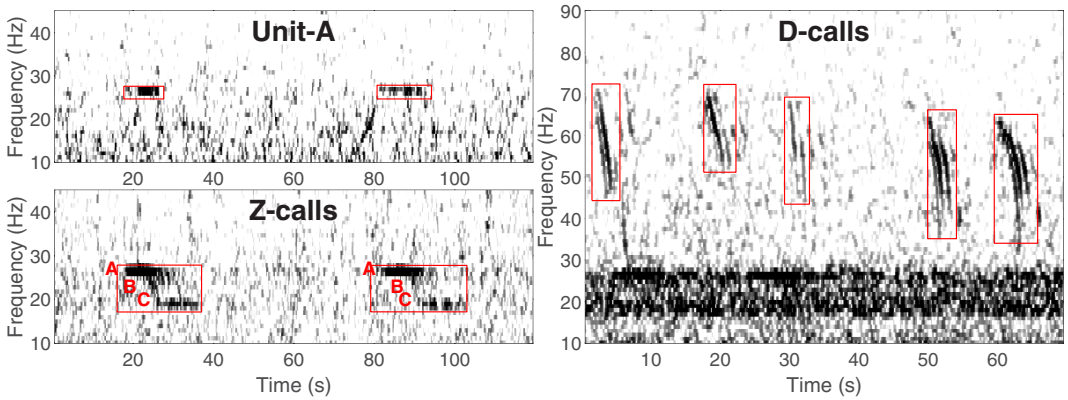


FIGURE 1
Spectrograms illustrating the different calls of Antarctic blue whales: song unit-A (top-left), non-song D-calls (right), and Z-calls with units A, B and C labelled with red text preceding the start of each unit (bottom left). Red boxes indicate the portions of the spectrogram that contains the calls. Figure adapted from (Miller et al., 2021c original figure licensed under creative commons).

of blue whales may be of greater interest and relevance in the context of ecosystem-based management because they have been found to be produced by both sexes, are believed to be associated with feeding/foraging/groups of whales (McDonald et al., 2001; Oleson et al., 2007b; Lewis et al., 2018; Schall et al., 2020), and the number of callers has been found to be correlated with the number of sightings (Oleson et al., 2007a). Non-song calls of blue whales globally include calls known as D-calls (sometimes referred to as downswept calls or FM calls), as well as variable AM/FM calls (Thompson et al., 1996; Rankin et al., 2005; Berchok et al., 2006; Oleson et al., 2007b). Unlike song, the non-song calls of blue whales do not appear to be distinctive to particular populations. Thus, in areas such as the sub-Antarctic where ABW and pygmy blue whales are sympatric, the detection of non-song calls does not lead to an easy attribution to a particular population.

Taken together, song and non-song calls appear to be produced globally by blue whales throughout the year (Torterotot et al., 2020; Miller et al., 2021c; Torterotot et al., 2022; Wingfield et al., 2022). Due to low spatial coverage of high-latitude, year-round recording sites and limited understanding of seasonal distribution and migratory behaviour of ABWs, it remains an open question as to how call production rates (in contrast to call detection rates) of ABWs in particular, change over time.

The majority of contemporary passive acoustic studies of blue whales have been conducted using fixed (moored) recording devices. These devices typically have good temporal resolution and coverage (Van Parijs et al., 2009) often recording continuously over many years. However, the spatial coverage of these devices in the Southern Hemisphere has been uneven, and too sparse for most regions of the Antarctic to describe blue whale distribution with much fidelity and precision (Opzeeland et al., 2013).

In contrast to moored acoustic recorders used to obtain long time series of recordings, sonobuoy surveys from ships have been used to obtain short time series (hours) of recordings across broad spatial scales during Antarctic voyages. Over the past two decades, in-situ passive acoustic monitoring from sonobuoys has been conducted by the Australian Antarctic Division (AAD) on seven Antarctic voyages. The results from some of these sonobuoy surveys have been reported previously in peer reviewed literature (Gedamke and Robinson, 2010; Miller et al., 2015, 2016; Miller et al., 2019a). Others have only been included in institutional reports or multinational fora (Gales, 2010; Double et al., 2015; Miller et al., 2017), and the latest results from the TEMPO voyage in 2021 (Kelly et al., 2021) are presented here for the first time. This type of acoustic monitoring has been conducted for various purposes on each voyage, but typically with one of the goals being to obtain a synoptic view of blue whale distribution along the voyage track.

Taken together, these seven AAD sonobuoy surveys span approximately 330 degrees of longitude throughout sub-Antarctic and Antarctic latitudes (which we define here as 50-60°S and >60°S respectively). These short duration passive acoustic recordings (typically 1-3 h long) were conducted with a sampling interval of around 30 nmi, predominantly from late January through mid-March. Thus, these sonobuoy surveys comprise a synoptic source of information about Antarctic blue whale distribution in the summer on the feeding grounds. Furthermore, this information is considerably more up-to-date, than other data sources on ABWs, such as industrial whaling catches (spanning 1930-1965), IDCR-SOWER visual surveys (spanning 1978-2004) (Branch, 2007) and SOWER passive acoustic surveys (spanning 1997-2009) (Shabangu et al., 2017; Shabangu, 2020). Contemporary sonobuoy data may be useful for understanding the present-day distribution of ABWs in a changing climate (Read, 2023; Stewart et al., 2023), or in the context of changing krill abundance, distribution, and fishing practices in the Southern Ocean (Jefferies, 2018; Kawaguchi and Nicol, 2020; Pallin et al., 2023; Trathan, 2023a, b).

Methods

Sonobuoy deployments and recording

Sonobuoys on AAD surveys were deployed under roughly the same spatial and temporal sampling regimes on research voyages in 2006, 2010, 2013, 2015, 2017, 2019, and 2021. The spatial sampling

regime was roughly every 30 nmi along the voyage track in order to acoustically cover the entire trackline. The temporal sampling regime was roughly every 3-6 hours around the clock. Sonobuoy deployments were weather dependent with deployments ceasing in heavy ice, when Beaufort Sea State was 7 or greater, or when wind speeds exceeded 30 knots as these conditions exceeded the limits at which sonobuoys can function reliably.

Two different calibrated recording setups were used to monitor radio signals transmitted from the sonobuoys (Miller et al., 2014c). The first setup was used in 2006 and 2010. This setup used a National Instruments data acquisition board with modified ICOM radio receivers, and is described in detail by Gedamke and Robinson (2010). The second set of recording equipment was in operation from 2013-2021. This included WinRadio radio receivers and Fireface UFX sound board for acoustic data acquisition and is described in detail by Miller et al (Miller et al., 2015, 2017; Miller et al., 2019a).

The make and model of sonobuoys varied across and within voyages, with four models being used in total: Omnidirectional 57A/B, and DIFAR 53D, 53F, and HIDAR 955. However, all of these models follow very similar, if not the same, military specifications and have hydrophones with the nominal frequency response all calibrated to within ± 3 dB (MIL-S-81487, 1996; Maranda, 2001). Nearly all sonobuoys deployed (>99.3%) were directional sonobuoys operating in analog directional analysis and frequency recording (DIFAR) mode which has a shaped frequency response that increases logarithmically in frequency by 20 dB per decade from 10-1000 Hz, and with a reference pressure of 122 ± 3 dB re 1 uPa at 100 Hz (Maranda, 2001; Greene et al., 2004; Rankin et al., 2019).

Monitoring for blue whale calls

For all voyages except the TEMPO voyage in 2021, acoustic data received from sonobuoys were monitored in real-time by an acoustician and the results of this real-time in-situ monitoring during the voyage are what have been analysed and presented (Gales, 2010; Double et al., 2015; Miller et al., 2015, 2017; Miller et al., 2019a). However, recordings from 2006 were previously re-inspected systematically after the voyage by co-author JG and have been presented in (Gedamke and Robinson, 2010), so we have opted to use these observations instead of those collected in real time for that voyage. Recordings from the 2021 voyage were not monitored in real-time during the voyage and were only inspected after the voyage by co-author KR (Kelly et al., 2023). During monitoring and inspection acousticians both listened and looked at spectrograms of incoming data with the aim of detecting calls from blue whales and other species. Here we focus exclusively on ABW calls at latitudes higher than 50°S.

Calls from blue whales were classified into three categories: song unit-A, Z-calls, and D-calls as per Miller et al. (2021c). Accordingly, song unit-A consisted of only the first tonal unit of ABW song; Z-calls consisted of the full three unit call of ABW song (including unit-A); and D-calls included downswept calls as well as AM/FM calls that were believed to be from blue whales (Figure 1). D-calls that were detected south of 50°S were assumed to be produced by ABWs, whilst D-calls north of 50°S were assumed to be from pygmy blue whales. While this simple criterion may not perfectly resolve the ambiguity about which population produced D-calls in sympatric areas, it is in accord with boundaries suggested by results from prior sonobuoy and visual surveys (Branch et al., 2007; Miller et al., 2014b; Double et al., 2015; Miller et al., 2015), and tagging data (Double et al., 2014; Buchan and Quiñones, 2016; Möller et al., 2020; Andrews-Goff et al., 2022).

The presence or absence of each call type was summarised independently for each sonobuoy and the summarised results were also mapped to facilitate qualitative analysis of spatial trends. Additionally, the proportion of sonobuoys with detections were plotted as histograms in latitude, longitude, week of the year, and recording duration. Since spatial and temporal coverage was often opportunistic and uneven, we chose wide bin widths of 3 degrees in latitude, 30 degrees in longitude, 1 week in time since start of year, and 30 minutes in duration for these histograms. These choices aimed to focus the results on broad-scale spatial and temporal trends.

For all analyses we excluded sonobuoys deployed north of 50°S, and deployed during periods of acoustic targeting of whales which were conducted during the 2010, 2013, 2015, and 2019 voyages. This latter exclusion was applied because targeting of whales typically involves higher rates of deployment of sonobuoys in the vicinity of calling animals which would bias our results. These exclusions removed 13 sonobuoys from the 2010 voyage; the entirety of the 2013 voyage; recordings from 143 sonobuoys deployed predominantly in the Ross Sea from 8-14 Feb and 24 Feb - 2 Mar from the 2015 voyage; and a total of 100 sonobuoy recordings in 2019. Analyses were then conducted on the remaining 952 deployments. The acoustic recordings, summarised detections, and metadata for sonobuoy surveys from these voyages are all publicly available from the Australian Antarctic Data Centre (Table 1). The collated table of these data used for the analyses here is presented in the Supplementary Material.

Regional comparison of presence of detections over time

Three sets of voyages had spatial, but not temporal, overlap in the areas that were monitored. The three regions of comparison were 50-80°E (2006 vs. 2021); Dumont D'Urville (DDU) Sea (2017 vs. 2019); and Ross Sea (2010 vs. 2015 vs. 2017). As this spatial overlap occurred in different years, each set of voyages potentially offered an opportunity to look for changes in the presence of blue whale calls in those regions over time. For this very high level and simple, qualitative comparison, we used as our metric of presence the proportion of sonobuoys with detections for each category of call. Since these were all Antarctic surveys, the 60°S parallel was used as the northernmost boundary for all regional comparisons. For each site, planned pairwise comparisons of the proportions of buoys with detections across years were performed using the test for equality of proportions implemented in the R function prop.test from the stats package (R Core Team, 2022).

TABLE 1 Sonobuoy datasets from 2006-2021 used in this study.

Voyage	Year	Start, end (Month & Day)	Buoys included (excluded)	Duration (h): mean (SD)	Data citation: Publication
BROKE West	2006	J10-F27	139 (0)	1.70 (1.22)	(Gedamke, 2014): (Gedamke and Robinson, 2010)
AWE	2010	F03-M12	97 (13)	1.81 (1.20)	(Gedamke, 2011): (Gales, 2010)
ABW Voyage	2013	J30-M15	0 (321)	N/A	(Miller et al., 2014a): (Miller et al., 2015)
NZ.Aus.AntEco	2015	J29-M10	142 (143)	2.24 (1.57)	(Double and Miller, 2017): (Double et al., 2015)
ACE	2017	J23-M18	242 (44)	1.51 (1.45)	(Calderan et al., 2019): (Miller et al., 2017)
ENRICH	2019	J19-M03	170 (100)	2.76 (1.86)	(Miller et al., 2021b): (Miller et al., 2019a)
TEMPO	2021	J30-M23	162 (22)	2.36 (1.82)	(Kelly et al., 2023): this study

The number of sonobuoys that were excluded because they were deployed during acoustic targeting or were at latitudes > -50°S are indicated in parentheses. The Duration column indicates the mean and standard deviation (SD) of the recording durations of only the 'included' buoys.

Results

Spatial and temporal distribution of calls

During the Austral summer, the stand-alone unit-A calls of ABWs were the most detected call type, and these were detected throughout most longitudes in the Antarctic and sub-Antarctic Southern Ocean. Z-calls, which include unit-A as well as units B & C, were the least detected calls from ABWs. These were observed mostly at high latitudes (Figures 2, 3). Blue whale D-calls were detected on more sonobuoys than Z-calls, but on fewer sonobuoys than unit-A (Figures 2, 3). These relative trends among call types were sustained across regions.

Within the survey months of January-March, there were subtle differences in the timing of call types across surveys (Figure 3, third column of panels). Unit-A was detected from the start through the end of the survey effort and appeared to increase throughout the year. Z-calls were detected intermittently and least often in January, but were detected consistently from the start of February all the way through the end of voyage data collection (in early-mid March). D-calls showed the opposite of Z-calls, that is they were detected from the start of the voyages in mid-late January through February, but seemed to taper off with decreasing detection rates over March.

Recording duration did not show a strong effect on detection for unit-A, but it did seem to strongly affect probability of detecting Z-calls with proportion of buoys with detections increasing with longer recording duration. An increase in proportion of sonobuoys with presence of D-calls was also found with increasing duration, however the relationship for D-calls appeared noisier and less pronounced than that observed for Z-calls (Figure 3, fourth column of panels).

Regional comparison of detections (presence) across years

Across the three call types and three regions, 15 comparisons could be made (Figures 4, 5). Across seven of these comparisons, the proportion of sonobuoys with detections was significantly higher in the later sample at the 0.05 level. These included all call types in the Indian Sector from voyages in 2006 vs. 2021; for unit-A and Z-calls in the DDU sea in 2017 vs. 2019; and for unit-A in the Ross Sea between 2010 vs 2015 and D-calls in the Ross Sea in 2010 vs. 2017). Six of these seven comparisons yielded no statistically significant differences at the 0.05 level. One of the 15 comparisons yielded a statistically significant decrease in the more recent sample: unit-A decreased in the Ross Sea from a proportion of 1 (70/70) in 2015 to 0.906 (29/32) in 2017. See Supplementary Material for further details of the results of the tests of proportions for each pairwise comparison.

Discussion

Spatial and temporal distribution of calls

The aggregate results from our passive acoustic surveys represent the most up-to-date synoptic data on the summer distribution of Antarctic blue whales (ABWs). The results indicate that ABWs still appear to have a circumpolar distribution throughout our study area, which included large portions of their historic Antarctic and sub-Antarctic feeding grounds. Furthermore, each of the three call types we detected had a different spatial distribution. Unit-A was the most widely distributed and was detected on the highest proportion of sonobuoys throughout the Antarctic and sub-Antarctic; Z-calls had the smallest and most discrete distribution concentrated at higher latitudes; and D-calls were intermediate between the two.

This relative spatial distribution among these call types is the same that was described by Miller et al. (2015) and Double et al. (2015) using data collected from sonobuoys deployed in 2013 and 2015, respectively. The 2013 voyage was not included here, and while the 2015 voyage was included in our circumpolar maps of distribution, large portions were excluded from our analysis of regional trends to avoid bias. During these 2013 and 2015 voyages, sonobuoys were predominantly used to track and find whales, instead of being deployed along designed survey tracks or during vessel transits between non-ABW-related destinations. The similarity in the results across the different surveys conducted over the years, regardless of whether sonobuoys were deployed during systematic spatial transects; transits from platforms of

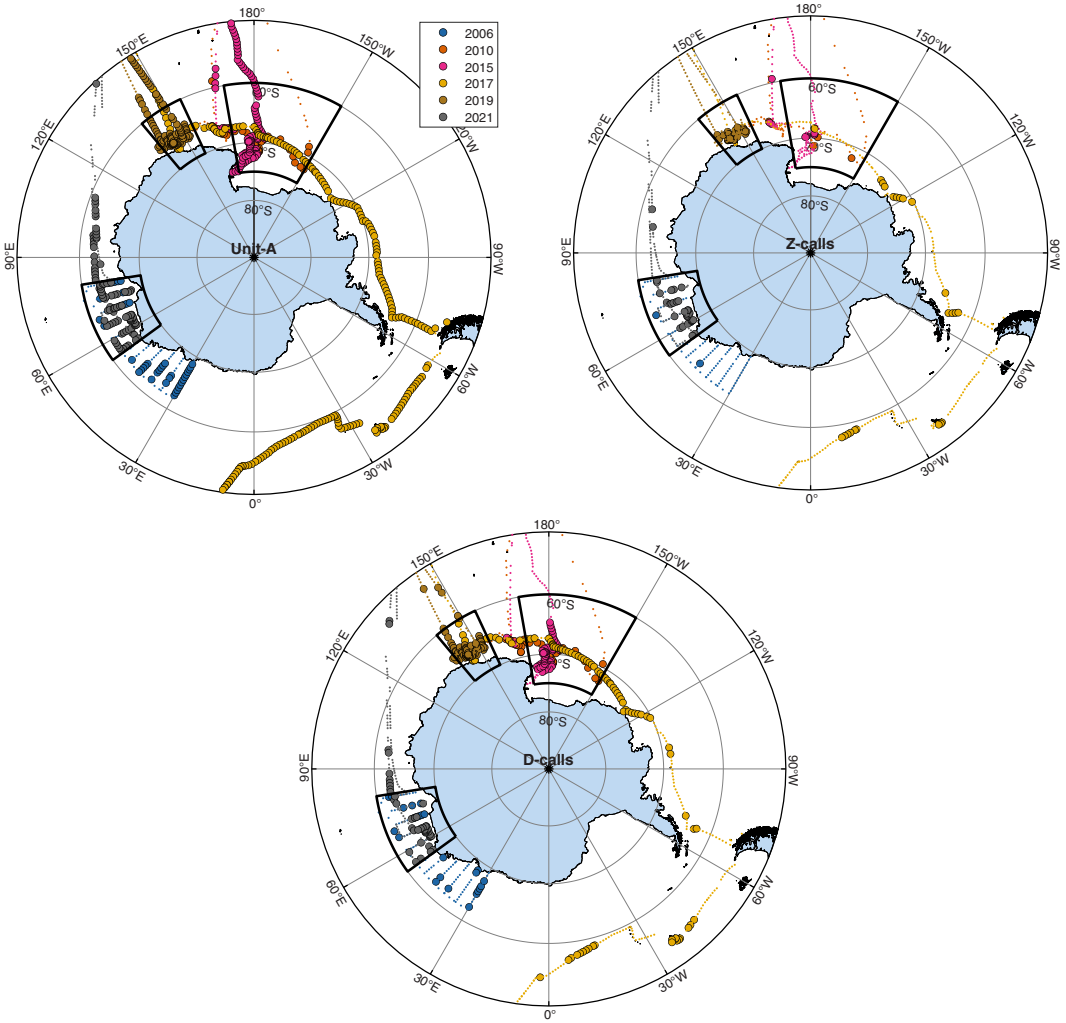


FIGURE 2
Maps illustrating sonobuoy deployment locations (small dots) and sonobuoys with detections present (circles with black outlines). Black boxes indicate areas used for regional comparisons over time. Panels from top-to-bottom indicate unit-A, Z-calls, and D-calls respectively. Maps created using M_Map software (Pawlowicz, 2019) with coastline data from the Global Self-consistent, Hierarchical, High-resolution Geography Database (Wessel and Smith, 1996).

opportunity; or whale tracking for acoustically assisted mark-recapture, suggest that the relative probability of detection of these call types (compared to other call types in that voyage) is independent of survey design. That is to say that across all voyages and survey types Z-calls were always the least detected call type, unit-A the most detected call type, and D-calls intermediate between the two.

Furthermore, on the voyages that tracked down groups of ABWs in 2013, 2015, and 2019, there was a strong correlation among Z-calls, D-calls and sightings, but not unit-A and sightings (Double et al., 2015; Miller et al., 2015; Miller et al., 2019a). Thus, it would appear that these differences among call types are likely driven by different detectability, with unit-A being especially detectable. Bouffaut et al. (2021), estimated that unit-A and unit-C had the same source level, though only from calls from a single individual. Assuming those results are indicative of source levels of the whole population, then the higher detectability of unit-A could be driven by the fact that unit-A is a pure tone, whereas unit-B is a downsweep, and unit-C is usually slightly downswept. It is possible that the pure tone of unit-A may provide additional constructive interference via multipath arrivals that does not occur with the shorter duration downsweep, hence resulting in higher probability of detection for unit-A. Alternatively, the enhanced detectability of unit-A in our study might arise from an artefact or limitation of the sonobuoys themselves that results in some negative perception bias for unit-C. A known source of such a bias against unit-C and therefore also detection of full Z-calls, is the shaped filter contained within each sonobuoy (MIL-S-81487, 1996; Greene et al., 2004; Rankin et al., 2019). This filter nominally reduces signal power at 18 Hz (the frequency of unit-C) by 3.2 ± 3 dB compared to 26 Hz (the frequency of unit-A). How such a reduction in received levels at these two frequencies translates into detection range or probability of detection further depends in turn on the noise levels and transmission losses at each frequency. Both noise levels and transmission losses can vary considerably throughout and across surveys, so measurement and estimation of these are beyond the

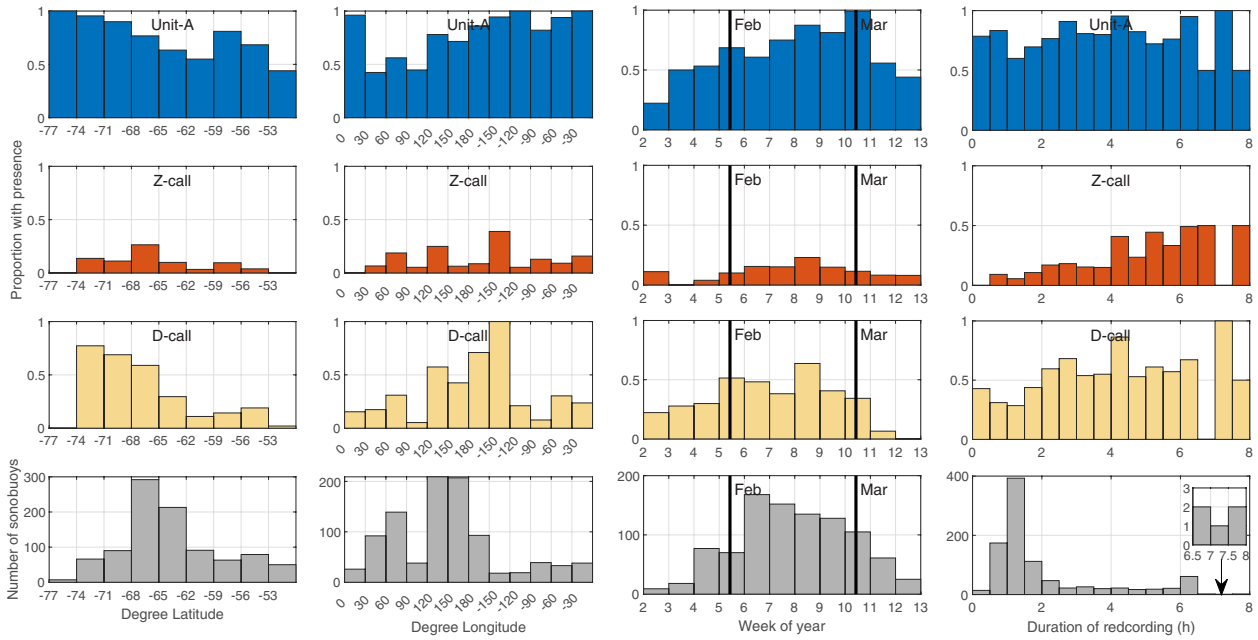


FIGURE 3
Proportion of sonobuoys with detection of Unit-A, Z-calls, and D-calls (blue, red, yellow bars respectively) by latitude in 3° bins (left column), longitude in 30° bins (second column) week of the year (third column) and recording duration (right column). Bottom panels indicate effort in the number of sonobuoys in each histogram bin. Thick black lines in the third column indicate the start of February and March. The inset in the bottom right panel shows a zoom of the histogram bins between 6.5-8 h.

scope of this study. Nevertheless, our results highlight the question: what proportion of the detections of unit-A are truly produced as a "stand-alone" call, and what proportion are part of Z-calls that have less detectable units B and C? In addition to obtaining more source level measurements of unit-C, this question could potentially be answered by modelling the probability of detection of each unit, or by conducting focal follows and/or acoustic tagging studies to estimate the cue rates of both types of calls. We discuss both of these solutions further in the sections below.

In addition to spatial trends, there was also apparent seasonality of song and non-song calls observed in the Antarctic, with D-calls trending towards higher proportion of detections earlier in the summer feeding season, and song trending towards later in the summer, and early autumn. These trends were in accord with observations of seasonality of blue whale song and D-calls observed in the Eastern North Pacific (Oleson et al., 2007a).

Regional comparison of presence of detections over time

Our regional, qualitative comparison of the proportion of sonobuoys with detections revealed a significantly higher proportion with detections in later years for seven out of 15 call types and regions ($p<0.05$; Figure 5). A further seven comparisons were found not to have statistically significant differences. In only one instance, unit-A in the Ross Sea, was there a statistically significant decline in the more recent sample. Here the percentage of buoys with detections went from 100% in 2015 to 90% in 2017. The call types and regions without a difference in detection rate in the more contemporary voyages were the proportion of Z-calls in the Ross Sea and D-calls in the Dumont D'Urville (DDU) Sea. Respectively, these appeared to remain the same in 2017 as 2010 and decrease very slightly from 2017 to 2019. Although these changes in proportional presence of call types could be associated with changes in ABW abundance, it is important to acknowledge that this is only one of many possible explanations for the acoustic differences in these datasets, which include changes in probability of detection, whale behaviour, and distribution. These factors, and how future studies might address them, are discussed in the following section below.

The surveys in the Indian sector (50-80E) were the most systematic relative to the surveys in the other two regions. The Indian sector surveys followed the same transects, and thus covered the same area in the same manner 15 years apart (2006 vs 2021). These results showed the largest magnitude of changes in presence for all three call types. Further analysis of these surveys would seem to provide the best prospect of investigating changes attributable to distribution and/or abundance over time. At lower latitudes in the Indian Ocean around Australia, other studies have revealed that the acoustic power in the ABW song band (25-29 Hz) has also increased over time (McCauley et al., 2018). However, these low latitude increases over time could potentially be driven by the same multitude of factors as our Antarctic results.

In contrast to the surveys in the Indian sector, the 2019 ENRICH survey through the DDU Sea region aimed for systematic transects across bathymetric and latitudinal gradients, and these transects were adaptively centred on an area where calls of

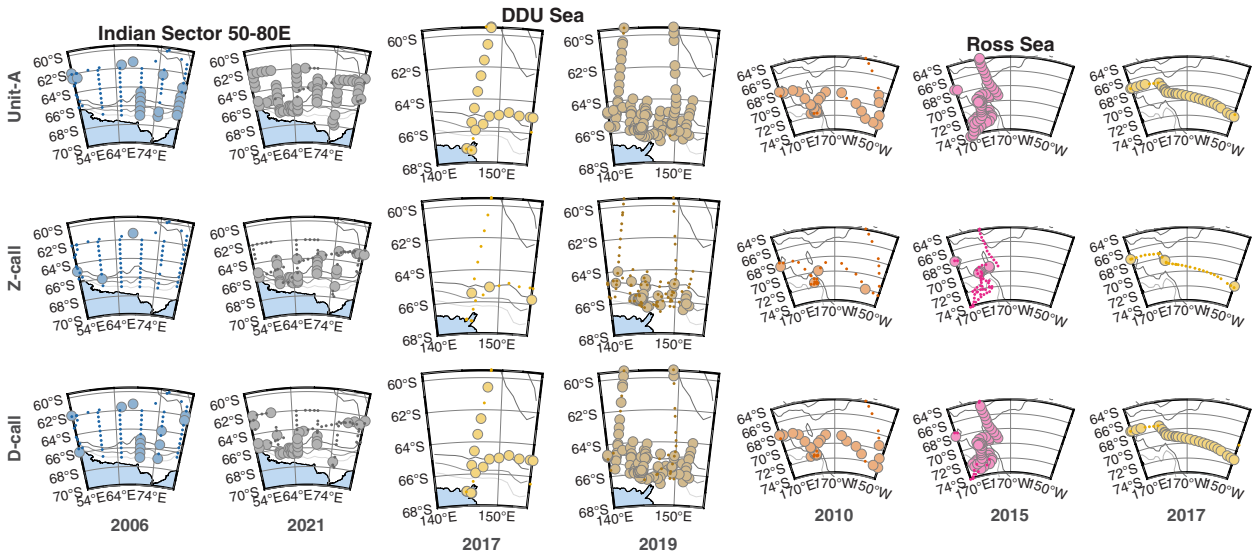


FIGURE 4
Three regional series of maps illustrating the sonobuoy deployment locations (small dots) and presence (large circles) of detections of three call types: Unit-A (top row), Z-calls (middle row), and D-calls (bottom row) across regions and voyages. Left and right panels in each pair show the oldest and most contemporary voyages respectively. Each set of six or nine panels represents a different area, with the first set (columns 1 & 2) representing the Indian Sector (50-80E), the second set (columns 3 & 4) representing the Dumont d'Urville (DDU) Sea, and the last set (columns 5, 6, & 7) representing the Ross Sea. Colours of symbols correspond to the year of survey (same as Figure 2) with each symbol 50% transparent to help indicate overplotting. Gray to black lines show the 1000, 2000, and 3000 m depth contours. Maps created using the software M_Map (Pawlowicz, 2019) and the Global Coastline Database (Wessel and Smith, 1996).

ABWs were initially detected. However, the sonobuoy deployments during the 2017 ACE voyage (contributing the sonobuoys used for the DDU Sea region comparison) were opportunistic, and the voyage track was planned to accommodate direct travel between various points of interest, predominantly glaciers and Antarctic Islands. No attempt was made to obtain uniform spatial coverage. Furthermore, the 2017 ACE voyage and the 2019 ENRICH voyage were conducted only two years apart. Thus it is unlikely that any differences associated with population changes would be detected given that maximum possible population growth rates are low

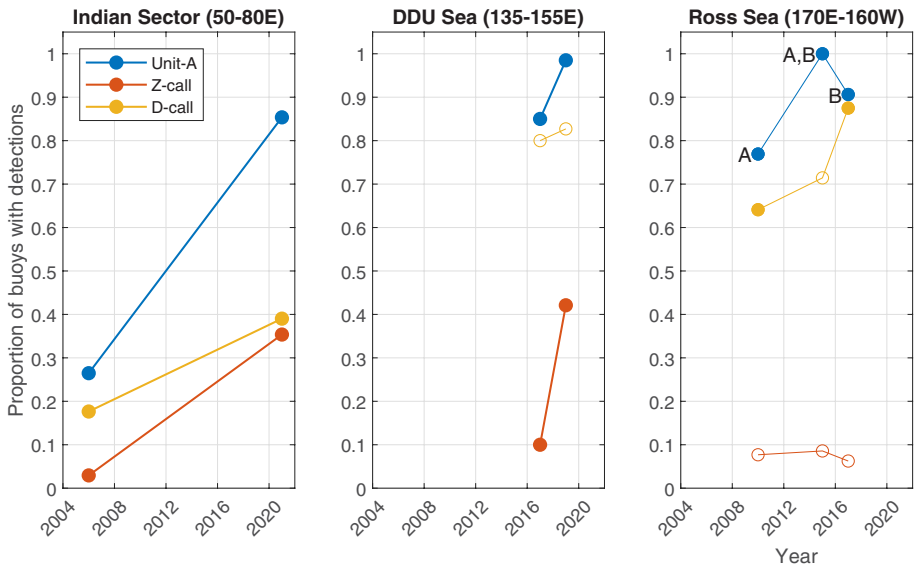


FIGURE 5
Regional comparisons from different voyages illustrating the proportion of sonobuoys with detections of Antarctic blue whale calls. Each panel shows a region with each line representing a call type. Filled circles indicate pairwise comparisons with statistically significant differences (where $p<0.05$). Letters A and B are used to identify which pairs were significantly different for unit-A in the Ross sea (i.e. 2010 and 2017 were each significantly different than 2015, but not each other).

(Branch, 2007). Additionally, there is a large disparity in the duration of the surveys, with the 2017 survey spending only a few days in the region, while the 2019 survey spent 30 days in the region. Further frustrating comparisons, the mean recording duration of sonobuoys deployed during the 2017 was the shortest of all the voyages we analysed, while that of the 2019 voyage was the longest. Thus, it is likely that any differences in detection between these voyages may be driven more by sampling artefacts or inter-annual variability in distribution and behaviour rather than changes in population abundance.

Focal follows of ABWs during the 2013, 2015, and 2019 voyages provide some evidence of different behaviours among these years. In particular, ABW movement rates in the DDU Sea in 2019 differed from those observed in the DDU and Ross Seas in 2013 and from those observed in the Ross Sea in 2015 (Calderan et al., 2023). Furthermore, high inter-annual variability in acoustic detections of fin whales has been observed from long-term acoustic recordings in the DDU Sea compared to other East Antarctic Seas (Aulich et al., 2022). Like blue whales, fin whales feed on Antarctic krill at high latitudes in the summer. Thus, the interannual variability of acoustic detections by both species, along with the high movement rates of blue whales in 2019 suggest that the DDU Sea may have habitat that is favourable to ABWs in some years, and unfavourable in others, and that their observable behaviours may reflect these conditions.

Similar to the 2017 ACE voyage, the 2010 AWE survey through the Ross Sea region was also opportunistic. But instead of direct transits among Antarctic glaciers and Islands, the 2010 AWE voyage focused primarily on humpback whales - collecting biopsy samples, photo-identification images and attaching satellite tags (Gales, 2010). The seven years between the AWE and ACE voyages was long enough that changes in ABW population abundance could potentially be detected. However, the drivers may also have been natural inter-annual variability in distribution, or the different spatial and temporal coverage of the surveys within the region. For example, the 2017 ACE voyage travelled through the Ross Sea from west to east via direct point-to-point travel, whereas the 2010 AWE voyage travelled from east to west via a meandering track in search of humpback whales. Though not included in our regional comparisons due to potential bias, the voyages in 2013 and 2015 both visited the western portion of the Ross Sea with numerous acoustically-assisted encounters of ABWs on both voyages. Across all these voyages, the Ross Sea had the highest effort of all the regions visited. This relatively high effort yielded a consistently high proportion of sonobuoys with detections of unit-A and D-calls. Movement rates of ABWs in the Ross Sea in 2015 were significantly slower than those in the DDU Sea in 2019, and this was due to higher rates of turning, suggestive of area restricted search behaviours typically associated with foraging (Calderan et al., 2023). Furthermore, krill swarm biomass, depth, and height were found to be good predictors of ABW presence in the Ross Sea in 2015 (Miller et al., 2019b). Taken together, this suggests that the Ross Sea was consistently an important foraging area for ABWs over these surveys. The longitude bin with the highest proportion of detections of all call types was also found to the east of the Ross Sea in the adjacent Amundsen Sea. However, the Amundsen Sea had the lowest survey effort, with data only collected during the 2017 voyage. In general, the central Pacific sector of the Antarctic remains scantily sampled for ABWs compared to most other parts of the Southern Ocean, so further data collection would be required to better understand the importance of this region to ABWs.

Drivers of acoustic trends in relation to future research and knowledge gaps

As we have already indicated, there are a number of factors that could be responsible for the changes in acoustic presence (or lack thereof) across regions and call types. These include change in the probability of call detection, change in whale behaviour, change in whale distribution, and change in whale abundance. These potential explanations are not mutually exclusive and can also interact in complex ways. Nevertheless, it is important that future work explores the drivers of acoustic trends and their link to ABW abundance, and that of other cetacean species, because passive acoustics likely present our best, most cost-effective and non-invasive method for monitoring populations long-term and in the face of environmental and climate change. However, in order to achieve this, resources will be required to overcome technological, logistical, biological and analytical challenges.

Fully accounting for all the possible drivers of each of these explanations would require additional efforts that are well beyond the scope of this manuscript. However, it is important to note that the means to address each of these explanations already exist. With further work, each of these potential drivers of acoustic trends could be considered as a hypothesis and could be investigated and accounted for in order to yield better knowledge of this critically endangered subspecies. Therefore, in the next section we briefly explore each of these factors in more detail and outline how they might be addressed with future research. This not only includes new and/or additional analysis of existing datasets, but also proposals for further at-sea studies of ABWs.

Changes in probability of detection

Estimating probability of detection of underwater sounds is challenging, with many factors that can strongly influence the results. These factors can be difficult to measure or even estimate, but include *inter-alia*: the perception bias of the detectors, source levels of the calls, and the noise levels from wind, ice, other animals, and manmade sounds, as well as factors that affect acoustic propagation which in turn includes: distance, depths, bathymetry, seabed composition, and speed of sound all along the pathway that sound travels between the whale and detector. However, there are an increasing number of studies that demonstrate a variety of methods to measure, model, or otherwise account for these factors to better estimate probability of detection of whale calls. In general, these methods usually involve using an automated detector to count calls, and then application of a suite of additional methods to obtain call densities (Harris et al., 2013; Marques et al., 2013; Helble et al., 2013a; Harris et al., 2018; Thode et al., 2020).

Call densities are counts of calls per unit area and per unit time, and these are also typically corrected for observer bias and effort.

Call densities can yield a more detailed picture of spatial and temporal acoustic trends than the simple presence of detections that we have reported here. Obtaining call densities requires application of complex statistical methods that model the observation process, e.g., the passive sonar equation (Küsel et al., 2011; Harris, 2012; Helble et al., 2013b; Harris et al., 2018) and/or implementation of a fundamentally different survey design, e.g. point or line-transect acoustic distance sampling (Marques et al., 2013). Future studies could leverage the ongoing work on acoustic distance sampling or spatially explicit capture-recapture methods when designing surveys and data collection protocols (Harris et al., 2013; Thode et al., 2020; Blackwell et al., 2021; Oedekoven et al., 2021). These methods require arrays of concurrently deployed hydrophones, and would therefore require fundamentally different survey designs to those applied in the Antarctic to date, i.e. where a single-sonobuoy was deployed at each listening station.

Methods that model the observation process, such as sonar equation-based methods, are referred to as auxiliary information methods (Marques et al., 2013). These require knowledge or estimation of a substantial amount of additional information about sound production, propagation through the environment, and detection processes that can in turn be used to model the probability of detection. This information typically includes the key drivers of the parameters of the sonar equation, namely the relationship between signal-to-noise ratio and detection of individual calls; detector/observer bias; transmission loss of sound as it propagates through the environment; distribution of source level of calls; and distribution of noise levels throughout the survey. More recent advances in these techniques also allow for the use of bearing information, similar to those from the DIFAR sonobuoys used here, to estimate fine-scale call density surfaces within the areas monitored (Harris et al., 2018). If knowledge of the call production rates and proportion of population calling is available, then call densities can be multiplied by these quantities in order to estimate animal density or local abundance in the survey area.

It is likely that both distance sampling and auxiliary information methods will be necessary to maximise value from historic and future acoustic surveys. Sonar equation (auxiliary information) based methods would provide a pathway for obtaining call densities from the existing datasets presented here. While new survey platforms, such as fleets of uncrewed underwater or surface vehicles (USVs), potentially each with reusable dipping DIFAR sensors or towed hydrophone arrays, might be better able to accommodate distance-sampling based methods. Additionally, the use of USVs could eliminate any issues of waste that might arise from the non-recovery of sonobuoys. But the success of such a fleet would be contingent on self-noise from the vessel and hydrophones being brought down to sufficiently low levels in the low frequency bands of ABW calls – a feat which could be quite an engineering challenge in itself. It is worth noting that despite the different approaches, both methods produce the same output: call densities. The key benefits of call densities obtained from these methods are that they can: 1) be made statistically robust, 2) be compared directly to each other, and 3) account for all factors except behaviour and abundance (assuming surveys have been appropriately designed). These benefits make call densities more suitable for drawing conclusions about the biology of these animals compared to the call presence per sonobuoy as we have presented here. Given the potential value-add to existing datasets, as well as the potential for even more efficient passive acoustic surveys in the future, the development, refinement, and application of these methods should be considered a priority area of focus for future acoustic work on ABWs. Development of these methods would also have value for other blue whale populations as well as other vocal baleen whale species, not just in the Antarctic, but potentially in all oceans.

Change in abundance

Acoustic assisted mark-recapture surveys (Peel et al., 2014) are likely to remain the most cost-effective way to account for changes in population abundance in ABWs (Peel et al., 2015). In brief, the acoustic assisted surveys proposed by Peel et al. (2015) involve using passive acoustics to more efficiently locate animals for (traditional) mark-recapture surveys using photographic or genetic identification of individual animals. The acoustic targeting of ABWs during the sonobuoy voyages in 2013, 2015, and 2019 were all examples of the acoustically assisted surveys described by Peel et al. (Peel et al., 2014, Peel et al., 2015). USVs, described above, would also likely provide excellent acoustic assistance in the form of near real-time detection, localisation, and call density estimation of ABWs. In many scenarios, particularly in the Antarctic, acoustic surveys from fleets of USVs could be more cost effective than in-situ deployment of sonobuoys from the limited number of crewed research, cargo, and icebreaking vessels that transit this remote region. The photographic and genetic estimates of whale abundance from acoustically-assisted capture-recapture studies could also be compared with acoustically-derived estimates of whale abundance (which in turn would be derived by multiplying the above described call densities from sonobuoys and/or moored recorders by the cue rates obtained from the tagging studies described below).

Change in whale behaviour

Sonobuoy surveys ultimately provide limited capacity to understand changes in whale behaviour. The sorts of behavioural changes that can be detected with sonobuoys are factors such as the duration of bouts of detections, or changes in the structure or nature of calls and call units. These types of changes are not fully representative of the behavioural changes that could drive acoustic trends over time. For example, sonobuoy surveys alone would provide no means of discerning whether the proportion of vocalising animals has changed. However, such studies have been successfully conducted on blue whales in other oceans using concurrent acoustic and visual focal follows and suction-cup acoustic recording tags (Oleson et al., 2007a, b; Lewis et al., 2018). In addition to the proportion of vocalising animals, such studies can also provide knowledge of call production rates and demographics of vocalising animals. Such knowledge is unlikely to be obtained purely from stand-alone acoustic studies, but could heavily influence detection rates, metrics of acoustic presence, and interpretation of trends. These studies also provide information about the depth distribution of vocalising animals, which is important for modelling detection range from acoustic propagation models (e.g. see Miller et al., 2021a). Near real-time detection, localisation, and call density estimation from a network of USVs, as

proposed in the previous section, could greatly assist in locating both densely and sparsely aggregated groups of vocalising ABWs for such tagging and focal follow studies. However, care would need to be taken to ensure that targeting groups of vocalising whales does not bias the results.

Change in distribution

Assuming that probability of detection, changes in whale behaviour, and changes in population abundance can be, or have already been addressed, then changes in distribution would be the most likely remaining explanation for any residual changes over time. Such changes could be addressed by additional passive acoustic surveys at increasingly finer scales in regions of interest with increasing spatial and temporal coverage. Additionally or alternatively, further analysis of distribution with respect to environmental covariates could be conducted in a manner similar to analyses of the SOWER sonobuoy data (Shabangu et al., 2017). While such analyses could be conducted solely with presence of calls, a clearer signal would likely emerge from using call densities, or acoustically derived ABW densities as the response variable.

Synergies among proposed future research paths

The factors that might affect acoustic trends such as probability of detection, whale behaviour, abundance, and distribution may interact in complex ways. However, we have outlined above several proposed research paths that could potentially address all of these factors. Furthermore, there are many synergies among these proposed solutions. Addressing all of these factors would expand and add value to two decades' of existing data, and would substantially improve our understanding of the distribution, life history, and population recovery of Antarctic blue whales and also be applicable to other species. Additionally, the proposed solutions to address these issues would also synergize with addressing knowledge gaps regarding whale abundance and distribution, and consumption rates and krill swarm preferences, to support management decisions undertaken by CCAMLR (CCAMLR, 2019 paragraph 5.17) and the IWC (Leaper and Childerhouse, 2014). For example, acoustic recording & accelerometry tags not only provide an estimate of acoustic cue rates, but can also be used to understand lunge (feeding) rates, a proxy for consumption (Nowacek et al., 2016). Further inter-disciplinary synergies beyond research on ABWs would also be highly tractable. For example, our proposed fleet of USVs could also be equipped with scientific echosounders to obtain information on krill in the vicinity of vocalising whales. This information could then be used to better understand the relationship between ABWs and krill (abundance, distribution, and swarm characteristics), via investigations similar to that described in previous studies of ABWs (Miller et al., 2019b) and other Antarctic whale species (Santora et al., 2010; Nowacek et al., 2011; Herr et al., 2016; Baines et al., 2022).

Conclusion

Sonobuoy surveys have provided the most contemporary data on the summer distribution of Antarctic blue whales (ABWs) on their Antarctic feeding grounds. The three classifications of calls that we investigated had different distributions relative to each other, but all appear to have a circumpolar distribution around the Antarctic and through the sub-Antarctic, but with Z-calls concentrated towards higher latitudes in the summer. Over multi-year to decadal timescales, the proportion of sonobuoys with presence of these three call types was predominantly higher in more recent surveys in the three regions where comparisons were viable.

To better understand these results and add value to these and other long-term datasets, we have outlined an efficient and holistic plan for future studies of ABWs. We propose continued synoptic passive acoustic surveys, but also several additional data collection and analytical methods that are synergistic. These methods include: refinement and application of call density analyses to existing sonobuoy and long-term acoustic datasets; development and deployment of fleets of USVs with reusable dipping DIFAR sensors or low-frequency towed hydrophone arrays for future passive acoustic data collection; tagging a substantial number of ABWs with high-resolution hydrophone accelerometry tags to understand acoustic cue rates and foraging rates; and acoustically assisted photographic identification and genetic capture-recapture studies to estimate population abundance. Thus, passive acoustic monitoring is poised to play a crucial role in future research addressing knowledge gaps about ABWs. These acoustic methods provide an efficient, cost-effective means for long-term monitoring of this endangered species, other species, and environmental variables, such as ice and waves, in the face of environmental change.

Data availability statement

The original contributions presented in the study are included in the article/Supplementary Material, further inquiries can be directed to the corresponding author/s.

Ethics statement

Data collection from sonobuoys during these studies was conducted under Notices of Determination and Authorisation provided by the Australian Antarctic Division for Australian Antarctic Science (AAS) projects #2655; 2683; 2941; 4102; 4512; 4600; 4636 as per the Antarctic Treaty (Environmental Protection) Act 1980 of Australia.

Author contributions

BM: Writing – review & editing, Writing – original draft, Visualization, Software, Project administration, Methodology, Investigation, Funding acquisition, Data curation, Conceptualization. VA-G: Writing – review & editing, Writing – original draft, Project administration, Funding acquisition. JB: Writing – review & editing, Writing – original draft, Methodology, Investigation, Data curation. EB: Writing – review & editing, Writing – original draft, Project

administration, Funding acquisition. SC: Writing – review & editing, Writing – original draft, Methodology, Investigation, Data curation. MD: Writing – review & editing, Writing – original draft, Project administration, Funding acquisition. JG: Writing – review & editing, Software, Project administration, Methodology, Investigation, Funding acquisition, Data curation. NK: Writing – review & editing, Writing – original draft, Project administration, Funding acquisition, Conceptualization. SL: Writing – review & editing, Writing – original draft, Project administration, Methodology, Investigation, Data curation. RL: Writing – review & editing, Writing – original draft, Methodology, Investigation, Data curation. EM: Writing – review & editing, Writing – original draft, Project administration, Methodology, Investigation, Data curation. KR: Writing – review & editing, Writing – original draft, Methodology, Investigation, Data curation. AŠ: Writing – review & editing, Writing – original draft, Methodology, Investigation, Funding acquisition, Data curation. KS: Writing – review & editing, Writing – original draft, Methodology, Investigation, Funding acquisition, Data curation.

Funding

The author(s) declare financial support was received for the research, authorship, and/or publication of this article. This work was made possible with the support of numerous Australian Antarctic Science (AAS) Projects with gracious and excellent support from personnel at the Australian Antarctic Division. These projects include: AAS Project 2655: An integrated survey of the waters between 30 and 80 degrees East (CCAMLR Division 58.4.2); AAS Project 2683: Passive acoustic monitoring of Antarctic marine mammals; AAS Project 2941: Conservation and Management Science of Marine Mammals; AAS Project 4102: Population abundance, trend, structure and distribution of the endangered Antarctic blue whale; AAS Project 4512: Ensuring sustainable management of the krill fishery in waters off the Australian Antarctic Territory; AAS Project 4600: Conservation and management of Australian and Antarctic whales – post-exploitation status, distribution, foraging ecology and their role in the Southern Ocean ecosystem; AAS Project 4636: Sustainable Management of Antarctic Krill and Conservation of the Krill-based Ecosystem. The 2017 ACE voyage was a scientific expedition carried out under the auspices of the Swiss Polar Institute, supported by funding from the ACE Foundation and Ferring Pharmaceuticals with major funding provided by the Swiss Polar Institute and the Australian Antarctic Division. AŠ and KS were supported by grants from the US National Science Foundation Office of Polar Programs (1745930) and the International Whaling Commission's Southern Ocean Research Partnership (IWC-SORP). Thanks to the CSIRO Marine National Facility (MNF) for its support in the form of sea time on RV Investigator, support personnel, scientific equipment and data management on the voyages in 2019 and 2021.

Acknowledgments

We thank the excellent crews and support staff of all the ships that were used to conduct these voyages: the RV Aurora Australis, FV Amaltal Explorer, RV Tangaroa, MV Akademik Treshnikov, and RV Investigator. Special thanks to the TEMPO ad-hoc sonobuoy team, Jez Bird, Derek Hamer, Angus Henderson, Joshua Smith, Maria Isabel Garcia Rojas, Rob King, Alicia Burns, Jessica Melvin, Madeleine Brasier, Christine Weldrick, Olivia Johnstone who all undertook sonobuoy preparation, deployment, and data acquisition during the 2021 voyage on top of their other full-time duties on the visual observation team and krill team. Thanks to Voyage Chief Scientists: Steve Nicol (2006), Nick Gales (2010), Richard O'Driscoll (2015), David Walton (2017), and So Kawaguchi (2021) for their patience and support at sea for this work. Thanks to Simon Wotherspoon for advice and code on implementing the log-odds statistical tests.

Conflict of interest

The authors declare that the research was conducted in the absence of any commercial or financial relationships that could be construed as a potential conflict of interest.

The reviewer JR declared a past co-authorship with the author JG.

Publisher's note

All claims expressed in this article are solely those of the authors and do not necessarily represent those of their affiliated organizations, or those of the publisher, the editors and the reviewers. Any product that may be evaluated in this article, or claim that may be made by its manufacturer, is not guaranteed or endorsed by the publisher.

Supplementary material

The Supplementary Material for this article can be found online at: https://www.frontiersin.org/articles/10.3389/fmars.2024.1324816/full#supplementary-material

References

Andrews-Goff, V., Bell, E., Miller, B., Wotherspoon, S., and Double, M. (2022). Satellite tag derived data from two Antarctic blue whales (Balaenoptera musculus intermedia) tagged in the east Antarctic sector of the Southern Ocean. *Biodivers. Data J.* 10, e94228. doi: 10.3897/BDJ.10.e94228

Aulich, M. G., Mccauley, R. D., Miller, B. S., Samaran, F., Giorli, G., Saunders, B. J., et al. (2022). Seasonal distribution of the fin whale (Balaenoptera physalus) in antarctic and Australian waters based on passive acoustics. *Front. Mar. Sci.* 9, 1–15. doi: 10.3389/fmars.2022.864153

Baines, M., Jackson, J. A., Fielding, S., Warwick-Evans, V., Reichelt, M., Lacey, C., et al. (2022). Ecological interactions between Antarctic krill (Euphausia superba) and baleen whales in the South Sandwich Islands region – Exploring predator-prey biomass ratios. *Deep Sea Res. Part I: Oceanogr. Res. Pap.* 189, 103867. doi: 10.1016/j.dsr.2022.103867

Baines, M., Kelly, N., Reichelt, M., Lacey, C., Pinder, S., Fielding, S., et al. (2021). Population abundance of recovering humpback whales Megaptera novaeangliae and other baleen whales in the Scotia Arc, South Atlantic. *Mar. Ecol. Prog. Ser.* 676, 77–94. doi: 10.3354/meps13849

Balcazar, N. E., Tripovich, J. S., Klinck, H., Nieukirk, S. L., Mellinger, D. K., Dziak, R. P., et al. (2015). Calls reveal population structure of blue whales across the southeast Indian Ocean and southwest Pacific Ocean. *J. Mammal.* 96 (6), 1184–1193. doi: 10.1093/jmammal/gyv126

Berchok, C. L., Bradley, D. L., and Gabrielson, T. B. (2006). St. Lawrence blue whale vocalizations revisited: Characterization of calls detected from 1998 to 2001. *J. Acoust. Soc. America* 120, 2340. doi: 10.1121/1.2335676

Blackwell, S. B., Thode, A. M., Conrad, A. S., Ferguson, M. C., Berchok, C. L., Stafford, K. M., et al. (2021). Estimating acoustic cue rates in bowhead whales, Balaena mysticetus, during their fall migration through the Alaskan Beaufort Sea. *J. Acoust. Soc. America* 149, 3611–3625. doi: 10.1121/10.0005043

Bouffaut, L., Landrø, M., and Potter, J. R. (2021). Source level and vocalizing depth estimation of two blue whale subspecies in the western Indian Ocean from single sensor observations. *J. Acoust. Soc. America* 149, 4422–4436. doi: 10.1121/10.0005281

Branch, T. A. (2007). Abundance of Antarctic blue whales south of 60 S from three complete circumpolar sets of surveys. *J. Cetacean Res. Manage.* 9, 253–262. doi: 10.47536/jcrm.v9i3

Branch, T. A., and Butterworth, D. S. (2001). Estimates of abundance south of 60° S for cetacean species sighted frequently on the 1978/79 to 1997/98 IWC/IDCR-SOWER sighting surveys. *J. Cetacean Res. Manage.* 3, 251–270. doi: 10.47536/jcrm.v3i3

Branch, T. A., Stafford, K. M., Palacios, D. M., Allison, C., Bannister, J. L., Burton, C. L. K., et al. (2007). Past and present distribution, densities and movements of blue whales *Balaenoptera musculus* in the Southern Hemisphere and northern Indian Ocean. *Mammal Rev.* 37, 116–175. doi: 10.1111/j.1365-2907.2007.00106.x

Buchan, S., and Quiñones, R. (2016). First insights into the oceanographic characteristics of a blue whale feeding ground in northern Patagonia, Chile. *Mar. Ecol. Prog. Ser.* 554, 183–199. doi: 10.3354/meps11762

Calderan, S., Miller, B. S., Leaper, R. C., and Miller, E. (2019). *Passive acoustic recordings from sonobuoys deployed during the Antarctic Circumnavigation Expedition 2017*. Australian Antarctic Data Centre. doi: 10.4225/15/59D5A05F6050F

Calderan, S. V., Leaper, R., Andrews-Goff, V., Miller, B. S., Olson, P. A., Reyes, M. V. R., et al. (2023). Surfacing rates, swim speeds, and patterns of movement of Antarctic blue whales. *Front. Mar. Sci.* 10. doi: 10.3389/fmars.2023.1087967

Carroll, G., Hedley, S., Bannister, J., Ensor, P., and Harcourt, R. (2014). No evidence for recovery in the population of sperm whale bulls off Western Australia, 30 years post-whaling. *Endangered Species Res.* 24, 33–43. doi: 10.3354/esr00584

CCAMLR. (1980). *Convention on the Conservation of Antarctic Marine Living Resources*. Hobart, Tasmania, Australia: Commission for the Conservation of Antarctic Marine Living Resources.

CCAMLR. (2019). *Report of the Thirty-eighth Meeting of the Commission (CCAMLR-38)* (Hobart, Australia: CCAMLR). Available at: https://meetings.ccamlr.org/en/system/files?file=e-cc-38_0.pdf (Accessed October 13, 2023).

Cooke, J. G. (2018). *Balaenoptera musculus ssp. intermedia* (Cambridge, UK: The IUCN Red List of Threatened Species), e.T41713A50226962. doi: 10.2305/IUCN.UK.2018-2.RLTS.T41713A50226962.en

Double, M. C., Andrews-Goff, V., Jenner, K. C. S., Jenner, M.-N., Laverick, S. M., Branch, T. A., et al. (2014). Migratory Movements of Pygmy Blue Whales (Balaenoptera musculus brevicauda) between Australia and Indonesia as Revealed by Satellite Telemetry. *PloS One* 9, e93578. doi: 10.1371/journal.pone.0093578

Double, M., and Miller, B. S. (2017). *Passive acoustic recordings from sonobuoys deployed during the NZ-Aus Antarctic Ecosystems Voyage 2015*. Australian Antarctic Data Centre. doi: 10.4225/15/59BA06898FD65

Double, M. C., Miller, B. S., Leaper, R., Olson, P., Cox, M. J., Miller, E., et al. (2015). "Cruise report on blue whale research from the NZ/Aus Antarctic Ecosystems Voyage 2015 of the Southern Ocean Research Partnership," in Paper submitted to the Scientific Committee of the International Whaling Commission. *SC/66a/SH7*. Cambridge, UK: International Whaling Commission, 1–22.

Gales, N. (2010). "Antarctic Whale Expedition: Preliminary science field report and summary," in Submitted to the Scientific Committee of the International Whaling Commission *SC/62/O12*. Ed. R. V. Tangaroa Cambridge, UK: International Whaling Commission, 21.

Gaskin, D. E. (1976). The evolution, zoogeography and ecology of cetacea. *Oceanog. Mar. Biol. Ann. Rev.* 14, 247–346.

Gavrilov, A. N., McCauley, R. D., and Gedamke, J. (2012). Steady inter and intra-annual decrease in the vocalization frequency of Antarctic blue whales. *J. Acoust. Soc. America* 131, 4476–4480. doi: 10.1121/1.4707425

Gedamke, J. (2011). *Passive acoustic monitoring of Antarctic marine mammals*. Australian Antarctic Data Centre. doi: 10.26179/4Z72-8984

Gedamke, J., and Robinson, S. (2014). *Marine mammal acoustic survey data from sonobuoy deployments on the BROKE-WEST Survey, Ver. 2*. Australian Antarctic Data Centre. doi: 10.4225/15/53F54E16A74A1. Accessed: 2024-04-16.

Gedamke, J., and Robinson, S. M. (2010). Acoustic survey for marine mammal occurrence and distribution off East Antarctica (30-80°E) in January-February 2006. *Deep Sea Res. Part II: Topic. Stud. Oceanogr.* 57, 968–981. doi: 10.1016/j.dsr2.2008.10.042

Greene, C. R. Jr., McLennan, M. W., Norman, R. G., McDonald, T. L., Jakubczak, R. S., and Richardson, W. J. (2004). Directional frequency and recording (DIFAR) sensors in seafloor recorders to locate calling bowhead whales during their fall migration. *J. Acoust. Soc. America* 116, 799–813. doi: 10.1121/1.1765191

Harris, D. V. (2012). *Estimating whale abundance using sparse hydrophone arrays*. Available at: https://research-repository.st-andrews.ac.uk/handle/10023/3463 (Accessed May 23, 2023).

Harris, D., Matias, L., Thomas, L., Harwood, J., and Geissler, W. H. (2013). Applying distance sampling to fin whale calls recorded by single seismic instruments in the northeast Atlantic. *J. Acoust. Soc. America* 134, 3522–3535. doi: 10.1121/1.4821207

Harris, D. V., Miksis-Olds, J. L., Vernon, J. A., and Thomas, L. (2018). Fin whale density and distribution estimation using acoustic bearings derived from sparse arrays. *J. Acoust. Soc. America* 143, 2980–2993. doi: 10.1121/1.5031111

Helble, T. A., D'Spain, G. L., Campbell, G. S., and Hildebrand, J. A. (2013a). Calibrating passive acoustic monitoring: Correcting humpback whale call detections for site-specific and time-dependent environmental characteristics. *J. Acoust. Soc. America* 134, EL400–EL406. doi: 10.1121/1.4822319

Helble, T. A., D'Spain, G. L., Hildebrand, J. A., Campbell, G. S., Campbell, R. L., and Heaney, K. D. (2013b). Site specific probability of passive acoustic detection of humpback whale calls from single fixed hydrophones. *J. Acoust. Soc. America* 134, 2556–2570. doi: 10.1121/1.4816581

Herr, H., Viquerat, S., Siegel, V., Kock, K.-H., Dorschel, B., Huneke, W. G. C., et al. (2016). Horizontal niche partitioning of humpback and fin whales around the West Antarctic Peninsula: evidence from a concurrent whale and krill survey. *Polar Biol.* 39, 799–818. doi: 10.1007/s00300-016-1927-9

Jefferies, C. S. (2018). International whale conservation in a changing climate: the ecosystem approach, marine protected areas, and the international whaling commission. *J. Int. Wildl. Law Policy* 21, 239–280. doi: 10.1080/13880292.2018.1547867

Kawaguchi, S., and Nicol, S. (2020). "Krill Fishery," in *Fisheries and Aquaculture*, vol. 9. Eds. G. Lovrich and M. Thiel (New York, NY, USA: Oxford University Press). doi: 10.1093/oso/9780190865627.003.0006

Kawamura, A. (1980). A review of food of balaenopterid whales. *Sci. Rep. Whales Res. Inst. Tokyo* 32, 155–197.

Kelly, N., Bestley, S., Burns, A., Clarke, L., Collins, K., Cox, M., et al. (2021). "An overview of the ecosystem survey to quantify krill abundance for krill monitoring and management in Eastern Sector of CCAMLR Division 58.4.2: Trends in Euphausiids off Mawson, Predators, and Oceanography "TEMPO."," in *Paper submitted to the Scientific Committee of the Comission for the Conservation of Antarctic Marine Living Resources*, vol. 26. (Hobart, Tasmania, Australia: Working Group on Ecosystem Monitoring and Management).

Kelly, N., Collins, K., and Miller, B. S. (2023). *Cetacean acoustic presence by species: TEMPO 2021 Sonobuoys*. Australian Antarctic Data Centre. doi: 10.26179/z2zn-j090

Küsel, E. T., Mellinger, D. K., Thomas, L., Marques, T. A., Moretti, D., and Ward, J. (2011). Cetacean population density estimation from single fixed sensors using passive acoustics. *J. Acoust. Soc. America* 129, 3610–3622. doi: 10.1121/1.3583504

Leaper, R., and Childerhouse, S. (2014). "Present and Future Conservation Management of Antarctic Baleen Whales," in *Antarctic Futures: Human Engagement with the Antarctic Environment*. Eds. T. Tin, D. Liggett, P. T. Maher and M. Lamers (Springer Netherlands, Dordrecht), 97–112. doi: 10.1007/978-94-007-6582-5_4

Leroy, E. C., Samaran, F., Bonnel, J., and Royer, J. (2016). Seasonal and diel vocalization patterns of Antarctic blue whale (Balaenoptera musculus intermedia) in the Southern Indian Ocean: A multi-year and multi-site study. *PloS One* 11, e0163587. doi: 10.1371/journal.pone.0163587

Letsheleha, I. S., Shabangu, F. W., Farrell, D., Andrew, R. K., la Grange, P. L., and Findlay, K. P. (2022). Year-round acoustic monitoring of Antarctic blue and fin whales in relation to environmental conditions off the west coast of South Africa. *Mar. Biol.* 169, 41. doi: 10.1007/s00227-022-04026-x

Lewis, L. A., Calambokidis, J., Stimpert, A. K., Fahlbusch, J., Friedlaender, A. S., McKenna, M. F., et al. (2018). Context-dependent variability in blue whale acoustic behaviour. *R. Soc. Open Sci.* 5. doi: 10.1098/rsos.180241

Ljungblad, D. K., Clark, C. W., and Shimada, H. (1998). A comparison of sounds attributed to pygmy blue whales (Balaenoptera musculus brevicauda) recorded south of the Madagascar Plateau and those attributed to 'true' blue whales (Balaenoptera musculus) recorded off Antarctica. *Rep. Int. Whaling Commission* 48, 439–442.

Möller, L. M., Attard, C. R. M., Bilgmann, K., Andrews-Goff, V., Jonsen, I., Paton, D., et al. (2020). Movements and behaviour of blue whales satellite tagged in an Australian upwelling system. *Sci. Rep.* 10, 21165. doi: 10.1038/s41598-020-78143-2

Mackintosh, N. A. (1966). "The distribution of southern blue and fin whales," in *Whales, dolphins and porpoises*. Ed. K. S. Norris (University of California Press, Berkeley and Los Angeles), 125–145.

Mackintosh, N., Wheeler, J., and Clowes, A. (1929). Southern blue and fin whales. *Discovery Rep.* 1, 257–540.

Maranda, B. H. (2001). *Calibration Factors for DIFAR Processing. Technical Memorandum DREA TM 2001-197* (Dartmouth, NS, Canada: Defence Research Establishment Atlantic Canada).

Marques, T. A., Thomas, L., Martin, S. W., Mellinger, D. K., Ward, J. A., Moretti, D. J., et al. (2013). Estimating animal population density using passive acoustics. *Biol. Rev.* 88, 287–309. doi: 10.1111/brv.12001

McCauley, R. D., Gavrilov, A. N., Jolliffe, C. D., Ward, R., and Gill, P. C. (2018). Pygmy blue and Antarctic blue whale presence, distribution and population parameters in southern Australia based on passive acoustics. *Deep-Sea Res. Part II: Topic. Stud. Oceanogr.* 157-158, 154–168. doi: 10.1016/j.dsr2.2018.09.006

McDonald, M. A., Calambokidis, J., Teranishi, A. M., and Hildebrand, J. A. (2001). The acoustic calls of blue whales off California with gender data. *J. Acoust. Soc. America* 109, 1728–1735. doi: 10.1121/1.1353593

Miller, B. S., Barlow, J., Calderan, S., Collins, K., Leaper, R., Olson, P., et al. (2015). Validating the reliability of passive acoustic localisation: a novel method for encountering rare and remote Antarctic blue whales. *Endangered Species Res.* 26, 257–269. doi: 10.3354/esr00642

Miller, B. S., Calderan, S., Gillespie, D., Weatherup, G., Leaper, R., Collins, K., et al. (2016). Software for real-time localization of baleen whale calls using directional sonobuoys: A case study on Antarctic blue whales. *J. Acoust. Soc. America* 139, EL83–EL89. doi: 10.1121/1.4943627

Miller, B. S., Calderan, S., Leaper, R. C., Collins, K., Barlow, J., and Double, M. (2014a). *Passive acoustic data from sonobuoys deployed during the 2013 Antarctic Blue Whale Voyage*. Australian Antarctic Data Centre. doi: 10.4225/15/53EC41A5230B1

Miller, B. S., Calderan, S., Leaper, R., Miller, E. J., Širović, A., Stafford, K. M., et al. (2021a). Source level of Antarctic blue and fin whale sounds recorded on sonobuoys deployed in the deep-ocean off Antarctica. *Front. Mar. Sci.* 8. doi: 10.3389/fmars.2021.792651

Miller, B. S., Calderan, S., Miller, E., Širović, A., and Stafford, K. M. (2021b). *Recordings of underwater sound and detections of marine mammals from sonobuoys deployed during 2019 ENRICH Voyage*. Australian Antarctic Data Centre. doi: 10.26179/W901-B438

Miller, B. S., Calderan, S., Miller, E. J., Širović, A., Stafford, K. M., Bell, E., et al. (2019a). "A passive acoustic survey for marine mammals conducted during the 2019 Antarctic voyage on Euphausiids and Nutrient Recycling in Cetacean Hotspots (ENRICH)," in *Proceedings of ACOUSTICS 2019*, , Cape Schanck, Victoria, Australia. 1–10 (Australian Acoustical Society).

Miller, B. S., Collins, K., Barlow, J., Calderan, S., Leaper, R., McDonald, M., et al. (2014b). Blue whale vocalizations recorded around New Zealand: 1964-2013. *J. Acoust. Soc. America* 135, 1616–1623. doi: 10.1121/1.4863647

Miller, B. S., Gedamke, J., Calderan, S., Collins, K., Johnson, C., Miller, E., et al. (2014c). "Accuracy and precision of DIFAR localisation systems: Calibrations and comparative measurements from three SORP voyages," in *Submitted to the Scientific Committee 65b of the International Whaling Commission, Bled, Slovenia. SC/65b/SH08*, vol. 14. Cambridge, UK: International Whaling Commission.

Miller, B. S.IWC SORP Acoustic Trends Working Group, , Stafford, K. M., Van Opzeeland, I., Harris, D., Samaran, F., et al. (2021c). An open access dataset for developing automated detectors of Antarctic baleen whale sounds and performance evaluation of two commonly used detectors. *Sci. Rep.* 11, 806. doi: 10.1038/s41598-020-78995-8

Miller, B. S., Miller, E., Calderan, S., Leaper, R., Stafford, K., Širović, A., et al. (2017). "Circumpolar acoustic mapping of endangered Southern Ocean whales: Voyage report and preliminary results for the 2016/17 Antarctic Circumnavigation Expedition," in *Paper SC/67a/SH03 submitted to the Scientific Committee 67a of the International Whaling Commision*, vol. 18. (Cambridge, UK: International Whaling Commission).

Miller, E. J., Potts, J. M., Cox, M. J., Miller, B. S., Calderan, S., Leaper, R., et al. (2019). The characteristics of krill swarms in relation to aggregating Antarctic blue whales. *Sci. Rep.* 9, 16487. doi: 10.1038/s41598-019-52792-4

MIL-S-81487 (1996). *Military Specification for AN/SSQ-53D Sonobuoy, MIL-S-81487E(AS)*. Lakehurst, NJ USA: Naval Air Engineering Center, Systems Engineering and Standardization Department (SESD).

Noad, M. J., Kniest, E., and Dunlop, R. A. (2019). Boom to bust? Implications for the continued rapid growth of the eastern Australian humpback whale population despite recovery. *Popul. Ecol.* 61, 198–209. doi: 10.1002/1438-390X.1014

Nowacek, D. P., Christiansen, F., Bejder, L., Goldbogen, J. A., and Friedlaender, A. S. (2016). Studying cetacean behaviour: new technological approaches and conservation applications. *Anim. Behav.* 120, 235–244. doi: 10.1016/j.anbehav.2016.07.019

Nowacek, D. P., Friedlaender, A. S., Halpin, P. N., Hazen, E. L., Johnston, D. W., Read, A. J., et al. (2011). Super-aggregations of krill and humpback whales in Wilhelmina Bay, Antarctic Peninsula. *PloS One* 6, e19173. doi: 10.1371/journal.pone.0019173

Oedekoven, C. S., Marques, T. A., Harris, D., Thomas, L., Thode, A. M., Blackwell, S. B., et al. (2021). A comparison of three methods for estimating call densities of migrating bowhead whales using passive acoustic monitoring. *Environ. Ecol. Stat* 29, 101–125. doi: 10.1007/s10651-021-00506-3

Oleson, E. M., Calambokidis, J., Barlow, J., and Hildebrand, J. A. (2007a). Blue whale visual and acoustic encounter rates in the southern California bight. *Mar. Mammal Sci.* 23, 574–597. doi: 10.1111/j.1748-7692.2007.02303.x

Oleson, E. M., Calambokidis, J., Burgess, W. C., McDonald, M. A., LeDuc, C. A., and Hildebrand, J. A. (2007b). Behavioral context of call production by eastern North Pacific blue whales. *Mar. Ecol. Prog. Ser.* 330, 269–284. doi: 10.3354/meps330269

Opzeeland, I. V., Samaran, F., Stafford, K., Findlay, K., Gedamke, J., Harris, D., et al. (2013). Towards collective circum-Antarctic passive acoustic monitoring: The Southern Ocean Hydrophone Network (SOHN). *Polarforschung* 83, 47–61.

Pallin, L. J., Kellar, N. M., Steel, D., Botero-Acosta, N., Baker, C. S., Conroy, J. A., et al. (2023). A surplus no more? Variation in krill availability impacts reproductive rates of Antarctic baleen whales. *Global Change Biol.* 29, 2108–2121. doi: 10.1111/gcb.16559

Pawlowicz, R. (2019). *M_Map: A mapping package for Matlab. Version 1.4k*. Available at: https://www.eoas.ubc.ca/$\sim$rich/map.html.

Peel, D., Bravington, M., Kelly, N., and Double, M. C. (2015). "Designing an effective mark — recapture study of Antarctic blue whales," in *Ecological Applications*, vol. 25 . Eds. D. Peel, M. Bravington, N. Kelly and M. C. Double (Wiley on behalf of the Ecological Society of America Stable), 1003–1015. Available at: https://www.jstor.org/stable/24432105.

Peel, D, Miller, BS, Kelly, N, Dawson, S, Slooten, E, and Double, MC (2014). A simulation study of acoustic-assisted tracking of whales for mark-recapture surveys. *PloS One* 9 (5), e95602. doi: 10.1371/journal.pone.0095602

Rankin, S., Ljungblad, D. K., Clark, C. W., and Kato, H. (2005). Vocalisations of Antarctic blue whales, *Balaenoptera musculus intermedia*, recorded during the 2001/2002 and 2002/2003 IWC/SOWER circumpolar cruises, Area V, Antarctica. *J. Cetacean Res. And Manage.* 7, 13–20. doi: 10.47536/jcrm.v7i1

Rankin, S., Miller, B., Crance, J., Sakai, T., and Keating, J. L. (2019). *Sonobuoy Acoustic Data Collection during Cetacean Surveys.* NOAA Technical Memorandum NMFS *SWFSC614, 1–36.* San Diego, CA: U.S. Department of Commerce, NOAA Technical Memorandum NMFS-SWFSC614.

R Core Team. (2022). *R: A language and environment for statistical computing*. Available at: https://www.r-project.org/.

Read, A. J. (2023). The ecology of whales in a changing climate. *Science* 382, 159–160. doi: 10.1126/science.adk4244

Rocha, R. C. Jr., Clapham, P. J., and Ivashchenko, Y. (2015). Emptying the oceans: A summary of industrial whaling catches in the 20th century. *Mar. Fish. Rev.* 76, 37–48. doi: 10.7755/MFR

Samaran, F., Adam, O., and Guinet, C. (2010). Detection range modeling of blue whale calls in Southwestern Indian Ocean. *Appl. Acoust.* 71, 1099–1106. doi: 10.1016/j.apacoust.2010.05.014

Samaran, F., Stafford, K. M., Branch, T. A., Gedamke, J., Royer, J.-Y., Dziak, R. P., et al. (2013). Seasonal and geographic variation of Southern blue whale subspecies in the Indian Ocean. *PloS One* 8, e71561. doi: 10.1371/annotation/01e9ce55-8fc3-4eda-964d-755ad7e70e72

Santora, J. A., Reiss, C. C. S., Loeb, V. J. V., and Veit, R. R. R. (2010). Spatial association between hotspots of baleen whales and demographic patterns of Antarctic krill Euphausia superba suggests size-dependent predation. *Mar. Ecol. Prog. Ser.* 405, 255–269. doi: 10.3354/meps08513

Schall, E., Di Iorio, L., Berchok, C., Filún, D., Bedriñana-Romano, L., Buchan, S. J., et al. (2020). Visual and passive acoustic observations of blue whale trios from two distinct populations. *Mar. Mammal Sci.* 36, 365–374. doi: 10.1111/mms.12643

Shabangu, F. (2020). Overview of the IWC SOWER cruise circumpolar acoustic survey data and analyses of Antarctic blue whale calls within the dataset. *J. Cetacean Res. Manage. (special Issue)* 4, 21–37. doi: 10.13140/RG.2.2.20607.02720

Shabangu, F., Andrew, R., Yemane, D., and Findlay, K. (2020). Acoustic seasonality, behaviour and detection ranges of Antarctic blue and fin whales under different sea ice conditions off Antarctica. *Endangered Species Res.* 43, 21–37. doi: 10.3354/esr01050

Shabangu, F. W., Findlay, K. P., Yemane, D., Stafford, K. M., van den Berg, M., Blows, B., et al. (2019). Seasonal occurrence and diel calling behaviour of Antarctic blue whales and fin whales in relation to environmental conditions off the west coast of South Africa. *J. Mar. Syst.* 190, 25–39. doi: 10.1016/j.jmarsys.2018.11.002

Shabangu, F. W., Yemane, D., Stafford, K. M., Ensor, P., and Findlay, K. P. (2017). Modelling the effects of environmental conditions on the acoustic occurrence and behaviour of Antarctic blue whales. *PloS One* 12, e0172705. doi: 10.1371/journal.pone.0172705

Širović, A., and Hildebrand, J. A. (2011). Using passive acoustics to model blue whale habitat off the Western Antarctic Peninsula. *Deep Sea Res. Part II: Topic. Stud. Oceanogr.* 58, 1719–1728. doi: 10.1016/j.dsr2.2010.08.019

Sirovic, A., Hildebrand, J. A., and Thiele, D. (2006). Baleen whale spatial patterns in the Scotia Sea during January and February 2003. *J. Cetacean Res. Manage.* 8, 161–171. doi: 10.47536/jcrm.v8i2

Širović, A., Hildebrand, J. A., and Wiggins, S. M. (2007). Blue and fin whale call source levels and propagation range in the Southern Ocean. *J. Acoust. Soc. America* 122, 1208–1215. doi: 10.1121/1.2749452

Širović, A., Hildebrand, J. A., Wiggins, S. M., McDonald, M. A., Moore, S. E., and Thiele, D. (2004). Seasonality of blue and fin whale calls and the influence of sea ice in the Western Antarctic Peninsula. *Deep Sea Res. Part II: Topic. Stud. Oceanogr.* 51, 2327–2344. doi: 10.1016/j.dsr2.2004.08.005

Širović, A., Hildebrand, J. A., Wiggins, S. M., and Thiele, D. (2009). Blue and fin whale acoustic presence around Antarctica during 2003 and 2004. *Mar. Mammal Sci.* 25, 125–136. doi: 10.1111/j.1748-7692.2008.00239.x

Stewart, J. D., Joyce, T. W., Durban, J. W., Calambokidis, J., Fauquier, D., Fearnbach, H., et al. (2023). Boom-bust cycles in gray whales associated with dynamic and changing Arctic conditions. *Science* 382, 207–211. doi: 10.1126/science.adi1847

Thode, A. M., Blackwell, S. B., Conrad, A. S., Kim, K. H., Marques, T., Thomas, L., et al. (2020). Roaring and repetition: How bowhead whales adjust their call density and source level (Lombard effect) in the presence of natural and seismic airgun survey noise. *J. Acoust. Soc. America* 147, 2061–2080. doi: 10.1121/10.0000935

Thomisch, K. (2017). *Distribution patterns and migratory behavior of Antarctic blue whales* (Bremerhaven, Germany: Alfred-Wegener-Institut Helmholtz-Zentrum für Polar- und Meeresforschung Am). doi: 10.2312/BzPM_0707_2017

Thompson, P. O., Findley, L. T., Vidal, O., and Cummings, W. C. (1996). Underwater sounds of blue whales Balaenoptera musculus in the Gulf of California, Mexico. *Mar. Mammal Sci.* 12, 288–293. doi: 10.1111/j.1748-7692.1996.tb00578.x

Torterotot, M., Samaran, F., and Royer, J.-Y. (2022). Long-term acoustic monitoring of nonstereotyped blue whale calls in the southern Indian Ocean. *Mar. Mammal Sci.* 39 (2), 594–610. doi: 10.1111/mms.12998

Torterotot, M., Samaran, F., Stafford, K. M., and Royer, J.-Y. (2020). Distribution of blue whale populations in the Southern Indian Ocean based on a decade of acoustic monitoring. *Deep Sea Res. Part II: Topic. Stud. Oceanogr.* 179, 104874. doi: 10.1016/j.dsr2.2020.104874

Trathan, P. N. (2023a). The future of the South Georgia and South Sandwich Islands marine protected area in a changing environment: The choice between industrial fisheries, or ecosystem protection. *Mar. Policy* 155, 105773. doi: 10.1016/j.marpol.2023.105773

Trathan, P. N. (2023b). What is needed to implement a sustainable expansion of the Antarctic krill fishery in the Southern Ocean? *Mar. Policy* 155, 105770. doi: 10.1016/j.marpol.2023.105770

Tripovich, J. S., Klinck, H., Nieukirk, S. L., Adams, T., Mellinger, D. K., Balcazar, N. E., et al. (2015). Temporal segregation of the Australian and Antarctic blue whale call types (*Balaenoptera musculus* spp.). *J. Mammal.* 96 (3), 603–610. doi: 10.1093/jmammal/gyv065

Van Parijs, S., Clark, C. W., Sousa-Lima, R. S., Parks, S. E., Rankin, S., Risch, D., et al. (2009). Management and research applications of real-time and archival passive acoustic sensors over varying temporal and spatial scales. *Mar. Ecol. Prog. Ser.* 395, 21–36. doi: 10.3354/meps08123

Wessel, P., and Smith, W. H. F. (1996). A global, self-consistent, hierarchical, high-resolution shoreline database. *J. Geophys. Res.* 101, 8741–8743. doi: 10.1029/96JB00104

Wingfield, J. E., Rubin, B., Xu, J., Stanistreet, J. E., and Moors-Murphy, H. B. (2022). Annual, seasonal, and diel patterns in blue whale call occurrence off eastern Canada. *Endangered Species Res.* 49, 71–86. doi: 10.3354/esr01204

Zerbini, A. N., Adams, G., Best, J., Clapham, P. J., Jackson, J. A., and Punt, A. E. (2019). Assessing the recovery of an Antarctic predator from historical exploitation. *R. Soc. Open Sci.* 6, 190368. doi: 10.1098/rsos.190368

frontiers | Frontiers in Marine Science

TYPE Original Research
PUBLISHED 14 June 2024
DOI 10.3389/fmars.2024.1337080

Check for updates

OPEN ACCESS

EDITED BY
Ibon Galparsoro,
Technological Center Expert in Marine and Food Innovation (AZTI), Spain

REVIEWED BY
Geraint A. Tarling,
British Antarctic Survey (BAS), United Kingdom
Kim Hünerlage,
Thünen Institute, Germany

*CORRESPONDENCE
Camila Cataldo-Mendez
camila.cataldomendez@utas.edu.au

RECEIVED 12 November 2023
ACCEPTED 30 May 2024
PUBLISHED 14 June 2024

CITATION
Cataldo-Mendez C, Kawaguchi S, Cox MJ, Melvin J, Rae V and Swadling KM (2024) The energy content and demographic composition of Antarctic krill (*Euphausia superba*) swarms in East Antarctica. *Front. Mar. Sci.* 11:1337080. doi: 10.3389/fmars.2024.1337080

COPYRIGHT
© 2024 Cataldo-Mendez, Kawaguchi, Cox, Melvin, Rae and Swadling. This is an open-access article distributed under the terms of the Creative Commons Attribution License (CC BY). The use, distribution or reproduction in other forums is permitted, provided the original author(s) and the copyright owner(s) are credited and that the original publication in this journal is cited, in accordance with accepted academic practice. No use, distribution or reproduction is permitted which does not comply with these terms.

The energy content and demographic composition of Antarctic krill (*Euphausia superba*) swarms in East Antarctica

Camila Cataldo-Mendez[1,2]*, So Kawaguchi[2,3], Martin J. Cox[2,3,4], Jessica Melvin[1], Victor Rae[1] and Kerrie M. Swadling[1,2]

[1]Institute for Marine and Antarctic Studies, University of Tasmania, Hobart, TAS, Australia, [2]Australian Antarctic Program Partnership, University of Tasmania, Hobart, TAS, Australia, [3]Southern Ocean Ecosystems Program, Australian Antarctic Division, Department of Climate Change, Energy, The Environment and Water, Kingston, TAS, Australia, [4]Integrated Digital East Antarctica Program, Australian Antarctic Division, Department of Climate Change, Energy, The Environment and Water, Kingston, TAS, Australia

Antarctic krill (*Euphausia superba*) aggregations are important in the Southern Ocean ecosystem; however, the amount of energy that krill swarms contain is unknown. We assessed the population structure of *E. superba* swarms in East Antarctica for two different sectors corresponding to the study areas of the ENRICH (2019) and TEMPO (2021) voyages. We also estimated swarm energy content based on calorific values for whole animals and key tissues (gonads, digestive gland, and muscle). A relationship between the energy content of muscle and gonads in gravid and adult females was detected: The higher the energy content in muscle tissue, the lower the energy content in the gonad tissue. This relationship was consistent for different female maturity stages, suggesting a trade-off in energy allocation between somatic growth and reproduction. Females will redirect energy to gonad development at the expense of somatic growth. Total swarm energy was calculated using the volumetric density of each swarm estimated from an acoustic survey. Four swarm types (A-D) were determined based on the body length and maturity stage of the individuals. The highest energy contents were found in Type B swarms, composed predominantly of adult males and females, and Type D swarms, comprising mostly gravid females. Trends in swarm demographic composition and energy content were consistent between surveys. We recommend swarm energy be incorporated into ecosystem models to represent energy transfer to top predators.

KEYWORDS

bomb calorimetry, energy content, swarm, summer, partitioning

1 Introduction

Antarctic krill (*Euphausia superba*, hereafter "krill") is a vital component of the Southern Ocean ecosystem, having both ecological and commercial importance. Krill plays a central role in carbon export (Cavan et al., 2019) and is a key species in the food web south of the Polar Front in the East Antarctic ecosystem, providing a link between primary production and higher trophic levels. Gaining knowledge about the energy availability and flow from mid-trophic to top trophic levels is critical for ecosystem modelling and management. Krill has a high lipid content (up to 40% of dry mass; Atkinson et al., 2002), and it has been determined that, on average, an adult individual has an energy content between 15.24 and 22.6 KJ g dry mass^{-1} during the summer season (Schaafsma et al., 2018). Furthermore, krill energy content varies with size, sex, and maturity stage (Färber-Lorda et al., 2009; Färber-Lorda and Ceccaldi, 2020).

Krill form large aggregations commonly called swarms, which is a key behavioral and ecological trait. Swarming behavior has been previously attributed to environmental cues such as temperature, oxygen saturation, chlorophyll *a* concentration and/or water column dynamics (Ritz, 2011; Leonori et al., 2017). The formation of swarms has further been linked to predator avoidance, reproduction, and improved fitness by increasing swimming speeds and saving energy for other physiological activities (Hamner and Hamner, 2000; Brierley and Cox, 2010). Physical characteristics of swarms have been at the center of previous classification schemes (e.g. Tarling et al., 2009; Bestley et al., 2018), and studies have primarily focused on attributes such as swarm shape (Cox et al., 2009), packing density, position in the water column and size (Kohut et al., 2019; Miller et al., 2019). However, other characteristics can be useful. For example, the sex ratio or stage composition of swarms can vary from 100% adults to 50:50 adults:juveniles, or an even distribution of juveniles, gravid females, adult males, and sub-adults (Watkins et al., 1986, 1990, 1992). It has been theorized that the physical characteristics of swarms might vary in accordance with the biological characteristics of the krill within a swarm (Amakasu et al., 2011); e.g., swarm shape and packing density might differ for different maturity stages (Tarling et al., 2009). Furthermore, as energy content varies between different developmental stages, it is reasonable to hypothesize that different swarms will have different energy content, not only based on size but also their demographic composition.

The relationships of krill with its predators have been studied from multiple angles, including predator avoidance in space and time (Alonzo and Mangel, 2001; Alonzo et al., 2003), predator energy intake (Friedlaender et al., 2019), and physical characteristics of swarms being targeted (Tarling et al., 2009). Despite extensive research on krill biology and ecology, some aspects with respect to energy availability have been overlooked. Although it is known that krill are a key species in the Southern Ocean food web (Alurralde et al., 2019), the amount of energy that krill swarms contribute to this complex system is unknown. Important questions around this topic are how much energy krill has to offer predators, and how swarm composition affects energy content? That is, what are the specific characteristics of krill swarms that most influence their energy content? Firstly, this study describes the population structure of krill swarms and calculates their energy content. Secondly, it utilizes swarm demographic composition to distinguish between swarm types to ultimately examine which swarm type offers the most energy to predators. As energy content varies between developmental stages, and swarms of equal demographic composition are yet to be found, here it is hypothesized that different swarms have different energy content not only based on swarm size but also their demographic composition.

2 Materials and methods

2.1 Data collection

This study used krill acoustic surveys and biological samples collected during two voyages to the east Antarctic. The Euphausiids and Nutrient Recycling in Cetacean Hotspots (ENRICH) research voyage was carried out between 19 January and 6 March, 2019, with the goal of studying the availability of Antarctic krill to large predators and their role in biogeochemical recycling in the Southern Ocean. The Trends in Euphausiids of Mawson, Predators, and Oceanography (TEMPO) research voyage occurred between 29 January and 24 March, 2021 (Figure 1). The area of operation spanned from 64°S to 63°S and 138°E to 155°E for ENRICH and from 62°S to 68°S and 55°E to 80°E for TEMPO. To detect krill swarms, active acoustic data were collected using a calibrated downward-facing split-beam echosounder (Simrad EK60) operating at 38 and 120 kHz. In this paper we use the term 'swarm' as a broad reference to each patch detected in the acoustic survey and the aggregations sampled during trawls.

Biological samples were collected from a total of 41 trawls during ENRICH and 59 during TEMPO along the pre-determined survey transects (for both voyages). Krill samples were collected using a Rectangular Midwater Trawl (RMT) towed for 7–15 min, with RMT 1 + 8 nets (8 m^2: mesh size 4.5 mm; 1 m^2; mesh size 300 µm) (Everson and Bone, 1986). Once on board, each individual krill was sexed and staged (classified as adult female (not gravid), adult male, sub-adult female, sub-adult male, spent female, gravid female, or juvenile). Finally, body morphometric characteristics (total length (mm), carapace length (mm), wet mass (g) and length of the digestive gland (mm)) were measured (Makarov and Denys, 1984). All specimens were stored in individual vials, snap-frozen in liquid nitrogen, and then stored at -86 °C for later use.

2.2 Sample processing

Krill were chosen from six randomly selected trawls (stations) to perform the energetic measurements. Thirty individuals were randomly chosen from each trawl, representing the population of the sampled swarm. First, all individuals were sexed, and the maturity stage was identified using a Makarov key (Makarov and Denys, 1984).

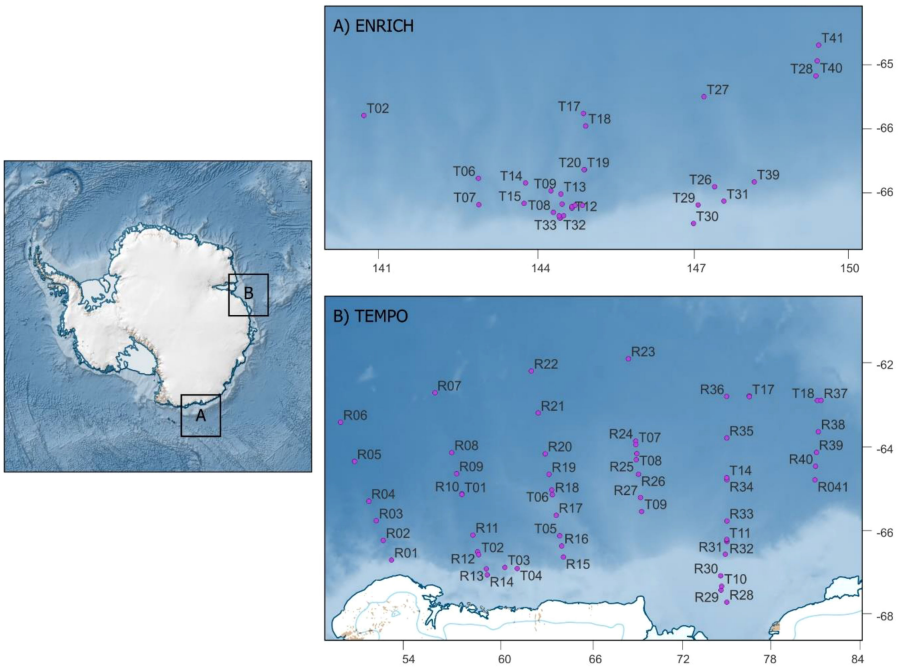


FIGURE 1
Map of study areas **(A)** ENRICH and **(B)** TEMPO. X and y axes on panels **(A, B)** correspond to degrees of longitude and latitude, respectively. Points represent trawl sampling stations. There was a combination of targeted (T) and routine (R) trawls during both voyages; target trawls represent responsive fishing when krill-like echoes were observed through echosounders, +and routine trawls are set locations.

The wet mass was recorded with an analytical balance (GR-200, 0.01 mg precision), and morphological measurements were made using a slide caliper (0.01 mm precision) following the descriptions for standard length 1 in Morris et al. (1988). The samples were defrosted at room temperature for 60 to 80 minutes. Using a dissecting microscope (Leica M12), each individual was then dissected to obtain samples of the following tissues: gonad, digestive gland, muscle, and remaining tissue (further detail in Annex 1). Lastly, the tissues were freeze-dried at -50°C for 48 hours.

2.3 Energy measurements

Bomb calorimetry was used to determine the calories (kilojoules per gram) in each tissue sample. A semi-micro bomb calorimeter (Parr 6725) equipped with a semi-micro-oxygen combustion vessel (Parr 1109A) and a thermometer (Parr 6722) was used for the energy measurements. Prior to each measurement the bomb was calibrated using calorimeter standard benzoic acid pellets (Parr 3418). Dried samples were pooled according to their trawl, sex, stage, and tissue. Then, micro pellets were made using a pellet press (Parr 2811). The pellet size was chosen based on the total dry mass of the samples. 25 mg of dry sample was used for each digestive gland and gonad pellet, 50 mg for the muscle samples and 100 mg for the remaining tissue.

Adult krill are known for their high calorific content (Hagen et al., 2001). However, when dissected, the capacity of some tissues to produce heat decreases causing incomplete sample combustion and leading to invalid results. To overcome this, benzoic acid spikes were used to ensure that complete combustion was achieved for each sample. To ensure the correct weight of spike was used, samples of different sizes were combusted with varying weights of spike, and then a linear regression was fitted to the data (Annex 4). No relationship was found between spike weight and sample heat of combustion, therefore, based on this information, a benzoic acid standard for calorimetry powder (Parr 3402) was used to supplement the spiked pellets, bringing the 'total sample' mass (krill tissue plus spike) to 250 mg. The estimates of gross heat or calorific value (H_c;$KJ\ g^{-1}$) were made using the following:

$$H_c = \frac{WT - e_1 - e_2 - e_3 - (H_{cs})(M_s)}{m} \quad (1)$$

where W is the energy equivalent of the calorimeter in use, T is the observed temperature rise, e_1 is the heat produced by burning the nitrogen portion of the air trapped in the bomb to form nitric acid, e_2 is the heat produced by the combustion of the fuse wire, e_3 corresponds to the fuse wire correction, m corresponds to the mass of the sample, H_{cs} is the heat of combustion of the spike and M_s the mass of the spike.

Equation 1 is based on the substitution procedure, which compares the heat obtained from the sample with the heat obtained by the combustion of a known material. The energy released by the sample during combustion is absorbed within the calorimeter and the resulting temperature change within the medium is recorded. The heat of combustion of the sample is then calculated by multiplying the temperature rise in the

calorimeter by the known heat equivalent of the benzoic acid standards. The formula makes any correction needed based on sample weight, accounting for fuse wire and spike combustion heat using the length of the remaining fuse wire after combustion and the weight of the spike used (further details in Parr 6725 semi-micro calorimeter instruction manual).

2.4 Data processing and analysis

For both surveys, hierarchical clustering was used to group stations with similar biometric and demographic characteristics based on krill total body length and development stage. Total body length, sex and maturity stage were used to determine the extent of similarity between the different stations. The cluster analysis was performed following the methods of Kawaguchi et al. (2010), using Ward distance and posterior multidimensional scaling (MDS) and Sammon mapping to project each station within the correspondent clusters using R and RStudio (RStudio, 2022; R version 4.2.2; packages: Wickham, 2023; MASS Venables and Ripley, 2002).

The mean energy measured in key tissues (gonad, digestive gland, and muscle) was used to calculate the energy content for each individual, grouped by stage, station, and cluster. One-way ANOVA and Tukey HSD *post hoc* tests were performed to evaluate the differences in energy content in tissues and total gross heat between the different stages. Linear regression models were used to assess the relationships between muscle and gonad energy content and total body length for the female stages. The mean energy of each cluster was calculated using the proportional mean energy of each stage, with their proportional standard errors, in units of kilojoules per gram of wet mass (KJ g^{-1} wet mass). This method takes into consideration the percentage of each stage within a swarm. Wet mass energy estimations were calculated based on the linear regression equation (y = a + bx) between whole dry mass and whole wet mass measurements.

To identify the geometrical attributes of swarms/trawls in accordance with their corresponding cluster, polygons were selected by grouping the acoustic line transects into lengths with similar demographics based on the hierarchical clustering results. This was achieved by constructing polygons encompassing areas that enclosed trawls with similar krill demographics. More than one polygon could exist for each cluster. The geometrical attributes of the polygons were described using QGIS (version 3.32.3 Lima), and acoustic transects were then matched to the polygon geometry to classify the acoustic data into clusters. Swarm detection and density estimations within the acoustic survey transects were undertaken as per Cox et al. (2011). In short, aggregations were classified as krill or non-krill using the SHAPES algorithm (Watkins and Brierley, 2002), following the mean volume backscatter strength (ΔS_v) technique with threshold value ΔS_v=120–38 kHz (Reiss et al., 2008), based on the length frequency collected from the net samples. Once an aggregation was determined to be a swarm, the ΔS_v = 120 kHz data were used to calculate the wet mass of krill per m^3 in each swarm (ρ_v) following Equation 2 (Demer and Conti, 2005).

$$\boldsymbol{\rho_v} = \mathbf{10}^{\frac{S_v - TS}{10}} \quad (2)$$

where S_v is the mean volume backscatter in units of *dB re 1* m^{-1}, and *TS* is the krill target strength in units of *dB re 1 kg*.

Swarm volumetric density (ρ_v) (g m^{-3}) was estimated following Cox et al. (2022), ρ_v was then used to calculate the biomass as grams of wet mass for each swarm, estimating volume by assuming that a swarm was detected by the echosounder along its longest length and that swarm shape was cylindrical. Biomass data were interpolated with the proportional mean energy data previously estimated for each swarm type. Swarms within the geometrical area of the polygon were used to determine the total proportional energy of each swarm in megajoules per swarm (MJ $swarm^{-1}$).

3 Results

3.1 Swarm demographic characteristics

Cluster analysis for ENRICH grouped the data into four clusters based on the developmental stage and body length of the individuals sampled in each trawl (Annex 2). All clusters contained the seven maturity stages examined in this study (sub-adult female and male, adult females and males, juveniles, spent females and gravid females), although in different proportions and body length distributions (Figure 2; Annex 3). Cluster 1 was composed predominately of sub-adult males (59%), with an average size of 44.8 ± 5.0 mm (average for sub-adult females and males). Cluster 2 was primarily composed of early life stages, sub-adult females (26%) and adult females (25%) and comprised a wide range of krill lengths as they were composed of all life stages from small juveniles to large gravid females. Cluster 3 was dominated by spent females (62%), and cluster 4 by 60% gravid females. As each cluster was composed of all stages, albeit in different proportions, body length ranged from small juveniles to large adults and gravid females. Cluster 4 was represented by larger individuals, with a mean body length (± standard deviation) of 48.6 ± 4.4 mm (range: 23.8 to 59.7 mm), while cluster 3 had a mean body length of 47.6 ± 4.3 mm (range: from 35.3 to 56.8 mm). Smaller sized krill were found in clusters 1 and 2, with averages of 43.1 ± 3.9 mm (range: 32.2 to 54.1 mm) and 40.9 ± 5.0 mm (range: 19.5 to 55.8 mm), respectively.

Similar results were found for the TEMPO dataset (Annex 2) but body length distribution for TEMPO swarms was overall smaller than observed for the ENRICH dataset, particularly the gravid females (46.1 ± 3.5 mm and 49.5 ± 3.9 mm, respectively). A different average swarm composition was found in cluster 3 for TEMPO. Juveniles with a mean size of 32.9 ± 5.4 mm and sub-adult stages (36.7 ± 3.7 mm females, 39.1 ± 4.8 mm males) dominated the swarm composition. This cluster did not fall into the categories (clusters) described for the ENRICH survey.

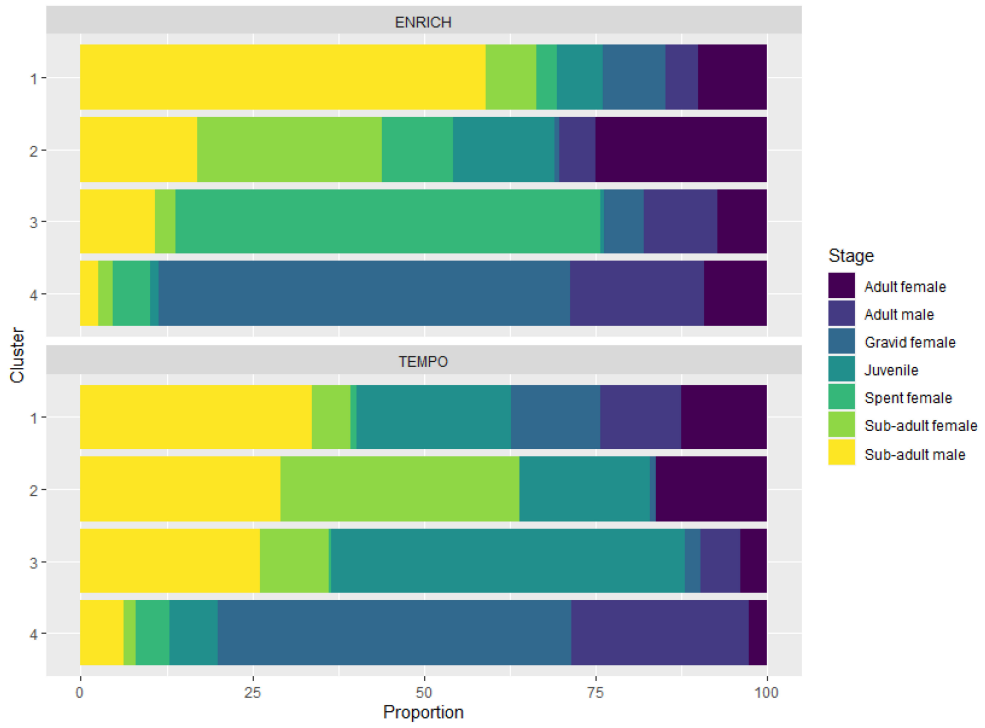


FIGURE 2
Krill stage composition of each cluster for ENRICH (top panel) and TEMPO (bottom panel). Each bar represents one cluster and the sections within a bar represent the percentage of each stage within a given cluster.

3.2 Energy content on different developmental stages

All stages had significantly different individual energy content (Figure 3E) (one-way ANOVA; $p = 0.0021$). Gravid females had a higher mean energy content than other stages, with a mean value of 3.8 KJ ind dry mass^{-1}. Adult males (3.2 KJ ind dry mass^{-1}) had a statistically significant lower energy content than adult females (3.4 KJ ind dry mass^{-1}) (Tukey's *post hoc* test, $p = 0.0241$). Juveniles had the lowest mean energy content (2.4 KJ ind dry mass^{-1}) among all stages. Finally, spent females had the lowest energy content among all female stages (3.2 KJ ind dry mass^{-1}). We standardized the energy content and expressed the results in mean kilojoules per gram of dry mass and found that adult females (21.19 KJ g dry mass^{-1}) had a higher energy content than other stages, followed by juveniles (21.15 KJ g dry mass^{-1}), adult males (21.14 KJ g dry mass^{-1}), spent females (20.37 KJ g dry mass^{-1}) and gravid females (20.36 KJ g dry mass^{-1}) (Figure 3F; Annex 6). The mean energy content for sub-adult females and males are 21.01 and 21.29 KJ g dry mass^{-1}, respectively.

3.3 Energy allocation

Energy allocation varied between the tissues of all stages (see details in Figures 3A–D and values in Annex 6 and 7). Gravid females partitioned more energy into the gonads, while adult females contained proportionally more energy in their digestive glands. In contrast to adult females, gravid females had higher mean energy in their gonads than their muscles when body mass was taken into consideration. For gravid females, the gonad represented 6.5% of the total body energy and the muscle 23%, while for adult females 4.5% corresponded to gonad energy and 29% to muscle. Only 0.3% of the energy in spent females was from the gonad, while muscle accounted for 29% and 8.5% was allocated to the digestive gland. The linear regression model showed a direct relationship between the muscle and the gonad energy content (linear regression $p = 0.004$, Annex 5): the higher the energy content of the gonad, the lower the energy content of the muscle. This trend was also observed in the dry mass of these tissues.

Clusters 1 and 2 had the highest mean energy, 5.41 ± 0.1 and 5.44 ± 0.1 KJ g wet mass^{-1}, respectively. Clusters 3 and 4 had similar mean energy contents but were lower than the other clusters: 5.32 ± 0.1 and 5.25 ± 0.1 KJ g wet mass^{-1}, respectively. A one-way ANOVA was performed on the swarm energy content data, showing significant differences between all cluster mean energy contents ($p = 0.0321$), validating the idea that different stage compositions of swarms translate to different energy contents of the swarms.

3.4 Swarm energy content

To enhance clarity and streamline the discussion of our findings, from this section we transition from referring to clusters numbered 1 through 4 to identifying them as swarm types A, B, C, and D, respectively. This renaming is intended to make our findings easier to understand and convey because of the unique makeup of

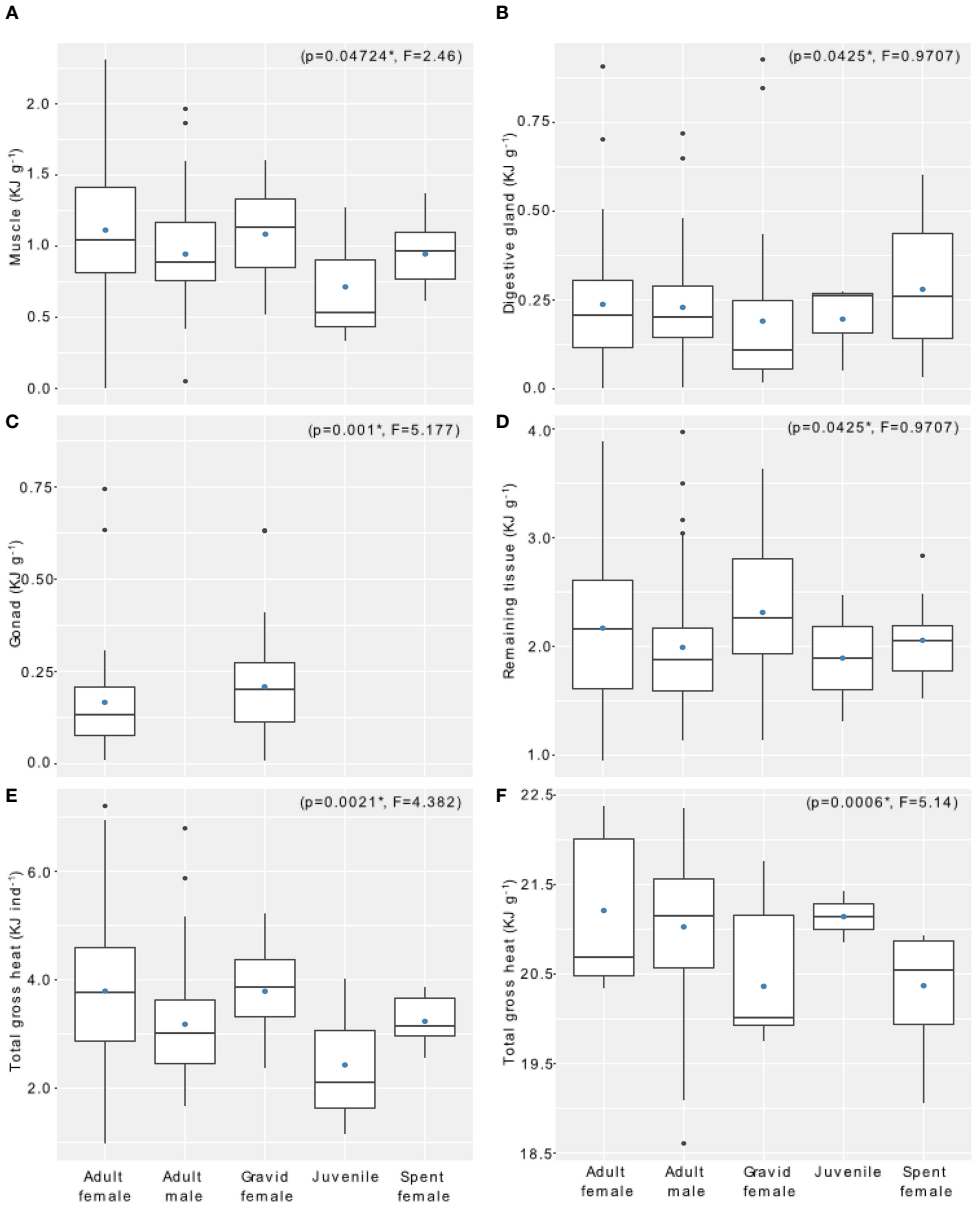


FIGURE 3
Mean energy content of key tissues in each developmental stage of krill for the ENRICH survey: **(A)** muscle, **(B)** digestive gland, **(C)** gonad, **(D)** remaining tissue, and **(E)** mean total gross heat by individual and by **(F)** gram of dried mass for the five stages. p and F values correspond to one-way ANOVA results, except for panel C where the values correspond to *post hoc* Tukey tests comparing the female stages only. Boxes represent the interquartile range, whiskers represent minimum and maximum values, horizontal line corresponds to the median, black dots correspond to outliers and blue dots represent the mean value. All units are in kilojoules per mass of dry weight, except for panel E, which is energy per individual. .

swarms, which is defined by the length and maturity stages of the individuals within each cluster.

1,675 and 4,219 krill swarms fell within the polygons selected using the krill acoustic survey area of ENRICH and TEMPO, respectively. Table 1 summarizes the number of swarms detected for each type, as well as the volume and energy of each swarm type. Type D swarms had both higher mean energy and higher overall total energy (sum of total energy of all swarm) of all four swarm types. Further, there was no correlation (Pearson, corr = -0.003, p=0.8122) between swarm biomass and swarm total energy. Swarm energy content varied in a geographical setting according to the volumetric density of the aggregations. Swarms with high energy content (MJ) were identified closer to the continental shelf (Figure 4).

4 Discussion

Krill swarms were grouped into four categories based on the size of the individuals and the proportion of the different stages within swarms. Higher energy contents (average mean energy per swarm type) were found in small swarms of types D and B, which were composed primarily of gravid females and equal proportions of all

10.3389/fmars.2024.1337080

TABLE 1 Summary of mean swarm dimensions (height[1] and length[2]), volumetric density (ρ_v) g wet mass/m3[3], mean swarm energy[4], and sum of total energy among swarms of the same type [5].

	Type	N	$\bar{x}$ height (m)	$\bar{x}$ length (m)	$\bar{x}\rho_v$ (g wet mass m^3)	Min	Max	$\bar{x}$swarm energy (MJ perswarm)	Min	Max	$\sum$swarm energy(MJ)
ENRICH	A	161	5.8 ± 3.4	331 ± 68	362 ± 50.19	17.96	1.9E+3	14.9E+6 ± 3.2E+6	32.6E+3	195.7E+6	2.4E+9
	B	501	8.55 ± 8.4	314 ± 69	177 ± 312.28	15.61	3.8E+3	38.2E+6 ± 17.4E+6	23.4E+3	2.6E+9	19.2E+9
	C	67	6.93 ± 4.0	295 ± 49	140 ± 172.97	14.58	729.7E+0	11.6E+6 ± 2.7E+6	13.2E+3	162.3E+6	774.4E+6
	D	946	5.82 ± 4.8	417 ± 89	132 ± 245.96	15.40	2.4E+3	41.6E+6 ± 59.4E+6	11.5E+3	17.5E+9	39.3E+9
TEMPO	A	1441	4.9 ± 3.3	186 ± 35	8.76E+04 ± 1.7E+3	0.01	44.8E+6	36.4E+3 ± 1.4E+3	308.98	1.9E+6	52.5E+6
	B	92	6.0 ± 3.6	77.4 ± 45	84 ± 6.6	0.001	27.12	21.6E+3 ± 3.5E+3	462.69	132.3E+3	2.0E+6
	C	234	5.0 ± 2.8	72.6 ± 43	91 ± 18	0.02	172.30	12.1E+3 ± 2.2E+3	231.23	160.0E+3	2.8E+6
	D	2452	4.2 ± 2.6	846 ± 18	2.14E+05 ± 4.9E+3	1.2E-93	165.1E+6	13.1E+3 ± 7.0E+3	338.08	1.7E+6	32.1E+6

[1] $\bar{x}$ height: mean distance for the respective swarm type from the highest point to the base of the cylinder to the top of the cylinder at its highest in meters.
[2] $\bar{x}$ length: mean cylinder diameter for the respective swarm type in meters. $3\bar{x}\rho_v$: mean volumetric density for the respective swarm type on units of grams of wet mass for cubic meter of volume.
[4] $\bar{x}$ swarm energy: mean swarm energy content considering the total energy of the classified swarm for a given type.
[5] $\sum$swarm energy: sum of the energy content of all the swarms for a given type.
Results are reported as value ± standard deviation. Minimum and maximum values are shown as further evidence of the variability of swarm volumetric density and the estimated swarm energy content. N corresponds to the number of swarms described for each swarm type.

stages, respectively. This evidence shows that energy content in krill swarms is driven by the stage composition and not by the physical size of the swarm.

This study is the first to report on energy allocation for both sexes and all main maturity stages. The assessment of the energy allocation showed that the female stages, both gravid and immature adults, have the highest energy content among all the measured life stages. The energy contents measured in the present study were similar to those in previous studies for female and male individuals (Ichii et al., 2007; Ruck et al., 2014; Schaafsma et al., 2018). However, energy content varied significantly between life stages. This has been suggested before by Schaafsma et al. (2018) and Clarke (1984), due to variations in the biochemical compositions of krill at different stages. By comparing results from this study with previous reports of energy content in different krill stages, we infer that the krill energy content might be related to geographical distribution and time of year. For example, Ichii et al. (2007) reported an energy value of 20.08 KJ g^{-1} and 17.41 KJ g^{-1} for gravid females and immature adult females in the vicinity of Elephant Island, while Schaafsma et al. (2018) reported 22.27 KJ g^{-1} for immature adult females in the Lazarev Sea. The present study estimated that immature adult females had a mean energy value of 21.08 KJ g^{-1} dry mass and gravid females 20.36 KJ g^{-1} dry mass during the summer season in east Antarctica. Krill populations undergo seasonal ontogenetic migration, therefore seasonal distribution of maturity composition and individual? size vary considerably, which has implications for the dynamics of energy content of krill populations. In addition to this, we believe this study was the first to measure krill energy content in all sex and maturity stages of krill for one geographical area in the same time span, giving us an understanding of the variability between stages.

Trade-offs are part of the evolutionary history of all animals (Garland, 2014). Growth patterns, reproductive investments, and longevity are all qualities that may be shaped by trade-offs (Ou et al., 2020). However, as far as we are aware, reproductive trade-offs have only been reported twice before for krill: Male krill reduce lipid storage to use all incoming energy in reproduction, thereby increasing their mortality rate (Virtue et al., 1996), while Steinke et al. (2022) found through controlled laboratory experiments that the physiological condition of juvenile female krill declined in response to high metabolic requirements. The energetic cost of reproduction is high for both females and males (Ross and Quetin, 2000), and this cost in krill has been attributed primarily to the generation of lipid-rich oocytes (Quentin et al., 1994). As a result, lipid levels and composition vary significantly according to sex and maturation stage. Female reproductive krill can have up to twice the amount of lipid as males (Clarke, 1984) and female krill lose 34% of their body mass after laying eggs (Nicol et al., 1995). It has been estimated that phytoplankton concentration in the Southern Ocean is not high enough to support the energetic demand of reproductive female krill (Nicol et al., 1995). We observed that spent females allocated the highest energy content to their digestive gland coupled with low energy content in muscle tissues. This could be interpreted as females trying to increase their lipid reserves at the expense of muscle tissue post-spawning and in preparation to produce more eggs. Similar to our findings, Steinke et al. (2022) found that juveniles allocate their energy towards reproductive development in winter when their lipid levels and reproductively important fatty

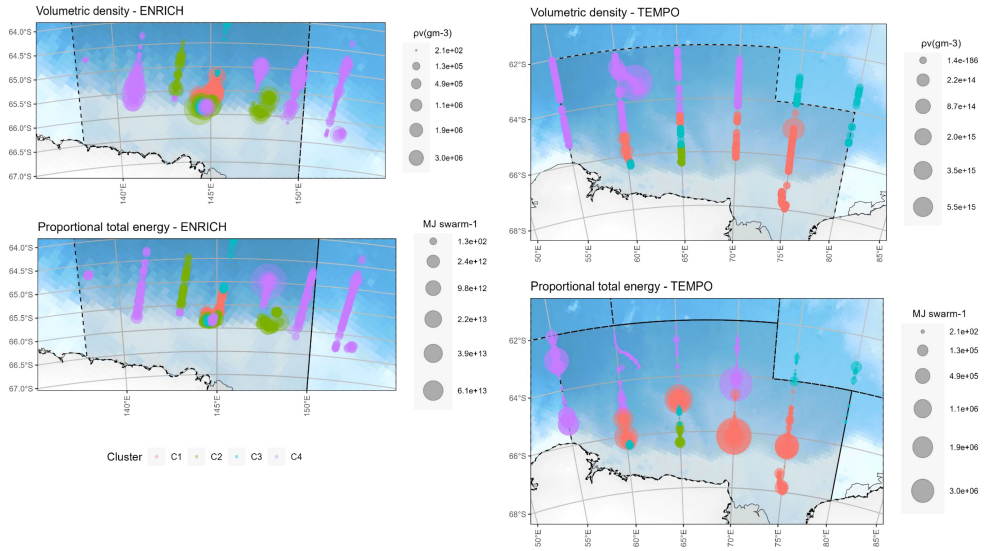


FIGURE 4
Maps of volumetric density (ρv(gm^{-3})) (top) and proportional total swarm energy (MJ per swarm) (bottom) for ENRICH (left) and TEMPO (right). Colors represent different clusters. Swarms located near the shelf break contained greater energy content; these swarms correspond to those of type D (C4).

acids supersede what is necessary for survival. Sexual development comes at a cost, as more mature juveniles were found to be in worse physiological condition. The trade-off between reproductive development and condition in juvenile krill is significant, as early maturation may better prepare krill for the spawning season but may also leave them more susceptible to suboptimal conditions in the environment. Juvenile krill has the capacity to utilize stored lipids throughout the autumn and winter, which can be used to initiate early reproductive development (Steinke et al., 2022). To confirm our trade-off hypothesis and to further understand the energy requirements of krill, the energy allocation of female krill at different times of the reproductive cycle needs to be evaluated.

Previous research has suggested that krill sometimes form swarms of individuals of the same maturity stage and that this composition changes depending on the season (Watkins, 1986; Watkins et al., 1992; Atkinson et al., 2006). However, our results differ as the swarms evaluated in this study were composed of all maturity stages. This may help increase fitness, whereby larger individuals can maintain faster swimming speeds (Ritz, 2011). It could be speculated that smaller individuals would also benefit by aggregating with larger krill due to the possibility that if the swarm moves faster, juveniles within a swarm composed of adults could also increase their swimming speed. This study proposes a classification of krill swarms based on their biological makeup. Larger gravid females dominated swarms of type D, and most swarms detected corresponded to this type. This is congruent with the time of the survey being peak breeding season. However, individuals of all stages were identified in all krill swarms. Tarling et al. (2009) previously classified krill swarms into two categories based on their density and horizontal length: type I swarms are those with densities below 10 ind m^{-3} and 50 m in length, and type II swarms are those above type I limits. If this classification system is applied to the swarms observed in the present study, type B and D swarms fall into Tarling et al.'s (2009) larger swarms (type II) and swarms A and C into type I. Based on our results and the previous swarm classification, larger swarms, defined as swarms with the longest height and length, correspond to swarms with high gravid female composition.

High energy swarms were found on the shelf break in this study. As there are no previous studies that estimate swarm or krill population energy content, we can put our results into context with previous estimations of krill density. High density values were found near the shelf break in both Kawaguchi et al. (2010) and the present study. On the other hand, much lower density values were found offshore, consistent with results for the Lazarev Sea reported by Siegel et al. (2016). The shelf break is of great importance to krill and its predators. For example, Adélie penguins forage at the shelf break during the breeding season (Alonzo et al., 2003), while dense aggregations of whales are found within the vicinities of the shelf break (Friedlaender et al., 2006), and some fish species also use the area all year round as a foraging ground (Hoddell et al., 2000). The shelf break is a region of high phytoplankton biomass, as upwelling in this region increases primary production (Wright and van den Enden, 2000), consequently boosting krill abundance (Atkinson et al., 2008) and leading to high swarm densities and high swarm energy content.

There are two important points in this study that should be carefully considered when interpreting the results. Firstly, while a swarm-based approach is suitable when managing krill fisheries, the way that biomass measurements are currently made could be biased as they assume that the swarm shape is a cylinder when obtaining volumetric density estimates. In the same way, our study also assumed swarm shapes to be cylindrical when calculating the volumetric density. Future research should focus on finding a way to estimate swarm volumetric density more accurately, perhaps by reconstructing the swarm shape detected with acoustic methods using multiple geometrical shapes.

Secondly, the swarm energy results from this study (even the individual energy contents) are only valid for the summer season in the east Antarctic. Both season and location should be considered as krill varies over temporal and spatial scales. Physical processes in the Southern Ocean also vary over time and space, although this study only focuses on one habitat of krill. Krill also resides under sea ice and may have different energy contents compared to krill from open waters. Moreover, different species of krill predators will be present in sea ice areas and their energetic needs could be different to those predators living and feeding in open waters. Understanding the transfer of energy from krill swarms to marine predators will require this information to be incorporated into ecosystem models.

5 Conclusion

This was the first study of its kind to describe the population structure of krill swarms coupled with energy. Swarms with high energy contents were identified, aiding in our understanding of the biological characteristics of krill swarms. This paper examines an important factor that should be considered when assessing Antarctic krill swarms: the maturity-stage composition of the swarms. Moreover, this paper reveals a reproductive trade-off in *E. superba*, suggesting that female krill invest most of their energy into gonadal development at the expense of muscle tissue. This paper is the first to quantify the energy content of krill individuals at different sex and maturity stages for the same region in the same time span. Measuring energy density using bomb calorimetry and proximate composition is a time-consuming process. Increased information on the relationships between energy density and other, easier to measure parameters could help in reducing the effort when estimating krill swarm energy density. If a sustained relationship between the physical, demographic, and energetic characteristics of krill swarms can be identified, then the makeup and energy content of the swarms could be estimated directly for swarms found with acoustic surveys without needing substantial laboratory work.

Data availability statement

Krill raw energy measurements are available in an open-source data set: https://data.aad.gov.au/metadata/SCAR_Diet_Energetics.

Ethics statement

The manuscript presents research on animals that do not require ethical approval for their study.

Author contributions

CCM: Conceptualization, Data curation, Formal analysis, Investigation, Methodology, Visualization, Writing – original draft, Writing – review & editing. SK: Supervision, Writing – review & editing. MJC: Formal analysis, Methodology, Supervision, Writing – review & editing. JM: Data curation, Writing – review & editing. VR: Data curation, Writing – review & editing. KMS: Conceptualization, Funding acquisition, Investigation, Supervision, Writing – review & editing.

Funding

The author(s) declare financial support was received for the research, authorship, and/or publication of this article. This project was funded by the Institute for Marine and Antarctic Studies at the University of Tasmania in collaboration with the Australian Antarctic Division. This project was supported and funded by Australian Antarctic Science Project 4512 and 4636 and received grant funding from the Australian Government as part of the Antarctic Science Collaboration Initiative program. This project also received financial support from Pew Charitable Trust and Antarctic Science Foundation. We acknowledge the use of the CSIRO Marine National Facility (https://ror.org/01mae9353) and grant of sea time on RV Investigator in undertaking this research.

Acknowledgments

This work could not have been accomplished without the support of the crew and scientists on the TEMPO and ENRICH voyages.

Conflict of interest

The authors declare that the research was conducted in the absence of any commercial or financial relationships that could be construed as a potential conflict of interest.

Publisher's note

All claims expressed in this article are solely those of the authors and do not necessarily represent those of their affiliated organizations, or those of the publisher, the editors and the reviewers. Any product that may be evaluated in this article, or claim that may be made by its manufacturer, is not guaranteed or endorsed by the publisher.

Supplementary material

The Supplementary Material for this article can be found online at: https://www.frontiersin.org/articles/10.3389/fmars.2024.1337080/full#supplementary-material

References

Alonzo, S. H., and Mangel, M. (2001). Survival strategies and growth of krill: avoiding predators in space and time. *Mar. Ecol. Prog. Ser.* 209, 203–217. doi: 10.3354/meps209203

Alonzo, S. H., Switzer, P. V., and Mangel, M. (2003). Ecological games in space and time: The distribution and aundance of Antarctic krill and penguins. *Ecology* 84, 1598–1607. doi: 10.1890/0012-9658(2003)084[1598:EGISAT]2.0.CO;2

Alurralde, G., Fuentes, V. L., Maggioni, T., Movilla, J., Olariaga, A., Orejas, C., et al. (2019). Role of suspension feeders in antarctic pelagic-benthic coupling: Trophic ecology and potential carbon sinks under climate change. *Mar. Environ. Res.* 152, 104790. doi: 10.1016/j.marenvres.2019.104790

Amakasu, K., Ono, A., Hirano, D., Moteki, M., and Ishimaru, T. (2011). Distribution and density of Antarctic krill (*Euphausia superba*) and ice krill (E. crystallorophias) off Adélie Land in austral summer 2008 estimated by acoustical methods. *Polar Sci.* 5, 187–194. doi: 10.1016/j.polar.2011.04.002

Atkinson, A., Meyer, B., Stübing, D., Hagen, W., Schmidt, K., and Bathmann, U. V. (2002). Feeding and energy budgets of Antarctic krill *Euphausia superba* at the onset of winter —II. Juveniles and adults. *Limnol. Oceanogr.* 47, 953–966. doi: 10.4319/lo.2002.47.4.0953

Atkinson, A., Shreeve, R. S., Hirst, A. G., Rothery, P., Tarling, G. A., Pond, D. W., et al. (2006). Natural growth rates in Antarctic krill (*Euphausia superba*): II. Predictive models based on food, temperature, body length, sex, and maturity stage. *Limnol. Oceanogr.* 51, 973–987. doi: 10.4319/lo.2006.51.2.0973

Atkinson, A., Siegel, V., Pakhomov, E. A., Rothery, P., Loeb, V., Ross, R. M., et al. (2008). Oceanic circumpolar habitats of Antarctic krill. *Mar. Ecol. Prog. Ser.* 362, 1–23. doi: 10.3354/meps07498

Bestley, S., Raymond, B., Gales, N. J., Harcourt, R. G., Hindell, M. A., Jonsen, I. D., et al. (2018). Predicting krill swarm characteristics important for marine predators foraging off East Antarctica. *Ecography* 41, 996–1012. doi: 10.1111/ecog.03080

Brierley, A. S., and Cox, M. J. (2010). Shapes of krill swarms and fish schools emerge as aggregation members avoid predators and access oxygen. *Curr. Biol.* 20, 1758–1762. doi: 10.1016/j.cub.2010.08.041

Cavan, E. L., Belcher, A., Atkinson, A., Hill, S. L., Kawaguchi, S., McCormack, S., et al. (2019). The importance of Antarctic krill in biogeochemical cycles. *Nat. Commun.* 10, 4742. doi: 10.1038/s41467-019-12668-7

Clarke, A. (1984). Lipid content and composition of Antarctic Krill, *Euphausia Superba* Dana. *J. Crustacean Biol.* 4, 285–294. doi: 10.1163/1937240X84X00660

Cox, M., Demer, D., Warren, J., Cutter, G., and Brierley, A. (2009). Multibeam echosounder observations reveal interactions between Antarctic krill and air-breathing predators. *Mar. EcologyProgress Ser.* 378, 199–209. doi: 10.3354/meps07795

Cox, M. J., Macaulay, G., Brasier, M. J., Burns, A., Johnson, O. J., King, R., et al. (2022). Two scales of distribution and biomass of Antarctic krill (*Euphausia superba*) in the eastern sector of the CCAMLR Division 58.4.2 (55°E to 80°E). *PloS One* 17, e0271078. doi: 10.1371/journal.pone.0271078

Cox, M. J., Watkins, J. L., Reid, K., and Brierley, A. S. (2011). Spatial and temporal variability in the structure of aggregations of Antarctic krill (*Euphausia superba*) around South Georgia 1997–1999. *Ices J. Mar. Sci.* 68, 489–498. doi: 10.1093/icesjms/fsq202

Demer, D. A., and Conti, S. G. (2005). New target-strength model indicates more krill in the Southern Ocean. *Ices J. Mar. Sci.* 62, 25–32. doi: 10.1016/j.icesjms.2004.07.027

Everson, I., and Bone, D. G. (1986). Effectiveness of the RMT8 system for sampling krill (*Euphausia superba*) swarms. *Polar Biol.* 6, 83–90. doi: 10.1007/BF00258257

Färber-Lorda, J., and Ceccaldi, H. J. (2020). Relationship of morphometrics, total carotenoids, and total lipids with activity and sexual and spatial features in *Euphausia superba*. *Sci. Rep.* 10, 13177. doi: 10.1038/s41598–020-69780–8

Färber-Lorda, J., Gaudy, R., and Mayzaud, P. (2009). Elemental composition, biochemical composition and caloric value of Antarctic krill: Implications in energetics and carbon balances. *J. Mar. Syst.* 78, 518–524. doi: 10.1016/j.jmarsys.2008.12.021

Friedlaender, A. S., Bowers, M. T., Cade, D., Hazen, E. L., Stimpert, A. K., Allen, A. N., et al. (2019). The advantages of diving deep: Fin whales quadruple their energy intake when targeting deep krill patches. *Funct. Ecol.* 34, 497–506. doi: 10.1111/1365-2435.13471

Friedlaender, A. S., Halpin, P., Qian, S., Lawson, G. L., Wiebe, P. H., Thiele, D., et al. (2006). Whale distribution in relation to prey abundance and oceanographic processes in shelf waters of Western Antarctic Peninsula. *Mar. Ecol. Prog. Ser.* 317, 297–310. doi: 10.3354/meps317297

Garland, T. (2014). Trade-offs. *Curr. Biol.* 24, R60–R61. doi: 10.1016/j.cub.2013.11.036

Hagen, W., Kattner, G., Terbrüggen, A., and Van Vleet, E. S. (2001). Lipid metabolism of the Antarctic krill *Euphausia superba* and its ecological implications. *Mar. Biol.* 139, 95–104. doi: 10.1007/s002270000527

Hamner, W. M., and Hamner, P. P. (2000). Behavior of Antarctic krill (*Euphausia superba*): schooling, foraging, and antipredatory behavior. *Can. J. Fisheries Aquat. Sci.* 57, 192–202. doi: 10.1139/f00-195

Hoddell, R. J., Crossley, A. C., Williams, R., and Hosie, G. W. (2000). The distribution of Antarctic pelagic fish and larvae (CCAMLR division 58.4.1). *Deep Sea Res. Part II: Topical Stud. Oceanogr.* 47, 2519–2541. doi: 10.1016/S0967–0645(00)00034–5

Ichii, T., Bengston, J., Boveng, P., Takao, Y., Jansen, J., Hiruki-Raring, L., et al. (2007). Provisioning strategies of Antarctic fur seals and chinstrap penguins produce different responses to distribution of common prey and habitat. *Mar. Ecology-Progress Ser.* 344, 277–297. doi: 10.3354/meps06873

Kawaguchi, S., Nicol, S., Virtue, P., Davenport, S. R., Casper, R., Swadling, K. M., et al. (2010). Krill demography and large-scale distribution in the Western Indian Ocean sector of the Southern Ocean (CCAMLR Division 58.4.2) in Austral summer of 2006. *Deep Sea Res. Part II: Topical Stud. Oceanogr.* 57, 934–947. doi: 10.1016/j.dsr2.2008.06.014

Kohut, J., Statscewich, H., Oliver, M., Fredj, E., Klinck, J., Dinniman, M., et al. (2019). Project SWARM: The application of an integrated polar ocean observing system to map the physical mechanisms driving food web focusing in an Antarctic biological hotspot. *OCEANS 2019 MTS/IEEE SEATTLE*, 1–7. doi: 10.23919/OCEANS40490.2019

Leonori, I., De Felice, A., Canduci, G., Costantini, I., Biagiotti, I., Giuliani, G., et al. (2017). Krill distribution in relation to environmental parameters in mesoscale structures in the Ross Sea. *J. Mar. Syst.* 166, 159–171. doi: 10.1016/j.jmarsys.2016.11.003

Makarov, R., and Denys, C. J. (1984). "Stages of sexual maturity of *Euphausia superba* Dana," in *BIOMASS Handbook*, vol. 11. (BIOMASS Handbook, Oban, United Kingdom), 1–11.

Miller, E., Potts, J., Cox, M., Miller, B., Calderan, S., Leaper, R., et al. (2019). The characteristics of krill swarms in relation to aggregating Antarctic blue whales. *Sci. Rep.* 9 (1), 16487. doi: 10.1038/s41598–019-52792–4

Morris, D., Watkins, J. L., Ricketts, C., Buchholz, F., and Priddle, J. (1988). An assessment of the merits of length and weight measurements of Antarctic krill *Euphausia superba*. *Br. Antarctic Survey Bull.* 79), 27–50.

Nicol, S., de la Mare, W. K., and Stolp, M. (1995). The energetic cost of egg production in Antarctic krill (*Euphausia superba* Dana). *Antarctic Sci.* 7, 25–30. doi: 10.1017/S0954102095000058

Ou, Q., Vannier, J., Yang, X., Chen, A., Mai, H., Shu, D., et al. (2020). Evolutionary trade-off in reproduction of Cambrian arthropods. *Sci. Adv.* 6, eaaz3376. doi: 10.1126/sciadv.aaz3376

Quentin, L. B., Ross, R. M., and Clarke, A. (1994). Krill energetics: seasonal and environmental aspects of the physiology of *Euphausia superba*. *South. Ocean Ecol. Biomass perspective*, 165–184.

Reiss, C. S., Cossio, A. M., Loeb, V., and Demer, D. A. (2008). Variations in the biomass of Antarctic krill (*Euphausia superba*) around the South Shetland Islands 1996–2006. *Ices J. Mar. Sci.* 65, 497–508. doi: 10.1093/icesjms/fsn033

Ritz, D. (2011). Is social aggregation in aquatic crustaceans a strategy to conserve energy? *Can. J. Fisheries Aquat. Sci.* 57, 59–67. doi: 10.1139/f00-170

Ross, R. M., and Quetin, L. B. (2000). "Reproduction in Euphausiacea," in *Krill*. Ed. I. Everson (Blackwell Science Ltd, Oxford, UK), 150–181. doi: 10.1002/9780470999493.ch6

RStudio, T (2022). *RStudio: Integrated Development Environment for R* (PBC, Boston, MA: RStudio).

Ruck, K. E., Steinberg, D. K., and Canuel, E. A. (2014). Regional differences in quality of krill and fish as prey along the Western Antarctic Peninsula. *Mar. Ecol. Prog. Ser.* 509, 39–55. doi: 10.3354/meps10868

Schaafsma, F. L., Cherel, Y., Flores, H., van Franeker, J. A., Lea, M.-A., Raymond, B., et al. (2018). Review: the energetic value of zooplankton and nekton species of the Southern Ocean. *Mar. Biol.* 165, 129. doi: 10.1007/s00227-018-3386-z

Siegel, V. (2016). *Biology and ecology of Antarctic krill* (Cham, Switzerland: Springer International Publishing AG). doi: 10.1007/978-3-319-29279-3

Steinke, K. B., Bernard, K. S., Fontana, J. M., Copeman, L. A., and Garcia, L. M. (2022). The energetic cost of early reproductive development in juvenile Antarctic krill at the Western Antarctic Peninsula. *Front. Mar. Sci.* 9. doi: 10.3389/fmars.2022.1009385

Tarling, G. A., Klevjer, T., Fielding, S., Watkins, J., Atkinson, A., Murphy, E., et al. (2009). Variability and predictability of Antarctic krill swarm structure. *Deep Sea Res. Part I: Oceanographic Res. Papers* 56, 1994–2012. doi: 10.1016/j.dsr.2009.07.004

Venables, W. N., and Ripley, B. D. (2002). *Modern applied statistics with S. 4th ed.* (New York: Springer), ISBN: .

Virtue, P., Nichols, P. D., Nicol, S., and Hosie, G. (1996). Reproductive trade-off in male Antarctic krill, *Euphausia superba*. *Mar. Biol.* 126, 521–527. doi: 10.1007/BF00354634

Watkins, J. L. (1986). Variations in the size of Antarctic krill, *Euphausia superba* Dana, in small swarms. *Mar. Ecol. Prog. Ser.* 31, 67–73. doi: 10.3354/meps031067

Watkins, J. L., and Brierley, A. S. (2002). Verification of the acoustic techniques used to identify Antarctic krill. *ICES J. Mar. Sci.* 59, 1326–1336. doi: 10.1006/jmsc.2002.1309

Watkins, J. L., Buccholz, F., Priddle, J., Morris, D. J., and Ricketts, C. (1992). Variation in reproductive status of Antarctic krill swarms; evidence for a size-related sorting mechanism? *Mar. Ecol. Prog. Ser.* 82, 163–174. doi: 10.3354/meps082163

Watkins, J. L., Morris, D. J., Ricketts, C., and Murray, A. W. A. (1990). Sampling biological characteristics of krill: Effect of heterogeneous nature of swarms. *Mar. Biol.* 107, 409–415. doi: 10.1007/BF01313422

Watkins, J. L., Morris, D. J., Ricketts, C., and Priddle, J. (1986). Differences between swarms of Antarctic krill and some implications for sampling krill populations. *Mar. Biol.* 93, 137–146. doi: 10.1007/BF00428662

Wickham, H., François, R., Henry, L., and Müller, K. (2023). *dplyr: A Grammar of Data Manipulation_* (R package version 1.0.9). Available at: https://CRAN.R-project.org/package=dplyr.

Wright, S. W., and van den Enden, R. L. (2000). Phytoplankton community structure and stocks in the East Antarctic marginal ice zone (BROKE survey, January–March 1996) determined by CHEMTAX analysis of HPLC pigment signatures. *Deep Sea Research Part II: Topical Studies in Oceanography 2000*. 47 (12), 2363–2400. doi: 10.1016/S0967-0645(00)00029-1

frontiers | Frontiers in Marine Science

TYPE Original Research
PUBLISHED 23 August 2024
DOI 10.3389/fmars.2024.1411130

Check for updates

OPEN ACCESS

EDITED BY
Kunio T. Takahashi,
National Institute of Polar Research, Japan

REVIEWED BY
Erica Jarvis Mason,
National Oceanic and Atmospheric Administration, United States
Franki Perry,
University of Exeter, United Kingdom

*CORRESPONDENCE
Fokje L. Schaafsma
fokje.schaafsma@wur.nl

†PRESENT ADDRESS
Ryan Driscoll,
National Oceanography Centre, Southampton, United Kingdom
Sara Driscoll,
National Oceanography Centre, Southampton, United Kingdom
Marin van Regteren,
Eneco, Rotterdam, Netherlands

RECEIVED 02 April 2024
ACCEPTED 25 July 2024
PUBLISHED 23 August 2024

CITATION
Schaafsma FL, Driscoll R, Matsuno K, Sugioka R, Driscoll S, van Regteren M, Sasaki H, Matsukura R, van Franeker JA and Murase H (2024) Demography of Antarctic krill (*Euphausia superba*) from the KY1804 austral summer survey in the eastern Indian sector of the Southern Ocean (80 to 150° E), including specific investigations of the upper surface waters.
Front. Mar. Sci. 11:1411130.
doi: 10.3389/fmars.2024.1411130

COPYRIGHT
© 2024 Schaafsma, Driscoll, Matsuno, Sugioka, Driscoll, van Regteren, Sasaki, Matsukura, van Franeker and Murase. This is an open-access article distributed under the terms of the Creative Commons Attribution License (CC BY). The use, distribution or reproduction in other forums is permitted, provided the original author(s) and the copyright owner(s) are credited and that the original publication in this journal is cited, in accordance with accepted academic practice. No use, distribution or reproduction is permitted which does not comply with these terms.

Demography of Antarctic krill (*Euphausia superba*) from the KY1804 austral summer survey in the eastern Indian sector of the Southern Ocean (80 to 150° E), including specific investigations of the upper surface waters

Fokje L. Schaafsma[1*], Ryan Driscoll[2†], Kohei Matsuno[3,4], Rikuto Sugioka[3], Sara Driscoll[2†], Marin van Regteren[1†], Hiroko Sasaki[5], Ryuichi Matsukura[5], Jan Andries van Franeker[1] and Hiroto Murase[6]

[1]Wageningen Marine Research, Den Helder, Netherlands, [2]Southwest Fisheries Science Center, National Oceanic and Atmospheric Administration, La Jolla, CA, United States, [3]Faculty/Graduate School of Fisheries Sciences, Hokkaido University, Hakodate, Japan, [4]Arctic Research Center, Hokkaido University, Sapporo, Japan, [5]Fisheries Resources Institute, Japan Fisheries Research and Education Agency, Yokohama, Japan, [6]Department of Ocean Sciences, Tokyo University of Marine Science and Technology, Tokyo, Japan

Antarctic krill (*Euphausia superba*) is a harvested species that has an important role in the Southern Ocean food web. Knowledge on the demography of Antarctic krill is necessary for a better understanding of the distribution of life stages and their relation with predator species. In addition, such information is essential for krill fisheries management by CCAMLR (Commission on the Conservation of Antarctic Marine Living Resources). A large part of the Indian sector of the Southern Ocean is understudied and large-scale krill surveys of this region are scarce. Therefore, a survey was carried out during the austral summer of 2018/2019 on board RV *Kaiyo-maru* in the region from 80 to 150° E. Krill was collected using a Rectangular Midwater Trawl (RMT). Previous studies suggest that part of the Antarctic krill population resides in the upper surface of the water column, but traditional trawls and echosounders have not been able to fully investigate this stratum due to sampling constraints. To overcome this knowledge gap, the upper surface (0-2 m) was sampled using a Surface and Under Ice Trawl (SUIT) in addition to the standard survey net. Results show that there were differences in the horizontal and vertical distribution of post-larval krill between the area west and east of approximately 120° E. These differences coincided with variation in environmental properties. Early calyptopis larvae were found throughout the survey area. Their relatively low numbers suggested ongoing spawning that started early in the season. Juveniles were found mainly in the western side of the sampling area and large densities of this

developmental stage were found to reside in the upper two meters of the water column. The quantitative estimation of krill in the upper surface indicated that undersampling this part of the population may influence estimates of, for example, recruitment.

KEYWORDS

Euphausiids, length-frequency, population structure, developmental stage, surface sampling, horizontal distribution, vertical distribution

1 Introduction

Knowledge of the population dynamics of Antarctic krill (*Euphausia superba*) is required to understand spatial and temporal variability in population structure and the biological characteristics of the species (Hill et al., 2006). Length- and/or stage-frequency distributions are necessary for estimating spawning biomass and recruitment indices or for modelling predator-prey interactions and ecosystem functioning (Hill et al., 2006; Kinzey et al., 2019; Wang et al., 2021), and, in relation to vertical and horizontal migration patterns, help to interpret results from acoustic surveys (Pauly et al., 2000; Jarvis et al., 2010; Cox et al., 2022; Abe et al., 2023). As Antarctic krill (hereafter "krill") is a harvested species, such information facilitates the effective management of stocks (Siegel, 2005; Hill et al., 2006; Nicol and Brierley, 2010). In addition, it is necessary for understanding the effects of potential fisheries not only on the krill population (Hill et al., 2006), but also on dependent predator species. Krill fishing currently occurs only in the Atlantic sector of the Southern Ocean, but historically also in the Pacific and Indian Sectors. Although fishing for krill has not been conducted in the latter area since 1995, precautionary catch limits are still established annually (CCAMLR, 2021).

Compared to the Atlantic sector, the Indian Sector of the Southern Ocean is an understudied region regarding the abundance, distribution and ecology of its biota. The region west of approximately 90°E, including the Prydz Bay region (Figure 1), has been investigated more extensively (e.g. Miller, 1985; Hosie et al., 1988; Miquel, 1991; Pakhomov, 1995; Kawaguchi et al., 2010), with

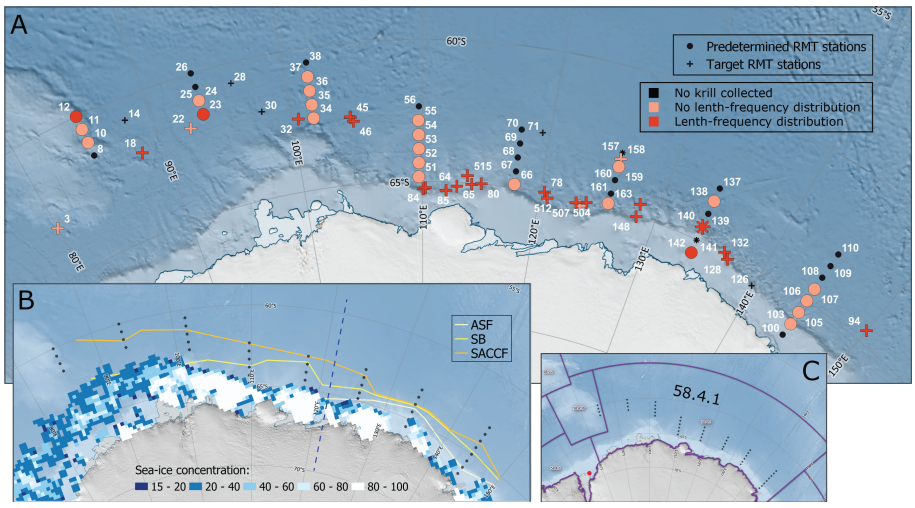


FIGURE 1
The main map **(A)** shows locations of predetermined (round points) and target (crosses) RMT stations during expedition KY1804 of RV *Kaiyo-maru* in the Indian sector of the Southern Ocean. A predetermined and a target haul was conducted at station 140 (red star). Red and light orange points indicate stations where post-larval Antarctic krill (*Euphausia superba*) were collected, but only at the red points there were sufficient numbers to obtain a length-frequency distribution. Black points indicate stations where no post-larval krill were caught. The inserted map **(B)** shows the pre-determined positions of RMT stations (grey dots) in relation to the sea-ice concentrations (% cover per 10 km grid) at the time of the survey, which were derived from the Advanced Microwave Scanning Radiometer-2 (AMSR-2) onboard the GCOM-W1 satellite, and were provided during the survey by the Arctic Data Archive System (ADS) of the National Institute of Polar Research, Japan (https://ads.nipr.ac.jp/dataset/A20170123-003). SACCF = Southern Antarctic Circumpolar Current Front, SB = the Southern Boundary of the Antarctic Circumpolar Current and ASF = Antarctic Slope Front. The dotted line indicates the division between Legs 1 and 2. The other inserted map **(C)** highlights CCAMLR Statistical Division 58.4.1 in relation to the predetermined RMT station grid. The Prydz Bay region was marked with a red dot.

usually a special interest for krill due to its importance in the food web and its commercial interest. These studies have provided information regarding the horizontal and vertical distribution of various life stages of the krill population using trawls and/or acoustics, and provide an idea of variation found in this distribution (e.g. Miller, 1985; Miquel, 1991; Jarvis et al., 2010; Cox et al., 2022). Diel Vertical Migration (DVM) was observed in some studies (Jarvis et al., 2010; Piccolin et al., 2020; Cox et al., 2022), while no difference in day/night catches were found in some others (Miller, 1985; Miquel, 1991). Jarvis et al. (2010) suspected that part of the population was likely residing in the upper 20 m of the water column which could not be detected using acoustic methods. As DVM was observed, krill were suspected to occupy this upper layer particularly during the night (Jarvis et al., 2010; Cox et al., 2022).

Distribution patterns of life stages in the region west of 90°E could partly be explained by oceanographic features, although results vary among studies. Natural boundaries, such as the Antarctic divergence, a region where upwelling of high-salinity water occurs, and the East Wind Drift have been suggested by some studies as the northern limit of post-larval krill distribution (Miller, 1985; Hosie et al., 1988) or as a separation between different stocks (Mackintosh, 1973; Pakhomov, 2000). Other studies suggested an influence of gyre systems on krill distribution (Pakhomov, 2000; Kawaguchi et al., 2010), although evidence of krill concentration due to circulation patterns was not always found (Miller, 1985). This may be due to inter-annual variation in circulation patterns in the entire Indian sector (Bryantsev et al., 1991; Pakhomov, 1995). Furthermore, some studies concluded that krill concentrated along the shelf break or that the increased abundance of post-larval krill in the south indicates a close association to the sea-ice edge (Miller, 1985). It is thus likely that factors influencing krill distribution are complex and influenced by bathymetry, currents and sea-ice dynamics, with large geographical and seasonal variation (Miller, 1985; Jarvis et al., 2010; Kawaguchi et al., 2010).

The part of the Indian sector from 80 to 150°E, which corresponds to the boundaries of CCAMLR Statistical Division 58.4.1 (Figure 1), has been investigated less extensively. Results of the 'Discovery' investigations suggested that krill were abundant between 80 and 120°E and extended far north in some areas (beyond 60°S), while krill was scarce between 120 and 150°E and only found further south (Marr, 1962; Mackintosh, 1973). Similar findings of a more coastal distribution of krill in the east (east of 120°E), and a wider latitudinal distribution in the west, was found during the BROKE (Baseline Research on Oceanography, Krill and the Environment) expedition in 1996, which was the last large-scale survey particularly designed for investigating *E. superba* (Nicol et al., 2000a). Differences in physical conditions were found between east and west of the survey area (Nicol et al., 2000b). Fronts associated with the eastward flowing Antarctic Circumpolar Current (ACC) turn southward in the eastern part of the area, resulting in the fronts lying closer together and closer to the Antarctic Slope Front (Figure 1), which is associated with the westward flowing Antarctic Slope Current (ASC) (Bindoff et al., 2000; Yamazaki et al., 2024).

Given the varying results on krill distribution patterns in the more regularly investigated area of the Indian sector (region west of 90°E), repeated surveys in the rest of this sector are essential to further elucidate distribution patterns, relationships with environmental properties and potentially annual and seasonal variation. Therefore, a multidisciplinary ecosystem survey was conducted in the area between 80 and 150°E with RV *Kaiyo-maru* in 2018/2019, during which main objectives were to estimate krill biomass and to perform oceanographic observations in the area (Murase et al., in review)[1]. The survey's short name is KY1804 (the fourth survey of *Kaiyo-maru* in Japanese fiscal year 2018).

The aim of this study is to make a general assessment of krill demography in the eastern Indian sector of the Southern Ocean during KY1804, and to gain knowledge on the vertical and horizontal distribution of the species. Distribution patterns are expected to vary among different life stages. Data on krill demography were collected on a predetermined grid of sampling stations with a Rectangular Midwater Trawl (RMT) and from target RMT catches that were conducted for the identification of species within echosigns recorded by an echosounder. Since standard trawls and acoustics do not sample the surface (Jarvis et al., 2010; Atkinson et al., 2012), the krill population occupying the upper two meters of the water column was additionally investigated using a Surface and Under Ice Trawl (SUIT). The surface waters are expected to be occupied by a notable part of the population. With this dedicated surface water sampling, we aim to increase our knowledge regarding the distribution of various life stages, in order to understand the consequences of undersampling this stratum for the biology of the species, and the understanding of Southern Ocean ecosystems.

2 Materials and methods

2.1 Sampling

Krill was collected during the KY1804 survey on board RV *Kaiyo-maru* (2942 GT, Fisheries Agency of Japan), which was conducted in the eastern Indian sector of the Southern Ocean between 80 and 150°E (west and east borders of CCAMLR Statistical Division 58.4.1), and approximately 60 and 66°S (Murase et al., in review). Specifically, the southern boundary was set at either the sea-ice edge or the 2000 m isobath. The latter is usually used as an approximate position of the shelf break in the Indian sector. The northern boundary was set approximately 120 nautical miles (222 km) to the north of the southern boundary although the distance varied among track lines. The survey was divided into two legs. Leg 1 was conducted from 15 December 2018 to 7 January 2019 during which sampling was performed from west to east (80 to 120°E) and Leg 2 was conducted from 26 January to 23 February 2019 during which sampling was performed from east to west (150 to 125°E). All net sampling was conducted in open water.

1 Murase, H., Abe, K., Schaafsma, F. L., and Katsumata, K. Overview of the multidisciplinary ecosystem survey in the eastern Indian sector of the Southern Ocean (80–150°E) by the Japanese research vessel Kaiyo-maru in the 2018–19 austral summer (KY1804 survey). *Progr. Oceanogr.*

Standard double oblique tows were conducted at 43 predetermined stations on eight transects using a multiple opening and closing RMT 1 + 8 (Baker et al., 1973; Roe and Shale, 1979), from the near surface (15-20 m depth) to 200 m depth (Figure 1; Supplementary Table S1). The RMT samples the upper 10 to 15 meters in the wake of the ship, where the surface water is displaced by the moving vessel and the ship's propellers (Everson and Bone, 1986; Methot, 1986; Flores et al., 2012, 2014). Therefore, although the RMT net is hauled up to the surface, it is presumed to undersample the upper 10-15 m. The RMT has been considered a standard sampling gear for krill by CCAMLR since 2000 (Siegel et al., 2004). The RMT 1 and RMT 8 are two nets mounted on top of each other which have mouth openings of 1 m^2 and 8 m^2, and mesh sizes of 0.33 mm and 4.5 mm, respectively. The vessel's speed was 2.5 knots (3.7 km/h) during the tow. Wire speeds during paying out and hauling were 0.7 to 0.8 m/sec and 0.3 m/sec, respectively. Distance between the stations was approximately 30 nautical miles. Of the 24 stations sampled during Leg 1, four were conducted during night-time (between sun set and sun rise) and 20 were conducted during day-time (between sun rise and sun set). Of the 19 stations conducted during Leg 2, 14 stations were conducted during the night and five were conducted during the day (Supplementary Table S1). The allocation of day- and night-time stations was arbitrary because it was difficult to predetermine the exact timing of the tows due to the comprehensive research program. In addition to predetermined stations, targeted tows were performed at the target depth, based on information from the echosounder (Abe et al., 2023; Figure 1). Target hauls were conducted at 33 stations (Supplementary Table S2). In a few instances, multiple aggregations were targeted in the same tow.

Horizontal tows at the upper two meters of the water column were performed using a SUIT (Van Franeker et al., 2009) at 27 stations located in the vicinity of predetermined RMT stations (Supplementary Table S3). The SUIT consisted of a 2 x 2 m steel frame with two nets attached. The first net was a 7 mm half-mesh commercial shrimp net attached over 1.5 m width. The rear 3 m of this shrimp net was lined with 0.3 mm plankton gauge. The second net was a 0.3 mm mesh plankton net, attached over 0.5 m width of the frame. The net was towed with 200 m wire at a constant speed of 2.5 to 3 kn, shearing out of the wake of the ship. Filtered water volume was measured during trawling using an Acoustic Doppler Current Profiler (ADCP, Nortek, Norway) mounted in the SUIT-net frame. Of the 16 stations sampled during Leg 1, 11 were conducted during day-time and five were conducted during night-time. During Leg 2, nine out of the 11 stations sampled were conducted during the day, and two during the night (Supplementary Table S3). In the western part of the study area, RMT and SUIT sampling was conducted further north compared to the eastern part due to sea-ice cover in the area (Figure 1). During the expedition, stations were numbered ascending regardless of the type of gear deployed, which is why numbering is not always consecutive. Numbers do, however, increase with the progression of time in both legs, so higher numbers were given to stations conducted later in time.

2.2 Krill density, stage, and length

After trawling, krill was sorted from the catch. In samples containing less than 150 krill, all individuals were staged and measured. For larger catches, a random subsample of at least 150 individuals was measured and staged. This random subsample was taken by splitting the sample one or multiple times using a Motoda box-type plankton sample splitter. On some occasions the catches were extremely large, and a 1-L sub-sample was taken with a measuring cup from a large container holding the catch, which was stirred until the sub-sample was collected. Due to time constrains, RMT 1 and SUIT samples were usually immediately preserved on 10% sodium tetraborate decahydrate-buffered formalin after trawling, and measurements and staging were done at the home laboratories, while RMT 8 samples were processed directly on board. It should be kept in mind that preservation can lead to shrinkage, which was estimated at 7.5% for post-larval krill (Quetin and Ross, 2003).

The standard length 1 (S1) was measured from the tip of the rostrum to the posterior end of the uropods (Mauchline, 1980). The maturity stage of post-larval krill was determined according to Makarov and Denys (1981). Briefly, Makarov and Denys (1981) distinguish one sub-adult female stage (F2) and five adult female stages (F3A to F3E) of which F3D are regarded as gravid, having a swollen thorax and abdominal segments due to enlarged ovaries, and F3E are regarded as spent, also having a swollen thorax and abdominal segments but with empty internal body cavities. Three stages of sub-adult males are distinguished (M2A to M2C), having different stadia of developing petasmas, and two stages of adults males (M3A and M3B), with fully developed petasmas and without or with fully developed spermatophores, respectively (Makarov and Denys, 1981). Krill that had lost one pair of post-lateral spines from their telson (Fraser, 1936), but did not show sexual characteristics yet (Makarov and Denys, 1981) were defined as juveniles. Larvae were staged according to Kirkwood (1982), distinguishing 12 developmental stages, namely nauplius I-II, metanauplius, calyptopis I-III (CI to CIII) and furcilia I-VI (FI to FVI).

Length-frequency distribution was based on 1-mm increments. Because the SUIT's shrimp net undersampled krill smaller than 20 mm (Siegel, 1986; Flores et al., 2012; Schaafsma et al., 2016), the densities per station were calculated using the data of the plankton net for krill smaller than 20 mm and from the shrimp net for krill of 20 mm and larger. A similar undersampling of krill <20 mm occurs in the RMT 8 net, while the RMT 1 net likely undersampled krill ≥20 mm (Siegel, 1986). However, as only larvae <5 mm were collected using RMT 1, all post-larval krill data from the RMT 8 was used in predetermined hauls, indicating that there may be a slight underestimation in the numbers of krill <20 mm. One exception was station 23, were FVI larvae and juveniles were collected using the RMT 1 net, while there was almost no krill in the RMT 8 net. For this station, the data from the RMT 1 net was used, indicating that there may be some underestimation of the numbers of krill ≥20 mm. For the target hauls, only results for post-larval krill were reported based on data from the RMT 8 net.

Results regarding larvae are presented separately, except for the abundance and distribution of FVI, since the length distribution of this stage largely overlaps with that of the juveniles and other furcilia stages were almost absent during the survey. The average number of krill per length class as collected by the SUIT was calculated by dividing the sum of volumetric densities per station by the number of stations. For the dominant life stages, the average size of krill was compared per station to obtain an indication of seasonal growth during the time of sampling, or to assess the potential presence of multiple spawning populations/events. These differences were investigated using an ANOVA followed by a non-parametric Tukey's HSD test. Statistical tests were performed with the R software, version 4.2.1 (R Core Team, 2022). Maps were generated using Quantarctica, version 3.22 (Matsuoka et al., 2021).

3 Results

3.1 General abundance from predetermined stations

In the epipelagic depth layer (15-200 m), the larval krill population consisted mainly of the stages CI, CII and CIII (Figure 2A), with mean densities of 3.45 ± 7.7, 1.33 ± 3.8 and

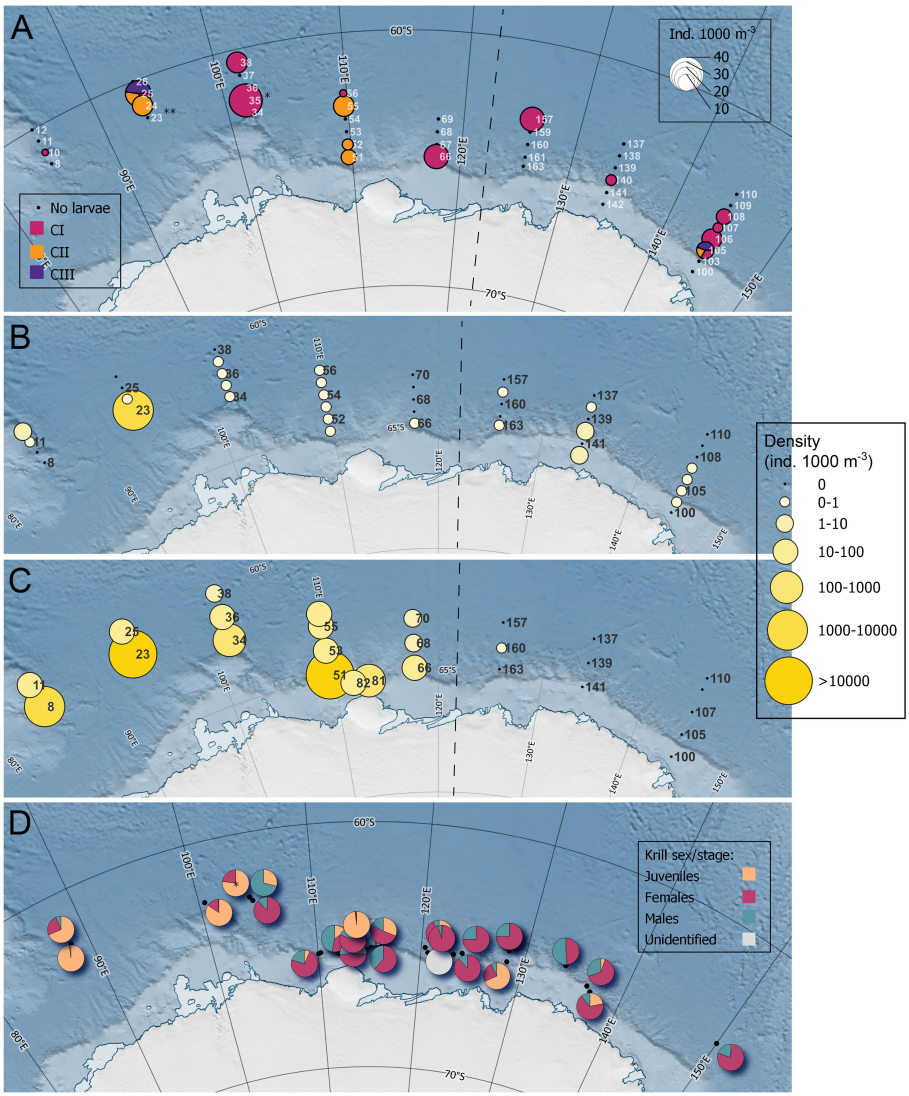


FIGURE 2
(A) Distribution and density of calyptopis larvae (CI, CII and CIII) of Antarctic krill *Euphausia superba*, collected using a Rectangular Midwater Trawl (RMT) at predetermined stations in the Indian sector of the Southern Ocean. * indicates the only location were furcilia II larvae were collected. ** indicates the only location were furcilia VI larvae were collected. Furcilia larvae were not taken into account in the depicted densities. **(B)** Volumetric density (ind. 1000 m^{-3}) of post-larval Antarctic krill per predetermined station collected at 15-200 m depth using the RMT. **(C)** Volumetric density (ind. 1000m^{-3}) of post-larval Antarctic krill per station collected at 0-2 m depth using the Surface and Under Ice Trawl. Note that not all stations numbers are depicted in maps **(B, C)**. **(D)** The proportional sex/developmental stage composition of Antarctic krill per targeted RMT station. For visibility, the charts were slightly dodged. The black points show the actual sampling location. The dotted lines indicate the division between Legs 1 and 2.

0.12 ± 0.6 ind. 1000 m^{-3}, respectively. CI larvae occurred throughout the sampling area. FII larvae (37.6 ind. 1000 m^{-3}) occurred only at station 35, while FVI larvae only occurred at station 23.

The number of post-larval krill from the epipelagic layer was very low. The initially calculated average density was 0.27 ind. 1000 m^{-3}, based on RMT 8 catches (Urabe et al., in review)[2]. Taking into account the large number of post-larval krill collected with the RMT 1 at station 23, the epipelagic contained, on average, 106.81 ± 690.43 ind. 1000 m^{-3}. This includes the small numbers of FVI collected at station 23 (1.6% of the catch). No krill were collected at 19 predetermined RMT stations.

The upper two meters of the water column contained, on average, 2457.02 ± 9031.34 ind. 1000 m^{-3} krill. This includes FVI larvae which were present in low numbers in the upper surface (1.6% of the population in this stratum). The number of krill collected in the upper two meters of the water column largely exceeded the average number of krill collected using the predetermined RMT (Figures 2B, C). Given the difference in size of the depth layers investigated and to aid comparison with echosounder results, the krill biomass, and both volumetric and areal densities per station are presented for both nets in Table 1. With one exception, the krill occupied the upper surface only in the waters west of 120˚E (Figure 2C).

3.2 Developmental stage distribution

At 21 predetermined RMT stations 10 or less individuals were caught. At only four predetermined RMT stations there were a sufficient number of individuals to establish a length-frequency distribution. At two of these stations, located on the two most western transect lines of the sampling area, the catch was dominated by juveniles (Supplementary Figure S1). At two stations east of 130˚E one catch (station 140) was dominated by gravid females (F3D) and adult males (M3B), while the other (station 142) was dominated by sub-adult females and males (Supplementary Figure S1).

Krill were collected during 36 target RMT hauls at 26 different stations. Of these hauls, 28 contained more than 20 individuals which were used for length-frequency distribution. The size structure of krill sampled varied across the survey area (Figure 2D). The length-frequency distribution of target hauls showed unimodal and bimodal peaks (Figures 3, 4). With some exceptions, the first peak usually consisted of juveniles and sub-adults males (M2A) and females (F2), while the second peak was often dominated by gravid females (F3D) and adults males (M3B). Some samples or peaks consisted of adult, non-gravid females (F3B and F3C) and late-stage sub-adult males (M2B and M2C). Small numbers of spent females (F3E) occurred only occasionally. Juveniles dominated the catches in 9 out of 16 measured stations

2 Urabe, I., Matsuno, K., Sugioka, R., Driscoll, R., Driscoll, S., Schaafsma, F. L., et al. Spatio-temporal changes in the macrozooplankton community in the eastern Indian sector of the Southern Ocean during austral summer: comparison between 1996 and 2018/2019. *Progr. Oceanogr.*

TABLE 1 Volumetric density, areal densities and wet mass of Antarctic krill (*Euphausia superba*) per predetermined station collected in the 15-200 m depth layer using RMT (Rectangular Midwater Trawl) and the 0-2 m depth layer using SUIT (Surface and Under Ice Trawl).

Station	Volumetric density (ind. 1000 m^{-3})		Areal density (ind. 100 m^{-2})		Wet mass (g 100 m^{-2})	
	RMT	SUIT	RMT	SUIT	RMT	SUIT
8	0	3925.21	0	785.04	0	119.00
10	0		0		0	
11	0.23	31.88	4.55	6.38	2.76	0.61
12	3.03		60.65		10.37	
23	4581.29	44144.14	91625.73	8828.83	4437.98	882.15
24	0.11		2.24		0.58	
25	0	43.01	0	8.60	0	0.35
26	0		0		0	
34	0.21	155.56	4.28	31.11	1.00	3.14
35	0.37		7.35		0.44	
36	0.33	23.66	6.62	4.73	1.43	0.50
37	0.06		1.18		0.12	
38	0	5.03	0	1.01	0	0.09
51	0.13	17898.92	2.61	3579.78	0.13	294.82
52	0.27		5.40		1.30	
53	0.25	45.08	5.08	9.02	2.29	0.57
54	0.12		2.36		3.07	
55	0.23	16.57	4.52	3.31	5.08	0.45
56	0.08	20.00	1.60	4.00	0.16	0.50
66	0.07	12.39	1.43	2.48	1.86	0.27
67	0		0		0	
68	0	2.51	0	0.50	0	0.04
69	0		0		0	
70	0	3.14	0	0.63	0	0.10
81		101.30		20.26		2.22
82		17.89		3.58		0.45
100	0	0	0	0	0	0
103	0.04		0.80		0.4	
105	0.65	0	12.93	0	11.07	0
106	0.51		10.29		5.76	
107	0.13	0	2.63	0	39.49	0
108	0		0		0	
109	0	0	0	0	0	0
110	0	0	0	0	0	0
137	0	0	0	0	0	0
138	0.22		4.33		3.03	

(Continued)

TABLE 1 Continued

Station	Volumetric density (ind. 1000 m^{-3})		Areal density (ind. 100 m^{-2})		Wet mass (g 100 m^{-2})	
	RMT	SUIT	RMT	SUIT	RMT	SUIT
139	0	0	0	0	0	0
140	2.43		48.57		68.26	
141	0	0	0	0	0	0
142	1.98		39.63		23.14	
157	0	0	0	0	0	0
159	0.07		1.37		1.09	
160	0	0.74	0	0.15	0	0.01
161	0		0		0	
163	0.06	0	1.16	0	0.7	0

It should be noted that post-larval krill densities were derived from the RMT 8 net, except for station 23 where krill were only collected in the RMT 1 net. Densities may include small numbers of furcilia VI, sizes of which overlapped with those of juveniles.

conducted west of 120 °E, which all sampled the upper 15-50 m of the water column (Figures 2D, 3; Supplementary Table S4). East of 120 °E, juveniles dominated at 2 out of 12 measured stations, one that sampled the upper 15-50 m and one that sampled below 300 m deep (Figure 4). Sub-adult and adult female and male krill occurred throughout the water column (Figures 3, 4).

The vast majority of, mainly post-larval, krill collected in the upper two meters of the water column were juveniles (92%), followed by early sub-adult females (F2B, 2.7%) and males (M2A1, 2.1%). The other stages were present in low numbers (Supplementary Table S5). Length-frequency distributions were similar across stations. An average length-frequency is shown in Figure 5. Late gravid (F3D) and spent (F3E) females were completely absent in the surface waters.

3.3 Krill size comparison

The average size of juveniles in the SUIT hauls ranged between 17.8 and 23.8 mm per station (Figure 6A; Supplementary Table S6). Although there were significant differences between some stations (($F_{13,616269}$ = 1264, p = < 0.0001), differences were not consistently higher or lower with seasonal progression (Figure 6A). The average size of juveniles in the target RMT hauls ranged from 21.1 to 36.3 mm, which was much a wider range compared to the average size of juveniles collected in the surface using the SUIT. Generally, the average size of juveniles per target station with >20 individuals increased as time progressed, but showed smaller krill again at station 64 after which size proceeded to increase with the progression of time (Figure 6B). Juveniles were significantly larger at stations 32 and 44 compared to station 64 ($F_{12,\ 980}$ = 219.9, p < 0.0001, Tukey HSD: p <0.006), although sampling was conducted five and eight days earlier, respectively. Stations 18 to 44 were conducted north of 64°S, in the vicinity of the ice edge. At these stations, the average size of juvenile increased from 21.1 mm to 27.7 mm in 7 days. The average size of two aggregations sampled at station 18 (averaging 21.1 and 24.1 mm) were significantly different from each other ($F_{12,\ 980}$ = 219.9, p < 0.0001, Tukey HSD: p <0.0001). Stations 64 onwards were conducted near the shelf break (Figure 6B). The average size of the juveniles collected at these stations increased from 23.6 to 36.3 mm in 48 days. The juveniles at station 515 were, on average, significantly larger compared to juveniles at all other stations ($F_{12,\ 980}$ = 219.9, p < 0.0001, Tukey HSD: p < 0.002).

There were no distinct patterns in the average size of gravid females (F3D) in the target RMTs (Figure 6C). Gravid females at station 83 were significantly smaller than the ones at all other stations ($F_{10,949}$ = 36.67, p = < 0.0001, Tukey p < 0.0001). The gravid females of stations 46, 80 and 85 were significantly smaller than the ones at some other stations ($F_{10,949}$ = 36.67, p = < 0.0001, Tukey p < 0.04). Two gravid female aggregations collected during a single RMT tow at station 80 differed significantly from each other in average size ($F_{10,949}$ = 36.67, p = < 0.0001, Tukey p < 0.0001). For adult males (M3B) some increase in average size seems to occur over periods of time, but this was not as consistent as with the juveniles and more variation was present (Figure 6D). Adults males at stations 83, 84 and 151 were significantly smaller than individuals at all other stations, except for from station 45 and each other ($F_{12,474}$ = 42.01, p = < 0.0001, Tukey p < 0.001). Two adult male aggregations collected during a single RMT tow at station 151 differed significantly from each other in average size ($F_{12,474}$ = 42.01, p = < 0.0001, Tukey p < 0.0001).

4 Discussion

4.1 Krill distributional patterns

Our study showed that a significant part of the krill population resided in the upper surface of the water column, which is not sampled by conventional trawls or echosounders. Although such upper-surface dwelling of mainly juveniles has been suspected (e.g. Jarvis et al., 2010; Atkinson et al., 2012), our study provides a quantitative estimate of density and length-frequency distribution of this part of the krill stock in the Indian sector of the Southern Ocean. The actual part of the stock in the undersampled surface layer may even be larger than the stock size estimated by SUIT, since the densities in the 0-2 m depth layer will likely gradually decrease to the densities as found below 15 m (Schaafsma et al., 2024).

The number of krill in the epipelagic layer, estimated using predetermined RMT catches, was low compared to the numbers encountered in the nets during BROKE (Nicol et al., 2000b). In contrast to the net data, echosounder data collected during our survey suggests that the total biomass of krill in the 20-200 m depth stratum was similar during KY1804 and BROKE (Pauly et al., 2000; Abe et al., 2023). Potential reasons for a lack of krill in the predetermined RMT hauls can be net avoidance or, more likely, the concentration of krill in aggregations, which were simply not encountered enough in the sampling design. This is a common

caveat in net-based sampling of schooling or swarming species (Mackintosh, 1973; Watkins, 2000; Nicol and Brierley, 2010).

The echosounder estimates of areal biomass densities reported from our survey showed that the horizontal distribution of krill seemed to vary between the areas west and east of 120˚E (Abe et al., 2023). In the west, echosounder data found krill relatively evenly distributed despite variation in latitude among transect lines sampled, with a peak in krill density at the transect furthest west (80˚E) (Abe et al., 2023). In the east, highest densities seemed to occur close to the shelf break, south of the southern boundary of the Antarctic Circumpolar Current, with the exception of the echosounder transect furthest east (150˚E) where high densities occurred along the entire transect (Abe et al., 2023). This distribution pattern is similar to those found in January to March during the Discovery expeditions (Mackintosh, 1973) and the BROKE expedition (Nicol et al., 2000b).

During BROKE, the differences in horizontal post-larval krill distribution between west and east were attributed to the more southward intrusion of warmer water in the eastern side of the sampling area, resulting from the southeastward flow of the ACC in the region, constraining the krill habitat closer to the coast (Bindoff et al., 2000; Nicol et al., 2000b). Such a geographic east-west difference in surface temperature was even more pronounced during the KY1804 expedition (Urabe et al., in review; Yamazaki et al., 2024). The temperature at the western side of the sampling area was generally between 0 and 1°C, with a few exceptions at the southernmost stations of certain transects were temperatures below 0°C occurred. At the eastern side of the sampling area, negative temperatures, down to -1.5°C, were found at the southern half of the transects, while temperatures in the northern half of the transects were generally higher than 1°C. Other environmental variables may have contributed to differences in distribution. The chlorophyll *a* concentration during our study was, on average, somewhat higher in the east than it was in the west, and retreating sea ice occurred more northernly on the western side of the sampling area while it already retreated to the vicinity of the shelf or beyond on the eastern side (Figure 1; Urabe et al., in review; Yamazaki et al., 2024).

The temperature differences between both sides of the sampling area, as well as the wider sea-ice extent resulting from transportation of formed sea ice found in the west, may be attributed to a series of subgyres, with several warmer water currents flowing southward and colder waters from the ASC flowing northward, in the region between 80 and 130˚E (Yamazaki et al., 2020; Hirano et al., 2021). The gyres are united with the ACC that travels in close proximity to the continental shelf (Yamazaki et al., 2020). In concurrence with conclusions from previous studies, differences in the population structure of post-larval krill between the areas west and east of 120˚E are likely a result of a combination of seasonality and physical factors, including time of sea-ice cover. The time gap between sampling in Leg 1 and 2 may have had an additional influence on distribution patterns. Growth and development may alter the vertical distribution of krill because the trade-off between food availability, energy budget and predation risk changes (Lampert, 1989; Quetin et al., 1996).

4.2 Krill size and developmental stage distribution

The number of individuals that could be measured from the predetermined RMT hauls was generally too small to obtain a reliable length-frequency distribution, which limited the analysis of temporal and spatial patterns in the distribution of different life stages in the 15-200 m depth layer. Target RMT hauls were mainly conducted to investigate the composition of acoustically detected targets and were performed opportunistically across a variety of locations and depths. These data on the horizontal and vertical distributions are thus, inherently biased (Watkins, 1999; Nicol et al., 2000b; Abe et al., 2023). However, combined with the SUIT net and acoustics, they can provide some information on distribution patterns of different life stages.

Target RMT hauls indicated that juveniles were often more dominant in the krill catches from the western side of the sampling area compared to the eastern side of the sampling area during our study (Figures 2D, 3, 4), which was similar to the findings of BROKE (Nicol et al., 2000b). This dominance of juveniles mainly occurred in the upper 15-50 m of the water column, with the exception of one deeper station in the eastern side of the sampling area. This corresponds with the findings from the surface water sampling which provided further evidence that juveniles remained close to the surface in this region, as the SUIT catches consisted mainly of juveniles. This upper surface dwelling occurred on the western side of the sampling area, and almost no krill was encountered in this stratum in the east (Figure 2C).

Patterns in horizontal distribution were only observed for post-larval krill, and perhaps for late stage furcilia on the verge of developing into juveniles. Predetermined RMT 1 hauls indicated that, during KY1804, younger calyptopis larval krill were distributed more evenly throughout the sampling area with densities ranging from 1.5 to 37.6 ind. 1000 m^{-3} (Figure 2A; Matsuno et al., in review)[3]. CI larvae were present in relatively small numbers throughout the sampling area during our survey, while stations with CII and CIII larvae occurred in various regions. This is different from results from BROKE, where very high larval densities were encountered in the eastern part of the sampling area with a mean density of 3186 ind. 1000 m^{-3}, and numbers were much lower west of 120˚E (Nicol et al., 2000b). Calyptopis stages were found throughout the survey area during BROKE, while early furcilia stages were mainly found in the east, which was attributed to seasonal progression (Nicol et al., 2000b).

Based on predetermined RMT 1 hauls, the CI larvae were encountered between 17 December and 13 February during our survey, indicating that spawning occurred between 17 November and 31 January, assuming that the developmental time of CI larvae is between 13 and 30 days depending on conditions that may influence

3 Matsuno, K., Sugioka, R., Maeda, Y., Driscoll, R., Schaafsma, F. L., Yamaguchi, A., et al. Spatial changes in the mesozooplankton and population structure of dominant species in the eastern Indian sector of the Southern Ocean during austral summer 2018/2019. *Progr. Oceanogr.*

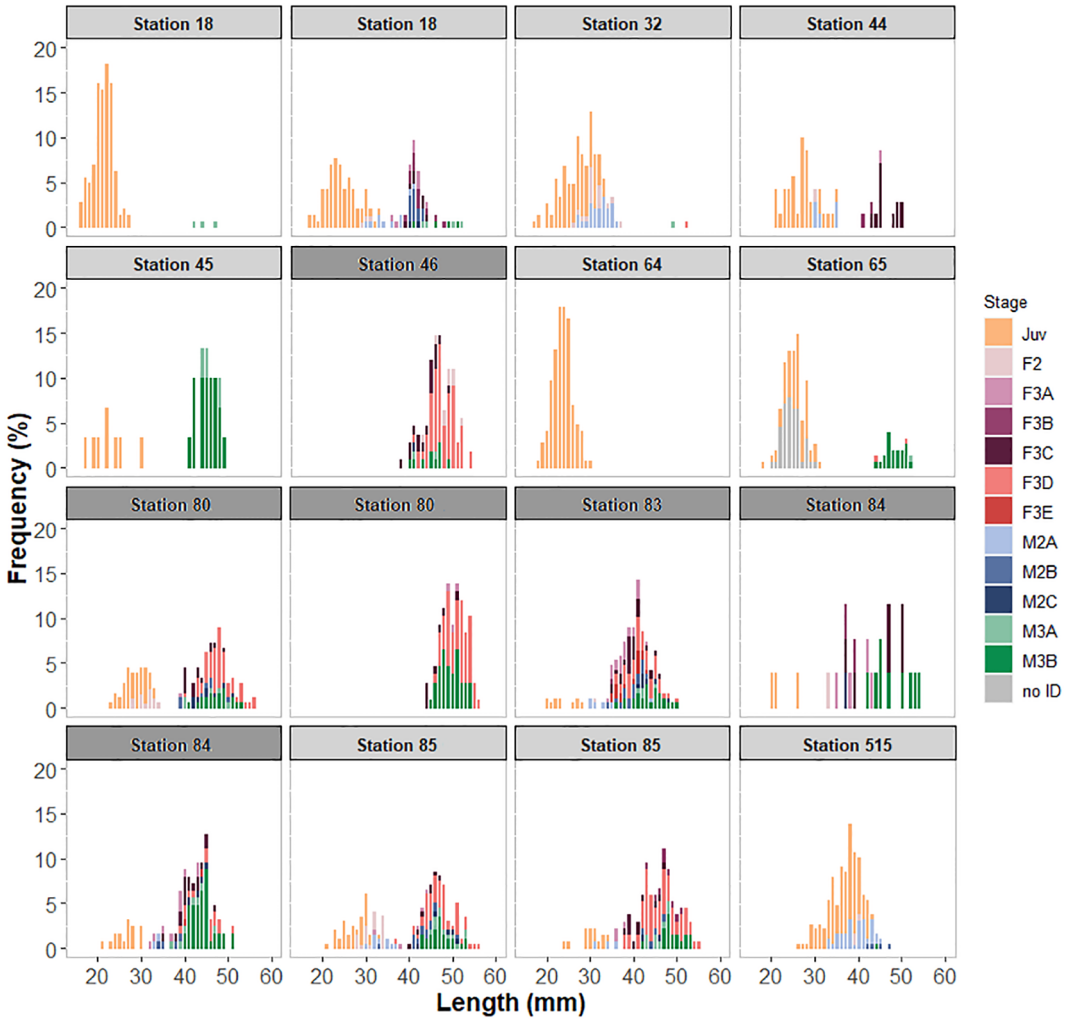


FIGURE 3
Length and stage distribution of Antarctic krill (*Euphausia superba*) at target RMT stations from trawls conducted west of 120 °E where >20 individuals could be measured. Trawls were conducted between 15 and 50 m depth (light grey headings), or between 50 and 75 m depth (grey headings). At some stations, multiple aggregations were collected during a single tow, indicated by plots with the same station number.

development such as temperature (Ikeda, 1984; Jia et al., 2014). CIII larvae occurred from 21 December to 31 January, indicating spawning potentially between 19 October and 18 December, assuming a developmental time between 40 and 63 days (Ikeda, 1984; Spiridonov, 1995; Jia et al., 2014). Considering the low numbers of larvae, the presence of gravid females in the target RMT hauls throughout the survey area and the almost total absence of spent females in these catches, this timing suggests that spawning occurred quite early (Spiridonov, 1995) and had not yet peaked. This could explain the low density of larvae compared to the findings of BROKE, which was conducted later in the season and during which high numbers in the east were mainly collected in the whole of March (Nicol et al., 2000b). During BROKE, gravid females were mainly found in targeted trawls conducted in the region west of 120°E while spent females were mainly found in the east, which could also be attributed to seasonal progression (Nicol et al., 2000b).

Results from target RMTs did not indicate a distinct temporal pattern in the size of gravid females indicating that their size remained similar throughout the survey (Figure 6C). This corresponds to earlier findings and can be due to a lack of growth because of energy investment in reproduction (Nicol et al., 2000b). Also similar to findings of previous studies (Nicol et al., 2000b), adult males showed some growth, although this was not consistent throughout the study area (Figure 6D). This could be a result of different populations sampled, a reflection of differences in feeding conditions or due to an increased energy investment in reproduction.

The size of juvenile krill twice increased with time in the 15-50 m depth layer sampled during target RMT hauls (Figure 6B). Assuming that these juveniles originate from two spawning populations or spawning events, and their increase in size comes from natural growth, the two groups would have been growing with 0.94 mm day^{-1} in the more northern stations and with 0.21 mm day^{-}

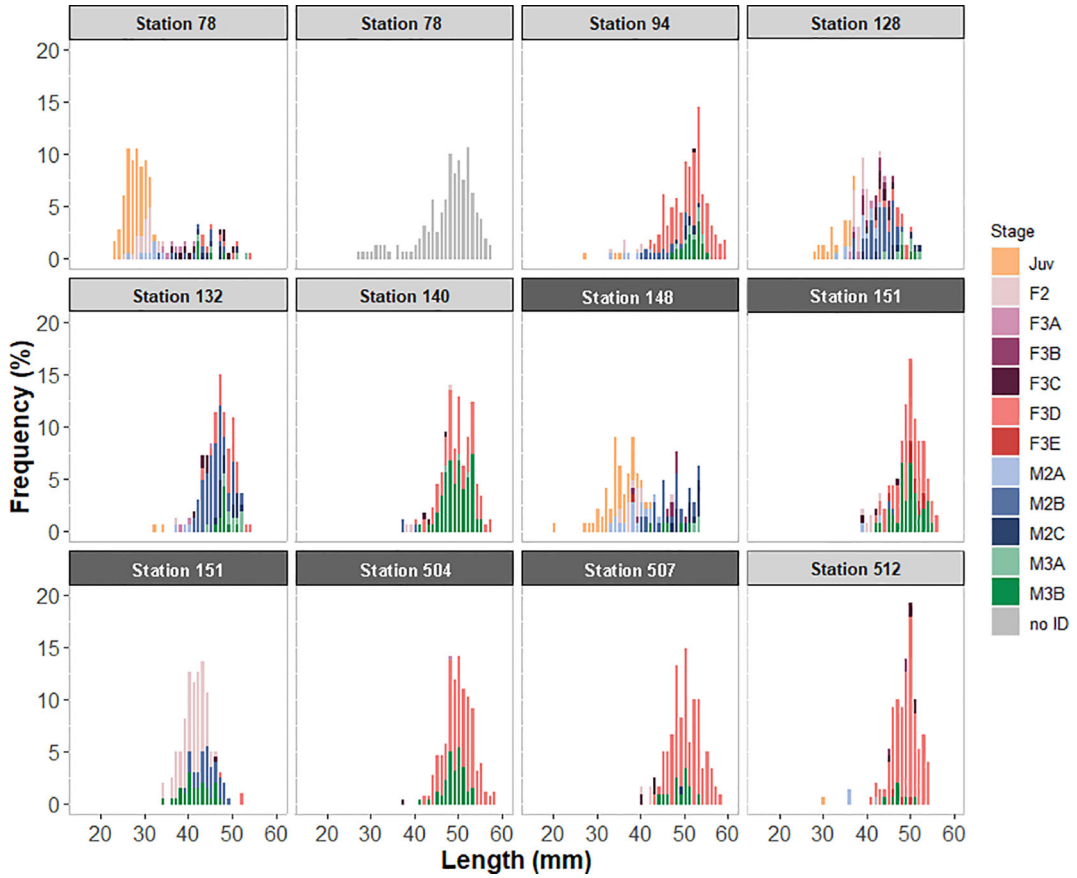


FIGURE 4
Length and stage distribution of Antarctic krill (*Euphausia superba*) at target RMT stations from trawls conducted east of 120 °E where >20 individuals could be measured. Trawls were conducted between 15 and 50 m depth (light grey headings) or between 200 and 600 m depth (dark grey headings). At some stations, multiple aggregations were collected during a single tow, indicated by plots with the same station number.

[1] at the more southern stations, located near the shelf break. Although this latter rate can be considered realistic, the former growth rate is much higher than maximum growth rates recorded (Atkinson et al., 2006; Tarling et al., 2006). It, therefore, seems likely that, at least in the part of the sampling area where transects were located north of ~62°S, juveniles originated from multiple spawning events. Alternatively, the juveniles may have originated from various locations, which could have resulted in different growth rates due to variable environmental conditions experienced.

The juveniles in the upper surface were all relatively small and their size remained similar over time and space, in contrast to the increasing size of juveniles from the target RMTs over time (Figure 6A). This may, again indicate various origins of the juveniles collected, perhaps resulting from the series of subgyres found in the area (Yamazaki et al., 2020). It may also indicate a small scale, gradual change in vertical distribution range within this developmental stage, with the vertical distribution range increasing with increasing size. Such a small-scale change in distribution was also suggested for furcilia larvae/age class 0 juveniles during winter (Schaafsma et al., 2016). Although these were caught under ice and their relationship with the environment is likely very different, such changes may be a result of similar mechanisms, such as saving energy by passive sinking, the speed of which increases with increasing size (Kils, 1982). However, further research is necessary to test such a hypothesis, especially since a previous study indicated that the vertical distribution of krill recruits (age 1+) depends on season (Pakhomov, 1995). In addition, it should be noted that krill were only collected in the surface during Leg 1, while length comparisons encompassed both legs for the target RMT catches.

4.3 Consequences of undersampling of the surface

The previously assumed distributional patterns of particularly juveniles may have been based on an incomplete picture. For example, several studies suggested a trend of younger individuals remaining south of the shelf break during summer, while older animals reside further offshore, north of the shelf break (Siegel, 1988; Lascara et al., 1999; Nicol et al., 2000b; Atkinson et al., 2008). However, the potential distribution in the upper surface waters was not taken into account in these studies. Knowledge on the presence

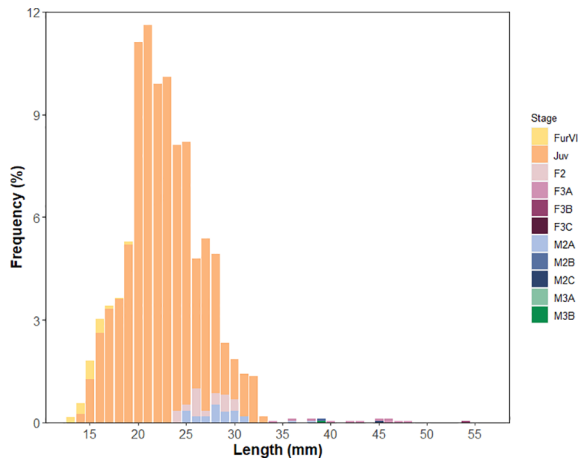


FIGURE 5
Average length-frequency distribution of Antarctic krill (*Euphausia superba*) in the upper two meters of the water column collected using the Surface and Under Ice Trawl.

of krill in the upper surface would aid in understanding smaller-scale and larger-scale distribution processes. For example, the aforementioned migration of different life-stages and the potential relation with oceanographic features such as gyres, that might aid in moving on- and off-shelf. Another example are circumpolar advection patterns that are expected to be greatly influenced by behavioural patterns (Hofmann et al., 1998; Murphy et al., 2004; Atkinson et al., 2008).

Length-frequency distributions of krill are often used to calculate an estimated recruitment value, which is used as a parameter in management models (Butterworth et al., 1991; Constable and de la Mare, 1996) and to assess the success of spawning in a certain year (Watkins, 1999). Because of the small numbers of krill collected in the predetermined RMT hauls, it was not possible to make an estimation for recruitment that is comparable to numbers from previous studies. Results from the SUIT sampling indicate that recruitment indices can be biased because obtained data is not fully representative of the entire stock due to the spatial segregations of life stages (Siegel and Loeb, 1995).

4.4 Knowledge gaps and future research

More information on the potential presence of DVM of krill is desirable to fully understand the consequences of the undersampling of the surface layer on biomass estimates and recruitment indices, as it cannot be excluded that surface krill move into water layers within the detection range of echosounders during certain times of the day. Analysis of the SUIT data provided some indication that DVM of *E. superba* was occurring during the survey, but the number of day and night hauls was unevenly distributed throughout the sampling area, potentially biasing comparison (Schaafsma et al., 2024). In addition, no obvious DVM patterns was found in the echosounder data (Abe et al., 2023). Thus, although this could be a result of krill performing only a shallow DVM, data collected during the survey does not provide conclusive evidence on the presence or absence of DVM. A similar conclusion was drawn from analyses performed on data collected during BROKE (Pauly et al., 2000).

It is important to note that very few krill was collected in the upper surface in the western side of the sampling area (Figures 2B, 6A). Therefore, it would be useful to increase knowledge on when and where juvenile krill accumulate in this layer, and to investigate the potential relationship with environmental and/or biological variables. This includes the distribution of juveniles in ice-covered waters, as sea ice was still present in the area at the time of sampling and is known to affect the distribution of various life stages (Flores et al., 2012). Such information would help to understand if a sampling bias occurs when parts of the potential krill habitat are not sampled (Quetin and Ross, 2003), and to assess if estimates of calculated recruitment indices are representative. For example, an underestimation of recruitment in the Antarctic Peninsula region was suspected in the Palmer LTER study (Quetin and Ross, 2003), which might be explained by undersampling of surface juveniles. In addition, although recruitment has been positively correlated with various aspects of sea-ice dynamics such as late sea-ice retreat (Siegel and Loeb, 1995) or an August maximum sea-ice extent (Quetin and Ross, 2003), a better understanding of relationships between successful spawning years and environmental variables or changes in transport mechanisms may have been hampered by a inaccurate estimation of the density of krill per year class (Siegel and Loeb, 1995; Watkins, 1999). Such knowledge would aid in understanding of natural variability of krill stocks (Siegel and Loeb, 1995) and the potential consequences of climate warming (Quetin and Ross, 2003).

More knowledge regarding the distribution of krill in the upper surface may also aid in understanding the distribution of top predator species. For example, a relationship between the distribution of 13-34 mm krill and the foraging grounds of humpback whales *Megaptera novaeangliae* has been demonstrated in the Antarctic Peninsula region (Santora et al., 2010). During our survey, humpback whales were also more abundant in the western side of the sampling area compared to the eastern side (Hamabe et al., 2024). In addition, depending on the method used, krill consumption by humpback whales exceeded the total krill biomass as established by echosounder data (Abe et al., 2023; Hamabe et al., 2024). This might be explained by the exclusion of a part of the krill stock in the biomass estimate, although juveniles would contribute less to total krill biomass compared to the same number of adults. A lack of knowledge on the distribution of krill in the upper surface may also explain discrepancies between stomach contents and net samples, as found in diet studies such as for the minke whale *Balaenoptera acutorostrata* (Ichii and Kato, 1991). The diet of this species has been found to regularly contain large proportions of one-year-old juvenile krill depending on the region of occurrence (Ichii and Kato, 1991; Ichii et al., 1998).

10.3389/fmars.2024.1411130

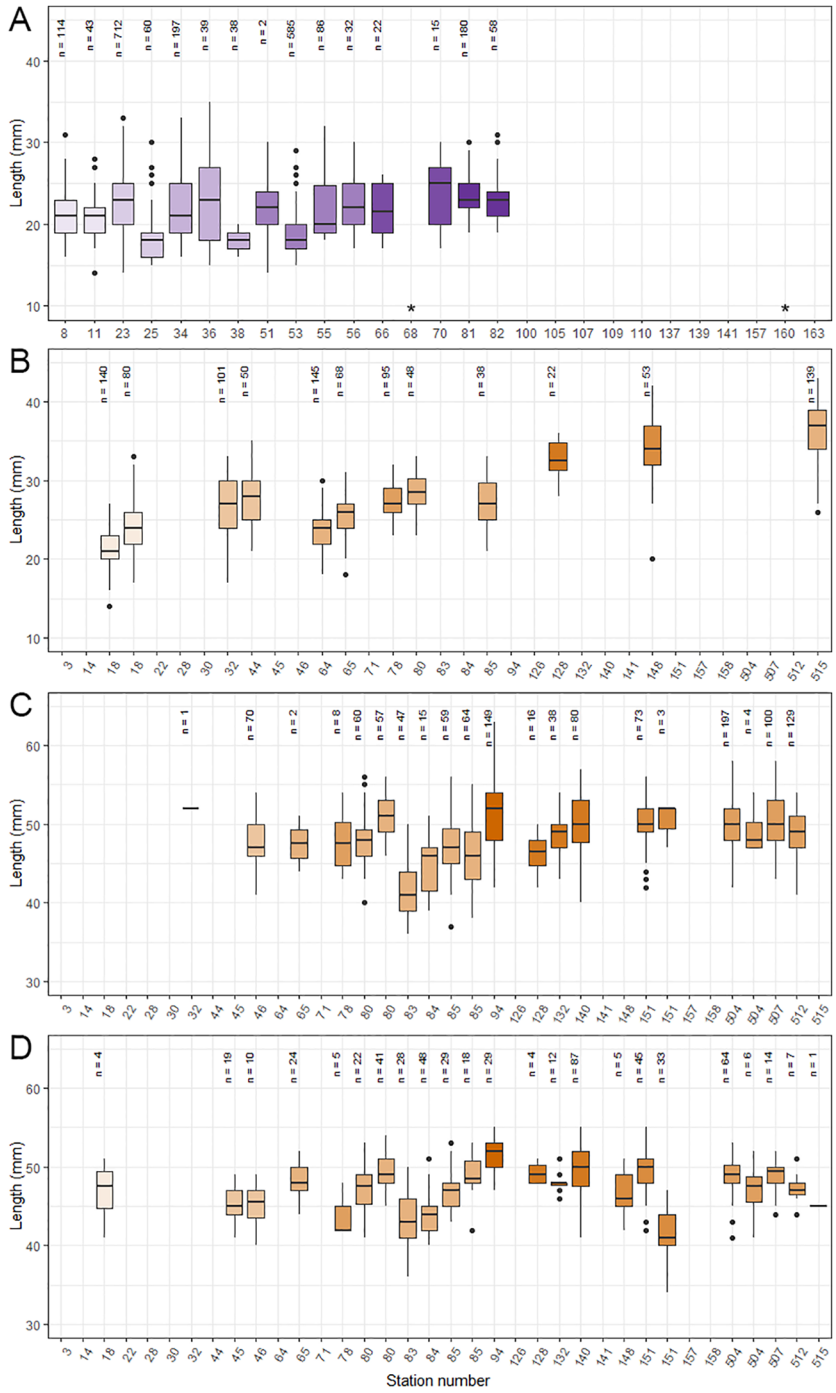


FIGURE 6
Average size per station of **(A)** juvenile Antarctic krill (*Euphausia superba*) collected in the 0-2 m depth layer using SUIT, **(B)** juvenile krill collected at target RMT hauls, **(C)** gravid females (F3D) collected at target RMT hauls and **(D)** adult male (M3B) collected at target RMT hauls. At some stations, multiple aggregations were collected during a single tow, indicated by the same station number. Station numbers are ascending with time, so the x-axis reflects seasonal progression. The colour gradients represent longitude, with colours transitioning from light to dark going from west to east. *n* is the number of individuals measured. The horizontal black lines show the median length in a station. The upper and lower limits of the squares indicated the 25th and 75th percentile. The upper and lower limits of the vertical line indicate the minimum and maximum length of juveniles in a station. Dots represent the true minimum and maximum lengths, but are numerically distant (percentile ± the interquartile range) from the other data points and therefore considered outliers. * indicates stations with low number of Antarctic krill for which no length measurements could be established; blank stations totally lacked krill.

Data availability statement

The raw data supporting the conclusions of this article will be made available by the authors, without undue reservation.

Ethics statement

The manuscript presents research on animals that do not require ethical approval for their study.

Author contributions

FS: Conceptualization, Formal analysis, Investigation, Methodology, Project administration, Visualization, Writing – original draft. RD: Formal analysis, Investigation, Methodology, Writing – review & editing. KM: Formal analysis, Funding acquisition, Supervision, Writing – review & editing. RS: Formal analysis, Investigation, Writing – review & editing. SD: Investigation, Writing – review & editing. MR: Investigation, Writing – review & editing. HS: Investigation, Supervision, Writing – review & editing. RM: Investigation, Supervision, Writing – review & editing. JF: Conceptualization, Funding acquisition, Writing – review & editing, Methodology. HM: Conceptualization, Funding acquisition, Investigation, Methodology, Project administration, Supervision, Writing – review & editing.

Funding

The author(s) declare that financial support was received for the research, authorship, and/or publication of this article. The KY1804 survey was supported by the Institute of Cetacean Research, the Japan Fisheries Research and Education Agency, and the Fisheries Agency of Japan. Antarctic research by Wageningen Marine Research is commissioned by the Netherlands Ministry of Agriculture, Nature and Food Quality (LNV) which funded this research under its Statutory Research Task Nature & Environment WOT-04-009-047.04.

Acknowledgments

We are very grateful to the officers, crew, and colleague researchers onboard RV *Kaiyo-maru* for their indispensable assistance with the biological sampling. Thanks to André Meijboom and Oliver Bittner (Wageningen Marine Research) for assistance with SUIT krill sample analysis, to Giulia Castellani (Alfred Wegener Institute) for processing ADCP data, and to Michiel van Dorssen (M. van Dorssen Metaalbewerking) for technical support using SUIT.

Conflict of interest

The authors declare that the research was conducted in the absence of any commercial or financial relationships that could be construed as a potential conflict of interest.

Publisher's note

All claims expressed in this article are solely those of the authors and do not necessarily represent those of their affiliated organizations, or those of the publisher, the editors and the reviewers. Any product that may be evaluated in this article, or claim that may be made by its manufacturer, is not guaranteed or endorsed by the publisher.

Supplementary material

The Supplementary Material for this article can be found online at: https://www.frontiersin.org/articles/10.3389/fmars.2024.1411130/full#supplementary-material

References

Abe, K., Matsukura, R., Yamamoto, N., Amakasu, K., Nagata, R., and Murase, H. (2023). Biomass of Antarctic krill (*Euphausia superba*) in the eastern Indian sector of the Southern Ocean (80–150°E) in the 2018–19 austral summer. *Progr. Oceanogr.* 218, 103107. doi: 10.1016/j.pocean.2023.103107

Atkinson, A., Nicol, S., Kawaguchi, S., Pakhomov, E., Quetin, L., Ross, R., et al. (2012). Fitting *Euphausia superba* into Southern Ocean food-web models: a review on data sources and their limitations. *CCAMLR Sci.* 19, 219–245.

Atkinson, A., Shreeve, R. S., Hirst, A. G., Rothery, P., Tarling, G. A., Pond, D. W., et al. (2006). Natural growth rates in Antarctic krill (*Euphausia superba*): II. Predictive models based on food, temperature, body length, sex, and maturity stage. *Limnol. Oceanogr.* 51, 973–987. doi: 10.4319/lo.2006.51.2.0973

Atkinson, A., Siegel, V., Pakhomov, E. A., Rothery, P., Loeb, V., Ross, R. M., et al. (2008). Oceanic circumpolar habitats of Antarctic krill. *Mar. Ecol. Prog. Ser.* 362, 1–8. doi: 10.3354/meps07498

Baker, A. D. C., Clarke, M. R., and Harris, M. J. (1973). The N.I.O. combination net (RMT 1 + 8) and further developments of rectangular midwater trawls. *J. Mar. Biol. Assoc. UK* 53, 167–184. doi: 10.1017/S0025315400056708

Bindoff, N. L., Rosenberg, M. A., and Warner, M. J. (2000). On the circulation and water masses over the Antarctic continental slope and rise between 80 and 150°E. *Deep-Sea Res. II* 47, 2299–2326. doi: 10.1016/S0967-0645(00)00038-2

Bryantsev, V. A., Kovalenko, L. A., and Bibik, V. A. (1991). "Hydrometeorological bases for forecasting of the Antarctic krill, *Euphausla superba* Dana, distribution and biomass in the Cooperation Sea," in *Document WG-KRILL-91/43* (CCAMLR, Hobart, Australia), 1–6.

Butterworth, D. S., Punt, A. E., and Basson, M. (1991). "A simple approach for calculating the potential yield of krill from biomass survey results," in *Selected Scientific Papers (SC-CAMLR-SSPI8)* (CCAMLR, Hobart, Australia), 207–217.

CCAMLR (2021). Available online at: https://www.ccamlr.org/en/fisheries/krill (Accessed 11 December 2023).

Constable, A. J., and de la Mare, W. K. (1996). A generalized model for evaluating yield and the long-term status of fish stocks under conditions of uncertainty. *CCAMLR Sci.* 3, 31–54.

Cox, M. J., Macauley, G., Brasier, M. J., Burns, A., Johnson, O. J., King, R., et al. (2022). Two scales of distribution and biomass of Antarctic krill (*Euphausia superba*) in

the eastern sector of the CCAMLR Division 58.4.2 (55°E to 80°E). *PloS One* 17, e0271078. doi: 10.1371/journal.pone.0271078

Everson, I., and Bone, D. G. (1986). Effectiveness of the RMT8 system for sampling krill (*Euphausia superba*) swarms. *Polar Biol.* 6, 83–90. doi: 10.1007/BF00258257

Flores, H., Hunt, B. P. V., Kruse, S., Pakhomov, E. A., Siegel, V., Van Franeker, J. A., et al. (2014). Seasonal changes in the vertical distribution and community structure of Antarctic macrozooplankton and micronekton. *Deep-Sea Res. I* 84, 127–141. doi: 10.1016/j.dsr.2013.11.001

Flores, H., Van Franeker, J. A., Siegel, V., Haraldsson, M., Strass, V., Meesters, E. H. W. G., et al. (2012). The association of Antarctic krill *Euphausia superba* with the under-ice habitat. *PloS One* 7, e31775. doi: 10.1371/journal.pone.0031775

Fraser, F. C. (1936). On the development and distribution of the young stages of krill (*Euphausia superba*). *Discovery Rep.* 14, 3–190. doi: 10.5962/bhl.part.3886

Hamabe, K., Miyashita, T., Nagata, R., Sasaki, H., and Murase, H. (2024). Abundance of humpback whales in the eastern Indian sector of the Southern Ocean in 2018/19 using opportunistic sighting survey data with a note on the occurrence of other cetaceans. *Progr. Oceanogr.* 226, 103296. doi: 10.1016/j.pocean.2024.103296

Hill, S. L., Murphy, E. J., Reid, K., Trathan, P. N., and Constable, A. J. (2006). Modelling Southern Ocean ecosystems: krill, the food-web, and the impacts of harvesting. *Biol. Rev. Cam. Philos. Soc* 81, 581–608. doi: 10.1017/S1464793106007123

Hirano, D., Mizobata, K., Sasaki, H., Murase, H., Tamura, T., and Aoki, S. (2021). Poleward eddy-induced warm water transport across a shelf break off Totten Ice Shelf, East Antarctica. *Commun. Earth Environ.* 2, 153. doi: 10.1038/s43247-021-00217-4

Hofmann, E. E., Klinck, J. M., Locarnini, R. A., Fach, B. A., and Murphy, E. J. (1998). Krill transport in the Scotia Sea and environs. *Antar Sci.* 10, 406–415. doi: 10.1017/S0954102098000492

Hosie, G. W., Ikeda, T., and Stolp, M. (1988). Distribution, abundance and population structure of the Antarctic krill (*Euphausia superba*) in the Prydz Bay region, Antarctica. *Polar Biol.* 8, 213–224. doi: 10.1007/BF00443453

Ichii, T., and Kato, H. (1991). Food and daily food-consumption of Southern minke whales in the Antarctic. *Polar Biol.* 11, 479–487. doi: 10.1007/BF00233083

Ichii, T., Shinohara, N., Fujise, Y., Nishiwaki, S., and Matsuoka, K. (1998). Interannual changes in body fat condition index of minke whales in the Antarctic. *Mar. Ecol. Progr. Ser.* 175, 1–12. doi: 10.3354/meps175001

Ikeda, T. (1984). Development of the larvae of the Antarctic krill (*Euphausia superba* Dana) observed in the laboratory. *J. Exper. Mar. Biol. Ecol.* 75, 107–117. doi: 10.1016/0022-0981(84)90175-8

Jarvis, T., Kelly, N., Kawaguchi, S., Van Wijk, E., and Nicol, S. (2010). Acoustic characterisation of the broad-scale distribution and abundance of Antarctic krill (*Euphausia superba*) off East Antarctica (30-80°E) in January-March 2006. *Deep-sea Res. II* 57, 916–933. doi: 10.1016/j.dsr2.2008.06.013

Jia, Z., Virtue, P., Swadling, K. M., and Kawaguchi, S. (2014). A photographic documentation of the development of Antarctic krill (*Euphausia superba*) from egg to early juvenile. *Polar Biol.* 37, 165–179. doi: 10.1007/s00300-013-1420-7

Kawaguchi, S., Nicol, S., Virtue, P., Davenport, S. R., Casper, R., Swadling, K. M., et al. (2010). Krill demography and large-scale distribution in the Western Indian Ocean sector of the Southern Ocean (CCAMLR Division 58.4.2) in Austral summer of 2006. *Deep-Sea Res. II* 57, 934–947. doi: 10.1016/j.dsr2.2008.06.014

Kils, U. (1982). Swimming behaviour, swimming performance and energy balance of Antartic krill, *Euphausia superba. Biomass Sci. Ser.* 3, 1–121.

Kinzey, D., Watters, G. M., and Reiss, C. S. (2019). Estimating recruitment variability and productivity in Antarctic krill. *Fish. Res.* 217, 98–107. doi: 10.1016/j.fishres.2018.09.027

Kirkwood, J. M. (1982). *A Guide to the Euphausiacea of the Southern Ocean* (Kingston: ANARE Research Notes 1, Australian Antarctic Division), 4.

Lampert, W. (1989). The adaptive significance of diel vertical migration of zooplankton. *Funct. Ecol.* 3, 21–27. doi: 10.2307/2389671

Lascara, C. M., Hofmann, E. E., Ross, R. M., and Quetin, L. B. (1999). Seasonal variability in the distribution of Antarctic krill, *Euphausia superba*, west of the Antarctic Peninsula. *Deep-Sea Res. I* 46, 951–984. doi: 10.1016/S0967-0637(98)00099-5

Mackintosh, N. A. (1973). Distribution of post-larval krill in the Antarctic. *Discovery Rep.* 36, 95–156.

Makarov, R. R., and Denys, C. J. (1981). Stages of sexual maturity of *Euphausia superba* Dana. *Biomass Handb.* 11, 2–13.

Marr, J. (1962). The natural history and geography of the Antarctic krill (*Euphausia superba Dana*). *Discovery Rep.* 32, 37–123.

Matsuoka, K., Skoglund, A., Roth, G., De Pomereu, J., Griffiths, H., Headland, R., et al. (2021). QuAntarctica, an integrated mapping environment for Antarctica, the Southern Ocean, and sub-Antarctic islands. *Environ. Modell. Software* 140, 105015. doi: 10.1016/j.envsoft.2021.105015

Mauchline, J. (1980). The biology of mysids and euphausiids. *Adv. Mar. Biol.* 18, 681.

Methot, R. D. (1986). Frame trawl for sampling pelagic juvenile fish. *California Coop. Ocean. Fish. Investig. Rep.* 27, 267–278.

Miller, D. G. M. (1985). The South African SIBEX I cruise to the Prydz Bay regio. *S. Afr. J. Antarct. Res.* 15, 33–41.

Miquel, J. C. (1991). Distribution and abundance of post-larval krill (*Euphausia superba* Dana) near Prydz Bay in summer with reference to environmental conditions. *Antarc. Sci.* 2, 279–292. doi: 10.1017/S0954102091000342

Murphy, E. J., Thorpe, S. E., Watkins, J. L., and Hewitt, R. (2004). Modeling the krill transport pathways in the Scotia Sea: spatial and environmental connections generating the seasonal distribution of krill. *Deep-Sea Res. II* 51, 1435–1456. doi: 10.1016/j.dsr2.2004.06.019

Nicol, S., and Brierley, A. S. (2010). Through a glass less darkly—New approaches for studying the distribution, abundance and biology of Euphausiids. *Deep-Sea Res. II* 57, 496–507. doi: 10.1016/j.dsr2.2009.10.002

Nicol, S., Kitchener, J., King, R., Hosie, G., and de la Mare, W. K. (2000b). Population structure and condition of Antarctic krill (*Euphausia superba*) of East Antarctica (80-150°E) during the Austral summer of 1995/1996. *Deep-Sea Res. II* 47, 2489–2517. doi: 10.1016/S0967-0645(00)00033-3

Nicol, S., Pauly, T., Bindoff, N. L., and Strutton, P. G. (2000a). BROKE" a biological/oceanographic survey of the coast of East Antarctica (80-150°E) carried out in January-March 1996. *Deep-Sea Res. II* 47, 2281–2298. doi: 10.1016/S0967-0645(00)00026-6

Pakhomov, E. A. (1995). Demographic studies of Antarctic krill *Euphausia superba* in the Cooperation and Cosmonaut Seas (Indian sector of the Southern Ocean). *Mar. Ecol. Progr. Ser.* 119, 45–61. doi: 10.3354/meps119045

Pakhomov, E. A. (2000). Demography and life cycle of Antarctic krill, *Euphausia superba*, in the Indian sector of the Southern Ocean: long-term comparison between coastal and open-ocean regions. *Can. J. Fish. Aq. Sci.* 57, 68–90. doi: 10.1139/f00-175

Pauly, T., Nicol, S., Higginbottom, I., Hosie, G., and Kitchener, J. (2000). Distribution and abundance of Antarctic krill (*Euphausia superba*) off East Antarctic (80-150°E) during the austral summer of 1995/1996. *Deep-Sea Res. II* 47, 2465–2488. doi: 10.1016/S0967-0645(00)00032-1

Piccolin, F., Pitzschler, L., Biscontin, A., Kawaguchi, S., and Meyer, B. (2020). Circadian regulation of diel vertical migration (DVM) and metabolism in Antarctic krill *Euphausia superba*. *Sci. Rep.* 10, 16796. doi: 10.1038/s41598-020-73823-5

Quetin, L. B., and Ross, R. M. (2003). Episodic recruitment in Antarctic krill *Euphausia superba* in the Palmer LTER study region. *Mar. Ecol. Progr. Ser.* 259, 185–200. doi: 10.3354/meps259185

Quetin, L. B., Ross, R. M., Frazer, T. K., and Haberman, K. L. (1996). Factors affecting distribution and abundance of zooplankton, with an emphasis on Antarctic krill, *Euphausia superba*. *Antarc. Res. Ser.* 70, 357–371. doi: 10.1029/AR070p0357

R Core Team (2022). *R: A language and environment for statistical computing* (Vienna, Austria: R Foundation for Statistical Computing).

Roe, H. S. J., and Shale, D. M. (1979). A new multiple rectangular midwater trawl (RMT 1 + 8M) and some modifications to the institute of oceanographic sciences' RMT 1 + 8. *Mar. Biol.* 50, 283–288. doi: 10.1007/BF00394210

Santora, J. A., Reis, C. S., Loeb, V. J., and Veit, R. R. (2010). Spatial association between hotspots of baleen whales and demographic patterns of Antarctic krill *Euphausia superba* suggests size-dependent predation. *Mar. Ecol. Progr. Ser.* 405, 255–269. doi: 10.3354/meps08513

Schaafsma, F. L., David, C., Pakhomov, E. A., Hunt, B. P. V., Lange, B. A., Flores, H., et al. (2016). Size and stage composition of age class 0 Antarctic krill (*Euphausia superba*) in the ice-water interface layer during winter/early spring. *Polar Biol.* 39, 1515–1526. doi: 10.1007/s00300-015-1877-7

Schaafsma, F. L., Matsuno, K., Driscoll, R., Sasaki, H., Van Regteren, M., Driscoll, S., et al. (2024). Zooplankton communities at the sea surface of the eastern Indian sector of the Southern Ocean during the austral summer of 2018/2019. *Progr. Oceanogr.* 226, 103303. doi: 10.1016/j.pocean.2024.103303

Siegel, V. (1986). Untersuchungen zur biologie des Antarkischen krill, *Euphausia superba*, in bereich der Bransfield Strabe und angrenzender Gebiete. *Mitt. aus dem Instit. für Seefischerei der Bundesforschungsanstalt für Fischerei* 38, 1–244.

Siegel, V. (1988). "A concept of seasonal variation of krill (*Euphausia superba*) distribution and abundance west of the Antarctic Peninsula," in *Antarctic Ocean and resources variability*. Ed. D. Sahrhage (Springer-Verlag, Berlin), 219–230.

Siegel, V. (2005). Distribution and population dynamics of *Euphausia superba*: summary of recent findings. *Polar Biol.* 29, 1–22. doi: 10.1007/s00300-005-0058-5

Siegel, V., Kawaguchi, S., Ward, P., Litvinov, F., Sushin, V., Loeb, V., et al. (2004). Krill demography and large-scale distribution in the southwest Atlantic during Janury/February 2000. *Deep Sea Res. II* 51, 1253–1273. doi: 10.1016/j.dsr2.2004.06.013

Siegel, V., and Loeb, V. (1995). Recruitment of Antarctic krill *Euphausia superba* and possible causes for its variability. *Mar. Ecol. Progr. Ser.* 123, 45–56. doi: 10.3354/meps123045

Spiridonov, V. A. (1995). Spatial and temporal variability in reproductive timing of Antarctic krill (*Euphausia superba* Dana). *Polar Biol.* 15, 161–174. doi: 10.1007/BF00239056

Tarling, G. A., Shreeve, R. S., Hirst, A. G., Atkinson, A., Pond, D. W., Murphy, E. J., et al. (2006). Natural growth rates in Antarctic krill (*Euphausia superba*): I. Improving methodology and predicting intermoult period. *Limnol. Oceanogr.* 51, 959–972. doi: 10.4319/lo.2006.51.2.0959

Van Franeker, J. A., Flores, H., and Van Dorssen, M. (2009). "The surface and under ice trawl (SUIT)," in *Frozen desert alive*. Ed. H. Flores (Groningen, The Netherlands: University of Groningen), 181–188.

Wang, R., Song, P. L. Y., and Lin, L. (2021). An integrated, size-structure stock assessment of Antarctic krill, *Euphausia superba*. *Front. Mar. Sci.* 8. doi: 10.3389/fmars.2021.710544

Watkins, J. L. (1999). A composite recruitment index to describe interannual changes in the population structure of Antarctic krill at South Georgia. *CCAMLR Sci.* 6, 71–84.

Watkins, J. (2000). "Sampling krill—direct sampling," in *Krill Biology, Ecology and Fisheries*. Ed. I. Everson (Blackwell Science, Oxford), 8–19.

Yamazaki, K., Aoki, S., Shimada, K., Kobayashi, T., and Kitade, Y. (2020). Structure of the subpolar gyre in the Australian-Antarctic basin derived from Argo floats. *J. Geophys. Res.: Oceans* 125, e2019JC015406. doi: 10.1029/2019JC015406

Yamazaki, K., Katsumata, K., Hirano, D., Nomura, D., Sasaki, H., Murase, H., et al. (2024). Revisiting circulation and water masses over the East Antarctic margin (80–150°E). *Progr. Oceanogr.* 225, 103285. doi: 10.1016/j.pocean.2024.103285

frontiers | Frontiers in Marine Science

TYPE Original Research
PUBLISHED 16 September 2024
DOI 10.3389/fmars.2024.1406678

Check for updates

OPEN ACCESS

EDITED BY
Michele Thums,
Australian Institute of Marine Science (AIMS), Australia

REVIEWED BY
Cristina D. S. Tollefsen,
Curtin University, Australia
Michael Noad,
The University of Queensland, Australia

*CORRESPONDENCE
Franciele R. de Castro
francielercastro@gmail.com

RECEIVED 26 March 2024
ACCEPTED 29 July 2024
PUBLISHED 16 September 2024

CITATION
de Castro FR, Harris DV, Buchan SJ, Balcazar N and Miller BS (2024) Beyond counting calls: estimating detection probability for Antarctic blue whales reveals biological trends in seasonal calling. *Front. Mar. Sci.* 11:1406678. doi: 10.3389/fmars.2024.1406678

COPYRIGHT
© 2024 de Castro, Harris, Buchan, Balcazar and Miller. This is an open-access article distributed under the terms of the Creative Commons Attribution License (CC BY). The use, distribution or reproduction in other forums is permitted, provided the original author(s) and the copyright owner(s) are credited and that the original publication in this journal is cited, in accordance with accepted academic practice. No use, distribution or reproduction is permitted which does not comply with these terms.

Beyond counting calls: estimating detection probability for Antarctic blue whales reveals biological trends in seasonal calling

Franciele R. de Castro[1,2]*, Danielle V. Harris[3], Susannah J. Buchan[1,4,5], Naysa Balcazar[6] and Brian S. Miller[7]

[1]Center for Oceanographic Research Centro de Investigación Oceanografica en el Pacifico Sur-Oriental (COPAS COASTAL), Universidad de Concepción, Concepción, Región del Bio, Concepción, Chile, [2]Aqualie Institute, Juiz de Fora, Minas Gerais, Brazil, [3]Centre for Research into Ecological and Environmental Modelling, University of St Andrews, St Andrews, United Kingdom, [4]Departamento de Oceanografía, Facultad de Ciencias Naturales y Oceanográficas, Universidad de Concepción, Concepción, Región del Bio, Concepción, Chile, [5]Centro de Estudios Avanzados en Zonas Áridas (CEAZA), La Serena, Chile, [6]Independent Researcher, Coolangatta, QLD, Australia, [7]Australian Antarctic Division, Kingston, TAS, Australia

We explore the utility of estimating the density of calls of baleen whales for better understanding acoustic trends over time. We consider as a case study stereotyped 'song' calls of Antarctic blue whales (*Balaenoptera musculus intermedia*) on their Antarctic feeding grounds over the course of a year-long, continuous recording from 2014. The recording was made in the Southern Ocean from a deep-water autonomous hydrophone moored near the seafloor in the Eastern Indian sector of the Antarctic. We estimated call density seasonally via a Monte-Carlo simulation based on the passive sonar equation, and compared our estimates to seasonal estimates of detection rate, which are commonly reported in acoustic studies of Antarctic blue whales. The resulting seasonal call densities at our Antarctic site were strongly influenced by seasonally varying noise levels, which in turn yielded seasonal differences in detection range. Incorporating the seasonal estimates of detection area into our analysis revealed a pattern of call densities in accord with historic (non-acoustic) knowledge of Antarctic blue whale seasonal distribution and migrations, a pattern that differed from seasonal detection rates. Furthermore, our methods for estimating call densities produced results that were more statistically robust for comparison across sites and time and more meaningful for interpretation of biological trends compared to detection rates alone. These advantages came at the cost of a more complex analysis that accounts for the large variability in detection range of different sounds that occur in Antarctic waters, and also accounts for the performance and biases introduced by automated algorithms to detect sounds. Despite the additional analytical complexities, broader usage of call densities, instead of detection rates, has the potential to yield a standardized, statistically robust, biologically informative, global investigation of acoustic trends in baleen whale sounds recorded on single hydrophones, especially in the remote and difficult to access Antarctic.

KEYWORDS

acoustic propagation modelling, Antarctic, Southern Ocean, Antarctic blue whale, single hydrophone, call density, acoustic trends

1 Introduction

Underwater passive acoustic monitoring has for decades been proposed as an efficient means of studying certain vocal marine species, particularly cetaceans (Mellinger et al., 2007; Van Parijs et al., 2009) with many applications focusing on understanding distribution and movement patterns of particular species. In more recent years, advances in computing, acoustic, and statistical methods have seen an increasing trend towards local density estimation from passive acoustics (Thomas and Marques, 2012; Wilcock, 2012; Harris et al., 2013, 2018; Helble et al., 2013; Hildebrand et al., 2015).

Density estimation can ultimately lead us to make assessments across multiple recording sites (Helble, 2013) that can lead to understanding broader population trends in space and time. Estimating animal density from underwater passive acoustic monitoring data can be a significant challenge given uncertainties in detection range of listening stations, acoustic behaviour of animals, and the performance of automatic detectors of animal sounds, among others.

A variety of acoustic techniques have been proposed and summarized in a review by Marques et al. (2013), and most of these methods are derived from widely used (predominantly visual) methods for estimating abundance (e.g. Borchers et al., 2002). Here we present an application of one of these methods: estimating density from single fixed passive acoustic sensors with a detection function estimated from auxiliary data (Küsel et al., 2011; Marques et al., 2013 Section IV.3). Specifically, our application focuses on estimating the seasonal density of calls, (henceforth call density) of Antarctic blue whales (*Balaenoptera musculus intermedia*; henceforth ABWs) on their Antarctic feeding grounds.

ABWs, the largest animal to have ever lived, are critically endangered (Cooke, 2018) after being hunted to the brink of extinction during industrial whaling (Rocha et al., 2015). They were subsequently encountered very rarely during three decades of visual surveys spanning the 1970s-2000s (Branch, 2007), and for the past two decades much of the primary data collection on this species has relied on passive acoustics (e.g. Ljungblad et al., 1998; Širović et al., 2004, 2009; Rankin et al., 2005; Širović and Hildebrand, 2011; Gavrilov et al., 2012; Balcazar et al., 2015; Miller et al., 2015, 2017, 2019; Rocha et al., 2015; Tripovich et al., 2015; Leroy et al., 2016; Shabangu et al., 2017, 2019, 2020; Thomisch, 2017; Dréo et al., 2019; Letsheleha et al., 2022). The low frequency sounds of baleen whales, particularly blue and fin whales, have long been known to be detectable over very large areas (Payne and Webb, 1971; Širović et al., 2007; Miller et al., 2015). Work to quantify site- and time-specific detection ranges (e.g., McDonald and Fox, 1999; McCauley et al., 2001; Samaran et al., 2010a; Shabangu et al., 2020), and this has confirmed that detection range can vary across sites and timespans. However, relatively few acoustic studies have focused on quantifying and accounting for this variability in detection range, despite the importance of these factors when interpreting counts of acoustic detections. More recently, several of the underwater acoustic studies that have taken detection range and its variability into account have done so via estimation of call densities (e.g. Helble et al., 2013; Harris et al., 2018; Miksis-Olds et al., 2019; Oedekoven et al., 2021; Warren et al., 2021), though none of these studies have focused on the calls of ABWs in the extremely variable Antarctic environment.

Call densities are one-step removed from acoustic estimates of animal density in that call densities do not account for vocal behaviour of animals. Therefore, call densities should be interpreted as indicative of a potential combination of animal density and animal behaviour. Call densities are similar to detection rates (call-counts per unit time), which have been commonly reported in many prior passive acoustic studies of ABWs (Širović et al., 2009; Samaran et al., 2013; Balcazar et al., 2015; Leroy et al., 2016; Thomisch, 2017; Dréo et al., 2019; Shabangu et al., 2020). However, unlike detection rate, call density is standardised by detection area yielding units of calls per unit area per unit time. Detection range of low-frequency whale sounds can be highly variable across sites and over time (Samaran et al., 2010a; Harris et al., 2018; Shabangu et al., 2020), so by accounting for all the main factors that influence detection, including the performance of an automated detector (i.e. false positives and missed-detections), resulting call densities do not suffer from one of the biggest hindrances to interpreting detection rates from these previous studies.

Here we describe a method to estimate seasonal call densities of ABW sounds, and results are standardized and suitable to assess trends in space and time. We also describe and apply methods to estimate the coefficient of variation (CV) of each of our call density estimates, and this in turn facilitates statistically robust comparisons among different regions and/or timespans.

2 Methods

2.1 Data collection

Acoustic recordings for our application come from the Australian Antarctic Division's long-term acoustic monitoring dataset (Miller et al., 2021c), which is part of the Southern Ocean Hydrophone Network (Opzeeland et al., 2013). We focus on the site located on the Southern Kerguelen Plateau (62.38°S, 81.79°E) and the year 2014, as this site and year contain near-continuous acoustic recording, and already contained a representative subset of 4298 ground-truth annotations of ABW song calls made by an expert analyst (Miller et al., 2020, 2021a). Recording for the full dataset started on February 10, 2014 and ended on February 7, 2015, totalling approximately 8700 hours of underwater sound.

2.2 Analysis

In general we follow the methods described in Harris et al. (2024, submitted), which were in turn extended from Küsel et al. (2011) to use auxiliary data to estimate the probability of detecting a call, which is a key parameter in density estimation methods. We apply the density estimation formula (Equation 1) for a single-sensor (a single fixed listening station with a single hydrophone) with call-counts, n_c, generated from an automated detector that has

10.3389/fmars.2024.1406678

a false discovery rate $\hat{f}$, such that:

$$\hat{D}_c = \frac{n_c(1-\hat{f})}{A\hat{p}_a T} \quad (1)$$

Here $\hat{D}_c$ is the estimated call density; A is the sum of the area for each transect; T is the duration of recording (in h); $\hat{p}_a$ is the probability of detection in the study area; and the circumflex or "hat operator" (^) indicates that a quantity is an estimated parameter. The following sections describe how each of these quantities were obtained.

2.2.1 Duration of recording (*T*)

Here we were interested in determining whether there were seasonal differences in call density, and how these compared to seasonal estimates of detection rate. To facilitate this we split the dataset into five time periods: four seasonal estimates and one annual estimate. Seasons were defined as summer comprising months: Dec, Jan, Feb; autumn: Mar, Apr, May; winter: Jun, Jul, Aug; and spring: Sep, Oct, Nov, and 'full year' included all of the data from each season. We opted for a conventional definition of seasons to enable comparisons with other ecological and biological studies using this approach, rather than relying on a physical oceanographic method, which can be region-specific. Each of the following quantities were then estimated independently for each time period, with *T* measured directly as the duration of recorded audio for each period.

2.2.2 Number of calls (n_c)

To count the number of calls we applied a spectrogram correlation detector to the entire duration of recorded data. This detector targets ABW song calls, also known as "Z-calls" (Širović et al., 2004), which are made up of unit A (the constant tone comprising the top of the Z), unit B, (the downsweep that connects units A & C), and unit C (the near-constant or slightly downswept tone comprising the bottom of the Z, Rankin et al., 2005). The detector we used is the same as the Antarctic blue whale "ABZ" call detector described by Miller et al. (2021a). According to the ground-truth detections (i.e., manual annotations made by an expert analyst), this spectrogram-correlation detector had mediocre performance (Miller et al., 2021a), but was capable of detecting calls composed of stand-alone unit-A, calls with only units A & B visible, and full Z-calls that contained all three units: A, B, and C (Figure 1). We chose a detection threshold that had a low false positive rate (approximately 2.5 false positives per hour), but also had a low true positive rate of approximately 0.27 for this site-year. Here, the true positive rate (AKA recall) was defined as the proportion of manually annotated detections found by the automated detector.

2.2.3 False discovery rate ($\hat{f}$)

False discovery rate for each season was calculated by expert inspection of every 50th automated detection throughout the dataset. We applied a fixed interval for manual inspection to ensure a consistent examination of a subset of automated detections across the dataset. The expert analyst, author FRC, viewed a spectrogram of the detection, and then determined whether or not that detection was true positive, or a false positive. The total number of true positives, TP, and false positives, FP, were then tabulated for each time period in order to estimate the false discovery rate (Equation 2):

$$\hat{f} = FP/(FP + TP) \quad (2)$$

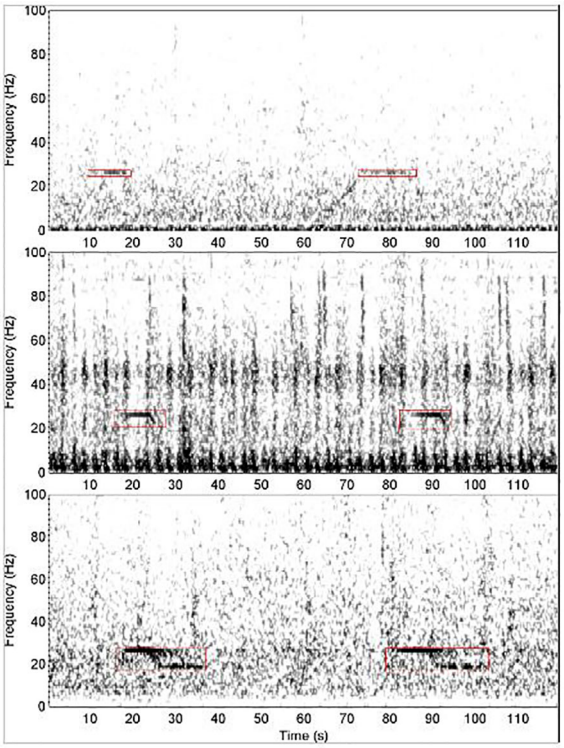


FIGURE 1
Examples of Antarctic blue whale song calls. Top: two detections of stand-alone unit-A. Middle: two detections that appear to consist solely of units A and B. Bottom: two Z-calls containing units A, B, & C. Image reproduced from (Miller et al., 2021a) under a creative-commons licence.

2.2.4 Probability of detecting a call within the study area ($\hat{p}_a$)

Detection probability was estimated with a Monte Carlo simulation using elements of the passive sonar equation. The method is described in full in Harris et al. (2024, submitted) and a summary is provided here. There were two main parts to the analysis: first, detection probability was modelled as a function of call signal-to-noise ratio (SNR) using a shape-constrained generalised additive model (GAM). Second, a Monte Carlo simulation was used to estimate the average detection probability $\hat{p}_a$ needed for Equation 1. The simulation was populated with virtual blue whale calls around a single omnidirectional hydrophone. All virtual calls were assigned source levels (SL), ambient noise levels (NL) and a transmission loss (TL), given their virtual position was known in relation to the hydrophone. The SNR (in dB) for unit-A of each simulated call was calculated using the expression from the passive sonar equation (Equation 3):

10.3389/fmars.2024.1406678

$$SNR = SL - TL - NL \quad (3)$$

A predicted detection probability for each call was estimated using the GAM results, and then the average detection probability, $\hat{p}_a$, was estimated from all the simulated calls (see section Monte Carlo method below for additional details).

2.2.4.1 Detector characterisation curves (SNR-detection functions)

The data from the IWC-SORP annotated library (Miller et al., 2020) for the site-year S. Kerguelen Plateau-2014 were used to estimate the probability of detection as a function of SNR (AKA detector characterisation curves, Figure 2), which illustrates the estimated relationship between SNR and probability of detection, essential for assessing how effective and reliable a detection system is under different levels of noise interference. As in Miller et al. (2021a) the 4298 detections of unit-A, units A-B and Z-calls from the manual analyst were treated as ground-truth, and false-positive detections from the automated detector were removed prior to modelling the relationship. The model here was similar to that presented by Miller et al. (2021a), however, here we estimated the SNR as SNR=RL-NL (in dB) and we did not divide by the variance of the noise as in the previous work (Miller et al., 2021a). Furthermore, here the relationships between SNR and automated detections were modelled independently for each season and the full year, whereas in the previous work only a single model was created for the full year. The detector characterisation curves were modelled as binomial shape-constrained GAMs with logit link functions and 5 'knots' using the package 'scam' (Pya, 2022) in R version 4.2.0 (R Core Team, 2019) using the formula (Equation 4):

$$detected \sim s(SNR) \quad (4)$$

Here, "detected" was a Boolean response variable with value 1 or 0 depending on whether or not the automated detector had any temporal overlap with a ground-truth manual annotation; SNR was the predictor variable, measured from the acoustic data as defined above.

2.2.4.2 Source levels

For the Monte Carlo simulation, SL was modelled as normally distributed (in dB), with a mean of 189 dB re 1 µPa @1m and standard deviation of 8.0. There have been very few studies of SL of ABW sounds, but they all report mean SL of unit-A that are very close to this value (Širović et al., 2007; Samaran et al., 2010b; Bouffaut et al., 2021; Miller et al., 2021b), despite these studies all being conducted in different seasons. Thus, the same distribution of SL was used for all time periods. The standard deviation of SL used was that reported by Miller et al. (2021a), which has the largest sample size of all these studies in terms of both number of calls (350) and likely number of whales.

2.2.4.3 Transmission-loss modelling

Transmission-loss (TL) was modelled by applying the parabolic equation method via the RAMGeo acoustic propagation algorithm (Collins, 2002, Figure 3). This was implemented via the software package AcTUP (Duncan, 2005), which is a user interface to the 2005 version of the Ocean Acoustics Library (Porter, 2020). TLs were modelled for a frequency of 26 Hz (corresponding to unit A of ABW calls) along 24 evenly-spaced radial transects originating at the recorder, and ending at distance w along each bearing with a

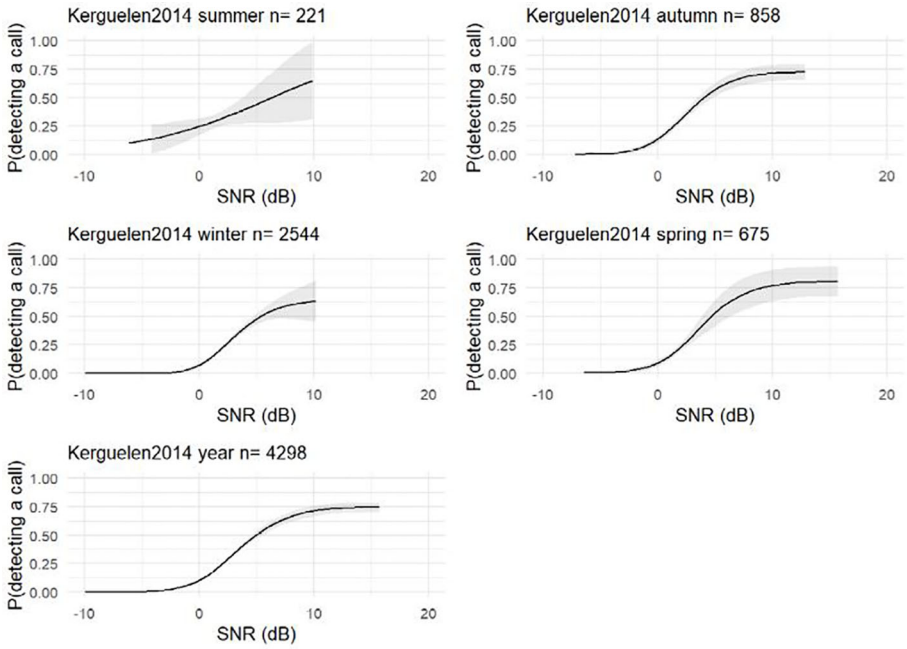


FIGURE 2
Probability of detecting a call given a signal-to-noise ratio (SNR) using a separate shape-constrained generalised additive model (GAM) for each time period. The grey area around each curve depicts the 95% confidence limits.

distance increment of 2 m following the principle of reciprocity of TL between source and receiver (Nghiem-Phu and Tappert, 1985; Jensen et al., 2011).

Parameters for the TL model included the depth at which the call was produced and received, bathymetry, seabed acoustic properties, and water-column sound-speed profile (Figure 4). The depth of the recorder was estimated to be 1800 m using the ship's echosounder during deployment, and the depth of calling was estimated to be 25 m, identical to that for which SL estimates were made (Miller et al., 2021b). We assumed that the effects of small variations in the depth of the calling whale, which can have large effects on the TL, were potentially counterbalanced by the SL adopted in this study, since such effects were taken into account in the SL estimation. Bathymetry was extracted for each transect from

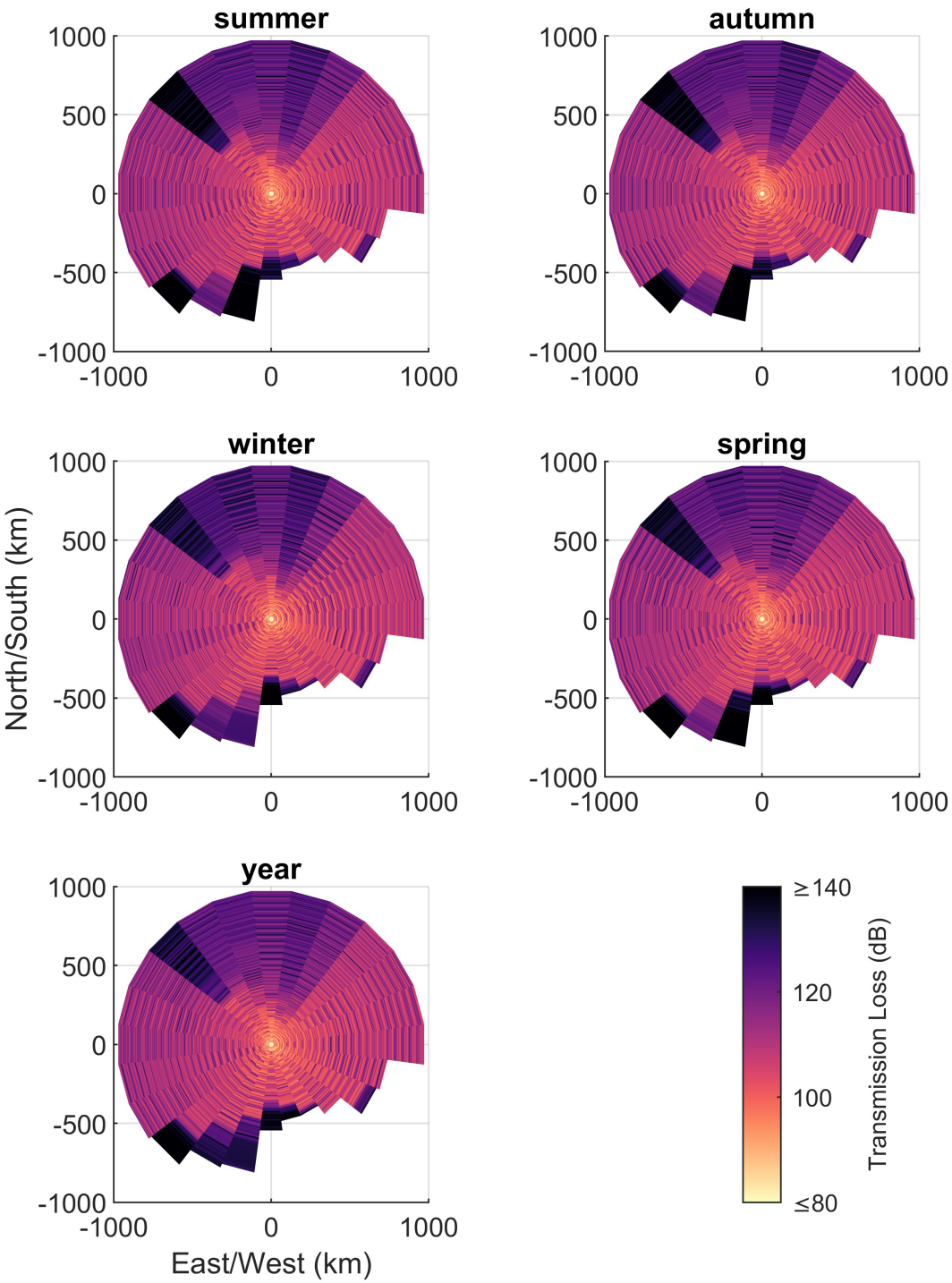


FIGURE 3
Transmission loss, TL, model per profile: 0-345° in 15° increments, respectively plotted for each season. TL were modelled at a frequency of 26 Hz assuming whale depth of 25 m and recorder depth of 1800 m.

10.3389/fmars.2024.1406678

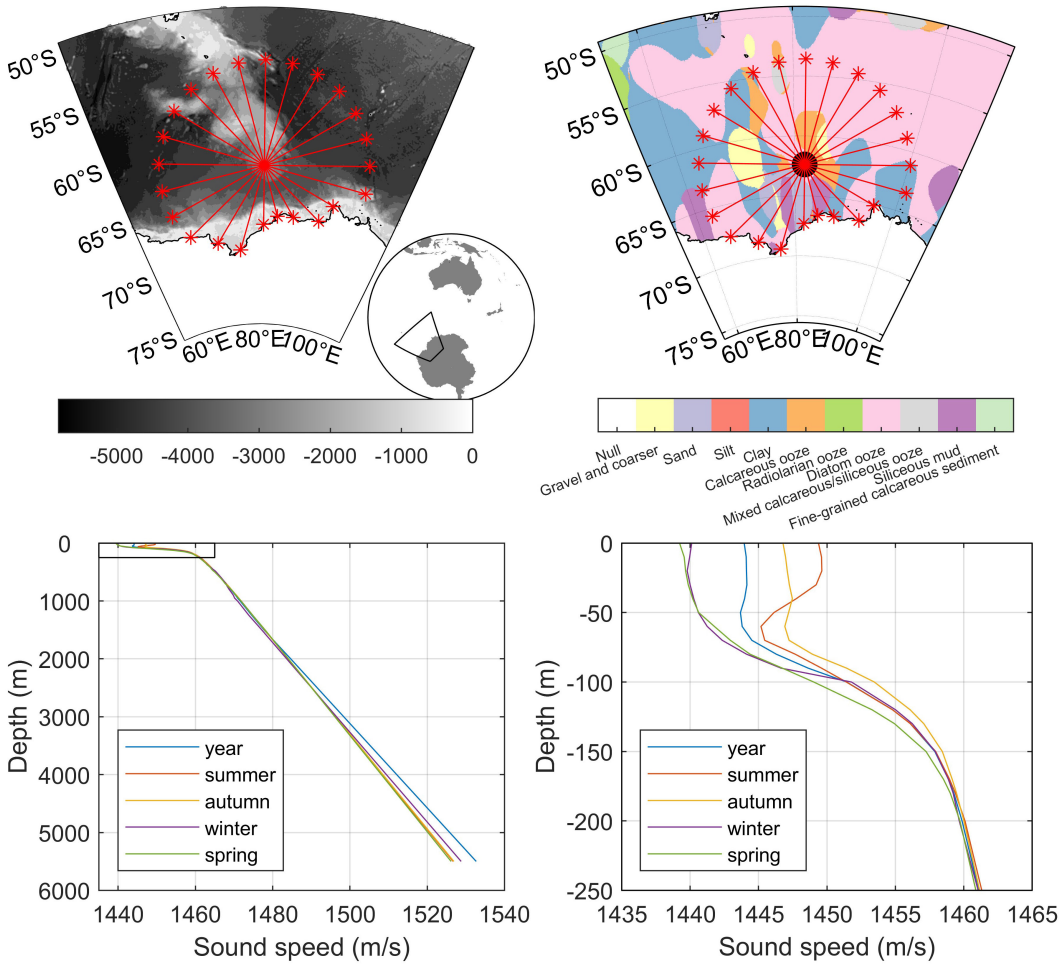


FIGURE 4
Maps of recording location (red circle) and transects used to estimate probability of detection in the study area (red lines). Top Left: bathymetry in m from etopo1 (Amante and Eakins, 2009). Top Right: sediment type from the Census of Seabed Sediments (Dutkiewicz et al., 2015) illustrating that the most common sediments are "clay" and "diatom ooze." Bottom: seasonal sound-speed profiles at the recording location as a function of depth derived salinity and temperatures from the World Ocean Atlas 2018 (Boyer et al., 2018). Bottom left panel shows full depth range, while the bottom right panel shows the same information, but focused on the first 250 m to better illustrate the details of this region.

the etopo1 database at 10 km distance increments (Amante and Eakins, 2009). Seabed acoustic properties were modelled as large-grain with a compressional sound speed of 1520 m/s and a density of 1200 kg/m3. These properties were similar to typical parameters for a homogenous seabed made of "clay" (Lurton, 2010). Only limited *in-situ* spatial information on geoacoustic properties of the seabed in the region could be found, but a 'clay' seabed seemed to be a reasonable choice according to the few data products available (Dutkiewicz et al., 2015) (Figure 4).

A single sound-speed profile (SSP) for each season (summer, autumn, winter, spring), and a single SSP for the full year was created from the World Ocean Atlas 2018 (Boyer et al., 2018) using the respective seasonal and yearly salinity and temperature water column profiles nearest in location to the instrument. The GSW Oceanographic Toolbox was used to calculate sound-speeds from salinity, temperature, and depth (McDougall and Barker 2011). Atmospheric seasons were chosen instead of physical oceanographic seasons as they are typically observed when discussing seasonality in marine mammals. However, the difference in SSP between atmospheric and oceanographic seasons, which are offset by a month, was not expected to substantially affect TL in this application and region. This is because Antarctic SSPs are upward refracting and contain shallow sound speed minima throughout the year, and thus are relatively stable across seasons compared to more temperate regions.

2.2.4.4 Noise levels

Noise levels were estimated for each manually annotated detection by calculating the mean power in dB re: 1 µPa in the 25-29 Hz frequency band of the spectrogram (i.e. the frequency band of SL measurements of unit-A of ABW song calls). The NL was measured 26 seconds (25 seconds + 1 second) prior to the onset of manual detection. When the annotation was at the beginning of the file, without 26 seconds of preceding audio, the noise was measured immediately following the detection. NL were measured for each call regardless of the presence or absence of other calls, and regardless of the presence or absence of a 'chorus' (i.e., elevated levels in the call band that arise from the hydrophone receiving

10.3389/fmars.2024.1406678

TABLE 1 Inputs into the call density equation for each season: number of detections (n_c), time of recording (T) in h, false discovery rate (f), probability of detection (p_a), and parameters for the distribution of noise level (NL) in dB re 1 μPa^2 RMS.

season	n_c	f	T	p_a	NLmean	NLsd
summer	13248	0.464	2075.4	0.0658	92.4	2.6
autumn	19123	0.243	2199.7	0.0192	96.8	3.7
winter	32631	0.265	2197.3	0.0701	87.5	3.5
spring	12903	0.388	2167.8	0.1836	81.0	2.4
year	77905	0.314	8640.2	0.0789	88.6	5.9

multiple overlapping calls from many non-localisable and/or distant animals). This decision can be viewed as a choice to explicitly include the effects of the 'chorus' and the potential effects of masking from other calls as noise in our estimates of call density. The mean and standard deviation of measured NL for each season and the full year were then used as input parameters (i.e., to generate normal distributions of NL) for Monte-Carlo simulations for the respective time-periods.

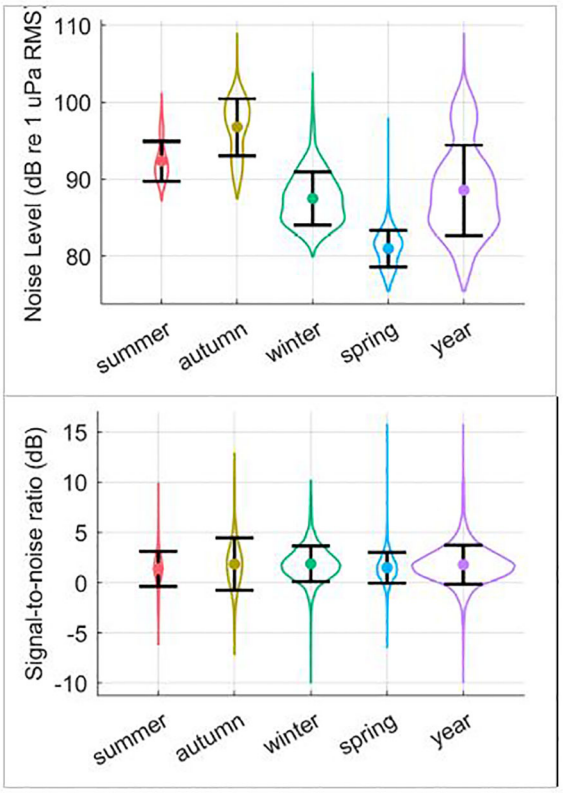


FIGURE 5
Top: Noise level (NL) and bottom: signal-to-noise ratio (SNR) distributions measured for unit-A of the manually annotated Antarctic blue whale A, B, and Z-calls (25-29 Hz band). Violin plots show the distributions of values from ground-truth detections, while error-bars show the standard deviation centred on the mean value.

2.2.4.5 Monte Carlo method

A Monte Carlo simulation similar to the method described in Harris et al. (2024, submitted) was used to estimate average detection probability, and is summarised here. The simulation has two stages referred to as the outer- and inner loops. The two stages are necessary to appropriately account for all sources of variability in the simulation.

In the outer loop, different source level and ambient noise level distributions were simulated, as well as a detector characterisation curve using parametric bootstraps. Normal distributions were assumed for the source- and noise level distributions with mean and standard deviations as described above, as the dB values were normally distributed in Miller et al. (2021b). A multivariate normal distribution was assumed for the model coefficients from the GAM. The estimated coefficient parameters were used as the mean values and the variance was derived from the GAM covariance matrix. The outer loop was run 1000 times, generating 1000 separate distributions for source- and noise level and 1000 detector characterisation curves. Each combination of simulated source- and noise level distributions, and the detector characterisation curve, were used to run the inner loop. The parametric bootstrap in the outer loop was intended to conservatively preserve variability and expand the range of uncertainty, particularly for SL. Though we used the best available estimates of SL, these estimates still came from a small number of whales and locations. The bootstrap aims to expand the 8 dB standard deviation around the mean SL to better model the uncertainty of these estimates.

In the inner loop, virtual whale calls were placed at 100 m range steps along each transmission loss transect (maximum range = 980 km, with land truncating some transects), resulting in a maximum of 9,800 virtual whale calls per transect. Each call was assigned a source level and an ambient noise level using a random draw from the simulated source- and noise level distributions. Then the relevant transmission loss value was used to estimate the simulated SNR of the call as expected at the hydrophone. The detector characterisation curve was then used to estimate the detection probability for each call, given their SNR values. An average detection probability, $\hat{p}_a$, was then estimable for each transect for each run of the inner loop (averaged across the maximum number of calls per transect, weighted by range, to account for the increasing area represented by calls at increased ranges along the radial). Additionally, we computed the overall detection probability as a weighted mean, with weights based on the area of each transect.

2.2.4.6 Estimation of CV

The delta method (Seber, 1982) was used to estimate an associated CV for each density estimate. For this, the CVs of each component of the analysis that contributed to the uncertainty in the eventual density estimate were combined to produce an overall CV for the D_c. These components were the probability of detection, the encounter rate and the false discovery rate. A CV is defined as the standard deviation divided by the mean estimate. Therefore, given $\hat{p}_a$ was a mean value, the standard error of $\hat{p}_a$ was divided by $\hat{p}_a$. The CV for $\hat{f}$ was estimated in the same way. For n_c, the standard deviation

10.3389/fmars.2024.1406678

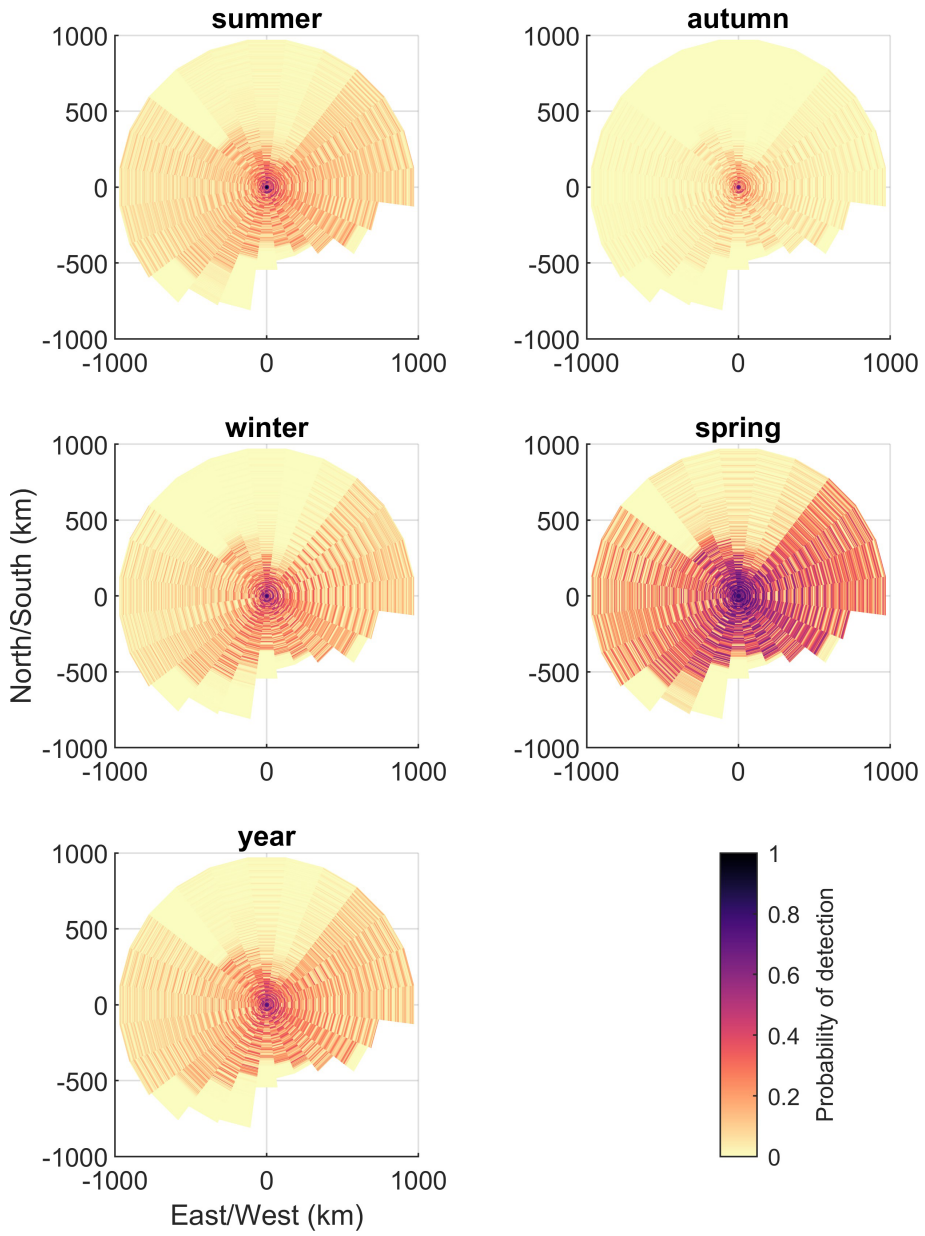


FIGURE 6
Probability of detection, $\hat{p}_a$, within study area for each radial transect.

was used since the encounter rate was not considered to be a mean estimate. For $\hat{f}$, CV was estimated computing the variance of a weighted mean following the definition of Cochran (1977).

3 Results

3.1 Pre-processing of data for call density estimates

The automatic detector yielded 77905 detections, across 8640.2 hours of recording, corresponding to the total time of deployment. Of these, 1559 automated detections were used to estimate false discovery rate, $\hat{f}$, with 313 from summer, 453 from autumn, 563 from winter, and 230 from spring. For the full year of deployment, $\hat{f}$ was 0.314. The detections per season, and other seasonal inputs into the call density estimates are presented in Table 1.

Noise levels showed strong differences over time yielding differences in seasonal mean NLs and respective standard deviations (Table 1; Figure 5). These seasonal differences in NL are in accord with what would be expected due to the seasonal effects of Antarctic sea-ice on underwater noise levels (Miller et al., 2016; Menze et al., 2017; Shabangu et al., 2020; Yun et al., 2021). However, the distribution of SNR of the annotated calls was relatively consistent over time (Figure 5). In contrast to NL, the SNR-detection functions for autumn, winter, and spring were all

10.3389/fmars.2024.1406678

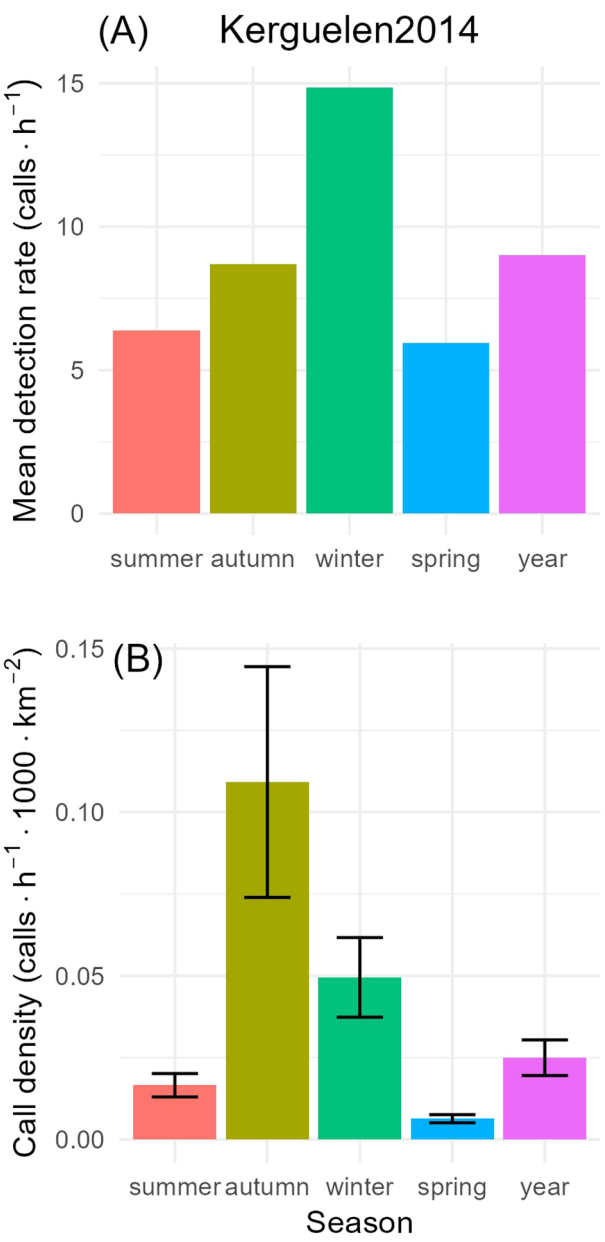


FIGURE 7
Top **(A)**: mean detection rate (in units of calls/h) of Antarctic blue whale tonal calls at S. Kerguelen Plateau 2014 for each time period. Mean detection rates were calculated by dividing the total number of detections by the total duration of monitoring in each time period. Bottom **(B)**: call densities (in units of calls/h/1000 km^2) for each time period with error-bars showing the 95% confidence intervals for each time period.

fairly similar to each other, but different than that for summer (Figure 2). In particular, the SNR-detection function for summer had a shallower slope than other seasons, and substantially wider confidence intervals.

The probability of detection produced by the Monte Carlo simulation decreased to a negligible value at the adopted maximum range of 980 km (Figure 3). Following the pattern set out by NL, the probability of detection within the study area, $\hat{p}_a$, varied substantially across the different time periods (Figure 6; Table 1). The lowest $\hat{p}_a$ occurred in autumn and the highest $\hat{p}_a$ values were in spring and, as would be expected, these were inversely correlated with NL.

3.2 Seasonal density estimates

Seasonal call densities, $\hat{D}_c$, ranged from 0.007 calls/h/1000 km^2 in spring to 0.128 in autumn. The CV of call density was highest in autumn (CV=0.153), and lowest in summer (CV=0.112), but with only small differences in CV among time periods (Figure 7; Table 2).

Detection rate peaked in winter at approximately 15 calls/h. In other seasons, these ranged from 5-8 calls/h (Figure 7). In contrast, maximum call densities occurred in autumn, followed by winter, and minimum call densities occurred in spring.

4 Discussion

4.1 Call density vs. detection rate

Here we present the first estimates of seasonal call densities of Antarctic blue whale song-calls from acoustic recordings made in the Antarctic. Previous passive acoustic studies of ABW calls in the Antarctic have focused on detection rate, and this has made it challenging to understand ecological and biological trends in detections over time and space. Our estimates of call density are more easily interpreted than estimates of detection rate – even if obtaining them is more complicated. By accounting for detection range and detector performance, we ensure that our call densities can be interpreted as some combination of animal density and animal behaviour – factors that are purely biological/ecological in nature. Detection rates, as they are usually presented, are simpler to estimate than call densities. However, within the detection rate the biological factors of interest are confounded with covariates from the physical environment (noise, propagation, detection range) and the detection process (detector performance). Accounting for variability in detection range and detector performance and propagating this variability throughout our call density estimate also provides a means of estimating the CV (and corresponding confidence intervals) of our seasonal call densities.

Plotting our seasonal call densities with confidence intervals reveals differences across seasons, without overlap in 95%

TABLE 2 Results of call density estimation for each season including: density of calls (D_c) in units of calls/h/1000 km^2, coefficient of variation for the parameters n_c, f, p_a, and D_c.

Season	D_c	CV.N_c	CV.$\hat{f}$	CV.p_a	CV.D_c
Summer	0.017	0.0022	0.010	0.110	0.110
Autumn	0.109	0.0010	0.014	0.164	0.165
Winter	0.050	0.0014	0.012	0.125	0.125
Spring	0.006	0.0034	0.012	0.100	0.100
Year	0.025	0.0010	0.003	0.111	0.111

confidence intervals. Furthermore, the seasonal pattern of call densities that we found was different from that of detection rate. Detection rate showed a maximum in the winter, with middling detection rates for summer, autumn, and spring that were all relatively indiscernible (within 2.5 in units of calls/h) from each other since they were confounded by greatly varying noise levels and thus $\hat{p}_a$. Our call densities peaked at a maximum in autumn, falling to a clear minimum in spring. Thus, our data demonstrate that there is a quantifiable seasonal difference in call density, and that this difference was driven by some combination of seasonal changes in ABW density, and/or acoustic behaviour.

The apparent seasonal pattern in call density can serve, alongside other independently derived knowledge of blue whale life history, to develop and test further hypotheses about the biological function of these sounds. For example, it has long been hypothesized, with no evidence to the contrary, that blue whale song calls are produced by males (Oleson et al., 2007; Lewis et al., 2018), and are linked to breeding. Furthermore, there is some evidence from early studies that ABWs have a prolonged and temporally diffuse breeding season over autumn and winter, and that this correlates with a prolonged and temporally diffuse migration to lower latitudes in these seasons (Brown, 1954; Mackintosh, 1966). The seasonal pattern of call density from our high-latitude Southern Indian Ocean site in 2014 appears to be in accord with these facets of ABW life-history, whereas detection rates would at best be considered ambiguous or inconclusive for testing this hypothesis.

Our interpretation of our acoustic data is that the peak in call density in autumn corresponds to the start of the (relatively prolonged) breeding period. We suspect the second-highest call densities in winter correspond to a potential behavioural peak in calling. However, this behavioural peak has a lower call density because fewer animals are within the detection range of our Antarctic recording site, potentially because the site is heavily ice-covered during winter, and potentially because a large proportion of calling animals have already migrated to lower latitudes, beyond even the very large detection range afforded by lower winter noise levels. The lowest call densities in spring correspond to time periods when ABWs switch their behaviour from breeding (and calling) to returning to the Antarctic to feed, and this reduced calling behaviour combined with largest values for $\hat{p}_a$, and high-detection range (due to reduced noise level from ice-covered seas, e.g. observed by Shabangu et al. (2020), and from reduction in the blue and fin whale choruses), results in a minimum call density at our Antarctic recording site. The higher call densities in summer would correspond to a time when most of the population have returned to the Antarctic feeding grounds and more are in proximity to our recording site. As the summer progresses into autumn and the breeding season approaches their energetic needs are met, and then some of the animals begin to alter their behaviour from feeding (and not calling much) back towards calling again. Further studies of seasonal calling behaviour, particularly estimates of the acoustic-cue rate (call production rate of an individual), and the proportion of individuals that are making calls, could serve to help test these hypotheses. Furthermore, collection of these data would provide for estimation of ABW (animal) density from our call densities.

4.2 Variability and confidence intervals

The CVs of our seasonal call densities ranged from 0.11 - 0.15. These are reasonable CV values and are lower compared to other methods of estimating abundance of Antarctic blue whales. For example, line-transect abundance estimates of ABWs reported by Branch and Butterworth (2001) from circumpolar sightings surveys ranged from 0.41- 0.52. However, the CVs from Branch and Butterworth were for estimates of global population abundance, whereas our CVs were for local call density where variability over a shorter time period and study area may be inherently reduced. Further, information on the relationship between call density and animal density (e.g., the Z call production rate of ABW, and the proportion of the ABW population that make Z calls) would be required to convert our call densities into animal densities. Previous studies have shown that the CV associated with such behavioural parameters can contribute the largest amount to an animal density CV (e.g., Harris et al., 2018). So, the relatively good CVs from our call density estimate could still increase by a large amount when scaling up the study area and time period to population abundance, and including the additional behavioural parameter(s) (see Fregosi et al., 2022, for another example).

Variability in $\hat{p}_a$ appeared to be the overwhelmingly dominant driver of the overall CV for our call densities (Table 2). The CV of $\hat{p}_a$ was driven by variability in NL, SL and TL, but predominantly by the distributions of SL. For our study, the same SL distribution was used across all seasons with a mean of 189 dB and standard deviation of 8 dB. The high variability in our SL distribution comes from a study that applied the sonar equation and modelled TL in a similar manner: i.e. using the software RAMGeo to model a deep water Antarctic environment similar to that of our site. The variability in SL thus includes both localisation error, and model mismatch including errors in TL. So as not to double count the uncertainty in TL, we assumed that it was already included amongst our highly variable SL. While variability in SL was the main driver of the CV of our call densities, the seasonal differences in our mean call densities were driven by noise.

Our distributions of NL showed substantial variability by season (Figure 5), with NL variation primarily linked to ice cover and chorusing. Autumn had the largest CV (of D_c and $\hat{p}_a$), with the remaining seasons CVs relatively similar (within 0.02).

We chose shape constrained GAMs because our dataset produced GAMs that exhibited unrealistic behaviour at very high and low SNR without constraints. In future studies, it would be worth testing whether annotating a larger amount of data would improve the precision of our SNR-detection function, and subsequent estimates of CV of $\hat{p}_a$ and of call density. This could be achieved in practice by adaptively annotating additional hours of summer recordings to supplement the distribution of summer SNR. Additionally, the spectrogram correlation detector that we used had poor recall for an acceptable level of precision, see (Miller et al., 2021a), so it would be worth exploring in a future study the extent to which using a better (i.e., less variable) detector could lower the CVs. The use of deep learning algorithms in conjunction with closed population capture-recapture models (Miller et al., 2022) has emerged as a novel approach to achieving improved results in call

detection. Also, Schall et al. (2024), presented a deep learning benchmark for the detection of blue and fin whale vocalizations in marine long-term PAM dataset.

4.3 Further exploration and advancement of call density methods

The analysis that we presented here represents an initial first-step toward a standardized measure of bioacoustic detections of ABWs recorded on single instruments that is suitable for comparison across different timespans, in addition to sites. Future work can focus on transforming extant estimates of detection rates into call densities, but we also expect that there will be further modifications and hopefully improvements to the various steps that comprise this method. Such improvements and modifications might include: improved detectors with better recall, lower $\hat{f}$, less variability in SNR-detection curves. A natural extension might also be to investigate call density over shorter time periods than annual & seasonal: e.g. monthly or weekly (though care has to be taken regarding sharing parameters between smaller time periods). Further, a key limitation of our method is that we have to assume a uniform call density across the area, thus it would be preferable to account for heterogeneity in spatial distribution of calls, if *a priori* knowledge is available (e.g., Harris et al., 2018). For example, in winter, large portions of our study area are covered by sea ice. Fully ice-covered areas may be less likely to contain whale calls than open water, so a simulation that included such effects of ice-cover and any other spatial covariates would be an important improvement.

Additionally, there is scope for improvement in estimation of TL, particularly via populating TL models with more accurate and higher-resolution environmental parameters, and accounting for uncertainty in model inputs where necessary. For example: higher-resolution and more accurate bathymetry than etopo1 could be used where available. Similarly, more accurate local SSPs than those derived from decadal & broad-spatial averages could also be used where available. Ideally, this would involve using *in-situ* data from argos floats and scientific surveys that occur in the vicinity of the monitoring sites (spatially and in time). Furthermore, it might also include modifications to vary the SSP spatially along each radial (in the same manner as bathymetry). And lastly, our assumption of homogenous seabed geoacoustics could be improved upon. In the Antarctic, little is known about density and sound-speed of the seabed at any location, but once measures are made at a location, these are likely to remain stable for a long time, so such data do have good potential for longevity/legacy, as well as retrospective re-analysis of call density should they become available. Such analysis would be important when comparing across different sites, but is less important for analyses comparing different time periods at a single site (like our seasonal analysis here) since these properties are not likely to vary much over time.

Compared to the potential improvements in estimating TL, there are fewer avenues for improvements in measuring NL. The main NL-related modification that would be useful to consider in future studies would be excluding times with very high noise from call density estimates. This would be analogous to going 'off-effort,' when conditions are unsuitable for detection, as is commonly done when estimating animal abundance with distance sampling. For example, during at-sea line-transect distance sampling surveys, visual observers stop data collection when the sightability is poor (e.g. sea-state is > Beaufort 5). This saves them time looking for animals in conditions where they would be very unlikely to detect anything, and costs little in the way of a reduction in number of detections. More importantly it also reduces variability of their density estimates. Applying this analogy to acoustics would involve identifying periods when high levels of noise prohibit reliable detection, and then excluding these periods from the estimates of call density.

Finally, there appears to be some scope to modify and improve upon estimation of SNR, detector characterisation, and false discovery rates. Estimation of SNR is an often overlooked and/or over-simplified aspect of passive acoustics, and so further investigation into how best to estimate SNR for call density estimation may be warranted. Questions for such investigation might include the timeframe over which to estimate noise and signal, and whether level measurements should focus on measures of central tendency (e.g. RMS, L50 measurements), or maxima (e.g. peak, L90). For the tonal calls of ABWs in this study the frequency band of interest was narrow and clearly defined, but for frequency-modulated calls, like blue whale D-calls it may not be appropriate to calculate signal and noise levels over a simple rectangular time-frequency box. Thus, there may be further need to better define the call in the time-frequency plane, e.g. by tracing a contour, for such calls. Another potential improvement related to SNR would be to better understand the effects of floating ground-truth on detector characterisation. For example, adjudicated mark-recapture methods, like those proposed by Miller et al. (2022), might be better able to address issues of variability and subjectivity in the human analysts annotations, and reduce potential biases that flow through to the SNR-detection function and $\hat{f}$.

4.4 Implications for long-term monitoring (conclusions)

The methods that we have presented here represent a pathway to extract even more value from the increasingly large body of knowledge generated from worldwide long-term single sensor recordings of low-frequency baleen whales. These methods should be directly applicable not just to ABWs, but any subspecies or population of blue whales, fin whales. These methods potentially the low-frequency omnidirectional calls of minke, sei, and right whales, where other standard density estimation methods such as distance sampling and spatial-capture recapture cannot be applied. Further adaptations to the propagation modelling and source-level estimation could make these methods suitable for broadband calls of baleen whales, like

humpback whales – similar to the methods proposed by Helble et al. (2013), and the Monte Carlo simulation method using odontocete clicks has been applied in several studies (Küsel et al., 2011; Hildebrand et al., 2015; Frasier et al., 2016).

For ABWs, application of this method across a wider geographic and temporal span of sites throughout the Southern Hemisphere would represent a pathway to deliver a cost-effective, statistically-robust, and intuitively-interpretable, long-term, global investigation of bioacoustic trends for this critically endangered subspecies. The method would be cost-effective since there have already been millions of hours of long-term underwater recordings that have been collected worldwide over the past two decades, and this sort of data is continuing to become more affordable to collect and analyse as technology progresses. The results of this method are statistically robust, with variability of each component propagated through to the final estimates of call density. But most importantly, the method produces results, call densities, that can be directly compared independent of the recording equipment, site-specific environmental factors, and detection methods, and that are driven by biological factors: animal density and behaviour.

As large-scale changes occur in the global ocean, these can have potential impacts on the distributions and abundance of pelagic prey and the whales species that feed upon it e.g (Moore, 2008; Moore and Huntington, 2008). Monitoring baleen whale call densities across large areas and timescales, including the use of existing passive acoustic datasets like those collected by the Southern Ocean Research Partnership (Opzeeland et al., 2013; Miller et al., 2021c), the Preparatory Commission for the Comprehensive Nuclear-Test-Ban Treaty Organization, or the Global Ocean Observing System, can be a valuable source of information for understanding the dynamics of changing pelagic ecosystems and is a step forward for global ocean observation.

Data availability statement

The raw data supporting the conclusions of this article will be made available by the authors, without undue reservation.

Ethics statement

Ethical approval was not required for the study involving animals in accordance with the local legislation and institutional requirements because the study was purely observational.

Author contributions

FC: Data curation, Formal analysis, Writing – original draft, Writing – review & editing. DH: Conceptualization, Funding acquisition, Methodology, Supervision, Writing – original draft, Writing – review & editing. SB: Conceptualization, Funding acquisition, Methodology, Supervision, Writing – original draft, Writing – review & editing, Project administration. NB: Writing – review & editing, Data curation. BM: Data curation, Writing – review & editing, Conceptualization, Formal analysis, Funding acquisition, Methodology, Supervision, Writing – original draft.

Funding

The author(s) declare financial support was received for the research, authorship, and/or publication of this article. This research was funded by International Whaling Commission-Southern Ocean Research Partnership (IWC-SORP) to SB (IWC SORP Research Fund Project 17). This research was also made possible by Australian Antarctic Division (AAD) AAS projects 4102 & 4600.

Acknowledgments

We thank the other members of the Acoustic Trends Working Group (Dr. Ana Širović, Dr. Fannie Shabangu, Dr. Flore Samaran, Dr. Ilse Van Opzeeland, Dr. Kathleen Stafford, and Dr. Ken Findlay) which is part of the Southern Ocean Research Partnership (SORP), for sharing their thoughts and supporting each step of this research development. BM thanks Drs Nat Kelly and Simon Wotherspoon from the AAD for their patience, guidance, and many conversations on distance sampling and density estimation. SB thanks the Center for Oceanographic Research COPAS COASTAL at the University of Concepción, Chile, funded by the Chilean Agencia Nacional de Investigación y Desarrollo (ANID) grant FB210021.

Conflict of interest

The authors declare that the research was conducted in the absence of any commercial or financial relationships that could be construed as a potential conflict of interest.

Publisher's note

All claims expressed in this article are solely those of the authors and do not necessarily represent those of their affiliated organizations, or those of the publisher, the editors and the reviewers. Any product that may be evaluated in this article, or claim that may be made by its manufacturer, is not guaranteed or endorsed by the publisher.

References

Amante, C., and Eakins, B. W. (2009). *ETOPO1 1 Arc-Minute Global Relief Model: Procedures, Data Sources and Analysis. NOAA Technical Memorandum NESDIS NGDC-24* (National Geophysical Data Center, NOAA). doi: 10.7289/V5C8276M

Balcazar, N. E., Tripovich, J. S., Klinck, H., Nieukirk, S. L., Mellinger, D. K., Dziak, R. P., et al. (2015). Calls reveal population structure of blue whales across the southeast Indian Ocean and southwest Pacific Ocean. *J. Mammalogy* 96 (6), 1184-1193. doi: 10.1093/jmammal/gyv126

Borchers, D. L., Buckland, S. T., and Zucchini, W. (2002). *Estimating Animal Abundance* (London: Springer London). doi: 10.1007/978-1-4471-3708-5

Bouffaut, L., Landrø, M., and Potter, J. R. (2021). Source level and vocalizing depth estimation of two blue whale subspecies in the western Indian Ocean from single sensor observations. *J. Acoustical Soc. America* 149, 4422–4436. doi: 10.1121/10.0005281

Boyer, T. P., Garcia, H. E., Locarnini, R. A., Zweng, M. M., Mishonov, A. V., Reagan, J. R., et al. (2018). *World Ocean Atlas 2018* (NOAA National Centers for Environmental Information). Available online at: https://accession.nodc.noaa.gov/NCEI-WOA18 (Accessed August 3, 2021).

Branch, T. A. (2007). Abundance of Antarctic blue whales south of 60 S from three complete circumpolar sets of surveys. *J. Cetacean Res. Manage.* 9, 253–262. Available at: http://www.iwcoffice.co.uk/_documents/sci_com/sc59docs/sc-59-SH9.pdf.

Branch, T. A., and Butterworth, D. S. (2001). Estimates of abundance south of 60° S for cetacean species sighted frequently on the 1978/79 to 1997/98 IWC/IDCR-SOWER sighting surveys. *J. Cetacean Res. Manage.* 3, 251–270. doi: 10.47536/jcrm.v3i3

Brown, S. (1954). "Dispersal in blue and fin whales," in *Discovery Reports*, vol. 26. , 357–384. Available at: http://scholar.google.com/scholar?hl=en&btnG=Search&q=intitle:Dispersal+in+blue+and+fin+whales#0.

Cochran, W. G. (1977). *Sampling techniques* (New York, USA: John Wiley & Sons).

Collins, M. D. (2002). *User's Guide for RAM Version 1.0 and 1.0p*. Available online at: http://oalib.hlsresearch.com/AcousticsToolbox/. (accessed [August 7, 2024])

Cooke, J. G. (2018). *Balaenoptera musculus ssp. intermedia* (The IUCN Red List of Threatened Species), e.T41713A50226962. doi: 10.2305/IUCN.UK.2018-2.RLTS.T41713A50226962.en

Dréo, R., Bouffaut, L., Leroy, E., Barruol, G., and Samaran, F. (2019). Baleen whale distribution and seasonal occurrence revealed by an ocean bottom seismometer network in the Western Indian Ocean. *Deep-Sea Res. Part II: Topical Stud. Oceanography* 161, 132–144. doi: 10.1016/j.dsr2.2018.04.005

Duncan, A. (2005). *Acoustics Toolbox User interface and Post processor (AcTUP)*. Available online at: http://cmst.curtin.edu.au/products/underwater/. (accessed [August 7, 2024])

Dutkiewicz, A., Müller, R. D., O'Callaghan, S., and Jónasson, H. (2015). Census of seafloor sediments in the world's ocean. *Geology* 43, 795–798. doi: 10.1130/G36883.1

Frasier, K. E., Wiggins, S. M., Harris, D., Marques, T. A., Thomas, L., and Hildebrand, J. A. (2016). Delphinid echolocation click detection probability on near-seafloor sensors. *J. Acoust. Soc Am.* 140, 1918–1930. doi: 10.1121/1.4962279

Fregosi, S., Harris, D. V., Matsumoto, H., Mellinger, D. K., Martin, S. W., Matsuyama, B., et al. (2022). Detection probability and density estimation of fin whales by a Seaglider. *J. Acoustical Soc. America* 152, 2277–2291. doi: 10.1121/10.0014793

Gavrilov, A. N., McCauley, R. D., and Gedamke, J. (2012). Steady inter and intra-annual decrease in the vocalization frequency of Antarctic blue whales. *J. Acoustical Soc. America* 131, 4476–4480. doi: 10.1121/1.4707425

Harris, D., Matias, L., Thomas, L., Harwood, J., and Geissler, W. H. (2013). Applying distance sampling to fin whale calls recorded by single seismic instruments in the northeast Atlantic. *J. Acoustical Soc. America* 134, 3522–3535. doi: 10.1121/1.4821207

Harris, D. V., Clarke, T., Heaney, K., Mellinger, D. K., Miles, D., and Thomas, L. (2024, submitted). Estimating the detection probability of long-ranging baleen whale song using a single sensor: towards density estimation. *J. Acoustical Soc. Am.*

Harris, D. V., Miksis-Olds, J. L., Vernon, J. A., and Thomas, L. (2018). Fin whale density and distribution estimation using acoustic bearings derived from sparse arrays. *J. Acoustical Soc. America* 143 (5), 2980-2993. doi: 10.1121/1.5031111

Helble, T. A. (2013). Site specific passive acoustic detection and densities of humpback whale calls off the coast of California. Thesis. UC San Diego, CA, USA.

Helble, T. A., D'Spain, G. L., Campbell, G. S., and Hildebrand, J. A. (2013). Calibrating passive acoustic monitoring: Correcting humpback whale call detections for site-specific and time-dependent environmental characteristics. *J. Acoustical Soc. America* 134, EL400–EL406. doi: 10.1121/1.4822319

Hildebrand, J. A., Baumann-Pickering, S., Frasier, K. E., Trickey, J. S., Merkens, K. P., Wiggins, S. M., et al. (2015). Passive acoustic monitoring of beaked whale densities in the Gulf of Mexico. *Sci. Rep.* 5, 16343. doi: 10.1038/srep16343

Jensen, F. B., Kuperman, W. A., Porter, M. B., and Schmidt, H. (2011). *Computational Ocean Acoustics* (New York, NY: Springer New York). doi: 10.1007/978-1-4419-8678-8

Küsel, E. T., Mellinger, D. K., Thomas, L., Marques, T. A., Moretti, D., and Ward, J. (2011). Cetacean population density estimation from single fixed sensors using passive acoustics. *J. Acoustical Soc. America* 129, 3610–3622. doi: 10.1121/1.3583504

Leroy, E. C., Samaran, F., Bonnel, J., and Royer, J. (2016). Seasonal and diel vocalization patterns of Antarctic blue whale (Balaenoptera musculus intermedia) in the Southern Indian Ocean: A multi-year and multi-site study. *PloS One* 11, e0163587. doi: 10.1371/journal.pone.0163587

Letsheleha, I. S., Shabangu, F. W., Farrell, D., Andrew, R. K., la Grange, P. L., and Findlay, K. P. (2022). Year-round acoustic monitoring of Antarctic blue and fin whales in relation to environmental conditions off the west coast of South Africa. *Mar. Biol.* 169, 41. doi: 10.1007/s00227-022-04026-x

Lewis, L. A., Calambokidis, J., Stimpert, A. K., Fahlbusch, J., Friedlaender, A. S., McKenna, M. F., et al. (2018). Context-dependent variability in blue whale acoustic behaviour. *R. Soc. Open Sci.* 5 (8), 180241. doi: 10.1098/rsos.180241

Ljungblad, D. K., Clark, C. W., and Shimada, H. (1998). A comparison of sounds attributed to pygmy blue whales (Balaenoptera musculus brevicauda) recorded south of the Madagascar Plateau and those attributed to 'true' blue whales (Balaenoptera musculus) recorded of Antarctica. *Rep. Int. Whaling Commission* 48, 439–442.

Lurton, X. (2010). *An Introduction to Underwater Acoustics: Principles and Applications* (London ; New York: Springer Science & Business Media).

Mackintosh, N. A. (1966). "The distribution of southern blue and fin whales," in *Whales, dolphins and porpoises*. Ed. K. S. Norris (University of California Press, Berkeley and Los Angeles), 125–145.

Marques, T. A., Thomas, L., Martin, S. W., Mellinger, D. K., Ward, J. A., Moretti, D. J., et al. (2013). Estimating animal population density using passive acoustics. *Biol. Rev.* 88, 287–309. doi: 10.1111/brv.12001

McCauley, R. D., Jenner, C., Bannister, J. L., Burton, C. L. K., Cato, D. H., and Duncan, A. (2001). Blue whale calling in the Rottnest Trench – 2000, western Australia. Report R2001-6, Centre for Marine Science and Technology, Curtin University of Technology, Perth, Western Australia.

McDonald, M. A., and Fox, C. G.. (1999). Passive acoustic methods applied to fin whale population density estimation. *J. Acoustical Soc. Am* 105, 2643–2651.

Mellinger, D. K., Stafford, K. M., Moore, S. E., Dziak, R. P., and Matsumoto, H. (2007). An overview of fixed passive acoustic observation methods for cetaceans. *Oceanography* 20, 36–45. doi: 10.1109/PASSIVE.2008.4786981

Menze, S., Zitterbart, D. P., van Opzeeland, I., and Boebel, O. (2017). The influence of sea ice, wind speed and marine mammals on Southern Ocean ambient sound. *R. Soc. Open Sci.* 4, 160370. doi: 10.1098/rsos.160370

Miksis-Olds, J. L., Harris, D. V., and Mouw, C. (2019). Interpreting fin whale (balaenoptera physalus) call behavior in the context of environmental conditions. *Aquat. Mammals* 45, 691–705. doi: 10.1578/AM.45.6.2019.691

Miller, B. S., Balcazar, N., Nieukirk, S., Leroy, E. C., Aulich, M., Shabangu, F. W., et al. (2021a). An open access dataset for developing automated detectors of Antarctic baleen whale sounds and performance evaluation of two commonly used detectors. *Sci. Rep.* 11, 806. doi: 10.1038/s41598-020-78995-8

Miller, B. S., Barlow, J., Calderan, S., Collins, K., Leaper, R., Olson, P., et al. (2015). Validating the reliability of passive acoustic localisation: a novel method for encountering rare and remote Antarctic blue whales. *Endangered Species Res.* 26, 257–269. doi: 10.3354/esr00642

Miller, B. S., Calderan, S., Leaper, R., Miller, E. J., Širović, A., Stafford, K. M., et al. (2021b). Source level of antarctic blue and fin whale sounds recorded on sonobuoys deployed in the deep-ocean off Antarctica. *Front. Mar. Sci.* 8. doi: 10.3389/fmars.2021.792651

Miller, B. S., Calderan, S., Miller, E. J., Širović, A., Stafford, K. M., Bell, E., et al. (2019). "A passive acoustic survey for marine mammals conducted during the 2019 Antarctic voyage on Euphausiids and Nutrient Recycling in Cetacean Hotspots (ENRICH)," in *Proceedings of ACOUSTICS 2019*, Cape Schanck, Victoria, Australia: Australian Acoustical Society. 1–10.

Miller, B. S., Madhusudhana, S., Aulich, M. G., and Kelly, N. (2022). Deep learning algorithm outperforms experienced human observer at detection of blue whale D-calls: a double-observer analysis. *Remote Sens Ecol. Conserv.* 9 (1), 104-116. doi: 10.1002/rse2.297

Miller, B. S., Miller, E., Calderan, S., Leaper, R., Stafford, K., Širović, A., et al. (2017). "Circumpolar acoustic mapping of endangered Southern Ocean whales: Voyage report and preliminary results for the 2016/17 Antarctic Circumnavigation Expedition," in *Paper SC/67a/SH03 submitted to the Scientific Committee 67a of the International Whaling Commision*, Bled Slovenia, Vol. 18.

Miller, B. S., Milnes, M., and Whiteside, S. (2021c). Long-term underwater acoustic recordings 2013-2019. *Ver.* 4. doi: 10.26179/h7xa-y729

Miller, B. S., Milnes, M., Whiteside, S., Double, M. C., and Gedamke, J. (2016). "Calibrated underwater sound levels at two Antarctic recording sites : the seasonality of sounds from wind, ice, and marine mammals," in *Paper submitted to the Scientific Committee of the International Whaling Commission. SC66B. Bled, Slovenia. SC/66B/SH19*. 1–13.

Miller, B. S., Stafford, K. M., Van Opzeeland, I., Harris, D., Samaran, F., Širović, A., et al. (2020). An annotated library of underwater acoustic recordings for testing and training automated algorithms for detecting Antarctic blue and fin whale sounds. doi: 10.26179/5e6056035c01b. (Accessed [August 7, 2024])

Moore, S. E. (2008). Marine mammals as ecosystem sentinels. *J. Mammalogy* 89, 534–540. doi: 10.1644/07-MAMM-S-312R1.1

Moore, S. E., and Huntington, H. P. (2008). Arctic marine mammals and climate change: impacts and resilience. *Ecol. Appl.* 18, S157–S165. doi: 10.1890/06-0571.1

Nghiem-Phu, L., and Tappert, F. (1985). Modeling of reciprocity in the time domain using the parabolic equation method. *J. Acoustical Soc. America* 78, 164–171. doi: 10.1121/1.392553

Oedekoven, C. S., Marques, T. A., Harris, D., Thomas, L., Thode, A. M., Blackwell, S. B., et al (2021). A comparison of three methods for estimating call densities of migrating bowhead whales using passive acoustic monitoring. *Environ. Ecol. Statistics*. doi: 10.1007/s10651-021-00506-3

Oleson, E. M., Calambokidis, J., Burgess, W. C., McDonald, M. A., LeDuc, C. A., and Hildebrand, J. A. (2007). Behavioral context of call production by eastern North Pacific blue whales. *Mar. Ecol. Prog. Ser.* 330, 269–284. Available at: http://escholarship.org/uc/item/5xk9k7bp.pdf.

Opzeeland, I. V., Samaran, F., Stafford, K., Findlay, K., Gedamke, J., Harris, D., et al. (2013). Towards collective circum-Antarctic passive acoustic monitoring: The Southern Ocean Hydrophone Network (SOHN). *Polarforschung* 83, 47–61.

Payne, R., and Webb, D. (1971). Orientation by means of long range acoustic signaling in baleen whales. *Ann. New York Acad. Sci.* 188, 110–141. doi: 10.1111/j.1749-6632.1971.tb13093.x

Porter, M. B. (2020). *Acoustics Toolbox. Acoustics Toolbox*. Available online at: http://oalib.hlsresearch.com/AcousticsToolbox/ (Accessed August 2, 2021).

Pya, N. (2022). *scam: Shape Constrained Additive Models*. Available online at: https://CRAN.R-project.org/package=scam. (accessed [August 7, 2024])

Rankin, S., Ljungblad, D. K., Clark, C. W., and Kato, H. (2005). Vocalisations of Antarctic blue whales, Balaenoptera musculus intermedia, recorded during the 2001/2002 and 2002/2003 IWC/SOWER circumpolar cruises, Area V, Antarctica. *J. Cetacean Res. And Manage.* 7, 13–20. doi: 10.47536/jcrm.v7i1

R Core Team (2019). *R: A language and environment for statistical computing*. Available online at: https://www.r-project.org/. (accessed [August 7, 2024])

Rocha, J. R.C., Clapham, P. J., and Ivashchenko, Y. (2015). Emptying the oceans: A summary of industrial whaling catches in the 20th century. *Mar. Fisheries Rev.* 76, 37–48. doi: 10.7755/MFR

Samaran, F., Adam, O., and Guinet, C. (2010a). Detection range modeling of blue whale calls in Southwestern Indian Ocean. *Appl. Acoustics* 71, 1099–1106. doi: 10.1016/j.apacoust.2010.05.014

Samaran, F., Guinet, C., Adam, O., Motsch, J.-F., and Cansi, Y. (2010b). Source level estimation of two blue whale subspecies in southwestern Indian Ocean. *J. Acoustical Soc. America* 127, 3800–3808. doi: 10.1121/1.3409479

Samaran, F., Stafford, K. M., Branch, T. A., Gedamke, J., Royer, J.-Y., Dziak, R. P., et al. (2013). Seasonal and geographic variation of Southern blue whale subspecies in the Indian Ocean. *PloS One* 8, e71561. doi: 10.1371/journal.pone.0071561

Schall, E., Kaya, I. I., Debusschere, E., Devos, P., and Parcerisas, C. (2024). Deep learning in marine bioacoustics: a benchmark for baleen whale detection. *Remote Sensing in Ecology and Conservation*doi: 10.1002/rse2.392

Seber, G. (1982). The estimation of animal abundance and related parameters. Macmillan, New York, USA.

Shabangu, F., Andrew, R., Yemane, D., and Findlay, K. (2020). Acoustic seasonality, behaviour and detection ranges of Antarctic blue and fin whales under different sea ice conditions off Antarctica. *Endangered Species Res.* 43, 21–37. doi: 10.3354/esr01050

Shabangu, F. W., Findlay, K. P., Yemane, D., Stafford, K. M., van den Berg, M., Blows, B., et al. (2019). Seasonal occurrence and diel calling behaviour of Antarctic blue whales and fin whales in relation to environmental conditions off the west coast of South Africa. *J. Mar. Syst.* 190, 25–39. doi: 10.1016/j.jmarsys.2018.11.002

Shabangu, F. W., Yemane, D., Stafford, K. M., Ensor, P., and Findlay, K. P. (2017). Modelling the effects of environmental conditions on the acoustic occurrence and behaviour of Antarctic blue whales. *PloS One* 12, e0172705. doi: 10.1371/journal.pone.0172705

Širović, A., and Hildebrand, J. A. (2011). Using passive acoustics to model blue whale habitat off the Western Antarctic Peninsula. *Deep Sea Res. Part II: Topical Stud. Oceanography* 58, 1719–1728. doi: 10.1016/j.dsr2.2010.08.019

Širović, A., Hildebrand, J. A., and Wiggins, S. M. (2007). Blue and fin whale call source levels and propagation range in the Southern Ocean. *J. Acoustical Soc. America* 122, 1208–1215. doi: 10.1121/1.2749452

Širović, A., Hildebrand, J. A., Wiggins, S. M., McDonald, M. A., Moore, S. E., and Thiele, D. (2004). Seasonality of blue and fin whale calls and the influence of sea ice in the Western Antarctic Peninsula. *Deep Sea Res. Part II: Topical Stud. Oceanography* 51, 2327–2344. doi: 10.1016/j.dsr2.2004.08.005

Širović, A., Hildebrand, J. A., Wiggins, S. M., and Thiele, D. (2009). Blue and fin whale acoustic presence around Antarctica during 2003 and 2004. *Mar. Mammal Sci.* 25, 125–136. doi: 10.1111/j.1748-7692.2008.00239.x

Thomas, L., and Marques, T. (2012). Passive acoustic monitoring for estimating animal density. *Acoustics Today* 8, 35–44. Available at: http://link.aip.org/link/?ATCODK/8/35/1.

Thomisch, K. (2017). *Distribution patterns and migratory behavior of Antarctic blue whales* (Bremerhaven, Germany: Alfred-Wegener-Institut Helmholtz-Zentrum für Polar- und Meeresforschung Am). doi: 10.2312/BzPM_0707_2017

Tripovich, J. S., Klinck, H., Nieukirk, S. L., Adams, T., Mellinger, D. K., Balcazar, N. E., et al. (2015). Temporal segregation of the Australian and Antarctic blue whale call types (Balaenoptera musculus spp.). *J. Mammalogy* 96 (3), 603-610. doi: 10.1093/jmammal/gyv065

Van Parijs, S., Clark, C. W., Sousa-Lima, R. S., Parks, S. E., Rankin, S., Risch, D., et al. (2009). Management and research applications of real-time and archival passive acoustic sensors over varying temporal and spatial scales. *Mar. Ecol. Prog. Ser.* 395, 21–36. doi: 10.3354/meps08123

Warren, V. E., Širović, A., McPherson, C., Goetz, K. T., Radford, C. A., and Constantine, R. (2021). Passive acoustic monitoring reveals spatio-temporal distributions of Antarctic and pygmy blue whales around central New Zealand. *Front. Mar. Sci.* 7. doi: 10.3389/fmars.2020.575257

Wilcock, W. S. D. (2012). Tracking fin whales in the northeast Pacific Ocean with a seafloor seismic network. *J. Acoustical Soc. America* 132, 2408–2419. doi: 10.1121/1.4747017

Yun, S., Lee, W. S., Dziak, R. P., Roche, L., Matsumoto, H., Lau, T.-K., et al. (2021). Quantifying soundscapes in the Ross sea, Antarctica using long-term autonomous hydroacoustic monitoring systems. *Front. Mar. Sci.* 8. doi: 10.3389/fmars.2021.703411

frontiers | Frontiers in Marine Science

TYPE Original Research
PUBLISHED 30 September 2024
DOI 10.3389/fmars.2024.1473471

Check for updates

OPEN ACCESS

EDITED BY
Kunio T. Takahashi,
National Institute of Polar Research, Japan

REVIEWED BY
Taiki Katsumata,
The Insitute of Cetacean Research, Japan
Yu Kanaji,
Japan Fisheries Research and Education Agency (FRA), Japan

*CORRESPONDENCE
Virginia Andrews-Goff
Virginia.Andrews-Goff@aad.gov.au

RECEIVED 31 July 2024
ACCEPTED 04 September 2024
PUBLISHED 30 September 2024

CITATION
Andrews-Goff V, Smith JN, Irvine LG and Double MC (2024) Ship-based RPA operations for cetacean research in Antarctica: progress, opportunities and challenges.
Front. Mar. Sci. 11:1473471.
doi: 10.3389/fmars.2024.1473471

COPYRIGHT
© 2024 Andrews-Goff, Smith, Irvine and Double. This is an open-access article distributed under the terms of the Creative Commons Attribution License (CC BY). The use, distribution or reproduction in other forums is permitted, provided the original author(s) and the copyright owner(s) are credited and that the original publication in this journal is cited, in accordance with accepted academic practice. No use, distribution or reproduction is permitted which does not comply with these terms.

Ship-based RPA operations for cetacean research in Antarctica: progress, opportunities and challenges

Virginia Andrews-Goff[1]*, Joshua N. Smith[1], Lyn G. Irvine[2,3] and Michael C. Double[1]

[1]Department of Climate Change, Energy, The Environment and Water, Australian Antarctic Division, Kingston, TAS, Australia, [2]Institute for Marine and Antarctic Studies, University of Tasmania, Kingston, TAS, Australia, [3]Irvine Marine Fauna Research, Perth, WA, Australia

Data collection facilitated by remotely piloted aircraft (RPA) has proven to be revolutionary in many disciplines including for research in extreme environments. Here we assess current use and utility of small multirotor remotely piloted aircraft (RPAs) for the challenging role of facilitating ship-based cetacean research in Antarctica. While such aircraft are now used routinely in sheltered environments in and off Antarctica, a comprehensive literature review found that RPA-mediated cetacean research conducted from ships at sea and outside of the Antarctic Peninsula region was relatively uncommon. In order to determine the potential utility of ship-based multirotor RPA operations for cetacean research, we repeatedly deployed small RPAs during a multidisciplinary research voyage in maritime East Antarctica to collect scientific data contributing to an understanding of krill and krill predator interactions. RPA flight metrics (duration, height, length, speed, distance from ship, battery drainage, satellites acquired) were compared to ship underway environmental sampling data. At a mean duration of 12 minutes, these 139 RPA flights were relatively short yet adequate to achieve the science intended, namely a range of cetacean related data streams including photogrammetry, photo identification, behavioural observations and whale blow sampling in addition to water sampling and collection of general scenic imagery. RPA flight operations were constrained by wind speed but not by air temperature with flights undertaken throughout the full range of air temperatures experienced (down to −9.5°C) but not throughout the full range of wind speeds experienced. For a 12-minute flight duration, battery drainage was around 60% indicating that the RPAs were rarely pushed to their operational limit. There was little evidence that the cold impacted RPA lithium battery performance with estimated maximum flight time within approximately 10% of expected flight time for the RPA platforms most used. Whist small multirotor RPAs are rarely applied to cetacean related research in maritime East Antarctica, we demonstrate their value and potential to deliver data critical to address knowledge gaps that challenge the effective management of both krill and their predators.

KEYWORDS

drone, whale, Antarctic blue whale, Southern Ocean, multirotor

1 Introduction

Remotely piloted aircraft (RPA) have proven revolutionary in a range of disciplines, especially where access to remote, extreme, hazardous and/or inaccessible environments is required (for example Di Stefano et al., 2018; Shahmoradi et al., 2020; Vargas Tamayo et al., 2020; Häusermann et al., 2023). Whilst RPAs have become integral to logistics (Xi et al., 2018), surveillance (Alvear et al., 2017), search and rescue (Lyu et al., 2023), media (Harvard et al., 2020) and other non-science applications (Mahadevan, 2010), their uptake within science disciplines has been particularly rapid due to the benefits and opportunities associated with the myriad of payload options (for example (Harris et al., 2019; Burgués and Marco, 2020; Butcher et al., 2021; Shelare et al., 2021). RPAs applied within a conservation and management context (Bersaglio et al., 2023) are proving to be an improved, faster and less invasive option than traditional methods (Howell et al., 2022; Alejandro et al., 2023; Hodgson et al., 2023) and particularly powerful for threatened species research (Gallego and Sarasola, 2021; Varela-Jaramillo et al., 2023; Zhang et al., 2023) or for marine species that are difficult to access (Barreto et al., 2021; Butcher et al., 2021; Hodgson et al., 2023).

Aerial observations to understand cetacean presence and behaviour has been a common scientific method employed since the whaling era (Carroll et al., 2014; Nowacek et al., 2016). Sighting surveys from planes and helicopters have been used globally to monitor cetacean species recovery (Stewart et al., 1987; Clark et al., 2010; Bannister, 2001; Herr et al., 2022b) with the logical potential for RPAs to generate a complementary data stream identified since at least 2008 (Schoonmaker et al., 2008). Subsequently, long range, fixed-wing RPAs have been used for line and strip transect surveys to derive cetacean abundance estimates (Hodgson et al., 2017) including in extreme environments (Aniceto et al., 2018) and also for research on Antarctic wildlife (Zmarz et al., 2018; Pfeifer et al., 2019; Pina and Vieira, 2022) and the physical Antarctic environment (Bello et al., 2022; Pina and Vieira, 2022). In addition to using RPAs to undertake aerial surveys (Angliss et al., 2018), RPAs and multirotor RPAs in particular, have been employed as a cetacean research tool to undertake photogrammetry (Durban et al., 2015; Christiansen et al., 2018), collect photo identification images (Koski et al., 2015; Ryan et al., 2022; Young et al., 2022), investigate energetics and kinematics (Christiansen et al., 2016; Werth et al., 2019), sample whale blow (Apprill et al., 2017; Pirotta et al., 2017), assess anthropogenic interactions (Ramp et al., 2021; Pirotta et al., 2022), sample faecal matter (Baird et al., 2022) and undertake behavioural observation (Torres et al., 2018; Fiori et al., 2020).

Whilst the majority of RPA-associated cetacean research occurs in relatively accessible regions, RPAs have also been used successfully in remote, polar regions (Johnston et al., 2022; Pallin et al., 2022), providing an alternative method to more efficiently facilitate the collection of data in locations that have historically added a degree of challenge (Hyun et al., 2020) to the study of a taxa that are already notoriously difficult to study (Nowacek et al., 2016). In Antarctica, the use of RPAs for cetacean research has increased in recent years (Durban et al., 2021; Bierlich et al., 2022; Pallin et al., 2022), primarily in the relatively sheltered regions of the Antarctic Peninsula where multirotor RPAs have been launched and recovered from small boats (around 6 m) to collect cetacean related data in nearshore waters. Larger (> 20 m), vessel based multirotor RPAs operations are less common but have successfully collected cetacean imagery and blow samples (Kennedy et al., 2020; Herr et al., 2022a, b). To the best of our knowledge, the use of fixed-wing RPAs for long range visual survey for cetaceans is yet to be described within the scientific literature for Antarctica but is likely imminent (Katsumata and Yoshida, 2023).

Both multirotor and fixed-wing RPAs provide an excellent opportunity to facilitate a contemporary understanding of cetacean abundance, distribution and habitat use in Antarctic waters particularly if flights can be conducted from large vessels and conducted simultaneously with other activities. Such data can be used for many purposes including: assessing the recovery of whale populations from past whaling activities; assessing the impacts of a rapidly changing environment; and informing the management of the Antarctic krill fishery. Antarctic baleen whales forage primarily on Antarctic krill, consuming large quantities of prey (Savoca et al., 2021). While most krill fishing effort is currently centred around the Antarctic Peninsula region, krill fishing recommenced off East Antarctica in 2016 (Kawaguchi and Nicol, 2020). The krill fishery in Antarctica is managed by the Commission for the Conservation of Antarctic Marine Living Resources (CCAMLR). This international body implements a precautionary, ecosystem-based fisheries management approach, which aims to prevent adverse, irreversible long-term impacts from fishing activities on target species and the ecosystem. Ecosystem-based management requires an understanding of both krill and krill predators. Krill cannot be sustainably managed without considering the needs of krill predators through knowledge of their abundance, distribution, phenology, prey requirements and foraging behaviour. Vessel based RPAs provide an excellent opportunity to generate data that addresses knowledge gaps in East Antarctica and elsewhere.

Between January and March 2019, a multi-disciplinary marine science voyage (the *ENRICH* Voyage – ***E**uphausiids and **N**utrient **R**ecycling **I**n **C**etacean **H**otspots*) was conducted off East Antarctica, from 64°S to 67°S and between 138°E and 154°W. During the voyage, the utility of small multirotor RPAs was assessed operationally and scientifically. Multirotor RPA flights were conducted for cetacean photogrammetry, photo-identification and blow sampling in order to contribute to the overarching aim of the voyage – to describe the characteristics of Antarctic krill swarms and determine whether these characteristics predict the distribution and behaviour of Antarctic predators, particularly Antarctic blue whales, and how these predators interact with krill in time and space. Here, we conduct a high-level review of cetacean research related RPA activities in Antarctica and specifically, we describe the multirotor RPA activities during the *ENRICH* voyage. We characterise the operating envelope of successful multirotor RPA use in maritime East Antarctica, highlighting the limitations, challenges and opportunities that RPA technology presents for future cetacean research.

2 Materials and methods

2.1 Literature review

To determine how and where RPAs are currently used for research in Antarctica, we used Web of Science to search for scientific publications, applying the search to all possible fields using the combination of the keywords: 'Antarctica' OR 'Antarctic' AND 'RPAS' OR 'UAV' OR 'UAS' OR 'unmanned aerial vehicle' OR 'unoccupied aerial vehicle' OR 'unmanned aerial system' OR 'unoccupied aerial system' OR 'remotely piloted aircraft' OR 'remotely piloted system' OR 'drone.' We then applied the same search within Google Scholar to cross-check and detect additional references. We manually verified the adequacy of the references and removed false positives. The list of publications was current to 2023. Building on Pina and Vieira (2022), publications were classified according to the dominant thematic area presented in the publication: i) technology and development (including methods), ii) atmosphere, iii) cryosphere, iv) hydrosphere, v) terrestrial, vi) wildlife and vii) other (includes review and regulatory related papers). Within the 'wildlife' category we then specifically identified papers that described RPA use for cetacean research.

2.2 Multirotor RPA activities in East Antarctica

The 49-day *ENRICH* voyage departed from Hobart, Tasmania on the 19 January and returned to the same port on the 5 March 2019 aboard the Marine National Facility's 93.9 m research vessel, *RV Investigator*[1]. The overarching aim of the research voyage was to describe the characteristics of Antarctic krill swarms and determine whether these characteristics predict the distribution and behaviour of Antarctic predators, particularly Antarctic blue whales, and how these predators interact with krill in time and space. Multi-disciplinary marine science was conducted off Antarctica from 64°S to 67°S and between 138°E and 154°W and included the use of a scientific multibeam echosounder (Simrad ME70) and a downward-facing split-beam echosounder (Simrad EK60) to measure the 3D geometry of krill swarms, target trawls to determine krill size and maturity stage composition, Integrated Growth Rate experiments to determine krill morphometric data and growth rates, sonobuoy deployments to undertake cetacean passive acoustic monitoring and real-time tracking, visual sightings for cetaceans and biogeochemistry deployments including CTDs (Conductivity Temperature Depth), Trace Metal Rosettes (TMRs), eXpendable BathyThermographs (XBTs) and drifters.

The ENRICH voyage also planned to use multiple small multirotor RPAs to undertake photogrammetry, photo-identification, whale 'blow' sampling, surface water sampling or to collect general whale and scenic imagery. Given the likely high number of RPA flights planned, the voyage also provided an opportunity to assess the feasibility and limitations of routinely using such aircraft for ship-based cetacean research in Antarctica.

Three multirotor RPAs: i) the DJI Inspire 2, ii) the DJI Phantom 4 Pro and iii) the DJI Phantom 4, were flown by a science team (two pilots flying the DJI Phantom 4 Pro and the DJI Phantom 4 to collect whale imagery and sample whale blow and water) and a documentary team (two pilots flying the DJI Inspire 2 to collect whale and scenic imagery) authorised under the Australian Antarctic Program Animal Ethics Committee and with Australian Government EPBC cetacean permit CP17-0004. All voyage activities were authorised under the Australian Government Antarctic Treaty (Environment Protection) Act. RPA pilots were licensed, holding an Australian Remote Pilots Licence (RePL), and operated under a Remotely Piloted Aircraft Operators Certificate (ReOC). The combined RPA flying experience of the documentary team included hundreds of hours flying in remote locations including Antarctica, flying to collect imagery of whales and operating from vessels at sea. The science team had also flown RPAs around whales and off of small boats with a combined RPA flying experience of < 100 hours at the time. RPA operation planning was informed by the Australian Antarctic Division's *Environmental Guidelines for operation of Remotely Piloted Aircraft Systems (RPAS) in Antarctica (v 1.1)* as well as relevant permit conditions. At the time, the Australian Government Civil Aviation Safety Authority (CASA) advised that it had no jurisdiction over these Southern Ocean operations because they occurred outside the 12 nautical mile territorial limit.

RPAs were flown in "ATTI" mode (Attitude Mode – a DJI-specific mode that allows drone flight without the use of Global Navigation Satellite Systems (GNSS) or Vision Position Systems) to remove conflict between the onboard magnetic compass, GNSS information, and autopilot logic caused by proximity to the south magnetic pole. RPAs were launched from the *RV Investigator* on days where whales were sighted within a suitable distance (~ < 1500m) of the vessel, mean wind speeds were less than 15 knots (27.8 kmh^{-1}) and with permission from the Bridge Officer and the Chief Scientist. RPAs were hand launched from the foredeck of deck 2 (the bow; from a location approximately 10.1 m above the water line at the time), which was roped off from other crew and scientists and cleared of ice daily. The RPA was held by the co-pilot, equipped with appropriate PPE (clear face-shield, safety glasses and gloves), with arms raised, 2 m above the deck level therefore launching from a height of approximately 12 m above sea level (registered as 0 m by the RPA). RPA launch sequences were announced over the ship intercom to ensure no unauthorised personnel entered the foredeck area. When the RPA achieved flight, it was released to hover and then flown in the direction of the whales(s) whilst the pilot (focused on the screen and keeping the whale(s) in the frame) maintained communications with the co-pilot (focused on the whale(s) and the position of the RPA) and vessel crew/Bridge on the whales(s) location and activities. When the RPA was in position above the whale(s), it collected vertical aerial pictures/video using a camera mounted vertically under the RPA. A live video link, providing the pilot with a live feed from the camera was used to correct the position of the RPA and confirm that photos/video of adequate quality were obtained. The RPA was then flown back to the research vessel with retrieval initiated following communication with the Bridge and crew.

1 https://www.csiro.au/en/about/facilities-collections/MNF/Research-vessel-Equipment-Data/RV-Investigator/Specifications

The co-pilot, equipped with appropriate PPE (clear face-shield, safety glasses and gloves), positioned with hands outstretched, retrieved the RPA by holding the landing gear once the RPA was in range. RPA flights were conducted in strict coordination with whale scientists onboard the vessel, including via feedback with whale observers on whether RPA operations were impacting whale behaviour and in order to keep track of whales in the area. The minimum approach distance to the whale varied depending on the research objective but was never less than 5m.

To characterise the environmental operating envelope of RPA use on this voyage, we derived RPA flight metrics (duration, height, length, speed, distance from ship, battery drainage, satellites acquired, flight turnaround times) and underway environmental sampling data collected concurrently by the *RV Investigator* including GPS location, air temperature and wind speed in addition to Beaufort scale as estimated by the whale observation team. We also derived additional environmental parameters known to impact RPA navigation and flight control including the geomagnetic Kp index (to characterise geomagnetic activity; Matzka et al., 2021), distance to the south magnetic pole, and magnetic declination and inclination (magneticField function in R package: oce). RPA flight metrics were obtained by decoding the RPA flight log files with both Flight Reader (https://www.flightreader.com/) and Airdata UAV (https://airdata.com/). All data manipulation and visualisations were undertaken in R 4.3.2 (R Core Team, 2023).

3 Results

3.1 Literature review

The literature review generated 206 peer-reviewed publications published between 2004 and 2023 in various forms including journal articles (n = 174), conference proceedings (n = 29), book sections (n = 2) and a report (n = 1) demonstrating RPA use in Antarctica including location, RPA type and scientific application and including 18 review articles. For these Antarctic related references, the dominant application was 'wildlife' followed by 'technology and development' (Figure 1). Amongst the wildlife publications, thirteen were specifically cetacean related focussing on a range of species including Antarctic minke, humpback, killer, sei, fin and southern right whales. One additional article was cetacean related however described the detection of whale bones via land survey and another additional article was a review (see Supplementary Material). Given that the intention of the literature review undertaken was to gain an understanding of RPA operations around cetaceans in Antarctica, we note an additional five technical reports (not peer reviewed) that described at-sea vessel-based RPA operations around cetaceans in Antarctica. All references are detailed in the Supplementary Material.

Across the thirteen peer reviewed publications and the five technical reports, six different multirotor RPA models were used, with fourteen references reporting the use of more than one RPA model. The commercially available DJI Phantom (n=11) and Inspire (n=9) models were the most commonly used followed by the LemHex-44 (n=7), the FreeFly Alta 6 (n=7), the APH-22 (n=3) and the Swellpro Splashdrone (n=1). Excluding the single review publication and another publication detailing the mapping of whale bones on land, the majority of RPA activities were undertaken in nearshore waters of the Antarctic Peninsula region (n=10) and off islands (n=5; Auckland Islands, Falkland Islands, Elephant Island, South Georgia; Figure 2.) Flying UAVs off of small boats (around 6m) was common practice (n=9 references), especially along the Antarctica Peninsula (n=8 references). RPAs were also flown off a range of larger vessels including ~20m (n=2 vessels), ~40m (n=1 vessel), ~70m (n=1 vessel) and ~120m (n=1 vessel) in length. Relatively few vessel-based RPA operations for cetacean science were reported for the East Antarctic sector (n=2 between 0°E – 30°

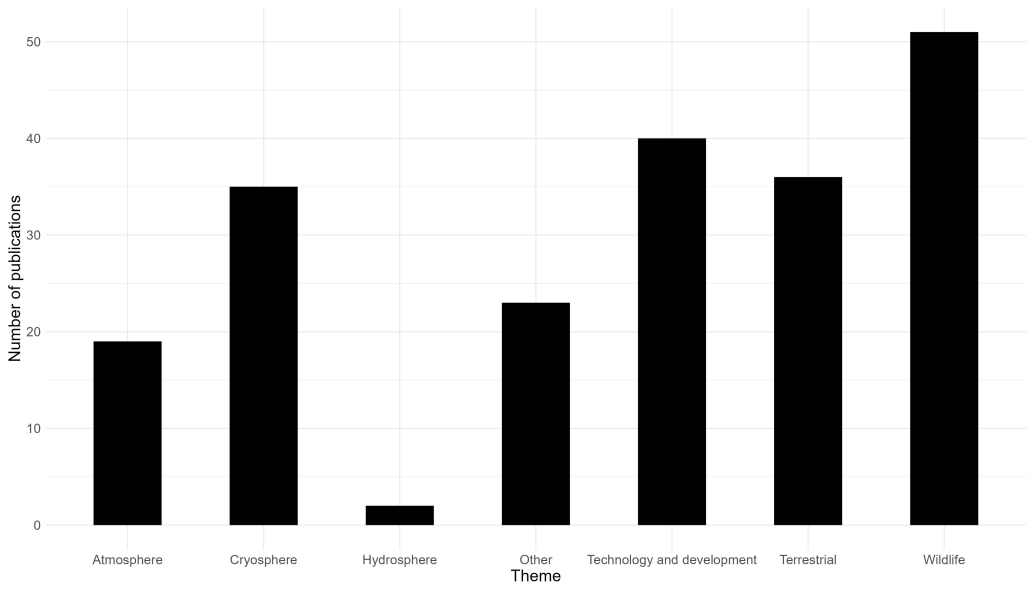


FIGURE 1
The number of publications in each literature review category.

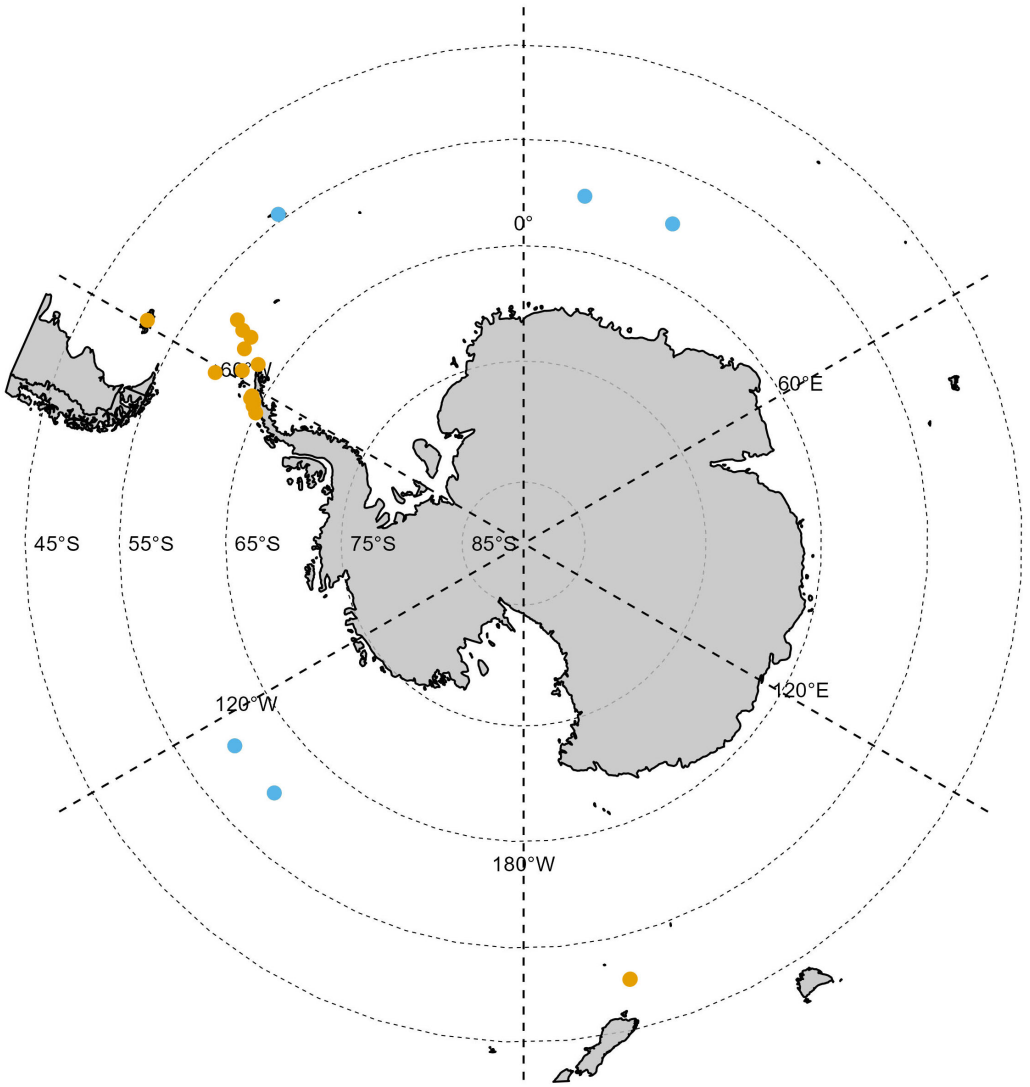


FIGURE 2
The general geographic location of multirotor RPA use around cetaceans in Antarctica and at subantarctic islands between 2004 and 2023. Orange locations represent RPA operations described in peer-reviewed publications, blue locations represent RPA operations described in technical reports. See Supplementary Material for list of references.

E, n=2 at the Auckland Islands). Only one reference provided operational details regarding RPA use (Dawson et al., 2017) but this did not extend to defining the environmental conditions under which flights occurred.

3.2 Multirotor RPA activities in maritime East Antarctica

On the Antarctic ENRICH voyage, 139 multirotor RPA flights were undertaken between the 25th January 2019 and the 25th February 2019 using a DJI Inspire 2 (n=119), DJI Phantom 4 (n=15) or a DJI Phantom 4 Pro (n= 5) using the operational settings described in Table 1. Flights occurred over the open water of maritime east Antarctica in the region bounded by 138.5°E – 152.6°E and 63.3°S – 66.3°S (Figure 3). The RPAs were used for whale photogrammetry, whale blow sampling, whale photo identification, surface water sampling for trace metal analysis, visual survey of whale behaviour and the collection of whale imagery for a documentary. During these flights, data was collected on Antarctic blue whales, fin whales and humpback whales. Data streams derived from RPA flights included photo identification (n = 12 Antarctic

TABLE 1 RPA settings used for flights occurring throughout the ENRICH voyage.

RPA configuration option	Setting used for ship-based flights
Flight mode	"ATTI" (or manual mode, GNSS disabled – note, in this mode, the barometer is used to maintain altitude)
Obstacle sensors	Disabled
Return to home	Disabled (or the ability to update home point during flight)

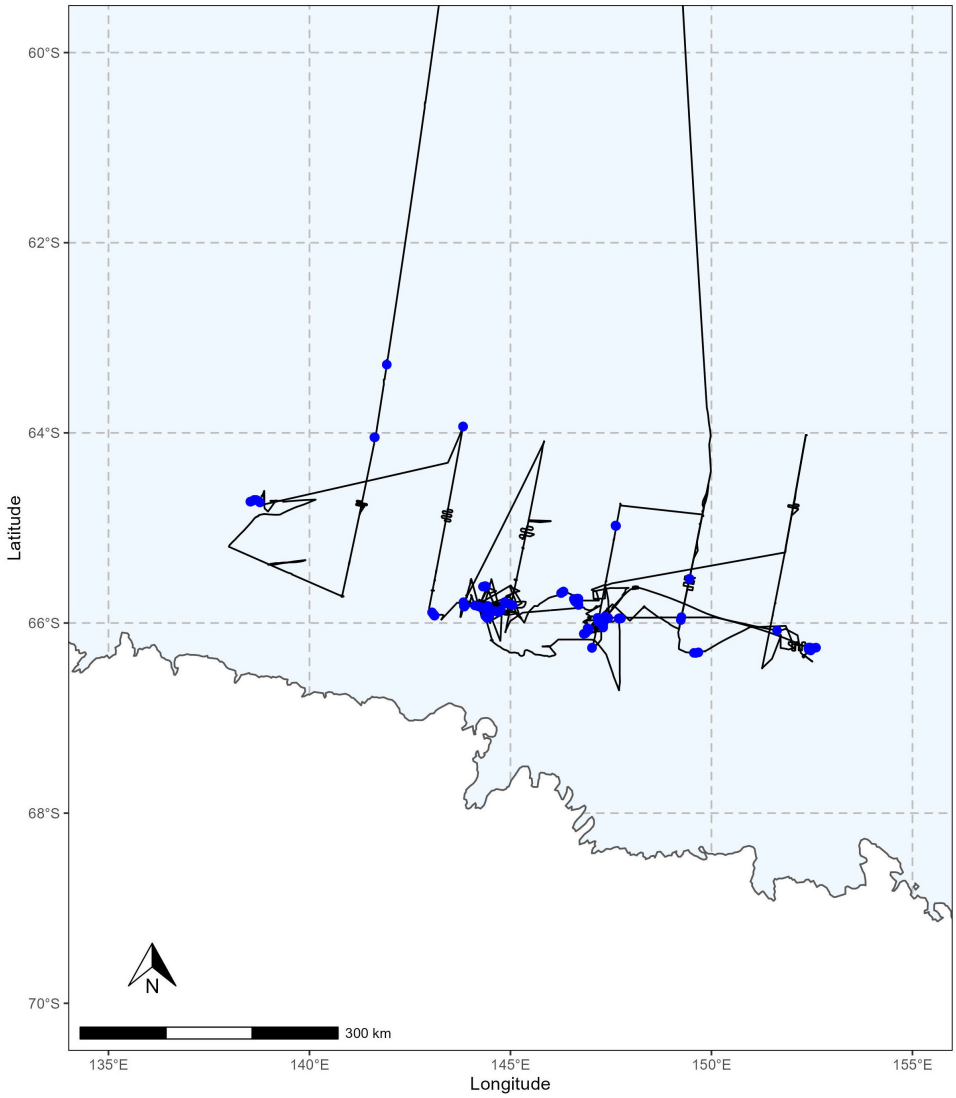


FIGURE 3
Map detailing the area of RPA operations throughout the ENRICH voyage. 139 flights (blue points) occurred along the ship track line (black line). The Antarctic continent is included in white to the south of the RPA operations.

blue whales), photogrammetry (n = 7 Antarctic blue whales, n = 1 fin whale, n = 3 humpback whales) and observations of feeding behaviour (n = 2 Antarctic blue whales, n = 2 fin whales, n = 2 humpback whale groups). Additionally, a single Antarctic blue whale blow sample was taken, and six flights were conducted to collect surface water samples (n=17) for trace metal analysis. Four flights collected 11 samples of surface seawater near two icebergs (< 300 m and ~50 m distance from the ship) and two flights collected 6 samples close to the ship to undertake a quality control analysis of the influence of the ship on trace metal samples. RPA flights occurred on 17 separate days over the 32-day period with 1 to 19 flights occurring in any day.

Flights were on average 12 minutes in duration (range: 3 min to 18 min), covering an average distance of 4.6 km (range: 0.5 km to 8.2 km) and flown at an average flight speed of 6.5 ms^{-1}/12.6 knots (median speed of 4.5 ms^{-1}/8.7 knots). The average flight height achieved was around 29 m/95 ft (median flight height approximately 30 m/98 ft; maximum flight height: approximately 71 m m/233 ft). The DJI Inspire 2 was flown at a slightly greater height (median: 32 m/105 ft) than the DJI Phantom 4 (median: 21 m/69 ft) and DJI Phantom 4 Pro (median: 20 m/66 ft), largely due to differences in camera lens capabilities and flight objectives. The average amount of battery drained per flight was 60% (median: 66%; in the case of the DJI Inspire 2, battery drainage value was averaged across both batteries). Being a larger RPA, the amount of battery drained was consistently higher for the DJI Inspire 2 than the DJI Phantom 4 and the DJI Phantom 4 Pro, however, battery drainage rates were similar at around 4% per minute (Figure 4). Estimates derived from the regression line equations describing the relationship between battery drainage and flight duration for each RPA platform indicated that at 100% battery drainage, flight durations would be around 21.8 min for the DJI Inspire 2 (manufacturer specifications indicated an expected flight duration of 23 to 27 minutes), 25.5 min for the DJI Phantom 4 (manufacturer

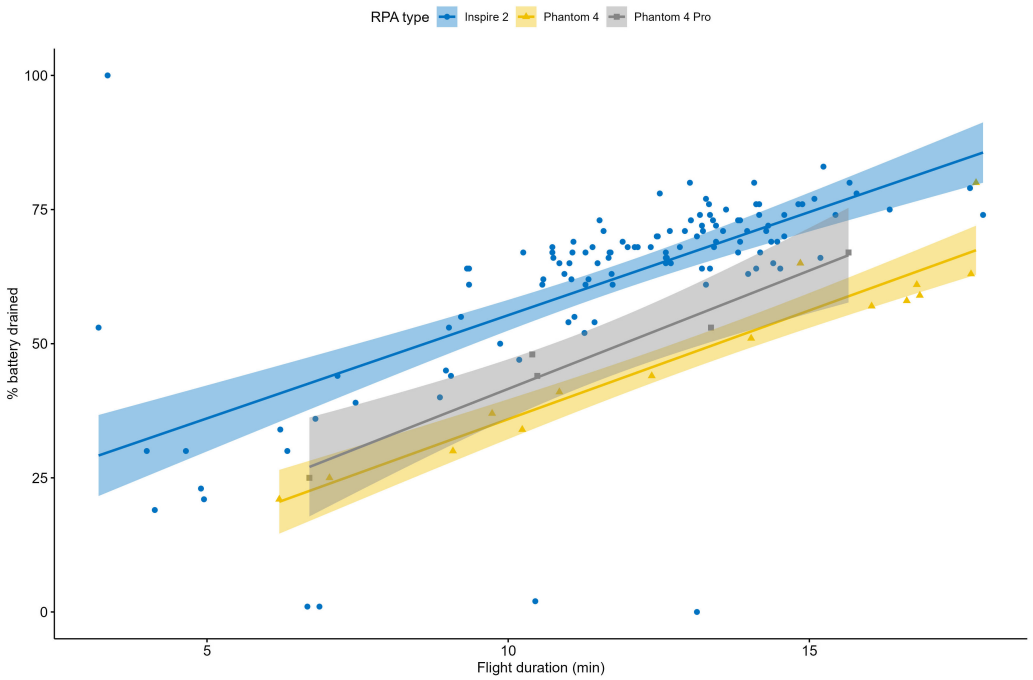


FIGURE 4
Battery drainage (%) in relation to flight duration (minutes) for the three RPA types used (DJI Inspire 2 – blue line, DJI Phantom 4 – orange line, DJI Phantom 4 Pro – grey line). Regression lines are included and shaded areas are the 95% confidence interval.

specifications indicated an expected flight duration of 28 minutes) and 23.3 min for the DJI Phantom 4 Pro (manufacturer specifications indicated an expected flight duration of 30 minutes) platforms.

A minimum of 14 and a maximum of 22 satellites were acquired for each of the 139 RPA flights. Compass calibration issues for the DJI Phantom 4 platforms were regularly noted by pilots during the 32-day period of flying. There was no evidence of strong geomagnetic activity during that time as evidenced by Kp index values (the activity level classification for geomagnetic storms) between 0 and 4 (mean = 1.3, median = 1). Flights were on average 506 km from the south magnetic pole (range 147 km to 816 km) where magnetic inclination (the angle made with the horizontal by Earth's magnetic field lines; range −90° at the south magnetic pole to 90° at the north magnetic pole) and declination (the angle between magnetic north and true north at a particular location on the Earth's surface) were on average, −88° (range: −86° to −89°) and 100° (57° to 115°) respectively.

The ship was underway throughout RPA flights, travelling at an average speed of 3.3 knots (median: 3.1 knots, range: 0 knots to 9.2 knots). Maximum distance from the ship did not exceed 2.2 km (median: 880 m). The larger maximum flight distance from the ship values are predominantly driven by the DJI Inspire 2 flights. The DJI Inspire 2 median maximum flight distance from the ship was 996 m (maximum: 2.2 km), the DJI Phantom 4 median maximum flight distance from the ship was 298 m (maximum: 1.2 km) and the DJI Phantom 4 Pro median maximum flight distance from the ship was 194 m (maximum 509 m).

The average air temperature across the 139 flights was −3.6°C (median: −3.0°C; Table 2). The air temperature encountered across the 32-day period throughout which flights occurred did not limit flying operations: the coldest air temperature recorded was −9.7°C and the coldest air temperature encountered during RPA flights was −9.5°C (Figure 5).

The wind speed recorded during UAV flights ranged from 0.1 knots to 23.9 knots, but on average, was 10 knots (median: 10.3 knots; Table 2). Wind speeds of up to 55.6 knots were encountered during the 32-day period throughout which flights occurred with a median wind speed of 13.5 knots. Higher wind speeds limited RPA use with the RPA clearly not operated throughout the full range of wind speeds encountered (Figure 6). Flights did not occur above Beaufort scale 5 with 52% of flights occurring at Beaufort scale 3 (Table 2).

The average time between RPA flight end and the initiation of the subsequent RPA flight following battery exchange or other RPA configuration requirements was 19 minutes (median: 16 minutes) but could be as low as 5 minutes (Figure 7).

Finally, RPAs were flown without incident. No RPA was lost and no collisions occurred despite RPAs flying in close proximity to the ship superstructure. No injuries occurred due to hand capture

TABLE 2 Environmental conditions encountered throughout RPA flights in maritime East Antarctica.

Environmental condition	Mean	Maximum
Air temperature (at the vessel, underway data)	−3.6°C	−9.5°C
Wind speed (at the vessel, underway data)	10 knots	24 knots (95^{th} quantile = 15.5 knots)
Beaufort scale (at the vessel, observer derived)	3	5

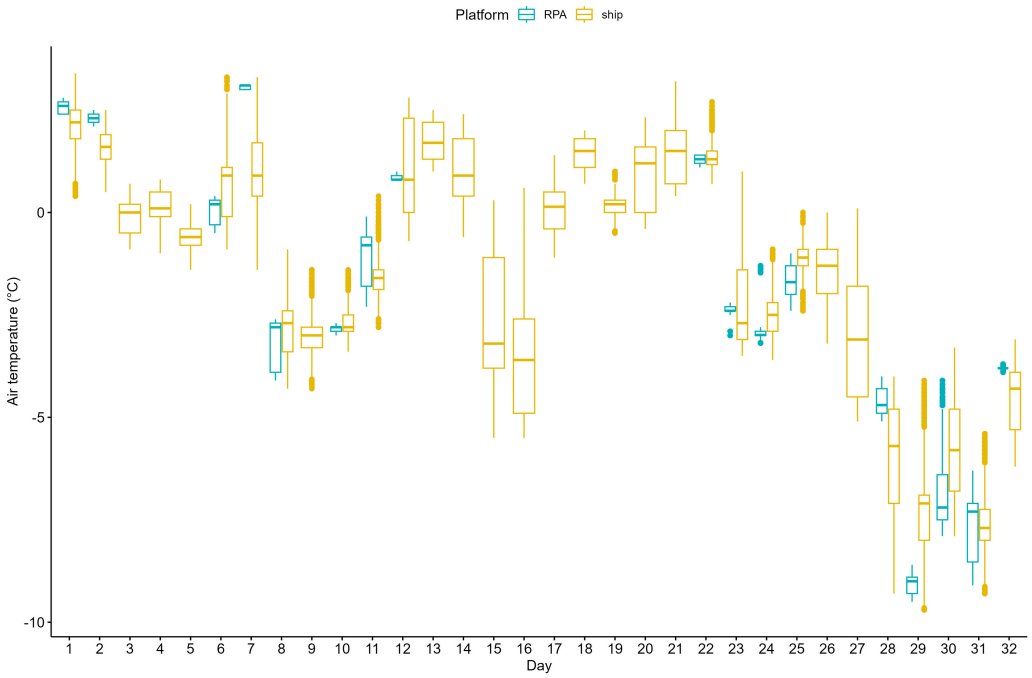


FIGURE 5
Boxplot detailing the daily air temperature (°C) encountered, derived from ship underway data (yellow), and air temperature encountered during RPA flights (blue). Day 1 is January 25, 2019 (UTC).

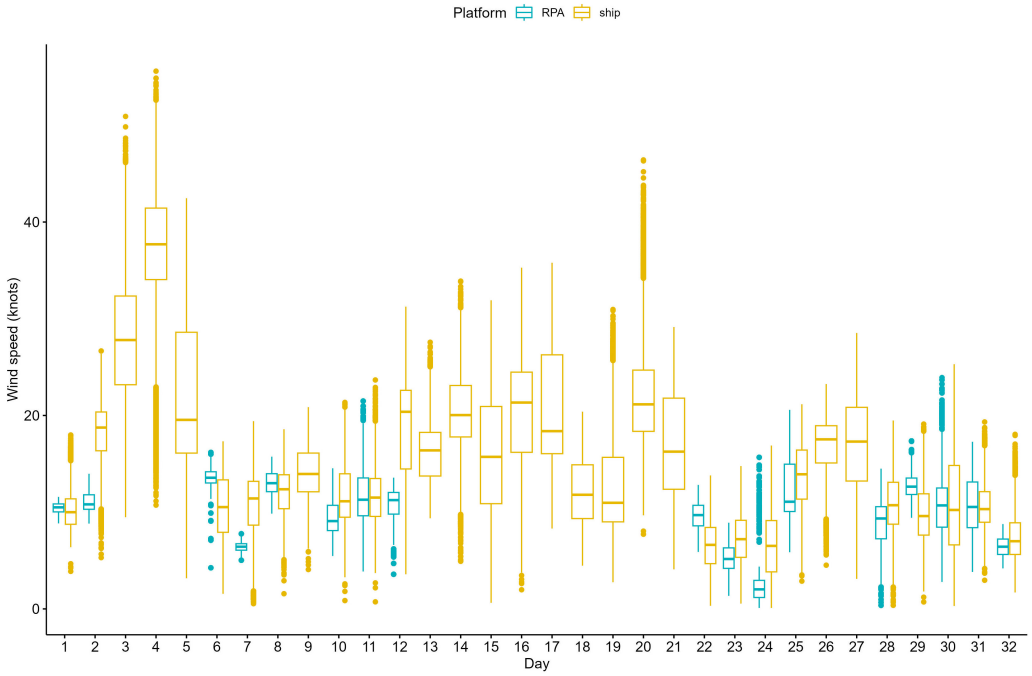


FIGURE 6
Boxplot detailing the daily wind speed (knots) encountered, derived from ship underway data (yellow) and wind speed encountered during RPA flights (blue). Day 1 is January 25, 2019.

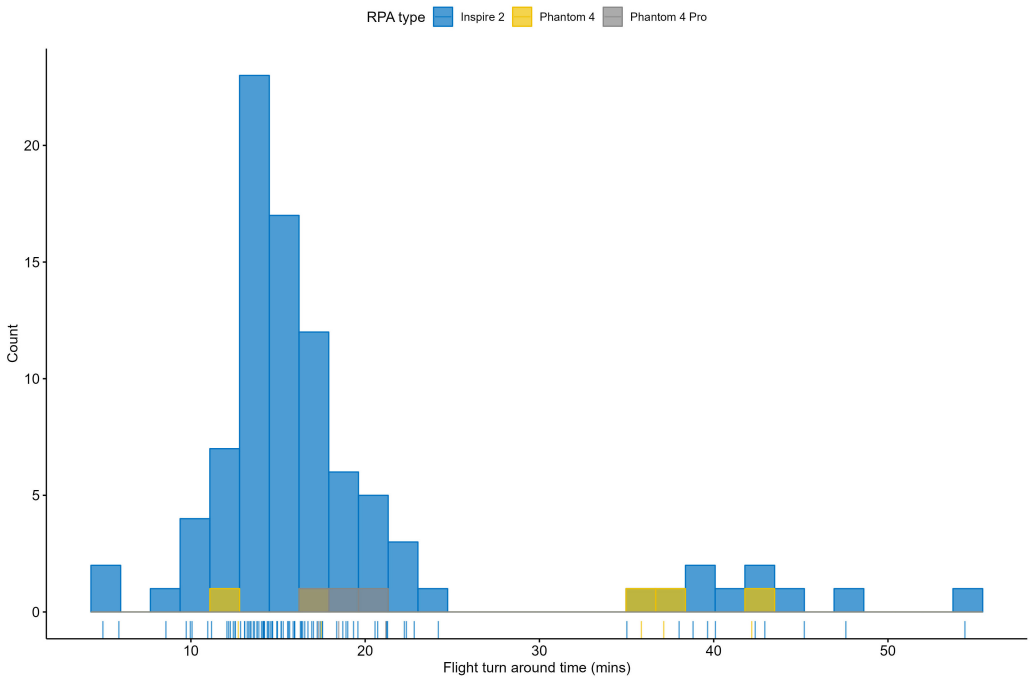


FIGURE 7
Turnaround times (the time between RPA flight end and the initiation of the subsequent RPA flight; in minutes) for the three RPA types (DJI Inspire 2 – blue, DJI Phantom 4 – orange, DJI Phantom 4 Pro – grey).

and release. RPAs were recalled once to avoid an aggregation of birds roosting on an iceberg.

4 Discussion

We demonstrate the successful use of ship-based small multirotor RPAs for cetacean research in maritime Antarctica. This research was carried out as a component of a multidisciplinary research voyage to study Antarctic krill and the distribution and behaviour of their predators with a particular focus on critically endangered Antarctic blue whales. The successful RPA flights generated data related to photogrammetry, photo identification and feeding behaviour of Antarctic blue whales, fin whales and humpback whales.

The literature review found that RPAs have been used extensively across most scientific disciplines for Antarctic based research with wildlife research via multirotor RPAs the dominant application. Publications describing the use of RPAs on ships to study wildlife at sea in Antarctica were relatively uncommon (in comparison to nearshore waters of the Antarctic Peninsula and islands) with the review highlighting, in particular, how rare Antarctic ship-based cetacean related research via multirotor RPA is in the East Antarctic sector. RPA flights for wildlife and cetacean research tended to be focused around the nearshore and protected waters of the Antarctic Peninsula and Antarctic or subantarctic islands. Whilst this highlights a gap in the geographic range of RPA related cetacean research effort, it is not unsurprising given the high concentration of Antarctic stations and tourist vessels, sheltered waters and high krill biomass located consistently and continuously throughout the nearshore waters of the Antarctic Peninsula (Atkinson et al., 2017; Green et al., 2023). The high biomass of krill in the region is the basis of the Antarctic krill fishery with the overlap between fishing effort and krill predators (e.g. Weinstein et al., 2017) necessitating the focus on collection of relevant scientific data. Amongst this literature, the base for RPA operations described was often a small boat launched from land or tourist vessel, via a day trip-type scenario following whale sightings (for example, Durban et al., 2021; Bierlich et al., 2022). Outside of this region, the offshore distribution of cetaceans such as Antarctic blue whales (see Andrews-Goff et al., 2022; Miller et al., 2024) imposes logistical constraints on the field operations designed to study them and this day-trip model via small boat launch is logistically and operationally challenging with increased safety risk. Some of these challenges can clearly be overcome via the use of RPAs at sea, launched from a research vessel and hence the importance of characterising and reporting ship-based operations of multirotor RPAs in Antarctica. Under the search terms applied, we found no publications that discussed, in detail, the operational use (pre-flight settings, RPA operating procedures and environmental operating conditions) of RPAs off large vessels to study cetaceans in Antarctica.

The vessel-based RPA flights undertaken on the ENRICH voyage were constrained by wind speed but not by air temperature. Flights were undertaken throughout the full range of air temperatures experienced (down to –9.5°C) but not throughout the full range of wind speeds experienced. Over the 32-day period when RPAs were operated, wind speeds reached > 2 times the strength of wind speeds occurring throughout the RPA flights

undertaken. Flights were undertaken up to Beaufort scale 5 indicating a wave height of up to approximately 3m was acceptable for safe RPA operations from the foredeck.

Whilst it is well established that temperatures below 0°C impact lithium battery performance resulting in significant power loss (Wang et al., 2016), the cold impacted battery performance to only a small degree, if at all. Estimated maximum flight time was within approximately 10% of expected flight time (as derived from manufacturer specifications for conditions above 0°C) for both the DJI Inspire 2 and DJI Phantom 4 and within 22% of expected flight time for the DJI Phantom 4 Pro (though few flights were undertaken on this platform). However, the RPA flights undertaken were relatively short at an average duration of 12 minutes. If RPA flights were longer, cold would likely begin to play a limiting role on operations primarily through the influence of cold on the comfort and dexterity of the RPA pilot rather than via the influence of cold on the battery given the existence of self-heating battery systems (Wang et al., 2016) and the ability to insulate batteries from extreme external temperatures (Häusermann et al., 2023). Often RPA flights occurred when the vessel was underway, at times flying out to around 2 km from the vessel but mostly much closer at just under 900 m from the vessel.

Whilst the RPA flights undertaken were relatively short in duration, they could be frequent given short turnaround times so often were adequate to achieve the science intended, namely photogrammetry, photo identification, behavioural observation, whale blow sampling, and water sampling. For a 12-minute flight duration, battery drainage was around 60% indicating that the RPAs were rarely pushed to their operational limit. Instead, RPAs were returned to the vessel for battery or payload exchange in line with whale surfacing behaviour and down times informed and coordinated by ongoing communications between pilots and whale observers. However, even if pushed to their operational limit to achieve flight times of up to approximately 30 minutes (as indicated by the manufacturer), the range achieved by these commercial multirotor RPAs is unlikely to enable extensive visual surveys which are so critical to an understanding of cetacean abundance and distribution. Long range, fixed wing drones that can be launched and retrieved from the deck of the ship are not only logistically and methodologically capable of undertaking these types of surveys (Hodgson et al., 2017) but can access areas that vessels cannot, such as regions of heavy ice inhabited by some Antarctic cetacean species (for example, Double et al., 2015; Herr et al., 2019; El-Gabbas et al., 2024).

RPAs were operated by both a science team and a documentary team throughout the voyage. The documentary team applied their extensive flying experience to the operation of the larger DJI Inspire 2 which was also relatively more robust to wind, able to undertake longer flights and easier to see at a distance due to its large size and darker colour than the other RPA platforms. The science team, flying off a large vessel and in Antarctica for the first time, were flying the smaller white DJI Phantom 4 RPAs which could also be difficult to see in the cloudy conditions that dominated despite the addition of colourful tape and flashing LEDs. The documentary team flying the DJI Inspire 2 therefore undertook around 80% of all flights. This demonstrates the opportunity that proficient pilots across disciplines offer for the collection of scientific data but also the need to consider RPA specifications relative to the operating environment.

The RPAs employed during the research voyage, like all RPAs, used GNSS signals to aid navigation and positioning. There are four GNSS with global coverage: GPS, GLONASS, BDS, and Galileo (Zheng et al., 2022). GNSS signal availability is governed by the altitude of satellite orbit, the inclination angle of the satellite and the Earth ground-level 'field of view' width of the signal transmitter attached to the satellite with the spacing, altitude and attitude of satellites all critical components when minimising error (Sheridan, 2020). For all GNSS, coverage of high latitudes is low (relative to equatorial regions) and this is especially true for GPS at latitudes > 75° due to satellite flight orbital inclination and altitude resulting in poor observation geometry. For all GNSS, at least four satellites are required for a full position fix and time or altitude fix. All RPA flights acquired at least 14 satellites despite all deployments occurring at high latitudes. The RPAs used both GPS and GLONASS, a GNSS combination resulting in the best estimate accuracy at high latitudes (Zheng et al., 2022). High precision and accuracy GNSS technologies have become available since this voyage occurred (Hodgson, 2020) and provide further confidence that high latitude RPA operations can occur with low position and navigation error.

The voyage's proximity to the south magnetic pole meant there was high magnetic declination angles and steep magnetic inclination angles which can affect multirotor RPAs, which rely heavily on the magnetic compass and magnetometer for flight control. Initial testing of the ability to fly the RPAs in P-mode (GNSS positioning mode) determined that sometimes the software prevented launches and flight control at times was unreliable. Pilots also suspected that the large steel structure of the vessel was interfering with the RPA compass. All RPA flights, therefore, were undertaken in ATTI-mode (manual mode). The influence of the south magnetic pole and associated magnetic declination/inclination are unlikely to be an ongoing issue for contemporary flights using RPAs with dual GNSS to override the compass function. Flying RPAs in manual flight modes continues to be recommended for high latitude operations to mitigate the influence of high magnetic declination and steep magnetic inclination on the compass.

Other considerations when flying small multirotor RPAs off a ship include ensuring that the ship superstructure is not positioned in between the flight controller and the RPA (which could happen if a whale travels behind the ship, for example) or risk loss of connection between the RPA and flight controller. Pilots should also consider disabling obstacle avoidance sensors when flying from vessels that have complex and cluttered deck space or emit signals such as Automatic Dependent Surveillance–Broadcast (for ships that also carry aircraft such as helicopters). Finally, for vessel-based RPA operations when the vessel is underway, the return to home feature should either be disabled or updated regularly to avoid early automatic return of the RPA (due to on board calculations indicating battery power is too low relative to distance from home) or return of the RPA to the take-off/home location that no longer aligns with the actual vessel location.

Prior to the voyage, the Australian Government's Civil Aviation Safety Authority (CASA) advised that they did not have jurisdiction over the RPA operations planned outside of Australian territory. Operations of Australian RPA outside of Australian territory must comply with Australia's international obligations. The international convention covering RPA use in international waters is the Convention on International Civil Aviation (the Chicago Convention), which Australia signed in 1944. Australian RPA operations must comply with the standards and recommended practices set out in annexes to the Chicago Convention. Currently, there is work underway to achieve the safe, secure and efficient integration of RPAs into global aviation frameworks so, temporarily, RPA operations in east Antarctic waters (12 nautical mile Australian Antarctic Territory coastline) will not be authorised by CASA. Contemporary flight management via CASA is likely to be far more stringent than that applied in 2019. Flights occurring typically within 500m of the pilot where the pilot maintains visual contact with the RPA without relying on any visual aids are classified as a visual line of sight (VLOS) operations. Extended visual line of sight operations (EVLOS) occur when the RPA is flown beyond the pilot's visual line of sight. EVLOS operations generally involve at least one visual observer placed within VLOS of the RPA or using a device, such as binoculars, to observe the RPA and general operating area. The flights we describe here are likely on the cusp of EVLOS and contemporary requirements for research such as this would include submission of documented practices and procedures to CASA, additional flying hours, proof of operational concept under VLOS conditions and a pilot proficiency check (Civil Aviation Safety Regulations, 1998).

Regardless of the regulatory setting and requirements associated with EVLOS operations, the ability to undertake RPA operations to study the largest of krill predators, taking advantage of a somewhat reliable surfacing behaviour (Calderan et al., 2023) and swimming speeds equivalent to RPA flight speed (Andrews-Goff et al., 2022) clearly presents significant opportunities to facilitate research in a hostile, remote environment. The research on the ENRICH voyage was undertaken with the specific goal to characterise Antarctic krill swarms, determine whether these characteristics predict the distribution and behaviour of Antarctic predators, particularly Antarctic blue whales, and characterise the predator–prey interactions. The RPAs employed collected vision associated with feeding and photogrammetry. Whilst there are alternative methods to collect similar data (for example, biologging tags; Cade et al., 2022), the data that can be derived from these feeding events observed are a step towards characterising prey field interactions and feeding kinematics (Goldbogen et al., 2017) and did not require dedicated ship time and additional personnel to launch a small boat for tag deployment. The ability for photogrammetry to provide critical information on health via body condition assessment is well proven (for example, Bierlich et al., 2022) and an expected outcome from this research also.

However, it is exceedingly clear that RPAs are a platform that can offer more than the collection of visual data alone. For cetaceans, RPAs have been used to deploy biologging tags using a gravity drop system (Wiley et al., 2023) with further innovation to develop a drone-based platform for biopsy sampling and type C (Andrews et al., 2019) small implantable satellite tag deployment underway (Andrews-Goff et al., 2024). Combining the use of biopsy samples (for an assessment of foraging strategy, pregnancy status and stock identity), with RPA derived imagery (to determine body condition) and satellite tag deployment (to ascertain foraging behaviour along with spatial and temporal occupancy of Antarctic feeding grounds) will provide entirely novel opportunities to study cetaceans.

RPA derived data streams can provide the basis of a robust monitoring program in the face of a changing climate, and address key knowledge gaps for management bodies such as CCAMLR and the International Whaling Commission (IWC). Critical to the sustainable management of krill is the adoption of a precautionary and ecosystem approach to fisheries management, which accounts for the predation needs of krill predators (Kelly et al., 2017, 2018). Data informed estimates of krill consumption rates (derived from metrics such as temporal and spatial occupancy and foraging performance) by cetaceans is critical to CCAMLR's ecosystem fisheries management approach.

This paper describes the extensive use of small, ship-based, multirotor RPAs for cetacean research in Antarctica. The RPAs delivered a range of cetacean related data streams including photogrammetry, photo identification, behavioural observations and whale blow sampling in addition to water sampling and collection of general scenic imagery. Despite the harsh environmental conditions encountered with air temperatures routinely well below 0°C and high winds, the RPAs performed exceptionally well to deliver the desired scientific outcomes safely within short, wide-ranging flights. In the period since these flights occurred, both the regulatory space and RPA development have advanced, and future research opportunities will benefit from improved battery and flight performance while accounting for more stringent flight management requirements. Regardless, the potential for RPAs to deliver critical data to address the knowledge gaps that challenge effective management of both krill, and their predators cannot be overstated. Harnessing the ability of these platforms to passively collect data and actively deploy sampling devices will be revolutionary for cetacean research globally, especially in isolated and remote regions such as maritime Antarctica.

Data availability statement

The datasets presented in this study can be found in online repositories. The names of the repository/repositories and accession number(s) can be found below: Australian Antarctic Data Centre: https://doi.org/10.26179/zs9v-ak70 or https://data.aad.gov.au/metadata/AAS_4101_RPA_ops_summ.

Ethics statement

This research was reviewed and approved by the Australian Antarctic Ethics Committee under Australian Antarctic Science Project 4101 and complied with all relevant permits including the Australian Government Environment Protection and Biodiversity Conservation Act Cetacean Permit (C12-0006, 2017-004) and the

Australian Government Antarctic Treaty (Environment Protection) Act provided specifically for Australian Antarctic Science Project 4101 as part of the 2019 Investigator Voyage.

Author contributions

VA: Conceptualization, Data curation, Formal analysis, Investigation, Methodology, Visualization, Writing – original draft, Writing – review & editing. JS: Conceptualization, Data curation, Investigation, Methodology, Resources, Writing – original draft, Writing – review & editing. LI: Conceptualization, Data curation, Investigation, Methodology, Resources, Writing – original draft, Writing – review & editing. MD: Conceptualization, Data curation, Formal analysis, Funding acquisition, Investigation, Methodology, Resources, Writing – original draft, Writing – review & editing.

Funding

The author(s) declare financial support was received for the research, authorship, and/or publication of this article. This work was made possible with the support of numerous Australian Antarctic Science (AAS) Projects with gracious and excellent support from personnel at the Australian Antarctic Division. These projects include: AAS Project 4101: Antarctic baleen whale habitat utilisation and linkages to environmental characteristics; AAS Project 4102: Population abundance, trend, structure and distribution of the endangered Antarctic blue whale; AAS Project 4512: Ensuring sustainable management of the krill fishery in waters off the Australian Antarctic Territory; AAS Project 4600: Conservation and management of Australian and Antarctic whalespost-exploitation status, distribution, foraging ecology and their role in the Southern Ocean ecosystem; AAS Project 4636: Sustainable Management of Antarctic Krill and Conservation of the Krill-based Ecosystem. Thanks to the CSIRO Marine National Facility (MNF) for its support in the form of sea time on RV Investigator, support personnel, scientific equipment and data management.

Acknowledgments

The ENRICH research voyage would not have been possible without the tenacity, hard work and support of many. In particular, we thank Karen Westwood for project management and Natalie Kelly for being the driving force behind the survey design and voyage Science Plan. We greatly appreciate the hard work and support of our AAD colleagues in the Science Branch, Science Technical Support, Operations, the Executive, Science Planning and Coordination, Human Resources, Media and Public Affairs, IT, the Polar Medicine Unit and the Australian Antarctic Data Centre. We thank Captain Adrian Koolhof and his crew, Lisa Woodward, Linda Gaskell and MNF staff. We would like to particularly acknowledge the significant contribution of both Alexander Vail and James Cox whose expert RPA abilities enabled the collection of much of the data discussed here and to who we are most grateful. Sincere thanks to all the scientists on board who worked long hours in often tough conditions to maximise what was achieved. Many thanks to Dr Brian Miller and Dr Elanor Bell for their feedback on earlier versions of this manuscript and to Dr Doug Thost for running his expert eye over the technical RPA components, in particular. Huge thank you also to Simon Wotherspoon who assisted with analyses to finalise the quality control of the original data set. Thank you to the reviewers for their constructive comments.

Conflict of interest

The authors declare that the research was conducted in the absence of any commercial or financial relationships that could be construed as a potential conflict of interest.

Publisher's note

All claims expressed in this article are solely those of the authors and do not necessarily represent those of their affiliated organizations, or those of the publisher, the editors and the reviewers. Any product that may be evaluated in this article, or claim that may be made by its manufacturer, is not guaranteed or endorsed by the publisher.

Supplementary material

The Supplementary Material for this article can be found online at: https://www.frontiersin.org/articles/10.3389/fmars.2024.1473471/full#supplementary-material

References

Alejandro, C.-C., Francesco, S., Lucio, P., Emiliano, V., and Roberto, G. V. (2023). Faster and better: comparison between traditional and drone monitoring in a cryptic species, the purple heron *Ardea purpurea*. *Acta Ornithologica* 57, 134–142. doi: 10.3161/00016454AO2022.57.2.002

Alvear, O., Zema, N. R., Natalizio, E., and Calafate, C. T. (2017). Using UAV-based systems to monitor air pollution in areas with poor accessibility. *J. Adv. Transp.* 2017. doi: 10.1155/2017/8204353

Andrews, R. D., Baird, R. W., Calambokidis, J., Goertz, C. E. C., Gulland, F. M. D., Heide-Jorgensen, M. P., et al. (2019). Best practice guidelines for cetacean tagging. *J. Cetacean Res. Manage.* 20, 27–66. doi: 10.47536/jcrm.v20i1.237

Andrews-Goff, V., Bell, E. M., Miller, B. S., Wotherspoon, S. J., and Double, M. C. (2022). Satellite tag derived data from two Antarctic blue whales (*Balaenoptera musculus intermedia*) tagged in the east Antarctic sector of the Southern Ocean. *Biodiversity Data J.* 10, e94228. doi: 10.3897/BDJ.10.e94228

Andrews-Goff, V., Double, M., Zerbini, A., Williams, G., Harcourt, R., Kelly, N., et al. (2024). "PROJECT 26. Remote aerial deployment and sampling: development of a new sampling platform for large cetaceans," in *IWC-SORP Research Fund: 2024 progress reports from funded projects, Paper presented to the Scientific Committee of the International Whaling Commission: SC/69B/SH/06Rev1: 24-28*. (Cambridge, UK: International Whaling Commission)

Angliss, R. P., Ferguson, M. C., Hall, P., Helker, V., Kennedy, A., and Sformo, T. (2018). Comparing manned to unmanned aerial surveys for cetacean monitoring in the Arctic: methods and operational results. *J. Unmanned Vehicle Syst.* 6, 109–127. doi: 10.1139/juvs-2018-0001

Aniceto, A. S., Biuw, M., Lindstrøm, U., Solbø, S. A., Broms, F., and Carroll, J. (2018). Monitoring marine mammals using unmanned aerial vehicles: quantifying detection certainty. *Ecosphere* 9, e02122. doi: 10.1002/ecs2.2018.9.issue-3

Apprill, A., Miller, C. A., Moore, M. J., Durban, J. W., Fearnbach, H., and Barrett-Lennard, L. G. (2017). Extensive core microbiome in drone-captured whale blow supports a framework for health monitoring. *Msystems* 2. doi: 10.1128/mSystems.00119-17

Atkinson, A., Hill, S. L., Pakhomov, E. A., Siegel, V., Anadon, R., Chiba, S., et al. (2017). KRILLBASE: a circumpolar database of Antarctic krill and salp numerical densities 1926–2016. *Earth Syst. Sci. Data* 9, 193–210. doi: 10.5194/essd-9-193-2017

Baird, R. W., Lerma, J. K., Cornforth, C. J., and Wood, K. A. (2022). An unexpected benefit from drone-assisted fecal sample collection: picking up subsurface poop after it floats to the surface. *Aquat. Mammals* 48, 565–567. doi: 10.1578/AM.48.6.2022.565

Bannister, J. (2001). Status of southern right whales off Australia. *J. Cetacean Res. Manage.* (special issue) 2, 103–110. doi: 10.47536/jcrm.vi.273

Barreto, J., Cajaíba, L., Teixeira, J. B., Nascimento, L., Giacomo, A., Barcelos, N., et al. (2021). Drone-monitoring: improving the detectability of threatened marine megafauna. *Drones* 5, 14. doi: 10.3390/drones5010014

Bello, A. B., Navarro, F., Raposo, J., Miranda, M., Zazo, A., and Álvarez, M. (2022). Fixed-wing UAV flight operation under harsh weather conditions: A case study in Livingston island glaciers, Antarctica. *Drones* 6, 384. doi: 10.3390/drones6120384

Bersaglio, B., Enns, C., Goldman, M., Lunstrum, L., and Millner, N. (2023). Grounding drones in political ecology: understanding the complexities and power relations of drone use in conservation. *Global Soc. Challenges J.* 2, 47–67. doi: 10.1332/HNEK4485

Bierlich, K. C., Hewitt, J., Schick, R. S., Pallin, L., Dale, J., Friedlaender, A. S., et al. (2022). Seasonal gain in body condition of foraging humpback whales along the Western Antarctic Peninsula. *Front. Mar. Sci.* 9. doi: 10.3389/fmars.2022.1036860

Burgués, J., and Marco, S. (2020). Environmental chemical sensing using small drones: A review. *Sci. total Environ.* 748, 141172. doi: 10.1016/j.scitotenv.2020.141172

Butcher, P. A., Colefax, A. P., Gorkin, III RA, Kajiura, S. M., López, N. A., Mourier, J., et al. (2021). The drone revolution of shark science: A review. *Drones* 5, 8. doi: 10.3390/drones5010008

Cade, D. E., Kahane-Rapport, S. R., Wallis, B., Goldbogen, J. A., and Friedlaender, A. S. (2022). Evidence for size-selective predation by Antarctic humpback whales. *Front. Mar. Sci.* 9. doi: 10.3389/fmars.2022.747788

Calderan, S. V., Leaper, R., Andrews-Goff, V., Miller, B. S., Olson, P. A., Reyes, M. V. R., et al. (2023). Surfacing rates, swim speeds, and patterns of movement of Antarctic blue whales. *Front. Mar. Sci.* 10. doi: 10.3389/fmars.2023.1087967

Carroll, G., Hedley, S., Bannister, J., Ensor, P., and Harcourt, R. (2014). No evidence for recovery in the population of sperm whale bulls off Western Australia, 30 years post-whaling. *Endangered Species Res.* 24, 33–43. doi: 10.3354/esr00584

Christiansen, F., Dujon, A. M., Sprogis, K. R., Arnould, J. P. Y., and Bejder, L. (2016). Noninvasive unmanned aerial vehicle provides estimates of the energetic cost of reproduction in humpback whales. *Ecosphere* 7 (10), e01468. doi: 10.1002/ecs2.1468

Christiansen, F., Vivier, F., Charlton, C., Ward, R., Amerson, A., Burnell, S., et al. (2018). Maternal body size and condition determine calf growth rates in southern right whales. *Mar. Ecol. Prog. Ser.* 592, 267–281. doi: 10.3354/meps12522

Civil Aviation Safety Regulations. (1998). *Statutory Rules No. 237, 1998 made under the Civil Aviation Act 1988*. Australian Government. Available at: https://www.legislation.gov.au/F1998B00220/latest/text.

Clark, C. W., Brown, M. W., and Corkeron, P. (2010). Visual and acoustic surveys for North Atlantic right whales, *Eubalaena glacialis*, in Cape Cod Bay, Massachusetts 2001–2005: management implications. *Mar. Mammal Sci.* 26, 837–854. doi: 10.1111/j.1748-7692.2010.00376.x

Dawson, S. M., Bowman, M. H., Leunissen, E., and Sirguey, P. (2017). Inexpensive aerial photogrammetry for studies of whales and large marine animals. *Front. Mar. Sci.* 4. doi: 10.3389/fmars.2017.00366

Di Stefano, G., Romeo, G., Mazzini, A., Iarocci, A., Hadi, S., and Pelphrey, S. (2018). The Lusi drone: A multidisciplinary tool to access extreme environments. *Mar. Pet. Geol.* 90, 26–37. doi: 10.1016/j.marpetgeo.2017.07.006

Double, M. C., Miller, B. S., Leaper, R., Olson, P., Cox, M. J., Miller, E., et al. (2015). "Cruise report on blue whale research from the NZ/Aus Antarctic ecosystems voyage 2015 of the Southern Ocean research partnership," in *Paper SC/66a/SH/7 presented to the IWC Scientific Committee*. (Cambridge, UK: International Whaling Commission).

Durban, J. W., Fearnbach, H., Barrett-Lennard, L. G., Perryman, W. L., and Leroi, D. J. (2015). Photogrammetry of killer whales using a small hexacopter launched at sea. *J. Unmanned Vehicle Syst.* 3, 131–135. doi: 10.1139/juvs-2015-0020

Durban, J., Fearnbach, H., Paredes, A., Hickmott, L., and LeRoi, D. (2021). Size and body condition of sympatric killer whale ecotypes around the Antarctic Peninsula. *Mar. Ecol. Prog. Ser.* 677, 209–217. doi: 10.3354/meps13866

El-Gabbas, A., Thomisch, K., Van Opzeeland, I., Burkhardt, E., and Boebel, O. (2024). Dynamic species distribution models of Antarctic blue whales in the Weddell Sea using visual sighting and passive acoustic monitoring data. *Diversity Distributions* 30, 87–105. doi: 10.1111/ddi.13790

Fiori, L., Martinez, E., Orams, M. B., and Bollard, B. (2020). Using Unmanned Aerial Vehicles (UAVs) to assess humpback whale behavioral responses to swim-with interactions in Vava'u, Kingdom of Tonga. *J. Sustain. Tourism* 28, 1743–1761. doi: 10.1080/09669582.2020.1758706

Gallego, D., and Sarasola, J. H. (2021). Using drones to reduce human disturbance while monitoring breeding status of an endangered raptor. *Remote Sens. Ecol. Conserv.* 7, 550–561. doi: 10.1002/rse2.v7.3

Goldbogen, J. A., Cade, D. E., Calambokidis, J., Friedlaender, A. S., Potvin, J., Segre, P. S., et al. (2017). How baleen whales feed: the biomechanics of engulfment and filtration. *Annu. Rev. Mar. Sci.* 9, 367–386. doi: 10.1146/annurev-marine-122414-033905

Green, D. B., Titaud, O., Bestley, S., Corney, S. P., Hindell, M. A., Trebilco, R., et al. (2023). KRILLPODYM: a mechanistic, spatially resolved model of Antarctic krill distribution and abundance. *Front. Mar. Sci.* 10. doi: 10.3389/fmars.2023.1218003

Harris, J. M., Nelson, J. A., Rieucau, G., and Broussard, III WP (2019). Use of drones in fishery science. *Trans. Am. Fisheries Soc.* 148, 687–697. doi: 10.1002/tafs.2019.148.issue-4

Harvard, J., Hyvönen, M., and Wadbring, I. (2020). Journalism from above: drones and the media in critical perspective. *Media Communication* 8, 60–63. doi: 10.17645/mac.v8i3.3442

Häusermann, D., Bodry, S., Wiesemüller, F., Miriyev, A., Siegrist, S., Fu, F., et al. (2023). FireDrone: multi-environment thermally agnostic aerial robot. *Adv. Intell. Syst.* 5, 2300101. doi: 10.1002/aisy.202300101

Herr, H., Hickmott, L., Viquerat, S., and Panigada, S. (2022a). First evidence for fin whale migration into the Pacific from Antarctic feeding grounds at Elephant Island. *R. Soc. Open Sci.* 9, 220721. doi: 10.1098/rsos.220721

Herr, H., Kelly, N., Dorschel, B., Huntemann, M., Kock, K.-H., Lehnert, L. S., et al. (2019). Aerial surveys for Antarctic minke whales (Balaenoptera bonaerensis) reveal sea ice dependent distribution patterns. *Ecol. Evol.* 9, 5664–5682. doi: 10.1002/ece3.2019.9.issue-10

Herr, H., Viquerat, S., Devas, F., Lees, A., Wells, L., Gregory, B., et al. (2022b). Return of large fin whale feeding aggregations to historical whaling grounds in the Southern Ocean. *Sci. Rep.* 12, 9458. doi: 10.1038/s41598-022-13798-7

Hodgson, M. E. (2020). On the accuracy of low-cost dual-frequency GNSS network receivers and reference data. *GIScience Remote Sens.* 57, 907–923. doi: 10.1080/15481603.2020.1822588

Hodgson, A. J., Kelly, N., and Peel, D. (2023). Drone images afford more detections of marine wildlife than real-time observers during simultaneous large-scale surveys. *PeerJ* 11, e16186. doi: 10.7717/peerj.16186

Hodgson, A., Peel, D., and Kelly, N. (2017). Unmanned aerial vehicles for surveying marine fauna: assessing detection probability. *Ecol. Appl.* 27, 1253–1267. doi: 10.1002/eap.2017.27.issue-4

Howell, L. G., Clulow, J., Jordan, N. R., Beranek, C. T., Ryan, S. A., Roff, A., et al. (2022). Drone thermal imaging technology provides a cost-effective tool for landscape-scale monitoring of a cryptic forest-dwelling species across all population densities. *Wildlife Res.* 49, 66–78. doi: 10.1071/WR21034

Hyun, C.-U., Park, M., and Lee, W. Y. (2020). Remotely piloted aircraft system (RPAS)-based wildlife detection: A review and case studies in maritime Antarctica. *Animals* 10, 2387. doi: 10.3390/ani10122387

Johnston, D. R., Rayment, W., and Dawson, S. M. (2022). Morphometrics and body condition of southern right whales on the calving grounds at Port Ross, Auckland Islands. *Mamm. Biol.* 102, 1525–1536. doi: 10.1007/s42991-021-00175-6

Katsumata, T., and Yoshida, T. (2023). Development progress of a long-range vertical takeoff and landing UAV for the improvement of ship-based cetacean sighting surveys. *Cetacean Population Stud.* 4, 45–47. doi: 10.34331/cpops.2022O001

Kawaguchi, S., and Nicol, S. (2020). "Krill fishery," in Fisheries and aquaculture: Volume 9. Eds. G. Lovrich and M. Thiel (New York: Oxford Academic). doi: 10.1093/oso/9780190865627.003.0006 (accessed 17 Sept. 2024).

Kelly, N., Cox, M., Emmerson, L., Kawaguchi, S., Raymond, B., Southwell, C., et al. (2017). "Towards an ecological risk assessment of krill fishing in East Antarctica (CCAMLR Divisions 58.4.1 and 58.4.2)," in *Ecosystem Monitoring and Management Working Group, CCAMLR, WG-EMM-17/20*. (Hobart, Tasmania, Australia: Commission for the Conservation of Antarctic Marine Living Resources), 32pp.

Kelly, N., Emmerson, L., Kawaguchi, S., Southwell, C., and Welsford, D. (2018). "An ecological risk assessment of current conversation measures for krill fishing in East Antarctica," in *Ecosystem Monitoring and Management Working Group, CCAMLR, WG-EMM-18/37*. (Hobart, Tasmania, Australia: Commission for the Conservation of Antarctic Marine Living Resources), 27pp.

Kennedy, A. S., Carroll, E. L., Baker, C. S., Bassoi, M., Buss, D., Collins, M. A., et al. (2020). "Whales return to the epicentre of whaling? Preliminary results from the 2020 cetacean survey at South Georgia (Islas Georgias del Sur)," in *Paper presented to the Scientific Committee of the International Whaling Commission: SC/68B/CMP/22*. (Cambridge, UK: International Whaling Commission).

Koski, W. R., Gamage, G., Davis, A. R., Mathews, T., LeBlanc, B., and Ferguson, S. H. (2015). Evaluation of UAS for photographic re-identification of bowhead whales, *Balaena mysticetus*. *J. Unmanned Vehicle Syst.* 3, 22–29. doi: 10.1139/juvs-2014-0014

Lyu, M., Zhao, Y., Huang, C., and Huang, H. (2023). Unmanned aerial vehicles for search and rescue: A survey. *Remote Sens.* 15, 3266. doi: 10.3390/rs15133266

Mahadevan, P. (2010). The military utility of drones. *CSS Analyses Secur. Policy* 78, 1–3. doi: 10.3929/ethz-a-006253833

Matzka, J., Bronkalla, O., Tornow, K., Elger, K., and Stolle, C. (2021). *Geomagnetic Kp index. V. 1.0* (GFZ Data Services). doi: 10.5880/Kp.0001

Miller, B. S., Andrews-Goff, V., Barlow, J., Bell, E., Calderan, S., Double, M. C., et al. (2024). Antarctic sonobuoy surveys for blue whales from 2006-2021 reveal contemporary distribution, changes over time, and paths to further our understanding of their distribution and biology. *Front. Mar. Sci.* 11. doi: 10.3389/fmars.2024.1324816

Nowacek, D. P., Christiansen, F., Bejder, L., Goldbogen, J. A., and Friedlaender, A. S. (2016). Studying cetacean behaviour: new technological approaches and conservation applications. *Anim. Behav.* 120, 235–244. doi: 10.1016/j.anbehav.2016.07.019

Pallin, L., Bierlich, K. C., Durban, J., Fearnbach, H., Savenko, O., Baker, C. S., et al. (2022). Demography of an ice-obligate mysticete in a region of rapid environmental change. *R. Soc. Open Sci.* 9, 220724. doi: 10.1098/rsos.220724

Pfeifer, C., Barbosa, A., Mustafa, O., Peter, H.-U., Rümmler, M.-C., and Brenning, A. (2019). Using fixed-wing UAV for detecting and mapping the distribution and abundance of penguins on the South Shetlands Islands, Antarctica. *Drones* 3, 39. doi: 10.3390/drones3020039

Pina, P., and Vieira, G. (2022). UAVs for science in Antarctica. *Remote Sens.* 14, 1610. doi: 10.3390/rs14071610

Pirotta, V., Hocking, D. P., Iggleden, J., and Harcourt, R. (2022). Drone observations of marine life and human-wildlife interactions off Sydney, Australia. *Drones* 6 (3), 75. doi: 10.3390/drones6030075

Pirotta, V., Smith, A., Ostrowski, M., Russell, D., Jonsen, I. D., Grech, A., et al. (2017). An economical custom-built drone for assessing whale health. *Front. Mar. Sci.* 4. doi: 10.3389/fmars.2017.00425

Ramp, C., Gaspard, D., Gavrilchuk, K., Unger, M., Schleimer, A., Delarue, J., et al. (2021). Up in the air: drone images reveal underestimation of entanglement rates in large rorqual whales. *Endangered Species Res.* 44, 33–44. doi: 10.3354/esr01084

R Core Team (2023). *R: A language and environment for statistical computing* (Vienna, Austria: R Foundation for Statistical Computing). Available at: https://www.R-project.org/.

Ryan, K. P., Ferguson, S. H., Koski, W. R., Young, B. G., Roth, J. D., and Watt, C. A. (2022). Use of drones for the creation and development of a photographic identification catalogue for an endangered whale population. *Arctic Sci.* 8 (4), 1191–1201.doi: 10.1139/as-2021-0047

Savoca, M. S., Czapanskiy, M. F., Kahane-Rapport, S. R., Gough, W. T., Fahlbusch, J. A., Bierlich, K. C., et al. (2021). Baleen whale prey consumption based on high-resolution foraging measurements. *Nature* 599, 85–90. doi: 10.1038/s41586-021-03991-5

Schoonmaker, J., Wells, T., Gilbert, G., Podobna, Y., Petrosyuk, I., and Dirbas, J. (2008). "Spectral detection and monitoring of marine mammals," in *Proc. SPIE 6946, Airborne Intelligence, Surveillance, Reconnaissance (ISR) Systems and Applications V*, 694606 (14 April 2008). doi: 10.1117/12.777740

Shahmoradi, J., Mirzaeinia, A., Roghanchi, P., and Hassanalian, M. (2020). "Monitoring of inaccessible areas in GPS-denied underground mines using a fully autonomous encased safety inspection drone," in *AIAA 2020-1961. AIAA Scitech 2020 Forum. January 2020.*

Shelare, S. D., Aglawe, K. R., Waghmare, S. N., and Belkhode, P. N. (2021). Advances in water sample collections with a drone – a review. *Materials Today: Proc.* 47, 4490–4494. doi: /10.1016/j.matpr.2021.05.327

Sheridan, I. (2020). Drones and global navigation satellite systems: Current evidence from polar scientists. *R. Soc. Open Sci.* 7, 191494. doi: 10.1098/rsos.191494

Stewart, B. S., Karl, S. A., Yochem, P. K., Leatherwood, S., and Laake, J. L. (1987). Aerial surveys for cetaceans in the former Akutan, Alaska, whaling grounds. *Arctic* 40, 33–42. doi: 10.14430/arctic1744

Torres, L. G., Nieukirk, S. L., Lemos, L., and Chandler, T. E. (2018). Drone up! Quantifying whale behavior from a new perspective improves observational capacity. *Front. Mar. Sci.* 5. doi: 10.3389/fmars.2018.00319

Varela-Jaramillo, A., Rivas-Torres, G., Guayasamin, J. M., Steinfartz, S., and MacLeod, A. (2023). A pilot study to estimate the population size of endangered Galápagos marine iguanas using drones. *Front. Zool.* 20, 4. doi: 10.1186/s12983-022-00478-5

Vargas Tamayo, L., Thron, C., Fendji, J. L. K. E., Thomas, S.-K., and Förster, A. (2020). Cost-minimizing system design for surveillance of large, inaccessible agricultural areas using drones of limited range. *Sustainability* 12, 8878. doi: 10.3390/su12218878

Wang, C.-Y., Zhang, G., Ge, S., Xu, T., Ji, Y., Yang, X.-G., et al. (2016). Lithium-ion battery structure that self-heats at low temperatures. *Nature* 529, 515–518. doi: 10.1038/nature16502

Weinstein, B. G., Double, M., Gales, N., Johnston, D. W., and Friedlaender, A. S. (2017). Identifying overlap between humpback whale foraging grounds and the Antarctic krill fishery. *Biol. Conserv.* 210, 184–191. doi: 10.1016/j.biocon.2017.04.014

Werth, A. J., Kosma, M. M., Chenoweth, E. M., and Straley, J. M. (2019). New views of humpback whale flow dynamics and oral morphology during prey engulfment. *Mar. Mammal Sci.* 35, 1556–1578. doi: 10.1111/mms.12614

Wiley, D. N., Zadra, C. J., Friedlaender, A. S., Parks, S. E., Pensarosa, A., Rogan, A., et al. (2023). Deployment of biologging tags on free swimming large whales using uncrewed aerial systems. *R. Soc. Open Sci.* 10, 221376. doi: 10.1098/rsos.221376

Xi, Z., Lou, Z., Sun, Y., Li, X., Yang, Q., and Yan, W. (2018). "*A* vision-based inspection strategy for large-scale photovoltaic farms using an autonomous UAV," in *2018 17th International Symposium on Distributed Computing and Applications for Business Engineering and Science (DCABES)*, Wuxi, China, pp. 200–203. doi: 10.1109/DCABES.2018.00059.

Young, B. G., Koski, W. R., Kilabuk, R., Watt, C. A., Ryan, K. P., and Ferguson, S. H. (2022). Collaborative field research using drones for whale photo-identification studies in Cumberland Sound, Nunavut. *Drone Syst. Appl.* 10, 256–265. doi: 10.1139/dsa-2021-0026

Zhang, H., Turvey, S. T., Pandey, S. P., Song, X., Sun, Z., and Wang, N. (2023). Commercial drones can provide accurate and effective monitoring of the world's rarest primate. *Remote Sens. Ecol. Conserv.* 9, 775–786. doi: 10.1002/rse2.341

Zheng, Y., Zheng, F., Yang, C., Nie, G., and Li, S. (2022). Analyses of GLONASS and GPS+GLONASS precise positioning performance in different latitude regions. *Remote Sens.* 14, 4640. doi: 10.3390/rs14184640

Zmarz, A., Rodzewicz, M., Dąbski, M., Karsznia, I., Korczak-Abshire, M., and Chwedorzewska, K. J. (2018). Application of UAV BVLOS remote sensing data for multi-faceted analysis of Antarctic ecosystem. *Remote Sens. Environ.* 217, 375–388. doi: 10.1016/j.rse.2018.08.031

frontiers | Frontiers in Marine Science

TYPE Original Research
PUBLISHED 04 October 2024
DOI 10.3389/fmars.2024.1456207

Check for updates

OPEN ACCESS

EDITED BY
Zhaomin Wang,
Hohai University, China

REVIEWED BY
Andrew Meijers,
British Antarctic Survey (BAS),
United Kingdom
Chengyan Liu,
Southern Marine Science and Engineering Guangdong Laboratory (Zhuhai), China

*CORRESPONDENCE
Annie Foppert
annie.foppert@utas.edu.au

RECEIVED 01 July 2024
ACCEPTED 23 August 2024
PUBLISHED 04 October 2024

CITATION
Foppert A, Bestley S, Shadwick EH, Klocker A, Vives CR, Liniger G and Westwood KJ (2024) Observed water-mass characteristics and circulation off Prydz Bay, East Antarctica. *Front. Mar. Sci.* 11:1456207. doi: 10.3389/fmars.2024.1456207

COPYRIGHT
© 2024 Foppert, Bestley, Shadwick, Klocker, Vives, Liniger and Westwood. This is an open-access article distributed under the terms of the Creative Commons Attribution License (CC BY). The use, distribution or reproduction in other forums is permitted, provided the original author(s) and the copyright owner(s) are credited and that the original publication in this journal is cited, in accordance with accepted academic practice. No use, distribution or reproduction is permitted which does not comply with these terms.

Observed water-mass characteristics and circulation off Prydz Bay, East Antarctica

Annie Foppert[1,2]*, Sophie Bestley[1,2], Elizabeth H. Shadwick[1,3], Andreas Klocker[2,4], Clara R. Vives[2,5,6,7], Guillaume Liniger[2,5,8] and Karen J. Westwood[1,7]

[1]Australian Antarctic Program Partnership, Hobart, TAS, Australia, [2]Institute for Marine and Antarctic Studies, University of Tasmania, Hobart, TAS, Australia, [3]Environment, CSIRO, Hobart, TAS, Australia, [4]NORCE Norwegian Research Centre, Bjerknes Centre for Climate Research, Bergen, Norway, [5]Australian Research Council Centre of Excellence for Climate Extremes, University of Tasmania, Hobart, TAS, Australia, [6]Globe Institute, University of Copenhagen, Copenhagen, Denmark, [7]Australian Antarctic Division, Department of Climate Change, Energy, the Environment and Water, Kingston, TAS, Australia, [8]Monterey Bay Aquarium Research Institute, Moss Landing, CA, United States

Circulation and water masses in the greater Prydz Bay region were surveyed in the austral summer 2021 (January-March) during the 'Trends in *Euphausiids* off Mawson, Predators and Oceanography' (TEMPO) experiment, and are described in this paper. The Southern Antarctic Circumpolar Current Front is found in the northern part of the survey area, generally near 63-64°S, whereas the Southern Boundary Front is located between 64 and 65.5°S. The westward flowing Antarctic Slope Front (ASF) is found in the southern part of the survey area near the continental slope on most transects. Highest concentrations of oxygen (> 300 μmol kg^{-1}) are found in shelf waters at stations in Prydz Bay, south of 67°S along 75°E, whereas the lowest oxygen values are found in the Circumpolar Deep Water layer, with an average of roughly 215 μmol kg^{-1}. North of the northern extension of the ASF, surface mixed layers are between 20 and 60 m deep. Mixed layers tend to deepen slightly in the northern part of the survey, generally increasing north of 64°S where the ocean has been ice-free the longest. We find evidence of upwelling of waters into the surface layers, based on temperature anomaly, particularly strong along 80°E. Enhanced variability of biogeochemical properties - nutrients, DIC, DO - in the AASW layer is driven by a combination of sea-ice and biological processes. Antarctic Bottom Water, defined as water with neutral density > 28.3 kg m^{-3}, was sampled at all the offshore full-depth stations, with a colder/fresher variety along western transects and a warmer/saltier variety in the east. Newly formed Antarctic Bottom Water – the coldest, freshest, and most recently ventilated – is mostly found in the deep ocean along 65°E, in the base of the Daly Canyon.

KEYWORDS

Southern Ocean fronts, Antarctic margin, Prydz Bay Gyre, water masses, Antarctic Bottom Water, carbon cycling, summer stratification, upwelling

1 Introduction

The Southern Ocean plays a crucial role in Earth's climate system through the modulation of the global meridional overturning circulation, global biogeochemical cycling, and biological productivity (Rintoul, 2018; Henley et al., 2020). The upwelling of nutrient-rich deep water supports primary production and the Southern Ocean ecosystem as a whole. The strong seasonal cycle in the upper ocean – dominated by the yearly growth and melt of sea ice – is a major control on light and phytoplankton growth, thereby influencing Southern Ocean ecosystem structure and function. The formation and export of Antarctic Bottom Water makes up a crucial limb of the meridional overturning circulation that is critical for the sequestration of anthropogenic heat and carbon, and the ventilation of the deep ocean.

Within the Southern Ocean, the eastward flowing Antarctic Circumpolar Current (ACC) connects all three major ocean basins, and separates the warm subtropical waters from the cold polar waters to the south (Orsi et al., 1995). The circumpolar flow of the ACC is steered by major bathymetric features, leading to complex circulation at the regional scale with localized hot spots of poleward heat fluxes and upwelling (Foppert et al., 2017; Tamsitt et al., 2017), and some recirculation within regional-scale subpolar gyres and smaller scale subgyres (McCartney and Donohue, 2007; Yamazaki et al., 2020). The greater Prydz Bay Gyre is located in the Indian Ocean sector within the Weddell-Enderby basin ~55-80°E. This area lies to the east of the Weddell Gyre extension and to the southwest of the southern Kerguelen Plateau. Here, the two southernmost ACC fronts, the Southern ACC Front (SACCF) and Southern Boundary (SB) intrude into the domain from the northwest, and are steered southward by the Kerguelen Plateau and through the Princess Elizabeth Trough (e.g. Heywood et al., 1999). The subpolar gyre is partially closed by the westward flow of the Antarctic Slope Current along the Antarctic shelf break and continental slope. The regional circulation, alongside upper-ocean structure, plays an important role in structuring regional productivity and the marine ecosystem.

Within Prydz Bay, the Amery Ice shelf is also an important regional feature, feeding shelf and ice-shelf water into the survey region. These waters play an important preconditioning role (Herraiz-Borreguero et al., 2016; Williams et al., 2016), supporting a known region of Antarctic Bottom Water (AABW) formation at Cape Darnley Polynya on the western side of the bay (Ohshima et al., 2013). Recent work by Blackensee et al. (in review)[1] provides a detailed review of AABW formation at Cape Darnley using a suite of available observations. Overall, the area between 55-80°E is known to be highly productive (Westwood et al., 2010; Wright et al., 2010; Pinkerton et al., 2021; Heidemann et al., 2024), especially relative to the overall Southern Ocean. While the Antarctic Slope Front (ASF) primarily acts as a barrier between shelf and oceanic environments, and the export of waters offshore from Prydz Bay, the additional influence of the West Ice Shelf near 80°E, and the interaction of fronts with the submarine Kerguelen Plateau (Bestley et al., 2018; Schallenberg et al., 2018) all serve to support heightened regional productivity.

In the Southern Ocean, phytoplankton growth is primarily limited by light and micro-nutrient availability, mainly iron (Nelson and Smith Jr., 1991; Boyd and Ellwood, 2010; Feng et al., 2010; Vives et al., 2022; Bazzani et al., 2023) and in some cases manganese (Latour et al., 2021). Characterization of the upper-ocean is therefore important when considering drivers that may influence productivity. Offshore, Circumpolar Deep Water (CDW) is the primary source of nutrients to surface waters through upwelling, with lateral advection also suggested for the Kerguelen Plateau region (Schallenberg et al., 2018). Closer to the Antarctic coast, melting sea ice, sediment resuspension, and melting glaciers and ice shelves may serve as additional nutrient inputs, leading to increased primary productivity (Westwood et al., 2010; Lannuzel et al., 2016; Dinniman et al., 2020; Smith et al., 2021; Herraiz-Borreguero et al., 2016). Light availability is largely controlled by mixed layer depths and sea ice cover, both of which are strongly influenced by the melting and formation of sea ice (e.g. Williams et al., 2010). Phytoplankton circulating in shallow mixed layers receive significantly higher light doses than those in deep mixed layers Morel (1991); Morel and Maritorena (2001). The ratio of mixed layer depth to euphotic depth also determines the extent to which phytoplankton are photo-limited (Westwood et al., 2010). At the retreating ice edge, light doses can be particularly high due to the formation of a meltwater lens that shallows the mixed layer (Arrigo et al., 2012). Thus, seasonal sea-ice retreat is particularly important for phytoplankton growth in the Southern Ocean.

The seasonal formation and melt of sea ice also exerts a dominant control on the carbonate chemistry of surface waters in Antarctic coastal regions (e.g. Roden et al., 2013; Shadwick et al., 2014), and contributes to the large seasonal variability observed there (e.g. Bates et al., 1998; DeJong et al., 2017). As described above, the return of sunlight in austral spring triggers the onset of under-ice and open water phytoplankton blooms (e.g. Arrigo and van Dijken, 2003; Sweeney, 2003), which convert inorganic carbon to organic carbon and promote the uptake of atmospheric CO2 (e.g. Shadwick et al., 2013). The delivery of carbon-rich CDW to the surface and/or the continental shelf influences the seasonality of the carbonate system, as does subsurface respiration of organic material produced during the productive season, with the balance of these processes determining the size of the ocean sink for CO2 in these regions (e.g. Arroyo et al., 2019; Roden et al., 2016; Shadwick et al., 2014).

This work describes the water-mass characteristics and frontal structure in the greater Prydz Bay region (55-80°E and south of 62°S) based on oceanography data collected during the 'Trends in *Euphausiids* off Mawson, Predators and Oceanography' (TEMPO) voyage in the austral summer of 2021. Section 2 describes the multidisciplinary survey, which repeated the eastern part of the BROKE-West survey (Meijers et al., 2010; Williams et al., 2010) at higher spatial resolution. Physical and biogeochemical water-mass properties and distribution of the regional oceanographic fronts are presented in Sections 3.2 and 3.3, respectively. Upper-ocean structure

1 Blackensee, S. N., Gwyther, D. E., Galton-Fenzi, B. K., Gunn, K. L., Herraiz-Borreguero, L., Ohshima, K. I., et al. A review of the oceanography and Antarctic Bottom Water formation offshore Cape Darnley, East Antarctica. *J. Geophysical Research: Oceans*.

and its spatial variability is detailed in Section 3.4. Section 3.5 describes deep ocean properties and inferred pathways of locally formed Antarctic Bottom Water. This paper provides the physical environmental context for the TEMPO survey, including biogeochemical components (oxygen, carbon, nutrients), and discusses the system state in 2021 compared with the BROKE-West survey 15 years prior (Section 4).

2 Data and methods

2.1 Oceanographic survey

Data for this study were collected on the R/V *Investigator* in the austral summer of 2021, between January and March. The TEMPO survey occupied 66 stations mainly along six north-south transects in the greater Prydz Bay region. We surveyed from 62°S or 63°S to the Antarctic slope, every 5° of longitude from 55°E to 80°E (Figure 1), as well as a few stations offset from the main transect lines. Along 75°E, the survey extended well into Prydz Bay, to 68°S. Note that the R/V *Investigator* does not have ice-breaking capabilities, so the survey extended no further than the sea-ice edge and all stations can be considered to be in the seasonal ice zone. The maximum depth of the profiles varied throughout the survey region, with one to roughly 300 dbar in a krill super-swarm (slightly east of the 75°E line), nine to 1500 dbar, three to 2250 dbar, and 52 to full-depth (i.e. within 5-10 m from the seafloor). Shallow profiles (i.e. those not sampling to full-depth) are shown as white dots in Figure 1.

Conductivity-temperature-depth (CTD, SBE9plus) profiles were collected at all stations and calibrated onboard against bottle samples to meet the Global Ocean Ship-based Hydrographic Investigations Program (GO-SHIP) standards; the accuracies of temperature and salinity were 0.002°C and 0.002 psu, respectively. Similarly, sensor measurements of dissolved oxygen (μmol l^{-1}) were made with an SBE43 optode sensor and are within 1% of measurements on discrete bottle samples. This study also presents macro-nutrients (μmol l^{-1}) – including nitrate (NO_3, 1160 samples) and silicate (Si, 1164 samples) – from discrete bottle measurements following methods described in Rees et al. (2019). We convert the DO and nutrient data from μmol l^{-1} to μmol kg^{-1} based on potential density of the seawater referenced to the surface (σ_0).

Measurements of dissolved inorganic carbon (DIC, 508 samples) and total alkalinity (TA, 287 samples) were made for samples collected at discrete bottle depths. After sampling, a saturated solution of mercuric chloride was used to preserve the samples. The concentrations of DIC and TA were determined by coulometric and potentiometric titration, respectively following established procedures at CSIRO in Hobart (e.g. Dickson et al., 2007). All analyses were referenced to certified materials and have

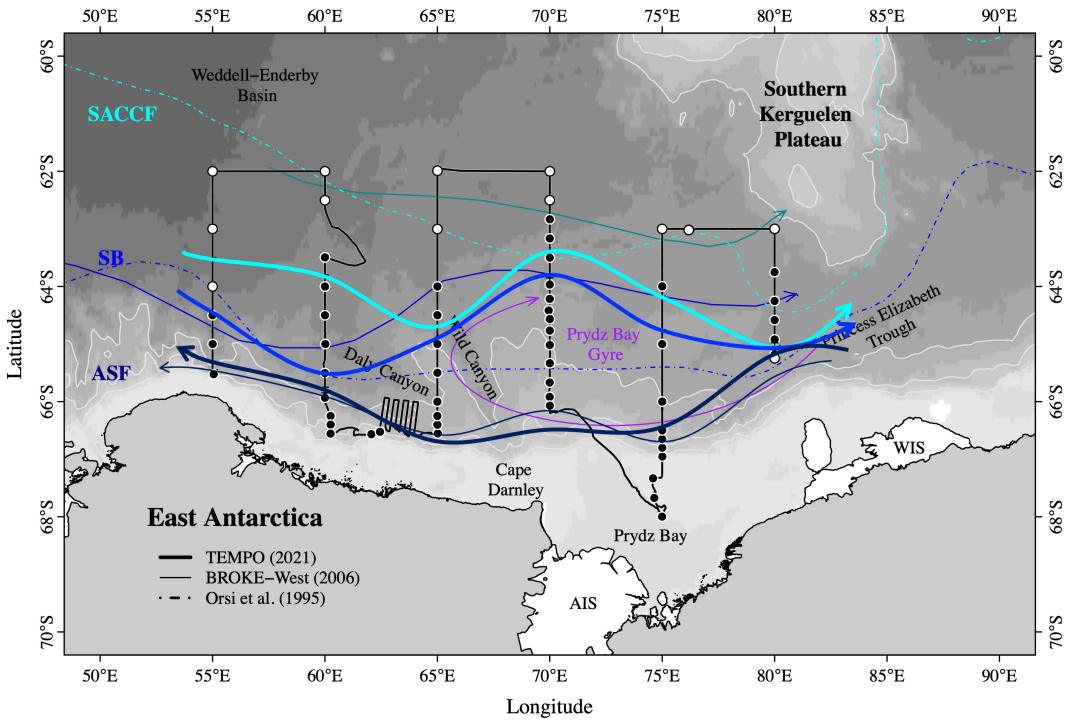


FIGURE 1
Map of the TEMPO survey region. Cruise track (black) proceeded from west to east 55-80°E. CTD station locations (circles) indicate full depth (black) and shallow (white) casts. Location of regional oceanic features compiled from this and previous studies. Major fronts shown include: the Antarctic Slope Front (ASF), the Southern Boundary (SB) and the Southern ACC Front (SACCF). Fronts are grouped by color with the line styles indicating associated references (bold lines – this study; dashed lines – Orsi et al. (1995); solid lines – BROKE-West (Meijers et al., 2010)). Background displays bathymetry at 500m intervals, with the 1000m, 2000m and 3000m isobaths (white contours) highlighting the submarine Southern Kerguelen Plateau and the Antarctic shelf break and foot of slope. Major geographical features are named, with the Antarctic continent and major ice features shown in grey and white, respectively. AIS, Amery Ice Shelf; WIS, West Ice Shelf.

uncertainty (accuracy and precision) of less than 2 μmol kg^{-1}. While a detailed partitioning of variability in DIC and TA across physical and biological drivers are beyond the scope of this work, some evaluation of these processes was done via the normalization to a constant salinity. Salinity-normalized DIC and TA (nDIC and nTA) were computed using a reference salinity of 35 (e.g. Friis et al., 2003; Shadwick et al., 2014). Additionally, once corrected for changes in salinity (which we are here assuming accounts for changes in horizontal and vertical mixing), potential alkalinity (pTA) was computed following Brewer and Goldman (1976), allowing relative variations in DIC and TA to be evaluated in the context of photosynthesis (respiration) and calcium carbonate ($CaCO_3$) formation (dissolution).

Horizontal ocean current velocities were measured by a hull-mounted shipboard Acoustic Doppler Current Profiler (SADCP, RDI Ocean Surveyor 150kHz). The data were collected and post-processed onboard using the University of Hawaii's Data Acquisition System (UHDAS) and the Data and Common Ocean Data Access System (CODAS), respectively. We only analyze velocity data while on station, and quasi-stationary, as the SADCP had reduced ping frequency – and therefore reduced data quality – during transit between stations when it was synchronized to the EK80 echo sounder for the krill biomass survey. We present zonal velocity data, averaged over the time the ship was on station, in the upper 350 m where the data is of high quality. We have not performed any detiding procedure on the data, as previous studies have observed tidal velocities to be small and have minimal impact on the velocity structure in the region, including both offshore in greater Prydz Bay (Meijers et al., 2010) and the continental slope and shelf (Ohshima et al., 2013; Liu et al., 2023)

2.2 Environmental data

We use satellite remote sensing data, synoptically available over greater spatial and temporal scales, to contextualize the TEMPO survey. We investigate how the seasonal cycle in 2020/2021 compared with other years by looking at area average monthly climatologies of sea-ice concentration (SIC; Cavalieri et al., 1996; http://nsidc.org) and chlorophyll-a (Chla; ESA Globcolour; https://www.globcolour.info/). SIC and Chla data have 25-km and 4-km spatial resolution, respectively. Monthly climatological Chla and SIC time series spanning 1998 to 2021 were calculated by averaging over the study area for each month (latitude ranging from 69°S to 61°S and longitude ranging from 54°E to 81°E). Monthly Chla and SIC timeseries for 2020/2021 were similarly calculated over the same region.

Sea surface temperature (SST) provides information about the spatial structure of the surface ocean. We use monthly Optimum Interpolation Sea Surface Temperature (OISST.v2) high resolution dataset (0.25°) from the National Oceanic and Atmospheric Administration (Banzon et al., 2016).

The 2-minute gridded bathymetry dataset of ETOPO2v2, available from NOAA's National Centers for Environmental Information (National Geophysical Data Center, N, 2006), provides seafloor depth in the region.

3 Results

3.1 Oceanographic setting

Water masses that were sampled during the TEMPO survey are Antarctic Surface Water (AASW), Circumpolar Deep Water (CDW) and modified CDW (mCDW), Antarctic Bottom Water (AABW), and Shelf Water (SW). Water masses are defined based on temperature and density criteria, as listed in Table 1. Several previous studies have defined the regional water masses in this area (e.g. Meijers et al., 2010; Bestley et al., 2020), each with slightly different definitions based on a combination of density, temperature, salinity, and dissolved oxygen concentration thresholds. Here, we use these studies as a guide and choose definitions accordingly. In the East Antarctic, the 1.5°C isotherm is typically used to demarcate between CDW and mCDW, with mCDW being colder. In this study, we discuss CDW and mCDW together as CDW/mCDW. Some shelf studies have gone further to include a heavily modified CDW with waters as cold as -1.85°C, distinct from Ice Shelf Water that is below the surface freezing point (e.g. Herraiz-Borreguero et al., 2015, 2016; Williams et al., 2016). As we have very few stations on the shelf in Prydz Bay, we use a more generic definition of SW that does not distinguish between heavily modified CDW, Ice Shelf Water, and Dense Shelf Water. Given the limited data on the shelf collected during TEMPO, our focus is on data from the slope and farther offshore; a recent review of observed water-mass properties on the shelf in this region can be found in Blackensee et al. (in review)[1]. AASW is defined here as all waters with $\gamma^N > 28.0$ kg m^{-3}. In the northern part of our study region, i.e. generally north of the Southern Boundary, this includes water with characteristics in the subsurface temperature-maximum layer that are typical of Upper CDW, whereas in the southern part of our study region, this includes water in the subsurface temperature-minimum layer. For simplicity and consistency with other studies, we do not make a latitudinal distinction when describing this water mass. However, we examine specific properties of the layers important in setting the summer stratification when investigating the spatial variability of upper-ocean properties, rather than using density-based definitions (Section 3.4).

The Southern Ocean fronts relevant to this work are the Southern ACC Front (SACCF), Southern Boundary Front (SB), and Antarctic Slope Front (ASF). Table 2 summarizes the frontal definitions that we use and their observed locations throughout the TEMPO survey region. We define the SACCF and SB as the

TABLE 1 Definitions of water masses sampled during the TEMPO survey.

	γ^N[kg m^{-3}]	CT [°C]
AASW	$\gamma^N < 28.0$	
CDW/mCDW	$28.0 < \gamma^N < 28.3$	$CT > -1.6$
AABW	$\gamma^N > 28.3$	$CT > -1.6$
SW	$28.0 > \gamma^N$	$CT < -1.6$

AASW, Antarctic Surface Water; CDW, Circumpolar Deep Water; mCDW, modified CDW; AABW, Antarctic Bottom Water; SW, Shelf Water.

TABLE 2 Locations of the Southern Ocean fronts sampled during the TEMPO survey.

	SACCF (CT_{max} = 1.8°C)	SB (CT_{max} = 1.5°C)	ASF-N (0°C at 200 m)	ASF (0°C at 400 m)
55°E	63.5°S	64.45°S	65.22°S	65.3°S
60°E	63.8°S	65.53°S	65.7°S	65.85°S
65°E	64.5°S	64.68°S	64.9°S	–
70°E	63.38°S	63.85°S	–	–
75°E	64.17°S	64.75°S	65.55	66.5
80°E	64.925	64.98	65.05	65.05

Frontal definitions are in parentheses below the front names. SACCF, Southern Antarctic Circumpolar Current Front; SB, Southern Boundary; ASF-N, northern limit of the ASF; and ASF, Antarctic Slope Front.

southernmost location where the subsurface temperature maximum equals 1.8°C and 1.5°C, respectively. These definitions are based on Meijers et al. (2010), who refined the circumpolar definitions of Orsi et al. (1995) for this region. We further refine the frontal definitions of Meijers et al. (2010), and consider the ASF to be where the base of the Winter Water layer (i.e. where the 0°C isotherm below the temperature minimum) reaches 400 m depth. We define the northern limit of the ASF (ASF-N) – which is relevant for biological studies and ecosystem processes – as the location where the base of the temperature minimum layer reaches 200 m depth.

Satellite remote sensing data provide a regional perspective of the greater Prydz Bay area during TEMPO (Figure 2). There are large surface blooms of chlorophyll-a (Chla) in the western and eastern parts of the study region, with low values of 0.1 mg m^{-3} found at 65°E and 70°E (Figure 2A). The largest values of Chla, reaching 5 mg m^{-3}, are found along the 75°E and 80°E. Here, elevated SST values are found further south than in the western part of the survey, with values of 0.5°C found near 66°S on the 75°E transect (Figure 2B). There are also lower sea-ice concentrations (SIC < 20%) near the mouth of Prydz Bay relative to the other coastal regions where SIC reaches 80% (Figure 2C).

The satellite observations of surface conditions during TEMPO are very close to the long-term climatologies of Chla and SIC for this region (Figure 3). There were no major anomalies evident leading up to, during, or immediately following the 2021 survey. Chla and SIC in February 2021 were slightly higher and lower, respectively, than climatological February values over the previous 24 years (Figure 3). Further, regional Chla and SIC are very close to historical record all year-round, and both can be considered normal for the 2020/2021 season. April 2021 Chla values are an exception, with slightly elevated values compared to the historical record, however, satellite observations are very limited during April as the sea ice expands and covers the ocean surface.

3.2 Water-mass characteristics

Figure 4A shows the temperature and salinity distribution observed in the CTD data throughout the entire survey area, colored by DO concentrations. The AASW layer at the ocean's surface is the lightest water mass, defined as waters lighter than 28.0 kg m^{-3}. It is the freshest of all the regional water masses and spans the largest temperature range (Figure 4A; Table 3). Across the survey region, AASW exhibits the highest oxygen concentrations (with local concentrations > 300 μmol kg^{-1}) and freshest salinities (SA < 34 g kg^{-1}). Very fresh waters were found along 60°E and 80°E (SA < 33 g kg^{-1}), associated with a surface meltwater lens from recent sea-ice melt. The variability of biogeochemical properties-nutrients, DIC, DO - is highest in the AASW layer (Table 3), reflecting the seasonal variations in these properties. This variability is driven by a combination of sea-ice processes (e.g. ice melt that also drives the large variations in salinity seen in the AASW) and biological processes (phytoplankton growth consuming inorganic carbon and nutrients to produce organic carbon).

Property plots of DIC, TA, salinity-normalized DIC (nDIC) and potential alkalinity (pTA) are shown in Figure 5. The relationship

TABLE 3 Mean water-mass characteristics, as observed during the TEMPO survey, with uncertainty represented by the standard deviation.

	AASW (*n* =63)	CDW/mCDW (*n* =47)	AABW (*n* =39)	SW (*n* =3)
γ^N [kg m^{-3}]	27.795 ± 0.047	28.191 ± 0.031	28.321 ± 0.010	28.208 ± 0.010
CT [°C]	-0.008 ± 1.227	0.391 ± 0.302	-0.288 ± 0.064	-1.838 ± 0.056
SA [g kg^{-1}]	34.503 ± 0.128	34.846 ± 0.038	34.831 ± 0.006	34.647 ± 0.006
DO [μmol kg^{-1}]	256.6 ± 43.7	215.1 ± 12.7	230.9 ± 4.1	313.8 ± 2.5
Thickness [m]	327 ± 134	2198 ± 672	657 ± 315	249 ± 15
Nitrate [μmol kg^{-1}]	28.9 ± 4.2	31.9 ± 0.5	32.3 ± 0.4	30.6 ± 0.3
Silicate [μmol kg^{-1}]	55.2 ± 23.0	106.6 ± 14.3	126.9 ± 12.8	67.9 ± 5.7
DIC [μmol kg^{-1}]	2197.9 ± 43.6	2255.6 ± 4.6	2256.5 ± 2.8	2239.1 ± 7.5
TA [μmol kg^{-1}]	2302.3 ± 25.21	2352.8 ± 6.0	2353.1 ± 2.6	2332.0 ± 2.4

The number of profiles included in the averages are shown in parentheses next to the water mass. Note that only profiles that sampled to the base of the water mass was included. AASW, Antarctic Surface Water; CDW, Circumpolar Deep Water; mCDW, modified CDW; AABW, Antarctic Bottom Water; SW, Shelf Water.

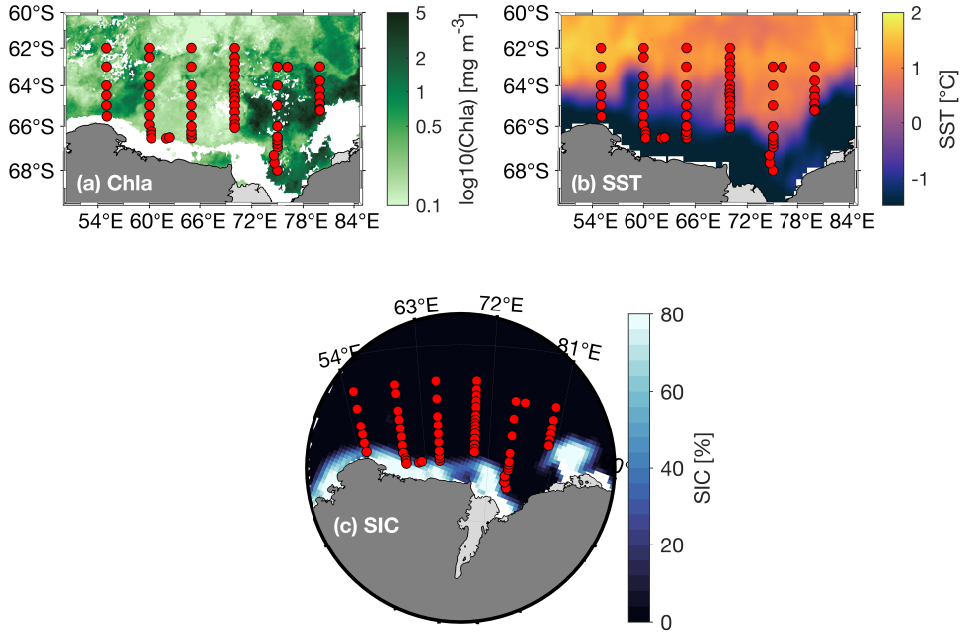


FIGURE 2
Regional remote sensing in February 2021: **(A)** Chlorophyll-a (Chla), **(B)** sea surface temperature (SST), and **(C)** sea-ice concentration (SIC). The red dots indicate the CTD sampling locations as in Figure 1. Note that SST data are present even in high sea-ice conditions because of the product that we used, which was gap-free interpolated.

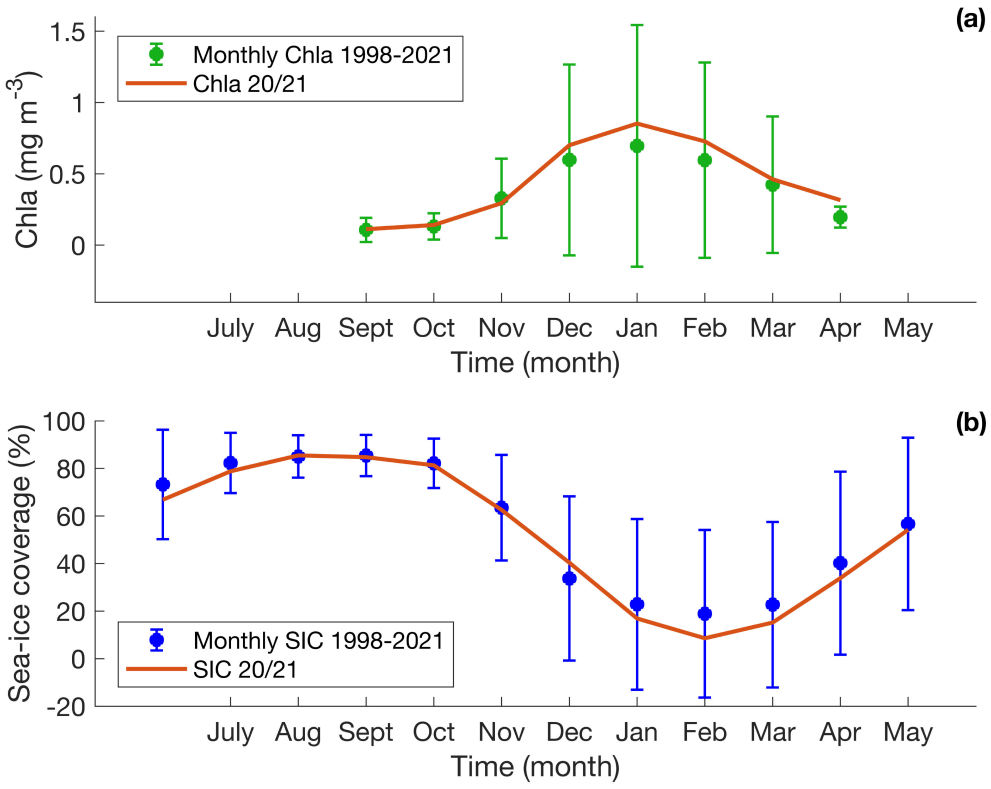


FIGURE 3
Monthly climatologies of **(A)** chlorophyll-a (Chla) and **(B)** sea-ice concentration (SIC) in the region defined as 61-69°S and 54-81°E during the 1998-2021 time period. The error bars represent the monthly standard deviation. The solid red lines represent the 2021 time series, showing that surface Chla and SIC state during the TEMPO voyage fit well within the historical spread.

10.3389/fmars.2024.1456207

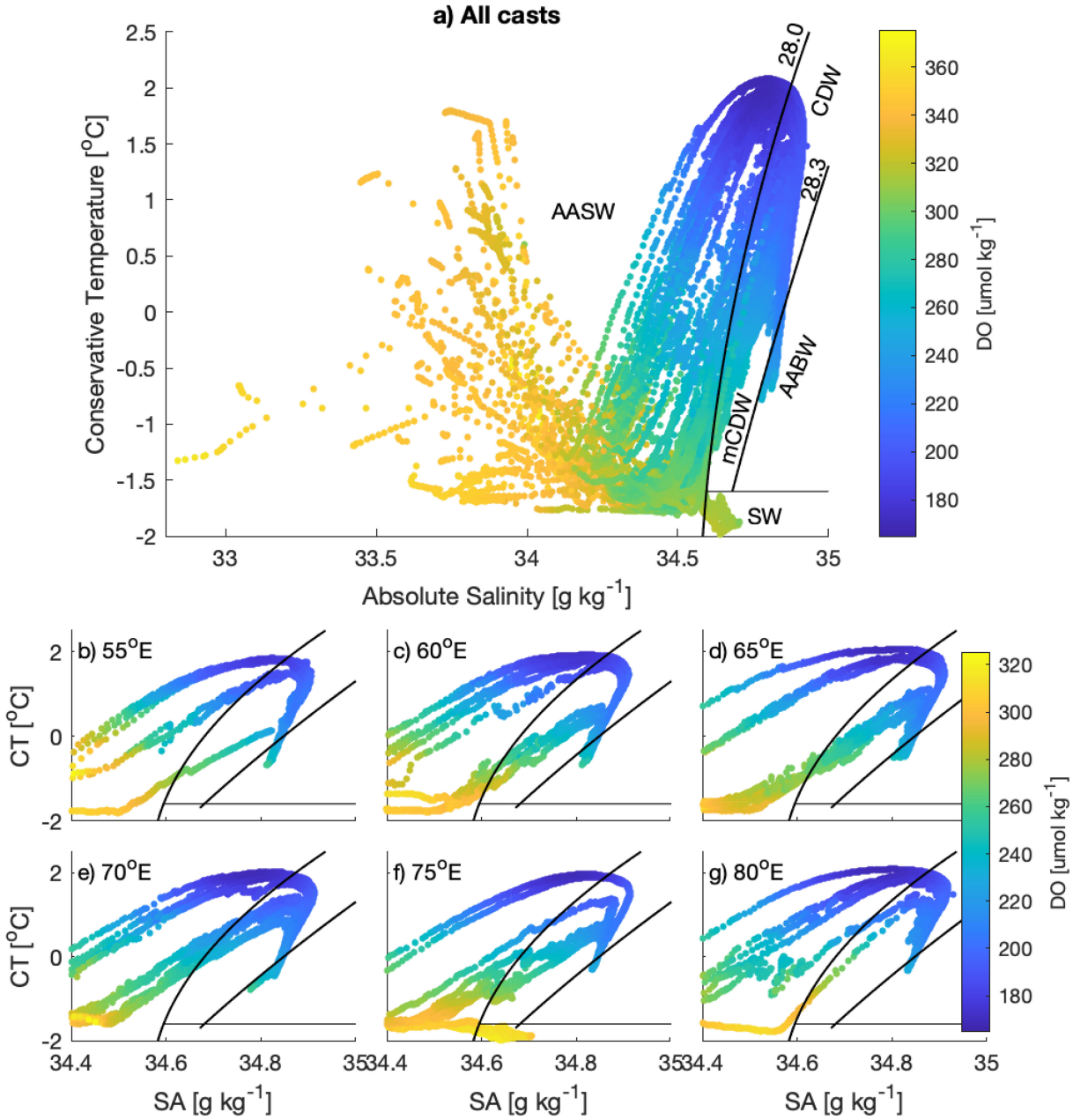


FIGURE 4
Temperature-salinity diagrams colored by dissolved oxygen concentrations (DO, [μmol kg^{-1}]). **(A)** All profiles over the entire survey. **(B–G)** Profiles along individual transects. Note the different colorbar for the transect panels. Neutral density contours (γ^N =28 and 28.3 kg m^{-3}) are drawn in each panel and labelled in **(A)** The -1.6°C isotherm is also shown in waters denser than 28 kg m^{-3} to distinguish Shelf Water (SW). Water masses, as defined in Table 1, are labelled in **(A)** Antarctic Surface Water (AASW), Circumpolar Deep Water (CDW), modified Circumpolar Deep Water (mCDW), Antarctic Bottom Water (AABW), and Shelf Water (SW).

between TA and salinity is nearly conservative, as seen by its near-linear dependence, with low TA values associated with low salinity found in the upper ocean (Figure 5B). The relationship between DIC and salinity is similar, though the influence of biological processes, particularly in the AASW as described above, results in larger variability with respect to salinity (Figure 5A). The relationship between salinity normalized DIC and potential TA in the upper ocean indicates a dominance of photosynthesis which reduces nDIC without changing the pTA (Figure 5D), and causes the variable concentrations of both parameters in the AASW (relative to deeper waters) as described above. While quantifying the impact of calcification, or the formation of $CaCO_3$ to the variability of the carbonate system goes beyond the scope of this work, the relationship between nDIC and pTA suggests that this process may also influence the upper ocean variability. Furthermore, when brine is rejected during sea ice formation, DIC may be expelled more efficiently than TA, resulting in ratios of DIC: TA in sea ice that are different from those observed in the underlying seawater (Rysgaard et al., 2007; Geilfus et al., 2012), and carbonate mineral precipitation during ice formation may have

10.3389/fmars.2024.1456207

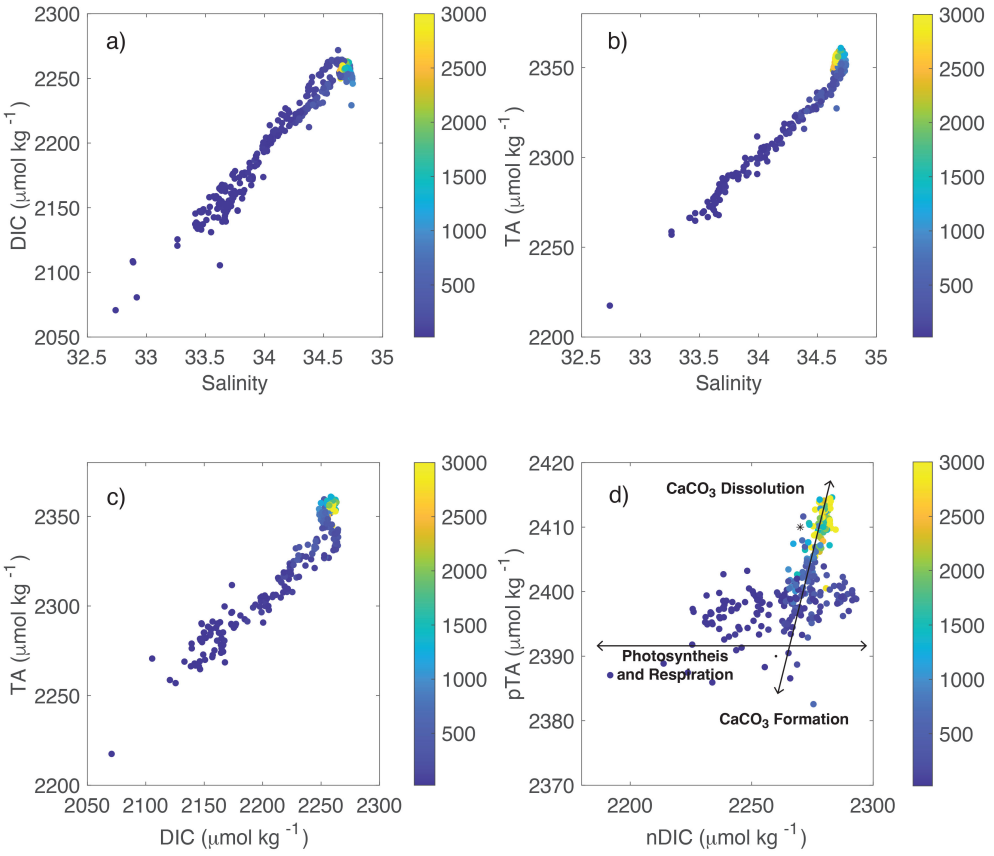


FIGURE 5
Property plots of the carbonate system. **(A)** DIC versus salinity, **(B)** TA versus salinity, **(C)** DIC versus TA, and **(D)** salinity-normalized DIC (nDIC) versus potential alkalinity (pTA). In **(D)** the effects of biological production and carbonate mineral processes are also shown schematically. Note that the colors represent depth of the samples.

implications for TA concentrations in the upper ocean (e.g. Dieckmann et al., 2008; Moreau et al., 2016).

The largest water mass in the region is CDW/mCDW, shown between the two gray lines in all panels of Figure 6, and found at every station with its characteristic maximum in salinity, low DO concentration, and relatively warm temperature. It occupies over 2000 m of the water column, on average, and is the most saline water mass in the region, with mean SA= 34.846 g kg $^{-1}$ (Table 3). Note that profiles at shallow stations on the northern end of the transects (Figure 1, white dots) did not sample the entire CDW layer; only profiles that sampled to the base of the layer were included in these averages. It is not clear from many of the transects whether or not the CDW/mCDW layer is accessing the continental shelf, as the transects do not extend far enough south. Yet, there is a clear inhibition of CDW/mCDW access to the slope along 55°E, where the top of the CDW/mCDW layer (γ^N = 28.0 kg m^{-3} isopyncal) clearly intersects with the continental slope at roughly the 500 m isobath (Figure 6, top row). Interestingly, the γ^N =28.0 kg m^{-3} isopyncal is present on the continental shelf along 75°E where we surveyed well into Prydz Bay (Figure 6, fifth row). However, this water is classified as Shelf Water, as it is too cold to be CDW/mCDW (CT < −1.6°C).

In contrast to the AASW described above, the variability in the biogeochemistry of the subsurface CDW/mCDW is much smaller, reflecting the dominance of processes occurring over longer than a single season. CDW/mCDW has elevated concentrations of inorganic carbon and nutrients (Figure 7), and minimum concentrations of dissolved oxygen resulting from both the respiration of organic matter in the interior ocean and the reduced ventilation of this water mass (see Table 3).

At the salinity maximum, there are elevated concentrations of TA, without associated maxima in DIC (Figures 5A, B). In contrast to the relationship between nDIC and pTA described in Section 3.4, the deeper waters (e.g., CDW/mCDW and AABW) indicate a dominance of $CaCO_3$ dissolution (Figure 5D). This is consistent with the broad enrichment of the Southern Ocean with pTA (relative to the other ocean basins) which can be considered a proxy for water mass age, i.e., the CDW has accumulated TA (relative to DIC) due to carbonate dissolution occurring over long timescales.

The AABW layer, the densest layer in the deep ocean, is present along every transect (Figure 6), and is particularly evident in the western transects, west of Prydz Bay (55-65°E). The mean thickness of the AABW layer over the survey area is 663 ± 316 m (Table 3). Note that the quoted uncertainty here represents the standard deviation and only profiles to the seafloor, i.e. profiles that sampled the entire AABW layer, were included in these statistics. AABW is generally thicker further to the north, as shown by the

10.3389/fmars.2024.1456207

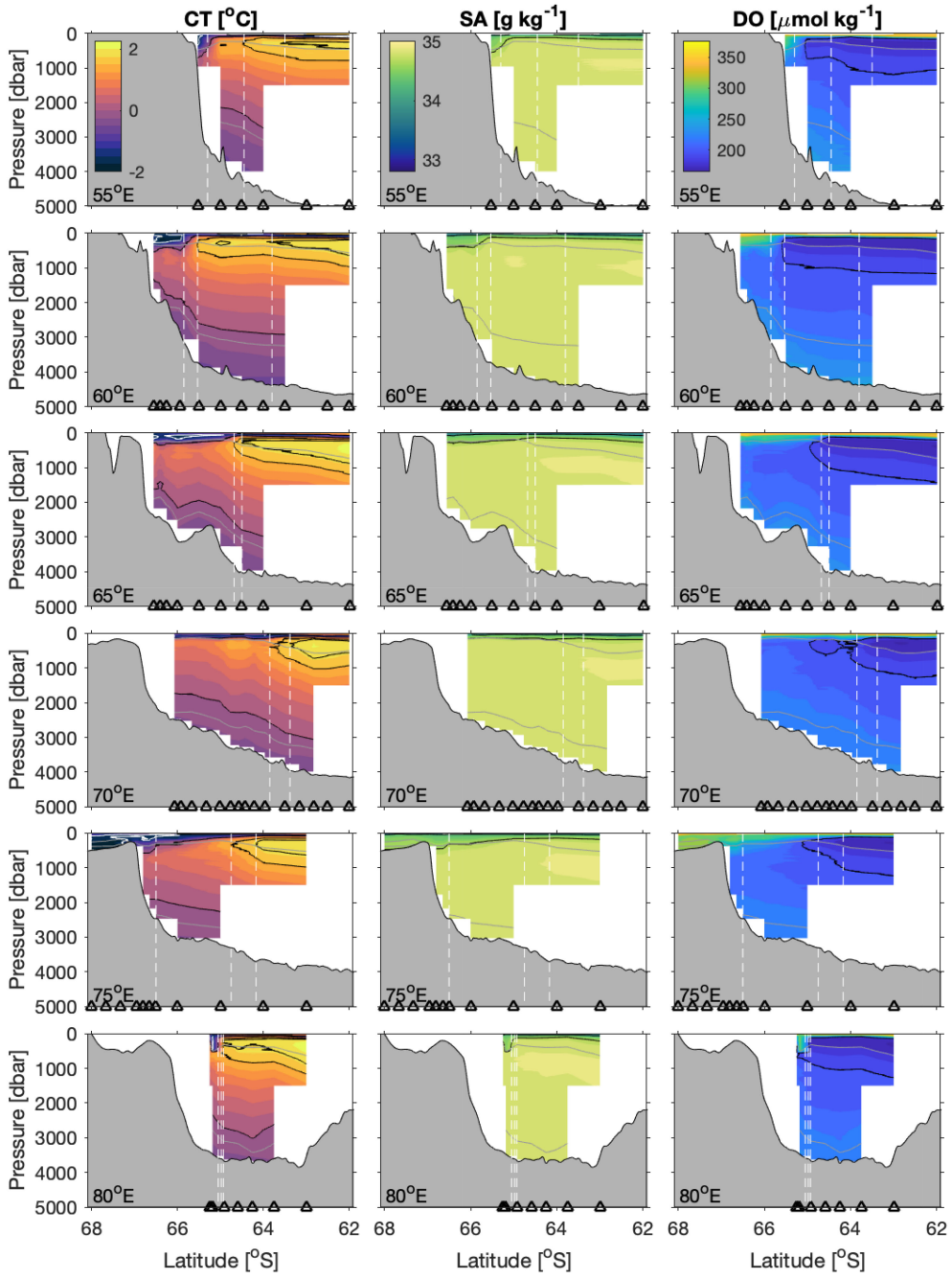


FIGURE 6
CTD data – temperature (left), salinity (center), and dissolved oxygen (right) – along the six transects. The transects are ordered with the western-most transect along the top row and eastern-most transect along the bottom row, with longitude denoted in bottom left corner. CT is contoured every 0.25°C, with the 0°C, 1.5°C, and 1.8°C isotherms as thin black lines and the -1.6°C as a thin white line; SA every 0.1 g kg^{-1}, with the 34 and 34.7 g kg^{-1} isohalines as thin black lines; and DO every 10 μmol kg^{-1}, with the 200 μmol kg^{-1} contour as a thin black line. Gray lines represent the γ^N = 28.0 and 28.3 kg m^{-3} isopycnals. Vertical dashed lines, from north to south, represent the Southern ACC Front, Southern Boundary, and Antarctic Slope Front (if sampled). The triangles along the bottom indicate station locations.

γ^N = 28.3 kg m^{-3} isopycnal (Figure 6, gray line). This is especially clear along 60°E, where the layer goes from over 1000 m depth at 63.5°S to intersecting the seafloor near 66°S. The thickest AABW layers are found in the western transects. This is likely the signature of local AABW formation at Cape Darnley (western side of Prydz Bay) resupplying the abyss and/or a pooling of AABW to the west due to the deepening of the bathymetry (as found in the Australian Antarctic Basin by, e.g., Foppert et al. (2021). Along 75°E, very cold SW was present at the bottom of the profiles where the survey extended onto the shelf in Prydz Bay (CT < -1.6°C; Figure 4F).

Both AABW and SW have elevated concentrations of DIC (and nutrients), relative to the other water masses, which is likely associated with the higher salinity of these waters resulting from their formation in the winter season at a time of net sea ice

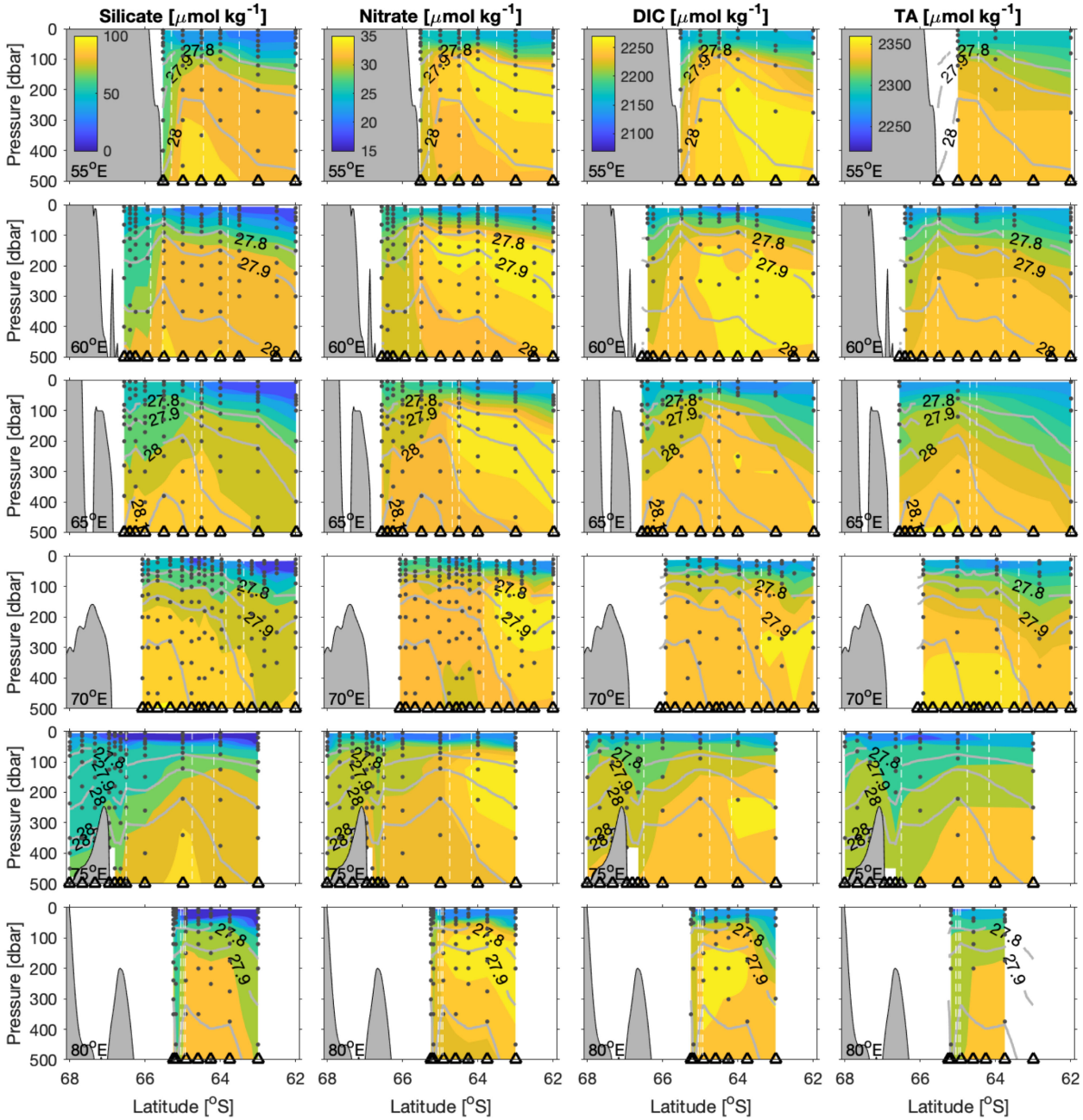


FIGURE 7
Upper-ocean biogeochemical properties – nitrate (left), silicate (center-left), DIC (center-right), TA (right) – along the six transects. The transects are ordered with the western-most transect along the top row and eastern-most transect along the bottom row, with longitude denoted in bottom left corner. Gray lines represent the isopycnals, as labeled. Black dots indicated bottle depths of the discrete samples taken for the respective quantities. Vertical dashed lines, from north to south, represent the Southern ACC Front, Southern Boundary, and Antarctic Slope Front (if sampled). The triangles along the bottom indicate station locations.

formation and brine rejection (which includes rejection of both DIC and salinity; e.g. Shadwick et al., 2014). The silicate concentration is notably higher in AABW than in CDW/mCDW (Table 3). This reflects both that the source of AABW is south of the Polar Front while CDW/mCDW is likely to have originated further north, i.e. north of the 'silica trap' (e.g. Boyd et al., 2024), and the fact that while nitrate is remineralized throughout the water column, resulting in similar concentrations in both layers, most of the biogenic silicate will be transported to depth and remineralized close to the seafloor. The elevated oxygen concentration in the SW water indicates recent ventilation through interactions with the atmosphere.

3.3 Frontal distribution and transport

Evidence of an oceanographic front is present and manifests as a gap in the temperature-salinity diagram in Figure 4A (from

roughly 1.5°C, 34.6 g kg^{-1} to -1.4°C, 34.4 g kg^{-1}). The fronts become more clear in the individual transects, where water-mass properties exhibit large differences between stations (Figures 4B–G), and especially in the CDW/mCDW layer where water masses are more stable. Two fronts are clear in the temperature-salinity diagrams along some transects, e.g. 55°E and 75°E, whereas other transects only exhibit one clear front, e.g. 60°E and 70°E.

Frontal locations are found in Table 2 and are shown in Figures 6, 8 (white dashed lines). In all six transects, the SACCF and SB are found between 63°S and about 65.5°S. The SACCF is always farther north than the SB, by definition, and the distance between the two fronts varies; they can be separated by nearly 200 km (e.g. along 60°E) or be located between the same two stations (e.g. along 80°E).

The SACCF is considered the southern limit of the Antarctic Circumpolar Current's eastward flow, while the SB is the southern limit of the CDW in the meridional overturning circulation (Orsi et al., 1995). Therefore, we expect enhanced zonal flow at the SACCF and not at the SB. Figure 9 shows the zonal velocity in the upper ocean along the six transects. Note that the SADCP data shown here is measured while on station, and does not reflect continuous measurements along the entire transect. In general, there is a relatively strong eastward velocity at, or near, the SACCF, with speeds greater than 0.1 m s^{-1}. This is evident along 65°E and 75°E. However, along 60°E, the SACCF is co-located with weak westward flow. Figure 8 shows that there is an eddy found along 60°E, seen as a detached closed contour in the temperature field near 65°S. This warm-core eddy is associated with anticyclonic circulation, i.e. westward flow to its north and eastward flow to its south. The westward flow of the eddy is therefore likely acting to reduce the eastward flow of the SACCF and the zonal velocity seen along 60°E reflects the interaction of this eddy with SACCF (Figure 9).

The ASF-N and ASF, defined as the location where the subsurface 0°C isotherm reaches 200 m and 400 m, respectively, are found farther south between roughly 65°S and 66.5°S (Table 2). The ASF and ASF-N were not sampled on the 70°E transect; nor was the ASF sampled on 65°E. Note that the ASF and ASF-N are generally located in between the same stations, indicating a strong horizontal (north-south) temperature gradient extending throughout the upper ocean. The exceptions are along 65°E, where there is a strong horizontal temperature gradient associated with the ASF-N near 64.9°S, yet the 0°C isotherm doesn't reach 400 m within our survey; and along 75°E, where the 0°C isotherm gradually descends poleward across about 2° of latitude (Figure 8).

The ASF is often associated with the westward flowing Antarctic Slope Current (ASC), that is generally found hugging the shelf break towards the southern flank of the ASF (e.g., see Figure 6 of Meijers et al., 2010). We find relatively strong westward flow at 55°E, with speeds of about 0.1 m s^{-1} (Figure 9). Along 75°E, there is weak westward flow at the ASF. Note that Meijers et al. (2010) found a strongly bottom-intensified ASC at 70°E, with much stronger westward flows at depth than near the surface. The weak upper-ocean speeds (around 0.05 m s^{-1}) observed at 75°E in BROKE-West by Meijers et al. (2010) are similar to those seen here at 70°E in Figure 9. Along 60°E and 80°E, we did not reach the shelf break (see Figure 6), and therefore likely did not survey far enough south to measure the ASC.

3.4 Upper-ocean variability

The development of the upper ocean structure in the seasonal ice zone is described by Williams et al. (2010) as follows. During winter, strong convection due to brine rejection creates a deep mixed layer. As summer approaches and the sea ice melts, the surface layer freshens and warms, and a seasonal mixed layer is formed above a layer of remnant Winter Water (WW). Those authors identified two features in the upper ocean that are important for setting the summertime stratification: the seasonal mixed layer depth (MLD) and the base of the WW, or temperature minimum, layer. The latter which is generally associated with the permanent pycnocline and the former with the seasonal pycnocline (or thermocline). Here, we discuss the characteristics of the seasonal mixed layer and underlying WW in the TEMPO survey. Note that we only present data from stations north of the ASF-N, where the summer stratification is well developed and there is a clear signature of the summertime stratification with a seasonal mixed layer overlying a distinct temperature minimum layer.

Mixed-layer depths (MLD) are shown by the white lines in Figure 8. MLD is defined as the depth at which neutral density is 0.03 kg m^{-3} greater than its near-surface value, following de Boyer Montégut et al. (2004). Here, we use 15 dbar as the near-surface reference level, except in the few cases where the profile starts deeper we use the top of the profile. Figure 10A shows MLD at stations north of the ASF-N in plan view over the survey region. The average MLD north of the ASF-N is 38 ± 10 m (mean ± 1 standard deviation), and values range from approximately 20-60 m deep. The deepest mixed layers are generally found at the northern end of the transects (Figure 8, white line), where the surface ocean has been ice-free the longest. Yet, relatively deep mixed layers are also found just north of the ASF-N along 55°E and 70°E.

Across the survey region, the average temperature in the mixed layer, $\overline{CT}_{MLD}$, generally decreases to the south (Figure 10B), as clearly seen along 70°E. The largest exception is on the 60°E transect, where the station at 64°S is colder than the two stations to the south of it. Note that this station is found to the north of the warm-core eddy observed along this transect and the cold anomaly may be associated with the anticyclonic circulation of the eddy bringing cooler waters up from the south. The warmest seasonal mixed layers are found in the northwest corner of the survey region, where $\overline{CT}_{MLD}$> 1.5°C.

The WW core, i.e. depth of the temperature minimum, generally deepens to the north (Figure 10C). The WW core is deepest in the northwest corner, with temperature minimum depths here being greater than 80 m. On average, the temperature minimum is -1.38 ± 0.22°C. The WW layer is warmest at the southern end (i.e. immediately north of the ASF-N) along 55°E and 80°E, reaching temperatures greater than -1°C (Figure 10D) whereas on other lines, the core of the WW cools to the south (i.e. 70°E and 75°E). The base of the WW layer – defined as the 0°C isotherm below to the temperature minimum – is notably deeper along the southern portion of 70°E (150-200m) than elsewhere (Figure 10E).

Williams et al. (2010) use temperature anomaly at 100 m depth as a proxy for local upwelling. Here, we consider the temperature

10.3389/fmars.2024.1456207

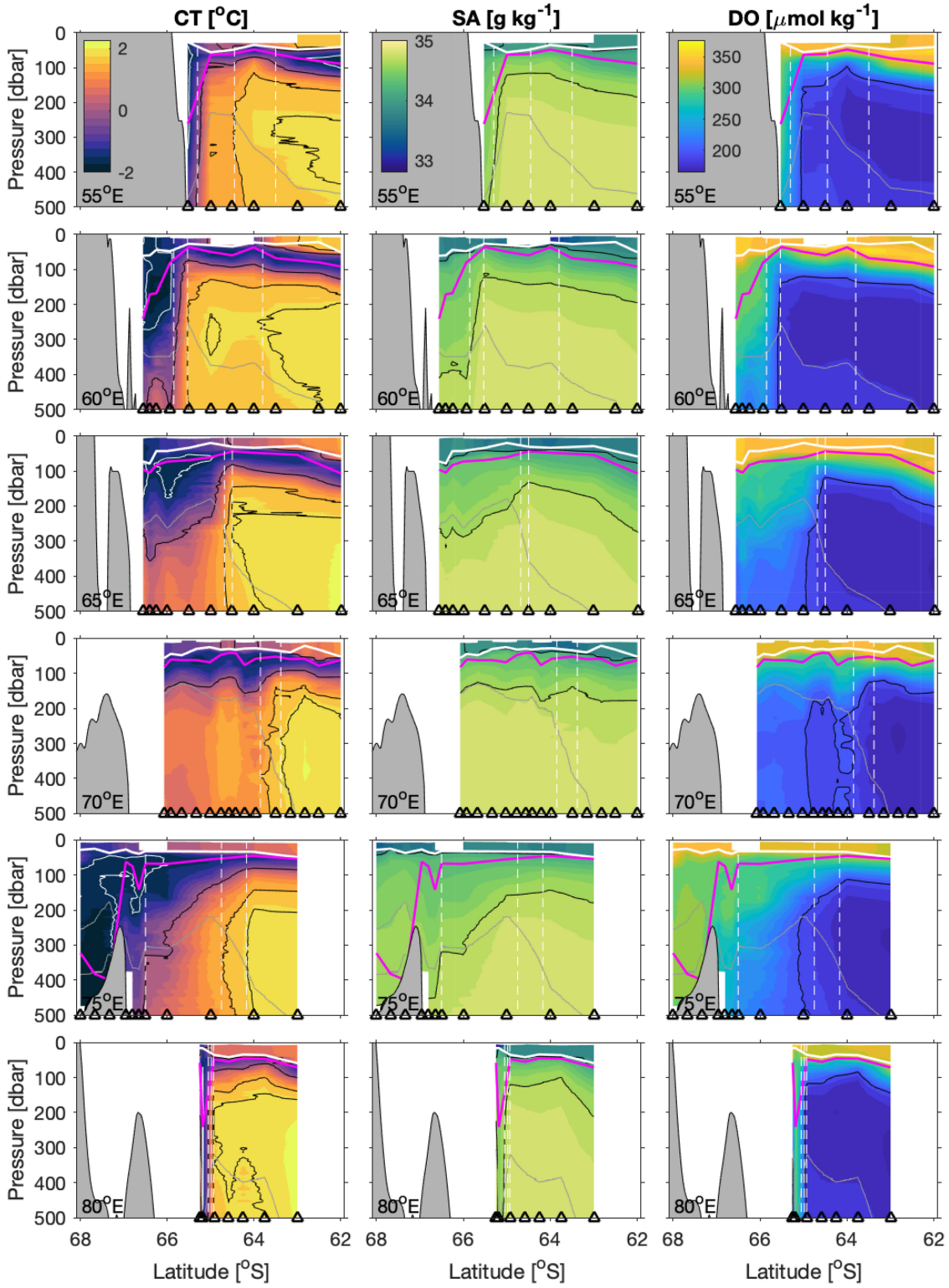


FIGURE 8
Upper-ocean CTD data – temperature (left), salinity (center), and dissolved oxygen (right) – along the six transects. The transects are ordered with the western-most transect along the top row and eastern-most transect along the bottom row, with longitude denoted in bottom left corner. CT is contoured every 0.25°C, with the 0°C, 1.5°C, and 1.8°C isotherms as thin black lines and the -1.6°C as a thin white line; SA every 0.1 g kg^{-1}, with the 34 and 34.7 g kg^{-1} isohalines as thin black lines; and DO every 10 μmol kg^{-1}, with the 200 μmol kg^{-1} contour as a thin black line. Mixed-layer depth is shown by the thick white line and temperature minimum by the thick magenta line. Gray lines represent the γ^N = 28.0 and 28.3 kg m^{-3} isopycnals (note the denser isopycnal only present along 75°E). Vertical dashed lines, from north to south, represent the Southern ACC Front, Southern Boundary, and Antarctic Slope Front (if sampled). The triangles along the bottom indicate station locations.

10.3389/fmars.2024.1456207

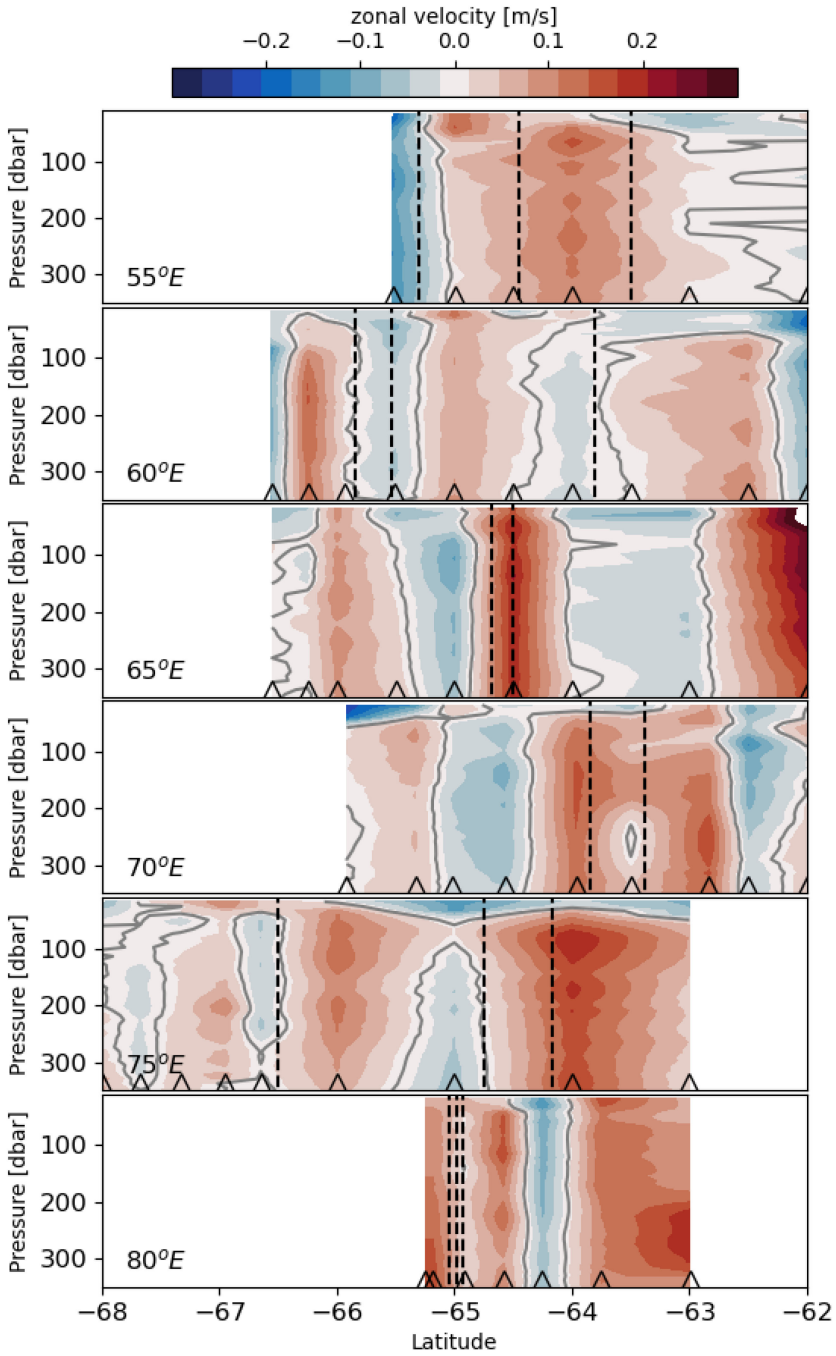


FIGURE 9
Zonal velocity in the upper ocean (upper 350 m) as measured by the shipboard ADCP while on station. Frontal locations are shown as dashed black lines. The grey line marks the zero contour. Vertical dashed lines, from north to south, represent the Southern ACC Front, Southern Boundary, and Antarctic Slope Front (if sampled). The triangles along the bottom indicate station locations. Note that the SADCP was only on and measuring velocities while on station, not during transit between stations.

anomaly at the mean depth of the WW core (60 m) and the temperature anomaly is therefore calculated from the mean temperature at 60 m across the survey region (-1.005°C). Relatively warm water in Figure 10F highlights areas where the water at the mean WW core is warmer than the survey average. There is a strong signal of anomalously warm water along 80°E. This, along with the depth of the WW base being relatively shallow there (Figure 10E), suggests localized upwelling at 80°E. There is some variability in the depth of the WW base along 70°E, with a shoaling of the WW base near 65°S, associated with warmer water at the mean WW core. The temperature field along 70°E shows the presence of a subsurface eddy here composed of CDW/mCDW (anomalously warm and low DO; Figure 8), associated with the upwelling and shoaling of isopycnals locally in the surface layers.

10.3389/fmars.2024.1456207

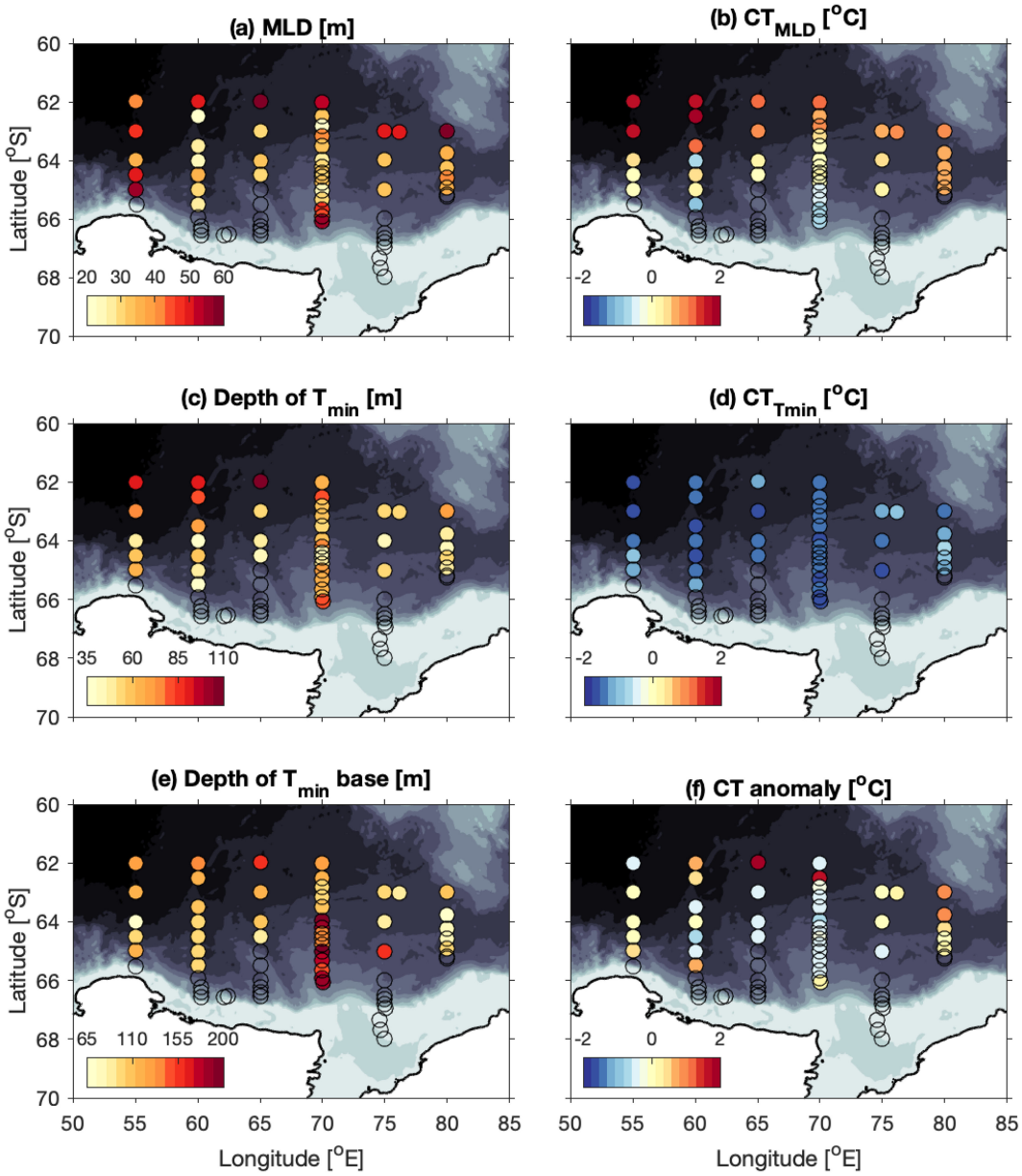


FIGURE 10
Upper-ocean characteristics. **(A)** Mixed layer depth, MLD [m]; **(B)** mean temperature in the mixed layer [°C]; **(C)** depth of the temperature minimum [m], indicative of the depth of the core of Winter Water; **(D)** minimum temperature [°C], indicative of the temperature at the WW core; **(E)** depth of the base of the temperature-minimum, or WW, layer [m]; **(F)** temperature anomaly [°C] at the mean depth of the WW core across the survey, with warm anomalies indicative of localized upwelling. Note that these maps only show data from stations north of the ASF (stations south of the ASF-N are shown as open circles.

3.5 Deep-ocean variability

Figure 11 shows the bottom properties of each full-depth CTD cast located in waters deeper than 500 m. Overall, there is an east-west pattern with colder, fresher, and more oxygen-rich waters found along the western transects (55-65°E) than the eastern transects (70-80°E). This illustrates the disparity in the two flavors of AABW in this region, with older AABW in the eastern part of the survey and newly formed AABW – likely formed locally in the Cape Darnley Polynya (Ohshima et al., 2013) – in the western part of the survey. Note that stations on the shelf along 75°E (not shown) had even higher DO concentrations (DO > 300 μmol kg^{-1}) as these shelf waters are actively ventilated through interactions with the atmosphere.

The most oxygen-rich bottom waters (DO > 250 μmol kg^{-1}) are found in the deep ocean along 60°E and at the southern end of 70°E (Figures 11C, D). There is also a single station near the 4000-m isobath on 55°E with higher DO relative to its neighboring stations. The oxygen-rich waters at these stations are also colder and fresher than surrounding waters (Figures 11A, B) and trace the pathway of AABW from the Cape Darnley Polynya into the abyssal ocean.

These results indicate the main AABW export pathway from the Cape Darnley Polynya to be through the Daly Canyon, as the

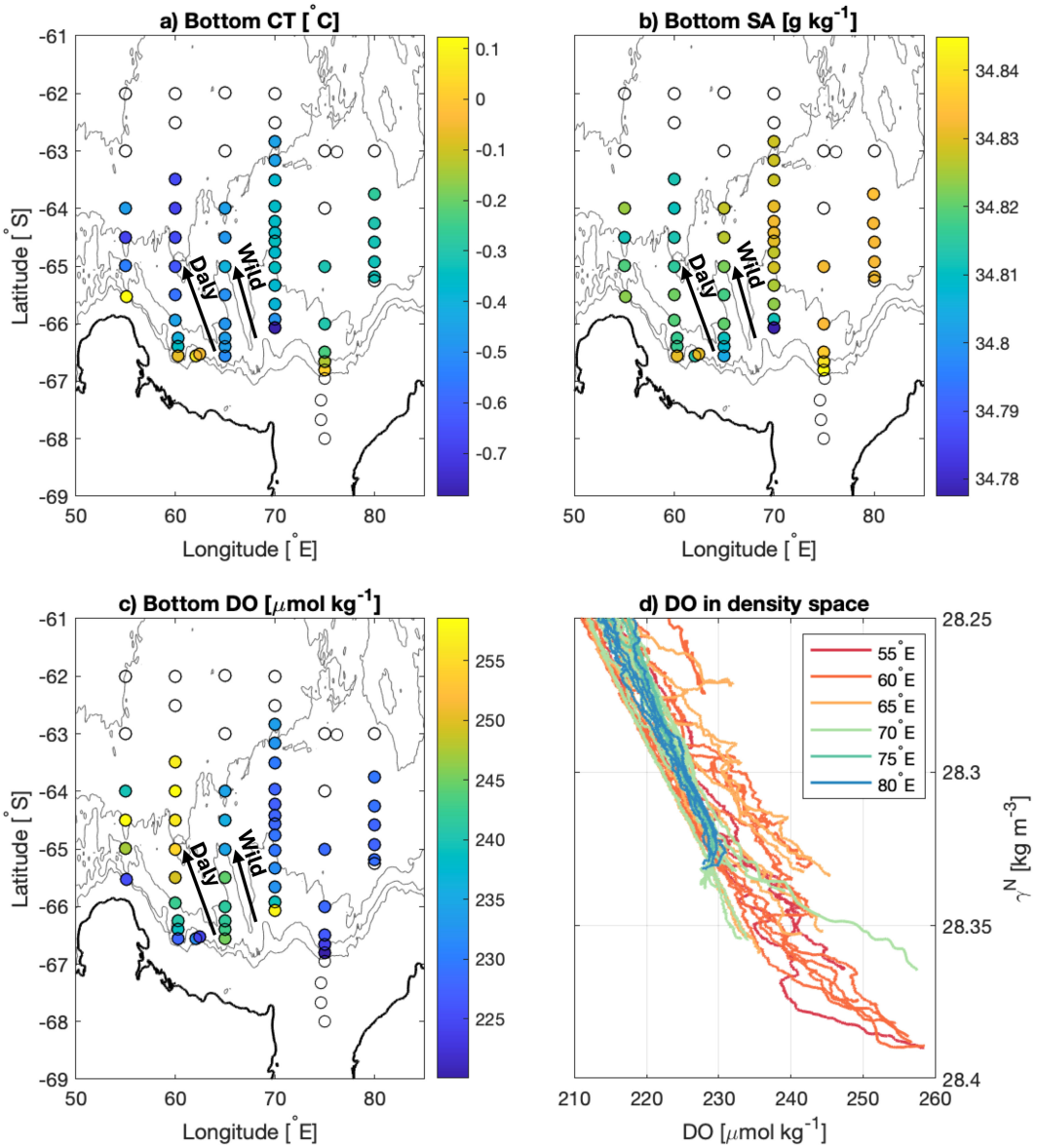


FIGURE 11
Bottom properties. **(A)** Conservative temperature [CT, °C], **(B)** absolute salinity [SA, g kg^{-1}], and **(C)** dissolved oxygen concentration [DO, μmol kg^{-1}] at the deepest point of the CTD profile. **(D)** Bottom of the DO profiles as a function of neural density [γ^N, kg m^{-3}]. For all panels, only information from full-depth profiles off the shelf (i.e. with maximum pressures greater than 500 dbar) are shown. The Wild and Daly Canyons are shown schematically with arrows.

bottom waters near its base are highly oxygenated, and more oxygenated than the bottom waters at the base of the Wild Canyon to its east. It appears some Dense Shelf Water might spillover of the shelf break near 70°E, as there are also highly oxygenated waters deeper than 2000 meters there. Note that the enhanced DO at the station on 55°E (DO> 250 μmol kg^{-1} in water about 4300 m deep) is comparable to the DO concentrations in the deep ocean along 60°E. This suggests the AABW on 55°E was potentially funneled locally into the abyssal ocean, likely through a narrow canyon west of the Daly Canyon (as stations to its north and south show lower DO concentrations).

4 Discussion and conclusions

A shipboard oceanographic survey of the greater Prydz Bay region was conducted in the austral summer 2021 (January-March) as part of the 'Trends in *Euphausiids* off Mawson, Predators and Oceanography' (TEMPO) study undertaken on the R/V Investigator. This paper characterizes the regional water masses and circulation from direct measurements of physical and biogeochemical properties, and upper-ocean horizontal velocities. We describe the spatial variability of the upper-ocean and features important for setting the summertime stratification that, in turn,

have a strong influence on regional primary productivity. Observations of deep ocean properties also provide insights regarding AABW formation and export pathways.

The fronts of the Southern Ocean separate the warmer waters to the north from the colder waters around Antarctica, acting as a barrier to poleward heat transport. Thus, a southward shift in the location of the fronts is associated with warm water moving south and impinging into the Antarctic margins, with implications for heat available for transport onto the shelf and basal melting of Antarctic Ice Shelves (e.g. Herraiz-Borreguero and Naveira Garabato, 2022). While the SB has widely been found to be trending southward, the location of the ASF has recently been posited to have shifted north in parts of East Antarctica Yamazaki et al. (2024). However, those conclusions only consider two surveys, more than 20 years apart, making a long-term trend tenuous in light of frontal meandering. It is well observed that Southern Ocean fronts meander latitudinally and can span 1-2 degrees of latitude at some locations (e.g. Sokolov and Rintoul, 2002).

Figure 1 shows the locations of the fronts observed during TEMPO in 2021 relative to the locations observed during the 2006 BROKE-WEST survey by Meijers et al. (2010) and in the historic climatology of Orsi et al. (1995). The longitudinal resolution of the CTD transects of TEMPO was twice that of BROKE-West (every 5°E compared to every 10°E), allowing for a greater detail in understanding the frontal structure and meandering. We find the SACCF entering the survey region earlier (i.e. intruding into the south farther west) than during BROKE-West and with a meander northward near 70°E that was not previously observed. At both 60°E and 80°E, we find the SACCF more than 1.5 degrees of latitude (over 150 km) farther south than documented by Meijers et al. (2010) and Orsi et al. (1995); it was found at a similar latitude to both previous studies at 70°E. The SB in 2021 was similar to its position during BROKE-West, with both surveys documenting a more northerly position along 70°E, by 1-2° latitude, than its position in the Orsi et al. (1995) climatology (Figure 1). This is likely due to the northward flow of the greater Prydz Bay Gyre, as suggested by Meijers et al. (2010). Note that there was a dearth of hydrographic data to support the early Orsi et al. (1995) climatology in this vicinity (see their Figure 2), potentially forcing interpolation across the Prydz Bay Gyre region.

The ASF was identified at roughly similar locations during TEMPO and BROKE-West (Figure 1). Note here that we have revisited the BROKE-West CTD data (available at 60, 70, and 80°E) and recalculated the ASF locations using the refined definition for consistency between surveys. The largest difference in ASF location was observed at 80°E, where the front was identified roughly 60 km farther north in 2021 compared to 2006. At 70°E, where sea ice prohibited the 2021 TEMPO survey from going beyond 66°S, the TEMPO survey did not encounter the ASF or ASF-N; that is, both were located south of this latitude. Therefore, both were located farther south in 2021 relative to their 2006 position, being 65°S (ASF-N), and 66°S (ASF), respectively (again, applying our refined ASF-N definition to BROKE-West data). These observed displacements of the ASF in 2021 relative to 2006 are likely due to frontal meandering, and associated eddy variability (e.g. Foppert et al., 2019), yet we cannot rule out a long-term change in frontal position as suggested by Yamazaki et al. (2024).

In the BROKE-West survey, Williams et al. (2010) found that mixed layer depths varied both meridionally and zonally within their survey area (average 29 ± 15 m; 30-80°E). Mixed layer depths were influenced by the number of ice free days, combined with accumulated wind stress once the ice had melted leading to exposure. Stations that had less ice free days had less time for mixed layer development, with the mixed layer also being cooler due to a higher proportion of ice and less time for warming from solar radiation. For BROKE-West, shallowest mixed layers were observed to the south near the retreating ice edge, and to the west where sampling was conducted earlier leading to shorter ice-free days compared to the east. In contrast, TEMPO mixed layer depths averaged 38 ± 10 m, with no obvious pattern across the survey area apart from the most northerly stations generally having deeper mixed layers (Figures 8, 10A). However, the TEMPO survey was conducted approximately a month later than BROKE-West, which meant that mixed layer depths had more time for development and influences from wind events. TEMPO mixed layer depths were most similar to eastern stations from BROKE-West (36 ± 15 m Legs 7-9, Westwood et al., 2010) which were conducted at a similar time in the season. Average temperatures within the mixed layer were also cooler to the south for TEMPO, similar to BROKE-West. Noticeably deeper mixed layers were found along 65°E compared to other eastern transects during BROKE-West, which was associated with a convergence of ocean circulation in this region Williams et al. (2010). However, this was not observed during the TEMPO survey.

Through the use of potential temperature anomalies, both the BROKE-West and TEMPO surveys showed evidence of localized upwelling of MCDW/CDW along 80°E in the area north of 64°S (north of the SACCF and SB). The upwelling of CDW is associated with increased nutrient availability to surface waters, including iron (Moreau et al., 2019; Smith et al., 2021), which may stimulate primary production (Westwood et al., 2010). While elevated values of surface chl-a are seen in this region in February (Figure 2A), Heidemann et al. (2024) showed that primary production in this region during TEMPO was noticeably lower than elsewhere within the survey, based on *in-situ* phytoplankton pigment data. However, large krill swarms and feeding whales (approximately 50) were observed in this region (M. Cox and S. Kawaguchi, pers. comm. March 2021), suggesting high production in terms of secondary and higher order predators. Heidemann et al. (2024) further showed strong evidence that the phytoplankton in this region had been grazed by krill, with clear depletion of large diatoms in surface waters and high phaeophytin:chlorophyll-*a* ratios (> 0.75; Wright et al., 2010). It is likely that high primary production here earlier in the season (February) was sustained through upwelling of nutrient-rich CDW and that the phytoplankton were grazed down by the time the TEMPO survey arrived at the eastern end of the survey (March).

A large phytoplankton bloom was observed on the slope and offshore along 70°E to 80°E, south of the SB (Heidemann et al., 2024). These southerly waters generally had a cold mixed layer and cold WW temperatures (i.e. cold minimum temperatures). We speculate that the influence of the West Ice Shelf and associated sea ice, and the cold shelf waters exported from Prydz Bay, is

extended offshore via advection associated with the Prydz Bay Gyre circulation. Heidemann et al. (2024) showed this bloom to be late phase (high iron depletion i.e., high Si:N and high phaeo:chl ratios) suggesting these waters coming from the West Ice Shelf region may originally have been iron rich, to support the high phytoplankton biomass bloom still evident during the survey period. Another distinct bloom was observed north of the sACCF across 55°E to 65°E (Heidemann et al., 2024). This bloom may have had its origins farther west, and there was evidence of large diatoms sinking from surface waters to below the mixed layer as waters flowed from west to east.

The characteristic concentrations of DIC, TA, and nutrients observed during the TEMPO surveys are broadly consistent with the earlier BROKE-West survey (Roden et al., 2016). As described above, biological activity over the shelf and slope, along with input of freshwater from sea ice melt, resulted in low concentrations of DIC in the upper ocean, associated with AASW. The TEMPO observations indicated minimum surface concentrations of ≈2070 μmol kg^{-1}, which is slightly lower than the minimum observed during the BROKE-West survey, as is the TA, though the density and temperature criteria used to define water masses also differed slightly (Roden et al., 2016). The conservative relationship between salinity and TA in the TEMPO observations is consistent with the BROKE-West observations, and while quantification of anthropogenic carbon accumulation in the deeper water masses (i.e., CDW and AABW) goes beyond the scope of the work presented here, the TEMPO observations do indicate characteristic concentrations of DIC in the deep ocean that are elevated relative to BROKE-West survey which occurred 15 years earlier.

We observed newly formed AABW concentrated along 60°E, at the base of the Daly Canyon, with considerably higher oxygen values there relative to farther east at 65°E (Figure 11). High oxygen waters were also found along 60°E during the BROKE-West survey (Meijers et al., 2010), however they did not survey 65°E and therefore could not make the distinction of where the newly formed AABW entered the deep basin. This recent oxygenation is indicative of Cape Darnley Bottom Water, formed locally in the Cape Darnley Polynya (Ohshima et al., 2013). While we cannot trace a continuous AABW pathway back to the shelf, Figure 11 strongly implies that the Dense Shelf Water is entering the deep basin mainly via the Daly Canyon, as opposed to the Wild Canyon (as suggested by mooring data in Ohshima et al., 2013). Gao et al. (2022) observed warming, freshening, and increasing dissolved oxygen in the Daly Canyon between 2003-2006 and 2013–2020, and attributed those changes to increased cascading of Dense Shelf Water plumes down Daly Canyon. Those results, along with the results shown in Figure 11, suggest the main pathway of Dense Shelf Water from Cape Darnley into the abyss is potentially shifting from the Wild to the Daly Canyon.

Data availability statement

The datasets presented in this study can be found in online repositories. The CTD, nutrient, and SADCP data used for this study can be found in the MNF Data Trawler https://www.cmar.csiro.au/data/trawler/survey_details.cfm?survey=IN2021_V01. Carbon data is available through personal communication with E. H. Shadwick. All environmental data (sea ice concentrations, surface cholorphyll-a, sea surface temperature, and bathymetry) are all publicly available. Monthly SIC data from the Nimbus-7 SMMR and SSMI/SSMIS passive microwave sensors were downloaded from the National Snow and Ice Data Center (http://nsidc.org; Cavalieri et al., 1996). Monthly surface satellite Chla were obtained from the European Space Agency (ESA) Globcolour website (https://www.globcolour.info/). Data consist of case 1 merged product from the SeaWiFS, MODIS-Aqua, VIIRS and MERIS sensors.

Author contributions

AF: Conceptualization, Data curation, Formal analysis, Investigation, Methodology, Visualization, Writing – original draft, Writing – review & editing. SB: Conceptualization, Data curation, Formal analysis, Investigation, Methodology, Visualization, Writing – original draft, Writing – review & editing. ES: Conceptualization, Data curation, Formal analysis, Investigation, Visualization, Writing – original draft, Writing – review & editing. AK: Visualization, Writing – review & editing. CV: Investigation, Writing – review & editing. GL: Visualization, Writing – review & editing. KW: Formal analysis, Investigation, Methodology, Project administration, Resources, Supervision, Writing – original draft, Writing – review & editing.

Funding

The author(s) declare financial support was received for the research, authorship, and/or publication of this article. This work was funded by the Australian Antarctic Program Partnership – a partnership of Australia's leading Antarctic research institutions supported by the Australian Government Antarctic Science Collaboration Initiative. This project was also supported and funded by Australian Antarctic Science Project 4512 and 4636, and received financial support from Pew Charitable Trust and Antarctic Science Foundation. We acknowledge the use of the CSIRO Marine National Facility (MNF, https://ror.org/01mae9353) and grant of sea time on RV Investigator in undertaking this work. GL and CV would like to thank the University of Tasmania and the Australian Research Council (ARC) Centre of Excellence for Climate Extremes (CE170100023) for their financial support.

Acknowledgments

We would like to thank chief scientist So Kawaguchi and deputy-chief scientist Rob King for leading the voyage, and Linda Gaskell for voyage management. We thank Abe Passmore and the CSIRO Carbon Lab for the analysis of DIC and alkalinity samples. The authors also thank the captain and crew of the R/V Investigator, and all those who supported the TEMPO survey both onboard and ashore. We acknowledge the use of the CSIRO

Marine National Facility (https://ror.org/01mae9353) and grant of sea time on RV Investigator in undertaking this research.

Conflict of interest

The authors declare that the research was conducted in the absence of any commercial or financial relationships that could be construed as a potential conflict of interest.

Publisher's note

All claims expressed in this article are solely those of the authors and do not necessarily represent those of their affiliated organizations, or those of the publisher, the editors and the reviewers. Any product that may be evaluated in this article, or claim that may be made by its manufacturer, is not guaranteed or endorsed by the publisher.

References

Arrigo, K. R., Lowry, K. E., and van Dijken, G. L. (2012). Annual changes in sea ice and phytoplankton in polynyas of the Amundsen Sea, Antarctica. *Deep Sea Res. Part II: Topical Stud. Oceanography* 71-76, 5–15. doi: 10.1016/j.dsr2.2012.03.006

Arrigo, K. R., and van Dijken, G. L. (2003). Phytoplankton dynamics within 37 Antarctic coastal polynya systems. *J. Geophysical Research: Oceans* 108. doi: 10.1029/2002JC001739

Arroyo, M. C., Shadwick, E. H., and Tilbrook, B. (2019). Summer carbonate chemistry in the dalton polynya, east Antarctica. *J. Geophysical Research: Oceans* 124, 5634–5653. doi: 10.1029/2018JC014882

Banzon, V., Smith, T. M., Chin, T. M., Liu, C., and Hankins, W. (2016). A long-term record of blended satellite and in *situ* sea-surface temperature for climate monitoring, modeling and environmental studies. *Earth System Sci. Data* 8, 165–176. doi: 10.5194/essd-8-165-2016

Bates, N. R., Hansell, D. A., Carlson, C. A., and Gordon, L. I. (1998). Distribution of CO2 species, estimates of net community production, and air-sea CO2 exchange in the Ross Sea polynya. *J. Geophysical Research: Oceans* 103, 2883–2896. doi: 10.1029/97JC02473

Bazzani, E., Lauritano, C., and Saggiomo, M. (2023). Southern ocean iron limitation of primary production between past knowledge and future projections. *J. Mar. Sci. Eng.* 11. doi: 10.3390/jmse11020272

Bestley, S., Raymond, B., Gales, N. J., Harcourt, R. G., Hindell, M. A., Jonsen, I. D., et al. (2018). Predicting krill swarm characteristics important for marine predators foraging off east Antarctica. *Ecography* 41, 996–1012. doi: 10.1111/ecog.03080

Bestley, S., van Wijk, E., Rosenberg, M., Eriksen, R., Corney, S., Tattersall, K., et al. (2020). Ocean circulation and frontal structure near the southern Kerguelen Plateau: The physical context for the Kerguelen Axis ecosystem study. *Deep-Sea Res. Part II: Topical Stud. Oceanography* 174, 104479. doi: 10.1016/j.dsr2.2018.07.013

Boyd, P. W., Arrigo, K. R., Ardyna, M., Halfter, S., Huckstadt, L., Kuhn, A. M., et al. (2024). The role of biota in the Southern Ocean carbon cycle. *Nat. Rev. Earth Environ.* 5, 390–408. doi: 10.1038/s43017-024-00531-3

Boyd, P. W., and Ellwood, M. J. (2010). The biogeochemical cycle of iron in the ocean. *Nat. Geosci.* 3, 675–682. doi: 10.1038/ngeo964

Brewer, P. G., and Goldman, J. C. (1976). Alkalinity changes generated by phytoplankton growth. *Limnology Oceanography* 21, 108–117. doi: 10.4319/lo.1976.21.1.0108

Cavalieri, D. J., Parkinson, C. L., Gloersen, P., and Zwally, H. J. (1996). *Sea ice concentrations from nimbus-7 smmr and dmsp ssm/i-ssmis passive microwave data, version 1*. doi: 10.5067/8GQ8LZQVL0VL

de Boyer Montégut, C., Madec, G., Fischer, A. S., Lazar, A., and Iudicone, D. (2004). Mixed layer depth over the global ocean: An examination of profile data and a profile-based climatology. *J. Geophysical Research: Oceans* 109. doi: 10.1029/2004JC002378

DeJong, H. B., Dunbar, R. B., Koweek, D. A., Mucciarone, D. A., Bercovici, S. K., and Hansell, D. A. (2017). Net community production and carbon export during the late summer in the Ross Sea, Antarctica. *Global Biogeochemical Cycles* 31, 473–491. doi: 10.1002/2016GB005417

Dickson, A., Sabine, C., and Christian, J. E. (2007). Guide to best practices for ocean CO2 measurements. *PICES Special Publ.* 3. doi: 10.25607/OBP-1342

Dieckmann, G. S., Nehrke, G., Papadimitriou, S., Göttlicher, J., Steininger, R., Kennedy, H., et al. (2008). Calcium carbonate as ikaite crystals in Antarctic sea ice. *Geophysical Res. Lett.* 35. doi: 10.1029/2008GL033540

Dinniman, M. S., St-Laurent, P., Arrigo, K. R., Hofmann, E. E., and van Dijken, G. L. (2020). Analysis of iron sources in antarctic continental shelf waters. *J. Geophysical Research: Oceans* 125, e2019JC015736. doi: 10.1029/2019JC015736

Feng, Y., Hare, C., Rose, J., Handy, S., DiTullio, G., Lee, P., et al. (2010). Interactive effects of iron, irradiance and CO2 on Ross Sea phytoplankton. *Deep Sea Res. Part I: Oceanographic Res. Papers* 57, 368–383. doi: 10.1016/j.dsr.2009.10.013

Foppert, A., Donohue, K. A., Watts, D. R., and Tracey, K. L. (2017). Eddy heat flux across the Antarctic Circumpolar Current estimated from sea surface height standard deviation. *J. Geophysical Research: Oceans* 122, 6947–6964. doi: 10.1002/2017JC012837

Foppert, A., Rintoul, S. R., and England, M. H. (2019). Along-slope variability of cross-slope eddy transport in east Antarctica. *Geophysical Res. Lett.* 46, 8224–8233. doi: 10.1029/2019GL082999

Foppert, A., Rintoul, S. R., Purkey, S. G., Zilberman, N., Kobayashi, T., Sallèe, J.-B., et al. (2021). Deep argo reveals bottom water properties and pathways in the Australian-antarctic basin. *J. Geophysical Research: Oceans* 126. doi: 10.1029/2021JC017935

Friis, K., Körtzinger, A., and Wallace, D. W. R. (2003). The salinity normalization of marine inorganic carbon chemistry data. *Geophysical Res. Lett.* 30. doi: 10.1029/2002GL015898

Gao, L., Zu, Y., Guo, G., and Hou, S. (2022). Recent changes and distribution of the newly-formed Cape Darnley Bottom Water, East Antarctica. *Deep Sea Res. Part II: Topical Stud. Oceanography* 201, 105119. doi: 10.1016/j.dsr2.2022.105119

Geilfus, N.-X., Carnat, G., Papakyriakou, T., Tison, J.-L., Else, B., Thomas, H., et al. (2012). Dynamics of pCO2and related air-ice CO2 fluxes in the Arctic coastal zone (Amundsen Gulf, Beaufort Sea). *J. Geophysical Research: Oceans* 117. doi: 10.1029/2011JC007118

Heidemann, A. C., Westwood, K. J., Foppert, A., Wright, S. W., Klocker, A., Vives, C. R., et al. (2024). Drivers of phytoplankton distribution, abundance and community composition off East Antarctica, from 55-80°E (CCAMLR division 58.4.2 East). *Front. Mar. Sci.* 11, 1454421. doi: 10.3389/fmars.2024.1454421

Henley, S. F., Cavan, E. L., Fawcett, S. E., Kerr, R., Monteiro, T., Sherrell, R. M., et al. (2020). Changing biogeochemistry of the southern ocean and its ecosystem implications. *Front. Mar. Sci.* 7. doi: 10.3389/fmars.2020.00581

Herraiz-Borreguero, L., Church, J. A., Allison, I., Peña-Molino, B., Coleman, R., Tomczak, M., et al. (2016). Basal melt, seasonal water mass transformation, ocean current variability, and deep convection processes along the Amery Ice Shelf calving front, East Antarctica. *J. Geophysical Research: Oceans* 121, 4946–4965. doi: 10.1002/2016JC011858

Herraiz-Borreguero, L., and Naveira Garabato, A. C. (2022). Poleward shift of Circumpolar Deep Water threatens the East Antarctic Ice Sheet. *Nat. Clim. Chang.* 12, 728–734. doi: 10.1038/s41558-022-01424-3

Herraiz-Borreguero, L., R., C., Allison, I., Rintoul, S. R., Craven, M., and Williams, G. D. (2015). Circulation of modified Circumpolar Deep Water and basal melt beneath the Amery Ice Shelf, East Antarctica. *J. Geophysical Research: Oceans* 20, 3098–3112. doi: 10.1002/2015jc010697

Heywood, K. J., Sparrow, M. D., Brown, J., and Dickson, R. R. (1999). Frontal structure and Antarctic Bottom Water flow through the Princess Elizabeth Trough, Antarctica. *Deep Sea Res. Part I: Oceanographic Res. Papers* 46, 1181–1200. doi: 10.1016/S0967-0637(98)00108-3

Lannuzel, D., Vancoppenolle, M., van der Merwe, P., de Jong, J., Meiners, K. M., Grotti, M., et al. (2016). Iron in sea ice: Review new insights. *Elementa: Sci. Anthropocene* 4, 1–19. doi: 10.12952/journal.elementa.000130

Latour, P., Wuttig, K., van der Merwe, P., Strzepek, R. F., Gault-Ringold, M., Townsend, A. T., et al. (2021). Manganese biogeochemistry in the southern ocean, from tasmania to Antarctica. *Limnology Oceanography* 66, 2547–2562. doi: 10.1002/lno.11772

Liu, C., Wang, Z., Liang, X., Li, X., Cheng, C., Wu, Y., et al. (2023). Observed tidal currents in prydz bay and their contribution to the amery ice shelf basal melting. *Ocean-Land-Atmosphere Res.* 2, 20. doi: 10.34133/olar.0020

McCartney, M. S., and Donohue, K. A. (2007). A deep cyclonic gyre in the Australian-Antarctic Basin. *Prog. Oceanography* 75, 675–750. doi: 10.1016/j.pocean.2007.02.008

Meijers, A. J., Klocker, A., Bindoff, N. L., Williams, G. D., and Marsland, S. J. (2010). The circulation and water masses of the Antarctic shelf and continental slope between 30 and 80E. *Deep-Sea Res. Part II: Topical Stud. Oceanography* 57, 723–737. doi: 10.1016/j.dsr2.2009.04.019

Moreau, S., Lannuzel, D., Janssens, J., Arroyo, M. C., Corkill, M., Cougnon, E., et al. (2019). Sea ice meltwater and circumpolar deep water drive contrasting productivity in

three antarctic polynyas. *J. Geophysical Research: Oceans* 124, 2943–2968. doi: 10.1029/2019JC015071

Moreau, S., Vancoppenolle, M., Bopp, L., Aumont, O., Madec, G., Delille, B., et al. (2016). Assessment of the sea-ice carbon pump: Insights from a three-dimensional ocean-sea-ice biogeochemical model (NEMO-LIM-PISCES). *Elementa: Sci. Anthropocene* 4. doi: 10.12952/journal.elementa.000122

Morel, A. (1991). Light and marine photosynthesis: a spectral model with geochemical and climatological implications. *Prog. Oceanography* 26, 263–306. doi: 10.1016/0079-6611(91)90004-6

Morel, A., and Maritorena, S. (2001). Bio-optical properties of oceanic waters: A reappraisal. *J. Geophysical Research: Oceans* 106, 7163–7180. doi: 10.1029/2000JC000319

National Geophysical Data Center, N (2006). *National geophysical data center 2006. 2-minute gridded global relief data (ETOPO2) v2*. doi: 10.7289/V5J1012Q

Nelson, D. M., and Smith, W. Jr. (1991). Sverdrup revisited: Critical depths, maximum chlorophyll levels, and the control of Southern Ocean productivity by the irradiance-mixing regime. *Limnology Oceanography* 36, 1650–1661. doi: 10.4319/lo.1991.36.8.1650

Ohshima, K. I., Fukamachi, Y., Williams, G. D., Nihashi, S., Roquet, F., Kitade, Y., et al. (2013). Antarctic Bottom Water production by intense sea-ice formation in the Cape Darnley polynya. *Nat. Geosci.* 6, 235–240. doi: 10.1038/ngeo1738

Orsi, A. H., Whitworth, T., and Nowlin, W. D. (1995). On the meridional extent and fronts of the Antarctic Circumpolar Current. *Deep-Sea Res. Part I* 42, 641–673. doi: 10.1016/0967-0637(95)00021-W

Pinkerton, M. H., Boyd, P. W., Deppeler, S., Hayward, A., Höfer, J., and Moreau, S. (2021). Evidence for the impact of climate change on primary producers in the southern ocean. *Front. Ecol. Evol.* 9. doi: 10.3389/fevo.2021.592027

Rees, C., Pender, L., Sherrin, K., Schwanger, C., Hughes, P., Tibben, S., et al. (2019). Methods for reproducible shipboard SFA nutrient measurement using RMNS and automated data processing. *Limnology Oceanography: Methods* 17, 25–41. doi: 10.1002/lom3.10294

Rintoul, S. R. (2018). The global influence of localized dynamics in the Southern Ocean. *Nature* 558, 209–218. doi: 10.1038/s41586-018-0182-3

Roden, N. P., Shadwick, E. H., Tilbrook, B., and Trull, T. W. (2013). Annual cycle of carbonate chemistry and decadal change in coastal Prydz Bay, East Antarctica. *Mar. Chem.* 155, 135–147. doi: 10.1016/j.marchem.2013.06.006

Roden, N. P., Tilbrook, B., Trull, T. W., Virtue, P., and Williams, G. D. (2016). Carbon cycling dynamics in the seasonal sea-ice zone of East Antarctica. *J. Geophysical Research: Oceans* 121, 8749–8769. doi: 10.1002/2016JC012008

Rysgaard, S., Glud, R. N., Sejr, M. K., Bendtsen, J., and Christensen, P. B. (2007). Inorganic carbon transport during sea ice growth and decay: A carbon pump in polar seas. *J. Geophysical Research: Oceans* 112. doi: 10.1029/2006JC003572

Schallenberg, C., Bestley, S., Klocker, A., Trull, T. W., Davies, D. M., Gault-Ringold, M., et al. (2018). Sustained upwelling of subsurface iron supplies seasonally persistent phytoplankton blooms around the southern kerguelen plateau, southern ocean. *Journal of Geophysical Research: Oceans*, 123, 5986–6003. doi: 10.1029/2018JC013932

Shadwick, E. H., Rintoul, S. R., Tilbrook, B., Williams, G. D., Young, N., Fraser, A. D., et al. (2013). Glacier tongue calving reduced dense water formation and enhanced carbon uptake. *Geophysical Res. Lett.* 40, 904–909. doi: 10.1002/grl.50178

Shadwick, E. H., Tilbrook, B., and Williams, G. D. (2014). Carbonate chemistry in the Mertz Polynya (East Antarctica): Biological and physical modification of dense water outflows and the export of anthropogenic CO2. *J. Geophysical Research: Oceans* 119, 1–14. doi: 10.1002/2013JC009286

Smith, A. J. R., Ratnarajah, L., Holmes, T. M., Wuttig, K., Townsend, A. T., Westwood, K., et al. (2021). Circumpolar deep water and shelf sediments support late summer microbial iron remineralization. *Global Biogeochemical Cycles* 35, e2020GB006921. doi: 10.1029/2020GB006921

Sokolov, S., and Rintoul, S. R. (2002). Structure of Southern Ocean fronts at 140°E. *J. Mar. Syst.* 37, 151–184. doi: 10.1016/S0924-7963(02)00200-2

Sweeney, C. (2003). The annual cycle of surface water CO2 and O2 in the Ross Sea: A model for gas exchange on the continental shelves of Antarctica. *Biogeochemistry Ross Sea* Antarctica Research Series, 78, edited by: R. B. Dunbar and G. R. DiTullio AGU, Washington, D. C., 295–312. doi: 10.1029/078ars19

Tamsitt, V., Drake, H. F., Morrison, A. K., Talley, L. D., Dufour, C. O., Gray, A. R., et al. (2017). Spiraling pathways of global deep waters to the surface of the Southern Ocean. *Nat. Commun.* 8, 1–10. doi: 10.1038/s41467-017-00197-0

Vives, C. R., Schallenberg, C., Strutton, P. G., and Westwood, K. J. (2022). Iron and light limitation of phytoplankton growth off East Antarctica. *J. Mar. Syst.* 234, 103774. doi: 10.1016/j.jmarsys.2022.103774

Westwood, K. J., Brian Griffiths, F., Meiners, K. M., and Williams, G. D. (2010). Primary productivity off the Antarctic coast from 30°-80°E; BROKE-West surve. *Deep-Sea Res. Part II: Topical Stud. Oceanography* 57, 794–814. doi: 10.1016/j.dsr2.2008.08.020

Williams, G. D., Herraiz-Borreguero, L., Roquet, F., Tamura, T., Ohshima, K. I., Fukamachi, Y., et al. (2016). The suppression of Antarctic Bottom Water formation by melting ice shelves in Prydz Bay. *Nat. Commun.* 7. doi: 10.1038/ncomms12577

Williams, G. D., Nicol, S., Aoki, S., Meijers, A. J., Bindoff, N. L., Iijima, Y., et al. (2010). Surface oceanography of BROKE-West, along the Antarctic margin of the south-west Indian Ocean (30 - 80ring operator E). *Deep-Sea Res. Part II: Topical Stud. Oceanography* 57, 738–757. doi: 10.1016/j.dsr2.2009.04.020

Wright, S. W., van den Enden, R. L., Pearce, I., Davidson, A. T., Scott, F. J., and Westwood, K. J. (2010). Phytoplankton community structure and stocks in the Southern Ocean (30-80°E) determined by CHEMTAX analysis of HPLC pigment signatures. *Deep-Sea Res. Part II: Topical Stud. Oceanography* 57, 758–778. doi: 10.1016/j.dsr2.2009.06.015

Yamazaki, K., Aoki, S., Shimada, K., Kobayashi, T., and Kitade, Y. (2020). Structure of the subpolar gyre in the Australian-antarctic basin derived from argo floats. *J. Geophysical Research: Oceans* 125. doi: 10.1029/2019JC015406

Yamazaki, K., Katsumata, K., Hirano, D., Nomura, D., Sasaki, H., Murase, H., et al. (2024). Revisiting circulation and water masses over the East Antarctic margin (80–150°E). *Prog. Oceanography* 225, 103285. doi: 10.1016/j.pocean.2024.103285-P

frontiers | Frontiers in Marine Science

TYPE Original Research
PUBLISHED 23 October 2024
DOI 10.3389/fmars.2024.1454421

Check for updates

OPEN ACCESS

EDITED BY
Stelios Katsanevakis,
University of the Aegean, Greece

REVIEWED BY
Olga Mangoni,
University of Naples Federico II, Italy
Jun Sun,
China University of Geosciences, China

*CORRESPONDENCE
Karen J. Westwood
karen.westwood@aad.gov.au

†PRESENT ADDRESSES
Andreas Klocker,
NORCE Norwegian Research Centre, Bjerknes Centre for Climate Research, Bergen, Norway
Clara R. Vives,
Geobiology Department, Globe Institute, University of Copenhagen, Copenhagen, Denmark

‡These authors share first authorship

RECEIVED 25 June 2024
ACCEPTED 30 August 2024
PUBLISHED 23 October 2024

CITATION
Heidemann AC, Westwood KJ, Foppert A, Wright SW, Klocker A, Vives CR, Wotherspoon S and Bestley S (2024) Drivers of phytoplankton distribution, abundance and community composition off East Antarctica, from 55-80°E (CCAMLR Division 58.4.2 East). *Front. Mar. Sci.* 11:1454421. doi: 10.3389/fmars.2024.1454421

COPYRIGHT
© 2024 Heidemann, Westwood, Foppert, Wright, Klocker, Vives, Wotherspoon and Bestley. This is an open-access article distributed under the terms of the Creative Commons Attribution License (CC BY). The use, distribution or reproduction in other forums is permitted, provided the original author(s) and the copyright owner(s) are credited and that the original publication in this journal is cited, in accordance with accepted academic practice. No use, distribution or reproduction is permitted which does not comply with these terms.

Drivers of phytoplankton distribution, abundance and community composition off East Antarctica, from 55-80°E (CCAMLR Division 58.4.2 East)

Asta C. Heidemann[1,2‡], Karen J. Westwood[1,3*‡], Annie Foppert[1,2], Simon W. Wright[2], Andreas Klocker[2†], Clara R. Vives[2,3†], Simon Wotherspoon[3] and Sophie Bestley[1,2]

[1]Australian Antarctic Program Partnership, University of Tasmania, Hobart, TAS, Australia, [2]Institute for Marine and Antarctic Studies, University of Tasmania, Hobart, TAS, Australia, [3]Australian Antarctic Division, Department of Climate Change, Energy, the Environment and Water, Kingston, TAS, Australia

Southern Ocean phytoplankton form the base of the Antarctic food web, influencing higher trophic levels through biomass and community structure. We examined phytoplankton distribution and abundance in the Indian Sector of the Southern Ocean during austral summer as part a multidisciplinary ecosystem survey: Trends in *Euphausiids* off Mawson, Predators and Oceanography (TEMPO, 2021). Sampling covered six meridional transects from 55-80°E, and from 62°S or 63°S to the ice edge. To determine phytoplankton groups, CHEMTAX analysis was undertaken on pigments measured using HPLC. Diatoms were the dominant component of phytoplankton communities, explaining 56% of variation in chlorophyll *a* (Chl *a*), with haptophytes also being a major component. Prior to sampling the sea ice had retreated in a south-westerly direction, leading to shorter ice-free periods in the west (< 44 days, ≤65° E) compared to east (> 44 days, ≥70°E), inducing a strong seasonal effect. The east was nutrient limited, indicated by low-iron forms of haptophytes, and higher silicate:nitrate drawdown ratios (5.1 east vs 4.3 west), pheophytin *a* (phaeo) concentrations (30.0 vs 18.4 mg m^{-2}) and phaeo:Chl *a* ratios (1.06 vs 0.53). Biological influences were evident at northern stations between 75-80°E, where krill "super-swarms" and feeding whales were observed. Here, diatoms were depleted from surface waters likely due to krill grazing, as indicated by high phaeo:Chl *a* ratios (> 0.75), and continued presence of haptophytes, associated with inefficient filtering or selective grazing by krill. Oceanographic influences included deeper mixed layers reducing diatom biomass, and a bloom to the north of the southern Antarctic Circumpolar Current Front in the western survey area thought to be sinking as waters flowed from west to east. Haptophytes were influenced by the Antarctic Slope Front with high-iron forms prevalent to the south only, showing limited iron transfer from coastal waters. Cryptophytes were associated with meltwater, and greens (chlorophytes + prasinophytes) were prevalent below the mixed layer. The interplay of seasonal, biological and oceanographic influences on phytoplankton populations during TEMPO had

parallels with processes observed in the BROKE and BROKE-West voyages conducted 25 and 15 years earlier, respectively. Our research consolidates understanding of the krill ecosystem to ensure sustainable management in East Antarctic waters.

KEYWORDS

pigment analysis, CHEMTAX, chlorophyll, phytoplankton composition, Southern Ocean, Antarctic ecosystem, krill-based foodwebs

1 Introduction

Primary production in Southern Ocean waters provides the basis for the Antarctic food web, directly influencing krill populations and consequently higher predators such as penguins, seals and whales (Nicol et al., 2010; Bestley et al., 2018, 2020; Krause et al., 2022; Lohmann et al., 2023). Potential shifts in phytoplankton biomass and community structure may therefore have important implications for the entire ecosystem (Deppeler and Davidson, 2017; Kim et al., 2018). In East Antarctica, the area between 55-80°E is known to be highly productive (Pinkerton et al., 2021). With a krill fishery developing in this region (Antarctic krill, *Euphausia superba*), ecological processes here need to be better understood to ensure sustainable ecosystem management.

The Southern Ocean is a High-Nutrient-Low-Chlorophyll (HNLC) zone where macronutrients such as nitrate and silicate are overabundant, but essential micro-nutrients, particularly iron, limit phytoplankton productivity (Boyd and Ellwood, 2010; Bazzani et al., 2023). Iron is supplied to the Southern Ocean through various mechanisms including sea-ice melt (Lannuzel et al., 2016), resuspended sediments from the Antarctic shelf (de Jong et al., 2013; Smith et al., 2021), and meltwater from ice shelves, glaciers and icebergs (Death et al., 2014; Duprat et al., 2016; Herraiz-Borreguero et al., 2016). Thus, chlorophyll *a* (Chl *a*) biomass is often higher near the coast of Antarctica compared to the open ocean (Westwood et al., 2010; Wright et al., 2010). The upwelling of Circumpolar Deep Water may also increase iron availability (Moreau et al., 2019; Smith et al., 2021), as well as remineralization of organic matter through microbial processes (Smetacek et al., 2004; Cavan et al., 2019). Light can also limit productivity in Southern Ocean waters (Vives et al., 2022), with mixed layer depths controlling the average irradiance received by cells in surface waters (Mitchell et al., 1991; Nelson and Smith, 1991). Phytoplankton biomass may also form distinct bands below the mixed layer in this region (Wright and van den Enden, 2000; Gomi et al., 2007; Westwood et al., 2010) with euphotic depth therefore being particularly important for these populations.

Whilst Chl *a* measurements provide a general indication of food stocks for krill, it is vital that phytoplankton community composition is also assessed given that size classes are known to change the efficiency of food webs (Trebilco et al., 2020). Research from the Western Antarctica Peninsula (WAP) has already shown that global warming can impact communities, with a shift from diatoms to smaller cryptophytes (Moline et al., 2004; Montes-Hugo et al., 2008; Mendes et al., 2023). Ocean acidification may also cause a shift to smaller cells, as demonstrated experimentally for East Antarctic waters (Davidson et al., 2016; Westwood et al., 2018). Large diatoms are known to form the main diet of krill, whereas smaller species such as cryptophytes, haptophytes and prasinophytes generally remain ungrazed (Meyer and El-Sayed, 1983; Kopczynska, 1992; Pauli et al., 2021). The persistence of small cells is thought to be either due to inefficient filtering by krill (Kawaguchi et al., 1999; Conroy et al., 2024) or selective feeding (Haberman et al., 2003), though feeding efficiency can increase if small cells are aggregated (Haberman et al., 2003; Liu et al., 2019). In contrast, salps and microzooplankton such as copepods and pteropods are highly efficient at grazing small cells (Deibel, 1985; Madin and Kremer, 1995; Pakhomov and Froneman, 2004; Venkataramana et al., 2019). However, this increases the complexity of the food web and is associated with less efficient energy transfer (Murphy et al., 2016).

Biogeochemical cycles may also be influenced by phytoplankton composition (Boyd et al., 2012; Murphy et al., 2021). The biological pump is influenced by cell size which affects the rate of carbon export as phytoplankton become senescent and sink (Smetacek, 1985; Acevedo-Trejos et al., 2015; Fan et al., 2020; Irion et al., 2021). In addition, selective vs generalized feeding by krill and zooplankton on various phytoplankton groups influences the re-packaging of cells into fecal material, which can be exported rapidly (Cavan et al., 2019; Trebilco et al., 2020). Climate may also be influenced by phytoplankton composition, with some species such as *Phaeocystis antarctica* (*P. antarctica*, haptophyte) being strong producers of dimethylsulfoniopropionate (DMSP, DiTullio and Smith, 1995). DMSP leads to the production of sulfate aerosols, promoting cloud formation and influencing earth's radiative budget (Jang et al., 2022).

Whilst comprehensive studies on phytoplankton composition and environmental drivers have been undertaken in the WAP and Ross Sea regions (Smith et al., 2014; Schofield et al., 2017; Bolinesi et al., 2020; van Leeuwe et al., 2020), less is known for East Antarctica. Similar to the Ross Sea, diatoms are known to be the dominant group, with haptophytes (mainly *P. antarctica*) also forming a major component (Davidson et al., 2010; Takao et al., 2014; Takahashi et al., 2022). However, there is high spatial and temporal variation for these and other taxa (Kawamura and Ichikawa, 1984; Gomi et al., 2005, 2007;

Davidson et al., 2010; Wright et al., 2010; Iida and Odate, 2014; Takahashi et al., 2022; Matsuno et al., 2023). The 1996 BROKE multidisciplinary voyage spanning 80°-150°E (Nicol et al., 2000) provided several insights into environmental drivers influencing phytoplankton in East Antarctica. They included grazing by krill or salps (Hosie et al., 2000; Wright and van den Enden, 2000), season (Waters et al., 2000), and influence from the Southern Boundary (SB) which when closer to the coast was associated with decreased sea ice extent and less production (Nicol et al., 2000). Blooms were found within melting pack ice but had variable phytoplankton composition, whereas cryptophytes and some dinoflagellates were prominent in grazed zones near the ice edge (Wright and van den Enden, 2000). Offshore, there were distinct sub-surface Chl *a* maxima with prasinophytes and haptophytes often prevalent within the temperature minimum (Tmin) layer (Wright and van den Enden, 2000). Diatoms were also associated with stratified conditions, whereas haptophytes were prevalent under mixed conditions (Wright and van den Enden, 2000). Overall, the drivers for different phytoplankton taxa were varied.

The 2006 BROKE-West multidisciplinary voyage (Nicol et al., 2010) conducted between 30°-80°E was an extension of BROKE and provided further insight into phytoplankton dynamics in East Antarctica (Davidson et al., 2010; Westwood et al., 2010; Wright et al., 2010). Based on detailed datasets from this voyage, and building on observations from BROKE, Wright et al. (2010) proposed a temporal sequence of phytoplankton composition as light starts to reach the water column during sea ice melt. They hypothesized that a primary bloom forms around 35 days before complete disappearance of sea ice, mainly composed of diatoms, haptophytes *(P. antarctica)*, and cryptophytes (Wright et al., 2010), seeded from the ice. The primary bloom becomes nutrient-limited and light-limited at depth due to self-shading, but the latter is relieved by krill grazing and increased light following ice melt. This allows a secondary bloom of (mainly) low-iron haptophytes to form at depth. Krill grazing at the retreating ice edge, combined with sedimentation of phytoplankton, causes iron to be exported to depth via sinking fecal pellets and detrital aggregations. This causes iron depletion in surface waters and removes opportunities for iron recycling in the upper water column. Offshore, where sea ice has been absent for longer periods and surface iron is depleted, a nanoflagellate community develops at depth consisting of haptophytes, dinoflagellates, prasinophytes (greens) and cryptophytes, as well as some small diatoms. The offshore population forms a distinct deep chlorophyll maximum (DCM) and represents a shade flora, positioned at a depth with just enough light for growth and sustained by recycled iron as well as residual and upwelled sources. To date, the temporal sequence proposed by Wright et al. (2010) has not been re-visited.

In 2021, the TEMPO voyage (Trends in *Euphausiids* off Mawson, Predators and Oceanography) was undertaken to gain a krill biomass estimate for East Antarctica and improve our understanding of the ecosystem to inform sustainable management practices for krill fishing (Kawaguchi et al. this issue). In this paper, our aim is to determine the patterns and drivers of phytoplankton distribution, abundance and community composition within the TEMPO survey area, since phytoplankton are the main food source for krill. The survey focused on the Commission for the Conservation of Antarctic Marine Living Resources (CCAMLR) management area 58.4.2 East (55-80°E) and provided the opportunity to expand on findings from the BROKE and BROKE-West surveys conducted 25 and 15 years earlier, respectively. Specifically, we aim to determine:

- Spatial patterns of phytoplankton biomass (Chl *a*) within the survey area.
- Patterns of phytoplankton community composition and how these are shaped through seasonal, biological and oceanographic influences, considering previous BROKE and BROKE-West observations.
- Potential parallels in the temporal sequence of phytoplankton composition hypothesized by Wright et al. (2010) for further validation.

2 Materials and methods

2.1 Survey and oceanography

The survey was undertaken during austral summer from 13th February to 12th March 2021 (Figure 1). Six north-south transects (T1 to T6) were conducted from west to east (55-80°E) with each extending from 62°S or 63°S to the sea ice edge. Three transects (60°E, 70°E, 80°E) coincided with the eastern transects of the BROKE-West voyage that was undertaken in 2006 (Nicol et al., 2010). An additional station (CTD 59) was undertaken between 75°E and 80°E to the north, where a krill "super-swarm" was detected. This aggregation was > 1 km and c. 100 m deep (M. Cox pers. comm.). There was also a significant number of whales (approx. 50, mostly humpback and some fin whales) and a krill super-swarm at the northern end of 80°E in the vicinity of CTD 60 (S. Kawaguchi pers. comm.), labelled as a "whale hot-spot" station.

CTD operations were conducted using Sea-Bird SBE911 instrumentation and 31 x 12 L Niskin bottles on a rosette. Additional sensors attached to the rosette included a photosynthetically active radiation (PAR) sensor and an ECO-Triplet for fluorescence measurements. To gain a high resolution of Chl *a* throughout the water column, high performance liquid chromatography (HPLC) Chl *a* data (see below) was regressed against fluorescence measurements from the same depths to provide calibrated fluorescence profiles.

Oceanographic fronts within the survey region are shown in Figure 1, as determined by Foppert et al. (2024). The Southern Antarctic Circumpolar Current Front (sACCF) and Southern Boundary (SB) were defined as the southernmost extents of the subsurface 1.8°C and 1.5°C isotherms, respectively (Williams et al., 2010; Bestley et al., 2020b). The Antarctic Slope Front (ASF) was defined to be where the subsurface 0°C isotherm deepened below 200 dbar from north to south, and was present along all transects but one (70°E, Figure 1). Lack of the ASF at 70°E may have been due to the presence of the Prydz Bay gyre which is known to extend offshore to approximately 65°S (Vaz and Lennon, 1996, Figure 1), or alternatively the ship did not travel far enough south to sample it due to heavy sea ice presence. Mixed layer depths were calculated

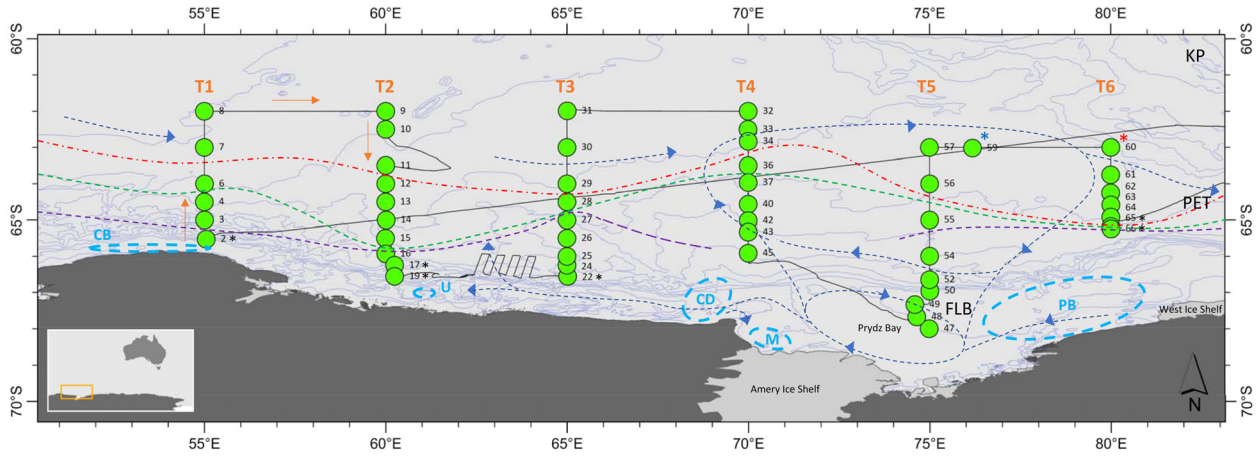


FIGURE 1
A schematic of the survey area showing CTD stations along Transects 1 - 6 (55-80°E), oceanographic fronts (after Foppert et al. (2024)), and 500 m depth contours. Red dashed line = sACCF, green dashed line = SB, purple dashed line = ASF. The approximate locations of gyres and currents are also indicated by blue dashed lines, after Smith and Trégure (1994), Vaz and Lennon (1996) and Williams et al. (2016). CTD station numbers are indicated and stations where ice was present are marked with a black asterisk. Sampling was undertaken from west to east. A krill super-swarm (defined as a dense aggregation > 1 km and c. 100 m deep) was located at CTD 59 – marked by a blue asterisk. A whale hot-spot (c. 50 whales) was located at CTD 60, with a krill super-swarm also present at this station – marked by a red asterisk. Locations of known polynyas are marked with light blue dashed circles; From west to east, CB = Cape Borle, U = Utstikkar Bay, CD = Cape Darnley, M = MacKenzie Bay, PB = Prydz Bay (consisting of Davis and Barrier polynyas combined), after Arrigo and van Dijken (2003) and Portela et al. (2021). The Kerguelen Plateau (KP), Princess Elizabeth Trough (PET), and Four Ladies Bank (FLB) are also indicated.

using a seawater density change of 0.03 kg m^{-3} from the near-surface (10 dbar, de Boyer Montégut et al., 2004, Foppert et al., 2024). The Tmin layer, where remnant winter water resides, was taken to be between the bottom of the mixed layer (as defined using the Δ 0.03 kg m^{-3} criterion) and the 0°C isotherm. For stations south of the ASF, Tmin was taken to be between the bottom of the mixed layer and 100 m. Euphotic depths were calculated as 1% incoming PAR, derived from vertical light extinction coefficients (K_d, Kirk, 1994).

Nutrients measured in Niskin bottle samples included silicate (Si), oxidized nitrogen (N), and ammonia, with sampling and analysis conducted according to standard procedures (Rees et al., 2019). As iron was not directly measured during the voyage, Si:N drawdown ratios were calculated as a proxy for iron limitation of phytoplankton, after Westwood et al. (2010), (see also Hutchins and Bruland, 1998). Briefly, average concentrations of Si and N in the mixed layer were subtracted from their respective average concentrations in the Tmin layer to determine nutrient drawdown by phytoplankton. Increased ratios are indicative of increased iron limitation.

2.2 Phytoplankton pigments

Pigments samples (1 L) were taken from Niskin bottles, filtered onto 13 mm GF/F filters in a darkened laboratory, then the filters placed in liquid nitrogen for later analysis. Six depths were sampled at each CTD station and always included the near-surface (5-10 m) and the depth of the DCM, as determined using real-time fluorescence data during downward CTD casts. In total 51 CTD stations were sampled. Pigments were later analyzed ashore using HPLC according to the method used in Wright et al. (2010). Briefly, filters were immersed in 300 µl 100% *N-N*-dimethylformamide and 50 µl methanol and incubated for 1 hour at -18°C. An internal standard (140 ng apo-8'-carotenal) was also added to improve analytical accuracy and to enable relative peak comparisons. Following incubation, the samples were mechanically disrupted using 0.7 mm zirconia beads in a mini-bead beater, then the extract was isolated from the filter/bead residue using centrifugation. The HPLC system used for analysis included a Gilson 233XL autosampler with 402 syringe pump, a Waters 1525 binary pump, a Symmetry C8 column maintained at 30°C by a water bath, a 2475 fluorescence detector and a 2998 photodiode array detector. For each HPLC run, 100 µl of sample was diluted with 25 µl water to improve peak quality (Jeffrey and Wright, 1997). Each sample injection was run for 40 minutes to allow sufficient time for solvent gradients to cycle through.

Pigments peaks were identified using Empower software (Waters) using known retention times determined through a standard mix (DHI) and a spectral absorption library (Zapata et al., 2000). Zeaxanthin and lutein peaks were difficult to distinguish due to interference from a smaller unknown peak that eluted at a similar time. These pigments were therefore analyzed under one peak named "ZeaLut". Chemotaxonomic analysis was undertaken using the software program CHEMTAX (Mackey et al., 1996; Wright et al., 1996). Nine phytoplankton taxa were initially chosen for analysis including chlorophytes, prasinophytes, cryptophytes, diatoms1, diatoms2, dinoflagellates1, dinoflagellates2, haptophytes8 high-iron, and haptophytes8 low-iron. This was based on previous experience within the survey region (Wright and van den Enden, 2000; Wright et al., 2010). Hierarchical clustering was undertaken on samples prior to analysis in CHEMTAX to reduce potential errors associated with

changes in pigment:Chl *a* ratios under varying environmental conditions such as light and nutrient availability (Wright et al., 2010). The R-Studio packages *cluster* and *dynamicTreeCut* were utilized, with the dynamic tree cutting method enabling detection of clusters dependent on their shape rather than the use of a fixed height cut-off (Langfelder et al., 2007; Hayward et al., 2023). The analysis resulted in 8 clusters sharing similar pigments.

To cross-check CHEMTAX outputs, light microscopy was undertaken on phytoplankton samples (1 L) that had been fixed in Lugol's iodine, taken at the same sites and depths as pigment samples. A total of 18 samples were examined, ensuring representation from each of the 8 clusters at the near-surface (5-10 m) and DCM, and from across each of the 6 transects. In some cases, it was clear that CHEMTAX was allocating a high proportion of Chl *a* to dinoflagellates2, whereas it should have been allocated to diatoms2. This was associated with the inclusion of gyroxanthin diester (gyrox) in the CHEMTAX analysis. There is evidence that gyrox may also be produced by haptophytes rather than solely dinoflagellates2 (Pettersen et al., 2011). Given high proportions of haptophytes in the samples it was decided to exclude gyrox and dinoflagellates2 from the CHEMTAX analysis and undertake a re-analysis. Chlorophytes and prasinophytes were also merged into "greens" for the re-analysis given the low biomass of these two groups. Table 1 shows revised phytoplankton groups and the initial pigment:Chl *a* ratios used for the second CHEMTAX run. Optimized ratios following the second run are also shown for Cluster 1, with values being within acceptable limits. As a further validation of CHEMTAX outputs, the pigment data was also analyzed using a new chemotaxonomic open-source R package *phytoclass* (Hayward et al., 2023) which uses a simulated annealing algorithm to derive phytoplankton groups. Results from the CHEMTAX and *phytoclass* analyses were strongly comparable with very little variance (Supplementary Figure 1).

Phaeophytin *a* (phaeo) pigment concentrations were also measured and utilized to gain insight into the growth stage of phytoplankton populations within the survey region. Phaeo is an oxidized degradation product of Chl *a* and thought to be a useful indicator of cell senescence (Gaffey et al., 2022), as well as grazing (Wright et al., 2010). The proportion of phaeo relative to Chl *a* can be used to indicate whether phytoplankton biomass reflects sampling during a growth phase, or during decline of the population. Comparisons of *in situ* samples with satellite-derived phenology have shown that phaeo:Chl *a* ratios < 28% suggest pre-peak growth, and higher values (> 0.28) a more senescent phase (Gaffey et al., 2022).

2.3 Ancillary data

Days since sea ice melt and distances to ice were determined from satellite. For sea ice calculations, daily passive microwave estimates of concentrations were obtained from the National Snow and Ice Data Centre SMMR-SSM/I polar product (Cavalieri et al., 1996; Maslanik and Stroeve, 1999), with ice cover <15% considered to be ice free. Data was obtained through the R package *raadtools* (Sumner, 2023). Maps of sea ice were produced using Nilas (Heil et al., 2023), showing daily 6 km concentrations using AMSR-E (Spreen et al., 2008, https://seaice.uni-bremen.de/sea-ice-

TABLE 1 (a) Initial pigment:Chl *a* ratios used in CHEMTAX, and (b) optimised ratios for Cluster 1 following analysis.

Class/Pigment	Chl c_3	Chl c_1	Peri	ButFuco	Fuco	19'-Hex	ZeaLut	Allo	Chl *b*	Chl *a*
(a) Initial										
Greens	0	0	0	0	0	0	0.012	0	0.31	1
Cryptophytes	0	0	0	0	0	0	0	0.36	0	1
Diatoms1	0	0.087	0	0	0.78	0	0	0	0	1
Diatoms2	0.065	0	0	0	1.02	0	0	0	0	1
Dinoflagellates1	0	0	0.54	0	0	0	0	0	0	1
Haptophytes8 high-iron	0.13	0	0	0.01	0.08	0.4	0	0	0	1
Haptophytes8 low-iron	0.27	0	0	0.12	0.02	1.1	0	0	0	1
(b) Optimised Cluster 1										
Greens	0	0	0	0	0	0	0.01	0	0.36	1
Cryptophytes	0	0	0	0	0	0	0	0.34	0	1
Diatoms1	0	0.07	0	0	0.68	0	0	0	0	1
Diatoms2	0.074	0	0	0	0.64	0	0	0	0	1
Dinoflagellates1	0	0	0.53	0	0	0	0	0	0	1
Haptophytes8 high-iron	0.05	0	0	0.01	0.08	0.51	0	0	0	1
Haptophytes8 low-iron	0.26	0	0	0.27	0.02	0.67	0	0	0	1

Pigment abbreviations are: Chl, chlorophyll; Peri, peridinin; ButFuco, 19'-butanoyloxyfucoxanthin; Fuco, fucoxanthin; 19'-Hex, 19'-hexanoyloxyfucoxanthin; Zea, zeaxanthin; Lut, lutein (ZeaLut pigment peaks combined); Allo, alloxanthin.

concentration/amsre-amsr2/). Maps of satellite-derived Chl *a* were produced via the ocean color climate change initiative (Sathyendranath et al., 2019) using merged products at 4 km resolution (OC-CCI ocean color data, Version 5, https://catalogue.ceda.ac.uk/uuid/1dbe7a109c0244aaad713e078fd3059a).

2.4 Models

Linear modelling, ANOVAs and General Additive Models (GAMs) were used to examine relationships between column-integrated phytoplankton and environmental variables. All modelling was undertaken in R (R Core Team, 2021). For linear modelling and ANOVAs, data was transformed where necessary based on box-cox and diagnostic plots. For 2-way ANOVAs, Tukey's HSD *post-hoc* tests were undertaken.

GAM analysis was undertaken using the R packages *mgcv* (Wood, 2017) and *visreg* (Breheny and Burchett, 2017). Parameters initially considered as predictors included mixed layer depth, days since ice melt, Tmin thickness, Tmin temperature, nitrogen concentrations in the Tmin layer and Si:N ratio. However, these needed to be reduced due to a high number of coefficients compared to a small sample size (n=51 stations). Following examination of separate GAMS for these parameters and the associated significance terms, a final GAM was fitted including mixed layer depth, days since sea ice melt, Si:N drawdown ratio (indicator of iron limitation) and nitrogen in the Tmin layer. Mixed layer depth and days since sea ice melt were found to be significant drivers of diatoms2 biomass (see below), so a similar GAM analysis was undertaken to also explore their effects on other phytoplankton taxa.

3 Results

3.1 Sea ice

Sea ice within the survey region retreated from north-east to south-west prior to the voyage commencing (Figures 2, 3). By mid-November the sea ice was already low to absent at the northern ends of 70-80°E. 55-65°E transects still had 100% ice cover along most of their length. The sea ice then retreated along the northern sections of 55-65°E throughout December. There was a gradual retreat south across all transects thereafter, with a minimum in February when voyage sampling commenced. By early to mid-March when sampling was being completed, the sea ice had started to re-form (Figure 2). As stations were undertaken from west to east, 55-65°E experienced more recent sea ice compared to other transects not only due to later melt, but also due to earlier sampling. 55-65°E and 80°E had sea ice present at southern-most stations at the time of sampling (Figure 3). The sea ice at the southern end of 80°E was newly formed. The southern stations on 70°E and 75°E did not have sea ice present at their sampling sites, though there was heavy sea ice in the surrounding area. Days since sea ice melt (defined as the number of days since a satellite pixel was 15% covered) ranged from 0-122 days at the time that samples were taken (Figure 3). The sACCF had a significant influence on the timing of sea ice melt with stations north of the sACCF melting earlier ($F_{1,49} = 45$, $p<0.001$, Figures 2, 3).

3.2 Chlorophyll distribution

Integrated Chl *a* concentrations (summed over 0-150 m) derived from high resolution fluorescence measurements ranged

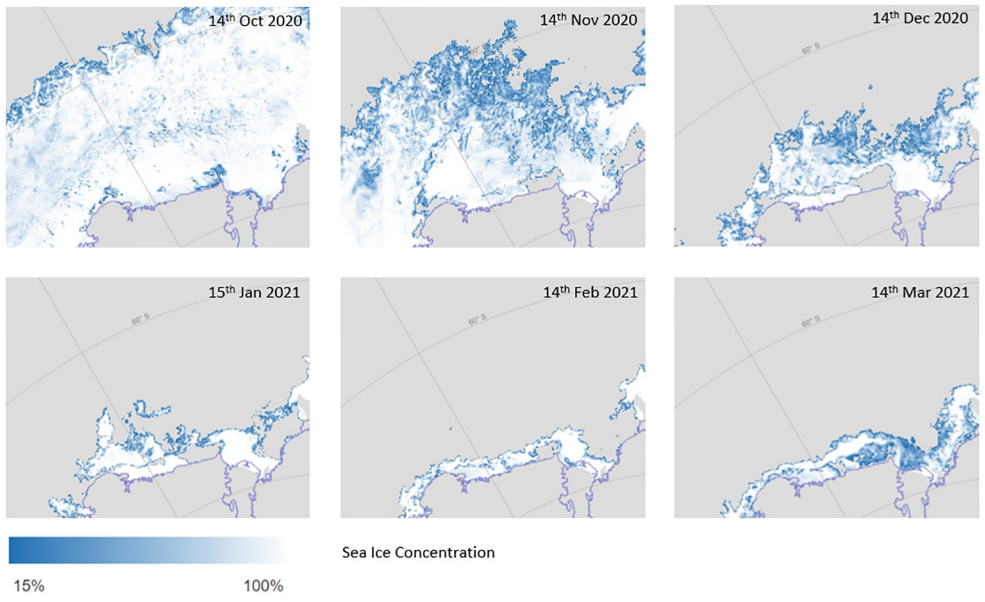


FIGURE 2
Sea ice concentrations (%) prior to and during the TEMPO voyage (Spreen et al., 2008).

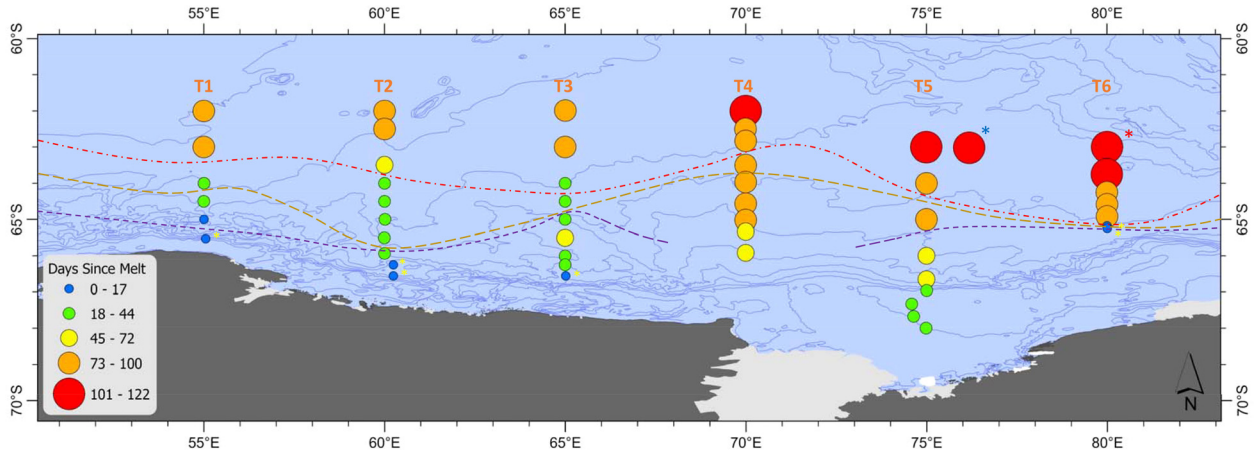


FIGURE 3
Days since sea ice melt at CTD stations along Transects 1-6 (55-80°E). Stations where sea ice was present are marked with a yellow asterisk. Red dashed line = sACCF, brown dashed line = SB, purple dashed line = ASF. The krill super-swarm station is marked by a blue asterisk. The whale hot-spot station is marked by a red asterisk.

from 18 to 102 mg m^{-2} (Figure 4). Chl *a* concentrations were elevated (> 61 mg m^{-2}) at the northern ends of 55°E and 60°E, the mid-section of 70°E, and the southern end of 80°E. At 75°E there were comparatively low Chl *a* concentrations (< 31 mg m^{-2}) on the shelf, but elevated concentrations at the continental slope and extending offshore. 65°E had relatively low Chl *a* along its length compared to the other transects. The krill super-swarm and whale hot-spot stations had notably low Chl *a* concentrations of < 24 mg m^{-2} (Figure 4).

Throughout the water-column Chl *a* concentrations ranged from 0.02 to 2.6 µg L^{-1}, with an average of 0.47 µg L^{-1} (Figure 5). Elevated Chl *a* concentrations at the northern end of 55°E were located within the mixed layer (Figure 5). In contrast, there was elevated Chl *a* below the mixed layer at 60°E and 65°E. The elevated Chl *a* stations across 55-65°E were all north of the sACCF (Figures 4, 5). South of the sACCF there were a number of Chl *a* "holes" (< 0.2 µg L^{-1}) within the mixed layer across 55-65°E (Figure 5). The well-defined nature of these holes, apparent at similar latitudes across transects, suggested that they may have been interlinked zonally, *i.e.* with the same hole spanning transects in association with currents.

The large offshore bloom along 75°E was located within the mixed layer (Figure 5) with Chl *a* concentrations as high as 2.6 µg L^{-1}. High Chl *a* along 70°E and 80°E were likely an east-west extension of this bloom. However, at 80°E most Chl *a* at the southern end was below the mixed layer rather than within it. This was due to shallow mixed layer depths associated with low salinity and temperature (Figure 5; Supplementary Figure 2), suggesting a meltwater lens at this location despite recent sea ice formation. 75°E showed an abrupt transition between the slope/offshore bloom and the shelf region, where comparatively low Chl *a* occurred throughout the water column (Figure 5). Elevated Chl *a* concentrations across 70-80°E

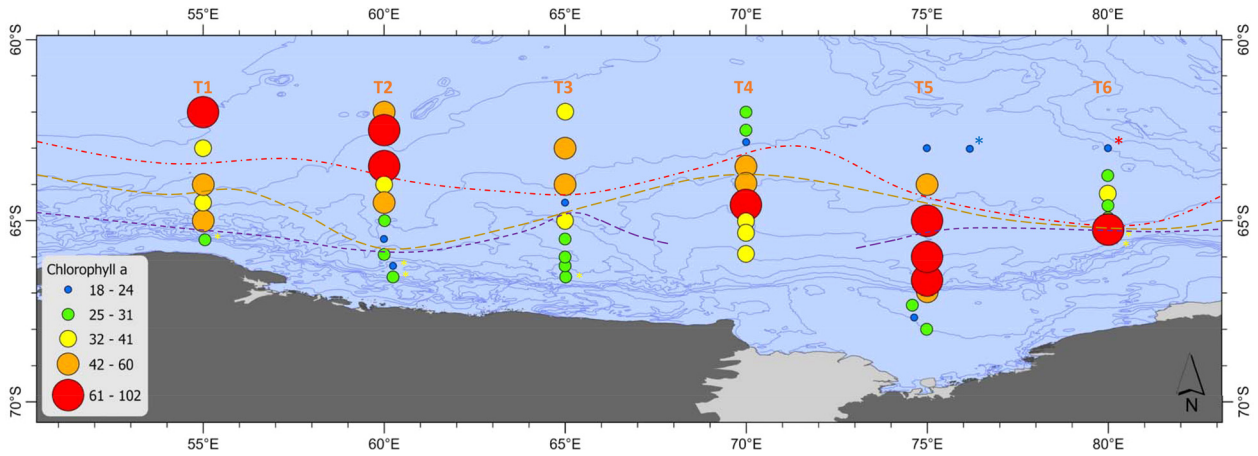


FIGURE 4
Integrated Chl *a* (10-150 m, mg m^{-2}) at stations along Transects 1 to 6 (55-80°E). Stations where sea ice was present are marked with a yellow asterisk. Red dashed line = sACCF, brown dashed line = SB, purple dashed line = ASF. The krill super-swarm station is marked by a blue asterisk. The whale hot-spot station is marked by a red asterisk.

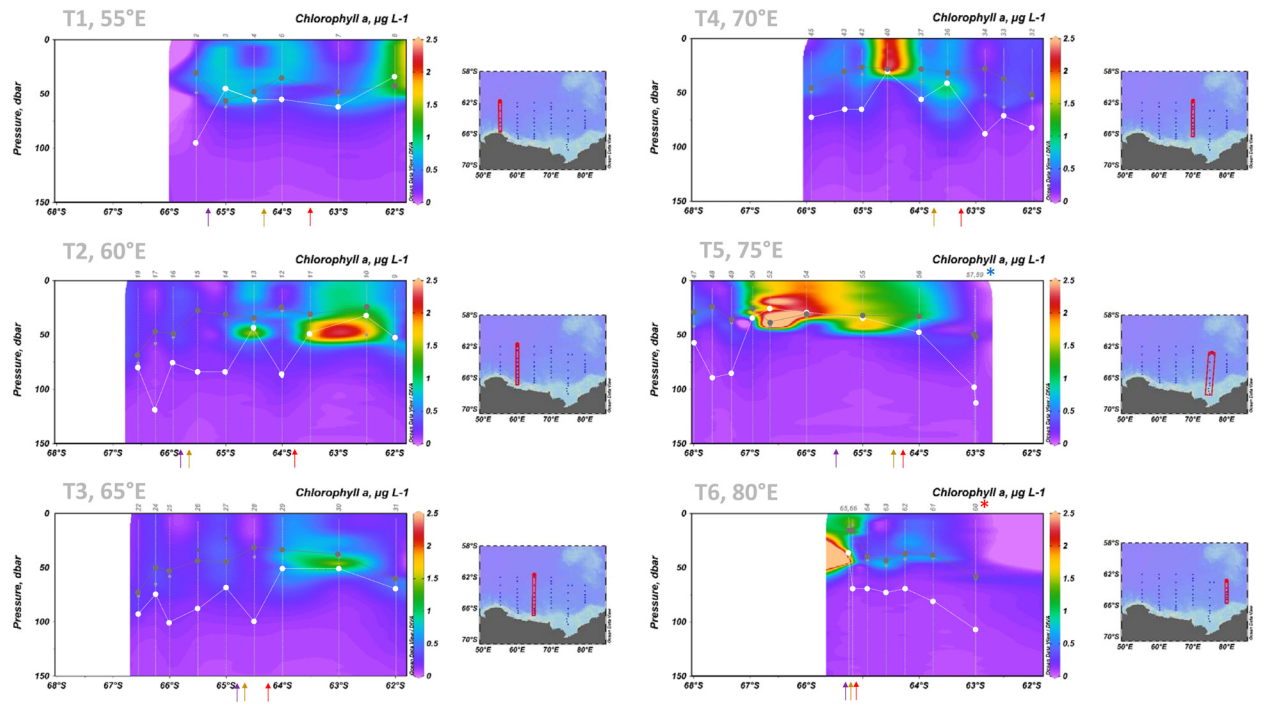


FIGURE 5
Chl *a* concentrations with depth (µg L^{-1}) along each transect (55-80°E). Dark grey circles with dashed lines are mixed layer depth calculated from density (kg m^{-3}), white circles with dashed lines are euphotic depth (m). Light grey circles are mixed layer depth calculated from maximum buoyancy frequency, for comparison with other studies. CTD station numbers are also shown. Data was interpolated between CTD stations using DIVA and plotted in Ocean Data View (Schlitzer, R., Ocean Data View, odv.awi.de, 2023). The krill super-swarm station is marked by a blue asterisk. The whale hot-spot station is marked by a red asterisk. Approximate frontal locations are indicated by arrows; red = sACCF, brown = SB, purple = ASF.

were all south of the SB (Figures 4, 5). North of the sACCF, there was low Chl *a* in surface waters at the krill super-swarm and whale hot-spot stations (Figures 4, 5).

Mixed layer depths ranged from 16 to 74 m (Figure 5), with shallowest depths at the southern end of 80°E due to the meltwater lens (see above). Euphotic depths ranged from 26-120 m (Figure 5), with depths of > 90 m at the krill super-swarm (75°E) and whale hot-spot (80°E) stations, as well as CTD 57 (in the vicinity of the krill super-swarm station) and CTDs 2, 17 and 25. These stations were all associated with low Chl *a*. At most stations, mixed layer depths were notably shallower than euphotic depths (Figure 5) so that cells circulating within the mixed layer would have experienced a high light environment. The exception was at stations where the 55-65°E and 70-80°E blooms occurred. At these locations, mixed depths were more similar to euphotic depths, and in some cases deeper, with circulating cells likely to experience periods of photo-limitation due to fluctuating light (Figure 5).

GAM analysis was used to further explore the major determinants of integrated Chl *a* stocks. The strongest association was a strong non-linear negative relationship with euphotic depth ($p < 0.001$, eff df= 3.23, R^2 adj=0.908, deviance explained=91.4%, Figure 6A). This clearly represented shading of the water column as biomass increased, rather than a negative response of phytoplankton to irradiance. There was also a non-linear relationship with days since sea ice melt ($p=0.014$, eff df = 3.46, R^2 adj=0.212, deviance explained=26.7%, n=51, Figure 6B). Biomass was high immediately following ice melt, slowly increased to a peak at 70 days, then declined. There were two high Chl *a* outliers evident (Figure 6B) – CTD 52 on the slope at 75°E, and CTD 66 at the southern end of 80°E. Both stations were associated with the 70-80°E bloom.

3.3 Satellite phenology

Ocean color data from satellites provided synoptic-scale patterns of Chl *a* in the lead up to, and during the voyage (Figure 7). The December composite showed there was elevated Chl *a* offshore (62-64°S) from 60-80°E in the vicinity of retreating sea ice. However, throughout February when sampling occurred this offshore Chl *a* was no longer visible. Similarly, the Prydz Bay polynya and West Ice Shelf were associated with consistently high Chl *a* on the shelf and offshore from December through to February (Figure 7), but by the time 70-80°E were sampled this visible surface Chl *a* had also decreased. Interestingly, there was a low Chl *a* band between the shelf and offshore in the Prydz Bay region during January and February, in the vicinity of the slope front (Figure 7). Ice cover hindered visibility in this region during March when *in situ* sampling was undertaken. The Cape Darnley and MacKenzie polynyas had peak Chl *a* concentrations in March, with the Cape Darnley autumn bloom achieving the highest surface concentrations evident within the survey area throughout the entire austral summer season. However, 70°E sampling in the vicinity of Cape Darnley was undertaken further offshore away from the polynya, and was also undertaken late February to early March so that these high Chl *a* concentrations

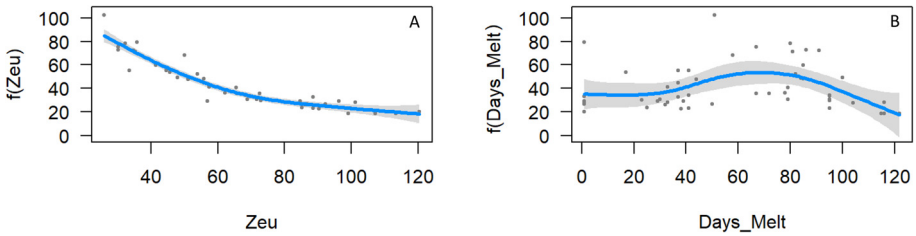


FIGURE 6
GAM analysis of integrated (10-150 m) Chl *a* showing the relationship with **(A)** euphotic depth, and **(B)** days since sea ice melt.

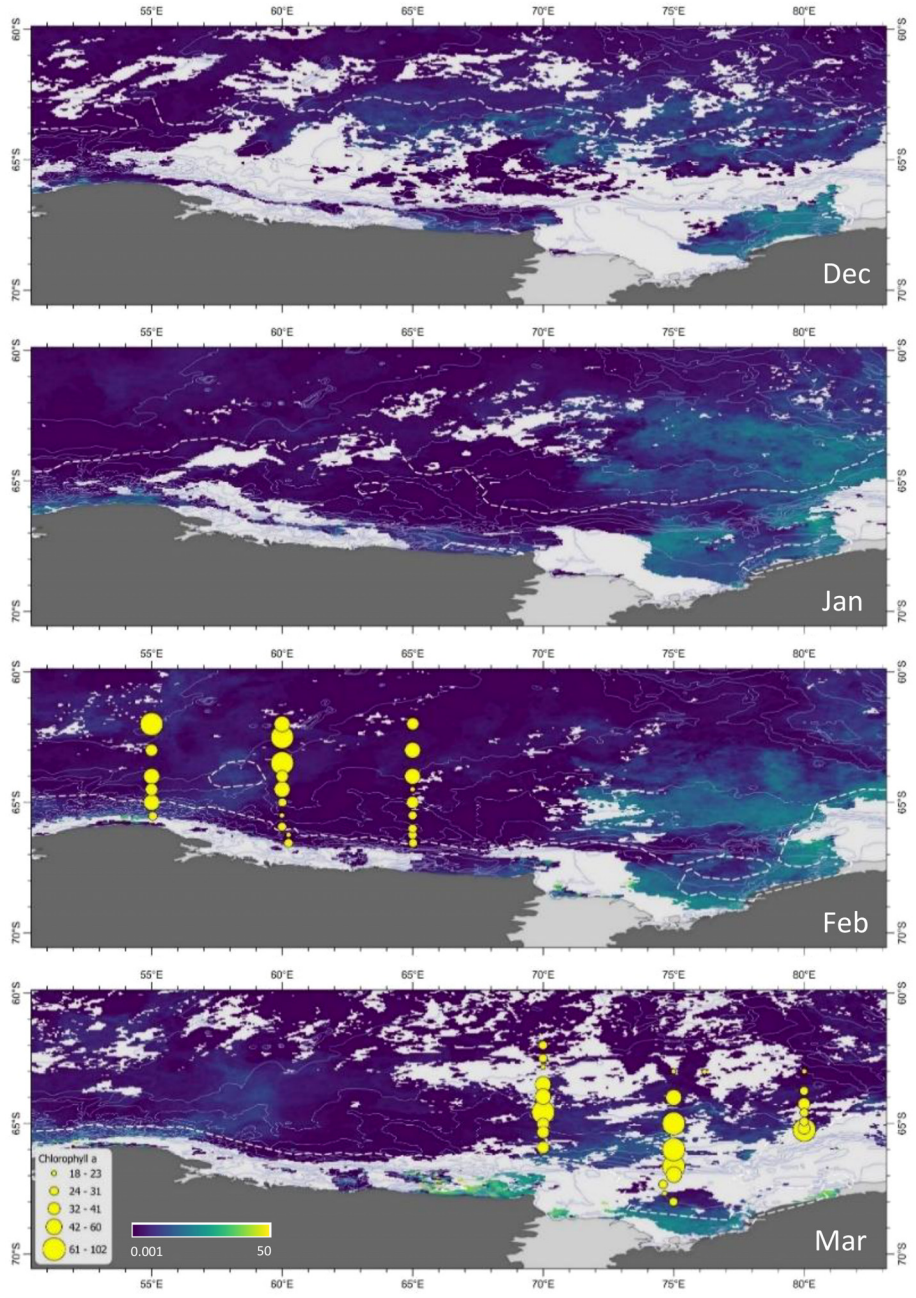


FIGURE 7
Chl *a* derived from monthly composites of ocean colour in the lead-up to and during the voyage (mg m^{-3}, Sathyendranath et al., 2019) and from HPLC pigment analysis during the voyage (mg m^{-2}, yellow circles). Depth contours (500 m) are shown as unbroken white lines. White dashed lines indicate 15% ice cover.

had likely not yet developed. Overall, *in situ* sampling of phytoplankton across the survey area appeared to occur post-peak of visible ocean color for most transects.

3.4 Phaeophytin and Si:N

Concentrations of phaeo ranged from 0 to 2.5 µg L^{-1} (Figure 8A). Measurements were significantly lower across 55-65° E (30.0 ± 16.4 mg m^{-2}) compared to 70-80°E (18.4 ± 12.5 mg m^{-2}, $F_{1,49}$ = 7.95, p=0.007), with a complete absence of phaeo at the southern end of 55°E. Concentrations did not noticeably change with depth for any given station. Phaeo:Chl *a* ratios showed that most phytoplankton populations in the survey area were in a decline phase, as indicated by proportions > 0.28 (Figure 8B). Cells in a growth phase (ratios < 0.28) were mainly in the western survey region across 55-65°E with these transects sampled earlier in the season (see above). Average ratios were significantly lower across 55-65°E (0.53 ± 0.3), compared to 70-80°E (1.06 ± 0.55, $F_{1,49}$ = 18.66, p< 0.005). Phaeo concentrations were not notably high at the krill super-swarm and whale hot-spot stations (Figure 8A), but this was likely associated with the very low biomass at these stations. In contrast, phaeo:Chl *a* ratios for these stations were high with values > 0.75 (Figure 8B).

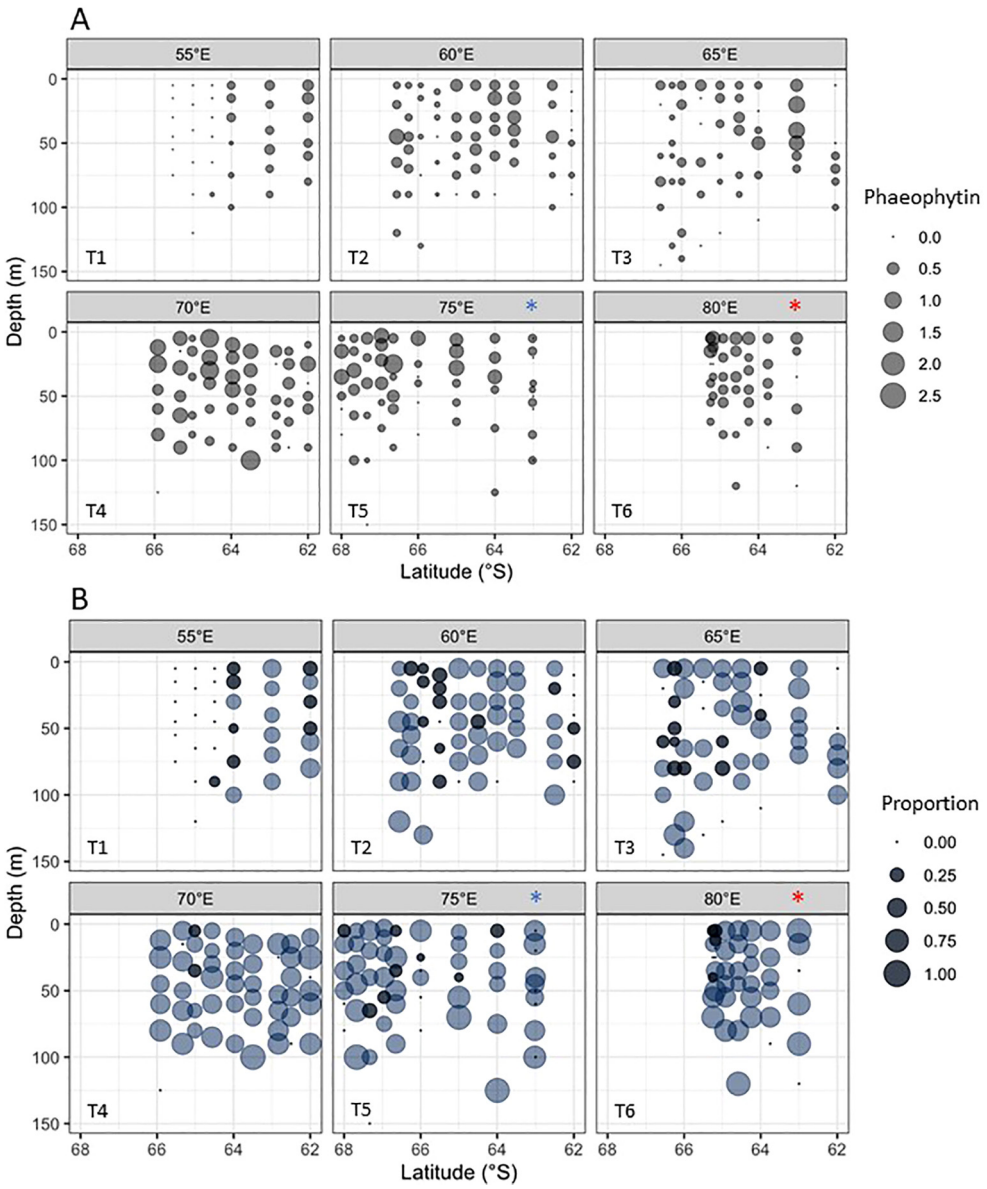


FIGURE 8
(A) Phaeophytin *a* (pheo) concentrations (µg L^{-1}), and **(B)** phaeo:Chl *a* ratios. Populations in a growth phase (ratios < 0.28) are indicated by dark blue circles. Light blue circles (ratios > 0.28) indicate populations in relative decline. Concentrations of 0 µg L^{-1} have been included to show locations where samples were taken. The krill super-swarm station is marked by a blue asterisk. The whale hot-spot station is marked by a red asterisk.

Macronutrient concentrations were generally non-limiting within the survey area, with nitrate ranging between 18.3-35.9 µM and silicate from 3.9-86.8 µM. The Si:N drawdown ratio was used as a proxy for iron limitation within the survey area (Hutchins and Bruland, 1998; Westwood et al., 2010), with higher ratios indicative of higher limitation. Si:N drawdown showed a similar pattern to phaeo:Chl *a* with ratios lower in the western survey area across 55-65°E (4.3 ± 0.7) compared to 70-80°E in the east (5.1 ± 0.7), with a one-way ANOVA showing that this difference was significant ($F_{1,49}$ = 8.9, p=0.004, Figure 9).

3.5 Phytoplankton community composition

Phytoplankton assemblages, determined using CHEMTAX analysis of pigments, had large spatial variations within the survey area (Figure 10). Diatoms2 was the most abundant group across all transects (Table 2), explaining 56% of variability in total Chl *a* with a strong linear relationship ($F_{1,49}$ = 65.5, R^2-adj= 0.56, p<0.001). Concentrations ranged from to 0.001 to 1.9 µg L^{-1}, with an average of 0.26 ± 0.34 µg L^{-1}. Microscopy showed that the pennate diatoms *Fragilariopsis* and *Pseudonitzschia* were the most represented genera within this group. The centric diatom *Thalassiosira* was also abundant as solitary cells. Haptophytes8 (high-iron and low-iron) were the second-most prevalent group, comprising almost 30% of total Chl *a*. There was variation as to which of the two iron groups dominated across the survey area, with a generally inverse relationship (Figure 10). Haptophytes8 high-iron were slightly more prevalent than low-iron overall, comprising 58% of the total haptophyte biomass. Concentrations of haptophytes8 high-iron ranged from 0 to 0.49 µg L^{-1}, with an average of 0.08 ± 0.08 µg L^{-1}. Haptophytes8 low-iron ranged from 0 to 0.45 µg L^{-1} with an average of 0.06 ± 0.06 µg L^{-1}. The primary species identified through light microscopy was *P. antarctica*, with both solitary cells and colonial forms present.

Diatoms1 were mainly found within the mixed layer across the survey region (Figure 10; Table 2). Concentrations ranged from 0 to 0.31 µg L^{-1} with an average of 0.016 ± 0.039 µg L^{-1}. In contrast, greens had highest biomass below the mixed layer (range 0 to 0.18 µg L^{-1}, average 0.02 ± 0.03 µg L^{-1}, Table 2) with their main prevalence at the southern ends of 65°E and 70°E, and off the shelf at 75°E. Similarly, dinoflagellates1 were more prevalent below the mixed layer, though biomass was relatively low (range 0 to 0.25 µg L^{-1}, average 0.014 ± 0.024 µg L^{-1}) and almost absent along 80°E. Cryptophytes were also low in biomass (range 0 to 0.14 µg L^{-1}, average 0.025 ± 0.017 µg L^{-1}) but were most prevalent at the southern-ends of 75°E (both on- and off-shelf) and 80°E. Cryptophyte populations were present both above and below the mixed layer (Figure 10; Table 2).

Elevated Chl *a* concentrations observed across the northern and mid-sections of 55-65°E (Figure 5) were associated with high abundances of diatoms2, north of the sACCF (Figure 10). The diatoms were clearly within the mixed layer at 55°E, but below the mixed layer at 60°E and 65°E. There were also elevated concentrations of haptophytes8 high-iron across 55-65°E, but cells were both above and below the mixed layer at 60°E and 65°E. Haptophytes8 high-iron were prevalent south of the ASF along most transects, particularly at 55°E, on the shelf at 75°E, and at 80°E (Figure 4). There were significantly lower densities of haptophytes8 high-iron north (6.3 ± 4.5 mg m^{-2}) compared to south of the ASF (9.5 ± 3.3 mg m^{-2}, $F_{1,49}$ = 6.11, p=0.017). Haptophytes low-iron were prevalent below the mixed layer across 55-65°E compared to surface waters (Figure 10; Table 2).

Elevated Chl *a* concentrations spanning 70-80°E south of the sACCF (Figure 5) were similarly associated with diatoms2 and haptophytes (Figure 10). However, in contrast to the bloom across 55-65°E, the haptophytes associated with the 70-80°E bloom in the eastern part of the survey area were predominantly low-iron rather than high-iron. Haptophytes low-iron were generally more prevalent in the eastern part of the survey area (70-80°E) compared to west (55-65°E).

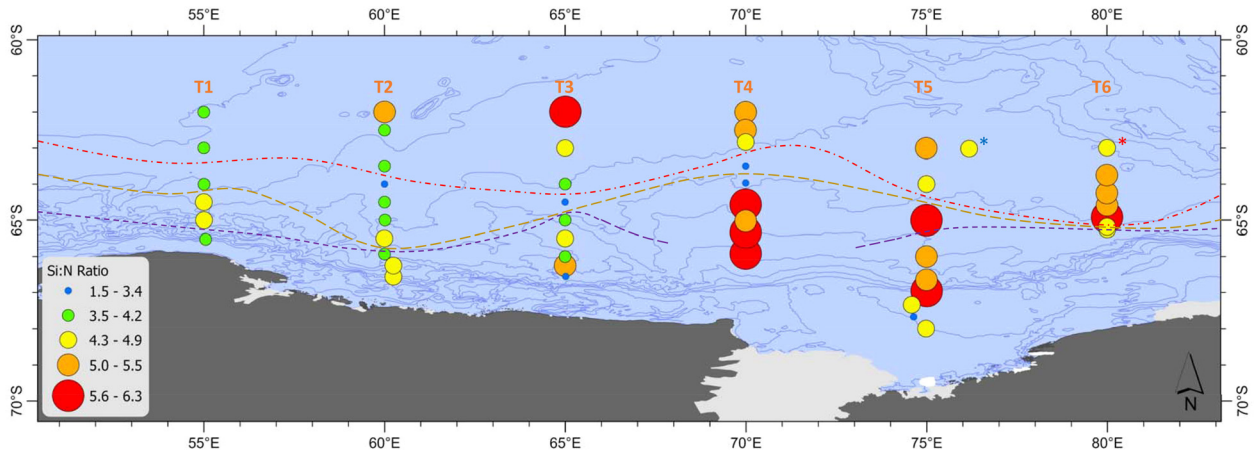


FIGURE 9
Silicate to nitrate ratios (Si:N) along Transects 1-6 (55-80°E). High ratios indicate high iron limitation and *vice versa*. Stations where sea ice was present are marked with a yellow asterisk. Red dashed line = sACCF, brown dashed line = SB, purple dashed line = ASF. The krill super-swarm station is marked by a blue asterisk. The whale hot-spot station is marked by a red asterisk.

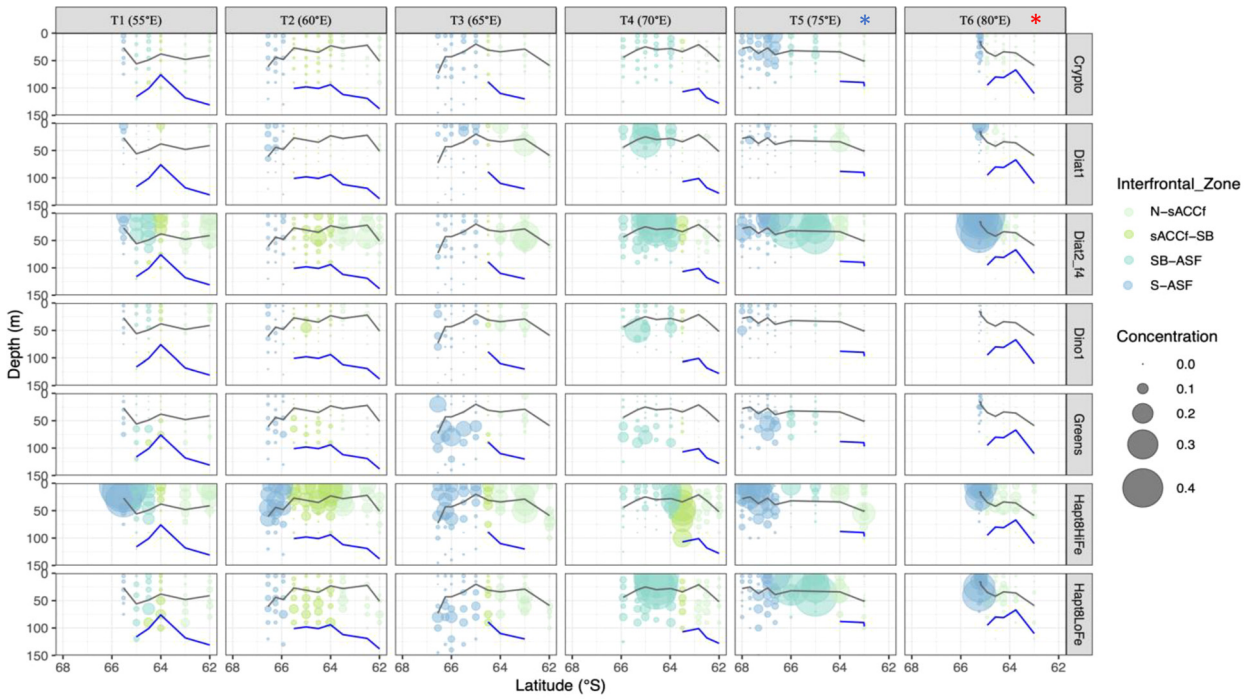


FIGURE 10
Depth profiles of phytoplankton taxa (μg L^{-1}) across the survey region. Mixed layer depths are shown as grey lines (Δ 0.03 kg m^{-3}), and the bottom of the Tmin layer shown as blue lines (note that deep values >150 m are not shown). Inter-frontal regions are coloured as per the key. Values of 0 μg L^{-1} have been included to show the locations where samples were taken. Due to high concentrations of diatoms2 they were reduced by a factor of 4 (f4) to improve visualisation. The krill super-swarm station is marked by a blue asterisk. The whale hot-spot station is marked by a red asterisk.

At the krill super-swarm station where there was low Chl *a* (see above), diatoms2 biomass was low throughout the water column (Figure 10). There was a high abundance of diatoms2 along 75°E, but an abrupt decrease in abundance where the krill were present. Similarly, at the whale hot-spot station there was low biomass of diatoms2 at the northern end of 80°E. Most other phytoplankton taxa were also absent at the krill super-swarm and whale hot-spot stations, except for haptophytes8 high iron.

3.6 Relationships with environmental variables

As diatoms2 were the dominant phytoplankton group and are the preferred food source for krill, the main modelling was undertaken on this taxon to further investigate relationships with environmental parameters. GAM analysis on column-integrated diatoms2 showed that mixed layer depth and days since sea ice melt were significant drivers of biomass (R^2-adj=0.36, deviance explained=46.9%, n=49, Figure 11). Diatoms2 biomass clearly decreased with deeper mixed layers (p=0.018, eff df=0.83). They also showed high biomass immediately following ice melt, a slight decrease, then similar to the Chl *a* model an increase between around 40 to 80 days post-melt, then a decline (p=0.022, eff df= 3.74). Nitrate concentration in the Tmin layer, Si:N drawdown and temperature of the Tmin layer had no significant influence on diatoms2.

For other phytoplankton taxa, mixed layer depth had a significant influence on two groups only; haptophytes8 low-iron (p=0.042, eff df=1.00, r2-adjusted=0.062, deviance explained=8.1%, Figure 12), and dinoflagellates1 (p=0.011, eff df=4.94, r2-adjusted=0.258, deviance explained=33.1%). However, the significant results were leveraged by the station with the deepest mixed layer (73 m at CTD 22). With this outlier removed the relationship for both taxa then became non-significant (p = 0.06 haptophytes8 low-iron, p=0.19 dinoflagellates1).

Days since ice melt influenced most phytoplankton groups, except dinoflagellates1 and diatoms1. Haptophytes8 high-iron decreased with days since melt (p=0.029, eff df=1.00, R^2-adjusted=0.075, deviance explained=9.4%, Figure 13), whereas haptophytes8 low-iron increased up until 70-80 days, then declined (p=0.036, eff df=2.69, R^2-adjusted=0.156, deviance explained=20.2%). Greens and cryptophytes remained relatively stable with days since ice melt, but started to decline at around 70 days post-melt (greens: p=0.003, eff df=2.34, R^2-adjusted=0.233, deviance explained=26.9%; cryptophytes: p=0.025, eff df=2.08, R^2-adjusted=0.150, deviance explained=18.5%). For all taxa, biomass declined at 95-120 days post-melt, with these stations all sampled 26th February or later, coinciding with the onset of austral autumn.

Overall, both mixed layer depth and days since ice melt had influences on phytoplankton populations within the survey region. One or both of these parameters influenced all taxa apart from dinoflagellates1 and diatoms1, noting that the influence of additional environmental parameters is not shown for taxa other

TABLE 2 Summary of key results for the seven major CHEMTAX phytoplankton groups.

Phytoplankton Group	Key Results
Cryptophytes	Low background concentrations across most of the survey area; Higher concentrations at southern stations on 75°E and 80°E; Biomass both above and below the mixed layer.
Diatoms1	Low background concentrations across most of the survey area; Most biomass within the mixed layer.
Diatoms2	The most abundant taxa comprising 56% of total Chl *a*; High abundances spanning 55-65°E north of the sACCF, and 70-80°E south of the sACCF and SB; Cells predominantly within the mixed layer at 55°E, 70°E and 75°E; Cells below the mixed layer at 60°E, 65°E and 80°E.
Dinoflagellates1	Low background concentrations across most of the survey area; Almost absent along 80°E; Highest concentrations found below the mixed layer at 70°E.
Greens	Prevalent below the mixed layer; High concentrations found at the southern ends of 65°E and 70°E, and off the shelf at 75°E.
Haptophytes8 high-iron	Prevalence south of the ASF along most transects; Associated with the 55-65°E bloom; Biomass both above and below the mixed layer; Cells still present at the krill super-swarm and whale hot-spot stations.
Haptophytes8 low-iron	Associated with the 70-80°E bloom; Biomass above and below the mixed layer across 70-80°E; Low concentrations in the western part of the survey area across 55-65°E, with cells prevalent in the Tmin layer.

than diatoms2. A preliminary analysis of additional parameters showed no meaningful patterns and were thus not pursued.

4 Discussion

The TEMPO survey off East Antarctica enabled the spatial distribution and temporal patterns of Chl *a* and phytoplankton communities to be described, as well as elucidating environmental drivers for these patterns. Variability was caused by an interplay of oceanographic, seasonal and biological influences that shaped populations. These are discussed further below. The survey also provided the opportunity to re-visit a similar region to the BROKE (Nicol et al., 2000) and BROKE-West (Nicol et al., 2010) voyages conducted 25 and 15 years earlier, respectively. The TEMPO survey differed from BROKE and BROKE-West in that it occurred about one month later and did not penetrate the sea ice zone. Nevertheless, the general patterns and features observed during TEMPO were similar to the previous voyages, and successional patterns relating to ice melt, krill grazing, and iron limitation were generally consistent with those described by Wright et al. (2010).

Chl *a* concentrations for TEMPO ranged from 0.02 to 2.6 μg L^{-1}, with an average of 0.47 μg L^{-1}, and integrated biomass from 18-102 mg m^{-2}. These concentrations were significantly lower than for BROKE-West (0.88-5.6 μg L^{-1}, average 1.2 μg L^{-1} and up to 328 mg m^{-2}, Wright et al., 2010), likely due to the ship being unable to enter sea ice where most productivity occurs (Strutton et al., 2000; Westwood et al., 2010). Maximum Chl *a* concentrations for BROKE (3.4 μg L^{-1}) were also higher than our study (Wright and van den Enden, 2000), though integrated concentrations were similar (27.4-103.0 mg m^{-2}). Diatoms2 was found to be the dominant taxon within the TEMPO survey region. This group therefore had a strong influence on Chl *a* distribution and explained 56% of variation. Haptophytes8 were the next dominant taxon and comprised 30% of Chl *a*. The dominance of diatoms and haptophytes was expected and agrees with other studies in the East Antarctic region (Davidson et al., 2010; Wright et al., 2010; Iida and Odate, 2014; Takao et al., 2014; Takahashi et al., 2022).

4.1 Oceanographic influences

There were two major blooms within the survey area, mainly consisting of diatoms2 and haptophytes8. The first bloom spanned 55-65°E north of the sACCF. Diatoms2 were within the mixed layer at 55°E, but below the mixed layer at 60°E and 65°E. Given the bloom was north of the sACCF this may suggest that the population was sinking as the current moved from west to east, with large and heavy cells observed such as *Fragilariopsis* and *Thalassiosira* having high export potential (Roca-Martí et al., 2017). Sinking may have been facilitated through nutrient limitation, though the northern sections of 55°E and 60°E were sampled closely in time. In contrast, haptophytes8 remained within the mixed layer across these transects, with the dominant species being motile cells of *P. antarctica*. The persistence of haptophytes8 in surface waters was therefore expected, given the small size of cells (< 5 μm) which

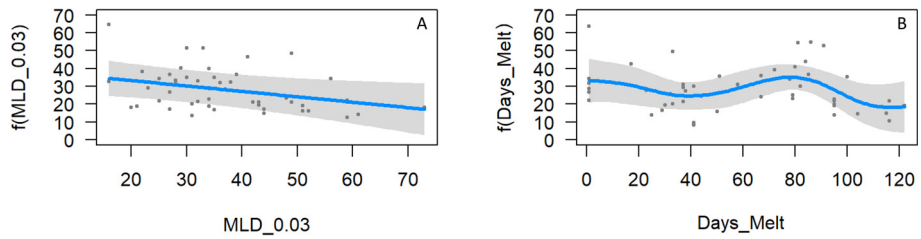


FIGURE 11
GAM analysis of diatoms2 showing the interactive relationship with **(A)** mixed layer depth, and **(B)** days since sea ice melt. Only parameters that had a significant influence are shown.

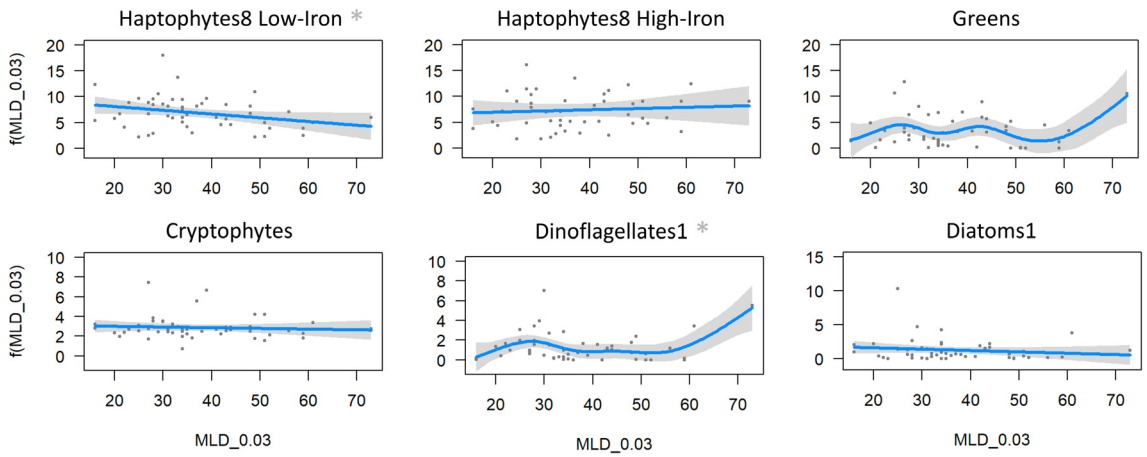


FIGURE 12
GAM analysis of the various phytoplankton taxa against mixed layer depth. Significant relationships are marked with an asterisk, but they are not significant when 73 m mixed layer depth is excluded.

hinders sinking, and evidence that the carbon flux of haptophytes is less efficient than for diatoms (Gowing et al., 2001; Wolf et al., 2016); although we note that rapid export of *P. antarctica* blooms can occur when cells are in colonial form (DiTullio et al., 2000). The second bloom spanned 70-80°E south of the SB. Again, this bloom was dominated by diatoms2 as well as haptophytes8, though in this case there was no evidence for the sinking of cells from surface waters. Satellite evidence suggested that the 70-80°E bloom was associated with advection from the Prydz Bay and West Ice Shelf regions. These regions may also be important for fueling blooms in the Princess Elizabeth Trough and Southern Kerguelen Plateau (Schallenberg et al., 2018). In the BROKE and BROKE-West surveys the SB was found to have an influence on production (Nicol et al., 2000; Wright et al., 2010). However, this was not found in our study given that blooms occurred both north and south of this front.

The main physical control on diatom2 populations was found to be mixed layer depth, with decreased biomass when mixed layer depth increased. Mixed layer depths were mostly shallower than euphotic depths throughout the survey area, so circulating cells did not experience photo-limitation. The preference of diatoms2 for shallower mixed layers and higher average irradiances agrees with the BROKE survey (Wright and van den Enden, 2000) and studies from other Antarctic regions including the Ross Sea (Arrigo et al., 1999), Western Antarctic Peninsula (Kopczynska, 1992; Schofield et al., 2017) and Northern Antarctic Peninsula (Costa et al., 2023). Diatoms are successful under stable light conditions due to low pigment concentrations per cell combined with high amounts of photoprotective pigment, allowing lower susceptibility to photoinhibition compared to other groups (Arrigo et al., 2010; Kropuenske et al., 2010). In fact, this group does not cope well with fluctuating light compared to other groups, due to slower photo acclimation processes (Larkum et al., 2003; Strzepek and Harrison, 2004; Kropuenske et al., 2010; van Leeuwe et al., 2020). Additional processes that may have contributed to decreased abundances included the entrainment of low Chl *a* water from depth (Smith

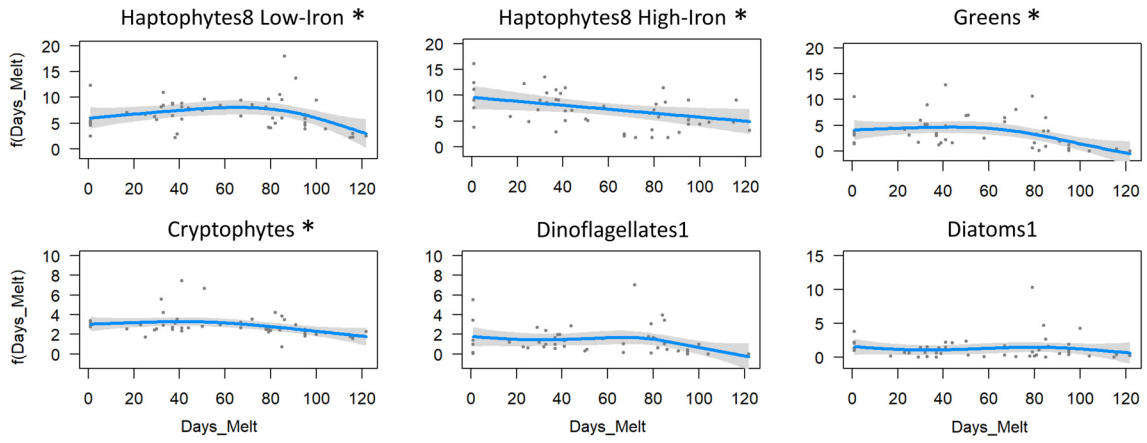


FIGURE 13
GAM analysis of the various phytoplankton taxa against days since ice melt. Significant relationships are marked with an asterisk.

et al., 2011), or increased particle aggregation from turbulence leading to export (Jones and Smith, 2017). Haptophytes were not affected by mixed layer depth in our study, but other studies have shown that they do favor mixed conditions (Wright and van den Enden, 2000). The main haptophyte, *P. antarctica*, is known to be highly adaptable to fluctuating light including under iron-limited conditions (Arrigo et al., 2010; van Leeuwe and Stefels, 2007; Kropuenske et al., 2010).

Haptophytes8 distribution was influenced by the ASF, in addition to seasonal influences described below. There were significantly higher concentrations of haptophytes8 high-iron south of the ASF across most transects, compared to north of the ASF. This pattern was very likely related to increased iron availability, with stations south of the ASF in closer vicinity to the Antarctic continental shelf and sea ice (Westwood et al., 2010). Shelf waters are known to supply sustained inputs of iron to surface waters through sediment resuspension (de Jong et al., 2013; Smith et al., 2021), with sea ice and melting from glaciers and ice shelves also being a significant source (Death et al., 2014; Duprat et al., 2016; Herraiz-Borreguero et al., 2016; Lannuzel et al., 2016). A significant change in haptophytes across the ASF confirms the physical influence of this front on nutrient availability, with reliance on cross-slope exchange processes such as frontal instabilities and eddies to influence transport (Heywood et al., 2014).

4.2 Seasonal effects

A second influence on haptophytes8 was season. North of the ASF there was a change in the relative proportion of high- and low-iron haptophytes8 from west to east across the survey area. Haptophytes8 high-iron were the prevalent form in the 55-65°E bloom and across the western survey region in general. In contrast, the 70-80°E bloom and general eastern survey region was dominated by low-iron forms, suggesting that this region was iron-limited. 55-65°E transects were sampled earlier in the season than 70-80°E. 55-65°E also experienced later sea ice melt, with retreat occurring across the survey area in a southwesterly direction. The combined influence of earlier sampling and later ice melt meant that most stations along 55-65°E were < 44 days post-melt. In contrast, the majority of 70-80°E stations were > 44 days post-melt (excepting stations on the shelf). Accordingly, GAM analysis showed that with increasing days since sea ice melt, haptophytes8 high-iron gradually decreased, whereas haptophytes8 low-iron increased, reflecting the differences observed between the western and eastern survey.

Pheophytin *a* (phaeo) concentrations and Si:N drawdown ratios further supported a strong seasonal influence on haptophytes8 and all other phytoplankton taxa within the survey area. Phaeo is a degradation product of Chl *a* (Jeffrey, 1997) and was significantly lower across 55-65°E compared to 70-80°E. It was also completely absent along sections of 55°E near the sea ice. Similarly, Si:N ratios were also significantly lower across 55-65°E suggesting less iron limitation of diatoms in this region (Hutchins and Bruland, 1998; Takeda, 1998; Franck et al., 2000). Finally, lower phaeo:Chl *a* ratios across 55-65°E compared to 70-80°E showed that 55-65°E populations to be in better health than 70-80°E populations. Interestingly however, most phaeo:Chl *a* ratios across the whole of the survey area were > 0.28 which suggested that cells were past their peak in growth at the time of sampling (Gaffey et al., 2022). This agreed with the satellite ocean color data which showed that by the time of sampling, Chl *a* that was previously present in surface waters had declined.

Despite clear changes in the health of phytoplankton between the western and eastern survey area, this was not reflected in column-integrated biomass for most taxa with days since sea ice melt only influencing the ratio of haptophytes high- and low- iron (see above) and diatoms2 over most of the growth season. This is discussed further in Section 4.5 below, in relation to the temporal sequence hypothesized by Wright et al. (2010). The main influence of days since sea ice melt was at the end of season with a decline in all taxa at > 95 days post-melt. These stations were all sampled 26th Feb or later, therefore coinciding with the onset of austral autumn. The last transect was completed on 12th March, by which time the sea ice had started to reform. Mixed layer depths for these final stations were not yet noticeably deeper. However, reduced daylength and lower angles of incoming light would have meant that cells were experiencing lower daily average irradiances, limiting productivity (Strutton et al., 2000). This would have allowed loss processes such as sinking and grazing to outweigh growth (Smith et al., 2000). Waters et al. (2000) also found decreased phytoplankton abundance with the onset of winter conditions during the BROKE survey.

4.3 Grazing

Large numbers of whales (c. 50) observed feeding at the northern end of 80°E (S. Kawaguchi pers. comm., April 2021), and krill super-swarms observed between 75°E and 80°E (M. Cox pers. comm., April 2021) indicated this region to be highly productive. Similarly, large numbers of humpback whales were previously observed feeding in the same vicinity in 2016 (A. Constable pers. comm. March 2016, K-Axis voyage, V3; 2015/16, RSV *Aurora Australis*), and tracking data has shown that Western Australian humpback whales visit this area from November to March (Bestley et al., 2019). Elevated climatological Chl *a* derived from satellite ocean color provides further evidence for high seasonal productivity here (Pinkerton et al., 2021). In addition, Foppert et al. (2024) found evidence of upwelling in this region during TEMPO, a process which likely increased nutrient availability for phytoplankton, and may support predictable foraging grounds for migrating baleen whales.

There was observational evidence for selective grazing of phytoplankton at the whale hot-spot and krill super-swarm stations located in this region. Diatoms2 had been stripped from surface waters, causing notably lower chlorophyll concentrations compared to the rest of the survey area. It is highly likely that diatoms2 had been grazed by krill, with their large cell size making them the preferred food source due to more efficient filtering (Meyer and El-Sayed, 1983). In contrast, small haptophytes remained within surface waters at both stations. This was likely

due either to inefficient filtering of small cells by krill (Kawaguchi et al., 1999; Conroy et al., 2024), or selective feeding on diatoms rather than haptophytes (Haberman et al., 2003). Phaeo: Chl *a* ratios at both stations were higher than elsewhere along these transects (> 0.75), also supporting the suggestion of heavy grazing. Interestingly, the haptophytes8 remaining in the water column at the whale hot-spot and krill super-swarm stations were high- rather than low-iron forms, despite these stations being off-shore and in the eastern survey area. This suggests nutrient recycling, possibly through bacterial remineralization of krill or whale fecal material which is known to be iron rich (Ratnarajah et al., 2018). Sloppy feeding by krill may also have been a source of iron (Cavan et al., 2019).

A series of "holes" in surface Chl a (< 0.2 µg L-1) occurred across 55-65°E. Similar holes were also observed north of the ice edge during BROKE and BROKE West (Wright and van den Enden, 2000; Wright et al., 2010), which, during the latter cruise, closely matched the distribution of krill swarms grazing the ice-edge bloom. Comparison of Chl *a* and integrated krill biomass data in the vicinity of CTD stations during TEMPO showed no relationship across the survey area (data not shown). However, krill swarms are actively motile and the biomass measured at a specific time in the vicinity of a CTD station does not necessarily represent recent grazing pressure. Cox et al. (2022) found during the TEMPO voyage that small scale krill surveys can provide a good representation of the statistical distribution of krill densities across a larger scale, but only within the same latitudinal band. This potentially supports the hypothesis of the Chl *a* holes being interconnected across transects due to bands of high krill density. However, the Chl *a* holes were not strictly within the same latitudinal band, showing minor shifts to the south from 55°E to 65°E. Given these holes were present both north and south of the sACCF, SB and ASF it does not seem that fronts were influential.

4.4 Shelf waters

The only shelf stations within the survey area were at the southern end of 75°E in Prydz Bay. Here, there was an abrupt transition to low Chl *a* compared to the slope and offshore phytoplankton bloom (60-80°E). This transition may have been partly related to circulation patterns. The shelf stations (CTDs 47-50) were located across Four Ladies Bank which is known to act as a barrier to water exchange between the continental shelf and offshore (Smith and Trégure, 1994; Xu et al., 2019). There is a gyre within Prydz Bay associated with the outflow of supercooled ice shelf water from underneath the Amery Ice Shelf. This water is channeled offshore through the Amery Depression, with a weak return flow thought to exist across Four Ladies Bank to the Amery (Williams et al., 2016). It was therefore likely that the 75°E shelf stations were experiencing quite different oceanographic influences compared to offshore.

Krill grazing may also have been partly responsible for the abrupt transition to low Chl *a*, particularly given that diatoms2 was the main group depleted. Satellite observations showed high Chl *a* in this region from December through to February, but this had decreased by the time of sampling in early March. Within Prydz Bay the krill species *Euphausiia crystallorophias* would likely have been the dominant taxon responsible for grazing (Thomas and Green, 1988; Hosie and Cochran, 1994). Zooplankton other than krill also require consideration as grazers, with microzooplankton, copepods, pteropods and salps also prominent in Prydz Bay (Pearce et al., 2010; Hosie and Cochran, 1994; Li et al., 2001; Yang et al., 2013). These zooplankton groups efficiently ingest small phytoplankton cells (Johnston et al., 2021) however there was no clear evidence of this in the current study. Whilst there was a decrease in haptophytes8 low-iron on the shelf compared to the slope and offshore, there was a marked increase in haptophytes8 high-iron likely due to increased iron availability (see above), so the overall biomass of haptophytes8 remained essentially the same. Small cryptophytes were also present over the Prydz Bay shelf in higher concentrations than other transects. Regardless of whether circulation patterns and/or grazing influenced the transition in Chl *a* between the shelf and offshore, these regions have previously been shown to be ecologically distinct (Hosie and Cochran, 1994; Davidson et al., 2010).

4.5 Comparison with the BROKE-West temporal sequence

The patterns of phytoplankton biomass and composition during the TEMPO survey were consistent with those of BROKE-West and the latter part of the hypothesized temporal sequence proposed by Wright et al. (2010). Wright et al. (2010) proposed that a primary bloom forms around 35 days before complete disappearance of sea ice, which is seeded from the ice community, and consists mainly of diatoms2, high- and low-iron haptophytes8 and, to a lesser extent, cryptophytes. This bloom quickly exhausts iron stocks and is consumed by krill, allowing a secondary bloom of low-iron haptophytes at depth due to increased light there. The surface waters are left iron-depleted as iron has been exported to depth via the sinking of detrital aggregates from the primary bloom and krill fecal pellets following grazing. A nanoflagellate shade community then develops at depth utilizing recycled iron (Boyd and Ellwood, 2010) as well as residual or upwelled sources.

Several observations during TEMPO matched this sequence. First, our study showed highest biomass of diatoms2 and haptophytes8 immediately following ice melt, noting that we were unable to sample prior to melt. These populations were likely residual from a primary bloom that had developed under the ice. Takahashi et al. (2022) also recently showed evidence for the seeding of the water column by diatoms from sea ice communities. Second, the observed change from predominantly high-iron to low-iron haptophytes8 and patterns of Si:N drawdown are consistent with exhaustion of iron by the bloom (see above). Third, our study showed the development of a deep nanoflagellate community, consisting of greens and haptophytes. Greens were prevalent below the mixed layer across most transects, particularly across 65-75°E. Haptophyte8 low-iron were prevalent below the mixed layer across 55-65°E. The success of nanoflagellates at depth in low-iron environments is likely due to their small cell size, with

efficient uptake of recycled iron due to high surface area to volume ratios (Sunda and Huntsman, 1997; Li et al., 2009; Marañón, 2015).

However, there were also some differences from BROKE-West, which may be partly explained by TEMPO occurring a month later in the season. In the BROKE-West temporal sequence, diatoms2 decreased rapidly after 20 days post-melt, whereas in our study there was a slow decline from 0 to 40 days, implying that loss processes were slower. There was also a secondary increase in diatoms2 from 40-80 days post-melt in our study. This may simply have represented sites with few loss processes, with cells that had grown earlier in the season remaining in the water-column but slowly becoming senescent. Increased Si:N drawdown ratios and phaeo in our study supported this suggestion. Sexual reproduction may also have occurred leading to an increase in cell size, as recently shown by Matsuno et al. (2023) at 90-100 days post-melt.

Our study was also different from BROKE-West in that cryptophytes were not prevalent during TEMPO, with an average concentration of only 0.025 μg L^{-1}. In the Western Antarctic Peninsula where cryptophytes are prevalent (Hayward et al., 2024), high biomass is associated with low salinity (32.5-33.75 psu) and colder (-1 to 1°C) coastal waters (Schofield et al., 2017), with plumes extending as far as 100 km offshore (Moline et al., 2004). We identified a meltwater lens at southern stations on 80°E during the TEMPO voyage with salinity and temperature as low as 32.7 psu and -1.3°C at the surface, respectively (Foppert et al., 2024). Accordingly, cryptophyte abundances were higher in this region. There were also higher abundances of cryptophytes at the southern end of 75°E on the shelf in Prydz Bay and extending offshore. Whilst there was no clear meltwater lens at this location (Foppert et al., 2024), salinity and temperature were low in the southernmost surface waters sampled (CTD 47, 33.3 psu, -1.2°C), with both parameters gradually increasing to the north. A gradual increase in salinity and temperature along 75°E (rather than the abrupt changes seen at 80°E), may have been related to mixing associated with the gyre (see above, Williams et al., 2016).

Lastly, dinoflagellates1 were present in the deep nanoflagellate community during the BROKE-West survey (Wright et al., 2010) but this was not seen during TEMPO, apart from at one station at the southern end of 70°E where there were high concentrations within the Tmin layer. In general, abundances of dinoflagellates1 were lower for TEMPO than for BROKE-West. An almost complete absence of dinoflagellates1 along 80°E suggested that this taxon was strongly influenced by season, leading to the lower concentrations for the TEMPO survey.

4.6 Conclusions

The TEMPO survey represented the first large multidisciplinary survey off East Antarctica since the BROKE and BROKE-West surveys conducted 25 and 15 years earlier, respectively. It offered the opportunity to re-examine processes at the base of the food web in a region where krill fishing may expand, and to further understand the interplay of seasonal, biological and oceanographic drivers. Our data was broadly consistent with the previous surveys, and supported a temporal sequence in phytoplankton biomass and composition proposed for ice edge blooms.

The dominant phytoplankton groups were diatoms2 and haptophytes8, the latter with pigments that represented high- and low-iron forms. The primary drivers of biomass and composition included mixed layer depth, the ASF, seasonal changes, and iron depletion. There was also clear evidence of krill grazing, with a number of "holes" in the distribution of phytoplankton along transects. These holes appeared to mainly affect diatoms2 with clear depletion in surface waters. Haptophytes8 remained at these sites, suggesting selective grazing of the large diatoms by krill, or inefficient grazing of the smaller haptophyte cells. Greens and haptophytes low-iron were prevalent below the mixed layer and represented a nanoflagellate shade community similar to that observed for BROKE-West.

Whilst we found that phytoplankton populations and processes over the past 25 years were comparable across studies, the predicted loss of sea ice with climate change will likely influence phytoplankton composition into the future. The potential effects of such changes on krill populations and dependent organisms, as well as on carbon export, warrants further study on bloom development, particularly within the sea ice early in the season. Such data is vital as a base for ecosystem and carbon models. From a methodological standpoint, our study showed that a combination of pigment analysis for phytoplankton taxa (particularly the high- and low-iron forms of haptophytes8), phaeo:Chl *a* ratios, and Si:N drawdown ratios, provides valuable insights into the growth and grazing of phytoplankton and can be used to refine modelling efforts.

5 Additional requirements

All voyage activities were undertaken under an approved Notice of Determination and Authorization, in compliance with the Antarctic Treaty (Environment Protection Act) 1980. Phytoplankton/pigment samples were collected under AMLR Permit 20-23-4512 in compliance with the Marine Living Resources Conservation Act 1981.

Data availability statement

The datasets presented in this study can be found in online repositories. The names of the repository/repositories and accession number(s) can be found in the article/Supplementary Material.

Author contributions

AH: Formal analysis, Investigation, Visualization, Writing – original draft, Writing – review & editing. KW: Conceptualization, Data curation, Formal analysis, Funding acquisition, Investigation, Methodology, Project administration, Resources, Supervision, Visualization, Writing – original draft, Writing – review & editing. AF: Conceptualization, Formal analysis, Investigation, Supervision, Visualization, Writing – review & editing. SW: Formal analysis, Supervision, Writing – review & editing. AK:

Investigation, Writing – review & editing. CV: Investigation, Writing – review & editing. SW: Formal analysis, Writing – review & editing. SB: Conceptualization, Formal analysis, Investigation, Project administration, Supervision, Visualization, Writing – review & editing.

Funding

The author(s) declare financial support was received for the research, authorship, and/or publication of this article. This project was supported and funded by Australian Antarctic Science Projects 4512 and 4636, and received grant funding from the Australian Government as part of the Antarctic Science Collaboration Initiative program. This project also received financial support from Pew Charitable Trust and the Antarctic Science Foundation. We acknowledge the use of the CSIRO Marine National Facility (MNF, https://ror.org/01mae9353) in the form of sea-time on RV *Investigator*, and provision of support personnel, scientific equipment and data management. All data and samples from the voyage are publicly available as per MNF policy.

Acknowledgments

We would like to thank chief scientist Dr So Kawaguchi and deputy-chief scientist Mr Rob King for leading the voyage, and Ms Linda Gaskell (MNF) for voyage management. We also thank the captain and crew of RV *Investigator*, and MNF technical personnel for their support on the voyage. Thanks also to Dr Michael Sumner for ocean color maps, Dr Ben Raymond for sea ice data, and Dr Alexander Hayward for comparison of CHEMTAX and *phytoclass* outputs.

Conflict of interest

The authors declare that the research was conducted in the absence of any commercial or financial relationships that could be construed as a potential conflict of interest.

Publisher's note

All claims expressed in this article are solely those of the authors and do not necessarily represent those of their affiliated organizations, or those of the publisher, the editors and the reviewers. Any product that may be evaluated in this article, or claim that may be made by its manufacturer, is not guaranteed or endorsed by the publisher.

Supplementary material

The Supplementary Material for this article can be found online at: https://www.frontiersin.org/articles/10.3389/fmars.2024.1454421/full#supplementary-material

References

Acevedo-Trejos, E., Brandt, G., Bruggeman, J., and Merico, A. (2015). Mechanisms shaping size structure and functional diversity of phytoplankton communities in the ocean. *Sci. Rep.* 5, 8918. doi: 10.1038/srep08918

Arrigo, K. R., Mills, M. M., Kropuenske, L. R., van Dijken, G. L., Alderkamp, A.-C., and Robinson, D. H. (2010). Photophysiology in two major Southern Ocean phytoplankton taxa: Photosynthesis and growth of *Phaeocystis Antarctica* and *Fragilariopsis cylindrus* under different irradiance levels. *Integr. Comp. Biol.* 50, 950–966. doi: 10.1093/icb/icq021

Arrigo, K. R., Robinson, D. H., Worthen, D. L., Dunbar, R. B., DiTullio, G. R., Vanwoert, M., et al. (1999). Phytoplankton community structure and the drawdown of nutrients and CO_2 in the Southern Ocean. *Science* 283, 365–367. doi: 10.1126/science.283.5400.365

Arrigo, K. R., and van Dijken, G. L. (2003). Phytoplankton dynamics within 37 Antarctic coastal polynya systems. *J. Geophys. Res. Oceans* 108, 3271. doi: 10.1029/2002JC001739

Bazzani, E., Lauritano, C., and Saggiomo, M. (2023). Southern Ocean iron limitation of primary production between past knowledge and future projections. *J. Mar. Sci. Eng.* 11, 272. doi: 10.3390/jmse11020272

Bestley, S., Andrews-Goff, V., van Wijk, E., Rintoul, S. R., Double, M. C., and How, J. (2019). New insights into prime Southern Ocean forage grounds for thriving Western Australian humpback whales. *Sci. Rep.* 9, 13988. doi: 10.1038/s41598-019-50497-2

Bestley, S., Raymond, B., Gales, N. J., Harcourt, R. G., Hindell, M. A., Jonsen, I. D., et al. (2018). Predicting krill swarm characteristics important for marine predators foraging off East Antarctica. *Ecography* 41, 996–1012. doi: 10.1111/ecog.03080

Bestley, S., Ropert-Coudert, Y., Bengtson Nash, S., Brooks, C. M., Cotté, C., Dewar, M., et al. (2020a). Marine ecosystem assessment for the southern ocean: birds and marine mammals in a changing climate. *Front. Ecol. Evol.* 8. doi: 10.3389/fevo.2020.566936

Bestley, S., van Wijk, E., Rosenberg, M., Eriksen, R., Corney, S., Tattersall, K., et al. (2020b). Ocean circulation and frontal structure near the southern Kerguelen Plateau: The physical context for the Kerguelen Axis ecosystem study. *Deep-Sea Res. II.* 174. doi: 10.1016/j.dsr2.2018.07.013

Bolinesi, F., Saggiomo, M., Ardini, F., Castagno, P., Cordone, A., Fusco, G., et al. (2020). Spatial-related community structure and dynamics in phytoplankton of the Ross Sea, Antarctica. *Front. Mar. Sci.* 7. doi: 10.3389/fmars.2020.574963

Boyd, P. W., Arrigo, K. R., Strzepek, R., and van Dijken, G. L. (2012). Mapping phytoplankton iron utilization: Insights into Southern Ocean supply mechanisms. *J. @ Geophys. Res. Oceans* 117, C06009. doi: 10.1029/2011JC007726

Boyd, P. W., and Ellwood, M. J. (2010). The biogeochemical cycle of iron in the ocean. *Nat. Geosci.* 3, 675–682. doi: 10.1038/ngeo964

Breheny, P., and Burchett, W. (2017). Visualization of regression models using *visreg*. *R. J.* 9, 56–71. doi: 10.32614/RJ-2017-046

Cavalieri, D. J., Parkinson, C. L., Gloersen, P., and Zwally, H. J. (1996). *Sea Ice Concentrations from Nimbus-7 SMMR and DMSP SSM/I-SSMIS Passive Microwave Data, Version 1* (NASA National Snow and Ice Data Center Distributed Active Archive Center).

Cavan, E. L., Belcher, A., Atkinson, A., Hill, S. L., Kawaguchi, S., McCormack, S., et al. (2019). The importance of Antarctic krill in biogeochemical cycles. *Nat. Commun.* 10, 4742. doi: 10.1038/s41467-019-12668-7

Conroy, J. A., Steinberg, D. K., Nardelli, S. C., and Schofield, O. (2024). Omnivorous summer feeding by juvenile Antarctic krill in coastal waters. *Limnol. Oceanogr.* 69, 874–887. doi: 10.1002/lno.12533

Costa, R. R., Ferreira, A., de Souza, M. S., Tavano, V. M., Kerr, R., Secchi, E. R., et al. (2023). Physical-biological drivers modulating phytoplankton seasonal succession along the Northern Antarctic Peninsula. *Environ. Res.* 231, 116273. doi: 10.1016/j.envres.2023.116273

Cox, M. J., Macaulay, G., Brasier, M. J., Burns, A., Johnson, O. J., King, R., et al. (2022). Two scales of distribution and biomass of Antarctic krill (Euphausia superba) in the eastern sector of the CCAMLR Division 58.4.2 (55°E to 80°E). *PloS One* 17, e0271078. doi: 10.1371/journal.pone.0271078

Davidson, A. T., McKinlay, J., Westwood, K., Thomson, P. G., van den Enden, R., de Salas, M., et al. (2016). Enhanced CO_2 concentrations change the structure of Antarctic marine microbial communities. *Mar. Ecol. Prog. Ser.* 552, 93–113. doi: 10.3354/meps11742

Davidson, A. T., Scott, F. J., Nash, G. V., Wright, S. W., and Raymond, B. (2010). Physical and biological control of protistan community composition, distribution and abundance in the seasonal ice zone of the Southern Ocean between 30 and 80°E. *Deep Sea Res. II* 57, 828–848. doi: 10.1016/j.dsr2.2009.02.011

Death, R., Wadham, J. L., Monteiro, F., Le Brocq, A. M., Tranter, M., Ridgwell, A., et al. (2014). Antarctic ice sheet fertilises the Southern Ocean. *Biogeosci.* 11, 2635–2643. doi: 10.5194/bg-11-2635-2014

de Boyer Montégut, C., Madec, G., Fischer, A. S., Lazar, A., and Iudicone, D. (2004). Mixed layer depth over the global ocean: An examination of profile data and a profile-based climatology. *J. Geophys. Res. Oceans* 109, C12003. doi: 10.1029/2004JC002378

Deibel, D. (1985). Clearance rates of the salp *Thalia democratica* fed naturally occurring particles. *Mar. Biol.* 86, 47–54. doi: 10.1007/BF00392578

de Jong, J., Schoemann, V., Maricq, N., Mattielli, N., Langhorne, P., Haskell, T., et al. (2013). Iron and land-fast sea ice of McMurdo Sound derived from sediment resuspension and wind-blown dust attributes to primary productivity in the Ross Sea, Antarctica. *Mar. Chem.* 157, 24–40. doi: 10.1016/j.marchem.2013.07.001

Deppeler, S. L., and Davidson, A. T. (2017). Southern Ocean phytoplankton in a changing climate. *Front. Mar. Sci.* 4. doi: 10.3389/fmars.2017.00040

DiTullio, G. R., Grebmeier, J. M., Arrigo, K. R., Lizotte, M. P., Robinson, D. H., Leventer, A., et al. (2000). Rapid and early export of *Phaeocystis Antarctica* blooms in the Ross Sea, Antarctica. *Nature* 404, 595–598. doi: 10.1038/35007061

DiTullio, G. R., and Smith, W. O. (1995). Relationship between dimethylsulfide and phytoplankton pigment concentrations in the Ross Sea, Antarctica. *Deep Sea Res. I Oceanogr. Res. Pap.* 52, 873–892. doi: 10.1016/0967-0637(95)00051-7

Duprat, L., Bigg, G., and Wilton, D. (2016). Enhanced Southern Ocean marine productivity due to fertilization by giant icebergs. *Nat. Geosci.* 9, 219–221. doi: 10.1038/ngeo2633

Fan, G., Han, Z., Ma, W., Chen, S., Chai, F., Mazloff, M. R., et al. (2020). Southern Ocean carbon export efficiency in relation to temperature and primary productivity. *Sci. Rep.* 10, 13494. doi: 10.1038/s41598-020-70417-z

Foppert, A., Bestley, S., Shadwick, E. H., Klocker, A., Vives, C. R., Liniger, G., et al (2024). Observed water-mass characteristics and circulation off Prydz Bay, East Antarctica. *Front. Mar. Sci.* 11, 1456207. doi: 10.3389/fmars.2024.1456207

Franck, V. M., Brzezinski, M. A., Coale, K. H., and Nelson, D. M. (2000). Iron and silicic acid concentrations regulate Si uptake north and south of the polar frontal zone in the Pacific Sector of the Southern Ocean. *Deep-Sea Res. II* 47, 3315–3338. doi: 10.1016/S0967-0645(00)00070-9

Gaffey, C. B., Frey, K. E., Cooper, L. W., and Grebmeier, J. M. (2022). Phytoplankton bloom stages estimated from chlorophyll pigment proportions suggest delayed summer production in low sea ice years in the northern Bering Sea. *PloS One* 17, e0267586. doi: 10.1371/journal.pone.0267586

Gomi, Y., Taniguchi, A., and Fukuchi, M. (2007). Temporal and spatial variation of the phytoplankton assemblage in the eastern Indian sector of the Southern Ocean in summer 2001/2002. *Polar Biol.* 30, 817–827. doi: 10.1007/s00300-006-0242-2

Gomi, Y., Umeda, H., Fukuchi, M., and Taniguchi, A. (2005). Diatom assemblages in the surface water of the Indian sector of the Antarctic surface water in summer of 1999/2000. *Polar Biosci.* 18, 1–15. doi: 10.15094/00006220

Gowing, M. M., Garrison, D. L., Kunze, H. B., and Winchell, C. J. (2001). Biological components of Ross Sea short-term particle fluxes in the austral summer of 1995–1996. *Deep-Sea Res. Part I: Oceanogr. Res. Papers* 48, 2645–2671. doi: 10.1016/S0967-0637(01)00034-6

Haberman, K. L., Ross, R. M., and Quetin, L. B. (2003). Diet of the Antarctic krill (*Euphausia superba* Dana): II. Selective grazing in mixed phytoplankton assemblages. *J. Exp. Mar. Biol. Ecol.* 283, 97–113. doi: 10.1016/S0022-0981(02)00467-7

Hayward, A., Pinkerton, M. H., and Gutiérrez-Rodriguez, A. (2023). *phytoclass*: A pigment-based chemotaxonomic method to determine the biomass of phytoplankton classes. *Limnol. Oceanogr. Methods* 21, 220–241. doi: 10.1002/lom3.10541

Hayward, A., Pinkerton, M. H., Wright, S. W., Gutiérrez-Rodriguez, A., and Law, C. S. (2024). Twenty-six years of phytoplankton pigments reveal a circumpolar Class Divide around the Southern Ocean. *Commun. Earth Environ.* 5, 92. doi: 10.1038/s43247-024-01261-6

Heil, P., Steketee, A., and Chua, S. (2023). Nilas Software - mapping tool for displaying multiple layers of physical and biogeochemical variables in the Southern Ocean. *Aust. Antarctic Data Centre*. doi: 10.26179/qh66-7p96

Herraiz-Borreguero, L., Lannuzel, D., van der Merwe, P., Treverrow, A., and Pedro, J. B. (2016). Large flux of iron from the Amery Ice Shelf marine ice to Prydz Bay. *J. Geophys. Res. Oceans* 121, 6009–6020. doi: 10.1002/2016JC011687

Heywood, K. J., Schmidtko, S., Hueze, C., Kaiser, J., Jickells, T. D., Queste, B. Y., et al. (2014). Ocean processes at the Antarctic continental slope. *Phil. Trans. R. Soc A* 372, 20130047. doi: 10.1098/rsta.2013.0047

Hosie, G. W., and Cochran, T. G. (1994). Mesoscale distribution patterns of macrozooplankton communities in Prydz Bay, Antarctica – January to February 1991. *Mar. Ecol. Prog. Ser.* 106, 21–39. Available at: http://www.jstor.org/stable/24844810.

Hosie, G. W., Schultz, M. B., Kitchener, J. A., Cochran, T. G., and Richards, K. (2000). Macrozooplankton community structure of East Antarctica (80-150°E) during the Austral summer of 1995/1996. *Deep-Sea Res. II* 47, 2437–2463. doi: 10.1016/S0967-0645(00)00031-X

Hutchins, D. A., and Bruland, K. W. (1998). Iron limited diatom growth and Si:N uptake ratios in a coastal upwelling regime. *Nature* 393, 561–564. doi: 10.1038/31203

Iida, T., and Odate, T. (2014). Seasonal variability of phytoplankton biomass and composition in the major water masses of the Indian Ocean sector of the Southern Ocean. *Polar Sci.* 8, 283–297. doi: 10.1016/j.polar.2014.03.003

Irion, S., Christaki, U., Berthelot, H., L'Helguen, S., and Jardillier, L. (2021). Small phytoplankton contribute greatly to CO_2-fixation after the diatom bloom in the Southern Ocean. *ISME J.* 15, 2509–2522. doi: 10.1038/s41396-021-00915-z

Jang, E., Park, K.-T., Yoon, Y. J., Kim, K., Gim, Y., Chung, H. Y., et al. (2022). First-year sea ice leads to an increase in dimethyl sulfide-induced particle formation in the Antarctic Peninsula. *Sci. Total Environ.* 803, 150002. doi: 10.1016/j.scitotenv.2021.150002

Jeffrey, S. W. (1997). "Application of pigment methods to oceanography," in *Phytoplankton Pigments in Oceanography: Guidelines to Modern Methods*. Eds. S. W. Jeffrey, R. F. C. Mantoura and S. W. Wright (UNESCO, Paris), 127–166, ISBN: .

Jeffrey, S. W., and Wright, S. W. (1997). "Qualitative and quantitative HPLC analysis of SCOR reference algal cultures," in *Phytoplankton Pigments in Oceanography: Guidelines to Modern Methods*. Eds. S. W. Jeffrey, R. F. C. Mantoura and S. W. Wright (UNESCO, Paris), 343–360, ISBN: .

Johnston, N. M., Murphy, E., Atkinson, A., Constable, A. J., Cotté, C., Cox, M., et al. (2021). Status, change and futures of zooplankton in the Southern Ocean. *Front. Ecol. Evol.* 17. doi: 10.3389/fevo.2021.624692

Jones, R. M., and Smith, W. O. (2017). The influence of short-term events on the hydrographic and biological structure of the southerwestern Ross Sea. *J. Mar. Syst.* 166, 184–195. doi: 10.1016/j.jmarsys.2016.09.006

Kawaguchi, S., Ichii, T., and Haganobu, M. (1999). Green krill, the indicator of micro- and nano-sized phytoplankton availability to krill. *Polar Biol.* 22, 133–136. doi: 10.1007/s003000050400

Kawamura, A., and Ichikawa, T. (1984). Distribution of diatoms in a small area in the Indian sector of the Antarctic. *Mem. Natn. Inst. Polar. Res. Spec. Issue* 32, 25–37.

Kim, H., Ducklow, H. W., Abele, D., Barlett, E. M. R., Buma, A. G. J., Meredith, M. P., et al. (2018). Inter-decadal variability of phytoplankton biomass along the coastal West Antarctic Peninsula. *Phil. Trans. R. Soc A* 376, 20170174. doi: 10.1098/rsta.2017.0174

Kirk, J. T. O. (1994). *Light and Photosynthesis in Aquatic Ecosystems. 2nd ed.* (Cambridge, United Kingdom: Cambridge University Press), ISBN: .

Kopczynska, E. E. (1992). Dominance of microflagellates over diatoms in the Antarctic areas of deep vertical mixing and krill concentrations. *J. Plankton Res.* 14, 1031–1054. doi: 10.1093/plankt/14.8.1031

Krause, D. J., Bonin, C. A., Goebel, M. E., Reiss, C. S., and Watters, G. M. (2022). The rapid population collapse of a key marine predator in the Northern Atlantic Peninsula endangers genetic diversity and resilience to climate change. *Front. Mar. Sci.* 8. doi: 10.3389/fmars.2021.796488

Kropuenske, L. R., Mills, M. M., van Dijken, G. L., Alderkamp, A.-C., Berg, G. M., Robinson, D. H., et al. (2010). Strategies and rates of photoacclimation in two major Southern Ocean phytoplankton taxa: *Phaeocystis Antarctica* (Haptophyta) and *Fragilariopsis cylindrus* (Bacillariophyceae). *J. Phycol.* 46, 1138–1151. doi: 10.1111/j.1529-8817.2010.00922.x

Langfelder, P., Zhang, B., and Horvath, S. (2007). Defining clusters from a hierarchical cluster tree: the Dynamic Tree Cut package for R. *Bioinformatics.* 24, 719–720. doi: 10.1093/bioinformatics/btm563

Lannuzel, D., Vancoppenolle, M., van den Merwe, P., de Jong, J., Meiners, K. M., Grotti., M., et al. (2016). Elementa. 4, 000130. doi: 10.12952/journal.elementa.000130

A. W. D. Larkum, S. E. Douglas and J. A. Raven (Eds.) (2003). *Photosynthesis in algae* (Dordrecht: Kluwer Academic Publishers), 480.

Li, W. K. W., McLaughlin, F. A., Lovejoy, C., and Carmack, E. C. (2009). Smallest algae thrive as the Arctic Ocean freshens. *Science* 326, 539. doi: 10.1126/science.1179798

Li, C., Sun, S., Zhang, G., and Ji, P. (2001). Summer feeding activities of zooplankton in Prydz Bay, Antarctica. *Polar Biol.* 24, 892–900. doi: 10.1007/s003000100292

Liu, M., Tao, Z., Zhang, Y., Yang, G., Sun, S., Li, C., et al. (2019). Feeding strategies of *Euphausia superba* in the eastern South Shetland Islands in austral summer. *Acta Oceanol. Sin.* 38, 75–83. doi: 10.1007/s13131-019-1392-8

Lohmann, A. C., Morton, J. P., Schofield, O. M., and Nowacek, D. P. (2023). Cyclical prey shortages for a marine polar predator driven by the interaction of climate change and natural climate variability. *Limnol. Oceanogr.* 68, 2668–2687. doi: 10.1002/lno.12453

Mackey, M. D., Mackey, D. J., Higgins, H. W., and Wright, S. W. (1996). CHEMTAX – a program for estimating class abundances from chemical markers: Application to HPLC measurements of phytoplankton pigments. *Mar. Ecol. Prog. Ser.* 144, 265–283. doi: 10.3354/meps144265

Madin, L., and Kremer, P. (1995). Determination of the filter-feeding rates of salps (Tunicata, Thaliacea). *ICES J. Mar. Sci.* 52, 583–595. doi: 10.1016/1054-3139(95)80073-5

Marañón, E. (2015). Cell size as a key determinant of phytoplankton metabolism and community structure. *Annu. Rev. Mar. Sci.* 7, 241–264. doi: 10.1146/annurev-marine-010814-015955

Maslanik, J., and Stroeve, J. (1999). *Near-Real-Time DMSP SSMIS Daily Polar Gridded Sea Ice Concentrations, Version 1* (NASA National Snow and Ice Data Center Distributed Active Archive Center).

Matsuno, K., Sumiya, K., Tozawa, M., Nomura, D., Sasaki, H., Yamaguchi, A., et al. (2023). Responses of diatom assemblages and life cycle to sea ice variation in the eastern Indian sector of the Southern Ocean during austral summer 2018/19. *Progr. Oceanogr.* 218, 103117. doi: 10.1016/j.pocean.2023.103117

Mendes, C. R. B., Costa, R. R., Ferreira, A., Jesus, B., Tavano, V. M., Dotto, T. S., et al. (2023). Cryptophytes: An emerging algal group in the rapidly changing Antarctic Peninsula marine environments. *Glob. Change Biol.* 29, 1791–1808. doi: 10.1111/gcb.16602

Meyer, M. A., and El-Sayed, S. (1983). Grazing of *Euphausia superba* Dana on natural phytoplankton populations. *Polar Biol.* 1, 193–197. doi: 10.1007/BF00443187

Mitchell, B. G., Brody, E. A., Holm-Hansen, O., McClain, C., and Bishop, J. (1991). Light limitation of phytoplankton biomass and macronutrient utilization in the Southern Ocean. *Limnol. Oceanogr.* 36, 1662–1677. doi: 10.4319/lo.1991.36.8.1662

Moline, M. A., Claustre, H., Frazer, T. K., Schofield, S., and Vernet, M. (2004). Alteration of the food web along the Antarctic Peninsula in response to a regional warming trend. *Glob. Change Biol.* 10, 1973–1980. doi: 10.1111/j.1365-2486.2004.00825.x

Montes-Hugo, M. A., Vernet, M., Martinson, D., Smith, R., and Iannuzzi, R. (2008). Variability on phytoplankton size structure in the western Antarctic Peninsula, (1997-2006). *Deep-Sea Res. Pt. II* 55, 2106–2117. doi: 10.1016/j.dsr2.2008.04.036

Moreau, S., Lannuzel, D., Janssens, J., Arroyo, M. C., Corkill, M., Cougnon, E., et al. (2019). Sea ice meltwater and circumpolar deep water drive contrasting productivity in three Antarctic polynyas. *JGR Oceans* 124, 2943–2968. doi: 10.1029/2019JC015071

Murphy, E. J., Cavanagh, R. D., Drinkwater, K. F., Grant, S. M., Heymans, J. J., Hofmann, E. E., et al. (2016). Understanding the structure and functioning of polar pelagic ecosystems to predict the impacts of change. *Proc. R. Soc B.* 283, 20161646. doi: 10.1098/rspb.2016.1646

Murphy, E. J., Johnston, N. M., Hofmann, E. E., Phillips, R. A., Jackson, J. A., Constable, A. J., et al. (2021). Global connectivity of Southern Ocean ecosystems. *Front. Ecol. Evol.* 9. doi: 10.3389/fevo.2021.624451

Nelson, D. M., and Smith, J. W. O. (1991). Sverdrup revisited: critical depths, maximum chlorophyll levels, and the control of Southern Ocean productivity by the irradiance-mixing regime. *Limnol. Oceanogr.* 36, 1650–1661. doi: 10.4319/lo.1991.36.8.1650

Nicol, S., Pauly, T., Bindoff, N. L., and Strutton, P. G. (2000). BROKE, a biological/oceanographic survey off the coast of East Antarctica (80-150°E) carried out in January-March 1996. *Deep Sea Res. II* 47, 2281–2298. doi: 10.1016/S0967-0645(00)00026-6

Nicol, S., Raymond, B., and Meiners, K. (2010). BROKE-West, a large ecosystem survey of the South West Indian Ocean sector of the Southern Ocean, 30°E-80°E (CCAMLR Division 58.4.2). *Deep-Sea Res. II.* 57, 693–700. doi: 10.1016/j.dsr2.2009.11.002

Pakhomov, E., and Froneman, P. (2004). Zooplankton dynamics in the eastern Atlantic sector of the Southern Ocean during the austral summer 1997/1998 - Part 2: Grazing impact. *Deep-Sea Res. Pt. II* 51, 2617–2631. doi: 10.1016/j.dsr2.2000.11.002

Pauli, N.-C., Metfies, K., Pakhomov, E. A., Neuhaus, S., Graeve, M., Wenta, P., et al. (2021). Selective feeding in Southern Ocean key grazers—diet composition of krill and salps. *Commun. Biol.* 4, 1061. doi: 10.1038/s42003-021-02581-5

Pearce, I., Davidson, A. T., Thomson, P. G., Wright, S., and van den Enden, R. (2010). Marine microbial ecology off East Antarctica (30-80°E): Rates of bacterial and phytoplankton growth and grazing by heterotrophic protists. *Deep-Sea Res.* 57, 849–862. doi: 10.1016/j.dsr2.2008.04.039

Pettersen, R., Johnsen, G., Berge, J., and Hovland, E. K. (2011). Phytoplankton chemotaxonomy in waters around the Svalbard archipelago reveals high amounts of Chl *b* and presence of gyroxanthin-diester. *Polar Biol.* 34, 627–635. doi: 10.1007/s00300-010-0917-6

Pinkerton, M. H., Boyd, P. W., Deppeler, S., Hayward, A., Höfer, J., and Moreau, S. (2021). Evidence for the impact of climate change on primary producers in the southern ocean. *Front. Ecol. Evol.* 9. doi: 10.3389/fevo.2021.592027

Portela, E., Rintoul, S. R., Bestley, S., Herraiz-Borreguero, L., van Wijk, E., McMahon, C. R., et al. (2021). Seasonal transformation and spatial variability of water masses within MacKenzie polynya, Prydz Bay. *J. Geophys. Res. Oceans* 126, e221JC017748. doi: 10.1029/2021JC017748

Ratnarajah, L., Nicol, S., and Bowie, A. R. (2018). Pelagic iron recycling in the Southern Ocean: Exploring the contribution of marine animals. *Front. Mar. Sci.* 29. doi: 10.3389/fmars.2018.00109

R Core Team (2021). "R: A language and environment for statistical computing version," in *R Foundation for Statistical Computing* (Vienna, Austria). Available at: https://www/R-project.org/.

Rees, C., Pender, L., Sherrin, K., Schwanger, C., Hughes, P., Tibben, S., et al. (2019). Methods for reproducible shipboard SFA nutrient measurement using RMNS and automated data processing. *Limnol. Oceanogr. Methods* 17, 25–41. doi: 10.1002/lom3.10294

Roca-Martí, M., Puigcorbé, V., Iversen, M. H., van der Loeff, M. R., Klaas, C., Cheah, W., et al. (2017). High particulate organic carbon export during the decline of a vast diatom bloom in the Atlantic sector of the Southern Ocean. *Deep Sea Res. II* 138, 102–115. doi: 10.1016/j.dsr2.2015.12.007

Sathyendranath, S., Brewin, R. J. W., Brockmann, C., Brotas, V., Calton, B., Chuprin, A., et al. (2019). An ocean-colour time series for use in climate studies: the experience of the ocean-colour climate change initiative (OC-CCI). *Sensors* 19, 4285. doi: 10.3390/s19194285

Schallenberg, C., Bestley, S., Klocker, A., Trull, T. W., Davies, D., Gault-Ringold, M., et al. (2018). Sustained upwelling of subsurface iron supplies seasonally persistent phytoplankton blooms around the southern Kerguelen plateau, Southern Ocean. *J. Geophys. Res. Oceans* 123, 5986–6003. doi: 10.1029/2018JC013932

Schofield, O., Saba, G., Coleman, K., Carvahlo, F., Couto, N., Ducklow, H., et al. (2017). Decadal variability in coastal phytoplankton community composition in a changing West Antarctic Peninsula. *Deep-Sea Res. I* 124, 42–54. doi: 10.1016/j.dsr.2017.04.014

Smetacek, V. S. (1985). Role of sinking in diatom life-history cycles: ecological, evolutionary and geological significance. *Mar. Biol.* 84, 239–251. doi: 10.1007/BF00392493

Smetacek, V., Assmy, P., and Henjes, J. (2004). The role of grazing in structuring Southern Ocean pelagic ecosystems and biogeochemical cycles. *Ant. Sci.* 16, 541–558. doi: 10.1017/S0954102004002317

Smith, W. O., Ainley, D. G., Arrigo, K. R., and Dinniman, M. S. (2014). The oceanography and ecology of the Ross Sea. *Annu. Rev. Mar. Sci.* 6, 469–487. doi: 10.1146/annurev-marine-010213-135114

Smith, W. O., Asper, V. L., Tozzi, S., Liu, X., and Stammerjohn, S. E. (2011). Surface layer variability in the Ross Sea, Antarctica as assessed by in *situ* fluorescence measurements. *Prog. Oceanogr.* 88, 28–45. doi: 10.1016/j.pocean.2010.08.002

Smith, W. O., Marra, J., Hiscock, M. R., and Barber, R. T. (2000). The seasonal cycle of phytoplankton biomass and primary productivity in the Ross Sea, Antarctica. *Deep-Sea Res. II* 47, 3119–3140. doi: 10.1016/S0967-0645(00)00061-8

Smith, A., Ratnarajah, L., Holmes, T., Wuttig, K., Townsend, A., Westwood, K., et al. (2021). Circumpolar Deep Water and shelf sediments support late summer microbial iron remineralisation. *Global Biogeochem. Cycles* 35, e2020GB00692. doi: 10.1029/2020GB006921

Smith, N., and Trégure, P. (1994). *Physical and chemical oceanography in the vicinity of Prydz Bay, Antarctica* (Cambridge: Cambridge University Press), 25–43.

Spreen, G., Kaleschke, L., and Heygster, G. (2008). Sea ice remote sensing using AMSR-E 89-GHz channels. *J. Geophys. Res. Oceans*. 113, C02S03. doi: 10.1029/2005JC003384

Strutton, P. G., Griffiths, F. B., Waters, R. L., Wright, S. W., and Bindoff, N. L. (2000). Primary productivity off the coast of East Antarctica (80-150°E): January to March 1996. *Deep-Sea Res. II* 47, 2327–2362. doi: 10.1016/S0967-0645(00)00028-X

Strzepek, R. F., and Harrison, P. J. (2004). Photosynthetic architecture differs in coastal and oceanic diatoms. *Nature* 431, 689–692. doi: 10.1038/nature02954

Sumner, M. (2023). "Raadtools: tools for synoptic environmental spatial data," in *R package version 0.6.0.9032*.

Sunda, W. G., and Huntsman, S. A. (1997). Interrelated influence of light, iron and cell size on marine phytoplankton growth. *Nature* 390, 389–392. doi: 10.1038/37093

Takahashi, K. D., Makabe, R., Takao, S., Kashiwasi, H., and Moteki, M. (2022). Phytoplankton and ice-algal communities in the seasonal ice zone during January (Southern Ocean, Indian sector). *J. Oceanogr.* 78, 409–424. doi: 10.1007/s10872-022-00649-2

Takao, S., Hirawake, T., Hashida, G., Sasaki, H., Hattori, H., and Suzuki, K. (2014). Phytoplankton community composition and photosynthetic physiology in the Australian sector of the Southern Ocean during the austral summer of 2010/2011. *Polar Biol.* 37, 1563–1578. doi: 10.1007/s00300-014-1542-6

Takeda, S. (1998). Influence of iron availability on nutrient consumption ratio of diatoms in oceanic waters. *Nature* 393, 774–777. doi: 10.1038/31674

Thomas, P. G., and Green, K. (1988). Distribution of *Euphausia crystallorophias* within Prydz Bay and its importance to the inshore marine ecosystem. *Polar Biol.* 8, 327–331. doi: 10.1007/BF00442023

Trebilco, R., Melbourne-Thomas, J., and Constable, A. J. (2020). The policy relevance of Southern Ocean food web structure: Implications of food web change for fisheries, conservation and carbon sequestration. *Mar. Policy* 115, 103832. doi: 10.1016/j.marpol.2020.103832

van Leeuwe, M. A., and Stefels, J. (2007). "Photosynthetic responses in *Phaeocystis Antarctica* towards varying light and iron conditions," in Phaeocystis, *major link in the biogeochemical cycling of climate-relevant elements*. Eds. M. A. van Leeuwe, J. Stefels, S. Belviso, C. Lancelot, P. G. Verity and W. W. C. Gieskes (Springer, Dordrecht). doi: 10.1007/978-1-4020-6214-8_6

van Leeuwe, M. A., Webb, A. L., Venables, H. J., Visser, R. J. W., Meredith, M. P., Elzenga, J. T. M., et al. (2020). Annual patterns in phytoplankton phenology in Antarctic coastal waters explained by environmental drivers. *Limnol. Oceanogr.* 65, 1651–1668. doi: 10.1002/lno.11477

Vaz, R. A. N., and Lennon, G. W. (1996). Physical oceanography of the Prydz Bay region of Antarctic waters. *Deep-Sea Res. I.* 43, 603–641. doi: 10.1016/0967-0637(96)00028-3

Venkataramana, V., Anilkumar, N., Naik, R. K., Mishra, R. K., and Sabu, P. (2019). Temperature and phytoplankton size class biomass drives the zooplankton food web

dynamics in the Indian Ocean sector of the Southern Ocean. *Polar Biol.* 42, 823–829. doi: 10.1007/s00300-019-02472-w

Vives, C. R., Schallenberg, C., Strutton, P. G., and Westwood, K. J. (2022). Iron and light co-limitation of phytoplankton growth off East Antarctica. *J. Mar. Syst.* 234. doi: 10.1016/j.jmarsys.2022.103774

Waters, R. L., van den Enden, R., and Marchant, H. J. (2000). Summer microbial ecology off East Antarctica (80-150°E): Protistan community structure and bacterial abundance. *Deep Sea Res. II Top. Stud. Oceanogr.* 47, 2401–2435. doi: 10.1016/S0967-0645(00)00030-8

Westwood, K. J., Griffiths, F. B., Meiners, K. M., and Williams, G. D. (2010). Primary productivity off the Antarctic coast from 30°-80°E; BROKE-West survey 2006. *Deep-Sea Res. II.* 57, 794–814. doi: 10.1016/j.dsr2.2008.08.020

Westwood, K. J., Thomson, P. G., van den Enden, R., Maher, L., Wright, S. W., and Davidson, A. T. (2018). Ocean acidification impacts primary and bacterial production in Antarctic coastal waters during austral summer. *J. Exp. Mar. Biol. Ecol.* 498, 46–60. doi: 10.1016/j.jembe.2017.11.003

Williams, G. D., Herraiz-Borreguero, L., Roquet, F., Tamura, T., Oshima, K. I., Fukamachi, Y., et al. (2016). The suppression of Antarctic bottom water formation by melting ice shelves in Prydz Bay. *Nat. Commun.* 7, 12577. doi: 10.1038/ncomms12577

Williams, G. D., Nicol, S., Aoki, S., Meijers, A. J. S., Bindoff, N. L., Iijima, Y., et al. (2010). Surface oceanography of BROKE-West, along the Antarctic margin of the south-west Indian Ocean (30-80°E). *Deep-Sea Res. II.* 57, 738–757. doi: 10.1016/j.dsr2.2009.04.020

Wolf, C., Iversen, M., Klaas, C., and Metfies, K. (2016). Limited sinking of *Phaeocystis* during a 12-day sediment trap study. *Mol. Ecol.* 25, 3428–3435. doi: 10.1111/mec.13697

Wood, S. (2017). *"Generalized Additive Models: An Introduction with R". 2nd edition* (Chapman and Hall/CRC).

Wright, S. W., Thomas, D. P., Marchant, H. J., Higgins, H. W., Mackey, M. D., and Mackey, D. J. (1996). Analysis of phytoplankton of the Australian sector of the Southern Ocean: Comparisons of microscopy and size frequency data with interpretations of pigment HPLC data using the CHEMTAX matrix factorisation program. *Mar. Ecol. Prog. Ser.* 144, 285–298. doi: 10.3354/meps144285

Wright, S. W., and van den Enden, R. L. (2000). Phytoplankton community structure and stocks in the East Antarctic marginal ice zone (BROKE survey, January-March 1996) determined by CHEMTAX analysis of HPLC pigment signatures. *Deep-Sea Res. II.* 47, 2363–2400. doi: 10.1016/S0967-0645(00)00029-1

Wright, S. W., van den Enden, R. L., Pearce, I., Davidson, A. T., Scott, F. J., and Westwood, K. J. (2010). Phytoplankton community structure and stocks in the Southern Ocean (30-80°E) determined by CHEMTAX analysis of HPLC pigment signatures. *Deep-Sea Res. Pt. II.* 57, 758–778. doi: 10.1016/j.dsr2.2009.06.015

Xu, S., Park, K., Wang, Y., Chen, L., Qi, D., and Li, B. (2019). Variations in the summer oceanic pCO_2 and carbon sink in Prydz Bay using the self-organising map analysis approach. *Biogeosciences* 16, 797–810. doi: 10.5194/bg-16-797-2019

Yang, G., Li, C., Sun, S., Zhang, C., and He, Q. (2013). Feeding of dominant zooplankton in Prydz Bay, Antarctica, during austral spring/summer: food availability and species responses. *Polar Biol.* 36, 1701–1707. doi: 10.1007/s00300-013-1387-4

Zapata, M., Rodriguez, F., and Garrido, J. L. (2000). Separation of chlorophylls and carotenoids from marine phytoplankton: a new HPLC method using a reversed phase C-8 column and pyridine-containing mobile phases. *Mar. Ecol. Prog. Ser.* 195, 29–45. doi: 10.3354/meps195029

frontiers | Frontiers in Marine Science

TYPE Original Research
PUBLISHED 22 November 2024
DOI 10.3389/fmars.2024.1360541

Check for updates

OPEN ACCESS

EDITED BY
Yuqiu Wei,
Chinese Academy of Fishery Sciences (CAFS), China

REVIEWED BY
Kusum Komal Karati,
Centre for Marine Living Resources and Ecology (CMLRE), India
Alexis Anne Bahl,
University of British Columbia, Canada

*CORRESPONDENCE
Christine K. Weldrick
christine.weldrick@utas.edu.au

RECEIVED 23 December 2023
ACCEPTED 23 October 2024
PUBLISHED 22 November 2024

CITATION
Weldrick CK, Brasier MJ, Burns A, Johnson OJ and Maschette D (2024) Zooplankton abundance and distribution along the Mawson coast, East Antarctica.
Front. Mar. Sci. 11:1360541.
doi: 10.3389/fmars.2024.1360541

COPYRIGHT
© 2024 Weldrick, Brasier, Burns, Johnson and Maschette. This is an open-access article distributed under the terms of the Creative Commons Attribution License (CC BY). The use, distribution or reproduction in other forums is permitted, provided the original author(s) and the copyright owner(s) are credited and that the original publication in this journal is cited, in accordance with accepted academic practice. No use, distribution or reproduction is permitted which does not comply with these terms.

Zooplankton abundance and distribution along the Mawson coast, East Antarctica

Christine K. Weldrick[1,2]*, Madeleine J. Brasier[1,2,3], Alicia Burns[4], Olivia J. Johnson[1,2] and Dale Maschette[1,2,3]

[1]Australian Antarctic Program Partnership, Institute for Marine and Antarctic Studies, University of Tasmania, Hobart, TAS, Australia, [2]Institute for Marine and Antarctic Studies, University of Tasmania, Hobart, TAS, Australia, [3]Southern Ocean Ecosystems Program, Australian Antarctic Division, Department of Climate Change, Energy, the Environment and Water, Kingston, TAS, Australia, [4]School of Life and Environmental Studies, University of Sydney, Sydney, NSW, Australia

During the summer of 2021, we conducted a comprehensive study on zooplankton communities along East Antarctica (55°E to 80°E) as part of the Trends in Euphausiids off Mawson, Predators, and Oceanography (TEMPO) survey program. Hierarchical agglomerative clustering identified three distinct zooplankton clusters based on environmental factors. Seven potential indicator taxa associated with specific clusters include copepods, pteropods, amphipods, and euphausiids. Mainly consisting of small copepods, chaetognaths and foraminifera, Cluster 1 (n = 34) was characterized by the highest abundance (74,386 ind./1000 m^3), spanning wide latitudinal and longitudinal gradients, deeper waters (mean depth = 3,475 m ± 739 m), and higher chlorophyll-*a* concentrations (mean = 49.13 mg m^{-2} ± 24.38 mg m^{-2}). Cluster 2 (n = 4) featured the lowest abundance (1,059 ind./1000 m^3) and the fewest sampling stations along the narrowest latitudinal range. Copepods, euphausiids, and foraminifera were among the most abundant in this group. Cluster 3 (n = 10), located near the ice edge, displayed a distinct temperature range (–1.46°C to 1.18°C) and moderate zooplankton abundance (22,629 ind./1000 m^3) consisting of copepods, euphausiids, and ostracods. IndVal analysis identified seven species as indicators of environmental conditions and Generalized Additive Models (GAMs) were used to model their abundance, as well as total zooplankton abundance. Across all models, significant drivers included chlorophyll-*a*, temperature, number of days since sea ice melt and mixed layer depth. The model for total zooplankton abundance explained 70.9% of the deviance, with number of days since ice melt and chlorophyll-*a* concentration emerging as the strongest predictors. These findings provide crucial insights into the ecological implications of changing climate conditions on East Antarctica zooplankton communities and their potential repercussions on the broader Southern Ocean ecosystem. This research enhances our understanding of the intricate relationship between environmental shifts and Southern Ocean ecology.

KEYWORDS

zooplankton, community structure, East Antarctica, distribution, abundance, multivariate analysis, Generalized Additive Models

1 Introduction

The Southern Ocean, a crucial component of global oceanic systems, is undergoing rapid transformations driven by climate change. These changes, including shifts in sea ice extent, ocean warming, and altered freshwater inputs, have widespread implications for the entire Antarctic marine food web (Constable et al., 2014; Massom et al., 2013; Poloczanska et al., 2016). Zooplankton, which serve as a critical link between primary producers and higher trophic levels, are particularly sensitive to these environmental shifts (Cavan et al., 2017; Yang et al., 2022). Fluctuations in sea ice extent, temperature regimes, and oceanographic processes can lead to changes in the abundance, distribution, and vertical structure of zooplankton communities, with significant consequences for both biogeochemical cycles and higher trophic levels (Smetacek et al., 2004).

Recent studies have identified shifts in zooplankton communities throughout the Southern Ocean, particularly in response to changing environmental conditions, such as sea ice melt and ocean warming. However, the Central Indian sector of East Antarctica, particularly the region along the Mawson coast, remains actively understudied compared to other sectors, such as the Western Antarctic Peninsula. Zooplankton communities in this region are sensitive to environmental fluctuations, particularly krill (*Euphausia superba*) and copepods, which serve as essential components of the Antarctic marine food web (Quetin et al., 1996; Reid et al., 2005; McCormack et al., 2020). Despite their ecological importance, gaps remain in understanding how environmental drivers such as temperature, sea ice melt, and primary productivity affect zooplankton distribution and abundance in this region.

Surveys conducted in the broader Southern Ocean, such as the BROKE-West (Nicol and Meiners, 2010) and Japanese-led krill biomass surveys (e.g., Murase et al., 2019), have provided valuable insights into the distribution and abundance of zooplankton and krill, but the Central Indian sector, including CCAMLR Division 58.4.2, has not been extensively studied. This region is vital for understanding the larger-scale implications of climate change on Antarctic ecosystems, especially given the significant role it plays in krill management and conservation efforts (Cox et al., 2022). The region's unique oceanographic conditions, including extensive landfast ice and variable sea ice dynamics, offer a critical setting for investigating how zooplankton communities respond to shifting environmental factors (Fraser et al., 2020).

The Commission for the Conservation of Antarctic Marine Living Resources (CCAMLR) recognizes the importance of Division 58.4.2 for managing krill fisheries and ensuring the long-term sustainability of this ecologically significant region. Previous surveys (Nicol and Meiners, 2010; Swadling et al., 2010) have informed krill management strategies, but ongoing research is necessary to assess the impact of climate change on krill and zooplankton communities in East Antarctica. The objective of this study is to contribute to that understanding by examining zooplankton distribution and environmental drivers along the Mawson coast, which could have broader implications for the management of krill and other key species in the Southern Ocean.

This study aims to address critical gaps in understanding how environmental conditions influence zooplankton communities along the Mawson coast in East Antarctica during the summer of 2021. We use a combination of environmental data, cluster analysis, and generalized additive models (GAMs) to identify patterns in the structure and key drivers of zooplankton dynamics. By investigating these relationships, we contribute valuable knowledge to inform future management and conservation efforts in this ecologically significant region.

2 Materials and methods

2.1 Sampling

Mesozooplankton net sampling was conducted aboard the RV *Investigator* as part of the multidisciplinary research voyage named Trends in Euphausiids off Mawson, Predators, and Oceanography (TEMPO). On 29 January 2021, the research vessel departed Hobart, Australia and was bound for the eastern half of the CCAMLR Division 58.4.2, spanning 62°S to 68°S and 55°E to 80°E (Figure 1). Active sampling along six north-south transects occurred within the seasonal ice zone between 13 February and 12 March 2021, starting at the southwest corner of the sampling region ('R01' in Figure 1). The vessel returned to Hobart on 24 March 2021.

A rectangular midwater trawl net (RMT1 + 8), with an 8 m^2 mouth opening and mesh size of 4.5 mm, was used to target larger plankton and nekton groups (e.g., Antarctic krill), and tapered to a mouth opening of 1.5 m^2 in the last 1.8 m of net (Hosie et al., 2000). Smaller plankton groups were sampled through a 1 m^2 mouth area with a 300 μm mesh size. Net trawls were either 'routine' where sampling occurred at pre-designated locations to match previous surveys (see Nicol and Meiners, 2010), or 'target' in which sampling was conducted based on observations using the vessel's echo sounders that suggested the presence of Antarctic krill swarms (see Kelly et al., 2021 for full survey details). All net trawling was conducted through a water speed of 2 knots, and routine trawls were deployed obliquely from surface to 200 m for up to 18 minutes. Nets during target trawls were kept open between 7 to 9 minutes. A flow meter was positioned at the mouth of the RMT8 net to measure the volume of seawater filtered. Antarctic krill from the RMT8 nets were sampled specifically for a distribution and biomass study by Cox et al. (2022). The samples from the RMT1 net were reserved for this study and preserved in 5% buffered formaldehyde and seawater solution prior to transportation to the Institute for Marine and Antarctic Studies in Hobart, Australia, for further analyses.

While in the laboratory, zooplankton samples were rinsed in seawater and split to a subsample of approximately n = 600 individuals using a Motoda box splitter (Motoda, 1985). Individuals at each station were identified to the lowest taxonomic level possible (henceforth taxon). Whilst this was usually to species or genus, some individuals were grouped at higher taxonomic level due to difficulties in identification (see Supplementary Table S1 for full list of taxonomic units). Individuals in each taxon were counted and, wherever possible, assigned life stage using a Leica M165 C stereoscopic microscope.

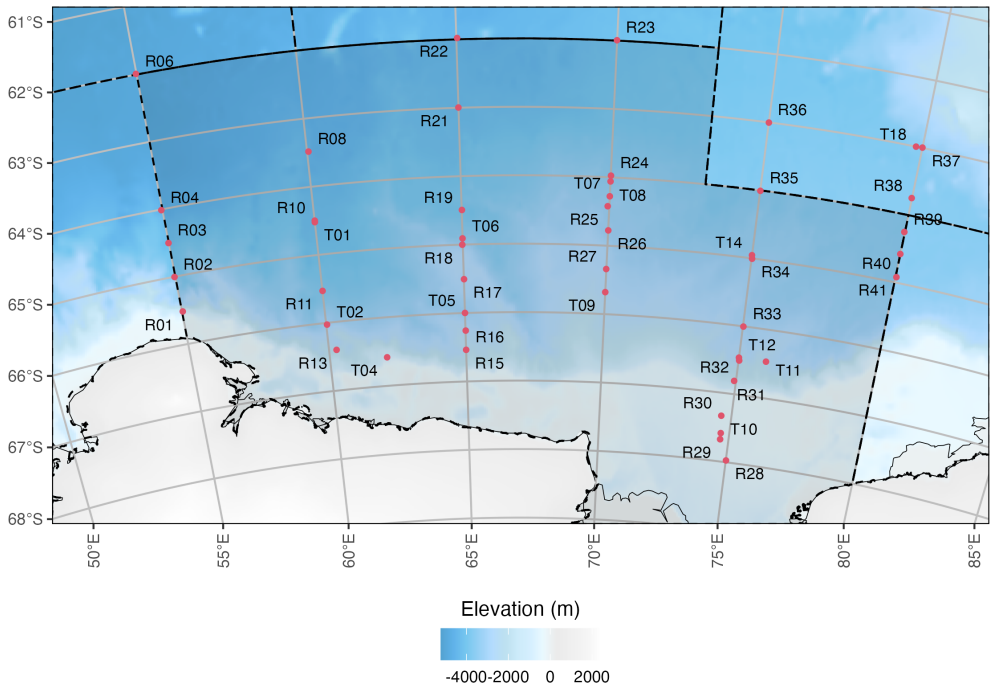


FIGURE 1
Locations of RMT1 + 8 plankton net deployments along six north-south transects. Deployment types were either routine or target, denoted in sampling site names by 'R' and 'T', respectively, which refers to planned and/or targeted trawls with reference to Antarctic krill sampling for biomass estimates (Cox et al., 2022). The background bathymetry grid is sourced from the GEBCO_2014 Grid, version 20150318, www.gebco.net.

Counts were divided by the splitting ratio then divided by the calibration value determined from the flowmeter. Abundances were calculated per taxon per sampling location and are reported as the number of individuals per 1000 m^3.

A Seabird SBE911 Plus CTD-mounted rosette sampler was deployed to perform full-depth profile water sampling at pre-determined depths throughout the water column and prior to each plankton net deployment. Profiles were created for temperature, salinity and fluorescence.

2.2 Environmental data

To investigate the relationships between environmental variables and zooplankton abundance, we used a suite of variables measured during the voyage, in the laboratory and additional satellite-derived datasets (Table 1). These variables were selected to provide a comprehensive understanding of the physical and biological factors influencing zooplankton abundance in our study area.

Chlorophyll-*a* concentration (mg m^{-2}), an essential indicator of phytoplankton biomass and, indirectly, primary productivity, was integrated over depths from 10 m to 200 m, aligning with the zooplankton sampling depth. This estimate was derived from *in situ* florescence measurements collected onboard from the CTD-mounted rosette sampler. For more details on how these values were derived, see Heidemann et al. (2024) in this issue.

Temperature and salinity were also collected using the CTD rosette sampler. Temperature (CT_200) was represented as absolute temperature (°C) averaged between the surface and 200 m, while salinity (SA_200) was represented as absolute salinity (g kg^{-1}) averaged over the same depth range. For temperature and salinity profiles, see Foppert et al. (2024) in this issue. The mixed layer depth (MLD_N2max) was determined as the depth where the maximum buoyancy frequency (N_2) occurred, i.e., the pycnocline. This method was chosen because pycnocline significantly influences the vertical distribution of zooplankton and their prey through the supply of nutrients (Priddle et al., 2003). The maximum buoyancy frequency was derived from CTD profiles of temperature and salinity (Foppert et al., 2024, this issue).

Bathymetric depth (m) at each sampling station was directly measured to understand the spatial distribution of zooplankton in relation to ocean depth. Ice concentration (%) and number of days since sea ice melted were obtained from satellite observations, specifically daily passive microwave estimated percent sea ice concentration from the National Snow and Ice Data Centre (NSIDC). Ice concentration represents the percentage of an area covered in sea ice at the time of sampling, while the days since ice melt provide temporal information on the recency of ice melt. Additionally, the distance from each sampling site to the edge of the ice was calculated using satellite-derived ice concentration data.

2.3 Analysis

2.3.1 Mesozooplankton community structure and indicator species analysis

As a preprocessing step, a fourth root transformation was applied to the abundance values to normalize the data, which is

TABLE 1 Environmental and spatial variables tested as zooplankton community predictors for generalized additive modeling (GAMs).

Variable abbreviation	Explanation
Chla	Integrated estimate of chlorophyll-*a* (mg m^{-2}) averaged at depths between 10 to 200 m, which aligns with the section of the water column where zooplankton were sampled.
CT_200	Absolute temperature (°C) averaged at depths between surface and 200 m maximum net sampling depth. Values are derived from *in situ* CTD measurements at each sampling site.
Depth	Bathymetric depth estimated at each sampling station.
IceConc	Actual ice concentration value (%). It is the percentage of an area covered in sea ice.
IceMeltDays	Number of days since sea ice melted calculated from daily passive microwave estimated percent sea ice concentration taken from the National Snow and IceData Centre.
m_to_Ice	Distance (m) estimated from sampling site to edge of ice
MLD_N2max	Mixed layer depth (m) where the N_2 maximum is found, i.e., the pycnocline.
SA_200	Absolute salinity (g kg^{-1}) averaged at depths between surface and 200 m maximum net sampling depth. Values were derived from *in situ* CTD measurements at each sampling site.

appropriate for minimizing the influence of a few highly abundant species (Quinn and Keough, 2002). Zooplankton community patterns were analyzed using Q-mode cluster analysis, which classified sampling sites based on Bray-Curtis dissimilarity. Hierarchical agglomerative clustering (UPGMA) was used to generate a cluster dendrogram, illustrating the similarity between sampling sites.

Non-metric multidimensional scaling (NMDS) was performed to complement the cluster analysis, providing a visual representation of similarity patterns among sites, also based on Bray-Curtis dissimilarities. The NMDS analysis was initialized with random starting configurations and iterated 1000 times to ensure the stability of the solution (Oksanen et al., 2022). Environmental vectors were fit onto the ordination to quantify how well each variable correlated with the site configuration in NMDS space (Table 1). The environmental variables included chlorophyll-*a* concentration, temperature, salinity, days since ice melt, mixed layer depth, latitude, longitude, sea ice concentration, distance to ice edge, and depth.

To assess the significance of community composition differences among clusters, we conducted a Permutational Multivariate Analysis of Variance (PERMANOVA), based on a Bray-Curtis dissimilarity matrix derived from the abundance data. The initial clustering identified 5 distinct clusters. Furthermore, a similarity profile (SIMPROF) analysis was conducted to validate the non-randomness of the similarity profiles within the cluster structure. We used this to test the number of significant clusters based on the Czekanowski distance measure. This combined approach highlights both the clustering structure and the multidimensional relationships within the data.

To determine the optimal number of clusters, we employed silhouette analysis, which measures how similar each sample is to its own cluster compared to others. The two-cluster solution yielded the highest silhouette width (asw = 0.24), indicating the strongest separation; however ecological systems are often complex, and selecting too few clusters may overlook important ecological variability. Therefore, we selected three clusters (asw = 0.18), balancing interpretability and clustering quality. This decision was made to capture more nuanced community distinctions that might be lost in a simpler two-cluster solution. The resulting cluster assignments were stored as a factor variable.

For each cluster, we first identified taxa contributing to the top 50% of the total abundance. This step focuses on determining the dominant taxa within each cluster, which allows us to characterize the general composition of the community. However, high abundance alone does not necessarily equate to a species being a good indicator of specific environmental conditions. To address this, we employed a separate Indicator Value (IndVal) analysis (De Cáceres et al., 2012) to statistically identify indicator species, which are taxa that are not only representative of a cluster but are also associated with specific environmental conditions or community compositions. The IndVal analysis provides a more refined approach by considering the fidelity and specificity of each taxon to the clusters, independent of their overall abundance. This allows us to identify taxa that may be less abundant but still serve as strong indicators of particular ecological settings. Thus, the identification of indicator species is based on a statistical representation of environmental conditions rather than abundance alone. A taxon is deemed a significant indicator if its associated *p*-value was less than 0.05, ensuring robustness in differentiating between clusters.

2.3.2 Environmental drivers of zooplankton abundance

To explore the relationship between environmental predictors and zooplankton abundance, we applied generalized additive models (GAMs) across all zooplankton data, regardless of cluster assignments. The GAMs focused on species-specific abundance (e.g., *Euphausia superba*, *Clausocalanus laticeps*, *Paraeuchaeta* sp.) as well as total zooplankton abundance. This approach allowed us to investigate how environmental factors, such as chlorophyll-*a* concentration, temperature, and mixed layer depth (MLD), influenced the abundance of key taxa across the entire dataset rather than within specific clusters.

Before fitting the GAMs, we tested for collinearity between environmental variables using Pearson's Correlation analysis, retaining variables with correlation coefficients below the threshold of 0.7 to avoid multicollinearity. Each GAM included smooth terms for predictor variables, such as chlorophyll-*a* concentration, sea surface temperature, and the number of days since sea ice melt, to capture potential non-linear relationships between environmental drivers and zooplankton abundance. The models were fitted using a Tweedie distribution with a log link function, which is appropriate for modeling non-negative, continuous data with skewness.

Model selection was based on the Akaike Information Criterion (AIC), where lower AIC values indicated better-fitting models with an optimal balance between goodness-of-fit and model complexity. A series of candidate models were constructed using various combinations of predictor variables, including chlorophyll-*a* concentration, sea surface temperature, salinity, and mixed layer depth. Each model included smooth terms to capture potential non-linear relationships between zooplankton abundance and the environmental predictors. The degree of smoothing (k) was selected to avoid overfitting while ensuring adequate flexibility to model non-linear patterns. All models were fitted using restricted maximum likelihood (REML) to provide more accurate parameter estimates, especially when comparing models with different levels of complexity.

All analyses were performed using R version 4.3.0 (R Core Team, 2023) with the following packages 'vegan' (Oksanen et al., 2022), 'cluster' (Maechler et al., 2023), 'indicspecies' (De Cáceres and Legendre, 2009), and 'mcgv' (Wood, 2017). All figures were made using SOmap (Maschette et al., 2019), 'GGally' (Schloerke et al., 2012) and ggplot (Wickham, 2016). Throughout this study, we considered results to be statistically significant at a 95% confidence level ($p < 0.05$).

3 Results

3.1 Oceanographic and hydrographic features

The southern Antarctic Circumpolar Current front (SACCF) enters the westernmost transect at 63.5°E in the northwest of the survey region. It extends poleward until the third transect (65°E) before heading northward to 63.38°E at the fourth transect (70°E). The SACCF then shifts poleward again across the fifth and sixth transects (75°E and 80°E). The Southern Boundary (SB) of the Antarctic Circumpolar Current enters the western transect at 64.45°E and progresses to its highest latitude of 65.53°E by the second transect (60°E) and its lowest latitude of 63.85°E at the 70°E transect. Closest to the Antarctic continent, the Antarctic Slope Front (ASF) enters the westernmost transect at 65.3°E and progressively heads as far south as 66.5°E at the fifth transect (75°E) before heading northwards to 65.05°E at the final transect (80°E), however there is uncertainty surrounding the exact location as there was likely an eddy located here, as well. There is also uncertainty surrounding the exact locations of the ASF at the third and fourth transects given the depths ranged across the sampling region, with a maximum depth of 4,992 m located at the north-westernmost station of the survey region (at trawl site R06; 62°S and 55°E), and a minimum depth of 451 m located at trawl site R30 (67°S and 74.6°E) towards Prydz Bay and north of the Amery Ice Shelf. The ASF is estimated near 65°S, where isotherms drop sharply.

The mixed layer depth (MLD) ranged from 20 m (trawl sites R18 and T06) (Figure 1) to 73 m at site R15, approximately 92 nm south and the closest sampling site to Mawson Coast. The pycnocline depth, i.e., the depth at which the maximum of buoyancy frequency (N_2 maximum) was found at the MLD, ranged across survey regions, where the shallowest pycnocline was 25 m, located at trawl sites R29 and T10 (towards the Amery Ice Shelf), and the deepest pycnocline depth at 88 m, located at T04 along the Mawson coast. Sea surface temperatures for the upper 200 m ranged from -1.73°C, at the south-westernmost station (R01), to 1.18°C, which was located at the northeast area of the survey region (site R38). Salinity values from the upper 200 m of the water column ranged from 34.57 (R02) to 34.10 (R22), which is the northernmost sampling site along the 65°E transect line where the freshest seawater was recorded. Integrated chlorophyll-*a* ranged widely throughout the survey region, where the smallest value recorded was 18.4 mg m^{-2} at trawl site R37, at the northern end of the easternmost transect (80°E), and 102.4 mg m^{-2} at trawl sites R32, T11 and T12, which are all located within the Cooperation Sea.

3.2 Mesozooplankton community composition and structure

Seventy-nine zooplankton taxa were identified from all 48 sampling sites. Total zooplankton abundances ranged from 115 to 59,970 ind./1000 m^3 with a mean abundance of 13,083 ind/1000 m^3 (± 15,670 ind./1000 m^3) that represent 17 broader taxonomic groups, of which 88% were copepods, 4% pteropods, 3% chaetognaths, 2% krill, 1% ostracods and 1% foraminifera (Supplementary Table S1 for a complete list of taxa identified). On 24 February 2021, the lowest abundance was recorded at site R18, located along the central transect of the survey region, on the 65°S line, with increasing abundance towards the east along the ASF (Figure 2). The maximum abundance was sampled on 27 February 2021 at trawl site R23 (62°S and 70°E), which was located north of the SACCF. Among the taxonomic groups, copepods dominated with the small sized species being the most dominant, including *Oithona similis* showing the highest estimated abundance (29,902 ind./1000 m^3), followed by *Microcalanus pygmaeus* (14,478 ind./1000 m^3). Large copepod species, *Calanoides acutus* and *Rhincalanus gigas*, were also dominant throughout the study region (21,181 ind./1000 m^3 and 9,300 ind./1000 m^3, respectively).

Q-mode cluster analysis identified three groups at approximately 45% similarity (Figure 3). Our study employed NMDS to visualize the underlying patterns in environmental data across various sampling sites (Figure 4). NMDS showed clear separation among three clusters (stress = 0.18). Ecological zones were differentiated according to chlorophyll-*a*, depth, temperature, salinity, MLD, sea ice concentration, and proximity to the ice edge. Our PERMANOVA analysis, based on a Bray-Curtis dissimilarity matrix calculated from the zooplankton abundance data, revealed a significant difference in community composition among the sampling sites (PERMANOVA, $p < 0.05$), and that the observed dissimilarity between groups was significantly higher than expected by change ($F = 1$). The SIMPROF analysis confirmed that 13 clusters were significantly distinct ($p < 0.05$ for each), suggesting that the observed groupings were not due to random chance.

3.2.1 Cluster 1

Cluster 1 included 34 sampling sites and was primarily associated with SACCF and SB frontal zones that exhibited high chlorophyll-*a* concentrations (49.13 ± 24.38 mg m^{-2}) and temperatures (0.02 ± 0.85°C) (Figure 5; Table 2). This cluster was

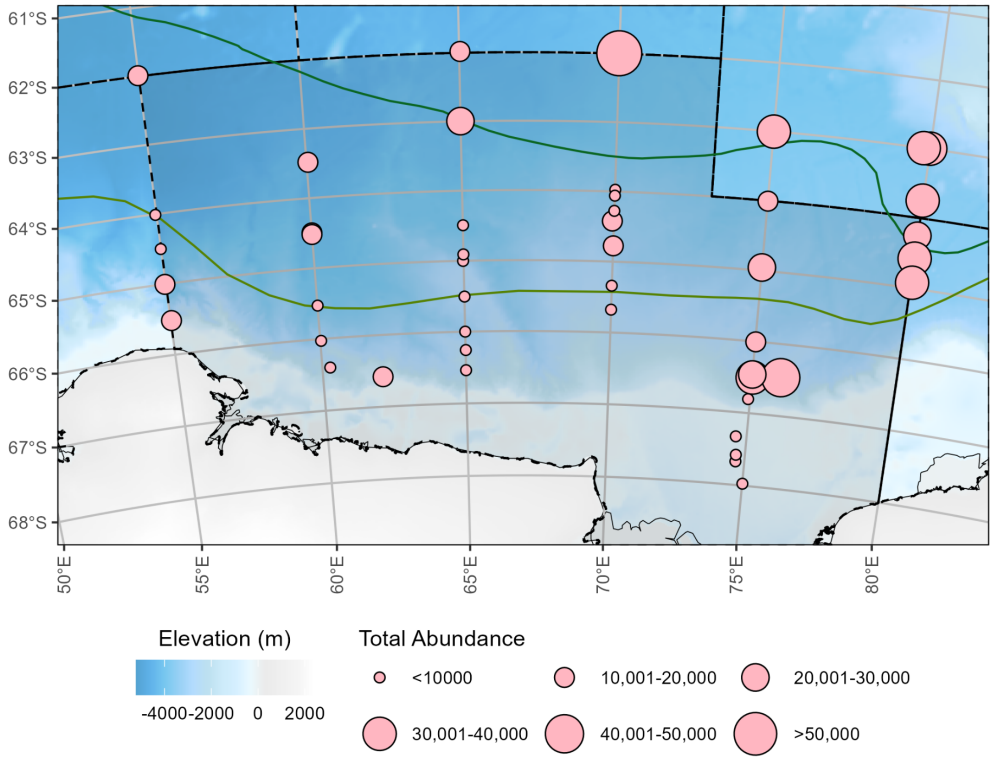


FIGURE 2
Total zooplankton abundance (ind./1000 m^3) at each sampling site. Solid border with darker regions indicates eastern sector of CCAMLR Division 58.4.2 from 55°E to 80°E. Dashed lines indicate other CCAMLR Division borders. Background bathymetry grid is from the GEBCO_2014 Grid, version 20150318, www.gebco.net. Solid, green lines represent oceanic frontal zones Southern Antarctic Circumpolar Current Front (SACCF), and the Antarctic Slope Front (ASF) determined through Orsi et al. (1995) and point estimates from Foppert et al. (2024).

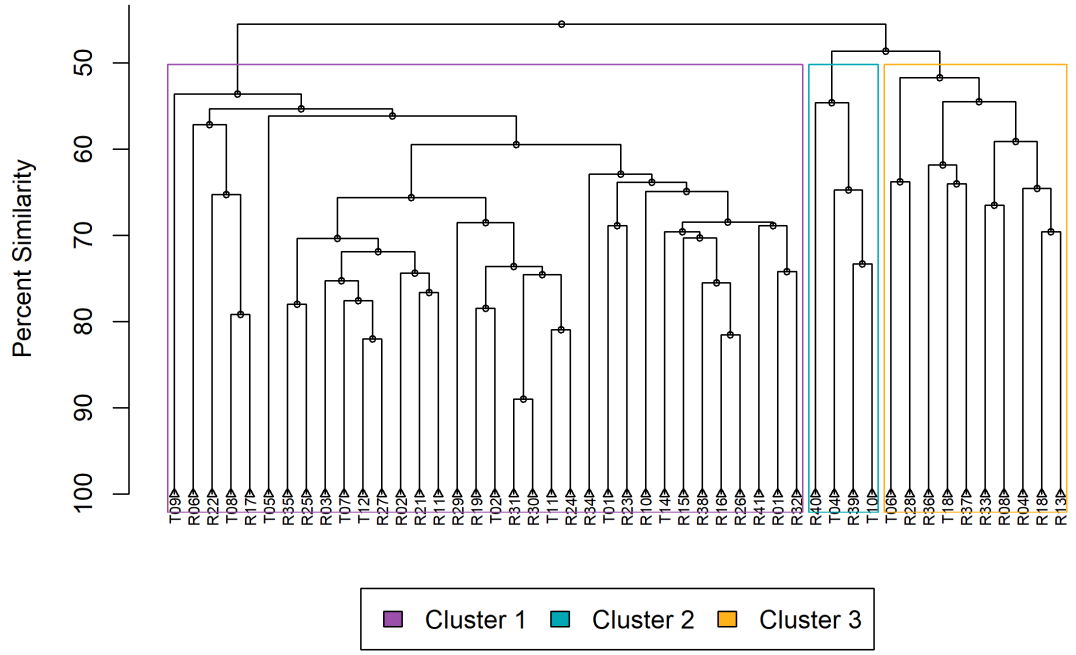


FIGURE 3
Dendrogram representing hierarchical clustering of sampling stations based on Bray-Curtis dissimilarity of zooplankton community compositions. Stations are labelled R or T and listed at the ends of the branches. Colored boxes around branches surround each of the three clusters. The length of the branches depicts percent similarity, illustrating the hierarchical structure of station similarities.

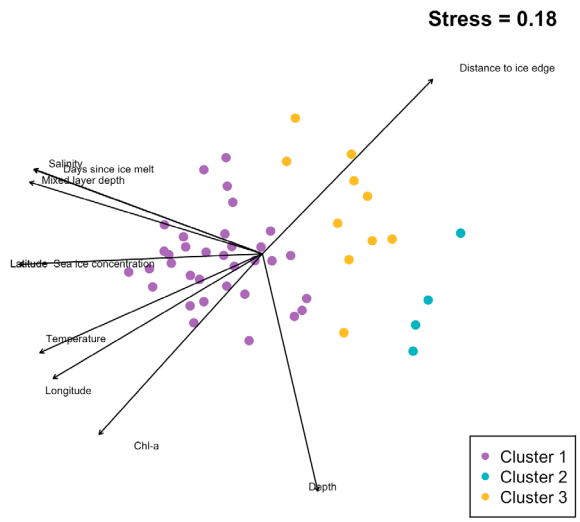


FIGURE 4
Non-metric Multidimensional Scaling (NMDS) plot displaying similarity patterns among sampling sites based on sampling sites, color-coded according to cluster assignment. Arrows indicate direction and strength of the relationship between environmental variables and the ordination space, with the length of each arrow proportional to the influence of the variable.

dominated by *Calanoides acutus* and *Rhincalanus gigas* that accounted for 78.6% (21,181 ± 681 ind./1000 m^3) and 20.7% (9,300 ± 938 ind./1000 m^3) of total abundance (Table 3).

This cluster also had the highest total abundance of zooplankton (74,386 ind./1000 m-3), with copepods contributing 58,524 ind./1000 m^3 (Table 3). Other significant taxa included chaetognaths (9,716 ind./1000 m^3), foraminifera (1,782 ind./1000 m^3), and ostracods (1,327 ind./1000 m^3). Overall, copepods dominated Cluster 1 with 78.6% of the community composition (Figure 6). Additionally, this cluster showed high species diversity, with 34 taxa, including *Clausocalanus breviceps* (4.50%), *Aetideops antarctica* (3.98%), and *Candacia* sp. (3.94%) (Figure 7; Table 4).

Environmental analysis revealed that Cluster 1 was characterized by deeper waters (3,475 ± 739 m) compared to Clusters 2 and 3, and its sites were primarily distributed across all northernmost regions (Table 2). This cluster appeared to have the greatest spatial distribution, spanning all transects from 55°E to 85°E.

3.2.2 Cluster 2

Cluster 2 included four sampling sites, which were located along transects 2 (60°E) and 3 (65°E) (Figure 5). This cluster was associated with mid-latitude regions and exhibited lower chlorophyll-a concentrations (30.04 ± 5.14 mg m^{-2}) and intermediate temperatures (-0.75 ± 0.86°C) compared to the other clusters (Table 2).

In terms of community composition, Cluster 2 had a more diverse array of species, with copepods contributing 72.5% of the total abundance (767 ind./1000 m^3) (Figures 6, 7; Table 3). The dominant species in this cluster included *Calanus simillimus* (30.12%), *Rhincalanus gigas* (25.31%), *Calanoides acutus* (23.39%), and *Calanus propinquus* (21.17%). This cluster exhibited the lowest overall zooplankton abundance (1,059 ind./1000 m^3).

The IndVal analysis identified several indicator species for Cluster 2, including the shelled pteropod *Clio pyramidata f. sulcata* (IndVal = 0.649, p = 0.024) and the pelagic worm *Rhynchonerella brongraini* (IndVal = 0.617, p = 0.026). *Clausocalanus laticeps* was also found to be significant across Clusters 1 and 2 (IndVal = 0.845, p = 0.018).

3.2.3 Cluster 3

Cluster 3 included ten sampling sites and was located in the southernmost regions of the survey, primarily along the Mawson coastline and within the Cooperation Sea (Figure 5). This cluster was most distinct from the others, separating at approximately 44%

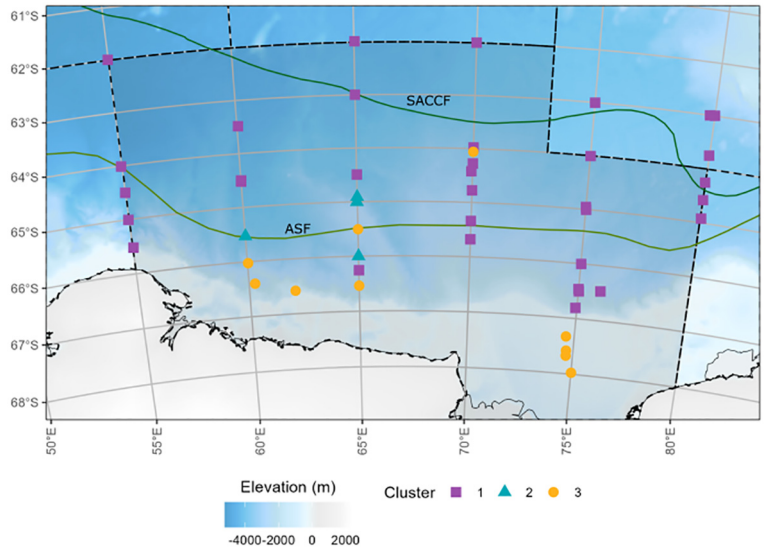


FIGURE 5
Station cluster groupings as determined by hierarchical agglomerative clustering analysis and NMDS. Solid, green lines represent oceanic frontal zones Southern Antarctic Circumpolar Current Front (SACCF) and the Antarctic Slope Front (ASF) determined through Orsi et al. (1995) and point estimates from Foppert et al. (2024).

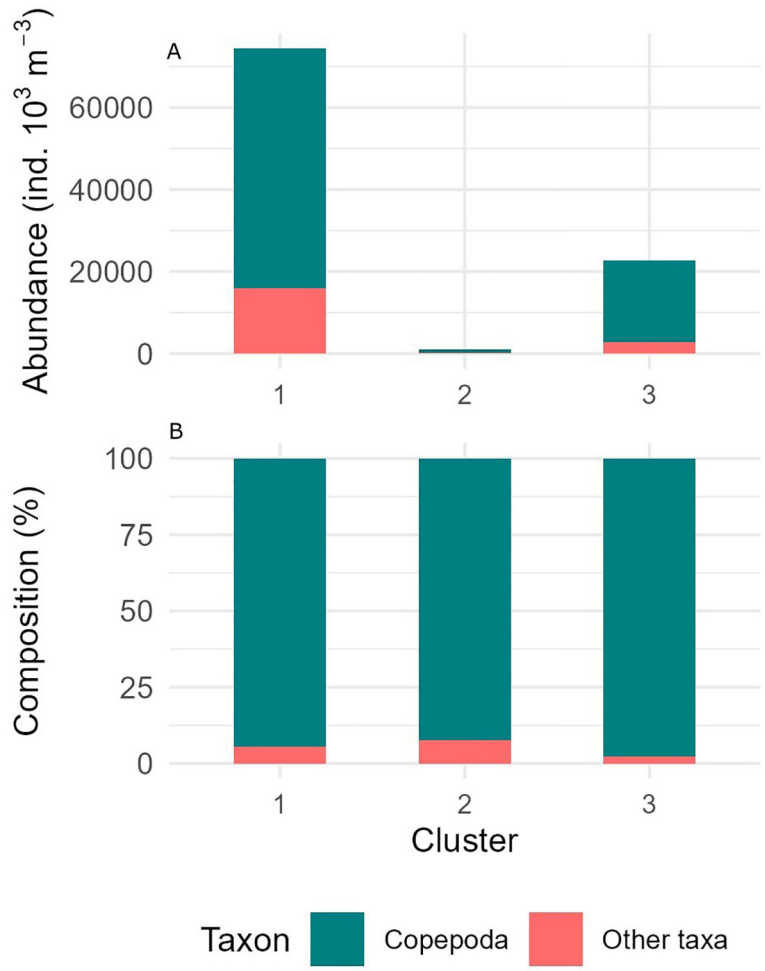


FIGURE 6
Abundance **(A)** and percent composition **(B)** of the taxonomic group Copepoda (teal color) and all other taxa (coral color) divided by clusters determined from Q-mode clustering analysis.

similarity. It was associated with lower chlorophyll-a concentrations (27.80 ± 7.79 mg m^{-2}) and colder temperatures (-1.43 ± 0.34°C) than Clusters 1 and 2 (Table 2).

The total zooplankton abundance for Cluster 3 was 22,629 ind./1000 m^3, with copepods contributing 19,743 ind./1000 m^3 and making up 87% of the community composition (Figure 6; Table 3). The dominant copepod species in this cluster were *Calanus simillimus* (13.89%), *Calanus propinquus* (12.66%), and *Oncaea antarctica* (10.70%). In addition, this cluster had notable proportions of euphausiids (1,044 ind./1000 m^3) and ostracods (Figure 7; Table 4).

The IndVal analysis identified *Paraeuchaeta* sp. as a statistically significant indicator species for Cluster 3, suggesting its strong association with the environmental conditions in this region.

3.3 Environmental drivers of zooplankton abundance

Pearson's Correlation analysis was run to assess collinearity between and among all environmental variables selected (Supplementary Figure S1 in Supplementary Materials for matrix). Since none of the correlations exceeded the 0.7 threshold, all predictor variables were retained for subsequent analysis. Due to insufficient abundance, three of the seven species identified previously as indicator species were excluded from further analysis: the pteropod *Clio pyramidata* f. *sulcata*, the pelagic worm *Rhynchonerella brongraini*, and the amphipod *Hyperiella* sp.

Generalized additive models (GAMs) were applied to examine how key environmental factors, such as chlorophyll-a, temperature, and MLD, influenced zooplankton abundance across the entire dataset. This analysis provided insights into how these environmental drivers impacted the abundance and distribution of key species, including copepods *Haloptilus* sp. (Supplementary Figure S2), *Clausocalanus laticeps* (Supplementary Figure S3), and *Paraeuchaeta* sp. (Supplementary Figure S4) and krill *Euphausia superba* (Supplementary Figure S5), as well as total zooplankton abundance (Supplementary Figure S6). Summary statistics for each model, including adjusted R^2, deviance explained, and significant smooth terms are provided in Supplementary Table S2 of

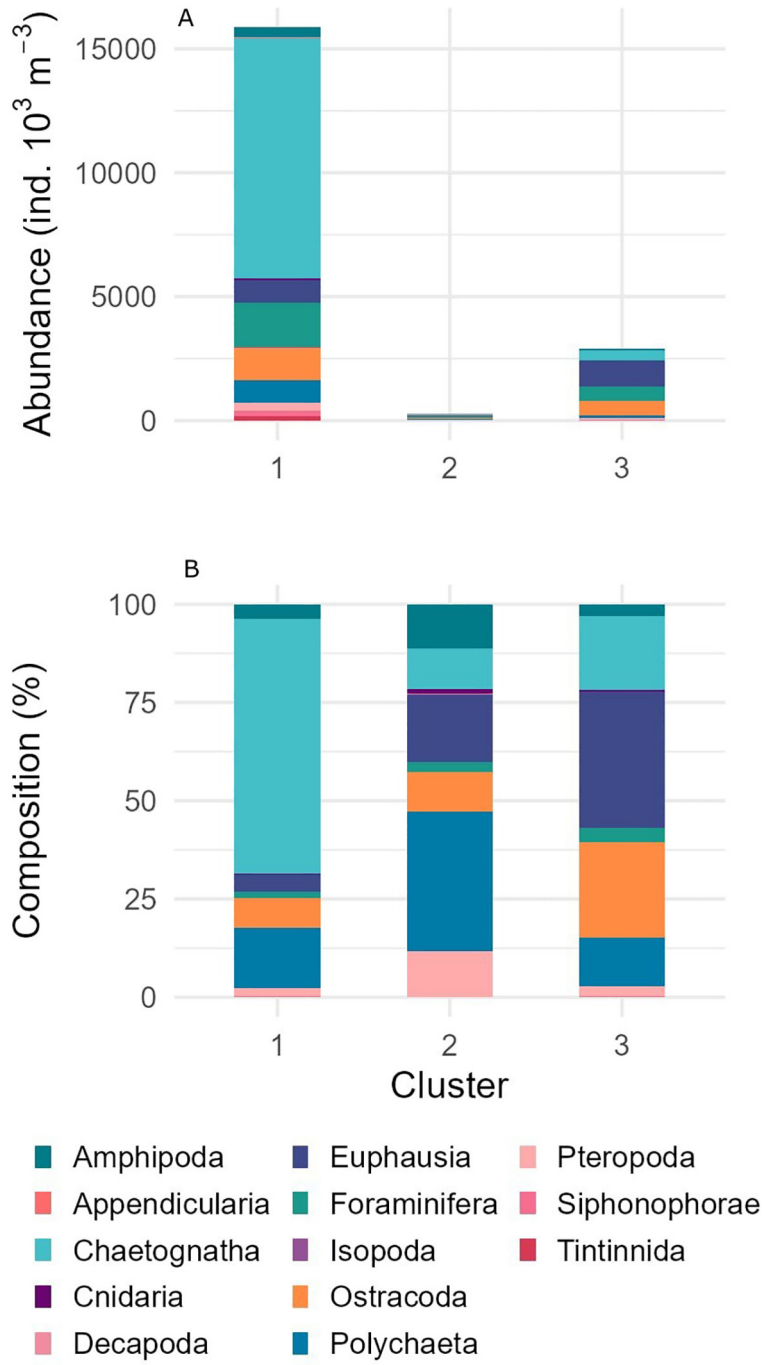


FIGURE 7
Abundance **(A)** and percent composition **(B)** of all taxa excluding Copepoda and divided by clusters determined from Q-mode clustering analysis.

Supplementary Materials. See Supplementary Figures (S2-S6) for the linear and response scale visualizations of these relationships for each of the species and total zooplankton abundances. The resultant models for each species and total zooplankton abundance are presented in Supplementary Table S3, which includes predictor variables and their AIC values, indicating model fit. Across all models, significant environmental drivers included chlorophyll-*a* concentration, temperature (integrated to 200 m), days since ice melt, and mixed layer depth (MLD).

For total zooplankton abundance, the model explained 70.9% of the deviance (adjusted $R^2 = 0.642$), suggesting that a substantial portion of zooplankton variability was driven by these factors (Supplementary Table S2), which included chlorophyll-*a* concentration, temperature, number of days since ice melt, and MLD. The smooth terms for days since ice melt was the most significant (*F*-value = 23.283; $p = 2.07\text{x}10^{-5}$), indicating a strong influence on total zooplankton abundance. Chlorophyll-*a* concentration was also highly significant (*F*-value = 15.478; $p = 3.10\text{x}10^{-3}$), reflecting its importance as a

TABLE 2 Mean ± standard deviation and range (minimum—maximum) values for environmental variables per cluster, as determined through hierarchical clustering.

Environmental variable	Cluster 1 (34)	Cluster 2 (4)	Cluster 3 (10)	$F_{between\ groups}$
Chl*a* $_{10\text{-}200m}$ mg m^{-2}	49.13 ± 24.38 18.42—102.35	30.04 ± 5.14 23.74—34.23	27.80 ± 7.79 20.10—48.21	4.72*
Depth (m)	3,475 ± 739 1,795—4,992	3,253 ± 581 2,456—3,806	1,499 ± 1207 451—3,530	19.35***
MLD N_2max (m)	43 ± 9 30—65	43 ± 13 27—58	50 ± 22 25—88	1.28
CT_{200} (°C)	0.02 ± 0.85 -1.46—1.18	-0.75 ± 0.86 -1.53—0.47	-1.43 ± 0.34 -1.71— -0.56	14.87***
SA_{200} (g kg^{-1})	34.41 ± 0.1 34.10—34.55	34.41 ± 0.11 34.32—34.56	34.31 ± 0.09 34.17—34.43	4.47*
Days since ice melt	77 ± 27 30—122	35 ± 8 25—41	-39 ± 151 -320—85	8.48***
Distance to ice edge (m)	197,325.56 ± 119,820.18 17,687.87—496,790.15	93,817.30 ± 62,246.81 37,961.95—147,705.81	79,154.88 ± 68,920.04 12,546.77—244,484.98	5.89**
Ice concentration (%)	0.00 0.00—0.00	0.00 0.00—0.00	7.34 ± 12.29 0.00—33.27	9.62***

Numbers in brackets refer to number of sampling sites (*n*).
One-way ANOVA Significant codes: $p < 0.05$(*), $p < 0.01$(**), $p < 0.001$(***); df = 2,43.

proxy for primary productivity. Temperature (F-value = 7.672, $p = 5.84 \times 10^{-5}$) and MLD (F-value = 5.282, $p = 2.68 \times 10^{-2}$) also showed significant effects. Similarly, *Clausocalanus laticeps* abundance was significantly influenced by temperature (F-value = 7.262, $p = 1.03 \times 10^{-2}$) and MLD (F-value = 14.126, $p = 5.60 \times 10^{-4}$).

For taxon-specific results, the GAM for the copepod *Clausocalanus laticeps* showed that environmental variables explained 81.6% of the variation in abundance (adjusted R^2 = 0.885; Supplementary Table S2), making it one of the best-fitting models in the analysis. The strongest predictors of *C. laticeps* abundance were chlorophyll-*a* concentration (F-value = 10.056; $p = 2.77 \times 10^{-4}$) and mixed MLD (F-value = 14.126; $p = 5.60 \times 10^{-4}$), suggesting that primary productivity and physical oceanographic conditions strongly influence this species. Days since ice melt also significantly affected abundance (F-value = 5.777; $p = 4.08 \times 10^{-3}$), indicating that seasonal variability in sea ice may play a role.

For *Haloptilus* sp., the environmental variables explained 37.6% of the variation in abundance (adjusted R^2 = 0.409; Supplementary Table S2), with latitude being the most significant predictor (F-value = 14.636; $p = 4.08 \times 10^{-4}$), highlighting the spatial distribution of this species. Salinity (integrated to 200 m) was also significant (F-value = 4.421; $p = 4.12 \times 10^{-2}$), while days since ice melt had a marginal effect (F-value = 3.862; $p = 6.24 \times 10^{-2}$).

For the krill *E. superba*, environmental variables explained 42.3% of the variation in abundance (adjusted R^2 = 0.151; Supplementary Table S2). Latitude was a significant predictor (F-value = 6.684; $p = 1.34 \times 10^{-2}$), indicating spatial patterns in krill distribution. Days since ice melt also significantly influenced krill abundance (F-value = 4.173; $p = 4.75 \times 10^{-2}$), while other variables, such as chlorophyll-a and temperature, did not significantly impact abundance.

Lastly, for *Paraeuchaeta* sp., the model explained 99.9% of the variation in abundance (adjusted R^2 = 0.999; Supplementary Table S2), though none of the predictors were statistically significant. Mixed layer depth was marginally non-significant (F-value = 1.975; $p = 6.62 \times 10^{-2}$), suggesting that deeper oceanographic processes may influence this species, but further research is needed to confirm these effects the observed dominance of certain species, such as *C. acutus* in warmer waters and *E. superba* in regions with earlier sea ice melt, highlights the nuanced interactions between zooplankton and their environmental. These species-specific patterns underscore the critical role of environmental gradients in structuring the overall community.

4 Discussion

Our study provides new insights into the distribution and abundance of mesozooplankton communities along the Mawson coast, East Antarctica, highlighting the roles of environmental variables such as temperature, primary productivity, and sea ice dynamics. These factors are critical in shaping the community structure and influencing the dominance of specific zooplankton species across environmental gradients.

4.1 Survey-wide mesozooplankton abundance and distribution

Mesozooplankton abundance across the survey ranged from 115 to 59,970 ind./1000 m^3, generally lower than in other Southern Ocean regions. This pattern likely reflects regional variations in environmental conditions, particularly temperature and chlorophyll-*a* concentrations. Areas with elevated chlorophyll-*a* and warmer waters, typically associated with oceanographic fronts such as the SACCF and ASF, supported higher zooplankton

10.3389/fmars.2024.1360541

TABLE 3 Taxa, abundance (ind./1000 m^3) and proportion (%) contributing to the top 50% of the total abundance for each cluster.

Cluster	Taxa	Total abundance	Percentage of cluster total
1	*Clausocalanus breviceps*	135.8	4.51
	Aetideopsis antarctica	119.8	3.98
	Candacia sp.	118.7	3.94
	Neocalanus gracilis	117.5	3.90
	Clausocalanus laticeps	117.4	3.89
	Solecithricella sp.	116.6	3.87
	Calanus propinquus	109.9	3.65
	Clausocalanus sp.	109.7	3.64
	Metridia sp.	100.7	3.34
	Paraeuchaeta sp.	98.7	3.27
	Gaidius tenuispinus	96.4	3.20
	Parathemisto sp.	94.8	3.15
	Neocalanus tonsus	93.5	3.10
	Gammaridean amphipod	93.2	3.09
	Ctenocalanus sp.	92.4	3.07
	Microcalanus pygmaeus	90.4	3.00
	Oncaea antarctica	90.0	2.99
	Themisto gaudichaudii	89.8	2.98
	Calanus simillimus	87.9	2.92
	Euchirella rostromanga	87.7	2.91
	Calanoides acutus	87.2	2.89
	Heterohabdus australis	87.1	2.89
	Rhincalanus gigas	83.4	2.77
	Oithona similis	76.6	2.54
	Oncaea spp.	74.4	2.47
	Heterohabdus sp.	71.0	2.36
	Oithona frigida	70.6	2.34
	Haloptilus sp.	66.1	2.19
	Metridia gerlachei	63.4	2.10
	Stephos longipes	61.9	2.05
	Aetidiopsis minor	59.8	1.99
	Pleuromamma sp.	54.8	1.82
	Heterostylites longicornis	51.3	1.70
	Harpacticoid copepod	45.1	1.50
2	*Calanus simillimus*	44.2	30.12
	Rhincalanus gigas	37.1	25.31
	Calanoides acutus	34.3	23.39
	Calanus propinquus	31.1	21.17
3	*Calanus simillimus*	80.8	13.89
	Calanus propinquus	73.7	12.66
	Oncaea antarctica	62.3	10.70
	Calanoides acutus	58.2	10.00
	Rhincalanus gigas	56.5	9.72
	Metridia sp.	55.9	9.60
	Pleuromamma sp.	55.2	9.48
	Metridia gerlachei	53.6	9.22
	Paraeuchaeta sp.	43.4	7.46
	Oncaea sp.	42.3	7.26

abundances. These results align with previous studies in the Southern Ocean, including the BROKE-West survey, which also identified similar patterns of enhanced zooplankton abundance in areas with increased primary productivity and nutrient availability (Nicol et al., 2000).

The zooplankton surveys from the BROKE-West study (Swadling et al., 2010) showed that abundances tended to be higher towards the northeast sector of the region, and our study aligns with these findings. Notably, the highest average chlorophyll-*a* concentration linked with the highest average zooplankton abundance in the BROKE-West survey. Our average estimates of chlorophyll-*a* concentration and zooplankton abundance were lower by an order of magnitude compared with the BROKE-West survey. This pattern suggests a complex dynamic between phytoplankton availability (i.e., food for zooplankton grazers), chlorophyll-*a* concentrations, and zooplankton grazing pressure. Further investigation into primary production rates and turnover is warranted to better understand these interactions in this region.

As reported by Swadling et al. (2010) across the same location, copepods emerge as the dominant group in our study, particularly the smaller species, such as *Oithona similis*, *Microcalanus pygmaeus* and *Ctenocalanus* sp. The dominance of large copepod species, like *Calanoides acutus* and *Rhincalanus gigas* observed here, has also been observed in previous studies across the same survey region and other regions of the Southern Ocean (Johnston et al., 2022). The large abundances of copepods in this region underscore their crucial role in the transfer of energy within the Antarctic food web, connecting primary productivity to higher trophic levels, as well as their conduit remineralization role (Swadling et al., 2010). Interestingly, Schaafsma et al. (2024) found that *C. propinquus* and *O. similis* were also dominant in surface waters, but with varying densities depending on the location and time of sampling. This suggests that surface conditions can significantly influence copepod distributions.

10.3389/fmars.2024.1360541

TABLE 4 Average abundances ± standard deviations (ind./1000 m^3) for all zooplankton taxa of each of the three clusters determined through agglomerative hierarchical clustering and NMDS analysis.

Species/taxon	Cluster 1 (34)	Cluster 2 (4)	Cluster 3 (10)
Aetideopsis antarctica	<1 ±<1	0	0
Aetideopsis minor	<1 ±<1	0	0
Calanoides acutus	858 ± 49	12 ±<1	41 ± 23
Calanus propinquus	75 ± 20	44 ± 6	31 ± 2
Calanus simillimus	27 ± 19	2 ±<1	81 ± 20
Candacia sp.	<1 ±<1	0	0
Clausocalanus breviceps	11_{a} ±14	$<1_{a}$ ±<1	<1 ±<1
Clausocalanus laticeps	**99** ± 14	**<1** ±<1	<1 ±<1
Clausocalanus sp.	<1 ±<1	0	<1 ±<1
Ctenocalanus sp.	39 ± 9	<1 ±<1	11 ± 6
Euchirella rostromanga	$<1_{b}$ ±<1	0	$<1_{b}$ ±<1
Gaedius tenuispinus	<1 ±<1	0	0
Haloptilus sp.	1 ± 4	**1** ±<1	<1 ±<1
Harpacticoid unidentified	<1 ±<1	0	<1 ±<1
Heterhabdus australis	$<1_{b}$ ±<1	0	$<1_{b}$ ±<1
Heterostylites longicornis	<1 ±<1	0	0
Heterhabdus sp.	$<1_{b}$ ±<1	0	$<1_{b}$ ±<1
Metridia gerlachei	256 ± 7	10 ±<1	28 ± 14
Metridia lucens	20 ± 25	<1 ±<1	10 ± 5
Microcalanus pygmaeus	1810 ± 18	6 ±<1	331 ± 1
Neocalanus gracilis	<1 ±<1	0	<1 ±<1
Neocalanus tonsus	<1 ±<1	0	0
Oithona frigida	1 ± 8	<1 ±<1	12 ± 2
Oithona similis	1936 ± 18	5 ±<1	123 ±<1
Oncaea antarctica	0	0	<1 ±<1
Oncaea sp.	465 ± 10	4 ±<1	11 ±<1
Paraeuchaeta sp.	<1 ±<1	0	**5** ± 2
Pleuromamma sp.	$<1_{b}$ ±<1	0	$<1_{b}$ ±<1
Rhincalanus gigas	832 ± 21	4 ± 1	7 ±<1
Solecithricella sp.	<1 ±<1	0	0
Stephos longipes	1 ± 2	<1 ±<1	14 ± 4
Gammaridean amphipod	<1 ±<1	0	0
Hyperia antarctica	<1 ±<1	<1 ±<1	0
Hyperia sp.	<1 ±<1	0	0
Hyperiella antarctica	<1 ±<1	0	0
Hyperiella dilatata	0	0	<1 ±<1
Hyperiella macronyx	0	0	<1 ±<1
Hyperiella sp.	0	$\mathbf{<1_{c}}$ ±<1	$\mathbf{<1_{c}}$ ±<1
Hyperoche medusarum	0	0	<1 ±<1
Parathemisto sp.	0	0	<1 ±<1
Primno macropa	4 ± 3	<1 ±<1	<1 ±<1
Themisto guadichaudii	<1 ±<1	< 1±<1	<1 ±<1
Euphausia crystallorophius	<1 ±<1	0	<1 ± 2
Euphausia superba	<1 ± 2	$\mathbf{<1_{c}}$ ±<1	$\mathbf{8_{c}}$ ±4
Thysanoessa macrura	57 ± 10	5 ± 1	4 ± 1
Clione antarctica	$<1_{b}$ ±<1	0	$<1_{b}$ ±<1
Clio pyramidata	<1 ±<1	**<1** ± 2	<1 ±<1
Gymnosome unidentified	0	<1 ±<1	<1 ±<1
Limacina helicina antarctica	110 ± 41	<1 ±<1	2 ±<1
Pteropod egg mass	<1 ±<1	0	0
Spongiobranchaea australis	$<1_{b}$ ±<1	0	$<1_{b}$ ±<1
Iospilidae worm	<1 ±<1	0	0
Pelagobia longicerrata	1 ± 3	<1 ±<1	<1 ±<1
Phalacrophorus pictus	$<1_{b}$ ±3	0	$<1_{b}$ ±<1
Phalacrophorus sp.	<1 ±<1	0	0
Polychaete unidentified	$<1_{b}$ ±<1	0	$<1_{b}$ ±<1
Rhynchonerella brongraini	<1 ±<1	**<1** ± 1	<1 ±<1
Rhynchonerella petersii	<1 ±<1	0	0
Rhynchonerella sp.	<1 ± 1	0	0
Tiarrana rotunda	0	0	<1 ±<1
Tomopteris septentrionalis	<1 ±<1	0	0
Tomopteris sp.	$<1_{b}$ ±1	0	$<1_{b}$ ±<1
Traviopsis/Typhloscolex	$<1_{b}$ ±<1	0	$<1_{b}$ ±<1
Vanadis antarctica	<1 ±<1	0	0
Vanadis longissima	0	<1 ±<1	0
Vanadis sp.	<1 ± 1	0	0
Eukrohnia hamata	$<1_{b}$ ±<1	0	$<1_{b}$ ±<1
Sagitta gazella	<1 ±<1	0	<1 ±<1
Sagitta marri	<1 ±<1	0	0
Sagitta maxima	<1 ±<1	<1 ±<1	0
Sagitta serratodentata	<1 ±<1	$<1_{c}$ ±<1	$<1_{c}$ ±2

(Continued)

(Continued)

10.3389/fmars.2024.1360541

TABLE 4 Continued

Species/taxon	Cluster 1 (34)	Cluster 2 (4)	Cluster 3 (10)
Sagitta sp.	<1 ± 1	0	<1 ± 2
Chaetognath unidentified	240 ± 7	5 ±<1	1 ± 1
Alacia hettacra	<1 ±<1	0	<1 ±<1
Austrinoecia isocheira	0	0	<1 ± 1
Boroecoa antipoda	0	0	<1 ±<1
Deeveyoecia arcuata	<1 ±<1	0	0
Metaconchoecia skogsbergi	0	0	<1 ±<1
Ostracod unidentified	31 ± 10	6 ±<1	4 ± 4
Appendicularian unidentified	$<1_b$ ±<1	0	$<1_b$ ±<1
Decapod unidentified	0	<1 ±<1	<1 ±<1
Isopod unidentified	<1 ±<1	<1 ±<1	0
Neogloboquadrina pachyderma	18 ± 13	9_c ±<1	32_c ±1
Siphonophore unidentified	<1 ± 1	$<1_c$ ±<1	$<1_c$ ±<1
Tintinnids unidentified	<1 ± 2	0	0
Total Abundance	**6893**	**133**	**838**

Values in brackets represent the number of sampling stations (*n*). Bold values correspond to statistically significant ($p < 05$) potential indicator species as determined through IndVal. Subscript a ($_a$) indicates species associated with the combination of Clusters 1 and 2, subscript b ($_b$) indicates species associated with Clusters 1 and 3, and subscript c ($_c$) indicates species associated with the combination of Clusters 2 and 3.
Values in bold correspond to indicator species.

4.2 Abundance patterns and community composition

The cluster analysis identified three distinct zooplankton communities, each characterized by dominant species and environmental conditions. Cluster 1, situated in warmer, northern waters, was dominated by *Calanoides acutus* (21,181 ± 681 ind./1000 m^3), a species known to thrive in regions with higher primary productivity. In contrast, *Euphausia superba* was more abundant in Cluster 3, associated with earlier sea ice melt and extended open-water periods conducive to phytoplankton growth. The significant variation in species abundance across clusters underscores the importance of environmental gradients in shaping zooplankton communities, with species responding differently to changes in temperature, sea ice, and nutrient availability.

The dominance of *Calanoides acutus* in Cluster 1, characterized by higher chlorophyll-*a* concentrations, mirrors findings from the BROKE-West survey, where similar species were found to dominate in regions of high primary productivity (Swadling et al., 2010). However, the lower abundances observed in our study compared to BROKE-West likely reflect regional differences in oceanographic conditions and temporal variability in phytoplankton blooms. The presence of *Euphausia superba* in Cluster 3, which is closely linked to areas of early sea ice melt, also aligns with observations from BROKE-West, where krill abundance was higher in regions with extended open-water periods following ice retreat.

Our findings also reveal the role of smaller copepod species, such as *Clausocalanus laticeps*, in driving community composition in Cluster 2, where environmental conditions were more moderate. These species-specific responses to environmental variability highlight the complexity of zooplankton community dynamics in this region, with key species occupying ecological niches that align with their physiological tolerances and feeding strategies.

4.3 Environmental drivers of zooplankton abundance

Generalized Additive Models (GAMs) provided species-specific insights into how environmental drivers shape zooplankton abundance, independent of the clustering analysis. Chlorophyll-*a* concentration and temperature emerged as significant predictors of abundance for *Clausocalanus laticeps*, while latitude and salinity were important for *Haloptilus* sp. The BROKE-West survey similarly highlighted the importance of these environmental drivers in structuring zooplankton communities, particularly the role of primary productivity in driving the distribution of key species across the region (Swadling et al., 2010; Nicol et al., 2000).

4.4 Influence of oceanographic fronts on zooplankton communities

Oceanographic features such as the Antarctic Circumpolar Current Front (SACCF), Southern Boundary (SB) and the Antarctic Slope Front (ASF) play a critical role in shaping the distribution of mesozooplankton communities in the Southern Ocean. These fronts and currents create distinct ecological boundaries, where enhanced mixing and nutrient availability influence the movement and abundance of zooplankton (Nicol and Meiners, 2010). Species such as *Calanoides acutus* and *Rhincalanus gigas* were more abundant near these frontal systems, which provide favorable feeding conditions. These patterns are consistent with other Southern Ocean studies, where zooplankton abundance and community composition have been linked to oceanographic fronts (Atkinson et al., 2008; Takahashi et al., 2002). The dynamic interaction of water masses in these areas leads to localized conditions that support different zooplankton assemblages, similar to patterns observed in other regions of the Southern Ocean (Atkinson et al., 2008; Pakhomov et al., 2000; Tarling et al., 2012). These features underscore the importance of oceanographic processes in structuring zooplankton communities and shaping broader ecosystem dynamics.

4.5 Caveats and future directions

While our study provides valuable insights into zooplankton distribution and abundance along the Mawson coast, several caveats

must be acknowledged. First, the temporal scope of our sampling was limited to the austral summer, which may not capture the full extent of seasonal variability in zooplankton communities. As zooplankton populations are known to exhibit significant changes across seasons due to shifts in sea ice cover and primary productivity (Swadling et al., 2023; Pinkerton et al., 2020), future studies should aim to include year-round sampling to better understand the temporal dynamics of these communities.

Second, our analysis primarily focused on surface environmental drivers, such as temperature and chlorophyll-*a* concentrations. However, deeper oceanographic processes, such as subsurface currents and nutrient upwelling, may also play a critical role in shaping zooplankton communities, particularly for species that undergo diel vertical migrations (Schaafsma et al., 2024). Future research should consider the influence of these deeper processes to provide a more comprehensive understanding of zooplankton ecology in the Southern Ocean.

Additionally, our study relied on Generalized Additive Models (GAMs) to explore species-environment relationships. While GAMs are powerful tools for identifying key environmental drivers, their application assumes a level of independence between variables that may not fully capture the complexity of ecosystem interactions (Dormann et al., 2013). Future studies may benefit from employing more complex ecological models, such as those that account for species interactions and multicollinearity between environmental predictors (Wisz et al., 2013).

Finally, our findings highlight the importance of understanding zooplankton responses to changing environmental conditions, particularly in light of climate change. Long-term monitoring programs will be essential for detecting shifts in zooplankton communities over time and assessing the resilience of Southern Ocean ecosystems. Further research into the functional roles of key zooplankton species, such as *Euphausia superba*, and their interactions with other trophic levels will be crucial for predicting future ecosystem responses.

4.6 Implications for Southern Ocean ecosystems under climate change

As the Southern Ocean continues to experience climate-driven changes in sea ice extent, temperature, and primary productivity, zooplankton communities will likely undergo significant shifts. Species like *Euphausia superba* may face disadvantages in regions with reduced sea ice cover, as earlier ice melt could disrupt the timing of phytoplankton blooms and krill recruitment (Atkinson et al., 2019; Flores et al., 2012). Conversely, species such as *Calanoides acutus*, which thrive in warmer waters, may benefit from these changing conditions. These shifts could have cascading effects on higher trophic levels, particularly krill-dependent predators like seabirds, fish, and marine mammals.

Our findings highlight the need for continued monitoring of zooplankton communities to better understand their responses to climate change. The significant role of environmental drivers in shaping taxon-specific abundance and community composition suggests that future changes in these drivers will alter the structure of Southern Ocean ecosystems. By identifying key environmental factors that influence zooplankton dynamics, this study contributes to the growing body of knowledge needed to predict the ecological impacts of climate change in polar regions.

Data availability statement

The original contributions presented in the study are included in the article/Supplementary Materials, further inquiries can be directed to the corresponding author.

Ethics statement

The manuscript presents research on animals that do not require ethical approval for their study.

Author contributions

CW: Conceptualization, Data curation, Formal Analysis, Investigation, Methodology, Project administration, Validation, Visualization, Writing – original draft, Writing – review & editing. MB: Methodology, Writing – review & editing. AB: Methodology, Writing – review & editing. OJ: Methodology, Writing – review & editing. DM: Data curation, Formal Analysis, Investigation, Methodology, Writing – review & editing.

Funding

The author(s) declare financial support was received for the research, authorship, and/or publication of this article. This research was supported by the Australian Antarctic Program Partnership - a partnership of Australia's leading Antarctic research institutions supported by the Australian Government Antarctic Science Collaborative Initiative. This project was also supported and funded by the Australian Antarctic Science Project 4512 and 4636, and received financial support from Pew Charitable Trust and the Antarctic Science Foundation.

Acknowledgments

We thank Dr. So Kawaguchi, Rob King, Jessica Melvin, Associate Professor Kerrie Swadling, and Dr. Karen Westwood for cruise and zooplankton sampling organization. Thanks to all crew and scientific team aboard the RV *Investigator*. We also thank Dr. Mike Sumner and Dr. Ben Raymond for providing distance to ice and ice concentration measurements, Dr. Annie Foppert for mixed layer depth estimates, and Dr. Karen Westwood for integrated chlorophyll-*a* values. Finally, we would also like to thank the reviewers whose input greatly improved the quality of this research output.

Conflict of interest

The authors declare that the research was conducted in the absence of any commercial or financial relationships that could be construed as a potential conflict of interest.

Publisher's note

All claims expressed in this article are solely those of the authors and do not necessarily represent those of their affiliated organizations, or those of the publisher, the editors and the reviewers. Any product that may be evaluated in this article, or claim that may be made by its manufacturer, is not guaranteed or endorsed by the publisher.

Supplementary material

The Supplementary Material for this article can be found online at: https://www.frontiersin.org/articles/10.3389/fmars.2024.1360541/full#supplementary-material

References

Atkinson, A., Hill, S. L., Pakhomov, E. A., Siegel, V., Reiss, C. S., Loeb, V. J., et al. (2019). Krill (*Euphausia superba*) distribution contracts southward during rapid regional warming. *Nat. Climate Change* 9, 142–147. doi: 10.1038/s41558-018-0370-z

Atkinson, A., Siegel, V., Pakhomov, E. A., Rothery, P., Loeb, V., Ross, R. M., et al. (2008). Oceanic circumpolar habitats of Antarctic krill. *Mar. Ecol. Prog. Ser.* 362, 1–23. doi: 10.3354/meps07498

Cavan, E. L., Henson, S. A., Belcher, A., and Sanders, R. (2017). Role of zooplankton in determining the efficiency of the biological carbon pump. *Biogeosciences.* 14, 177–186. doi: 10.5194/bg-14-177-2017

Constable, A. J., Melbourne-Thomas, J., Corney, S. P., Arrigo, K. R., Barbraud, C., Barnes, D. K. A. A., et al. (2014). Climate change and Southern Ocean ecosystems I: how changes in physical habitats directly affect marine biota. *Glob. Change Biol.* 20, 3004–3025. doi: 10.1111/gcb.12623

Core Team, R. (2023). *R: A Language and Environment for Statistical Computing* (Vienna, Austria: R Foundation for Statistical Computing). Available at: https://www.R-project.org/.

Cox, M. J., Macaulay, G., Brasier, M. J., Burns, A., Johnson, O. J., King, R., et al. (2022). Two scales of distribution and biomass of Antarctic krill (Euphausia superba) in the eastern sector of the CCAMLR Division 58.4.2 (55°E to 80°E). *PloS One* 17, 1–19. doi: 10.1371/journal.pone.0271078

De Cáceres, M., and Legendre, P. (2009). Associations between species and groups of sites: Indices and statistical inference. *Ecology* 90, 3566–3574. doi: 10.1890/08-1823.1

De Cáceres, M., Legendre, P., Wiser, S. K., and Brotons, L. (2012). Using species combinations in indicator value analyses. *Methods Ecol. Evol.* 3, 973–982. doi: 10.1111/j.2041-210X.2012.00246.x

Dormann, C. F., Elith, J., Bacher, S., Buchmann, C., Carl, G., Carré, G., et al. (2013). Collinearity: a review of methods to deal with it and a simulation study evaluating their performance. *Ecography* 36, 27–46. doi: 10.1111/j.1600-0587.2012.07348.x

Flores, H., Atkinson, A., Kawaguchi, S., Krafft, B., Milinevsky, G., Nicol, S., et al. (2012). Impact of climate change on Antarctic krill. *Mar. Ecol. Prog. Ser.* 458, 1–19. doi: 10.3354/meps09831

Foppert, A., Bestley, S., Shadwick, E. H., Klocker, A., Vives, C. R., Liniger, G., et al. (2024). Observed water-mass characteristics and circulation off Prydz Bay, Antarctica. *Front. Mar. Sci.* 11. doi: 10.3389/fmars.2024.1456207

Fraser, A. D., Massom, R. A., Ohshima, K. I., Willmes, S., Kappes, P. J., Cartwright, J., et al. (2020). High-resolution mapping of circum-Antarctic landfast sea ice distribution 2000–2018. *Earth Syst. Sci. Data* 12, 2987–2999. doi: 10.5194/essd-12-2987-2020

Heidemann, A. C., Westwood, K. J., Foppert, A., Wright, S. W., Klocker, A., Vives, C. R., et al. (2024). Drivers of phytoplankton distribution, abundance and community composition off East Antarctica, from 55-80°E (CCAMLR division 58.4.2 east). *Front. Mar. Sci.* 11. doi: 10.3389/fmars.2024.1454421

Hosie, G. W., Schultz, M. B., Kitchener, J. A., Cochran, T. G., and Richards, K. (2000). Macrozooplankton community structure off East Antarctica (80-150°E) during the Austral summer of 1995/1996. *Deep Sea Res. Part II* 47, 2437–2463. doi: 10.1016/S0967-0645(00)00031-X

Johnston, N. M., Murphy, E. J., Atkinson, A. A., Constable, A. J., Cotté, S., Cox, M., et al. (2022). Status, change and futures of zooplankton in the Southern Ocean. *Front. Ecol. Evol.* 9. doi: 10.3389/fevo.2021.624692

Kelly, N., Bestley, S., Burns, A., Clarke, L., Collins, K., Cox, M., et al. (2021). *An overview of the ecosystem survey to quantify krill abundance for krill monitoring and management in Eastern Sector of CCAMLR Division 58.4.2: Trends in Euphausiids off Mawson, Predators, and Oceanography "TEMPO"* (Working Group on Ecosystem Monitoring and Management (WG-EMM-2021/07).

Maechler, M., Rousseeuw, P., Struyf, A., Hubert, M., and Hornik, K. (2023). cluster: Cluster Analysis Basics and Extensions. R package version 2.1.4. Available at: https://CRAN.R-project.org/package=cluster.

Maschette, D., Raymond, B., and Hosie, G. (2019). SOmap: Southern Ocean Mapping Tools. *R package version 0.1.5*. https://CRAN.R-project.org/package=SOmap.

Massom, R., Reid, P., Stammerjohn, S., Raymond, B., Fraser, A., and Ushio, S. (2013). Change and variability in east antarctic sea ice seasonality 1979/80-2009/10. *PloS One* 8, e64756. doi: 10.1371/journal.pone.0064756

McCormack, S. A., Griffith, G., Hill, S. L., Hoover, C., Johnston, N. M., Marina, T. I., et al. (2020). Southern Ocean food webs: progress, prognoses, and future priorities for research and policy makers. *Front. Ecol. Evol.* 9, 624763. doi: 10.3389/fevo.2021.624763

Motoda, S. (1985). Devices of simple plankton apparatus–VII. *Bull. Mar. Sci.* 37, 776–777.

Murase, H., Abe, K., Matsukura, R., Sasaki, H., Driscoll, R., Schaafsma, F., et al. (2019). Cruise report of multidisciplinary ecosystem survey in the eastern Indian sector of the Antarctic (CCAMLR Division 58.4.1) with a focus on Antarctic krill during 2018/19 season by the Japanese survey vessel *Kaiyo-maru*. *CCAMLR Rep*.

Nicol, S., and Meiners, K. (2010). [amp]]ldquo;BROKE-West" a biological/oceanographic survey off the coast of east Antarctica (30-80oE) carried out in January-March 2006. *Deep-Sea Res.* 57, 693–992. doi: 10.1016/j.dsr2.2009.11.002

Nicol, S., Pauly, T., Bindoff, N. L., Wright, S., Thiele, D., Hosle, G. W., et al. (2000). Ocean circulation off east Antarctica affects ecosystem structure and sea-ice extent. *Nature* 406, 504–507. doi: 10.1038/35020053

Oksanen, J., Simpson, G., Blanchet, F., Kindt, R., Legendre, P., Minchin, P. R., et al. (2022). *vegan: Community Ecology Package* (R package version 2.6-4). Available at: https://CRAN.R-project.org/package=vegan.

Orsi, A. H., Whitworth, T.III, and Nowlin, W. D.Jr (1995). On the meridional extent and fronts of the Antarctic Circumpolar Current. *Deep-Sea Res. I* 42, 641–673. doi: 10.1016/0967-0637(95)00021-W

Pakhomov, E. A., Perissinotto, R., McQuaid, C. D., and Froneman, P. W. (2000). Zooplankton structure and grazing in the Atlantic sector of the Southern Ocean in late austral summer 1993: Part 1. Ecological zonation. *Deep-Sea Res. I* 47, 1663–1686. doi: 10.1016/S0967-0637(99)00122-3

Pinkerton, M. H., Décima, M., Kitchener, J. A., Takahashi, K. T., Robinson, K. V., Stewart, R., et al. (2020). Zooplankton in the Southern Ocean from the continuous plankton recorder: Distributions and long-term change. *Deep-Sea Res. I* 162, 103303. doi: 10.1016/j.dsr.2020.103303

Poloczanska, E. S., Burrows, M. T., Brown, C. J., Molinos, J. G., Halpern, B. S., Hoegh-Guldberg, O., et al. (2016). Responses of marine organisms to climate change across oceans. *Front. Mar. Sci.* 3. doi: 10.3389/fmars.2016.00062

Priddle, J., Whitehouse, M. J., Ward, P., Shreeve, R. S., Brierley, A. S., Atkinson, A., et al. (2003). Biogeochemistry of a Southern Ocean plankton ecosystem: Using natural variability in community composition to study the role of metazooplankton in carbon and nitrogen cycles. *J. Geo Res.* 103, 8082. doi: 10.1029/2000JC000425

Quetin, L. B., Ross, R. M., Frazer, T. K., and Haberman, K. L. (1996). Factors affecting distribution and abundance of zooplankton, with an emphasis on Antarctic krill, *Euphausia superba*. *Antarct Res. Ser.* 70, 357–371. doi: 10.1029/ar070p0357

Quinn, G. P., and Keough, M. J. (2002). *Experimental Design and Data Analysis for Biologists* (Cambridge, UK: Cambridge University Press).

Reid, K., Croxall, J. P., Briggs, D. R., and Murphy, E. J. (2005). Antarctic ecosystem monitoring: Quantifying the response of ecosystem indicators to variability in Antarctic krill. *ICES J. Mar. Sci.* 62, 366–373. doi: 10.1016/j.icesjms.2004.11.003

Schaafsma, F. L., Matsuno, K., Driscoll, R., Sasaki, H., van Regteren, M., Driscoll, S., et al. (2024). Zooplankton communities at the sea surface of the eastern Indian sector of the Southern Ocean during the austral summer of 2018/2019. *Prog. Ocean* 226, 103303. doi: 10.1016/j.pocean.2024.103303

Schloerke, B., Crowley, J., Cook, D., Hofmann, H., and Wickham, H. (2012). *GGAlly: Extension to ggplot2* (R package version 2.2.1).

Smetacek, V., Assmy, P., and Henjes, J. (2004). The role of grazing in structuring Southern Ocean pelagic ecosystems and biogeochemical cycles. *Antarctic Sci.* 16, 541–558. doi: 10.1017/S0954102004002317

Swadling, K. M., Constable, A. J., Fraser, A. D., Massom, R. A., Borup, M. D., Ghigliotti, L., et al. (2023). Biological responses to change in Antarctic sea ice habitats. *Front. Ecol. Evol.* 10. doi: 10.3389/fevo.2022.1073823

Swadling, K. M., Kawaguchi, S., and Hosie, G. W. (2010). Antarctic mesozooplankton community structure during BROKE-West (30°E-80°E), January-February 2006. *Deep Res. Part II Top. Stud. Oceanogr* 57, 887–904. doi: 10.1016/j.dsr2.2008.10.041

Takahashi, K. T., Kawaguchi, S., Kobayashi, M., Hosie, G. W., Fukuchi, M., and Toda, T (2002). Zooplankton distribution patterns in relation to the Antarctic Polar Front Zones recorded by Continuous Plankton Recorder (CPR) during 1999/2000 Kaiyo Maru cruise. *Polar Bioscience* 15, 97–107. doi: 10.15094/00006187

Tarling, G. A., Stowasser, G., Ward, P., Poulton, A. J., Zhou, M., Venables, H. J., et al. (2012). Seasonal trophic structure of the Scotia Sea pelagic ecosystem considered through biomass spectra and stable isotope analysis. *Deep Sea Research Part II: Topical Studies in Oceanography* 59, 222–236. doi: 10.1016/j.dsr2.2011.10.001

Wickham, H.. (2016). *ggplot2: Elegant Graphics for Data Analysis*. New York: Springer-Verlag. https://ggplot2.tidyverse.org

Wisz, M. S., Pottier, J., Kissling, W. D., Pellissier, L., Lenoir, J., Damgaard, C. F., et al. (2013). The role of biotic interactions in shaping distributions and realised assemblages of species: implications for species distribution modelling. *Biol. Rev.* 88, 15–30. doi: 10.1111/j.1469-185X.2012.00235.x

Wood, S. N. (2017). *Generalized Additive Models: An Introduction with R (2nd edition)* (Boca Raton, FL: Chapman and Hall/CRC).

Yang, G., Atkinson, A., Pakhomov, E. A., Hill, S. L., and Racault, M. F. (2022). Massive circumpolar biomass of Southern Ocean zooplankton: Implications for food web structure, carbon export, and marine spatial planning. *Limnol Oceanogr* 1–15, 2516-2530. doi: 10.1002/lno.12219

frontiers | Frontiers in Marine Science

TYPE Original Research
PUBLISHED 22 January 2025
DOI 10.3389/fmars.2024.1451997

Check for updates

OPEN ACCESS

EDITED BY
Toru Hirawake,
National Institute of Polar Research, Japan

REVIEWED BY
Keishi Shimada,
National Institute of Polar Research, Japan
Rachel Thomas,
Florida Department of Environmental Protection, United States

*CORRESPONDENCE
Annie Foppert
annie.foppert@utas.edu.au

RECEIVED 20 June 2024
ACCEPTED 19 December 2024
PUBLISHED 22 January 2025

CITATION
Liang M, Foppert A, Westwood KJ and Bestley S (2025) Observed upper-ocean structure and seasonal production in the southern Kerguelen Plateau region, 1994-2021.
Front. Mar. Sci. 11:1451997.
doi: 10.3389/fmars.2024.1451997

COPYRIGHT
© 2025 Liang, Foppert, Westwood and Bestley. This is an open-access article distributed under the terms of the Creative Commons Attribution License (CC BY). The use, distribution or reproduction in other forums is permitted, provided the original author(s) and the copyright owner(s) are credited and that the original publication in this journal is cited, in accordance with accepted academic practice. No use, distribution or reproduction is permitted which does not comply with these terms.

Observed upper-ocean structure and seasonal production in the southern Kerguelen Plateau region, 1994-2021

Man Liang[1], Annie Foppert[1,2]*, Karen J. Westwood[2,3] and Sophie Bestley[1,2]

[1]Institute for Marine and Antarctic Studies, University of Tasmania, Hobart, TAS, Australia, [2]Australian Antarctic Program Partnership, Hobart, TAS, Australia, [3]Australian Antarctic Division, Department of Climate Change, Energy, the Environment and Water, Kingston, TAS, Australia

In the Indian sector of the Southern Ocean, 80°E marks an important transition in ocean circulation between the greater Prydz Bay gyre to the west and the Australian Antarctic gyre to the east. Here, the submarine Kerguelen Plateau impedes the eastward flow of the Antarctic Circumpolar Current (ACC), topographically steering the flow. Enhanced biological productivity associated with the southern plateau supports an important marine ecosystem with many foraging marine predators. We collate ship-based hydrographic data on the vertical structure of the upper water column near 80°E from eight voyages spanning 1994 to 2021, from 58°S towards the Antarctic continent. The study aims to investigate the mixed layer oceanography, the implications for nutrient supply from deep to near-surface waters, and associated biological production. Our results show that the major oceanographic fronts are constrained within the narrow Princess Elizabeth Trough, between the southern Kerguelen Plateau and the Antarctic slope. Therefore, the Southern Boundary and the Southern ACC Front (SACCF) are often co-located, albeit with some interannual variability, with the location of the SACCF ranging from roughly 63°S to 65°S. The average depth of the seasonal mixed layer ranges from 34-49 m, typically deepening from south to north, in association with longer time since sea-ice melt. Below the mixed layer, Winter Water (WW) characteristics also vary across the observed latitudinal range; typically the temperature and thickness of the WW layer are inversely related, with warmer WW layers being thinner. Subsurface nitrate concentrations range from 20-40 μM, while silicate concentrations reach 100 μM. Nutrient drawdown is calculated based on mean concentrations in the mixed layer and WW layer, with drawdown values at individual stations reaching nearly 12 μM and 60 μM for nitrate and silicate, respectively, and a positive correlation between the two. Nutrient drawdown was higher in association with longer time since sea-ice melt and with thinner WW layers, while higher nitrate-based production was associated with deeper mixed layers. Observed relationships between upper water column characteristics and biological processes are discussed in terms of likely nutrient supply mechanisms and seasonal patterns of utilization.

KEYWORDS

Antarctic Circumpolar Current (ACC) fronts, summer stratification, seasonal mixed layer, nutrient availability, drawdown, biological productivity

1 Introduction

The Southern Ocean plays a central role in supporting the global climate, providing a direct link to global biogeochemical cycles through redistributing nutrients, carbon, and oxygen between the major ocean basins, and between the deep ocean, surface ocean, and atmosphere (Henley et al., 2020). It connects the Indian, Pacific, and Atlantic Oceans through the influence of the Antarctic Circumpolar Current (ACC) (Orsi et al., 1995). The eastward-flowing ACC is deflected by topography in different regions of the Southern Ocean (Lu et al., 2020; Talley, 2011; Williams et al., 2010); when passing through constrictive bathymetric troughs or around major submarine plateaus, the flow intensifies, and meridional meandering may occur downstream, facilitating enhanced mesoscale eddy activity associated with cross frontal exchange and upwelling (Foppert et al., 2017; Tamsitt et al., 2017; Rintoul, 2018). In the south Indian sector, the major obstacle is the submarine Kerguelen Plateau, which significantly influences the path of the ACC (Sparrow et al, 1996; Heywood et al., 1999; Vivier et al., 2015; Bestley et al., 2020). As the ACC approaches the southern Kerguelen Plateau (SKP), the Southern Boundary (SB) and Southern ACC Front (SACCF) are diverted to the south through the Princess Elizabeth Trough (PET). Further east, their flow is then deflected northward along the eastern flank of the SKP.

The Southern Ocean overall is known to be a high nutrient low chlorophyll (HNLC) region, due to low concentrations of iron that limit phytoplankton production despite the availability of macronutrients (Boyd et al., 2012; Henley et al., 2020). Iron is supplied through various mechanisms including dust deposition, sea-ice melt, redistribution of suspended sediments from shallow shelf areas, and glacial meltwater from ice shelves and icebergs (Gao et al., 2020; Laufkötter et al., 2018; Rintoul, 2018; Schallenberg et al., 2018). The sustained phytoplankton blooms observed in the SKP region are thought to result from a higher subsurface iron supply here than other regions (Schallenberg et al., 2018). This increased primary production may positively influence Antarctic krill (Nicol et al., 2000b; Nicol and Raymond, 2012; Bestley et al., 2018) and their dependent higher-order predators (Raymond et al., 2015; Patterson et al., 2016) including migratory species such as humpback whales (Bestley et al., 2019).

Physical features affecting the upper ocean structure can have a large influence on primary production given the reliance of phytoplankton cells on light and nutrients for growth (Pinkerton et al., 2021). Phytoplankton growth is constrained to within the euphotic zone (where incoming light is sufficient for photosynthesis). If the mixed layer is deeper than this, and cells are mixed below the euphotic zone, then growth may be sub-optimal due to periods of darkness. Mixed layer dynamics are therefore important for phytoplankton, as light limitation may reduce phytoplankton growth and overall primary productivity (Nelson and Smith, 1991; Westwood et al., 2010). The structure of the water column also influences macro- and micro-nutrient supply, including upwelling of nutrients into surface waters (Williams et al., 2010).

There are also significant seasonal influences on the control of phytoplankton growth (Arrigo et al., 2008). The high latitude of the Southern Ocean means that light availability shows a strong oscillation between limited daylight in winter and extended daylight hours in summer. The seasonal advance and retreat of sea ice also exerts an important control on upper ocean dynamics, influencing both light and nutrient availability. When sea ice melts, the release of low-salinity water stratifies the water column, and iron is also released (Person et al., 2021). This creates favorable conditions for phytoplankton growth and ice-edge blooms are often observed (Westwood et al., 2010; Williams et al., 2010). Seasonal summer warming serves to stratify the upper water column and stabilizes the mixed layer while in winter, the mixed layer again deepens (Sallée et al., 2010). In ice-free regions, decreasing temperatures and enhanced winds convect the water column and deepen the mixed layer; in the seasonal ice zone, brine rejection enhances convection and deepens the mixed layer (Williams et al., 2010). A clear signature in polar waters is the remnant winter mixed layer, or Winter Water, evident as a cold temperature minimum layer beneath the summer mixed layer above (e.g. van Wijk et al., 2010).

To understand how physical conditions may control biological dynamics, there have been several multi-disciplinary survey efforts to observe the structure and function of marine ecosystem components in the SKP region. Namely, the voyages are BROKE in 1996 (e.g. Nicol et al., 2000a; Wright and van den Enden, 2000); BROKE-West in 2006 (e.g. Williams et al., 2010; Meijers et al., 2010); KAXIS in 2016 (e.g. Schallenberg et al., 2018; Bestley et al., 2020); and TEMPO in 2021 (e.g. Cox et al., 2022; Heidemann et al., 2024). The SKP region is also sampled by international GO-SHIP efforts along repeat hydrography section I08S (https://www.go-ship.org/). This study collates data from eight occupations near or along 80°E – through the TEMPO, BROKE, BROKE-West, and GO-SHIP efforts – spanning from 1994 to 2021 to allow for a more comprehensive study of upper ocean dynamics and physical-biological linkages in this significant region. Newly recorded TEMPO data, from the 2021 survey, are placed into broader temporal context to investigate patterns within and between years. The main aims of the study are to 1) examine the upper water column structure across the eight voyages; 2) describe the variability of upper-ocean properties over time; and 3) examine relationships between key physical properties and their influence on nutrient availability and production.

2 Data

2.1 Oceanographic data

The project focuses on the area around 80°E, between 58°S and 68° S (Figure 1; Table 1). The study area includes the southern part of the Kerguelen plateau, the Princess Elizabeth Trough (PET), and south to the East Antarctic shelf break. The oceanographic data presented here were collected across eight different voyages, from as early as 1994 to the most recent TEMPO data in 2021. All data prior to 2021 can be

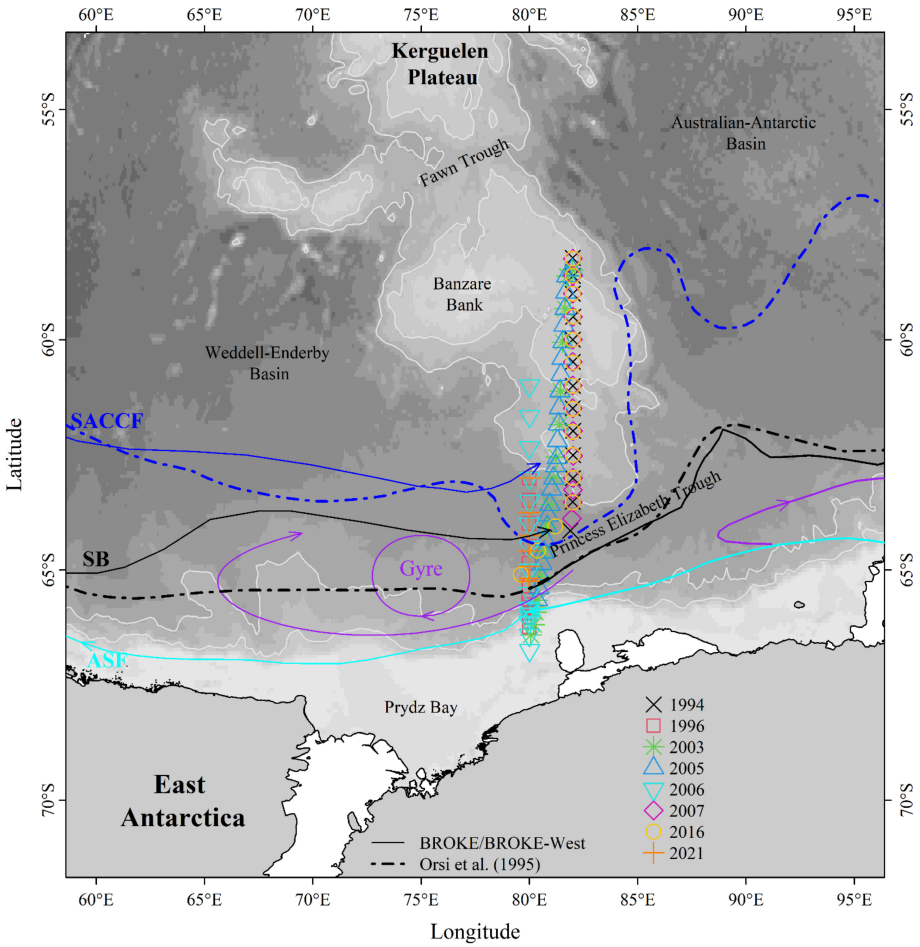


FIGURE 1
Map of study area. The eight oceanographic voyages are shown with different colored/shaped symbols (see legend). The major fronts in the study region include: the Southern Antarctic Circumpolar Current Front (SACCF), the Southern Boundary (SB), and the Antarctic Slope Front (ASF). All fronts are shown by lines [solid line – BROKE (Bindoff et al., 2000) and BROKE-West (Meijers et al., 2010; Williams et al., 2010); dash line – Orsi et al. (1995)]. The background shows bathymetry from GEBCO.

obtained from CCHDO (https://cchdo.ucsd.edu/); TEMPO data is available through the MNF portal (https://www.marine.csiro.au/data/trawler/survey_details.cfm?survey=IN2021_V01). We use a total of 121 CTD profiles across the eight surveys in this study.

In the northern part of the study region, north of about 64°S, repeat oceanographic transects along I08S are at 82°E (1994, 2003, 2005, 2007, 2016) and these transects traverse the submarine SKP before dog-legging west to 80°E (Figure 1). Other multidisciplinary marine surveys along 80°E include BROKE (1996), BROKE-West (2006) and TEMPO (2021). The southern extent of each occupation is generally determined by sea-ice extent or by the continental shelf break. Hence, the 1994 and 2007 cruises provided data mainly over the SKP to the north of around 64°S, while the surveys extended much further south in other years (to nearly 67°S; Figure 1).

All hydrographic data are from the austral summer, i.e. December to March. By coincidence, the year that each voyage was conducted roughly corresponds to the time throughout the summer season that the sampling occurred. That is, the 1994 voyage was conducted in early December, the 1996 voyage in January, the 2003-2016 voyages in February, and the 2021 voyage in March. The one exception is 2005, conducted at the end of January to early February (Table 1).

Ship-based CTD data provide temperature (°C), salinity (PSS-78), concentration of dissolved oxygen (DO; μmol kg^{-1}), and pressure (dbar) throughout the water column. Fluorescence measurements were not taken on every voyage and have therefore been excluded from this study. The data were examined over the upper 1000 m. Using the Gibbs Seawater toolbox (McDougall and Barker, 2011), we calculate the conservative temperature (CT, °C), absolute salinity (SA, g kg^{-1}), neutral density (γ^n, kg m^{-3}), potential density referenced to the surface (σ_0, kg m^{-3}), and the buoyancy frequency (N^2, s^{-2}). Potential density and buoyancy frequency are both used to calculate the mixed layer depth (as described in Section 3.2).

Each of the 121 CTD profiles had corresponding macronutrient data from discrete bottle samples. Within the upper 300 m these comprise a total of 900 nitrate and 929 silicate measurements (μM; Table 1), respectively. These data were combined with the CTD sensor data to estimate nutrient drawdown (μM) and primary production (mg Carbon m^{-2} d^{-1}; as described in Section 3.3).

TABLE 1 Voyage summary information for each oceanographic cruise and stations/samples included in this study.

Date	Voyage	Hydrographic Cruise ID	Ship	Latitudinal Range (°S)	Number of Stations	Bottles per station [min, max]		Total samples	
						Si	N	Si	N
3/2021*	TEMPO*	IN2021_V01	*Investigator*	63.00 – 65.25	7	[8,10]	[8,10]	63	63
2/2016	I08S 2016	33RR20160208	*Roger Revelle*	58.24 – 65.10	15	[7,13]	[7,13]	141	141
2/2007	I08S 2007	33RR20070204	*Roger Revelle*	58.24 – 63.88	14	[6,9]	[6,9]	107	107
2/2006*	BROKE-West*	09AR20060102	*Aurora Australis*	60.00 – 66.75	16	[9,12]	[9,12]	178	177
1-2/2005	I09S 2004	09AR20041223	*Aurora Australis*	58.48 – 65.65	25	[4,10]	[4,10]	158	158
2-3/2003	I08S 2003	09AR20030103	*Aurora Australis*	58.49 – 66.41	16	[4,9]	[0,9]	97	70
1-2/1996*	BROKE*	09AR9604_1	*Aurora Australis*	63.00 – 66.24	15	[4,9]	[4,9]	82	81
12/1994	I08S 1994	316N145_5	*KNORR*	58.22 – 64.15	13	[6,10]	[6,10]	103	103
Total					121			929	900

Date of stations, voyage name, CCHDO ID, and ship name are listed. The number of stations, number of bottles per station for nitrate and silicate, and the total number of bottle samples in the upper 300 m are also detailed. The dates marked with an asterisk (*) denote data collected off the Kerguelen Plateau at 63°S.

2.2 Ancillary environmental information

The National Snow and Ice Data Centre SMMR-SSM/I polar product, which is available for the Southern Hemisphere gridded at 25 km resolution, provided the daily passive microwave estimates of percentage of sea-ice concentration (Cavalieri et al., 1996; Maslanik and Stroeve, 1999). These data were used to calculate the ice-free days, defined as the time since the concentration of ice fell below 15%. Bathymetry data comes from the General Bathymetric Chart of the Oceans GEBCO_2014 Grid, version 20150318 (Weatherall et al., 2015; https://www.gebco.net/).

3 Methods

3.1 Definitions for water masses and major fronts

In this paper, we follow Bestley et al. (2020) (their Tables 1 and 2, and references therein) for the definitions of water masses and major fronts. The surface layer of the upper ocean is Antarctic Surface Water (AASW), defined where the neutral density is less than 28 kg m^{-3} and the temperature below 2°C. Within this water mass, Winter Water (WW) is the remnant deep winter mixed layer, defined subsurface where the temperature is less than 0.5°C beneath the overlying seasonal mixed layer (ML); the ML is determined according to the density method outlined in section 3.2.

Below AASW lies the warmer and more saline Circumpolar Deep Water (CDW). In this region, the area of lowest oxygen (e.g. DO< 200 µmol kg^{-1}) identifies Upper Circumpolar Deep Water (UCDW), and the signature of maximum salinity (e.g. SA > 34.7 g kg^{-1}) identifies Lower Circumpolar Current Deep Water (LCDW). As UCDW rises southwards and its properties are modified through mixing, the cooled and freshened form is called Modified Circumpolar Deep Water (mCDW).

Following Orsi et al. (1995), in this region we use the subsurface 1.5°C and 1.8°C isotherms to define the locations of the Southern Boundary (SB) and the Southern ACC Front (SACCF), respectively. The SB marks the location where CDW has cooled enough to be recognized as mCDW, i.e. south of SB the subsurface maximum temperature is less than 1.5°C.

Along the Antarctic shelf break, there is a strong sub-surface horizontal density gradient associated with the Antarctic Slope Front (ASF), which is often coincident with the vertical plunge of the 0°C isotherm (Ainley and Jacobs, 1981). Here, we define the ASF to be the location where the 0.5°C isotherm at the bottom of the temperature minimum layer reaches 200 m depth. This is similar to the northern extent of the ASF in the greater Prdyz Bay region used by Foppert et al. (2024).

3.2 Mixed layer depth calculation

To investigate the vertical structure of the upper ocean two methods were used to calculate mixed layer depth. The first defines it to be the depth at which the potential density difference ($\Delta\sigma_0$) is 0.03 kg m^{-3} from the near-surface (10 dbar), following the global approach of de Boyer Montégut et al. (2004). The second method defines the 'ecologically relevant' mixed layer depth using the maximum buoyancy frequency (N^2) following Carvalho et al. (2017). Figure 2 shows an example of the results based on both methods.

3.3 Nutrient drawdown and seasonal production

To understand the connection between physical properties and biological production, the drawdown of nitrate and silicate in the upper ocean was calculated from the bottle data, and the seasonal

TABLE 2 Summary of the upper-ocean features observed in the eight voyages, 1994 – 2021.

Year	SACCF Latitude (°S)	SB Latitude (°S)	ASF Latitude (°S)	MLD ($\Delta\sigma$) (m)	MLD (N^2) (m)	Winter Water thickness (m)
2021*	*64.93*	*64.95*	*65.05*	39.0 ± 12.4	47.4 ± 8.2	47.6 ± 10.7
2016	*63.6*	*63.9*	64.8	48.1 ± 11.6	53.7 ± 11.5	57.7 ± 48.8
2007	–	–	–	48.1 ± 12.4	59.0 ± 10.8	47.3 ± 15.4
2006*	63.3	64.3	65.0	42.4 ± 9.9	59.9 ± 3.4	92.0 ± 36.8
2005	64.4	64.8	65.3	33.9 ± 13.1	60.0 ± 22.3	94.0 ± 31.6
2003	*64.7*	*64.9*	65.2	49.2 ± 10.0	54.2 ± 10.0	66.3 ± 29.7
1996*	*64.5*	*64.6*	*64.7*	43.5 ± 11.5	67.5 ± 37.4	73.5 ± 16.1
1994	–	–	–	43.0 ± 10.9	67.0 ± 30.3	58.8 ± 17.0

See Methods for frontal definitions. Asterisks represent voyages with the data collected off the Kerguelen Plateau at 63°S. Fronts that were found between the same station-pair are in italics. Note that the mean mixed layer depths and WW thicknesses are for stations north of the ASF and error bars represent standard deviation.

production associated with them were quantified following Westwood et al. (2010). For drawdown, we first calculated the average concentration of nitrate and silicate within the (density-based) mixed layer and then subtracted this from the average concentration in the WW below (i.e. $[N]_{WW} - [N]_{ML}$ is the nitrate drawdown in units of μM). This represents the amount of nutrients that the phytoplankton had used since the previous winter. For this calculation we included only stations north of the Antarctic Slope Front, where WW is clearly observed, and those that have high quality nutrient data in both the mixed layer and WW. As outlined above, WW averages included all bottles located beneath the density-based mixed layer, where the CTD trace indicated temperature was ≤ 0.5°C, i.e., bottles above the base of the temperature-minimum (or WW) layer. This difference between the 0.5°C isotherm depth (WW base) and the mixed layer depth is considered the thickness of the WW layer.

Nutrient drawdown was converted to carbon drawdown using the ratios of Redfield (1958) and Copin-Montegut and Copin-

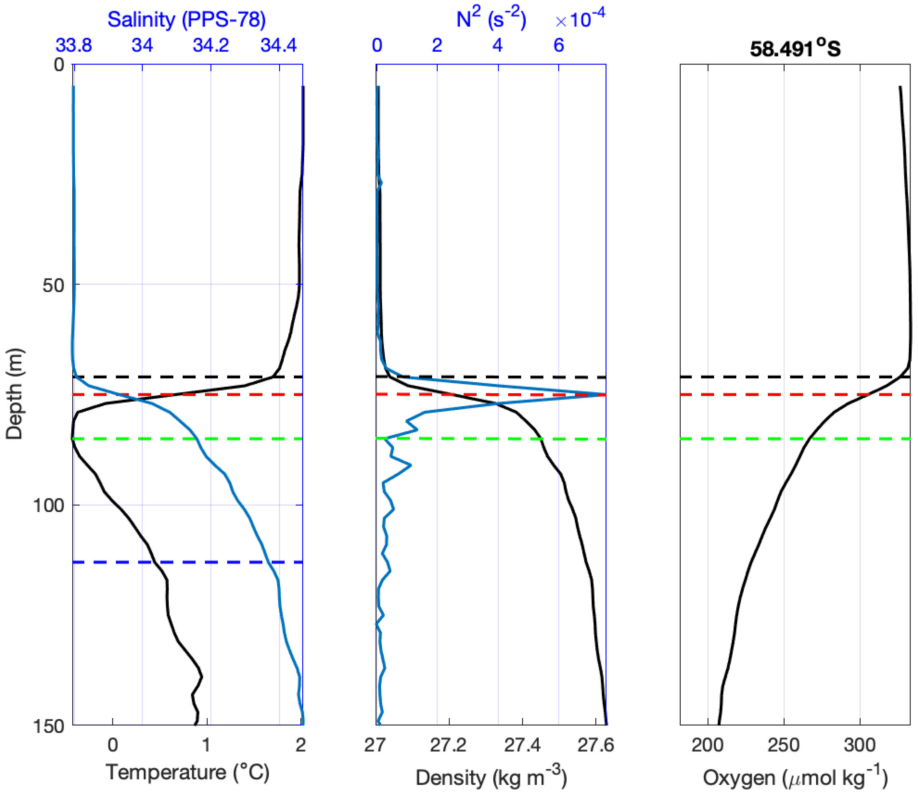


FIGURE 2
Example profiles of upper-ocean structure. Left: Temperature and salinity; Middle: potential density and buoyancy frequency (N^2); Right: dissolved oxygen. The dashed lines indicate mixed layer depth as determined by the density-based criterion (black) and the N^2 maximum (red). Below, the depth of temperature minimum (green) and the base of the Winter Water layer (blue; left panel) are shown.

Montegut (1978). That is, C:N = 6.6. and C:Si = 2.5, respectively. Seasonal production rates (mg C m^{-2} d^{-1}) were calculated by determining the number of growth days for phytoplankton over the season. Growth days were estimated through deriving the time since sea-ice melt from satellite data, at the time and location that stations were sampled (Westwood et al., 2010). Thus, seasonal production of carbon by nitrate, for example, is given by:

$$\text{Production}_N = [6.6 \times ([N]_{WW} - [N]_{ML})(MLD)/(T_{growth})] \times 12.01$$

where T_{growth} is the number of days since sea ice melt, 6.6 is the Redfield ratio, and 12.01 g mol^{-1} is the molecular weight of carbon. Recall $[N]_{WW} - [N]_{ML}$ is the nitrate drawdown in µM (or mmol m^{-3}) and MLD is the mixed layer depth based on the density criterion.

3.4 Relationships between physical and biological parameters

To explore relationships between upper water column structure, physical drivers, and biological processes we fitted a series of linear regression models using the freely available R statistical software version 4.3.2 (R Core Team, 2023). We fitted separate models to investigate each of the following response variables: a) winter water thickness, b) winter water nitrate, c) mixed-layer nitrate, d) nitrate-based drawdown and e) nitrate-based production. We firstly inspected the correlation between predictor variables and used variance inflation factors (VIFs) as a guide for selecting candidate variable combinations for any given model, aiming for VIFs of approximately 3 or below (Zuur et al., 2010). Candidate predictor variables considered are summarized in Electronic Supplementary Material Table S1. To identify the best set of predictor variables we used automatic model selection methods (Burnham and Anderson, 2002) ranking models based on AICc, as implemented via the *dredge()* function in the library (MuMIn) (Barton, 2023). The results shown are the predictor terms retained in the highest-ranked models based on AICc; in the case where the ΔAICc was< 2 the simplest (most parsimonious) model was selected. This aspect of the data analysis again excluded observations south of the ASF (n=29), as well as those stations immediately north of the ASF/south of the SB where the 'WW' was anomalously thick (≥130m) due to the ASF influence (n=6). Data from two cold core eddies, located at 63.6°S in 2005 and 64°S in 2006, were similarly excluded.

4 Results

The ocean characteristics and water column structure observed over the eight voyages, 1994-2021, are shown in Figures 3 and 4, with the latter focusing on the upper 1000 m. Occupying the deepest of these layers, LCDW is evident as a high salinity (SA > 34.7 g/kg) tongue underlying UCDW above. The core of the UCDW is characterized by high temperature (CT > 1.8°C) and low oxygen (< 180 µmol/kg) signatures, typically below 150 m and above 500 m in this region. The near surface is occupied by AASW, which during these summertime voyages is characterized by a warmed seasonal mixed layer overlying a cold WW layer (temperature minimum layer with CT< 0.5°C) that is a remnant of the deep winter mixed layer.

As the UCDW rises southward its properties are cooled and freshened. In this region, the southernmost extent of subsurface temperature maxima of 1.8°C and 1.5°C are used to demarcate the location of the SACCF and the Southern Boundary, respectively (yellow and green vertical lines, respectively, in Figures 4 and 5). Over the period that voyages were conducted, the SACCF was observed at latitudes from 63.3°S-64.93°S and the SB ranged between 63.9°S-64.95°S (Table 2). The SACCF and SB were identified between the same station pair in four of the six voyages that sampled the fronts (Table 2, italicized values), but were found more than 100 km apart in 2006. Thus, the SB and the SACCF were generally co-located in most years, with the exception of 2005 and 2006.

The ASF is evident as a strong meridional temperature gradient towards the southern end of some transects, characterized by the 0.5°C isotherm at 200 m. It was unable to be identified in all years, as voyages over the SKP (in 2007 and 1994) either terminated or turned eastward north of this feature. For voyages where the ASF was sampled it was located near 65°S, with a range of 64.7-65.3°S.

Figure 5 shows transects of temperature, salinity, and oxygen in the upper 300 m, allowing visibility of changes in the mixed layer and Winter Water layer. For stations north of the ASF, the average mixed layer depth based on density ranges from 33.9-49.2 m, while the average mixed layer depth based on maximum buoyancy frequency (N^2) is generally deeper, ranging from 47.4-67.5 m (Table 2). When including stations south of the ASF, the mean mixed layers are consistently shallower by up to 10 and 20 m for the density-based and N^2 maximum-based MLD definitions, respectively (not shown). Below the mixed layer, the WW layer (temperature below 0.5°C) ranges from 47.3-94.0 m in thickness at stations north of the ASF. Note that we present information in Table 2 for stations north of the ASF only, because those are the relevant stations for nutrient drawdown and seasonal production calculations.

At individual stations, the density-based MLDs vary between roughly 10 m and 70 m, while those calculated from buoyancy frequency vary between 10 m and 130 m (Figure 6). The latter are typically deeper by 10-20 m (Table 2), but can be up to almost 100 m deeper. There is a broad pattern of MLD deepening from the south to the north. In all years, there is considerable station-to-station variability using both methods. Time within season has no clear influence on MLD and there is no clear difference between years (Figures 6B, E). However, there is a relationship between MLD and the amount of ice-free time (i.e. number of days since sea-ice melt; Figures 6C, F). Mixed layers are generally deeper in regions where the ocean has been ice-free longer and, thus, exposed to local wind-driven mixing for longer. Overall, the variability appears dominated by latitude and time since sea-ice melt, which are largely correlated, as sea ice tends to melt from north to south.

Due to differences in cruise tracks (Figure 1), oceanographic observations are available across all voyages only at 63°S and 64°S. Figure 7 co-plots the major diagnostic features of the upper ocean structure at these two latitudes. Figure 7A shows that the mixed layer

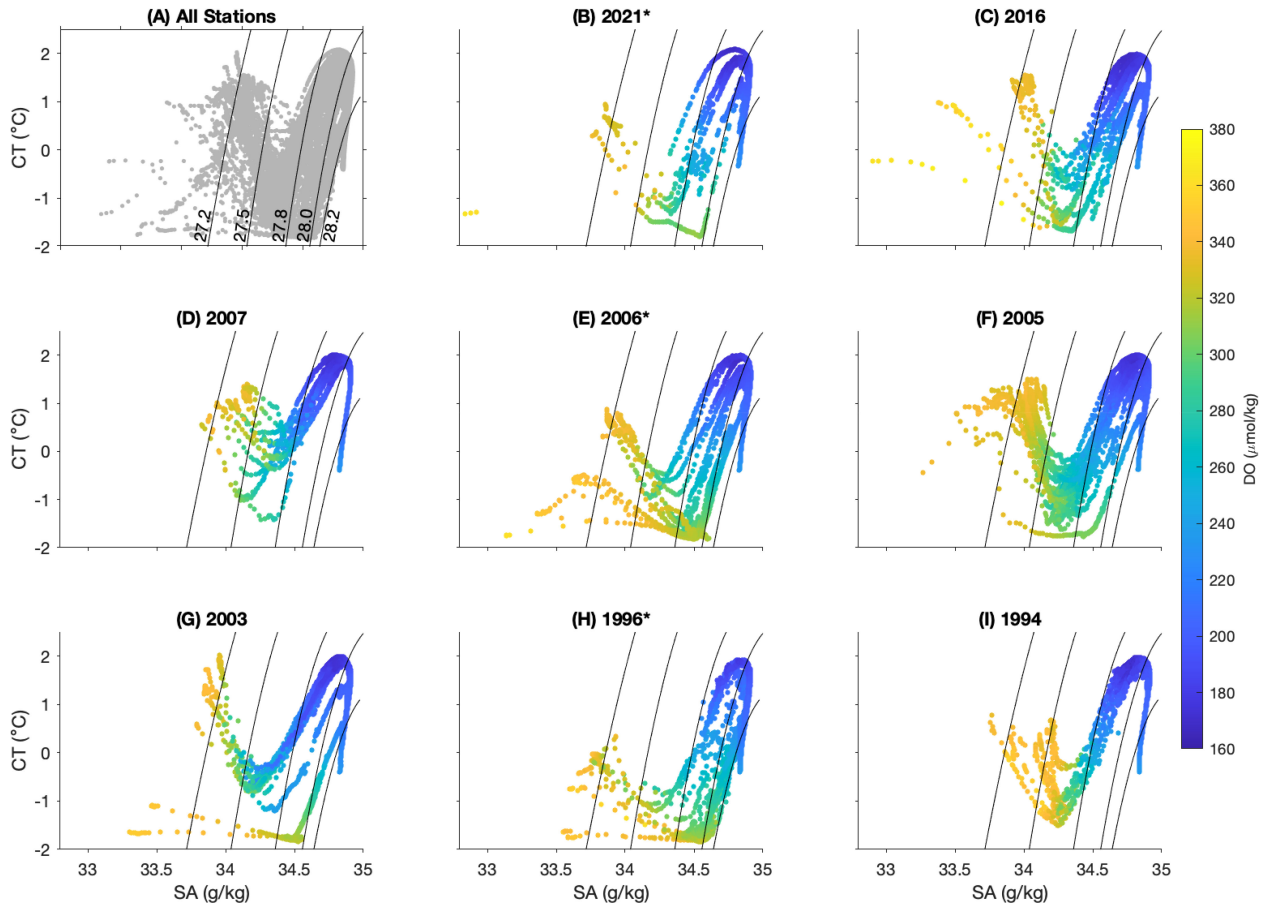


FIGURE 3
Conservative temperature and absolute salinity diagram. **(A)** T-S diagrams from all casts from the eight occupations. **(B–I)** T-S diagrams from the individual occupation, with year of occupation in the title.Colours represent the concentration of dissolved oxygen (DO, μmol kg^{-1}). Solid lines are neutral density contours with values of gn = 27.2, 27.5, 27.8, 28.0, and 28.2 kg m^{-3}, as labelled in **(A)**. The voyages marked with an asterisk (*) are those where data was collected off the Kerguelen Plateau at 63°S.

appears to be warming at 63°S, however this is likely due to the timing of the sampling in each year rather than a long-term trend. Recall, in 1994 the sampling occurred in December while in 2021 the sampling occurred in March (Table 1). This apparent warming pattern is not seen at 64°S (Figure 7A). There is no clear pattern in the depth of the mixed layer between years at either location (Figure 7B). In the WW, cooler temperature minima are generally found deeper in the water column (Figures 7C, D). Figures 7E, F shows that when the oxygen minimum layer lies deeper, oxygen concentrations are generally higher. Figure 7E shows that the oxygen minimum values at 63°S are very stable but slightly higher at stations off the plateau (1996, 2006 and 2021). Here, the oxygen minimum is also deeper (Figure 7F). In general, deep-water properties (O_{2min} and S_{max}) are much more stable at 63°S than 64°S.

Nitrate concentrations in the upper 300 m range from about 20-40 μM, and silicate concentrations reach values near 100 μM (Figure 8). Concentrations of both nutrients generally increase with depth and are distinctly lower in the mixed layer compared to the WW below. Stations south of ~65°S, i.e. south of the ASF, have lower concentrations of nutrients at depth compared to stations on the northern side of the ASF.

Nutrient drawdown values reach nearly 12 μM for nitrate and 60 μM for silicate at individual stations (Figure 9; Table 3). There is a seasonal influence on drawdown for both nutrients (Figures 9B, E), with more ice-free days associated with higher nutrient drawdown. Voyage average production estimates range from 123.4-375.2 mg C m^{-2} d^{-1} for nitrate and 240.0-560.5 mg C m^{-2} d^{-1} for silicate (Table 3). Daily production values are normalized by days since sea ice melt and are therefore similar across the growing season (Figures 9H, K) and latitudes (Figure 9G, J). There is an indication that mixed layer depth may positively influence production (Figures 9I, L).

There is a clear linear relationship between silicate drawdown and nitrate drawdown, with silicate drawdown 4.6 times higher than that of nitrate (Figures 10A; Table 3). Seasonal production is also linearly related, with production calculated from silicate almost twice as high than that of nitrate-based production (Figure 10B).

The results from the fitted regression models reveal relationships between upper water column structure, physical drivers, and biological processes (Figure 11). Thicker Winter water layers (Figure 11A) are associated with shallower mixed layers (coef. est = -0.90 ± 0.16, t-value=-5.715, p-value<0.001) and colder Tmin values (coef. est = -14.14 ± 3.88, t-value=-3.643,

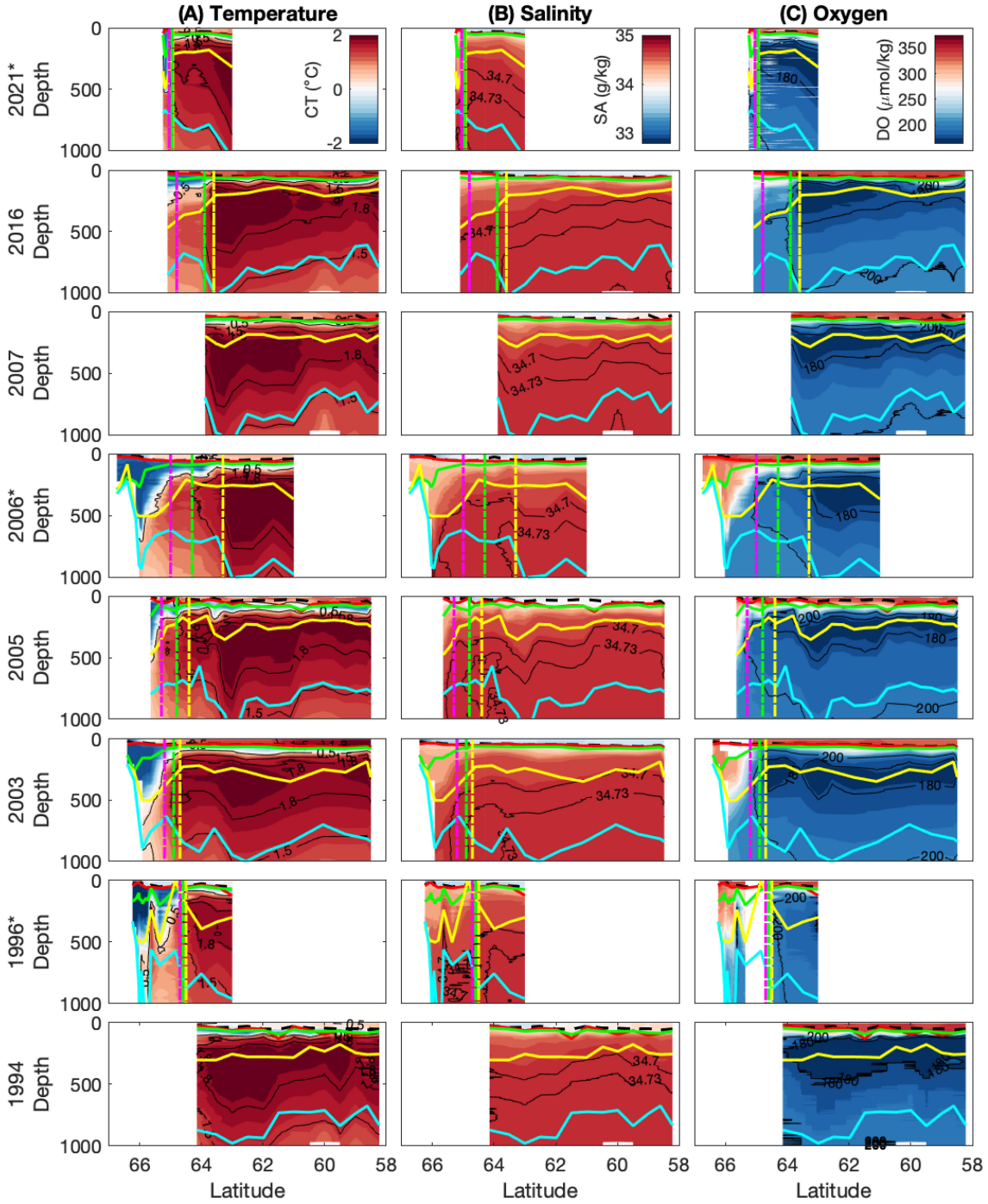


FIGURE 4
Transects of **(A)** temperature, **(B)** salinity and **(C)** oxygen in the upper 1000 m across eight voyages 1994 – 2021. Coloured lines represent the density-based MLD (black), the depth of maximum buoyancy frequency (N^2, red), temperature minimum (green), oxygen maximum (yellow), and salinity maximum (blue). Dashed vertical lines represent the fronts from south to north: ASF (magneta) SB (green) and SACCF (yellow). The voyages marked with an asterisk (*) are those where data was collected off the Kerguelen Plateau at 63°S.

p-value<0.001), while WW layers are thinner where UCDW (diagnostic signature is O2 minima) is shallower (coef. est = 0.08 ± 0.03, t-value=2.226, p-value=0.029). WW nitrate concentration is higher where the WW layer is thinner (coef. est = -0.03 ± 0.01, t-value=-2.96, p-value=0.004; Figure 11B), while mixed layer nitrate concentrations are higher within colder mixed layers (coef. est = -1.81 ± 0.41, t-value=-4.383, p-value<0.001) and where the WW core (i.e. the depth of the temperature minimum) is deeper (coef. est = 0.09 ± 0.02, t-value=5.461, p-value<0.001; Figure 11C). Nitrate drawdown is higher in association with longer time since sea-ice melt (coef. est = 0.04 ± 0.01, t-value=3.855, p-value<0.001) and shows a positive association with thinner WW layers (coef. est = -0.03 ± 0.01, t-value=-2.28, p-value=0.026; Figure 11D). Finally, higher nitrate-based production is associated

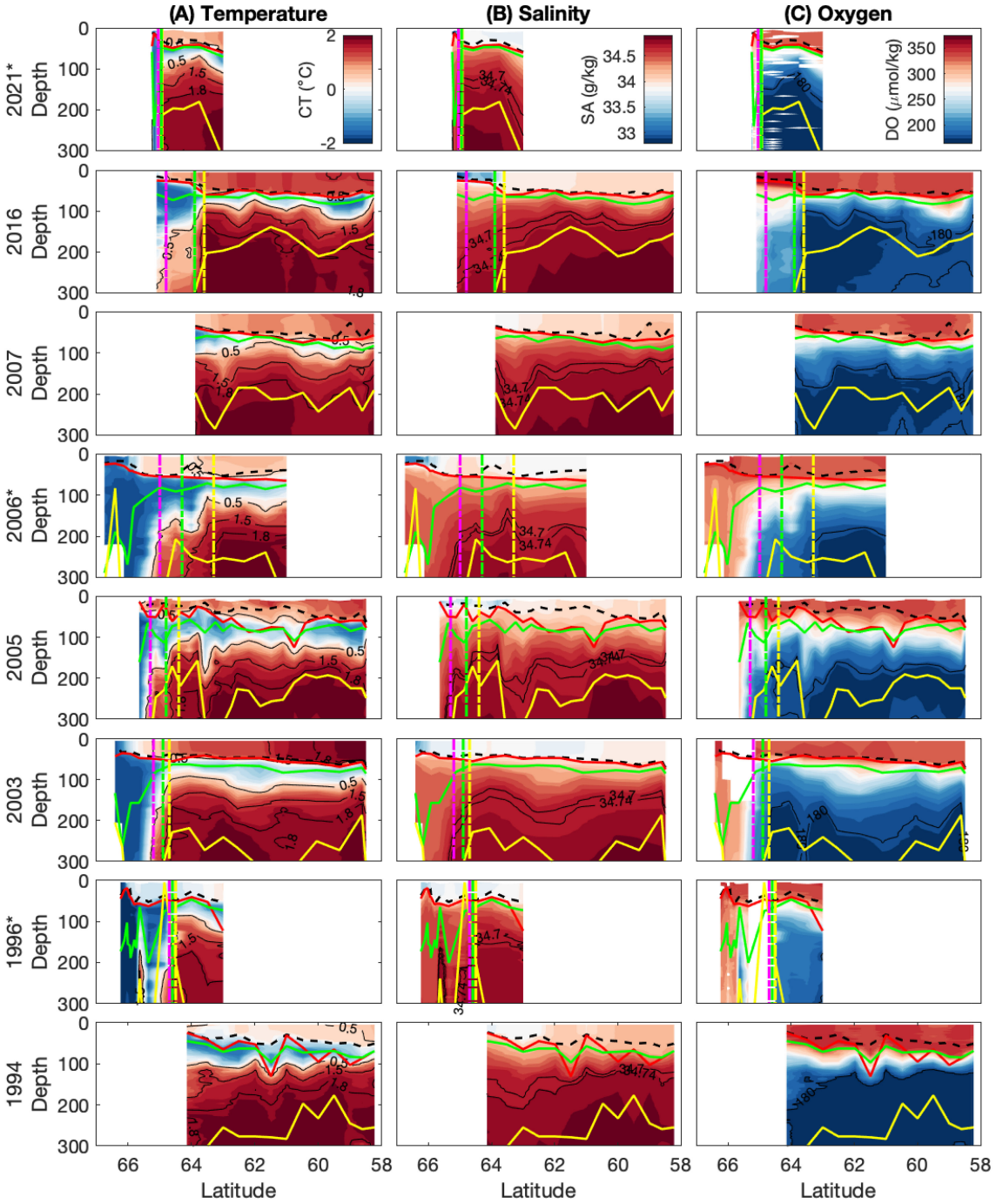


FIGURE 5
Transects of **(A)** temperature, **(B)** salinity and **(C)** oxygen in the upper 300 m across eight voyages, 1994 – 2021. Representation as for Figure 4.

with deeper mixed layers (coef. est = 3.68 ± 1.15, t-value=3.196, p-value=0.002; Figure 11E).

5 Discussion

The study investigated available hydrographic data (temperature, salinity, and oxygen concentration) in conjunction with spatiotemporal patterns in nutrient availability, drawdown and primary production, to examine the relationship between upper ocean vertical structure and ecosystem productivity in the region near 80°E. The upper ocean properties were largely consistent across the eight voyages 1994 – 2021, facilitating our ability to define water masses and fronts and compare them across years using uniform criteria. The spatial and temporal patterns in the biophysical properties enabled us to explore the physical processes that set the structure and nutrient supply within the seasonal mixed layer and the winter water below, and how these are utilized by phytoplankton throughout the season, thereby improving our

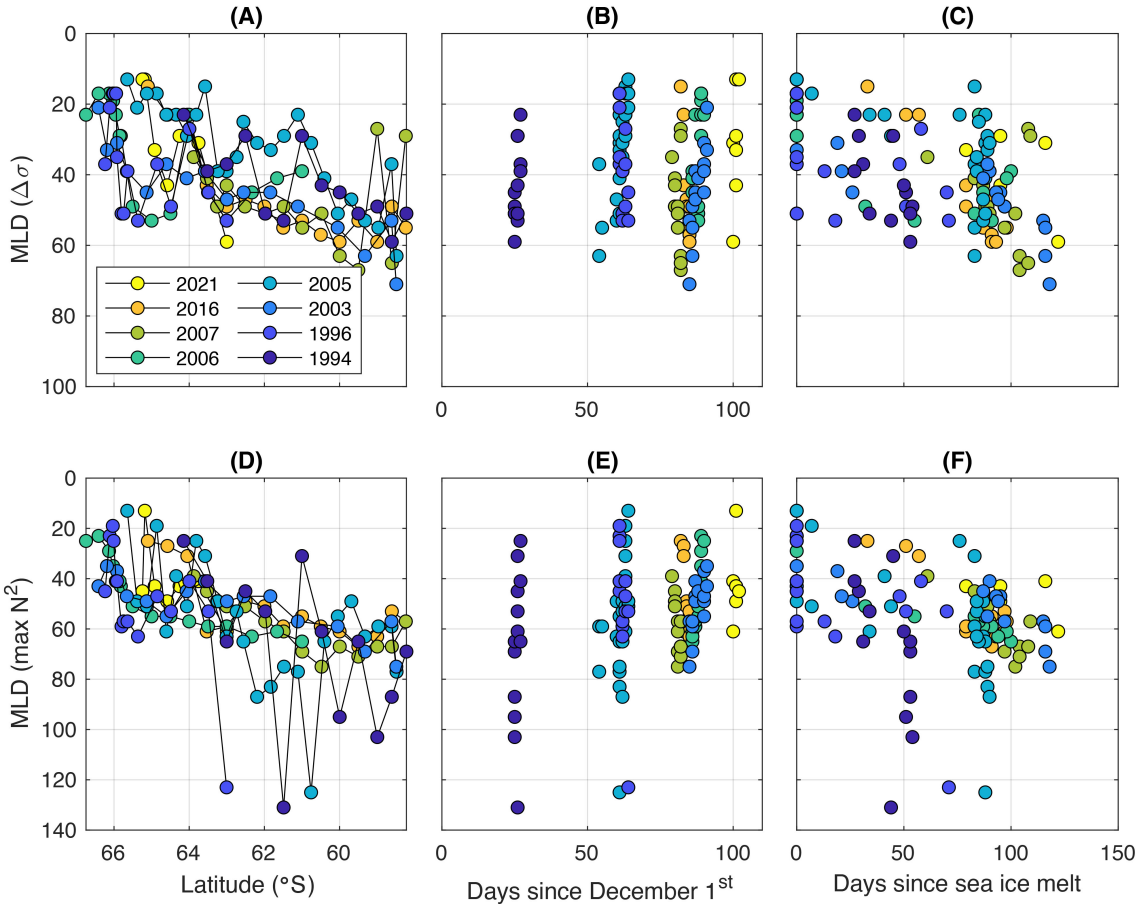


FIGURE 6
Mixed layer depth variation in space and time. The top row (panels **A–C**) shows density-based MLD variability as a function of (left) latitude, (middle) time within season, and (right) days since sea ice melt. The bottom row (panels **D–F**) shows the same for MLD defined as the N^2 maximum. Colour indicates voyage year.

understanding of the ecosystem function within the important southern Kerguelen plateau region.

In this region, the eastward flow of the ACC is constrained by the narrow PET, with the KP to the north and the Antarctic continental slope to the south. Hence, the two southernmost fronts of the ACC (Southern Boundary and SACCF) are often co-located in space, when defined by classical subsurface criteria (Table 2). However, the two fronts can be separated by up to a degree of latitude (~100 km) as observed in 2006. Across the different voyages, the frontal locations vary north-south across about 1-1.5 degrees of latitude, consistent with previous observations of meandering ACC fronts, which could be due to the recirculation of the Prydz Bay gyre and the increase in mesoscale eddy dynamics on approaching the PET (Bestley et al., 2020; Heywood et al., 1999).

Over the observation period 1994 to 2021, mixed layer depths calculated from either density or maximum buoyancy frequency, shallowed from north to south. This is likely a seasonal effect, being due to the earlier ice-free state in the northern part of the study domain, where seawater is exposed to wind mixing for a longer time. Stations at the northern end of the study region generally experienced about 100 days since sea ice melt while those on the southern end were only ice-free for about 30 days before sampling. As the mixed layer reflects the interaction between the ocean and the atmosphere, its depth is influenced by the wind in the atmosphere, with increased wind stress causing it to deepen (Carranza and Gille, 2015; Sallée et al., 2010). Williams et al. (2010) showed that there was a strong positive linear correlation between the mixed layer depth and ice-free days and wind stress in this area. The repeat observations at 63°S in our study showed that the mixed layer gradually increased in average temperature from early to late summer, accompanied by a general deepening overall (Figures 7A, B). The exceptions were in 1994 and 2007, with anomalous values likely due to local storms or mesoscale dynamics.

The mixed layer became much shallower south of 65°S in the vicinity of the ASF (the cold, V-shaped feature evident in Figure 5). South of the ASF the near surface often remains under the influence of sea ice, particularly associated with the West Ice shelf nearby. Westwood et al. (2010) noted that the mixed layer depth in the sea-ice region is shallower than in the open sea, which is consistent with our results near 80°E. Additionally, both the density-based and buoyancy-based mixed layer depths fluctuated greatly during 1994, possibly because these voyage data were mainly collected in early summer (December) before the seasonal mixed layer had a chance to form (Figure 1; Table 1).

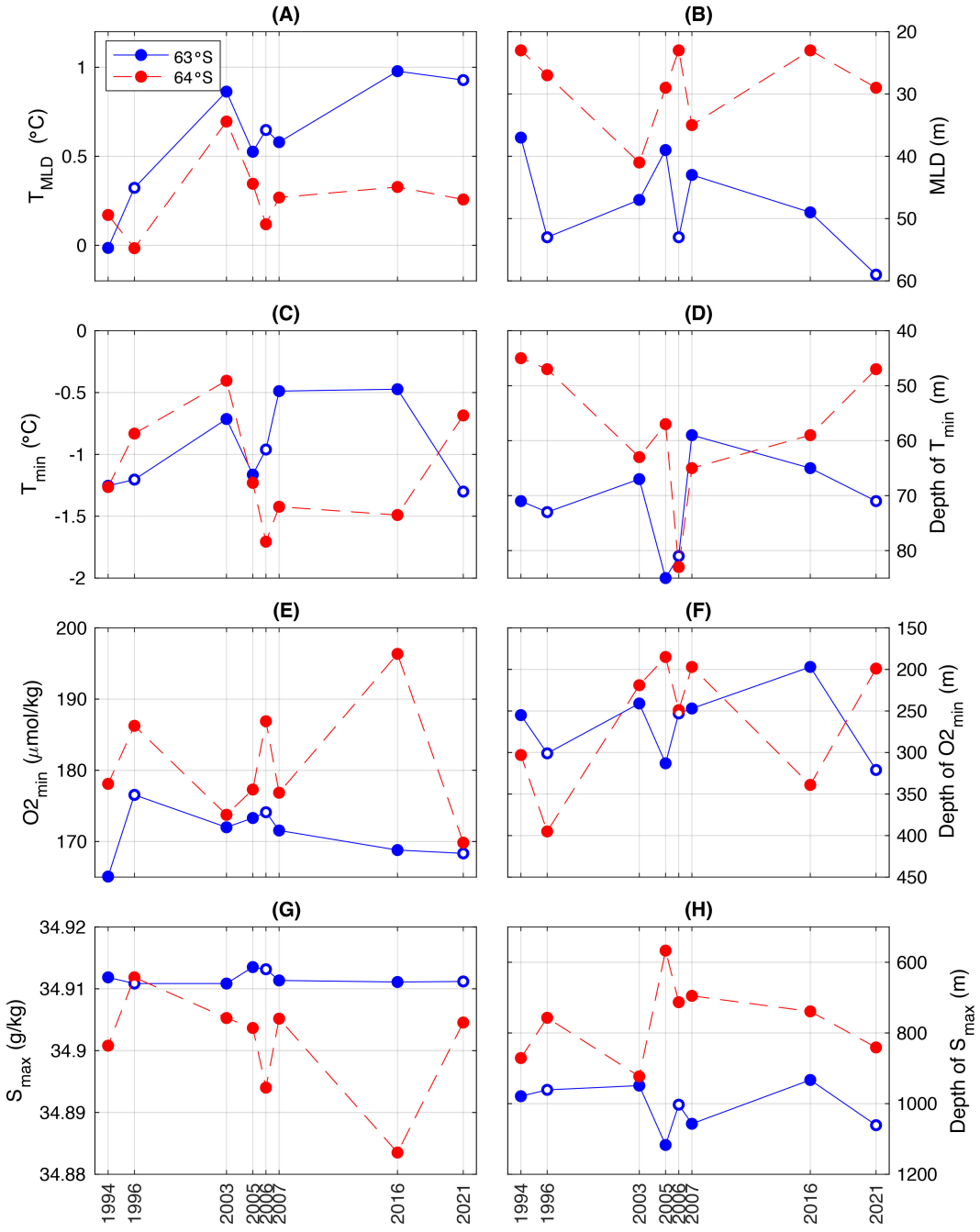


FIGURE 7
Upper-ocean water-mass characteristics at 63°S (blue) and 64°S (red) across eight voyages 1994 – 2021. **(A)** Mean MLD temperature; **(B)** MLD, calculated using the density-based criterion; **(C)** Minimum temperature; **(D)** Depth of temperature minimum; **(E)** Minimum oxygen concentration; **(F)** Depth of oxygen minimum; **(G)** Maximum salinity; **(H)** Depth of salinity maximum. Open circles in the blue line indicate the voyages that sampled west of the Southern Kerguelen Plateau (i.e. off-plateau) at 63°S. Note that the y-axes in the right column are inverse, such that depth is increasing downwards.

The oceanographic data showed relatively consistent spatial patterns in nutrient concentrations within the region (Figure 8). Nutrient concentrations are clearly lower in the surface layer relative to the deep. This is because the main source of macronutrients in the Southern Ocean is circumpolar deep water, which replenishes nutrients from below (Callahan, 1972). Also, nutrient drawdown by phytoplankton mainly occurs within the mixed layer where light availability for photosynthesis is high. As depth increases, the amount of light obtained by phytoplankton decreases, leading to less productivity and drawdown (Westwood et al., 2010).

Nutrient drawdown of both nitrate and silicate was generally related to time since sea-ice melt across the voyages (Figures 9B, E), with values increasing with time. This is because the total amount of nutrients used by phytoplankton accumulates gradually over the season. Stations sampled later in the season therefore had more time for nutrient uptake, and *vice versa*. Nitrate concentrations are lower

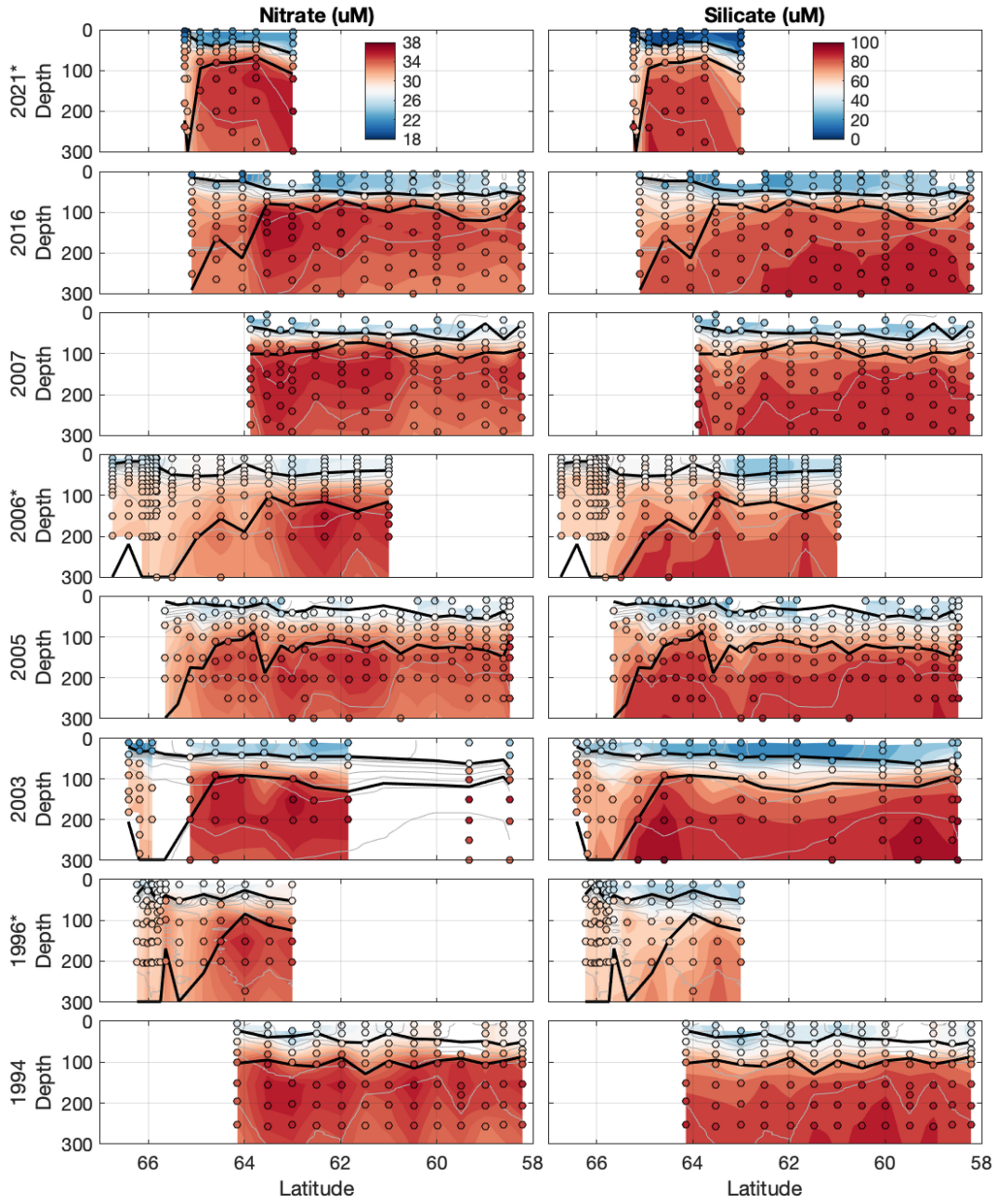


FIGURE 8
Transects of nutrients in the upper 300 m: nitrate (left) and silicate (right). Colored dots indicate nutrient concentrations from bottle samples. Background shading shows the nutrient data linearly interpolated onto an even pressure grid. Solid black lines, from shallower to deeper, represent the MLD and the bottom of the WW layer. The thin grey lines represent potential density contours at 0.1 kg m^{-3} intervals.

with warmer temperatures in the mixed layer (Figure 11C) and drawdown of nitrate is higher with more days since sea ice melt (Figure 11D), further supporting a seasonal effect with the mixed layer warming throughout the season. The exception to the general seasonal pattern was in 2016 when drawdown was higher than expected early in the season (~50 days since melt, Figure 9B). This may have been related to replenishment of nutrients, e.g. from upwelling of CDW or lateral advection (Westwood et al., 2010). The similar pattern of nitrate and silicate drawdown across voyages suggests that diatoms were the main phytoplankton group contributing to production – given that other taxa do not require silicate. The dominance of diatoms in Southern Ocean waters has been clearly shown in other studies from East Antarctica (e.g. Wright et al., 2010, average of 61% of total chlorophyll *a* in a primary bloom, 43% in a secondary bloom, 38.7% south of the SB outside bloom regions, 49% between the SB and sACCF, 60.6% north of the sACCF; Takao et al., 2014, 55-87% of total chlorophyll south of 55°S; Heidemann et al., 2024, 56% of total chlorophyll *a* south of 62°S).

Production was also related to days since melt but had the opposite pattern to drawdown, with highest values (up to 2000 mg C m^{-2} d^{-1})

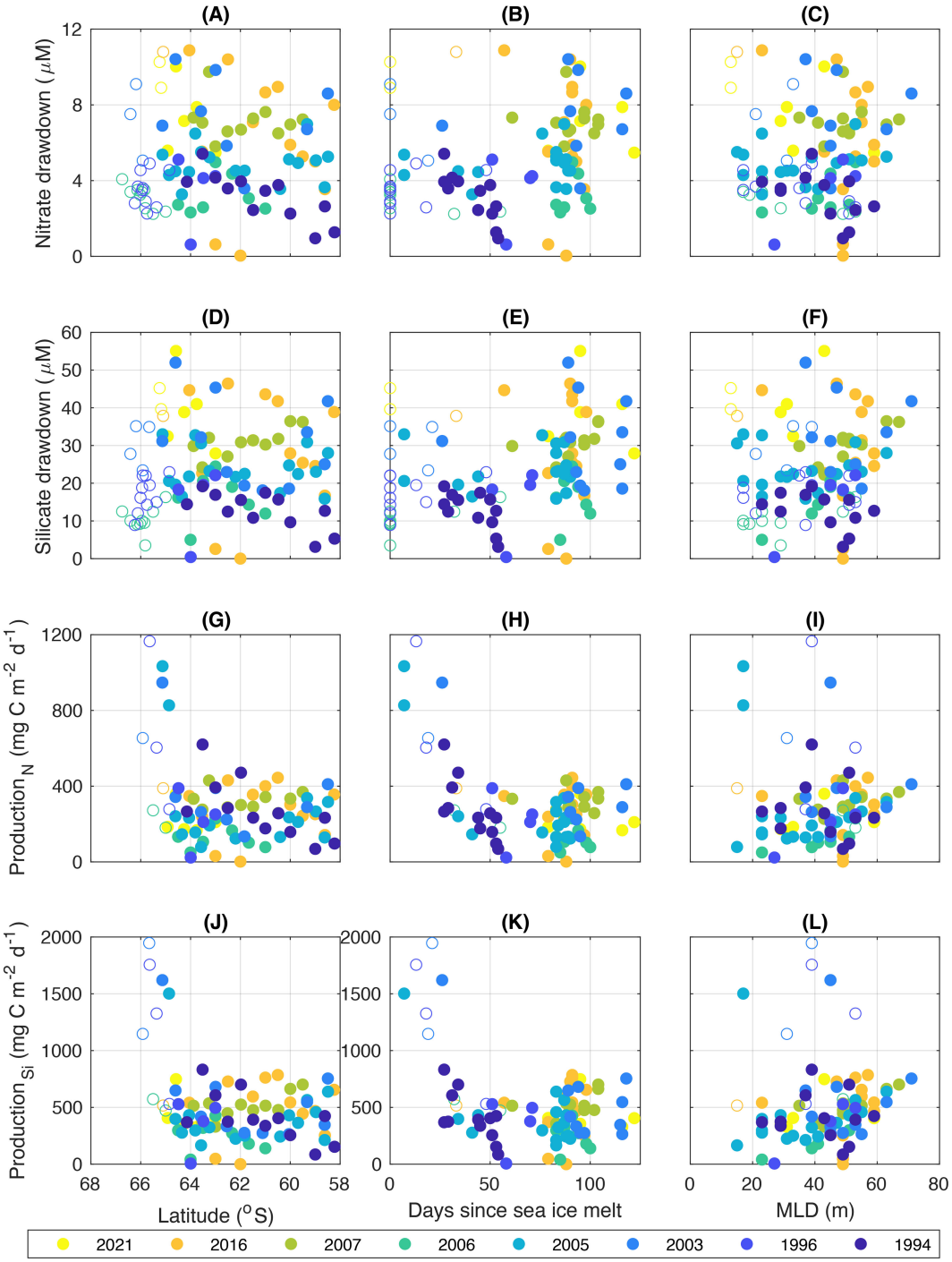


FIGURE 9
Nutrient drawdown and production. From top to bottom, the drawdown of nitrate (panels **A–C**) and silicate (panels **D–F**), and the corresponding production estimates based on nitrate and silicate drawdown (panels **G–I** and panels **J–L**, respectively). The drawdown and production values are shown as a function of (left) latitude, (middle) days since sea-ice melt, and (right) density-based MLD. Open symbols represent the stations located south of ASF.

occurring earliest in the season, within the first 40 days of melt (Figures 9H, K). Most high values are for stations south of the ASF, with latitude therefore also affecting production (Figures 9G, J). These stations south of the ASF, and with short days since melt, are likely reflective of the spring bloom that can occur at the retreating ice edge. This is associated with high iron input from ice melt (Lannuzel et al., 2016), combined with shallow mixed layer depths within the fresh meltwater lens creating a stable, high light environment. It should be noted that drawdown and production values are partly questionable south of the ASF in that there is no true Tmin to gain accurate WW nutrient concentrations. However, our data agrees with previous studies that clearly show highest production close to the Antarctic

TABLE 3 Nutrient drawdown and primary production estimates based on silicate and nitrate bottle data collected across eight voyages, 1994 – 2021.

Year	Nutrient Drawdown (μM)		Production (mg C m^{-2} d^{-1})	
	Nitrate	Silicate	Carbon (N)	Carbon (Si)
2021*	7.9 ± 2.0	40.0 ± 8.8	218.9 ± 80.5	449.2 ± 170.6
2016	6.5 ± 3.5	28.9 ± 14.9	272.7 ± 142.1	476.6 ± 252.9
2007	7.2 ± 1.0	30.2 ± 4.4	313.8 ± 56.2	504.1 ± 110.3
2006*	3.2 ± 0.8	12.8 ± 5.5	123.4 ± 59.7	240.0 ± 128.7
2005	4.9 ± 1.0	23.8 ± 5.5	281.8 ± 256.8	540.5 ± 569.4
2003	7.4 ± 2.1	30.8 ± 10.1	375.2 ± 247.8	560.5 ± 393.9
1996*	3.5 ± 1.2	16.6 ± 6.2	218.4 ± 151.1	352.0 ± 239.8
1994	3.2 ± 1.3	12.8 ± 4.9	271.5 ± 157.6	411.4 ± 214.3
Average	**5.5 ± 2.0**	**24.5 ± 9.8**	**259.5 ± 74.7**	**441.8 ± 106.0**

Values are the voyage average over the study area at stations north of the ASF and uncertainty is represented by the standard deviation. The long-term average values are presented at the bottom (in bold). The voyages marked with an asterisk (*) indicate the data are collected off the Kerguelen Plateau at 63°S.

coast compared to offshore waters, thought to be due to increased iron supply (Westwood et al., 2010; Wright et al., 2010).

North of the ASF production does not obviously vary with ice-free days. It may have been expected that production rates would decrease by late summer because phytoplankton cells may have been becoming senescent with time. However, this was not observed. Rather, production north of the ASF was positively influenced by increased mixed layer depth (Figure 11E). Accordingly, there was less nitrate in the mixed layer when the mixed layers were warmer (Figure 11C), both consistent with increased drawdown occurring in waters that experienced a longer time since sea-ice melt (Figure 11D). The positive influence of mixed layer depth on production may be unexpected given that increased mixed layer depths potentially mean less light availability for phytoplankton growth. However, in this area mixed layers typically ranged from 10-60 m across voyages and under low biomass euphotic depths can be as deep as 80-100 m, as demonstrated by Westwood et al. (2010) and Heidemann et al. (2024). This suggests that even within the deepest mixed layer depths observed there was still sufficient light for phytoplankton growth.

The positive influence of deeper mixed layers on production was likely associated with increased nutrient availability, allowing

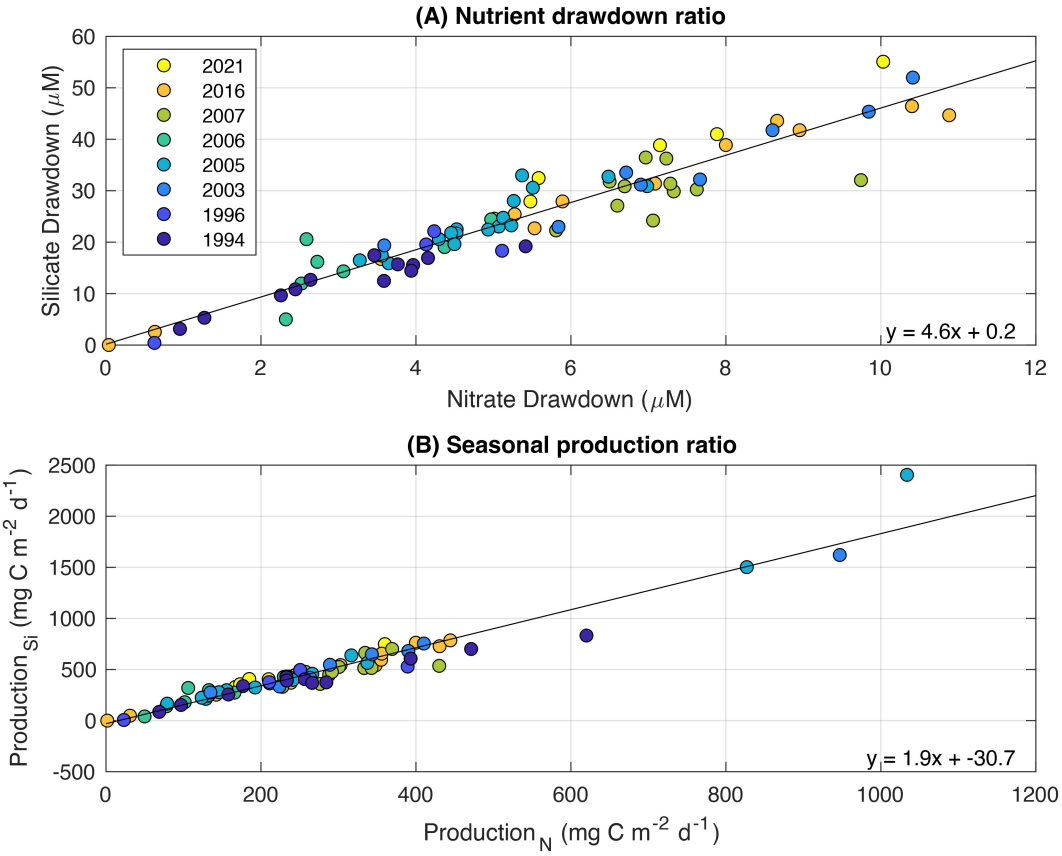


FIGURE 10
The relationship between nitrate and silicate **(A)** drawdown and **(B)** seasonal production from observations across eight voyages, 1994 – 2021. Note that only data from stations north of the ASF are shown. The solid lines represent linear regression, with equations shown in the lower right-hand corner of each panel.

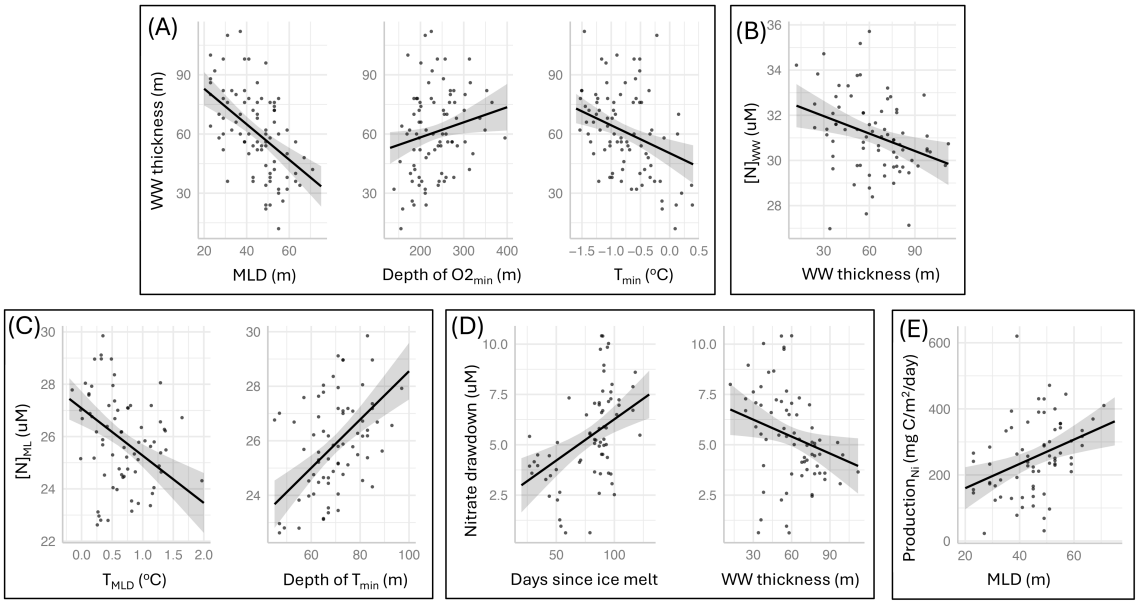


FIGURE 11
Results from fitted linear models exploring relationships between upper water column structure, physical drivers, and biological processes. Shown are the predictor terms retained in the highest ranked models for **(A)** Winter water thickness (m) (R^2_{adj} = 0.43), **(B)** winter water nitrate concentrations (μM) (R^2_{adj} = 0.09), **(C)** mixed layer nitrate concentrations (μM) (R^2_{adj} = 0.32), **(D)** the drawdown of nitrate (R^2_{adj} = 0.28), and **(E)** the production estimate based on nitrate drawdown (mg C m^{-2} d^{-1}) (R^2_{adj} = 0.12). All retained terms are considered significant (p-value< 0.05); model coefficient estimates are reported in Results text.

sustained phytoplankton growth throughout the season. Evidence to support increased nutrient availability comes from consideration of additional physical processes within the water column. Firstly, it was found that the availability of nitrate in WW was related to the thickness of this layer: decreased WW thickness means increased nitrate. Therefore, we consider any physical processes that enhance a decrease in WW thickness allows the potential for increased nutrient supply to surface waters. Shallower depths of UCDW (as indicated by the oxygen minimum) were related to decreased WW thickness. Therefore, it is likely that nitrate was increased due to upwelling from nutrient rich CDW. A thinner (and warmer) WW layer is caused not only by shallower CDW below but is also associated with deeper mixed layers overlying (Figure 11A, see also Figure 8). With a thinner WW layer, the mixed layer is therefore in closer proximity to CDW, as well as to increased nutrient availability within the WW layer. This may enable a reliable and sustained source of additional nutrients. For phytoplankton populations offshore there is high reliance on upwelled nutrient sources to replenish surface waters given a lack of input from continental sources.

The production values obtained in our study were within a similar range to other regions in East Antarctica. North of the ASF, voyage averages for nitrate-based production ranged from 127-309 mg C m^{-2} d^{-1} and silicate-based production from 243-533 mg C m^{-2} d^{-1} (Table 3). The average across all voyages and locations was 260 ± 75 and 442 ± 106 mg C m^{-2} d^{-1} for nitrate- and silicate-based production, respectively. In comparison, the BROKE-West region nitrate-based production averaged 410.3 ± 323.7 mg C m^{-2} d^{-1} and silicate-based production 302.5 ± 273.7 mg C m^{-2} d^{-1} (Westwood et al., 2010). For the BROKE region nitrate-based production was 50-750 mg C m^{-2} d^{-1} (Nicol et al., 2000a; Strutton et al., 2000). Our study also had similar production rates to the Weddell Sea (128 - 977 mg C m^{-2} d^{-1}), Ross Sea (124 - 638 mg C m^{-2} d^{-1}), and the Scotia Sea (30 - 250 mg C m^{-2} d^{-1}) in the open ocean (El-Sayed and Weber, 1982; Park et al., 1999; Saggiomo et al., 2002).

The ratio of silicate drawdown to nitrate drawdown was 4.6, and the ratio of silicate-based production to nitrate-based production was 1.9, with the carbon production based on silicate consumption being significantly higher than that based on nitrate. According to Richards (1958), we would expect phytoplankton to uptake silicate at about the same amount as nitrogen (ratio 1:1). The difference in our study could be due to recycling of nitrogen by bacteria in surface waters (Brzezinski et al., 2003; Mosseri et al., 2008). This forms ammonia and regenerated production may have occurred, whereby the diatoms use ammonia as a source of nitrogen rather than nitrate. As the diatoms are consuming silicate whilst using either nitrate or ammonia as a nitrogen source, this results in a silicate:nitrate uptake greater than 1. A second reason could be iron limitation. Under the condition of iron deficiency, the uptake of silicate has been shown to be greater than that of nitrate (Hutchins and Bruland, 1998; Takeda, 1998). Westwood et al. (2010) showed higher Si:N ratios offshore compared to coastal Antarctic waters where iron supply was likely greater.

A sustained seasonal phytoplankton bloom over and east of the SKP has been linked to subsurface iron supply, likely advected northwards offshore from the Antarctic shelf (Schallenberg et al., 2018). This regional productivity supports foraging grounds for higher order predators, including those migrating from Kerguelen

Island (Patterson et al., 2016; Bestley et al., 2016) and farther north. For example, tracking data for migratory Western Australian humpback whales (Bestley et al., 2019) showed occupancy of the dynamic western boundary current (~59°S, 83°E) earlier in the season (Nov-Dec) and southward movement thereafter including into this area near 80° E. Two recent voyages, in 2016 (KAXIS) and 2021 (TEMPO), directly observed large numbers of whales aggregating and feeding on krill at this "biological hotspot" near 63°S, 80° E; i.e. within the deep waters immediately west of the SKP. Todd and Williamson (2022) found that cetaceans sighted near the northern Kerguelen Plateau tended to occur in pelagic (depths > 600 m) rather than plateau waters. Thiele et al. (2000) proposed that cetacean distributions might be linked to areas where physical processes support extended surface water residence conditions for primary producers. Comparing repeat ocean observations available at 63°S and 64°S, we found the greatest differences to be evident in the deep-water properties (Figures 7G, H), these properties generally being more stable at 63°S. Because the major fronts (sACCf and SB) are farther to the south, the properties at 63°S are less influenced by the dynamic frontal meandering and exchange. It is possible that this quiescent area, nearby the dynamic fronts but with relatively weak geostrophic currents, may provide favorable conditions for retaining phytoplankton blooms (Park et al., 2008a, Park et al., 2008b) and krill swarms (Bestley et al., 2018). Todd and Williamson (2022) also found whales sightings to be associated with higher phytoplankton concentrations and higher dissolved oxygen. Whales are particularly dependent on predictable, productive conditions for their seasonal feeding in polar regions (Smetacek and Nicol, 2005; Tulloch et al., 2019).

This study used all available cruise data, which is of a certified standard quality but was intermittent over the 20-year period, providing an incomplete time series of the physical environment and biological exchange in the region. In the future, oceanographic data from animal tracking (https://imos.org.au/facility/animal-tracking) could be included in a more comprehensive analysis of the changes in seawater properties and associated biological activity in the region (e.g. Roquet et al., 2009). Increasing data streams from BGC-Argo floats (https://argo.ucsd.edu/expansion/biogeochemical-argo-mission/) can further document spatial and seasonal variations in physical-biogeochemical properties (fluorescence, backscatter, PAR) with high temporal and spatial resolution (Rembauville et al., 2017). Future work incorporating these new data sources could further examine the drivers of specific changes, for example, the interlinked roles of sea ice and the wind field to determine the importance of local and regional effects on mixed layer depth prior to sampling.

6 Conclusion

We provide a comprehensive study on the vertical structure of the upper ocean and associated primary production in the vicinity of 80°E East Antarctica, from a compilation of historical cruise data. The mixed layer depth varied with latitude, being deeper in the northern part of the study region where sea ice melt occurs earlier. Nutrient drawdown increased throughout the season, with more drawdown later in the summer. Silicate-based production was higher than nitrate-based production in this region, possibly due to efficient nitrate recycling and/or iron limitation. Deeper mixed layer depths had a positive influence on production north of the ASF, likely associated with the supply of nutrients from UCDW. Highest production was south of the ASF where nutrient availability is increased due to continental and ice inputs.

Data availability statement

All data are publicly available. Data prior to 2021 can be found on CCHDO (https://cchdo.ucsd.edu/), and the TEMPO data is available from the CSIRO's Marine National Facility data portal (https://www.marine.csiro.au/data/trawler/survey_details.cfm?survey=IN2021_V01).

Author contributions

ML: Formal analysis, Investigation, Visualization, Writing – original draft. AF: Conceptualization, Data curation, Formal analysis, Investigation, Methodology, Project administration, Supervision, Visualization, Writing – review & editing. KW: Conceptualization, Formal analysis, Investigation, Methodology, Project administration, Supervision, Writing – review & editing. SB: Conceptualization, Data curation, Formal analysis, Investigation, Methodology, Project administration, Supervision, Visualization, Writing – review & editing.

Funding

The author(s) declare financial support was received for the research, authorship, and/or publication of this article. This project was supported and funded by Australian Antarctic Science Project 4512 and 4636, and received grant funding from the Australian Government as part of the Antarctic Science Collaboration Initiative program. This project also received financial support from Pew Charitable Trust and Antarctic Science Foundation.

Acknowledgments

We acknowledge the use of the CSIRO Marine National Facility (https://ror.org/01mae9353) and grant of sea time on RV *Investigator* in undertaking part of this research. We thank the captains and crews for their efforts and support in the collection of these data. We also thank Michael Sumner and Ben Raymond from the Australian Antarctic Division for their assistance in providing estimates of days since sea ice melt for all stations.

Conflict of interest

The authors declare that the research was conducted in the absence of any commercial or financial relationships that could be construed as a potential conflict of interest.

Publisher's note

All claims expressed in this article are solely those of the authors and do not necessarily represent those of their affiliated organizations, or those of the publisher, the editors and the reviewers. Any product that may be evaluated in this article, or claim that may be made by its manufacturer, is not guaranteed or endorsed by the publisher.

Supplementary material

The Supplementary Material for this article can be found online at: https://www.frontiersin.org/articles/10.3389/fmars.2024.1451997/full#supplementary-material

References

Ainley, D. G., and Jacobs, S. S. (1981). Sea-bird affinities for ocean and ice boundaries in the Antarctic. *Deep Sea Res. Part A. Oceanographic Res. Papers* 28, 1173–1185. doi: 10.1016/0198-0149(81)90054-6

Arrigo, K. R., van Dijken, G. L., and Bushinsky, S. (2008). Primary production in the Southern Ocean 1997–2006. *J. Geophysical Research: Oceans* 113, C08004. doi: 10.1029/2007JC004551

Barton, K. (2023). "MuMIn: Multi-Model Inference," in *R package version 1.47.5*. Available at: https://CRAN.R-project.org/package=MuMIn.

Bestley, S., Andrews-Goff, V., van Wijk, E., Rintoul, S. R., Double, M. C., and How, J. (2019). New insights into prime Southern Ocean forage grounds for thriving Western Australian humpback whales. *Sci. Rep.* 9, 1–12. doi: 10.1038/s41598-019-50497-2

Bestley, S., Jonsen, I. D., Harcourt, R. G., Hindell, M. A., and Gales, N. J. (2016). Putting the behaviour into animal movement modelling: improved activity budgets from use of ancillary tag information. *Ecol. Evol.* 6, 8243–8255. doi: 10.1002/ece3.2016.6.issue-22

Bestley, S., Raymond, B., Gales, N., Harcourt, R., Hindell, M. A., Jonsen, I., et al. (2018). Predicting krill swarm characteristics important for marine predators foraging off East Antarctica. *Ecography* 41, 996–1012. doi: 10.1111/ecog.2018.v41.i6

Bestley, S., van Wijk, E., Rosenberg, M., Eriksen, R., Corney, S., Tattersall, K., et al. (2020). Ocean circulation and frontal structure near the southern Kerguelen Plateau: The physical context for the Kerguelen Axis ecosystem study. *Deep Sea Res. Part II: Topical Stud. Oceanography* 174. doi: 10.1016/j.dsr2.2018.07.013

Bindoff, N. L., Rosenberg, M. A., and Warner, M. J. (2000). On the circulation and water masses over the Antarctic continental slope and rise between 80 and 150 E. *Deep Sea Res. Part II: Topical Stud. Oceanography* 4, 2299–2326. doi: 10.1016/S0967-0645(00)00038-2

Boyd, P. W., Arrigo, K. R., Strzepek, R., and vanDijken, G. L. (2012). Mapping phytoplankton iron utilization: Insights into Southern Ocean supply mechanisms. *J. Geophysical Research: Oceans* 117, C06009. doi: 10.1029/2011JC007726

Brzezinski, M. A., Dickson, M.-L., Nelson, D. M., and Sambrotto, R. (2003). Ratios of Si, C and N uptake by microplankton in the Southern Ocean. *Deep Sea Res. Part II: Topical Stud. Oceanography* 50, 619–633. doi: 10.1016/S0967-0645(02)00587-8

Burnham, K. P., and Anderson, D. R. (2002). *Model selection and multimodel inference: a practical information-theoretic approach. 2nd ed* (New York: Springer-Verlag).

Callahan, J. E. (1972). "The structure and circulation of deep water in the Antarctic," in *Deep sea research and oceanographic abstracts*, 19, 563–575. doi: 10.1016/0011-7471(72)90040-X

Carranza, M. M., and Gille, S. T. (2015). Southern Ocean wind-driven entrainment enhances satellite chlorophyll-a through the summer. *J. Geophysical Research: Oceans* 120, 304–323. doi: 10.1002/2014JC010203

Carvalho, F., Kohut, J., Oliver, M. J., and Schofield, O. (2017). Defining the ecologically relevant mixedlayer depth for Antarctica's coastal seas. *Geophysical Res. Lett.* 44, 338–345. doi: 10.1002/2016GL071205

Cavalieri, D., Parkinson, C., Gloersen, P., and Zwally, H. (1996). Sea Ice Concentrations From Nimbus-7 SMMR and DMSP SSM/ISSMI Passive Microwave Data, January 1979 to August 2011. *Natl. Snow Ice Data Cent. Boulder Colo.,[Updated daily]*. doi: 10.5067/8GQ8LZQVL0VL

Copin-Montegut, C., and Copin-Montegut, G. (1978). The chemistry of particulate matter from the south Indian and Antarctic oceans. *Deep Sea Res.* 25, 911–931. doi: 10.1016/0146-6291(78)90633-1

Cox, M. J., Macaulay, G., Brasier, M. J., Burns, A., Johnson, O. J., King, R., et al. (2022). Two scales of distribution and biomass of Antarctic krill (Euphausia superba) in the eastern sector of the CCAMLR Division 58.4. 2 (55° E to 80° E). *PloS One* 17, e0271078. doi: 10.1371/journal.pone.0271078

de Boyer Montégut, C., Madec, G., Fischer, A. S., Lazar, A., and Iudicone, D. (2004). Mixed layer depth over the global ocean: An examination of profile data and a profile-based climatology. *J. Geophysical Research: Oceans* 109, C12. doi: 10.1029/2004JC002378

El-Sayed, S., and Weber, L. (1982). Spatial and temporal variations in phytoplankton biomass and primary productivity in the Southwest Atlantic and the Scotia Sea. *Polar Biol.* 1, 83–90. doi: 10.1007/BF00263804

Foppert, A., Bestley, S., Shadwick, E. H., Klocker, A., Vives, C. R., Liniger, G., et al. (2024). Observed water-mass characteristics and circulation off Prydz Bay, East Antarctica. *Front. Mar. Sci.* doi: 10.3389/fmars.2024.1456207

Foppert, A., Donohue, K. A., Watts, D. R., and Tracey, K. L. (2017). Eddy heat flux across the Antarctic Circumpolar Current estimated from sea surface height standard deviation. *J. Geophysical Research: Oceans* 122, 6947–6964. doi: 10.1002/2017JC012837

Gao, Y., Yu, S., Sherrell, R. M., Fan, S., Bu, K., and Anderson, J. R. (2020). Particle-size distributions and solubility of aerosol iron over the Antarctic peninsula during austral summer. *J. Geophysical Research: Atmospheres* 125, e2019JD032082. doi: 10.1029/2019JD032082

Heidemann, A., Westwood, K. J., Foppert, A., Klocker, A., Vives, C. R., Wotherspoon, S., et al. (2024). Drivers of phytoplankton distribution, abundance and community composition off East Antarctica, from 55-80°E (CCAMLR Division 58.4.2 East). *Front. Mar. Sci.* doi: 10.3389/fmars.2024.1454421

Henley, S. F., Cavan, E. L., Fawcett, S. E., Kerr, R., Monteiro, T., Sherrell, R. M., et al. (2020). Changing biogeochemistry of the Southern Ocean and its ecosystem implications. *Front. Mar. Sci.*, 581. doi: 10.3389/fmars.2020.00581

Heywood, K. J., Sparrow, M. D., Brown, J., and Dickson, R. R. (1999). Frontal structure and Antarctic bottom water flow through the Princess Elizabeth Trough, Antarctica. *Deep Sea Res. Part I: Oceanographic Res. Papers* 46, 1181–1200. doi: 10.1016/S0967-0637(98)00108-3

Hutchins, D. A., and Bruland, K. W. (1998). Iron-limited diatom growth and Si: N uptake ratios in a coastal upwelling regime. *Nature* 393, 561–564. doi: 10.1038/31203

Lannuzel, D., Vancoppenolle, M., van den Merwe, P., de Jong, J., Meiners, K. M., Grotti, M., et al. (2016). Iron and sea ice: Review and new insights. *Elementa* 4. doi: 10.12952/journal.elementa.000130

Laufkötter, C., Stern, A. A., John, J. G., Stock, C. A., and Dunne, J. P. (2018). Glacial iron sources stimulate the southern ocean carbon cycle. *Geophysical Res. Lett.* 45, 377–313,385. doi: 10.1029/2018GL079797

Lu, Z., Liu, D., Liao, J., Wang, J., Li, H., and Zhang, J. (2020). Characterizing spatial distribution of chlorophyll a in the Southern Ocean on a circumpolar cruise in summer. *Sci. Total Environ.* 708, 134833. doi: 10.1016/j.scitotenv.2019.134833

Maslanik, J., and Stroeve, J. (1999). "Near-real-time DMSP SSMIS daily polar gridded sea ice concentrations, version 1," in *NASA national snow and ice data center distributed active archive center*.

McDougall, T. J., and Barker, P. M. (2011). *Getting started with TEOS-10 and the Gibbs Seawater (GSW) Oceanographic Toolbox. Scor/Iapso WG*. SCOR/IAPSO WG127, 28pp.

Meijers, A., Klocker, A., Bindoff, N., Williams, G., and Marsland, S. (2010). The circulation and water masses of the Antarctic shelf and continental slope between 30 and 80E. *Deep Sea Res. Part II: Topical Stud. Oceanography*, 723–737. doi: 10.1016/j.dsr2.2009.04.019

Mosseri, J., Queguiner, B., Armand, L., and Cornet-Barthaux, V. (2008). Impact of iron on silicon utilization by diatoms in the Southern Ocean: A case study of Si/N cycle decoupling in a naturally iron-enriched area. *Deep Sea Res. Part II: Topical Stud. Oceanography* 55, 801–819. doi: 10.1016/j.dsr2.2007.12.003

Nelson, D. M., and Smith, W. Jr. (1991). Sverdrup revisited: Critical depths, maximum chlorophyll levels, and the control of Southern Ocean productivity by the

irradiance-mixing regime. *Limnology Oceanography* 36, 1650–1661. doi: 10.4319/lo.1991.36.8.1650

Nicol, S., Pauly, T., Bindoff, N., and Strutton, P. (2000a). BROKE" a biological/oceanographic survey off the coast of East Antarctica (80–150° E) carried out in January–March 1996. *Deep Sea Res. Part II: Topical Stud. Oceanography* 12-13, 09670645. doi: 10.1016/S0967-0645(00)00026-6

Nicol, S., Pauly, T., Bindoff, N. L., Wright, S., Thiele, D., Hosie, G. W., et al. (2000b). Ocean circulation off east Antarctica affects ecosystem structure and sea-ice extent. *Nature* 406, 504–507. doi: 10.1038/35020053

Nicol, S., and Raymond, B. (2012). Pelagic ecosystems in the waters off East Antarctica (30°E–150°E). *Antarctic ecosystems: an extreme environment in a changing world*. A. D. Rogers, N. M. Johnston, E. J. Murphy and A. Clarke Eds. Ch. 8 (Blackwell Publishing Ltd.), 243–254. doi: 10.1002/9781444347241.ch8

Orsi, A. H., Whitworth, T.III, and Nowlin, W. D.Jr. (1995). On the meridional extent and fronts of the Antarctic Circumpolar Current. *Deep Sea Res. Part I: Oceanographic Res. Papers* 42, 641–673. doi: 10.1016/0967-0637(95)00021-W

Park, Y.-H., Fuda, J.-L., Durand, I., and Naveira Garabato, A. C. (2008a). Internal tides and vertical mixing over the Kerguelen Plateau. *Deep Sea Res. Part II: Topical Stud. Oceanography* 55, 582–593. doi: 10.1016/j.dsr2.2007.12.027

Park, Y.-H., Roquet, F., Durand, I., and Fuda, J.-L. (2008b). Large-scale circulation over and around the Northern Kerguelen Plateau. *Deep Sea Res. Part II: Topical Stud. Oceanography* 55, 566–581. doi: 10.1016/j.dsr2.2007.12.030

Park, M. G., Yang, S. R., Kang, S.-H., Chung, K. H., and Shim, J. H. (1999). Phytoplankton biomass and primary production in the marginal ice zone of the northwestern Weddell Sea during austral summer. *Polar Biol.* 1, 251–261. doi: 10.1007/s003000050360

Patterson, T. A., Sharples, R. J., Raymond, B., Welsford, D. C., Andrews-Goff, V., Lea, M.-A., et al. (2016). Foraging distribution overlap and marine reserve usage amongst sub-Antarctic predators inferred from a multi-species satellite tagging experiment. *Ecol. Indicators vol. 70* pp, 531–544. doi: 10.1016/j.ecolind.2016.05.049

Person, R., Vancoppenolle, M., Aumont, O., and Malsang, M. (2021). Continental and sea ice iron sources fertilize the Southern Ocean in synergy. *Geophysical Res. Lett.* 48, e2021GL094761. doi: 10.1029/2021GL094761

Pinkerton, M. H., Boyd, P. W., Deppeler, S., Hayward, A., Höfer, J., and Moreau, S. (2021). Evidence for the impact of climate change on primary producers in the southern ocean. *Front. Ecol. Evol.* 9. doi: 10.3389/fevo.2021.592027

R Core Team (2023). "R: A Language and Environment for Statistical Computing," in *R Foundation for Statistical Computing*(Vienna, Austria). Available at: https://www.R-project.org/.

Raymond, B., Lea, M.-A., Patterson, T., Andrews-Goff, V., Sharples, R., Charrassin, J.-B., et al. (2015). Important marine habitat off east Antarctica revealed by two decades of multi-species predator tracking. *Ecography* 38, 121–129. doi: 10.1111/ecog.01021

Redfield, A. C. (1958). The biological control of chemical factors in the environment. *Am. scientist* 46, 230A–2221.

Rembauville, M., Briggs, N., Ardyna, M., Uitz, J., Catala, P., Penkerc'h, C., et al. (2017). Plankton assemblage estimated with BGC-Argo floats in the Southern Ocean: Implications for seasonal successions and particle export. *J. Geophysical Research: Oceans* 122, 8278–8292. doi: 10.1002/2017JC013067

Richards, F. (1958). "Dissolved silicate and related properties of some western north-Atlantic and Caribbean waters." *J. Mar. Res.* 17(1).

Rintoul, S. R. (2018). The global influence of localized dynamics in the Southern Ocean. *Nature* 558, 209–218. doi: 10.1038/s41586-018-0182-3

Roquet, F., Park, Y. H., Guinet, C., Bailleul, F., and Charrassin, J. B. (2009). Observations of the Fawn Trough Current over the Kerguelen Plateau from instrumented elephant seals. *J. Mar. Syst.* 78, 377–393. doi: 10.1016/j.jmarsys.2008.11.017

Saggiomo, V., Catalano, G., Mangoni, O., Budillon, G., and Carrada, G. C. (2002). Primary production processes in ice-free waters of the Ross Sea (Antarctica) during the austral summer 1996. *Deep Sea Res. Part II: Topical Stud. Oceanography* 49, 1787–1801. doi: 10.1016/S0967-0645(02)00012-7

Sallée, J.-B., Speer, K., and Rintoul, S. (2010). Zonally asymmetric response of the Southern Ocean mixed layer depth to the Southern Annular Mode. *Nat. Geosci.* 3, 273–279. doi: 10.1038/ngeo812

Schallenberg, C., Bestley, S., Klocker, A., Trull, T. W., Davies, D. M., Gault-Ringold, M., et al. (2018). Sustained upwelling of subsurface iron supplies seasonally persistent phytoplankton blooms around the southern Kerguelen plateau, Southern Ocean. *J. Geophysical Research: Oceans* 123, 5986–6003. doi: 10.1029/2018JC013932

Smetacek, V., and Nicol, S. (2005). Polar ocean ecosystems in a changing world. *Nature* 437, 362–368. doi: 10.1038/nature04161

Sparrow, M. D., Heywood, K. J., and Brown, J. (1996). Current structure of the south Indian Ocean. *J. Geophysical Research: Oceans* 101, 6377–6391. doi: 10.1029/95JC03750

Strutton, P. G., Griffiths, F. B., Waters, R. L., Wright, S. W., and Bindoff, N. L. (2000). Primary productivity off the coast of East Antarctica (80-150°E): January to March 1996. *Deep-Sea Res. II* 47, 2327–2362. doi: 10.1016/S0967-0645(00)00028-X

Takao, S., Hirawake, T., Hashida, G., Sasaki, H., Hattori, H., and Suzuki, K. (2014). Phytoplankton community composition and photosynthetic physiology in the Australian sector of the Southern Ocean during the austral summer of 2010/2011. *Polar Biol.* 37, 1563–1578. doi: 10.1007/s00300-014-1542-6

Takeda, S. (1998). Influence of iron availability on nutrient consumption ratio of diatoms in oceanic waters. *Nature* 393, 774–777. doi: 10.1038/31674

Talley, L. D. (2011). *Descriptive physical oceanography: An introduction* (Academic press).

Tamsitt, V., Drake, H. F., Morrison, A. K., Talley, L. D., Dufour, C. O., Gray, A. R., et al. (2017). Spiraling pathways of global deep waters to the surface of the Southern Ocean. *Nat. Commun.* 8, 172. doi: 10.1038/s41467-017-00197-0

Thiele, D., Chester, E. T., and Gill, P. C. (2000). Cetacean distribution off Eastern Antarctica (80–150 E) during the Austral summer of 1995/1996. *Deep Sea Res. Part II: Topical Stud. Oceanography* 47, 2543–2572. doi: 10.1016/S0967-0645(00)00035-7

Todd, V. L., and Williamson, L. D. (2022). Cetacean distribution in relation to oceanographic features at the Kerguelen Plateau. *Polar Biol.* 5, 113–126. doi: 10.1007/s00300-021-02977-3

Tulloch, V. J., Plagányi, ÉE., Brown, C., Richardson, A. J., and Matear, R. (2019). Future recovery of baleen whales is imperiled by climate change. *Global Change Biol.* 25, 1263–1281. doi: 10.1111/gcb.2019.25.issue-4

van Wijk, E. M., Rintoul, S. R., Ronai, B. M., and Williams, G. D. (2010). Regional circulation around Heard and McDonald Islands and through the fawn trough, central Kerguelen Plateau. *Deep Sea Res. Part I: Oceanographic Res. Papers* 57, 653–669. doi: 10.1016/j.dsr.2010.03.001

Vivier, F., Park, Y.-H., Sekma, H., and Le Sommer, J. (2015). Variability of the Antarctic Circumpolar Current transport through the Fawn trough, Kerguelen Plateau. *Deep-Sea Researt Part II: Topical Stud. Oceanography* 114, 12–26. doi: 10.1016/j.dsr2.2014.01.017

Weatherall, P., Marks, K. M., Jakobsson, M., Schmitt, T., Tani, S., Arndt, J. E., et al. (2015). A new digital bathymetric model of the world's oceans. *Earth Space Sci.* 2, 331–345. doi: 10.1002/2015EA000107

Westwood, K. J., Griffiths, F. B., Meiners, K. M., and Williams, G. D. (2010). Primary productivity off the Antarctic coast from 30° to 80° E; BROKE-West survey. *Deep-Sea Research II* 57, 794–814. doi: 10.1016/j.dsr2.2008.08.020

Williams, G. D., Nicol, S., Aoki, S., Meijers, A. J., Bindoff, N. L., Iijima, Y., et al. (2010). Surface oceanography of BROKE-West, along the Antarctic margin of the south-west Indian Ocean (30–80E). *Deep Sea Res. Part II: Topical Stud. Oceanography* 57, 738–757. doi: 10.1016/j.dsr2.2009.04.020

Wright, S. W., and van den Enden, R. L. (2000). Phytoplankton community structure and stocks in the East Antarctic marginal ice zone (BROKE survey, January-March 1996) determined by CHEMTAX analysis of HPLC pigment signatures. *Deep Sea Res. Part II: Topical Stud. Oceanography* 47, 2363–2400. doi: 10.1016/S0967-0645(00)00029-1

Wright, S. W., van den Enden, R. L., Pearce, I., Davidson, A. T., Scott, F. J., and Westwood, K. J. (2010). Phytoplankton community structure and stocks in the Southern Ocean (30-80°E) determined by CHEMTAX analysis of HPLC pigment signatures. *Deep Sea Res. Part II: Topical Stud. Oceanography* 57, 758–778. doi: 10.1016/j.dsr2.2009.06.015

Zuur, A. F., Ieno, E. N., and Elphick, C. S. (2010). A protocol for data exploration to avoid common statistical problems. *Methods Ecol. Evol.* 1, 3–14. doi: 10.1111/j.2041-210X.2009.00001.x

frontiers | Frontiers in Marine Science

TYPE Original Research
PUBLISHED 21 February 2025
DOI 10.3389/fmars.2025.1513013

Check for updates

OPEN ACCESS

EDITED BY
Martin Cox,
Australian Antarctic Division, Australia

REVIEWED BY
Sun-Yong Ha,
Korea Polar Research Institute, Republic of Korea
Abigail Jessica Rose Smith,
Australian Antarctic Division, Australia
Joanne Potts,
Pacific Community (SPC), New Caledonia

*CORRESPONDENCE
Yan Bai
baiyan@sio.org.cn

RECEIVED 17 October 2024
ACCEPTED 30 January 2025
PUBLISHED 21 February 2025

CITATION
Tan Y and Bai Y (2025) Antarctic krill habitat suitability variation in the Southern Ocean over 20 years.
Front. Mar. Sci. 12:1513013.
doi: 10.3389/fmars.2025.1513013

COPYRIGHT
© 2025 Tan and Bai. This is an open-access article distributed under the terms of the Creative Commons Attribution License (CC BY). The use, distribution or reproduction in other forums is permitted, provided the original author(s) and the copyright owner(s) are credited and that the original publication in this journal is cited, in accordance with accepted academic practice. No use, distribution or reproduction is permitted which does not comply with these terms.

Antarctic krill habitat suitability variation in the Southern Ocean over 20 years

Yiyang Tan[1,2,3] and Yan Bai[2]*

[1]Southern Marine Science and Engineering Guangdong Laboratory (Guangzhou), Guangzhou, China, [2]State Key Laboratory of Satellite Ocean Environment Dynamics, Second Institute of Oceanography, Ministry of Natural Resources, Hangzhou, China, [3]School of Oceanography, Shanghai Jiao Tong University, Shanghai, China

Antarctic krill (*Euphausia superba*) is a key species that sustains the biodiversity of the Southern Ocean and is a protected and restricted fishing target in this region. Considering the significant impacts of climate change on the ecological environment of the Southern Ocean, it is critical to understand the long-term spatio-temporal habitat distribution of Antarctic krill. This study integrates remote sensing and reanalysis data with Antarctic krill survey records to evaluate krill habitat suitability in the Southern Ocean. A novel habitat suitability model was developed using phytoplankton phenology and sea ice dynamics as key timing parameters, employing the Categorical Boosting (CatBoost) algorithm. This is the first time interannual variation in krill habitat distribution, spanning over 20 years (1997–2019), has been analyzed in relation to environmental parameters. Results show that the ice-free period in the Amundsen Sea has extended annually, while phytoplankton blooms have occurred earlier, lasted longer, and exhibited increasing chlorophyll a concentration (CHL), particularly in coastal regions. Additionally, the CatBoost model outperformed traditional species distribution models (SDMs) in handling large-scale presence-absence data (GCV = 0.16), demonstrating that bloom peak CHL and sea ice retreat timing are more effective indicators of krill habitat suitability than single-time environmental parameters. Based on long-term changes in highly suitable habitat areas for Antarctic krill and synchronized trends with the Southern Annular Mode (SAM) index, the overall area of suitable habitat for Antarctic krill in the Prydz sector has declined, likely linked to surface cooling caused by climate change. In contrast, the coastal region of the Atlantic sector, particularly the Western Antarctic Peninsula, a rapid warming area, has experienced an increase in krill habitat suitability. However, habitat suitability in the Weddell Sea has shown a marked decrease. Although climate change has produced mixed effects on krill habitats due to the varying responses of krill different life stages to environmental parameters, this study overall highlights a degradation of krill habitat in the Southern Ocean over the past two decades. These findings provide new insights into Antarctic krill habitat modeling and offer a long-term perspective on the climate change impacts, emphasizing the need for future under-ice investigations.

KEYWORDS

Antarctic krill (*Euphausia superba*), CatBoost, sea ice dynamics, phytoplankton bloom, Southern Ocean

1 Introduction

Antarctic krill (*Euphausia superba*) is a small, pelagic crustacean inhabiting the Southern Ocean, known for its enormous biomass, which plays a crucial role in sustaining the Southern Ocean food web and biodiversity (Croxall et al., 1999; Trathan and Hill, 2016). By feeding on large amounts of phytoplankton and conducting diel vertical migrations, Antarctic krill accelerates the downward export and transport of particles, thereby promoting marine biogeochemical cycles (Cavan et al., 2019). Krill are also sensitive to climate and environmental changes, serving as an indicator species for the fragile habitat of the Southern Ocean. For instance, increasing CO_2 concentrations, rising temperatures, and sea ice melting can trigger responses in krill related to egg hatching, spatial distribution, and abundance (Kawaguchi et al., 2013). Antarctic krill is a major food source for Southern Ocean predators (Croxall et al., 1999; Trathan and Hill, 2016) and an important target for commercial fisheries (Meyer et al., 2020). To preserve the biodiversity of the Southern Ocean ecosystem, the Commission for the Conservation of Antarctic Marine Living Resources (CCAMLR) has designated Antarctic krill as a key species under protection and introduced precautionary fishing limits (Siegel, 2016). Therefore, in light of the significant ongoing changes in the Southern Ocean's ecological environment, it is critical to assess the spatio-temporal distribution, trends, and habitat suitability of Antarctic krill.

Numerous studies have used environmental parameters derived from remote sensing and reanalysis models, in combination with krill population growth models, to predict habitat growth potential for Antarctic krill (Piñones and Fedorov, 2016) and assess habitat suitability in the Southern Ocean. Thorpe et al. (2019) developed a krill growth model for juveniles based on bathymetry, sea temperature, and sea ice concentration (SIC) data, finding that krill population growth in some nearshore areas is constrained by sea ice. Atkinson et al. (2006) incorporated remotely sensed chlorophyll concentrations (CHL) and sea surface temperature (SST) into a krill growth model, showing that remotely sensed CHL significantly improves the accuracy of daily krill growth rate predictions. Flores et al. (2012b) used mixed-layer depth (MLD) and related vertical profile parameters in a krill juvenile density prediction model, finding a positive correlation between juvenile krill density and MLD during the Antarctic summer when MLD is less than 12 m or ranges between 20-30 m. While these studies elucidate the relationships between Antarctic krill and environmental parameters, they lack discussions on the indicative role of temporal characteristics in habitat suitability. Some studies have explored the relationship between krill recruitment and sea ice phenology in the southwest Atlantic based on SIC-derived sea ice growth and retreat timing (Veytia et al., 2021), while others have provided distributions and trends of phytoplankton bloom phenological parameters in the Southern Ocean (Thomalla et al., 2023). These studies offer potential timing parameters for Antarctic krill habitat suitability models and phenological feature extraction.

The modeling and assessment of Antarctic krill habitat suitability are generally based on species distribution models (SDMs), including linear mixed models (LMM) (Kawaguchi et al., 2006; Brown et al., 2010; Candy, 2021), generalized additive models (GAMs) (Trathan et al., 2003; Murase et al., 2013; Trathan et al., 2022), and the maximum entropy model (Maxent) (Friedlaender et al., 2011; Nachtsheim et al., 2017; Lin et al., 2022), all of which have been applied in studies on krill distribution. These models have shown promising predictive and assessment outcomes, but their applicability and generalizability still require further improvement. Traditional SDM models, for instance, lack the ability to handle missing data, which is a common issue for environmental parameters such as CHL. And the missing data in CHL is in relation to krill density, as krill swarms could lead to zero values. Additionally, SDM models are subject to various limitations. Maxent, for example, is better suited for small presence-only datasets and is sensitive to spatial sampling bias and model complexity, which can result in prediction errors (Taylor et al., 2020; Lin et al., 2022). In this context, CatBoost (Categorical Boosting), a model capable of handling missing data, emerges as a suitable alternative. CatBoost is a gradient boosting framework, which is an ensemble learning technique that combines multiple decision trees to create a strong predictive model (Prokhorenkova et al., 2018). CatBoost automatically handles missing values in the input data by treating missing values as a separate category and learning a specific pattern for them during the training process. This approach allows CatBoost to capture the relationship between the missing values and the target variable, which can be particularly useful when the missingness itself carries important information. Therefore, CatBoost offers a novel approach for modeling the Antarctic krill habitat in the Southern Ocean, particularly under conditions where environmental variables are complex and contain missing values. Additionally, it addresses the issue of insufficient dataset matching that hampers larger-scale fitting. However, the application of CatBoost in species distribution modeling is still relatively limited.

Antarctic krill have a wide circum-Antarctic distribution, and their responses and adaptations to environmental changes are complex. Consequently, the response characteristics and mechanisms of krill distribution to environmental factors vary across different spatial and temporal scales. Existing studies have mainly focused on the Antarctic Peninsula and Scotia Sea in the western Southern Ocean, with relatively few studies evaluating habitat suitability in East Antarctica (Bibik et al., 1988; Lin et al., 2022). Research on the habitat suitability of Antarctic krill across the entire Southern Ocean primarily focuses on krill recruitment and their future responses to climate change, lacking historical reviews of krill habitat changes (Veytia et al., 2020). Moreover, few studies have assessed the spatio-temporal distribution of Antarctic krill habitat suitability based on long-term time series data (Candy, 2021).

This study, focusing on the entire Southern Ocean (45°S–90°S), integrates field observations and long-term remote sensing and reanalysis datasets spanning more than 20 years (1997-2019) at daily and 8-day averages. It introduces temporal parameters related to phytoplankton bloom phenology and sea ice dynamics to construct a krill habitat suitability model using the CatBoost algorithm. The study explores the relationship between krill spatial distribution and environmental factors through a

systematic comparison of four sectors: the Atlantic sector, Lazarev sector, Prydz sector, and Ross sector, identifying similarities and differences in the spatio-temporal variation of krill and its interactions with the marine ecological environment.

2 Data and methods

2.1 Study region and survey data

The study area is located in the Southern Ocean, covering the region between 45°S and 90°S surrounding Antarctica. To investigate the regional differences and characteristics of Antarctic krill habitat suitability across various sectors of the Southern Ocean, the study area was divided into 4 sectors (Yang et al., 2021): Atlantic sector (90°W–10°W), Lazarev sector (10°W–60°E), Prydz sector (60°E–150°E), and Ross sector (150°E–90°W) (Figure 1A).

The Antarctic krill data used in this study were sourced from the Global Biodiversity Information Facility (GBIF, https://www.gbif.org/) database on *Euphausia superba* Dana, 1850. Based on the raw dataset from GBIF, we conducted a validation and filtering process. First, we restricted the dataset to records from 1997 to 2020 and excluded entries lacking date information, including those record flagged as "record date unlikely" and "record date mismatch." Second, we retained only those records that contained latitude and longitude information, specifically within the latitude from 45°S to 90° S. Notably, some records were missing the negative sign for latitude; we corrected these by adding negative sign before retention. Next, we filtered the dataset to remove those data that were not derived from standardized observations (including acoustic and trawling investigation) or identified institutions (e.g. individual user-verified records from iNaturalist). We also examined the data source to exclude datasets that are not *in situ* observations, such as those related to stomach contents. We verified original source for each record to ensure the records pertained to Antarctic krill to avoid incorrect classification in GBIF. Finally, we removed duplicate records by merging them with identical dates and coordinates into a single one, retaining presence as occurrence status when both presence and absence data appear. Dataset after standardization is provided in the Supplementary Material (Supplementary Table 1).

Standardized dataset is composed of 12 original datasets and contains a total of 6,603 presence-absence records of Antarctic krill, with their distribution density across the Southern Ocean illustrated in Figure 1. Among these, there are 5,444 presence records and 1,143 absence records. The majority of the survey datasets present adult krill as dominant, with other life stages representing a smaller proportion. The sharp decline in the number of krill surveys after

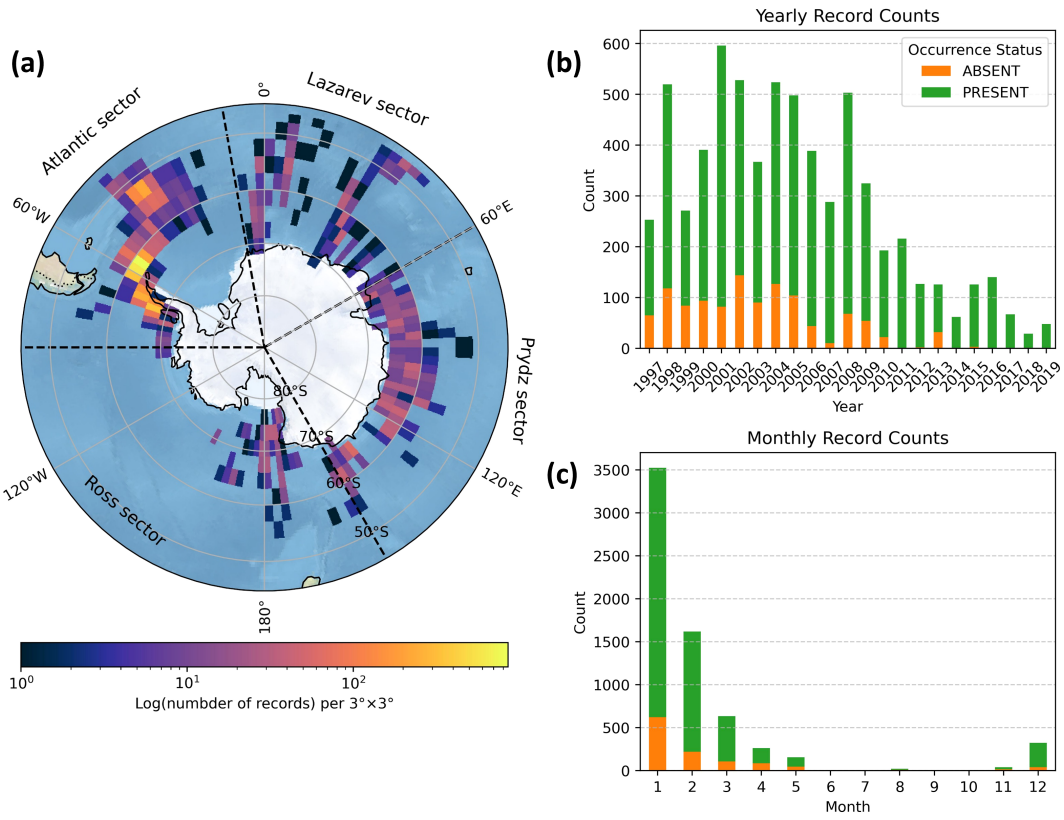


FIGURE 1
Antarctic krill survey data **(A)** density and Atlantic sector, Lazarev sector, Prydz sector, and Ross sector in the study region, and number of Antarctic krill survey records for **(B)** each year and **(C)** each month.

2010 primarily stems from CCAMLR's restrictions on Antarctic krill fishing (CCAMLR, 2008) (Figure 1B). Given that Antarctic krill migrate to surface waters during the Austral summer, making them easier to observe, this study focuses on the habitat suitability of Antarctic krill from November to April, during which 97.2% of the krill survey data were collected (Figure 1C).

2.2 Remote sensing data and reanalysis data

The remote sensing and reanalysis data used in this study are listed in Table 1. Sea surface temperature (SST) data were obtained from the Level 4 product of the Group for High-Resolution Sea Surface Temperature (GHRSST) dataset. This gridded product is derived from satellite, ship, and buoy observations, with the remote sensing data primarily sourced from the optimally interpolated global SST product based on the Advanced Very High-Resolution Radiometer (AVHRR) (Huang et al., 2021). The data are available at https://www.ncei.noaa.gov/data/sea-surface-temperature-optimum-interpolation.

Sea ice concentration (SIC) data were sourced from the National Snow and Ice Data Center (NSIDC). These data are obtained from observations by the Defense Meteorological Satellite Program (DMSP) and the Nimbus-7 satellite platform (Fetterer et al., 2017). Daily SIC products can be accessed at https://noaadata.apps.nsidc.org/NOAA/G02135/, and the product also provides the date of the minimum annual sea ice extent.

Sea surface chlorophyll concentration (CHL) data were obtained from the Ocean Colour Climate Change Initiative (OC-CCI), developed by the European Space Agency (ESA) Climate Change Initiative. This reanalysis dataset (version 5.0) integrates multi-sensor satellite observations, including data from MERIS, MODIS Aqua, Sentinel-3 OLC, SeaWiFS, and VIIRS, and is available at https://www.oceancolour.org/ (Sathyendranath et al., 2021). Due to significant interference from sea ice cover and clouds, there are substantial gaps in the ocean color data. To address this, we employed the gap-filling method developed by Thomalla et al. (2023) for the OC-CCI CHL product.

Mixed-layer depth (MLD) data were derived from the CMCC Global Ocean Physical Reanalysis System (C-GLORS) dataset. This dataset is produced using the NEMO ocean model coupled with the LIM2 sea ice model and calculated via the OceanVar data assimilation system (Storto and Masina, 2016). The data can be accessed at https://data.marine.copernicus.eu/product/.

TABLE 1 Summary information of remote sensing data and reanalysis data used in this study.

Parameters	Dataset	Time	Spatial Resolution
SST	AVHRR OI	daily	0.25°×0.25°
SIC	Sea Ice Index (G02135)	daily	25 km
CHL	OC-CCI	8-day	4 km
MLD	C-GLORS	daily	0.25°×0.25°

2.3 Timing parameters of phytoplankton bloom and sea ice dynamics

2.3.1 Phytoplankton bloom timing parameters

Phytoplankton blooms refer to the rapid proliferation and accumulation of phytoplankton, during which chlorophyll-a (CHL) concentrations increase significantly. Previous studies have shown that bloom phenology can affect fishery yields. For instance, variations in the timing and duration of spring blooms are closely correlated with the survival and development of juvenile fish (Platt et al., 2003). Antarctic krill larvae exhibit similar characteristics in population growth models (Kohlbach et al., 2017). Bloom phenology parameters include the onset and termination dates within a year, the bloom peak, and its duration, among others (Thomalla et al., 2023). In this study, we used Antarctic krill occurrence records and the corresponding CHL time series to construct bloom phenology parameters and analyze their temporal correlations (i.e., time lags) with krill occurrence. The schematic diagram of the phytoplankton bloom timing parameters is presented in the Supplementary Material (Supplementary Figure 1a). We used the calculation methods from (Ferreira et al., 2022) for the key bloom phenology parameters, which are presented below (Equations 1–7):

$$\boldsymbol{CHL_{BloomThreshold}} = (\boldsymbol{CHL_{max}} - \boldsymbol{CHL_{min}}) \times \mathbf{5\,\%} + \boldsymbol{CHL_{min}} \quad (1)$$

In Equation 1, $CHL_{BloomThreshold}$ (mg·m^{-3}) was calculated from the maximum (CHL_{max}, mg·m^{-3}) and minimum (CHL_{min}, mg·m^{-3}) CHL of timeseries during observation period (from July 1 of each year to June 30 of the following year). The 5% threshold was established through research by Siegel et al. (2002), determining a chlorophyll-a concentration level that corresponds just above the median biomass value on the bloom initiation day.

$$\boldsymbol{t_{BloomDur}} = \boldsymbol{t_{BloomTerm}} - \boldsymbol{t_{BloomInit}} \quad (2)$$

In Equation 2, the bloom duration ($t_{BloomDur}$) is the duration between bloom initiation and termination. The time at which CHL first exceeds the bloom threshold ($CHL_{BloomThreshold}$) marks the initiation of the bloom ($t_{BloomInit}$). The bloom termination ($t_{BloomTerm}$) is defined as the time when CHL falls below the bloom threshold after reaching its peak. The peak value of CHL timeseries during bloom ($CHL_{\mathrm{BloomPeak}}$) and the time ($t_{\mathrm{BloomPeak}}$) when CHL peaks are identified using the Python function find_peaks, searching for peaks in the CHL time series ($\{CHL_t\}_{t=1}^{T}$) during the bloom period. And the parameter "height" limits the minimum value of peak CHL.

$$\boldsymbol{CHL_{BloomInteg}} = \sum_{i=1}^{t_{BloomDur}} \boldsymbol{CHL_i} \quad (3)$$

In Equation 3, the cumulative chlorophyll-a concentration during the bloom period is estimated using the trapezoidal rule to integrate CHL during bloom ($CHL_{BloomInteg}$).

$$\boldsymbol{t_{DABloomInit}} = \boldsymbol{t_{AKO}} - \boldsymbol{t_{BloomInit}} \quad (4)$$

$$\boldsymbol{t_{DBBloomTerm}} = \boldsymbol{t_{BloomTerm}} - \boldsymbol{t_{AKO}} \quad (5)$$

$$\boldsymbol{t_{DBBloomPeak}} = \boldsymbol{t_{BloomPeak}} - \boldsymbol{t_{AKO}} \quad (6)$$

In Equations 4, 5, to determine the temporal relationship between the phytoplankton bloom and Antarctic krill observations (t_{AKO}), the number of days between the krill observation date and the bloom initiation date ($t_{DABloomInit}$) is calculated. "DABloomInit" here refers to days after bloom initiation. This implies that we assume observations of Antarctic krill typically occur during phytoplankton bloom periods, which is consistent with the phenology of the Antarctic krill. Thus, the difference between the krill observation date and the bloom termination date is calculated as $t_{DBBloomTerm}$ referring to days before bloom termination. And the difference between the krill observation and the CHL peak time date is calculated as $t_{DBBloomPeak}$ referring to days before CHL peak time in Equation 6 .

$$CHL_{BloomMean} = \frac{CHL_{BloomInteg}}{t_{BloomDur}} \tag{7}$$

Finally, in Equation 7, $CHL_{BloomMean}$ is calculated from $CHL_{BloomInteg}$ and $t_{BloomDur}$, representing mean CHL during phytoplankton bloom. The units and definitions of all the phytoplankton bloom timing parameters mentioned above can be found in Table 2.

2.3.2 Sea ice dynamics timing parameters

The sea ice phenology parameters, representing sea ice arrival and retreat, can be calculated from the SIC time series. The sea ice formation time, or time of arrival (TOA), is defined as the date when SIC first reaches or exceeds 15% in a given year; the sea ice retreat time, or time of retreat (TOR), is determined by searching backwards from the date of the minimum sea ice extent in the following year until SIC first reaches or exceeds 15% (Stammerjohn et al., 2008). The schematic diagram of the sea ice dynamics timing parameters is presented in the Supplementary Material (Supplementary Figure 1b). Since the Antarctic krill observations are primarily recorded in ice-free areas, the ice-free duration (IFDUR) is calculated to represent the length of time without sea ice. The time differences between sea ice dynamics and krill observations are calculated as the number of days after sea ice retreat (DATOR), measured as the days between krill occurrence (t_{AKO}) and the sea ice retreat time, and the number of days before sea ice formation (DBTOA), calculated as the days between krill occurrence and the sea ice arrival time. The sea ice phenology parameter calculations and their formulas are presented in Equations 8–10:

$$t_{IFDUR} = t_{TOA} - t_{TOR} \tag{8}$$

$$t_{DBTOA} = t_{TOA} - t_{AKO} \tag{9}$$

$$t_{DATOR} = t_{AKO} - t_{TOR} \tag{10}$$

2.4 Suitability model development and validation

In this study, the CatBoost algorithm was used to construct a habitat suitability model for Antarctic krill. The selected parameters were divided into 3 categories: (a) conventional single-moment environmental parameters, (b) sea ice and phytoplankton bloom phenology parameters, and (c) the time differences between krill observations and timing parameters. A total of 14 parameters were selected. Antarctic krill survey records were matched with the 14 environmental data parameters based on latitude, longitude, and date to create a matched dataset. Genuine cross-validation (GCV)

TABLE 2 Environmental parameters for Antarctic krill survey data.

Type	Definition	Short name/unit
Single moment environmental factors	Mixed layer depth	MLD/m
	Sea surface temperature	SST/°C
	Chlorophyll a concentration	CHL/mg·m^{-3}
	Sea ice concentration	SIC/‰
Timing parameters of phytoplankton bloom and sea ice dynamics	Ice-free duration	IFDUR/day
	Bloom duration	BloomDur/day
	Integrated CHL during bloom	BloomInteg/mg·m^{-3}
	Mean CHL during bloom	BloomMeanCHL/mg·m^{-3}
	CHL peak during bloom	BloomMaxCHL/mg·m^{-3}
Time difference between Antarctic krill observation and timing parameters	The number of days after the observation point to the retreat of sea ice	DATOR/day
	The number of days before the formation of sea ice from the observation point	DBTOA/day
	The number of days after the observation point to phytoplankton bloom initiation	DABloomInit/day
	The number of days before the observation point to phytoplankton bloom termination	DBBloomTerm/day
	The number of days before the observation point to phytoplankton bloom termination	DBBloomPeak/day

was employed to assess the model's overall performance. This dataset was divided into 2 parts for developing CatBoost model: for each year (starting from July 1st to ensure data continuity), data from that year were excluded for validation, and the remaining data were input for training. The model's performance is assessed by averaging the accuracy obtained from modeling and validating each year through a leave-one-out approach.

The model's classification accuracy was evaluated using three metrics: (a) mean squared error (MSE), (b) Area Under the Curve (AUC) of the Receiver Operating Characteristic (ROC), and (c) True Skill Statistic (TSS). Factors with low contribution to the model and strong collinearity will be filtered out for re-modeling in order to identify the optimal model. Additionally, a limitation was imposed on the number of non-null environmental parameters input to reduce the uncertainty in prediction results caused by excessive missing values. The predictive accuracy in different experiments were compared to determine the optimal model for reconstructing Antarctic krill habitat suitability. Finally, since extended daylight during the Austral summer boosts phytoplankton blooms, causing krill to migrate to surface waters, which align with both coverage of our survey records and the focus of our study, the model outputs were limited to the period from November to April of the subsequent year. The model produced daily habitat suitability distributions for Antarctic krill in the Southern Ocean from 1997 to 2019. The entire workflow of the modeling process is illustrated in the Supplementary Material (Supplementary Figure 2).

2.4.1 Matchup dataset for suitability model

Based on the obtained MLD, SST, SIC, and gap-filled CHL products, along with the calculated timing parameters for phytoplankton bloom and sea ice dynamics, the corresponding values for each survey record were extracted by matching the latitude, longitude, and date (year, month, and day) of the survey with the relevant environmental data. This process was applied to each survey record. The abbreviations, definitions, and classifications of the 14 environmental parameters are summarized in Table 2.

2.4.2 CatBoost algorithms and model development

The CatBoost (Categorical Boosting) algorithm has demonstrated robust resistance to overfitting and strong feature extraction capabilities in species distribution models and other ecological and climate prediction studies (Hancock and Khoshgoftaar, 2020; Chang et al., 2023). Fundamentally, CatBoost is an implementation of the gradient boosting decision tree (GBDT) algorithm, optimized specifically for datasets containing a large number of categorical variables. Its handling of missing values involves treating them as a distinct category, allowing estimation during the model training process. During training, CatBoost employs decision trees as base models, and by introducing random permutations and sequential updates, it reduces prediction bias, thus improving model generalization. Additionally, it calculates gradients using the models trained in previous iterations, which helps prevent target leakage (Prokhorenkova et al., 2018). In this study, the CatBoost classifier from the Python CatBoost package was used. The target variable was set to 1 for presence and 0 for absence, with 14 environmental parameters as predictors. The modeling parameters were set as: iterations = 1000, learning_rate = 0.1, depth = 6, and loss_function = 'Logloss' to build the habitat suitability model.

2.4.3 Model validation

In species distribution model (SDM) research, the receiver operating characteristic (ROC) curve and the area under the curve (AUC) are commonly used to evaluate the classification ability and accuracy of SDMs based on presence-absence data. The ROC-AUC allows for the simultaneous evaluation of the model's predictive accuracy for both presence and absence without requiring a threshold for positive and negative classifications (Manel et al., 2001). In this study, ROC-AUC was used to assess the model's accuracy. The ROC curve is a plot of different classification thresholds, with the true positive rate (TPR) on the vertical axis and the false positive rate (FPR) on the horizontal axis, defined as follows:

$$Sensitivity{=}TPR = \frac{TP}{TP + FN} \tag{11}$$

$$FPR = \frac{FP}{FP + TN} \tag{12}$$

$$\mathrm{AUC} = \int_0^1 \mathrm{TPR(FPR)}\, \mathrm{d(FPR)} \tag{13}$$

Here, AUC represents the area under the ROC curve, with values ranging from 0 to 1. The closer the AUC value is to 1, the stronger the model's classification performance. TP refers to true positives, TN to true negatives, FP to false positives, and FN to false negatives.

Additionally, this study evaluated the model's overall classification performance and its ability to distinguish negative classes using True Skill Statistic (TSS). TSS is a measure used to evaluate the performance of binary classification models, particularly useful for assessing imbalanced classes. The TSS ranges from -1 to 1, where 1 indicates perfect classification, 0 indicates the model's performance is no better than random guessing, and negative values suggest performance worse than random predictions. The formulas are as follows:

$$\mathrm{Specificity} = \frac{TN}{TN + FP} \tag{14}$$

$$TSS = Sensitivity + Specificity - 1 \tag{15}$$

Where, sensitivity (also known as True Positive Rate) is the proportion of actual positive cases correctly predicted by the model. Specificity (also known as True Negative Rate) is the proportion of actual negative cases correctly predicted by the model.

To evaluate the model's generalization ability across different years and independent datasets, we calculated the mean values of three validation metrics for each experiment that employed a leave-one-out approach, incorporating different selections of input variables and non-null limitations. GCV is calculated as the mean squared error (MSE) of leave-one-out prediction errors (Kvile et al.,

2018). We evaluated the modeling accuracy of each experiment using a combination of the three metrics and selected the optimal configuration for modeling and prediction.

3 Results

3.1 Environmental factors characteristics for Antarctic krill

3.1.1 Sea ice dynamics and bloom phytoplankton variation in the Southern Ocean

From 1997 to 2019, the average sea ice retreat time in the Southern Ocean ranged from August to February of the following year, showing an earlier retreat at lower latitudes and a later retreat at higher latitudes. Near the continental shelf, sea ice retreat times were concentrated in February, with the Weddell Sea having particularly late retreat times (Figure 2A). Over the same period, the Weddell Sea, Antarctic Peninsula, parts of the Bellingshausen Sea, and the D'Urville region experienced progressively later sea ice retreat, with a maximum delay of up to 4 days per year. In contrast, the Amundsen Sea showed a trend of earlier sea ice retreat, also with a maximum shift of 4 days per year, and certain areas in the Cosmonauts Sea exhibited a similar trend of earlier retreat (Figure 2D).

The average sea ice formation time in the Southern Ocean from 1997 to 2019 ranged from March to July, with earlier formation near the coast and later formation in the open ocean (Figure 2B). Unlike the retreat time, sea ice formation in the Amundsen Sea showed a significant delay, with formation occurring 4 days later per year (Figure 2E). The average ice-free duration during this period indicated year-round ice coverage near the continental shelf, while regions closer to 60°S and farther north displayed ice-free conditions throughout the year (Figure 2C). Similarly, the Amundsen Sea showed a trend of increasing ice-free duration, with a maximum extension of 6 days per year (Figure 2F).

From 1997 to 2019, the average bloom initiation time in the Southern Ocean ranged from August to February of the following year, with later initiation near the coast and earlier initiation in the open ocean. In the southwestern Antarctic region, bloom initiation generally occurred around February (Figure 3A). The trend shows a significant advancement in bloom initiation at lower latitudes, with an average shift of 5 days per year (Figures 3B, C). The average bloom termination time ranged from October to May, with little spatial variation across the Southern Ocean, and was predominantly concentrated around March (Figure 3D). The bloom termination time did not exhibit a significant trend from 1997 to 2019 (Figure 3F), but in the 60°S-70°S region of the southwestern Antarctic and the D'Urville Sea, it advanced by approximately 5 days per year (Figure 3E). The average bloom duration was shorter near the coast and longer in the open ocean (Figure 3G). There was

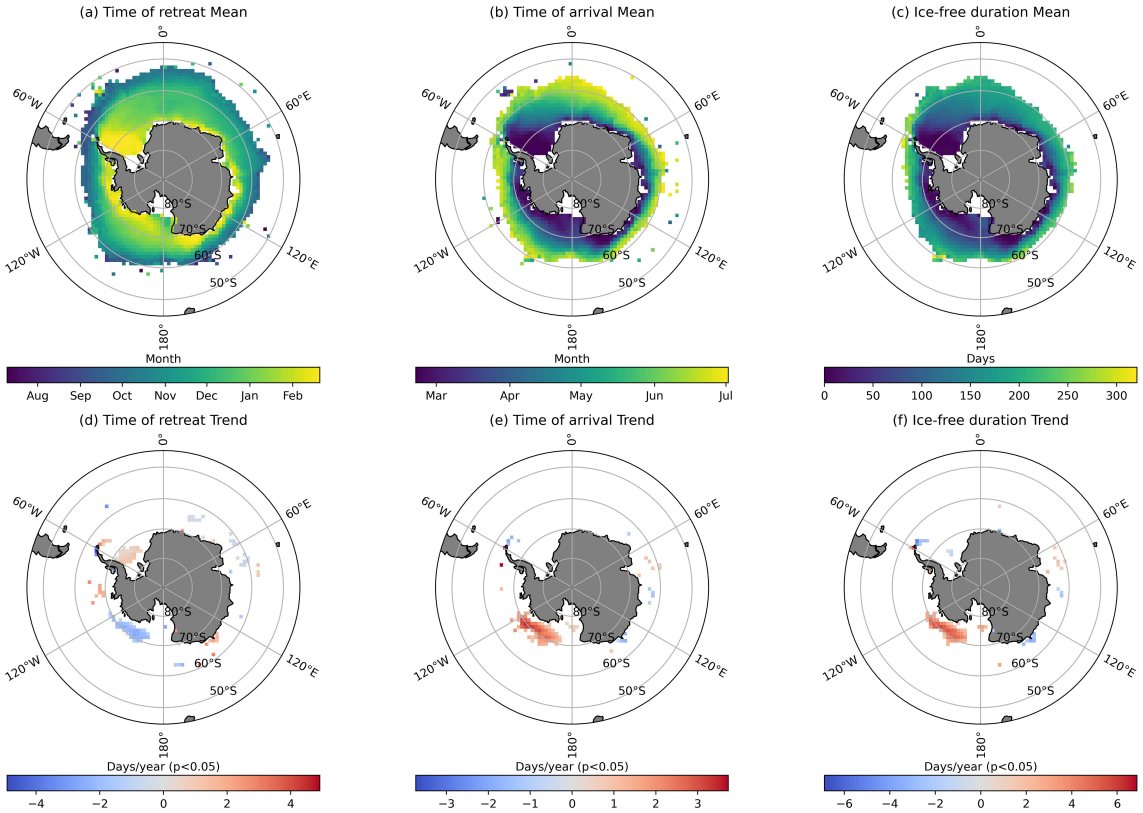


FIGURE 2
Mean and trend of sea ice dynamics timing parameters in 1997-2019. **(A)** Time of retreat annual mean. **(B)** Time of arrival annual mean. **(C)** Ice-free duration annual mean. **(D)** Time of retreat annual trend. **(E)** Time of arrival annual trend. **(F)** Ice-free duration annual trend.

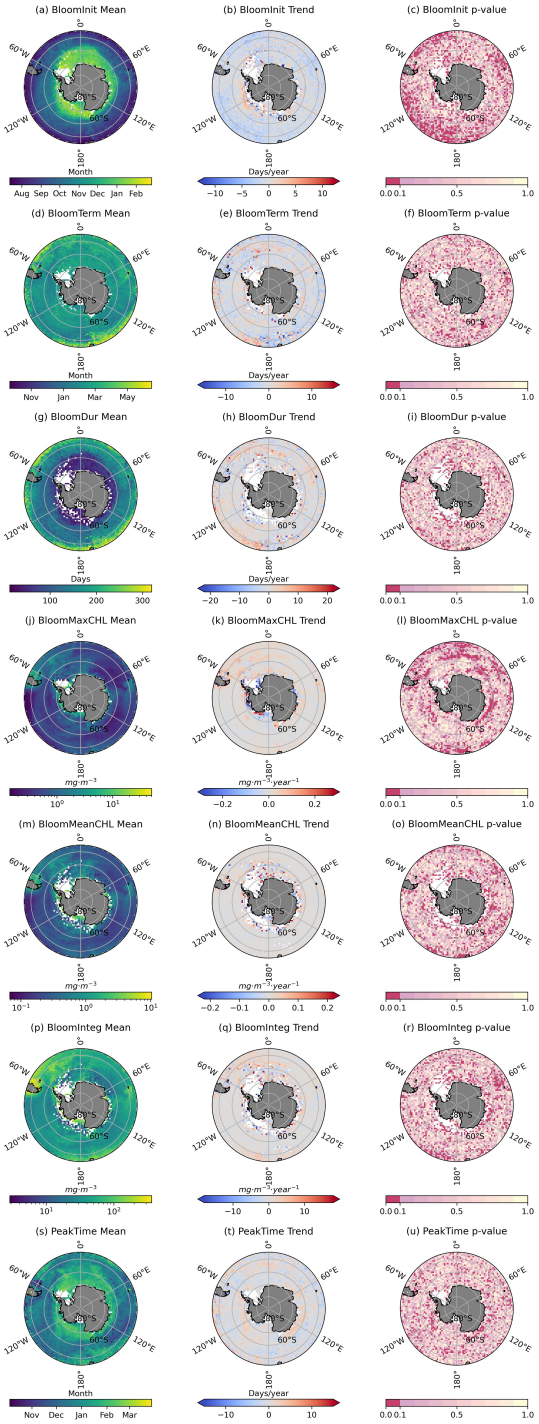


FIGURE 3
Mean and trend of algal bloom timing parameters in 1997-2019. **(A–C)** Bloom initiation date annual mean, trend, and p-value. **(D–F)** Bloom termination date annual mean, trend, and p-value. **(G–I)** Bloom duration annual mean, trend, and p-value. **(J–L)** Bloom maximum chlorophyll-a concentration annual mean, trend, and p-value. **(M–O)** Bloom mean chlorophyll-a concentration annual mean, trend, and p-value. **(P–R)** Bloom integrated chlorophyll-a concentration annual mean, trend, and p-value. **(S–U)** Bloom chlorophyll-a concentration peaking date annual mean, trend, and p-value.

an extension in bloom duration at lower latitudes (north of 50°S), while the bloom duration near the continental shelf remained relatively unchanged (Figures 3H, I).

During the 1997-2019 period, the peak, mean, and integrated CHL during the bloom were highest near the coast and lower in the open ocean (Figures 3J, M, P). Across the entire Southern Ocean, peak CHL during the bloom showed an upward trend, with a notable increase in the D'Urville Sea near the continental shelf, where the average CHL increased by approximately 0.05 mg·m^{-3} per year (Figures 3K, L). Similarly, integrated CHL during the bloom showed a significant upward trend in the Mawson Sea (Figures 3Q, R). The peak timing of CHL during blooms in the Southern Ocean exhibits a pattern where

coastal areas peak later than the open ocean. Typically, the peak date for coastal regions occurs around February (Figure 3S). At the same time, there is a notable delay in the peak timing of CHL during blooms in both the Amundsen Sea and the D'Urville Sea (Figures 3T, U).

3.1.2 Environmental factors characteristics for Antarctic krill presence

Based on the Antarctic krill presence data, matched with environmental parameters, kernel density plots were generated for four sectors (Figure 4). The results show that Antarctic krill generally appears when SST is between -2°C and 5°C. In the Ross sector, krill are concentrated in areas with SST below 0°C, with a peak at temperatures lower than 0°C. In the Lazarev sector, krill appear in both areas below 0°C and around 1°C. For the Prydz and Atlantic sectors, krill are found across a wider SST range. Specifically, in the Atlantic sector, krill are more commonly found in areas with SST above 1°C, while in the Prydz sector, krill tend to appear in areas with SST closer to 0°C (Figure 4A).

For MLD, Antarctic krill in the Prydz sector are more frequently found in waters with an MLD less than 20 meters, while in the other three sectors, krill are predominantly found in areas where the MLD is greater than 20 meters (Figure 4B). In terms of CHL, krill in the Atlantic sector are typically found in areas with CHL around 0.3 $mg{\cdot}m^{-3}$, in the Ross sector at around 0.2 $mg{\cdot}m^{-3}$, and in the Prydz sector at around 0.1 $mg{\cdot}m^{-3}$. The Lazarev sector does not show a distinct CHL peak (Figure 4C). It is important to note that krill surveys are usually conducted in ice-free regions, so the presence data are predominantly matched to areas with SIC near zero.

Regarding the time of sea ice retreat, Antarctic krill in the Ross and Lazarev sectors typically appear around 25 days after the sea ice has retreated, while in the Prydz sector, krill appear about 50 days after retreat. In the Atlantic sector, krill appear 50 to 120 days after sea ice retreat (Figure 4D). In relation to sea ice formation, krill in the Ross sector are observed about 30 days before ice formation, while in the Prydz sector, krill are found 60 days before formation. In the Atlantic sector, krill are observed 100 to 140 days before ice formation, while the Lazarev sector shows no clear peak (Figure 4E).

For the duration of the ice-free period, krill in the Ross sector experience the shortest duration, concentrated around 60 days. In contrast, krill in the Lazarev and Atlantic sectors experience the longest ice-free periods, around 180 days, while the Prydz sector has an ice-free period of approximately 150 days (Figure 4F).

In terms of phytoplankton bloom initiation, krill in the Atlantic sector typically appear about 100 days after bloom initiation, while in the Prydz sector, they appear around 75 days after bloom initiation. The other two sectors do not exhibit clear patterns (Figure 4G). Regarding bloom termination, krill in the Atlantic sector generally appear 20 to 50 days after bloom termination, while krill in the Prydz sector appear right as the bloom ends (Figure 4H). For bloom duration, krill in the Atlantic sector are more frequently found in areas where the bloom lasts 80 to 120 days, while in the Prydz sector, the bloom duration is around 75 days (Figure 4I). For the timing of CHL peaks during blooms, Antarctic krill in the Atlantic and Prydz sectors typically appear before the CHL peak, while in the Ross sector, they are observed after the CHL peak (Figure 4J).

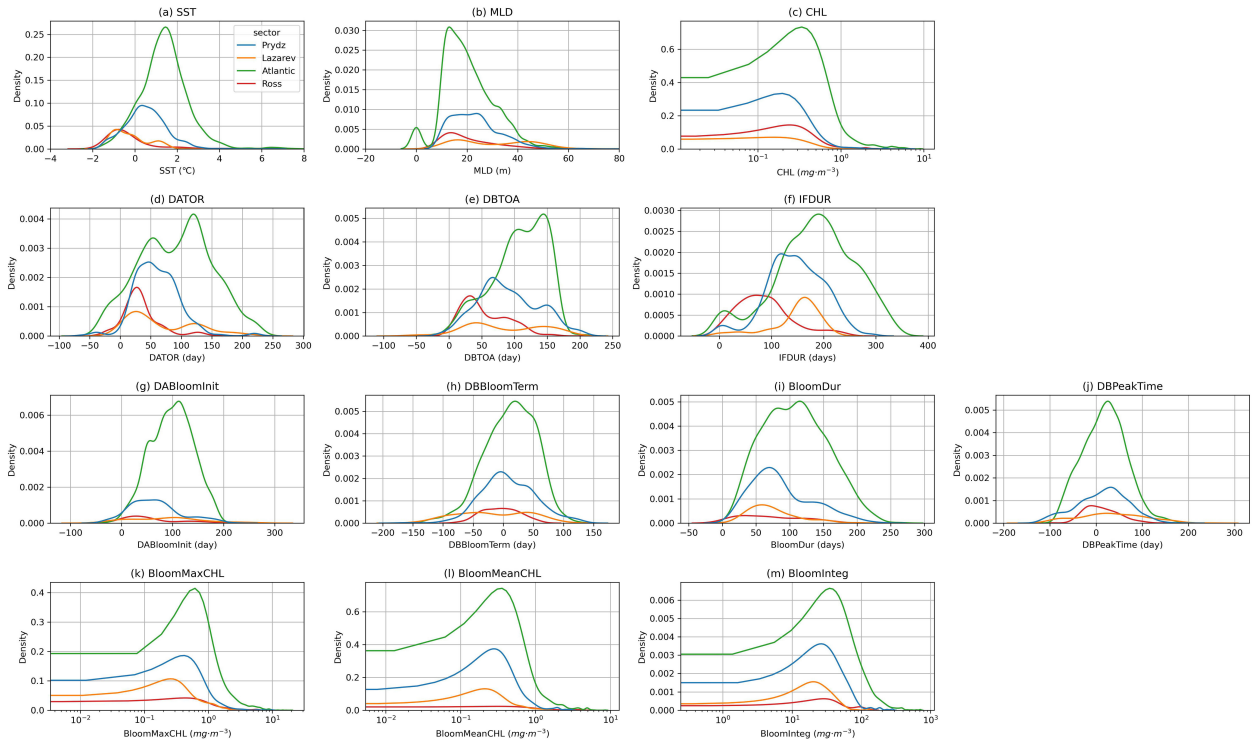


FIGURE 4
Kernal density estimation of krill presence matched environmental parameters: **(A)** SST, **(B)** MLD, **(C)** CHL, **(D)** DATOR, **(E)** DBTOA, **(F)** IFDUR, **(G)** DABloomInit, **(H)** DBBloomTerm, **(I)** BloomDur, **(J)** DBPeakTime, **(K)** BloomMaxCHL, **(L)** BloomMeanCHL, **(M)** BloomInteg.

When examining CHL peaks, mean values, and integrated CHL during the bloom, the results indicate the highest concentrations in the Atlantic sector, followed by the Prydz and Lazarev sectors, with the Ross sector showing no distinct peak (Figures 4K-M).

3.2 Suitability model validation and comparisons

For the original matched dataset, we tested the optimal combinations of 11–14 environmental parameters (with the minimum GCV for the same number of input parameters). Subsequently, we evaluated the optimal combination of environmental parameters by minimizing the number of non-null input factors required to predict suitability. Several model sets were constructed and compared for classification accuracy and generalization ability (Table 3). During the process of reducing the total number of input parameters to find the optimal variable combination, we observed that as the overall number of inputs decreased, the GCV continued to decline. However, when the input parameters were reduced from 12 to 11, both the AUC and TSS showed a decrease, indicating a decline in the model's classification ability, while the GCV only improved by 0.0001. Therefore, we chose the optimal combination with 12 input parameters for further training. Compared to the original model with 14 environmental parameters, the model performance increase when the factors with strong collinearity, BloomDur, and IFDUR, were removed, leading to an decrease in GCV and increase in AUC and TSS.

Since MLD, SIC, and SST had no missing data, we initially established a requirement of at least three non-null environmental variables for predicting suitability; otherwise, the output would be null. We gradually increased the minimum number of non-null input parameters from three to six and found that having at least four non-null values resulted in the lowest GCV (Table 3). Consequently, we set the final model to require a minimum of four non-null inputs from the optimal combination of 12 environmental parameters.

The final model, built using 12 environmental parameters, see Figure 5A for the detail inputs, which showed that the highest contributing factors were SST, TOR, BloomMaxCHL and MLD. Among them, the timing parameters of sea ice dynamics and phytoplankton bloom contributed significantly more to the model than single-time CHL and SIC values (Figure 5A). In contrast, BloomMeanCHL, BloomInteg, and SIC had the lowest contributions to the model. SIC has low effectiveness in distinguishing Antarctic krill habitats primarily because it consists mostly of zero values, particularly since most observational data were collected in areas without sea ice cover. Meanwhile, BloomMeanCHL and BloomInteg provide limited effective information due to their high collinearity with other chlorophyll parameters.

It is important to note that the optimal combinations of environmental parameters, under the constraint of a limited number of input variables, are derived from filtering all possible combinations based on the minimum GCV. Despite the AUC performing poorly according to the classification performance standards: failing (0.5–0.6), poor (0.6–0.7), fair (0.7–0.8), good (0.8–0.9), and excellent (0.9–1.0) (Phillips et al., 2006), some years could not calculate the AUC due to a single category and had a smaller MSE (Figure 5C). As a result, the actual classification accuracy should be AUC > 0.675 (Figure 5B). Overall, the model was effective in reconstructing the historical habitat suitability of Antarctic krill and could be reliably used for modeling their habitat suitability.

3.3 Predicted Antarctic krill habitat suitability

3.3.1 Highly suitable Antarctic krill habitat seasonal and annual variations

Based on the months included in the survey data and the life cycle of Antarctic krill, the habitat suitability model constructed using CatBoost was restricted to the period from November to April for reconstructing Antarctic krill habitat suitability. The monthly average habitat suitability for Antarctic krill from 1997 to 2019 was calculated (Figure 6). Habitat suitability was classified into four categories: Unsuitable (below 0.4), Marginally suitable (0.4-0.6), Moderately suitable (0.6-0.8), and Highly suitable (0.8-1.0).

In November, the average habitat suitability for Antarctic krill in the Southern Ocean showed higher suitability near the continental shelf, lower suitability near the 60°S latitude, and higher suitability north of 60°S. By December, the region with

TABLE 3 ROC-AUC, TSS and genuine cross validation scores for each modeling experiment.

Experiment No.	Model	GCV	AUC	TSS
1	14 factors, no restrictions on non-null inputs	0.1683	0.6673	0.2429
2	Drop BloomInteg based on **Exp. 1**	0.1616	0.6615	0.2514
3	Drop BloomDur and IFDUR based on **Exp. 1**	0.1588	0.6693	0.2501
4	Drop SIC, BloomMeanCHL, BloomInteg based on **Exp. 1**	0.1587	0.6476	0.2515
5	Least 3 non-null inputs for prediction based on **Exp. 3**	0.1670	0.6953	0.2595
6	**Least 4 non-null inputs for prediction based on Exp. 3**	**0.1616**	0.6751	0.3046
7	Least 5 non-null inputs for prediction based on **Exp. 3**	0.1748	0.7824	0.4197
8	Least 6 non-null inputs for prediction based on **Exp. 3**	0.1867	0.7633	0.5446

The bold values refer to the final parameter selection used for modeling.

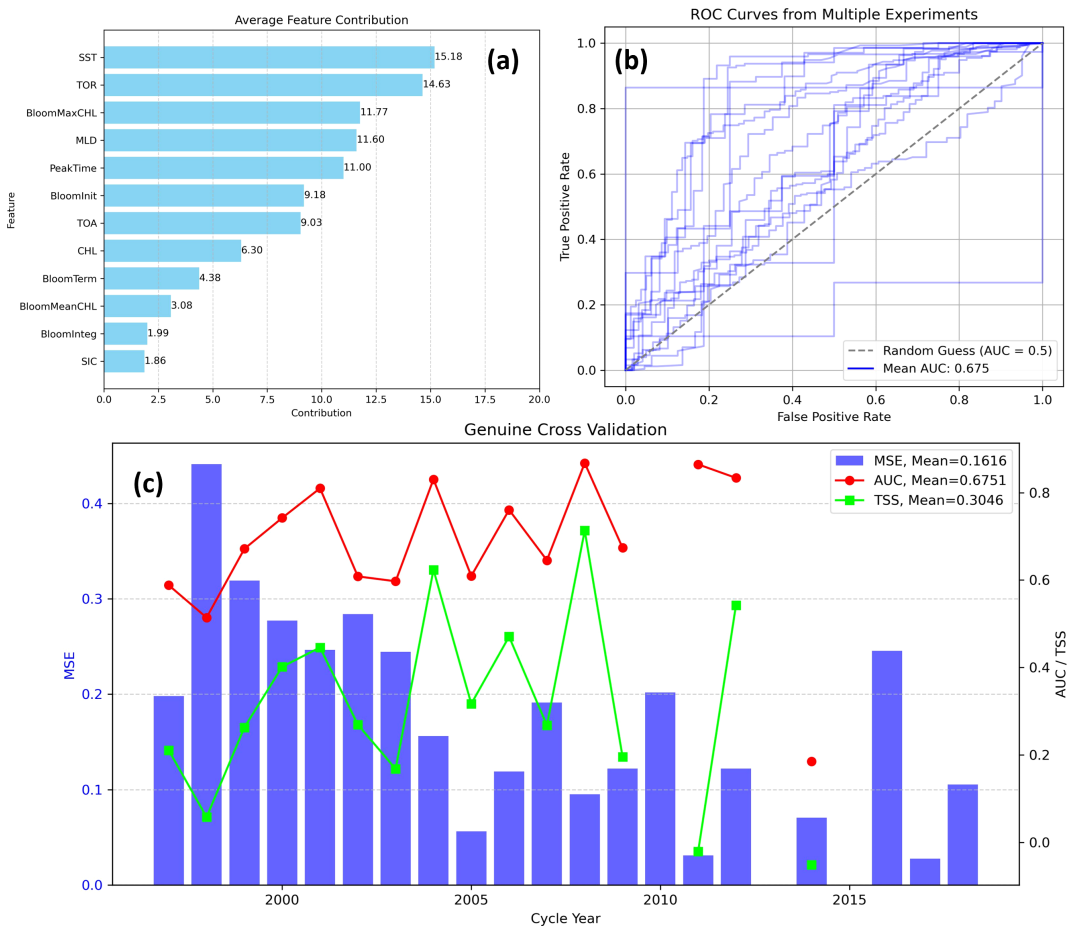


FIGURE 5
(A) Feature importance of CatBoost-based suitability model, **(B)** ROC curves from multiple time modeling, and **(C)** GCV-based model validation.

lower suitability in the middle had increased (Figures 6A, B). From January to March, the highly suitable habitat for Antarctic krill consistently remained in the waters south of 60°S near the continental shelf, and the moderately suitable habitat between 60°W and 180°W exhibited a dynamic shift toward higher latitudes. In the D'Urville Sea, the suitability of krill habitats increased and contracted towards higher latitudes near the coast. By April, the most suitable krill habitats were concentrated around the Antarctic continental shelf (Figures 6C-F).

The highly suitable regions for Antarctic krill (Suitability > 0.8) were extracted, and the annual area of Antarctic krill habitat was calculated for the four sectors (Figure 7). Notably, the highly suitable habitat area for Antarctic krill in the Atlantic Sector reached its maximum extent in 2005 but exhibited a significant decline by 2019. Similarly, the Lazarev Sector reached its peak one year later, in 2006, followed by a noticeable reduction. In contrast, the highly suitable habitat area in the Prydz Sector demonstrated a more prolonged declining trend. Meanwhile, the Ross Sector showed a peak in its highly suitable habitat area at a time similar to that of the Atlantic and Lazarev Sectors.

SAM has remained in a positive phase after 2010 except for 2016 (Figure 7E), leading to intensified of zonal winds that enhance warm deep waters upwelling near the Antarctic coast, thereby reducing sea ice extent and supporting increased primary production (Fogt and Marshall, 2020; Greaves et al., 2020). Although the trends in the other three sectors were not significant, all four sectors displayed a pattern of initial increase followed by a decline, which corresponded with the annual trend of the SAM index. This indicates a decline in the suitability of Antarctic krill habitat that is related with the positive SAM index after 2010. It is worth noting that the area of highly suitable habitat for Antarctic krill in the Prydz sector demonstrated a significant overall declining trend from 1997 to 2019.

3.3.2 Antarctic krill habitat suitability spatio-temporal patterns

Using the habitat suitability model predicted by CatBoost, the daily habitat suitability of Antarctic krill from November to April during the period 1997-2019 was obtained. Based on the daily distribution of Antarctic krill habitat suitability, annual distributions of habitat suitability were calculated, along with the multi-year averages, variances, trends, and the significance of these trends (p-values) for the period from 1997 to 2019 (Figure 8). The distribution of habitat suitability showed higher values along the continental shelf and lower values toward lower latitudes. Notably, the habitat suitability for Antarctic krill exhibits distinct maxima in

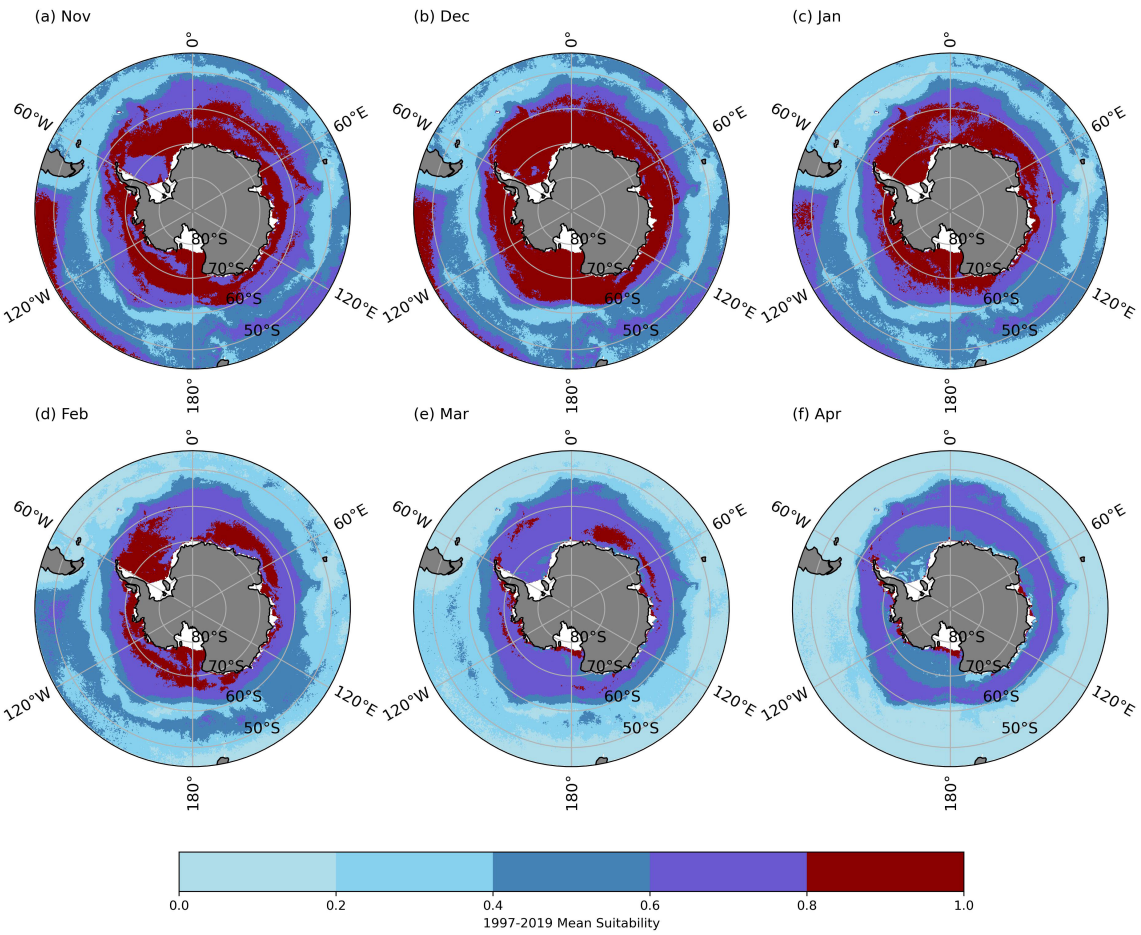


FIGURE 6
Monthly mean Antarctic krill habitat suitability in 1997-2019. **(A)** November; **(B)** December; **(C)** January; **(D)** February; **(E)** March; **(F)** April.

the coastal regions of the Ross Sea, Prydz Bay, Amundsen Sea, and the Western Antarctic Peninsula, while the habitat suitability in the Weddell Sea primarily indicates moderate suitability (Figure 8A). The zonal trend from the coastal regions towards lower latitudes shows a decrease in highly suitable habitat maxima, transitioning to moderately suitable habitats, followed by a gradual increase back to highly suitable habitats, before rapidly declining to marginally suitable habitats near 60°S. Moreover, the range of suitable habitat in the Southwestern Antarctic is significantly greater than that in the Southeastern Antarctic. Based on the multi-year variance of Antarctic krill habitat suitability, the differences in habitat suitability within the sea ice extent and the Antarctic Circumpolar Current (ACC) range are smaller compared to the variations observed at the ice edge (Figure 8B).

The trend analysis of annual mean habitat suitability for Antarctic krill from 1997 to 2019 reveals a non-significant increase in habitat suitability in the Southwestern Antarctic (Figures 8C, D). Significantly, habitat suitability has increased along the coastal region of the Western Antarctic Peninsula, Amundsen Sea, as well as in the nearshore areas of the Somov Sea. In contrast, the Weddell Sea exhibits a significant declining trend in habitat suitability. Besides, the habitat change trends in most other areas are not significant (Figure 8D).

4 Discussion

This study proposed a novel workflow for reconstructing the historical habitat suitability of Antarctic krill. Using remote sensing and reanalysis products, we calculated sea ice and phytoplankton bloom timing parameters and conducted multi-year trend analyses. Additionally, based on Antarctic krill survey data, we evaluated the habitat suitability characteristics of different regions in the Southern Ocean. For the first time, the CatBoost algorithm was applied to construct a species distribution model, offering a new approach for habitat suitability research and demonstrating the critical role of timing parameters among environmental drivers. Furthermore, we conducted a trend analysis of habitat changes over more than 20 years and identified a declining trend in Antarctic krill habitat suitability.

4.1 Impact of climate change on sea ice dynamics and phytoplankton bloom timing in the Southern Ocean

Based on the calculated sea ice parameters for 1997-2019, it was observed that the ice-free period in the Amundsen Sea has been extending (Figure 2F). Previous studies have shown that the sea ice

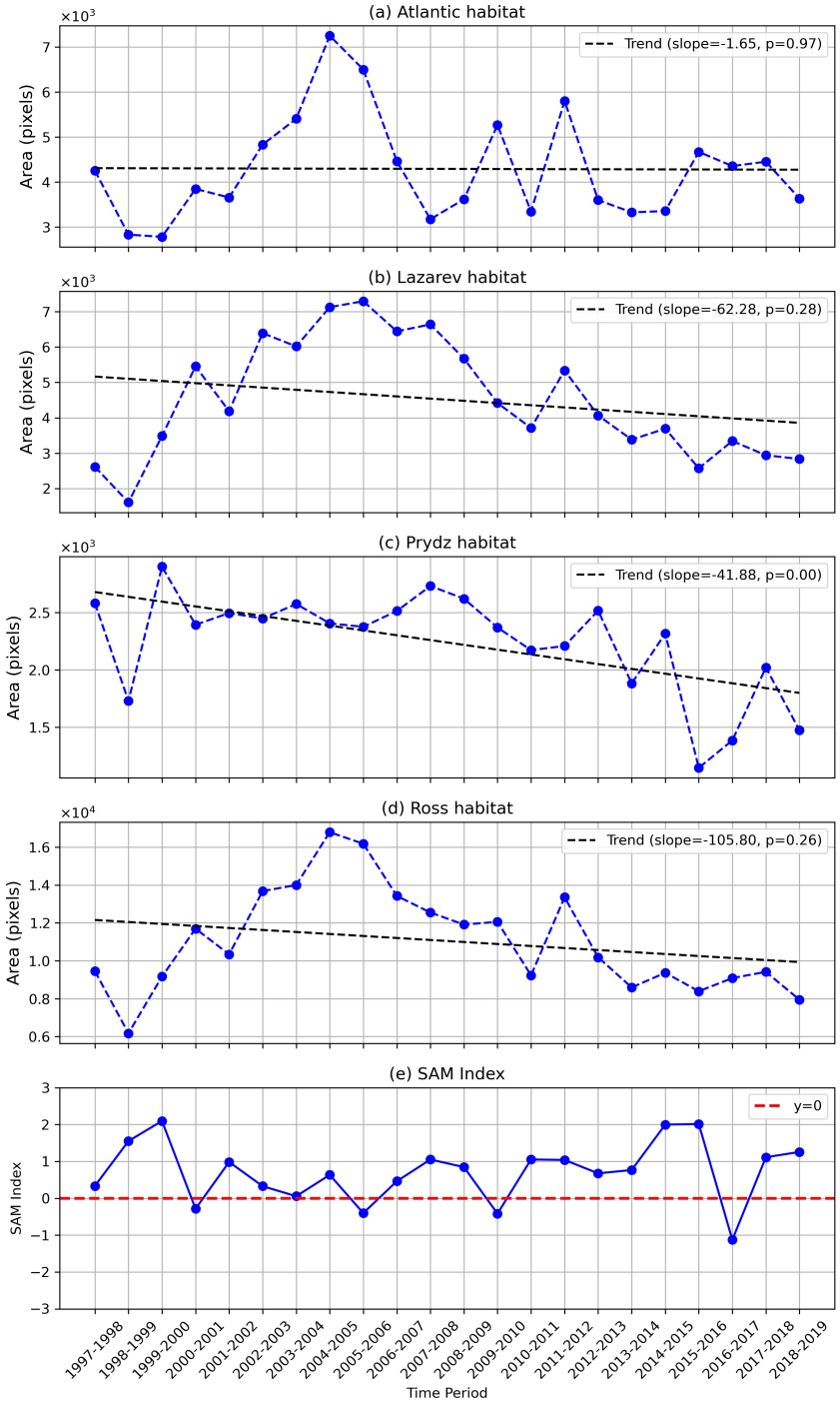


FIGURE 7
Antarctic krill highly suitable habitat area variation in 1997-2019 in 4 sectors: **(A)** Atlantic sector; **(B)** Lazarev sector; **(C)** Prydz sector; **(D)** Ross sector. **(E)** annual mean SAM index from November to April (calculated from Marshall, 2003).

in this region has been consistently decreasing during the Antarctic summer from 1979 to 2014 (Hobbs et al., 2016), with the timing of sea ice retreat advancing each year (Figure 4D). Although no direct cause has been identified for the earlier sea ice retreat and reduction in the Amundsen Sea, the phenomenon is closely linked to the influence of Southern Annular Mode (SAM), El Niño-Southern Oscillation (ENSO), and the Amundsen Sea low (ASL) on atmospheric circulation over the Southern Ocean (Hosking et al., 2013). Additionally, under the combined effects of ENSO and SAM, the extent of summer sea ice in the Southern Ocean is expected to increase (Pezza et al., 2012), which could explain the shortened ice-free period in the D'Urville Sea. Thus, further research of environmental factors interaction is necessary to better understand the specific physical processes and climate change effects on sea ice dynamics in different regions of the Southern Ocean in the future.

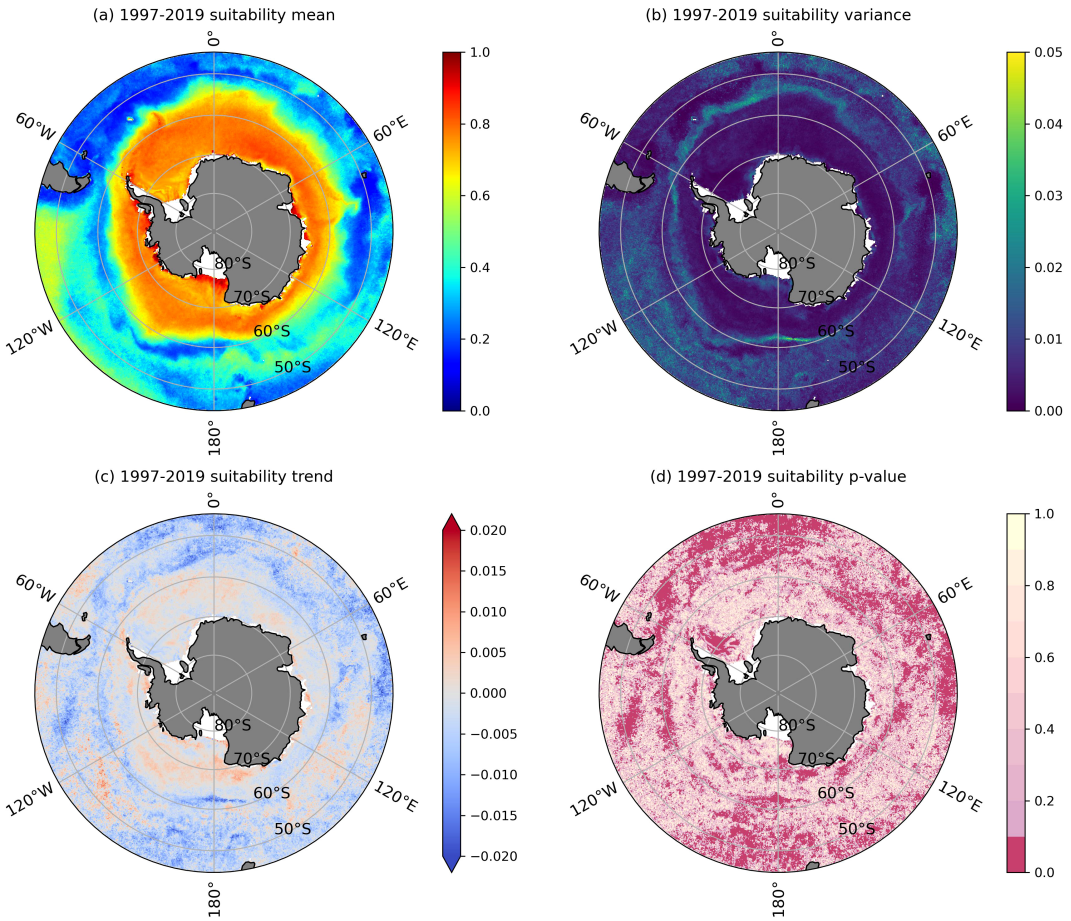


FIGURE 8
Mean **(A)**, variance **(B)**, trend **(C)**, and p-value **(D)** of Antarctic krill habitat suitability from 1997 to 2019.

Regarding the phytoplankton bloom timing parameters from 1997 to 2019, it was found that the onset of blooms in the Southern Ocean advanced (Figure 3D), the duration of blooms lengthened (Figure 3F), and CHL during blooms increased (Figures 3J-L). These trends are consistent with the previous research, although our study only calculated bloom parameters for the Antarctic krill investigated month rather than the entire year. Nevertheless, the parameterization of phytoplankton bloom timing during this period could regulate the primary food sources (e.g. diatoms, large dinoflagellates, and other armored flagellates) availability for Antarctic krill (Flores et al., 2012a). The increase in CHL during blooms is primarily associated with rising sea surface temperatures and deeper summer mixed layers (Thomalla et al., 2023). It should be noted that although the OC-CCI products have been interpolated, there are still missing values in the coastal area due to factors like sea ice coverage. As a result, the characteristics of phytoplankton blooms in that region can't be fully identified to provide references for predicting the distribution of Antarctic krill. Additionally, research on the Antarctic Peninsula has shown that the bloom initiation and peak dates of CHL during phytoplankton bloom in the marginal ice zone and shelf areas are delayed, which could be attributed to enhanced light limitation resulting from deeper mixing induced by increased wind speeds during spring (Turner et al., 2024). Ungapped CHL products covering the coastal areas of the Southern Ocean needs to be developed to better understand phytoplankton bloom variation.

The declining trend in SST in the Southern Ocean since 1980, attributed by many studies to SAM, contributes to Antarctic sea-ice expansion (Kostov et al., 2017; Kang et al., 2023). However, this surface cooling process in the Southern Ocean is more pronounced in the marginal ice zone in the Ross Sector (Kusahara et al., 2017; Kang et al., 2023), leading Antarctic krill in the Ross Sector stayed with lower SST. In the Lazarev Sector, while the surface cooling process in this region is not prominent, studies in the Lazarev Sea and Cosmonauts Sea have indicated that Antarctic krill in these areas are temperature-limited, tending to inhabit environments with sea temperatures below 0°C (Meyer et al., 2009; Lin et al., 2022). Simultaneously, Antarctic krill in these two sectors appear earlier following sea ice retreat compared to the other two sectors, indicating the critical role of the under-ice habitat as a primary residence and its importance in providing a colder thermal environment (Figure 4D). Antarctic krill in the Ross Sector typically inhabit areas with shorter ice-free periods (Figure 4F), despite the prolonged ice-free season in the Amundsen Sea, suggests a preference for environments with sea ice cover.

The Atlantic Sector has the most Antarctic krill survey records (Figure 1A). While fewer sampling records in the Weddell Sea due

to fishing restrictions, Antarctic krill investigations in the western Antarctic Peninsula and Scotia Sea regions are abundant. Many studies indicate that the Antarctic Peninsula, a region of rapid warming influenced by atmospheric circulation and oceanic anomalies, is distinguished from other sectors of the Southern Ocean by the retreat of sea ice and rising sea surface temperatures (Li et al., 2014; Sato et al., 2021). Therefore, in the Atlantic Sector, Antarctic krill appear at higher temperature ranges (1-2°C), experience the longest ice-free period, and the warmer seawater extends the duration of phytoplankton blooms. The Prydz Sector encompasses the waters of East Antarctica, and existing studies have reflected SST warming from 1996 to 2013 through diatoms collected in sediment cores from Prydz Bay (Huang et al., 2023). The anomalous warming in this region during 2016-2017 is also noteworthy, as it is expected to have a direct impact on the Antarctic krill populations in the area (Sabu et al., 2021). Meanwhile, the ice shelf melt in the D'Urville Sea cools and freshens the subsurface ocean while warming the upper layers (Huot et al., 2021). Therefore, the suitable temperature range for Antarctic krill in the Prydz Sector is second only to that in the Atlantic Sector, and the characteristics of sea ice and phytoplankton blooms follow a similar pattern.

4.2 The impact mechanisms of environmental drivers on the Antarctic krill habitat suitability

Based on the extracted habitat suitability of Antarctic krill (Figure 8), Pearson correlation coefficients were calculated between habitat suitability and the key environmental variables identified in the CatBoost model: SST, BloomMaxCHL, TOR, and MLD. SST showed varying correlations with krill habitat suitability across regions. In coastal areas along the continental shelf, lower sea surface temperatures were associated with higher habitat suitability, while south of 60°S, higher SST correlated with higher habitat suitability. Moreover, a negative correlation between krill and SST is observed in coastal areas, while the suitability of krill south of 60°S is positively correlated with SST (Figure 9A). Krill larvae prefer stable temperatures around −1-0°C for hatching, whereas adult krill thrive in warmer waters near 1°C or higher (Thorpe et al., 2019). Thus, while rising ocean temperatures may negatively affect krill hatching, they could benefit adult krill growth. This balance explains why the warming or cooling of sea surface in different sectors of the Southern Ocean from 1997 to 2019 did not result in a significant change in the suitable habitat area for Antarctic krill (Figure 7).

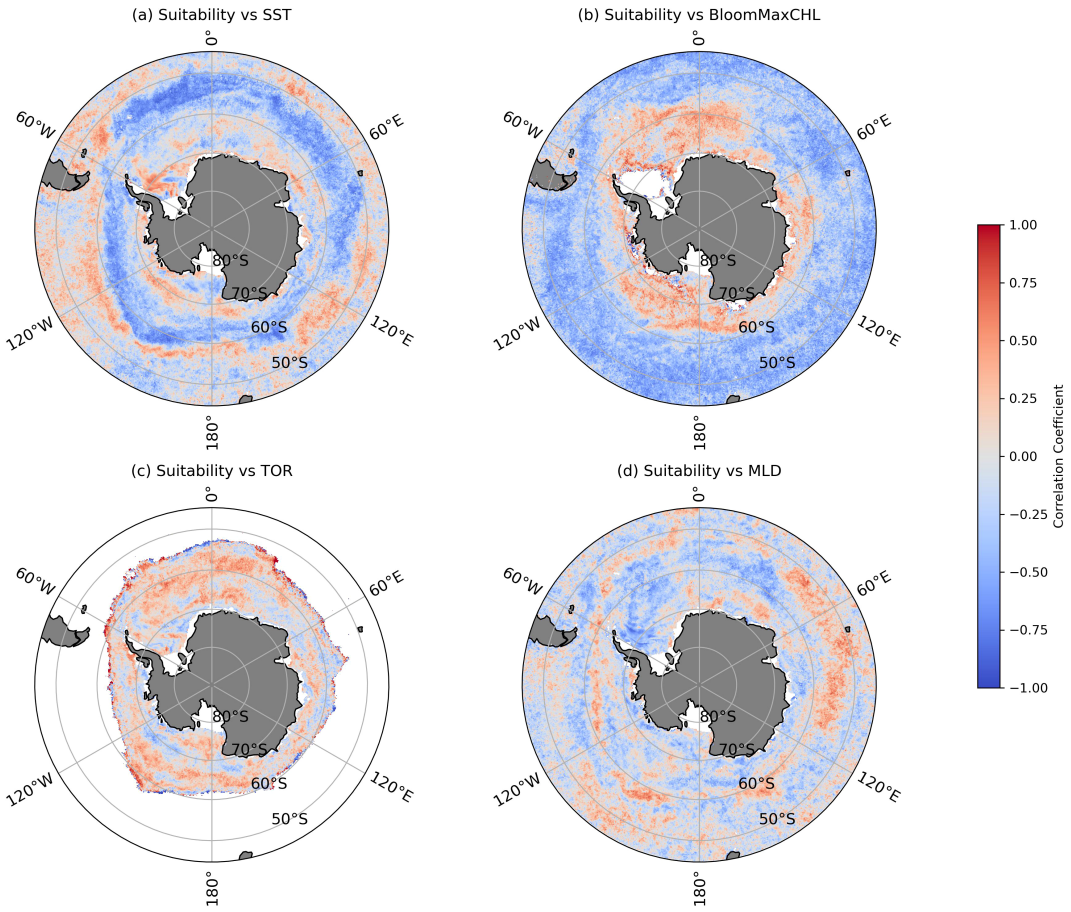


FIGURE 9
Key environmental factors correlation with Antarctic krill total presence days in 1997-2019: **(A)** SST, **(B)** BloomMaxCHL, **(C)** TOR, **(D)** MLD.

A positive correlation was also found between the BloomMaxCHL and krill habitat suitability south of 60°S, indicating that higher food availability supports higher habitat suitability. In contrast, in lower-latitude open ocean regions, significant negative correlations between BloomMaxCHL and krill suitability has been shown (Figure 9B). According to previous research, Antarctic krill exhibit distinct dietary structures between nearshore and open water environments: in nearshore areas, krill predominantly rely on diatoms as their primary food source, while in open waters, diatoms do not serve as the main food source for krill (Cleary et al., 2018). Although this does not rule out the possibility that Antarctic krill in open ocean environments may select diatoms as a primary food source when they are abundant, it is evident that krill gradually shift to copepods as their main food source after the postlarval growth stage (Schmidt et al., 2014). Therefore, we have reason to believe that the habitat suitability of Antarctic krill in open waters north of 60°S is less influenced by the overall abundance of phytoplankton, such as diatoms, due to their selective foraging, which is shaped by the foraging area, their growth stage, and the time of year. Seasonal variations significantly affect primary production and the accessibility of various phytoplankton groups throughout the year: when pelagic phytoplankton stocks, detected by satellite, are low, krill are more likely to seek alternative food sources such as sea ice algae, copepods, and detritus (Meyer et al., 2017).

Sea ice plays a crucial role in supporting phytoplankton reproduction, which in turn boosts krill larvae abundance in sea ice covered areas (Marrari et al., 2008). In the Weddell and Amundsen Seas, positive correlations were between sea ice retreat and habitat suitability, suggesting that later sea ice retreat corresponds to higher habitat suitability (Figure 9C). Longer durations of sea ice cover result in higher krill recruitment, as sea ice provides a source of overwintering influence and refuge for Antarctic krill larvae (Veytia et al., 2021). However, the early retreat of sea ice in the Amundsen Sea indicates a decrease in krill habitat suitability in this region. For larvae, sea ice serves as an essential food source, while it has less impact on adult krill (Walsh et al., 2020). However, the timing of sea ice retreat also determines the timing of phytoplankton blooms, making it a critical factor. The response of Antarctic krill to sea ice retreat may vary across different life stages, potentially even exhibiting opposite effects. This further highlights the differences in krill population structure between the Ross and Atlantic sectors compared to the other two sectors.

Regarding MLD, a positive correlation with krill habitat suitability was observed across most regions of the Southern Ocean, except for the Ross and Weddell Seas, where a negative correlation was found (Figure 9D). This could be caused by strong warming, leading to increased stratification and shallower MLD, which inhibits vertical mixing and limits the supply of oxygenated surface waters to deeper layers, restricting the habitat and reproductive activities of subsurface organisms (Schmidtko et al., 2017; Levin, 2018). Although studies have evaluated the relationship between MLD and krill abundance in the Ross Sea, they have not fully addressed the interannual variability of these factors (Davis et al., 2017). Furthermore, since the habitable range of MLD for Antarctic krill is often an inconsistent range in research studies, the specific biophysical processes in certain areas require further investigation.

Based on the responses of Antarctic krill habitat suitability to the 4 key variables across different regions, we can interpret the trends in Antarctic krill habitat suitability from 1997 to 2020 and their distribution characteristics in the Southern Ocean (Figure 8B). In the Atlantic Sector, the habitat suitability of Antarctic krill exhibited a growing trend in the Weddell Sea and the Antarctic Peninsula from 1997 to 2020. Although the Antarctic Peninsula is a region experiencing rapid warming, leading to a negative hatching environment for krill larvae due to rising sea temperatures, the increase in phytoplankton caused by these temperature rises has provided more food resources for Antarctic krill. In the Ross Sector, due to limitations in the Ross Sea data and the lack of a clear trend, we cannot ascertain the changes in Antarctic krill in this region. However, the suitable habitat area for Antarctic krill in this sector did experience an initial increase followed by a decrease from 1997 to 2020 (Figure 7D). In the Amundsen Sea, a region affected by climate change, despite surface cooling, the earlier retreat of sea ice has led to a decreasing trend near the continental shelf. Conversely, in the open waters at 60°S, Antarctic krill are showing an increasing trend. The reduction in sea ice provides a more prolonged growth window for phytoplankton (Arrigo et al., 2012), which can offer additional food resources for Antarctic krill in this area.

In the Lazarev Sector and Prydz Sector, the habitat suitability trend of Antarctic krill exhibits a pattern of increase, decrease, and then increase from coastal to open waters. The southeastern Antarctic region is experiencing surface cooling, which indicates an expansion of sea ice extent, a shortening of the ice-free period, and a reduction in the duration of summer phytoplankton blooms, ultimately leading to a decline in primary productivity of phytoplankton (Ludescher et al., 2019). Previous studies have documented a shift in the phytoplankton community in the Cosmonaut Sea towards smaller phytoplankton species, which may result in a transition in the zooplankton community structure from krill to salps (Li et al., 2024). Consequently, a declining trend in Antarctic krill is observed between 60°S and 70°S in the southeastern Antarctic, with a more pronounced reduction in habitat suitability for krill in the Prydz Sector since 2011 (Figure 7C). Therefore, the increasing trend of Antarctic krill habitat suitability in coastal areas and at 60°S may indicate a latitudinal migration of krill away from regions with declining phytoplankton productivity.

Overall, the impacts of climate change on the four sectors vary, resulting in different responses from Antarctic krill, making it challenging to explain these changes using a single response model. In the Atlantic Sector, warming and phytoplankton blooms have led to an increase in Antarctic krill. In the Ross Sector, the environmental dynamics of the Amundsen Sea are complex; it is influenced not only by climate factors such as the Southern Annular Mode (SAM) but is also experiencing surface cooling. Observations indicate that the timing of sea ice retreat is occurring earlier, and the ice-free period is extending, contributing to a decline in the krill population. In the Lazarev Sector and Prydz Sector, these areas follow the overall trend observed in the

southeastern Antarctic, characterized by surface cooling and an increase in sea ice extent. The limited growth window for phytoplankton in these regions fails to provide adequate food resources for Antarctic krill, leading to a decrease in their population and a latitudinal migration. Although surface cooling is evident throughout the Southern Ocean, except in the Atlantic Sector, the response to sea ice varies by region; overall, however, these changes present an unfavorable trend for the Antarctic krill population.

4.3 Influence of sea ice on the Antarctic krill distribution of different life stages

The Antarctic krill survey data used in this study were not modeled to assess the habitat of Antarctic krill based on their life stages. This limitation primarily arises from the scarcity of robust data on krill life stages, as well as the challenges in achieving accuracy and consistency in the observation methods. Consequently, there was insufficient data available to train the model with the target metric requiring information such as body length. In this study, a larger amount of available survey data without specifically considering the individual life stages was collected and standardized in order to review the historical habitat suitability of Antarctic krill. Thus, the applicability of this model is subject to specific limitations. By refining relevant indices such as growth potential and recruitment index, as done in other studies (Veytia et al., 2020, 2021), and distinguishing between life stages in the model, we could further improve the capability of the model and obtain a more detailed mechanistic interpretation. Additionally, the influence of sea ice coverage on habitat selection by Antarctic krill is critical; however, the sea ice parameters used in this study are limited. More parameters, such as those related to the marginal ice zone (MIZ), need to be incorporated into the model to enhance the interpretability of sea ice effects (Veytia et al., 2021).

As mentioned earlier, the majority of surveys in this study indicate that adults constitute the primary composition of trawl survey data, compared to the larval and juvenile stages. Eggs and furcilia are likely to occur in open waters as part of their developmental ascent, whereas juveniles are typically found in coastal areas where they are sheltered by sea ice. Given the strong dependency of these life stages on under-ice habitats, the lack of sufficient under-ice survey data in this study hinders a thorough analysis of habitat suitability for juvenile Antarctic krill in nearshore regions. Thus, the inclusion of under-ice survey data is essential in Antarctic krill research. Although previous studies have investigated under-ice environments and their impact on krill distribution (Flores et al., 2012b; Meyer et al., 2017), there remains a lack of integrated long-term data and standardized research from different datasets regarding under-ice surveys. Therefore, the use of autonomous platforms capable of observing hard-to-reach areas like the under-ice environment is necessary. This approach would extend our temporal coverage of krill observations and is required to gain accurate assessments of the relationship between krill and sea ice.

4.4 The CatBoost-based suitability model for presence-absence data

This study utilized the CatBoost algorithm, based on presence-absence data, to construct a habitat suitability model for Antarctic krill and classify their habitat suitability. Previous studies have primarily used the Maxent model with presence-only data to evaluate krill habitat suitability, which led to different classification criteria (Lin et al., 2022). Although Maxent has been widely applied in species distribution modeling (SDM) for krill, it is more suited to regional-scale studies, often failing to converge when applied to larger-scale habitat reconstructions.

Many existing models and predictions for Antarctic krill are based on abundance data, such as the Krill Recruitment Index or growth potential models. However, abundance data often lacks sufficient coverage across life stages and is difficult to standardize, while occurrence data, as used in this study, provides a more comprehensive dataset for model training (Thorpe et al., 2019; Veytia et al., 2021). Most krill abundance models focus on future distribution trends under various climate scenarios, with little focus on historical habitat reconstructions. However, historical reconstructions of Antarctic krill habitat are important as they help to reveal shifts in biogeochemical cycling and predator-prey relationships (Michelson et al., 2023), constrain models of future ecological changes, enhancing predictions about the impacts of ongoing climate change (Strugnell et al., 2022), and aid in managing the expanding krill fishery, ensuring that critical spawning areas are protected (Green et al., 2021). Thus, this study aims to address this gap by offering a broader evaluation of Antarctic krill habitat suitability (Veytia et al., 2020; Lin et al., 2022; Green et al., 2023).

Nevertheless, CatBoost also has limitations in habitat suitability assessment, particularly in the classification of suitability and its relation to abundance or biomass. Further comparisons with other SDM algorithms and validation using actual sampling data are needed to refine the model. Additionally, addressing under-sampled areas in the Southern Ocean is crucial for improving the accuracy and performance of habitat suitability models for Antarctic krill.

5 Conclusion

This study integrates remote sensing and reanalysis data with Antarctic krill survey records to assess habitat suitability for Antarctic krill in the Southern Ocean. Using phytoplankton bloom and sea ice dynamics as timing parameters, a habitat suitability model was constructed using the CatBoost algorithm. For the first time, the long-term interannual variation of Antarctic krill habitat suitability over a span of more than 20 years was obtained. By combining long-term data of Antarctic environmental parameters, the study reveals the mechanisms through which environmental changes influence krill distribution and habitat suitability.

From 1997 to 2019, the ice-free period in the Amundsen Sea extended annually. Simultaneously, the onset of phytoplankton blooms advanced, their duration lengthened, and chlorophyll

concentrations (CHL) during bloom periods steadily increased, particularly in coastal regions. These shifts in bloom timing and sea ice dynamics suggest that climate change is progressively impacting the Southern Ocean ecosystem. The habitat suitability of Antarctic krill is closely tied to these environmental parameters. Specifically, krill prefer areas with lower sea surface temperatures (SST), later sea ice retreat, and higher CHL during bloom periods. Krill juvenile, especially in coastal regions, are highly dependent on these conditions.

Compared to the traditional species distribution model (e.g. Maxent), CatBoost demonstrated superior ability to handle large-scale presence-absence data and provided more stable suitability predictions. The model revealed that timing parameters of bloom phenology and sea ice dynamics were more effective in explaining krill habitat suitability than conventional single-time environmental parameters. For the entire Southern Ocean, the contribution of bloom peak CHL was more indicative of krill habitat suitability than mean CHL, and sea ice retreat timing was more informative than sea ice concentration (SIC).

Model results show varying spatial and temporal trends in krill habitat suitability across different regions of the Southern Ocean between 1997 and 2019. For the four sectors, the area of high suitable habitat of Antarctic krill has shown a decline prior to Southern Annular Mode (SAM) remaining consistently positive. This trend is consistent with the positive state of SAM index. Notably, the area of highly suitable habitat for Antarctic krill in the Prydz sector has shown a significant overall decline over 20 years. The habitat suitability for Antarctic krill is generally higher in coastal areas, with a more extensive range often observed in the southwest Antarctic. In this context, the Weddell Sea has exhibited a noticeable downward trend in habitat suitability, while the Western Antarctic Peninsula has shown a significant upward trend, likely due to its status as a region experiencing rapid warming. The mechanisms of climate change effects in other sectors differ; the surface cooling that leads to increased sea ice and changes in phytoplankton communities has had varied impacts across different sectors.

In this study, we have calculated timing parameters of phytoplankton bloom and sea ice dynamic and developed a CatBoost-based suitability habitat model, reconstructing historical habitat suitability of Antarctic krill in the Southern Ocean over 20 years. The trends and patterns of phytoplankton bloom and sea ice dynamic in the Southern Ocean were identified, while also collecting characteristics on the environmental conditions associated with Antarctic krill presence. Based on predictions of historical habitat suitability, we analyze variations and trends in suitable habitat for Antarctic krill over the years, as well as their responses to climate change impacts, with a focus on four distinct sectors of the Southern Ocean. This study streamlines the standardization process of Antarctic krill survey data and employs innovative machine learning techniques to provide historical reconstruction of Antarctic krill habitat dynamics and fresh insights into the feedback mechanisms of Antarctic krill in response to climate change. By utilizing this approach, future survey data, regardless of the observational methods employed, can be integrated to reconstruct a comprehensive dataset of Antarctic krill observations in the Southern Ocean. This integration will yield a valuable overview of Antarctic krill habitats, inform fisheries management policies and protected area planning, and lay the groundwork for predicting changes in population dynamics and migrations of Antarctic krill under various climate change scenarios. Nevertheless, the application of CatBoost in species distribution modeling research can be further compared with other models to explore its suitability. In the future, under-ice Antarctic krill surveys should be widely utilized to construct a more complete dataset on the life cycle of Antarctic krill for habitat research.

Data availability statement

The original contributions presented in the study are included in the article/Supplementary Material. Further inquiries can be directed to the corresponding author.

Author contributions

YT: Conceptualization, Data curation, Formal analysis, Methodology, Software, Validation, Visualization, Writing – original draft, Writing – review & editing. YB: Conceptualization, Methodology, Writing – review & editing.

Funding

The author(s) declare financial support was received for the research, authorship, and/or publication of this article. This work was supported by the Impact and Response of Antarctic Seas to Climate Change program (grant number IRASCC2020-2022-No. 01-01-03A) and the National Naturel Science Foundation of China under Grant 42176177.

Acknowledgments

We would like to thank the Group for High-Resolution Sea Surface Temperature (GHRSST) for providing SST data (https://www.ncei.noaa.gov/data/sea-surface-temperature-optimum-interpolation), the National Snow and Ice Data Center (NSIDC) for SIC data (https://noaadata.apps.nsidc.org/NOAA/G02135/), and the European Space Agency (ESA) for Ocean Colour Climate Change Initiative (OC-CCI) products (https://www.oceancolour.org/). We also acknowledge the CMCC Global Ocean Physical Reanalysis System (C-GLORS) for providing MLD data (https://data.marine.copernicus.eu/product/) and the Global Biodiversity Information Facility (GBIF) for the Antarctic krill survey data (https://www.gbif.org/). We would also like to thank the staff of the satellite ground station, satellite data processing and sharing center, and marine satellite data online analysis platform (SatCO2) of the State Key Laboratory of Satellite Ocean Environment Dynamics, Second Institute of Oceanography, Ministry of Natural Resources of China (SOED/SIO/MNR) for their help with data processing. Finally, we sincerely thank the

reviewers for their valuable comments and suggestions, which greatly improved the quality of this manuscript.

Conflict of interest

The authors declare that the research was conducted in the absence of any commercial or financial relationships that could be construed as a potential conflict of interest.

Generative AI statement

The author(s) declare that no Generative AI was used in the creation of this manuscript.

Publisher's note

All claims expressed in this article are solely those of the authors and do not necessarily represent those of their affiliated organizations, or those of the publisher, the editors and the reviewers. Any product that may be evaluated in this article, or claim that may be made by its manufacturer, is not guaranteed or endorsed by the publisher.

Supplementary material

The Supplementary Material for this article can be found online at: https://www.frontiersin.org/articles/10.3389/fmars.2025.1513013/full#supplementary-material

References

Arrigo, K. R., Lowry, K. E., and Van Dijken, G. L. (2012). Annual changes in sea ice and phytoplankton in polynyas of the Amundsen Sea, Antarctica. *Deep Sea Res. Part II: Topical Stud. Oceanography* 71-76, 5–15. doi: 10.1016/j.dsr2.2012.03.006

Atkinson, A., Shreeve, R. S., Hirst, A. G., Rothery, P., Tarling, G. A., Pond, D. W., et al. (2006). Natural growth rates in Antarctic krill (Euphausia superba): II. Predictive models based on food, temperature, body length, sex, and maturity stage. *Limnology Oceanography* 51, 973–987. doi: 10.4319/lo.2006.51.2.0973

Bibik, V., Maslennikov, V., Pelevin, A., Petrova, N., Samyshev, E., SoliÂnkin, E., et al. (1988). *Distribution of Euphausia Superba Dana in Relation to Environmental Conditions in the Commonwealth and Cosmonaut Seas*. Moscow: VNIRO Publishers.

Brown, M., Kawaguchi, S., Candy, S., and Virtue, P. (2010). Temperature effects on the growth and maturation of Antarctic krill (Euphausia superba). *Deep Sea Res. Part II: Topical Stud. Oceanography* 57, 672–682. doi: 10.1016/j.dsr2.2009.10.016

Candy, S. G. (2021). Long-term trend in mean density of Antarctic krill (Euphausia superba) uncertain. *Annu. Res. Rev. Biol.* 36, 27–43. doi: 10.9734/arrb/2021/v36i1230460

Cavan, E. L., Belcher, A., Atkinson, A., Hill, S. L., Kawaguchi, S., Mccormack, S., et al. (2019). The importance of Antarctic krill in biogeochemical cycles. *Nat. Commun.* 10, 4742. doi: 10.1038/s41467-019-12668-7

CCAMLR (2008). *Precautionary Catch Limitation on Euphausia superba in Statistical Division 58.4.2* (Hobart, Australia: CCAMLR). Available at: https://cm.ccamlr.org/en/measure-51-03-2008 (Accessed January 06, 2024).

Chang, W., Wang, X., Yang, J., and Qin, T. (2023). An improved catBoost-based classification model for ecological suitability of blueberries. *Sensors* 23 (4), 1811. doi: 10.3390/s23041811

Cleary, A. C., Durbin, E. G., and Casas, M. C. (2018). Feeding by Antarctic krill Euphausia superba in the West Antarctic Peninsula: differences between fjords and open waters. *Mar. Ecol. Prog. Ser.* 595, 39–54. doi: 10.3354/meps12568

Croxall, J. P., Reid, K., and Prince, P. A. (1999). Diet, provisioning and productivity responses of marine predators to differences in availability of Antarctic krill. *Mar. Ecol. Prog. Ser.* 177, 115–131. doi: 10.3354/meps177115

Davis, L. B., Hofmann, E. E., Klinck, J. M., Piñones, A., and Dinniman, M. S. (2017). Distributions of krill and Antarctic silverfish and correlations with environmental variables in the western Ross Sea, Antarctica. *Mar. Ecol. Prog. Ser.* 584, 45–65. doi: 10.3354/meps12347

Ferreira, A., Brito, A. C., Mendes, C. R. B., Brotas, V., Costa, R. R., Guerreiro, C. V., et al. (2022). OC4-SO: A new chlorophyll-a algorithm for the western Antarctic peninsula using multi-sensor satellite data. *Remote Sens.* 14 (5), 1052. doi: 10.3390/rs14051052

Fetterer, F., Knowles, K., Meier, W. N., Savoie, M., and Windnagel, A. K. (2017). *Sea Ice Index, Version 3 Sea ice concentration* (Boulder, Colorado USA: National Snow and Ice Data Center).

Flores, H., Atkinson, A., Kawaguchi, S., Krafft, B. A., Milinevsky, G., Nicol, S., et al. (2012a). Impact of climate change on Antarctic krill. *Mar. Ecol. Prog. Ser.* 458, 1–19. doi: 10.3354/meps09831

Flores, H., Van Franeker, J. A., Siegel, V., Haraldsson, M., Strass, V., Meesters, E. H., et al. (2012b). The association of Antarctic krill Euphausia superba with the under-ice habitat. *PloS One* 7, e31775. doi: 10.1371/journal.pone.0031775

Fogt, R. L., and Marshall, G. J. (2020). The Southern Annular Mode: Variability, trends, and climate impacts across the Southern Hemisphere. *WIREs Climate Change* 11, e652. doi: 10.1002/wcc.v11.4

Friedlaender, A. S., Johnston, D. W., Fraser, W. R., Burns, J., Patrick N, H., and Costa, D. P. (2011). Ecological niche modeling of sympatric krill predators around Marguerite Bay, Western Antarctic Peninsula. *Deep Sea Res. Part II: Topical Stud. Oceanography* 58, 1729–1740. doi: 10.1016/j.dsr2.2010.11.018

Greaves, B. L., Davidson, A. T., Fraser, A. D., Mckinlay, J. P., Martin, A., Mcminn, A., et al. (2020). The Southern Annular Mode (SAM) influences phytoplankton communities in the seasonal ice zone of the Southern Ocean. *Biogeosciences* 17, 3815–3835. doi: 10.5194/bg-17-3815-2020

Green, D. B., Bestley, S., Corney, S. P., Trebilco, R., Lehodey, P., and Hindell, M. A. (2021). Modeling Antarctic krill circumpolar spawning habitat quality to identify regions with potential to support high larval production. *Geophysical Res. Lett.* 48, e2020GL091206. doi: 10.1029/2020GL091206

Green, D. B., Titaud, O., Bestley, S., Corney, S. P., Hindell, M. A., Trebilco, R., et al. (2023). KRILLPODYM: a mechanistic, spatially resolved model of Antarctic krill distribution and abundance. *Front. Mar. Sci.* 10. doi: 10.3389/fmars.2023.1218003

Hancock, J. T., and Khoshgoftaar, T. M. (2020). CatBoost for big data: an interdisciplinary review. *J. Big Data* 7, 94. doi: 10.1186/s40537-020-00369-8

Hobbs, W. R., Massom, R., Stammerjohn, S., Reid, P., Williams, G., and Meier, W. (2016). A review of recent changes in Southern Ocean sea ice, their drivers and forcings. *Global Planetary Change* 143, 228–250. doi: 10.1016/j.gloplacha.2016.06.008

Hosking, J. S., Orr, A., Marshall, G. J., Turner, J., and Phillips, T. (2013). The influence of the Amundsen–Bellingshausen seas low on the climate of west Antarctica and its representation in coupled climate model simulations. *J. Climate* 26, 6633–6648. doi: 10.1175/JCLI-D-12-00813.1

Huang, B., Liu, C., Banzon, V., Freeman, E., Graham, G., Hankins, B., et al. (2021). Improvements of the daily optimum interpolation sea surface temperature (DOISST) version 2.1. *J. Climate* 34, 2923–2939. doi: 10.1175/JCLI-D-20-0166.1

Huang, Y., Ma, R., Li, J., and Tu, S. (2023). Sea surface temperature changes reflected by diatoms in the P6-10 core from 1893 to 2013 from Prydz bay, Antarctica. *J. Mar. Sci. Eng.* 11 (7), 1428. doi: 10.3390/jmse11071428

Huot, P.-V., Fichefet, T., Jourdain, N. C., Mathiot, P., Rousset, C., Kittel, C., et al. (2021). Influence of ocean tides and ice shelves on ocean–ice interactions and dense shelf water formation in the D'Urville Sea, Antarctica. *Ocean Model.* 162, 101794. doi: 10.1016/j.ocemod.2021.101794

Kang, S. M., Yu, Y., Deser, C., Zhang, X., Kang, I.-S., Lee, S.-S., et al. (2023). Global impacts of recent Southern Ocean cooling. *Proc. Natl. Acad. Sci.* 120, e2300881120. doi: 10.1073/pnas.2300881120

Kawaguchi, S., Ishida, A., King, R., Raymond, B., Waller, N., Constable, A., et al. (2013). Risk maps for Antarctic krill under projected Southern Ocean acidification. *Nat. Climate Change* 3, 843–847. doi: 10.1038/nclimate1937

Kawaguchi, S., Steven, G. C., Robert, K., Mikio, N., and Stephen, N. (2006). Modelling growth of Antarctic krill. I. Growth trends with sex, length, season, and region. *Mar. Ecol. Prog. Ser.* 306, 1–15. doi: 10.3354/meps306001

Kohlbach, D., Lange, B. A., Schaafsma, F. L., David, C., Vortkamp, M., Graeve, M., et al. (2017). Ice algae-produced carbon is critical for overwintering of Antarctic krill Euphausia superba. *Front. Mar. Sci.* 4. doi: 10.3389/fmars.2017.00310

Kostov, Y., Marshall, J., Hausmann, U., Armour, K. C., Ferreira, D., and Holland, M. M. (2017). Fast and slow responses of Southern Ocean sea surface temperature to SAM in coupled climate models. *Climate Dynamics* 48, 1595–1609. doi: 10.1007/s00382-016-3162-z

Kusahara, K., Williams, G. D., Massom, R., Reid, P., and Hasumi, H. (2017). Roles of wind stress and thermodynamic forcing in recent trends in Antarctic sea ice and Southern Ocean SST: An ocean-sea ice model study. *Global Planetary Change* 158, 103–118. doi: 10.1016/j.gloplacha.2017.09.012

Kvile, K.Ø., Ashjian, C., Feng, Z., Zhang, J., and Ji, R. (2018). Pushing the limit: Resilience of an Arctic copepod to environmental fluctuations. *Global Change Biol.* 24, 5426–5439. doi: 10.1111/gcb.2018.24.issue-11

Levin, L. A. (2018). Manifestation, drivers, and emergence of open ocean deoxygenation. *Annu. Rev. Mar. Sci.* 10, 229–260. doi: 10.1146/annurev-marine-121916-063359

Li, X., Holland, D. M., Gerber, E. P., and Yoo, C. (2014). Impacts of the north and tropical Atlantic Ocean on the Antarctic Peninsula and sea ice. *Nature* 505, 538–542. doi: 10.1038/nature12945

Li, Y., Zhao, J., Li, D., Pan, J., He, J., Hu, J., et al. (2024). Factors controlling the phytoplankton crops, taxonomic composition, and particulate organic carbon stocks in the Cosmonaut Sea, East Antarctica. *J. Oceanology Limnology*. 42, 1859–1908. doi: 10.1007/s00343-024-3198-6

Lin, S., Zhao, L., and Feng, J. (2022). Predicted changes in the distribution of Antarctic krill in the Cosmonaut Sea under future climate change scenarios. *Ecol. Indic.* 142, 109234. doi: 10.1016/j.ecolind.2022.109234

Ludescher, J., Yuan, N., and Bunde, A. (2019). Detecting the statistical significance of the trends in the Antarctic sea ice extent: an indication for a turning point. *Climate Dynamics* 53, 237–244. doi: 10.1007/s00382-018-4579-3

Manel, S., Williams, H. C., and Ormerod, S. J. (2001). Evaluating presence–absence models in ecology: the need to account for prevalence. *J. Appl. Ecol.* 38, 921–931. doi: 10.1046/j.1365-2664.2001.00647.x

Marrari, M., Daly, K. L., and Hu, C. (2008). Spatial and temporal variability of SeaWiFS chlorophyll a distributions west of the Antarctic Peninsula: Implications for krill production. *Deep Sea Res. Part II: Topical Stud. Oceanography* 55, 377–392. doi: 10.1016/j.dsr2.2007.11.011

Marshall, G. J. (2003). Trends in the Southern Annular Mode from observations and reanalyses. *J. Clim.* 16, 4134-4143. doi: 10.1175/1520-0442(2003)016<4134:TITSAM>2.0.CO;2

Meyer, B., Atkinson, A., Bernard, K. S., Brierley, A. S., Driscoll, R., Hill, S. L., et al. (2020). Successful ecosystem-based management of Antarctic krill should address uncertainties in krill recruitment, behaviour and ecological adaptation. *Commun. Earth Environ.* 1, 28. doi: 10.1038/s43247-020-00026-1

Meyer, B., Freier, U., Grimm, V., Groeneveld, J., Hunt, B. P. V., Kerwath, S., et al. (2017). The winter pack-ice zone provides a sheltered but food-poor habitat for larval Antarctic krill. *Nat. Ecol. Evol.* 1, 1853–1861. doi: 10.1038/s41559-017-0368-3

Meyer, B., Fuentes, V., Guerra, C., Schmidt, K., Atkinson, A., Spahic, S., et al. (2009). Physiology, growth, and development of larval krill Euphausia superba in autumn and winter in the Lazarev Sea, Antarctica. *Limnology Oceanography* 54, 1595–1614. doi: 10.4319/lo.2009.54.5.1595

Michelson, C. I., Polito, M. J., Wunder, M. B., Emslie, S. D., Mccarthy, M. D., Patterson, W. P., et al. (2023). Holocene climate change shifted Southern Ocean biogeochemical cycling and predator trophic dynamics. *Limnology Oceanography* 68, 2642–2653. doi: 10.1002/lno.v68.12

Murase, H., Kitakado, T., Hakamada, T., Matsuoka, K., Nishiwaki, S., and Naganobu, M. (2013). Spatial distribution of Antarctic minke whales (Balaenoptera bonaerensis) in relation to spatial distributions of krill in the Ross Sea, Antarctica. *Fisheries Oceanography* 22, 154–173. doi: 10.1111/fog.2013.22.issue-3

Nachtsheim, D. A., Jerosch, K., Hagen, W., Plötz, J., and Bornemann, H. (2017). Habitat modelling of crabeater seals (Lobodon carcinophaga) in the Weddell Sea using the multivariate approach Maxent. *Polar Biol.* 40, 961–976. doi: 10.1007/s00300-016-2020-0

Pezza, A. B., Rashid, H. A., and Simmonds, I. (2012). Climate links and recent extremes in antarctic sea ice, high-latitude cyclones, Southern Annular Mode and ENSO. *Climate Dynamics* 38, 57–73. doi: 10.1007/s00382-011-1044-y

Phillips, S. J., Anderson, R. P., and Schapire, R. E. (2006). Maximum entropy modeling of species geographic distributions. *Ecol. Model.* 190, 231–259. doi: 10.1016/j.ecolmodel.2005.03.026

Piñones, A., and Fedorov, A. V. (2016). Projected changes of Antarctic krill habitat by the end of the 21st century. *Geophysical Res. Lett.* 43, 8580–8589. doi: 10.1002/2016GL069656

Platt, T., Fuentes-Yaco, C., and Frank, K. T. (2003). Spring algal bloom and larval fish survival. *Nature* 423, 398–399. doi: 10.1038/423398b

Prokhorenkova, L., Gusev, G., Vorobev, A., Dorogush, A. V., and Gulin, A. (2018). CatBoost: unbiased boosting with categorical features. *Adv. Neural Inf. Process. Syst.* 31, 6639–6649. doi: 10.5555/3327757.3327770

Sabu, P., Subeesh, M. P., Sivakrishnan, K. K., and Anilkumar, N. (2021). Causes and impacts of anomalous warming in the Prydz Bay, East Antarctica during austral summer 2016-17. *Polar Sci.* 30, 100660. doi: 10.1016/j.polar.2021.100660

Sathyendranath, S. J., Brockmann, C., Brotas, V., Calton, B., Chuprin, A., Clements, O., et al. (2021). *ESA Ocean Colour Climate Change Initiative (Ocean_Colour_cci): Version 5.0 Data. 5.0 ed* (NERC EDS Centre for Environmental Data Analysis). United Kingdom: Plymouth Marine Laboratory (Science Lead), Germany: Brockmann Consult and HEREON, France: Joint Research Centre in the EU, HYGEOS, Italy: CNR, Portugal: Foundation of the Faculty of Sciences of the University of Lisbon. doi: 10.5285/1dbe7a109c0244aaad713e078fd3059a

Sato, K., Inoue, J., Simmonds, I., and Rudeva, I. (2021). Antarctic Peninsula warm winters influenced by Tasman Sea temperatures. *Nat. Commun.* 12, 1497. doi: 10.1038/s41467-021-21773-5

Schmidt, K., Atkinson, A., Pond, D. W., and Ireland, L. C. (2014). Feeding and overwintering of Antarctic krill across its major habitats: The role of sea ice cover, water depth, and phytoplankton abundance. *Limnology Oceanography* 59, 17–36. doi: 10.4319/lo.2014.59.1.0017

Schmidtko, S., Stramma, L., and Visbeck, M. (2017). Decline in global oceanic oxygen content during the past five decades. *Nature* 542, 335–339. doi: 10.1038/nature21399

Siegel, V. (2016). "Introducing Antarctic krill Euphausia superba Dan," in *Biology and Ecology of Antarctic Krill* (Springer International Publishing, Cham), 1–19.

Siegel, D. A., Doney, S. C., and Yoder, J. A. (2002). The north Atlantic spring phytoplankton bloom and Sverdrup's critical depth hypothesis. *Science* 296, 730–733. doi: 10.1126/science.1069174

Stammerjohn, S. E., Martinson, D. G., Smith, R. C., Yuan, X., and Rind, D. (2008). Trends in Antarctic annual sea ice retreat and advance and their relation to El Niño–Southern Oscillation and Southern Annular Mode variability. *J. Geophysical Research: Oceans* 113, C03S90. doi: 10.1029/2007JC004269

Storto, A., and Masina, S. (2016). C-GLORSv5: an improved multipurpose global ocean eddy-permitting physical reanalysis. *Earth Syst. Sci. Data* 8, 679–696. doi: 10.5194/essd-8-679-2016

Strugnell, J. M., Mcgregor, H. V., Wilson, N. G., Meredith, K. T., Chown, S. L., Lau, S. C. Y., et al. (2022). Emerging biological archives can reveal ecological and climatic change in Antarctica. *Global Change Biol.* 28, 6483–6508. doi: 10.1111/gcb.v28.22

Taylor, A. T., Hafen, T., Holley, C. T., González, A., and Long, J. M. (2020). Spatial sampling bias and model complexity in stream-based species distribution models: A case study of Paddlefish (Polyodon spathula) in the Arkansas River basin, USA. *Ecol. Evol.* 10, 705–717. doi: 10.1002/ece3.v10.2

Thomalla, S. J., Nicholson, S.-A., Ryan-Keogh, T. J., and Smith, M. E. (2023). Widespread changes in Southern Ocean phytoplankton blooms linked to climate drivers. *Nat. Climate Change* 13, 975–984. doi: 10.1038/s41558-023-01768-4

Thorpe, S. E., Tarling, G. A., and Murphy, E. J. (2019). Circumpolar patterns in Antarctic krill larval recruitment: an environmentally driven model. *Mar. Ecol. Prog. Ser.* 613, 77–96. doi: 10.3354/meps12887

Trathan, P. N., Brierley, A. S., Brandon, M. A., Bone, D. G., Goss, C., Grant, S. A., et al. (2003). Oceanographic variability and changes in Antarctic krill (Euphausia superba) abundance at South Georgia. *Fisheries Oceanography* 12, 569–583. doi: 10.1046/j.1365-2419.2003.00268.x

Trathan, P. N., Fielding, S., Warwick-Evans, V., Freer, J., and Perry, F. (2022). Seabird and seal responses to the physical environment and to spatio-temporal variation in the distribution and abundance of Antarctic krill at South Georgia, with implications for local fisheries management. *ICES J. Mar. Sci.* 79, 2373–2388. doi: 10.1093/icesjms/fsac168

Trathan, P. N., and Hill, S. L. (2016). "The importance of krill predation in the Southern Ocean," in *Biology and Ecology of Antarctic Krill*. Ed. V. Siegel (Springer International Publishing, Cham), 321–350.

Turner, J. S., Dierssen, H., Schofield, O., Kim, H. H., Stammerjohn, S., Munro, D. R., et al. (2024). Changing phytoplankton phenology in the marginal ice zone west of the Antarctic Peninsula. *Mar. Ecol. Prog. Ser.* 734, 1–21. doi: 10.3354/meps14567

Veytia, D., Bestley, S., Kawaguchi, S., Meiners, K. M., Murphy, E. J., Fraser, A. D., et al. (2021). Overwinter sea-ice characteristics important for Antarctic krill recruitment in the southwest Atlantic. *Ecol. Indic.* 129, 107934. doi: 10.1016/j.ecolind.2021.107934

Veytia, D., Corney, S., Meiners, K. M., Kawaguchi, S., Murphy, E. J., and Bestley, S. (2020). Circumpolar projections of Antarctic krill growth potential. *Nat. Climate Change* 10, 568–575. doi: 10.1038/s41558-020-0758-4

Walsh, J., Reiss, C. S., and Watters, G. M. (2020). Flexibility in Antarctic krill Euphausia superba decouples diet and recruitment from overwinter sea-ice conditions in the northern Antarctic Peninsula. *Mar. Ecol. Prog. Ser.* 642, 1–19. doi: 10.3354/meps13325

Yang, G., Atkinson, A., Hill, S. L., Guglielmo, L., Granata, A., and Li, C. (2021). Changing circumpolar distributions and isoscapes of Antarctic krill: Indo-Pacific habitat refuges counter long-term degradation of the Atlantic sector. *Limnology Oceanography* 66, 272–287. doi: 10.1002/lno.11603

frontiers | Frontiers in Marine Science

TYPE Original Research
PUBLISHED 26 March 2025
DOI 10.3389/fmars.2025.1448250

Check for updates

OPEN ACCESS

EDITED BY
Steven Parker,
Commission for the Conservation of Antarctic Marine Living Resources (CCAMLR), Australia

REVIEWED BY
Erica Jarvis Mason,
National Oceanic and Atmospheric Administration, United States
Sisong Dong,
Shanghai Ocean University, China

*CORRESPONDENCE
Dale Maschette
Dale.Maschette@utas.edu.au

RECEIVED 13 June 2024
ACCEPTED 24 February 2025
PUBLISHED 26 March 2025

CITATION
Maschette D, Wotherspoon S, Murase H, Kelly N, Ziegler P, Swadling KM and Kawaguchi S (2025) Resource potential and maturity estimates of *Euphausia superba* in East Antarctica.
Front. Mar. Sci. 12:1448250.
doi: 10.3389/fmars.2025.1448250

COPYRIGHT
© 2025 Maschette, Wotherspoon, Murase, Kelly, Ziegler, Swadling and Kawaguchi. This is an open-access article distributed under the terms of the Creative Commons Attribution License (CC BY). The use, distribution or reproduction in other forums is permitted, provided the original author(s) and the copyright owner(s) are credited and that the original publication in this journal is cited, in accordance with accepted academic practice. No use, distribution or reproduction is permitted which does not comply with these terms.

Resource potential and maturity estimates of *Euphausia superba* in East Antarctica

Dale Maschette[1,2]*, Simon Wotherspoon[1], Hiroto Murase[3], Nat Kelly[1], Philippe Ziegler[1], Kerrie M. Swadling[2,4] and So Kawaguchi[1,4]

[1]Department of Climate Change, Energy, the Environment and Water, Australian Antarctic Division, Kingston, TAS, Australia, [2]Institute for Marine and Antarctic Studies (IMAS), University of Tasmania, Hobart, TAS, Australia, [3]Tokyo University of Marine Science and Technology, Tokyo, Japan, [4]Australian Antarctic Program Partnership, University of Tasmania, Hobart, TAS, Australia

The East Antarctic krill fisheries are spread across two Divisions of the Commission for the Conservation of Antarctic Marine Living Resources (CCAMLR), Division 58.4.1 between 80-150°E and Division 58.4.2 between 30-80°E. Each of these Divisions is further divided into East and West subregions with separate catch limits. In 2019, CCAMLR agreed to a revised krill fishery management strategy recommended by the Scientific Committee. This strategy consists of setting catch limits for *Euphausia superba* using three combined approaches; 1) an acoustic biomass estimate, 2) a precautionary harvest rate derived from a stock assessment and 3) a spatial allocation of catch limits based on overlap of predator needs. Using recent survey data we estimate 50% length at maturity for *E. superba* to be 41.67 mm and 42.29 mm for Divisions 58.4.1 and 58.4.2 respectively. In both areas females were estimated to reach 50% maturity at a smaller length than males. Using these updated estimates of *E. superba* length at maturity and a new implementation of the Generalized Yield Model (the Grym), we estimate precautionary harvest rates for krill in Divisions 58.4.1 and 58.4.2-East ranging between 0.0854 - 0.1201. These calculated harvest rates were then applied to the biomass estimates from recent surveys to estimate total precautionary catch limits for *E. superba* in Divisions 58.4.1 (391,754 tonnes) and 58.4.2 East (640,872 tonnes). These catch limits are based on biomass estimates from a 2019 survey conducted by Japan in Division 58.4.1 and a 2021 survey conducted by Australia in Division 58.4.2 East.

KEYWORDS

krill, fishery, precautionary catch limit, generalised yield model, Grym, CCAMLR, stock assessment

1 Introduction

Antarctic krill (*Euphausia superba*, hereafter krill) is a key species in Southern Ocean ecosystems. Krill is a major grazer of primary production and forms the main prey for many marine predators such as fish, penguins, flying seabirds, seals, and whales (Everson, 2000) as well as playing an important role in marine biogeochemical cycles in the region

(Cavan et al., 2019). Krill is also the target of the region's largest fishery which is managed by the Commission for the Conservation of Antarctic Marine Living Resources (CCAMLR) (Nicol et al., 2012). CCAMLR is divided into three statistical areas for management purposes: Area 48 (Atlantic Ocean Sector, 70°W–30°E), Area 58 (Indian Ocean Sector, 30°E–150°E) and Area 88 (Pacific Ocean Sector, 150°E–70°W). These areas are further subdivided into statistical Subareas and Divisions (Figure 1).

The krill fishery initially commenced in the 1970s in Area 58 in the Southern Ocean, then spread around the Antarctic continent to the Antarctic Peninsula in Area 48. Since the 1990s, the fishery has been almost exclusively focused in Area 48, and the fishing within this sector has further concentrated to only a few, relatively small locations (Kawaguchi and Nicol, 2020). Krill fishing has grown rapidly since ~ 2010, with recent increasing commercial interest in krill oil driving annual catches to levels previously recorded in the 1980s. Over the last few years, the krill fishery has regularly reached the catch limits on the main fishing ground in the Antarctic Peninsula region (Subarea 48.1) and expanded to other fishing grounds within the Southwest Atlantic sector (such as Subarea 48.2) in the middle of the season. There has also been interest in resuming krill fishing in Area 58, with some activity between 2016/17 and 2018/19 (CCAMLR, 2022).

The Antarctic environment is changing rapidly, and these changes are considered to affect the krill population in a range of ways, including shifts in habitat, physiology, and biomass (Kawaguchi et al., 2024). While CCAMLR's management procedure takes into account the uncertainty in the long-term dynamics of krill stocks through projections, overall catch limits are likely to be sensitive to changes in biological parameters (such as relationships of length to weight, maturity, and age), and hence management advice is likely to be more robust if derived from multiple surveys and/or more contemporary information. Spatial allocations of catch limits would also benefit from better understanding of variation in the spatial distribution of krill.

In Area 48, there has been recognition of the risk of concentrating krill fishing effort in small areas where central-place foragers also feed (Constable and Nicol, 2002; Watters et al., 2020). As a result, CCAMLR has adopted the concept of small-scale management units (SSMUs), which aim to break up large management areas into smaller areas with their own catch limits, in turn limiting concentrated fishing and spreading the risk of fishing across a broader spatial area (Hewitt et al, 2004). Since their introduction, however, CCAMLR has been unable to reach consensus on allocation of Subarea catch limits to the SSMUs. Notably, due to a lack of recent krill fishing, Area 58 has received less attention or emphasis in ensuring mechanisms are in place to avoid localized risks. Upon joining CCAMLR, member parties agree to be legally bound by 'Conservation Measures' (CM) which are agreed each year by the CCAMLR Commission (Constable, 2011). The CMs, among other things, outline the spatial areas and catch limits for all fisheries within the CCAMLR Convention Area. Specified within CM 51-02 and CM 51-03, the Area 58 krill fisheries (and subsequent catch limits) are subdivided into Division 58.4.1 (80–150°

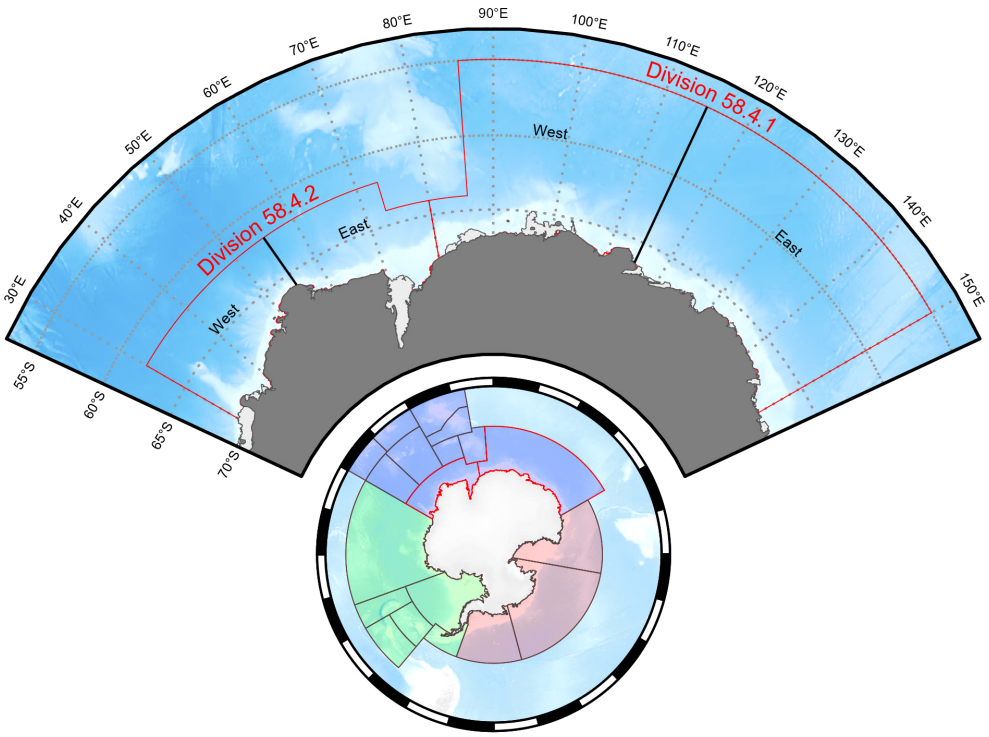


FIGURE 1
Management areas of the Commission of the Conservation of Antarctic Marine Living Resources (Bottom circle) showing Area 48 (green), Area 58 (blue) and Area 88 (red). Division 58.4.1 and Division 58.4.2 (Top arc) showing current management splits for the krill management into east and west regions in each Division. Maps produced with the SOmap package in R (Maschette et al., 2019).

E) and Division 58.4.2 (30–80°E) respectively. The current catch limits for these two areas are 440 000 tonnes in Division 58.4.1 and 2.645 million tonnes in Division 58.4.2.

Current precautionary catch limits and trigger levels in Area 58 have been set based on information collected through two large-scale surveys conducted by Australia, the BROKE (Baseline Research on Oceanography, Krill and the Environment) survey in Division 58.4.1 in 1996 (Nicol, 2000) and the BROKE West survey in Division 58.4.2 in 2006 (Nicol et al., 2010). Catch limits for each Division are further split into east and west subdivisions. In 2019, the CAMLR Commission endorsed a revised krill fishery management strategy recommended by the Scientific Committee (CCAMLR, 2019, para. 5.17). This management strategy consists of three elements:

1. a stock assessment to estimate precautionary harvest rates (defined as γ).
2. regular updates of biomass estimates, initially at the subarea scale, but potentially at multiple scales.
3. a spatial overlap analysis framework to inform the spatial allocation of catch.

Most of the work undertaken since then has focused on the areas covered by Conservation Measure 51-07, specifically Subarea 48.1. In Area 58, two surveys have been conducted recently, the first by Japan in Division 58.4.1 in 2018/19 (Abe et al., 2023) and the second by Australia in the eastern sector of Division 58.4.2 (55–80° E) in 2021 (Cox et al., 2022). These provide the necessary data for updating biological parameters (such as length, sex, or maturity; e.g., Schaafsma et al., 2024) and precautionary catch allocations in these Divisions. Here, we provide results from updated stock assessments for both Divisions 58.4.1 and 58.4.2, addressing the first element of the new krill management strategy, i.e., estimating precautionary harvest rates, in these areas.

The Generalised Yield Model (GYM) is an assessment model for assessing the status of stocks under various levels of uncertainty using either deterministic (for icefish) or stochastic (for other species) projections (Constable and de la Mare, 1996; Constable, 2004). The core functionality of the GYM is to project stock abundance, biomass, and yield in each age class forward in time over a single year. The GYM assumes the number, biomass, and yield of individuals of an age class, in a year, at specified timesteps within the year satisfy the system of differential equations with an adaptive Runge-Kutta scheme outlined in Constable and de la Mare (1996). Unlike more modern stock assessment models which integrate observation data to estimate population parameters within the model runs, GYM assessments for krill used pre-calculated parameter values with uncertainty to project the population forward. As noted by Thomson (2016) this provided CCAMLR with an innovative solution to the problem of calculating harvest rates for stock about which little was known, and for which fisheries data were absent. The GYM was reexamined by Maschette et al. (2023), the outcome of which was the development of the Grym model framework which provides same utility of the GYM but with a more exact solution by replacing the adaptive Runge-Kutta scheme with a composite trapezoidal rule. Additionally, by being implemented in an open-source language (Wotherspoon and Maschette, 2023) the Grym has overcome issues highlighted by Kinzey et al. (2013) of pre-termination in the GYM software, and allowed for further expansion of capability such as those implemented by Liu et al. (2023) on incorporating multiple fishing fleets into projections.

Within stock assessment models' maturity ogives are used to indicate for a given length (or age) class what proportion of individuals are mature (spawning), and ultimately the size of the spawning stock biomass (SSB). As such, changing the underlying shape or distribution used for estimating the ogive function implemented in a stock assessment may lead to quite different estimates of SSB when given the same data. To allow for stock assessments that reflect current population parameters we have re-estimated size at maturity using a ramped ogive function following the methods outlined in Maschette and Wotherspoon (2023) and expanded on these methods to estimate a logistic-based size at maturity for comparison with results using the ramped ogive function.

The results from our krill stock assessments provide precautionary harvest rates for Divisions 58.4.1 and 58.4.2. Similar to the process undertaken in 2021 for Subarea 48.1 (Maschette et al., 2021), these harvest rates are then applied to the recent survey estimates of biomass in Division 58.4.1 (Abe et al., 2023) and 58.4.2 East (Cox et al., 2022) to derive updated precautionary catch limits.

2 Methods

2.1 Maturity-at-length estimation

2.1.1 Modelling maturity within Grym projections

The Grym (Maschette et al., 2023) when used for krill currently models maturity-at-length with a ramp-shaped ogive function (rampOgive in the Grym R package; Wotherspoon and Maschette, 2023) to be consistent with the original Generalized Yield Model implementation (Constable and de la Mare, 1996):

$$p(l) = \begin{cases} 0 & l \leq L - \frac{w}{2} \\ \frac{l-L}{w} + \frac{1}{2} & L - \frac{w}{2} < \ l < L + \frac{w}{2} \\ 1 & l \geq L + \frac{w}{2} \end{cases}$$

where $p(l)$ represents the proportion of individuals of length l that are mature, L is the length at which 50% of all individuals are mature, and w is the width of the ramp.

For the krill stock assessments, within each projection L and w are held constant, but for each individual projection L is drawn from a uniform distribution with limits L_{min} and L_{max}:

$$L \sim U(L_{min}, L_{max}) .$$

Maschette et al. (2021) and Maschette and Wotherspoon (2023) used these to be consistent with previous assessments for krill performed within CCAMLR. Recently, however, functionality has been added to the Grym package to model selectivity and maturity using logistic ogive functions. For consistency with the stock

assessment framework CASAL (Bull et al., 2012), which is used for many fish stock assessments in CCAMLR, the logistic model is parameterized in terms of the 50% and 95% quantiles and uses a constant of 19 (See Bull et al., 2012 for details), so that:

$$p(l) = \left[1 + \exp\left(-\log(19)\frac{l - q_{50}}{d_{95}}\right)\right]^{-1}$$

where q_{50} and q_{95} are the 50% and 95% quantiles respectively and $d_{95} = q_{95} - q_{50}$ .Within an individual projection run q_{50} and d_{95} (and hence q_{95}) are held constant across years, between projection runs however, q_{50} and d_{95} are drawn from a multivariate normal distribution:

$$\begin{pmatrix} q_{50} \\ d_{95} \end{pmatrix} \sim \mathrm{N}(\boldsymbol{\mu}, \Sigma)$$

with mean μ and variance covariance matrix Σ. The use of d_{95} allows the stock assessment model to maintain the same shape for the logistic ogive relative to each randomly drawn value of q_{50} when a range of q_{50} values are provided.

2.1.2 Modelling maturity input parameters for the Grym

2.1.2.1 Available data

RMT 8 nets with 8m2 mouth opening and mesh size of 4.5mm were used for either 'target-trawls,' i.e., responsive fishing when krill-like echoes were observed using the vessel's echo sounders, or routine trawls (i.e., oblique tows at pre-planned survey stations). Trawls were hauled at approximately 2 knots through water speed and routine trawls sampled the upper 200 m of the water column. Because the total number of krill captured at predetermined stations was generally small, the length measurements of predetermined and targeted stations were both used. Total length of krill (Standard 1; Morris et al., 1988) for up to 150 individuals were measured per station.

Within Division 58.4.1, data collected on board the *RV Kaiyo-maru* during the Japanese KY1804 survey in 2018/19 (Figure 2, Abe et al., 2023) contain length and maturity observations from 4632 krill consisting of 1124 juveniles, 1245 males and 1824 females ranging from 14 - 63 mm collected in 45 hauls (Figure 3). For Division 58.4.2, data were collected on the *RV Investigator* TEMPO voyage in 2021 (Figure 2, Cox et al., 2022) and contain length and maturity observations from 2761 krill consisting of 714 juveniles, 1032 males and 1015 females ranging from 14 - 56 mm collected in 27 hauls (Figure 3).

In both data sets, krill exhibiting maturity stages F3B to F3E and M3 were considered mature individuals (Makarov and Denys, 1980). Additionally, all krill less than 30 mm in length were designated as immature (Tarling et al., 2016; Pakhomov, 1995a). For each region maturity was estimated for ramp and logistic o-gives for all sexes, and for males and females. Due to the inability to know whether juveniles were male or female, they were included in both the male and female maturity estimates.

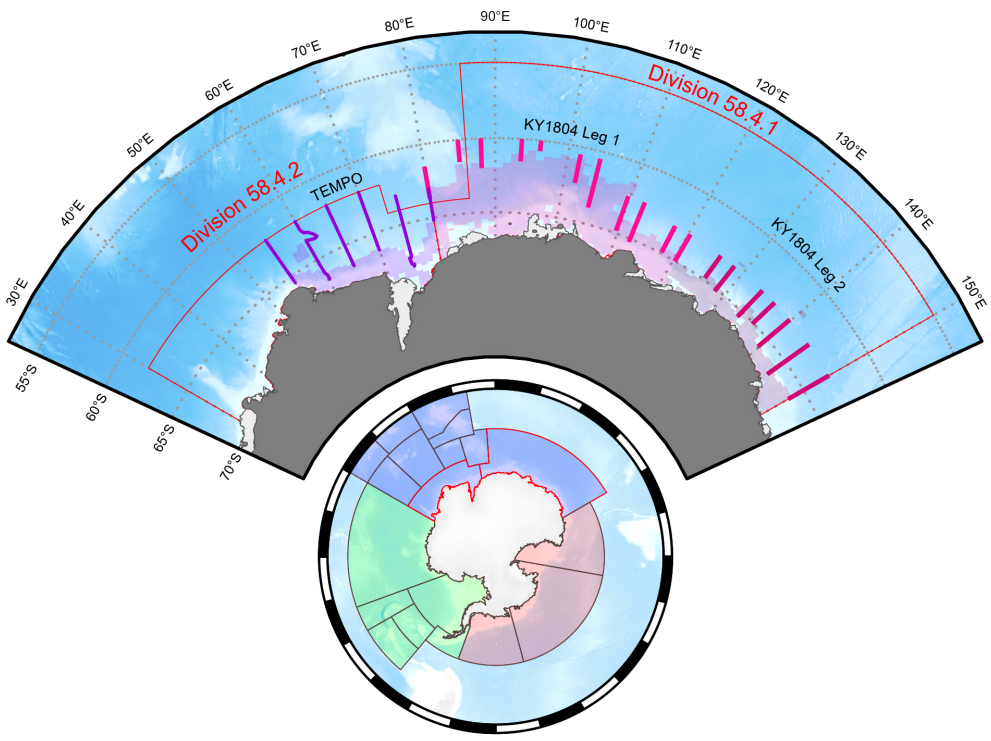


FIGURE 2
Survey transect locations for KY1804 in Division 58.4.1 split into two legs (pinks) and TEMPO survey transects in Divisions 58.4.2 (purple) showing average sea ice extent over survey periods (transparent colors). Management areas of the Commission of the Conservation of Antarctic Marine Living Resources (Bottom circle) showing Area 48 (green), Area 58 (blue) and Area 88 (red). Maps produced with the SOmap package in R (Maschette et al., 2019).

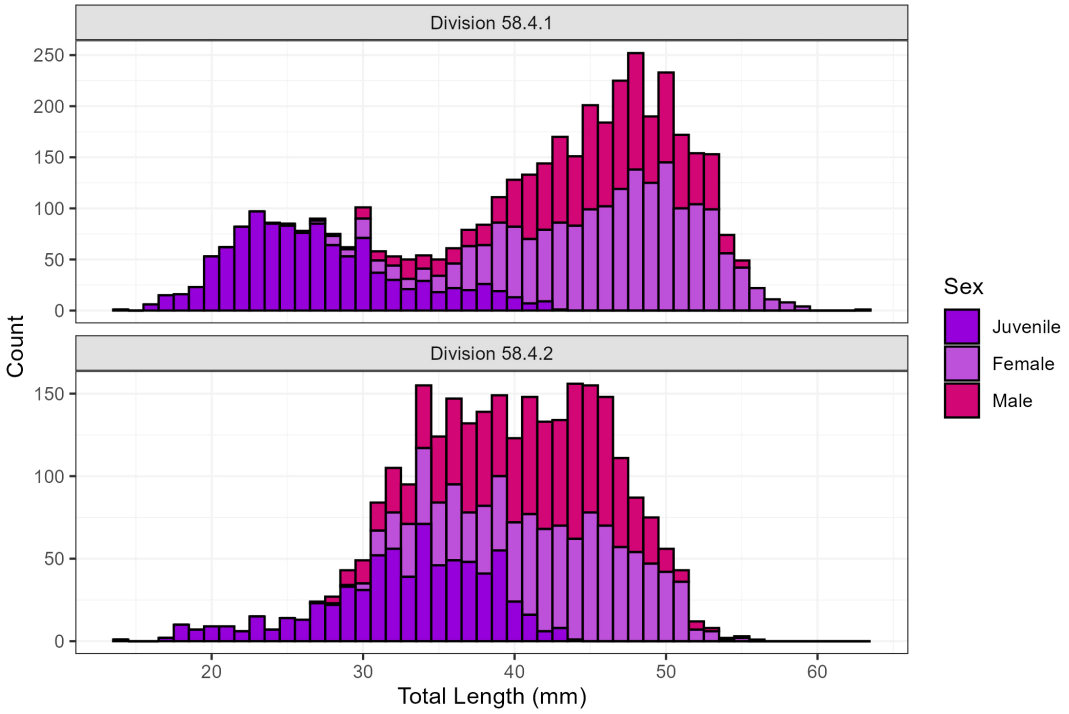


FIGURE 3
Euphausia superba length distribution measured during surveys in Divisions 58.4.1 and 58.4.2.

2.1.2.2 Estimating the ramp parameters:

The parameters L_{min}, L_{max} and w for the ramped ogive function are estimated by fitting a Bayesian nonlinear binomial model to maturity at length data observed in the survey. The model takes the form:

$$M_i \sim \text{Bin}(1, \pi_i)$$

$$\pi_i = \begin{cases} p_1 & l_i \le L - \frac{w}{2} \\ p_1 + (p_2 - p_1)\left(\frac{l_i - L}{w} + \frac{1}{2}\right) & L - \frac{w}{2} < l_i < L + \frac{w}{2} \\ p_2 & l_i \ge L + \frac{w}{2} \end{cases}$$

where M_i is a binary variable that is 1 if individual i is mature and 0 otherwise; l_i is the length of that individual; and π_i is the probability that an individual of that length observed in that year will be mature. Here, L is the length at which the probability of maturity is 0.5, and w is the width of the ramp. The parameters p_1 and p_2 represent the probabilities that the smallest and largest individuals will be mature. It is necessary that $p_1 > 0$ and $p_2 < 1$ to allow for the small number of individuals that mature unusually early or late, and any potential misidentification of maturity stage, and Beta priors are adopted that constrain p_1 to be near 0 and p_2 to be near 1

$$p_1 \sim \text{Beta}(1, 100)$$

$$p_2 \sim \text{Beta}(100, 1)$$

Diffuse Normal priors are chosen for L and w:

$$L \sim \text{N}(45, 0.01)$$

$$w \sim \text{N}(10, 0.01)$$

where again the normal distributions have been parameterized in terms of mean and standard deviation.

The upper and lower limits L_{min} and L_{max} for L are determined as the 2.5% and 97.5% quantiles for L, and w is determined as the 97.5% quantile for w.

2.1.2.3 Estimating the logistic parameters:

The input parameters q_{50} and q_{95} for the logistic ogive function are the 50th and 95th quantiles respectively. They are estimated by fitting a Bayesian nonlinear binomial model to maturity at length data observed in the survey. In this case:

$$M_i \sim \text{Bin}(1, \pi_i)$$

$$\pi_i = \left[1 + \exp\left(-\log(19)\frac{l_i - q_{50}}{d_{95}}\right)\right]^{-1}$$

where again M_i is a binary variable that is 1 if individual i is mature and 0 otherwise; l_i is the length of that individual; π_i is the probability that individual of that length observed in that year will be mature; and $d_{95} = q_{95} - q_{50}$.
Diffuse normal priors are chosen for q_{50} and d_{95}:

$$q_{50} \sim \text{N}(45, 0.01)$$

$$d_{95} \sim \text{N}(10, 0.1)$$

For the simulation, logistic ogive profiles are generated by drawing from a multivariate Normal distribution with mean and covariance matching the posterior distribution of q_{50} and d_{95}.

2.2 Stock assessments

2.2.1 Model parameters

The input parameters used in the stock assessment models for Divisions 58.4.1 and 58.4.2 East are shown in Table 1. The parameters are largely consistent with those used in previous assessments for these areas (SC-CAMLR, 2000; Delegation of Australia, 2007). Estimates of maturity were calculated in this paper, where possible, other parameters were obtained from the literature (Table 1). For these assessments, we have run two different scenarios for each Division based on the maturity models described above; the first using the maturity values fitted as a ramp function, the second with maturity implemented as a logistic function (Table 1). Model were fitted to the base parameters (Supplementary Material 1) of previous assessments first then one parameter updated in subsequent runs in the order of B0logSD, Length to weight relationship, and finally maturity (Table 1).

2.2.2 Model Configuration

The structure of the assessment model was configured to be consistent with those used in the krill assessment for Subarea 48.1 (see Maschette et al., 2021).

Natural mortality and recruitment in krill assessments are based on the proportional recruitment model outlined by de la Mare (1994) which was further developed by Pavez et al. (2023). These use the mean ($\hat{\mu}_R$) and standard deviation ($\hat{\sigma}_R^2$) of proportional recruitment from survey data (Table 1) to determine the associated

TABLE 1 Grym model parameters for *Euphausia superba* stock assessments in Divisions 58.4.1 and 58.4.2.

	Ramp Maturity		Logistic Maturity	
Parameter	Division 58.4.1	Division 58.4.2	Division 58.4.1	Division 58.4.2
First Age Class	1	1	1	1
Last Age Class	7	7	7	7
t_0	0	0	0	0
$L\infty$	60.8 mm	60.8 mm	60.8 mm	60.8 mm
k	0.45	0.45	0.45	0.45
Start growth period (dd/mm)	21/10	21/10	21/10	21/10
End growth period (dd/mm)	12/02	12/02	12/02	12/02
Weight-length parameter – A (g)	1.71E-6*	1.71E-6*	1.71E-6*	1.71E-6*
Weight-length parameter – B	3.41*	3.41*	3.41*	3.41*
Min length, 50% mature	**40.14 mm**	**42.24 mm**	**41.33 mm**	**41.99 mm**
Max length, 50% mature	**40.89 mm**	**42.99 mm**	**42.00 mm**	**42.59 mm**
Range over which maturity occurs	**18.83 mm**	**16.05 mm**	**10.27 mm**	**8.38 mm**
Start of spawning season (dd/mm)	1/12	1/12	1/12	1/12
End of spawning season (dd/mm)	28/02	28/02	28/02	28/02
Monitoring interval (dd/mm)	01/02	01/02	01/02	01/02
Mean proportional recruitment	0.557	0.557	0.557	0.557
SD of proportional recruitment	0.126	0.126	0.126	0.126
Min length, 50% Selected	30 mm	30 mm	30 mm	30 mm
Max length, 50% Selected	39 mm	39 mm	39 mm	39 mm
Range over which selection occurs	9 mm	9 mm	9 mm	9 mm
Fishing Season (dd/mm)	01/12 to 01/03	01/12 to 01/03	01/12 to 01/03	01/12 to 01/03
Reference Date (dd/mm)	01/10	01/10	01/10	01/10
Reasonable upper bound for Annual F	1.5	1.5	1.5	1.5
B0logSD	0.17†	0.289*	0.17†	0.289*

Values without notation come from Delegation of Australia (2007). *Cox et al. (2022), †Abe et al. (2023). Bold values are estimated within this paper.

annual natural mortality and distribution of random recruits which reproduce the recruitment values observed in the survey. The recruitment variance and natural mortality indices were pre-generated using an inverse-beta distribution following the method outlined in Pavez et al. (2023) to enable consistency between model runs. The overlap of mortality estimates across runs with expected values in published literature was used to evaluate the reliability of the generated estimates.

For the assessment models with logistic maturity, the rampOgive function within the projection function was changed to the logisticOgive function (see Supplementary Material 2). For each run, L50 values for maturity and selectivity were selected from their respective L_{min} and L_{max} ranges (Table 1) using a uniform distribution (See section 2.1.1).

The precautionary harvest rate is calculated following the CCAMLR decision rules developed for krill (SC-CAMLR, 1994). These specify that:

1. Choose a harvest rate, γ_1, so that the probability of the spawning biomass dropping below 20% of its median pre-exploitation level over a 20-year harvesting period is 10%.
2. Choose a harvest rate, γ_2, so that the median escapement at the end of a 20-year period is 75% of the median pre-exploitation level.
3. Select the lower of γ_1 and γ_2 as the precautionary harvest rate.

Initial precautionary harvest rates were determined by testing γ values between 0.05 and 0.13 in 0.0005 increments using 10,000 model iterations. Subsequent runs were conducted at 0.0001 increments for ranges ±0.01 of initial precautionary harvest rates using 100,000 iterations to determine final precautionary harvest rates. Using 100,000 iterations rather than the 10,000 used in the assessment for Subarea 48.1 allows for less variation between reruns of the same model caused by random number generation.

2.2.3 Precautionary catch limits

The harvest rates determined by applying the CCAMLR decision rules to the results from the updated stock assessments were multiplied with the recent krill survey biomass estimates in Divisions 58.4.1 and 58.4.2 East to determine updated precautionary catch limits (PCL). The PCL was calculated overall for Division 58.4.1, and at three smaller spatial scales within it referred to as 'West', 'Middle' and 'East' in Abe et al. (2023). Division 58.4.2 is divided into East and West sections. Recently updated biomass estimated for krill (Cox et al., 2022) only covered the 'East' region as defined in Conservation Measure 51-03. No recent biomass estimates to update the PCL for Division 58.4.2 West were available.

3 Results

3.1 Maturity-at-length estimation

3.1.1 Ramp parameters

In Division 58.4.1, the combined sex ramp model estimated L_{50} maturity to be 40.45 mm with 2.5% and 97.5% quantiles of 40.13 mm and 40.89 mm, respectively (Tables 1, 2). The slope of the ramp, or the 97.5% quantile interval over which maturity occurs, was estimated to be 18.82 mm (Figure 4A).

In Division 58.4.2, the combined sex ramp model estimated L_{50} maturity to be 42.64 mm with 2.5% and 97.5% quantiles of 42.24 mm and 42.99 mm, respectively (Tables 1, 2). The 97.5% quantile interval over which maturity occurs was estimated at 16.05 mm (Figure 4C).

In both Division 58.4.1 and Division 58.4.2 female krill were estimated to reach L_{50} maturity at a smaller size (39.00 and 40.00 mm respectively) than male krill (45.11 and 45.47 mm respectively, Table 2, Figure 5).

3.1.2 Logistic parameters

For both Divisions the combined sex logistic model estimated a similar value of L_{50} maturity compared to the respective ramp models. In Division 58.4.1, L_{50} maturity was estimated as 41.67 mm with 2.5% and 97.5% quantiles of 41.33 mm and 42.00 mm, respectively (Tables 1, 3). The d_{95}, which is used to define the shape of the curve, was estimated as 10.27 mm (Figure 4B).

In Division 58.4.2, L_{50} maturity was estimated as 42.29 mm with 2.5% and 97.5% quantiles of 41.99 mm and 42.59 mm respectively

TABLE 2 Estimates of *Euphausia superba* length at maturity (mm) from Divisions 58.4.1 and 58.4.2 fitted with ramp o-gives.

Division	58.4.1			58.4.2		
Sex	All	Males	Females	All	Males	Females
Individuals	4191	2369 (1124)	2946 (1124)	2761	1746 (714)	1729 (714)
Length at 50% maturity (L_{50})	40.45	45.11	39.00	42.65	45.47	40.00
L_{50} 2.5% quantile	40.14	44.59	38.67	42.24	45.10	39.37
L_{50} 97.5% quantile	40.89	45.54	39.46	42.99	45.91	40.55
Range over which maturity occurs	17.67	20.33	14.66	17.72	14.01	11.91
Range 2.5% quantile	16.69	18.96	13.11	13.64	13.07	9.57
Range 97.5% quantile	18.83	22.18	15.51	16.05	15.48	14.81

O-gives are fitted for all sexes (male, females and juveniles), and males with juveniles, and females with juveniles. Number of juveniles shown in parenthesis.

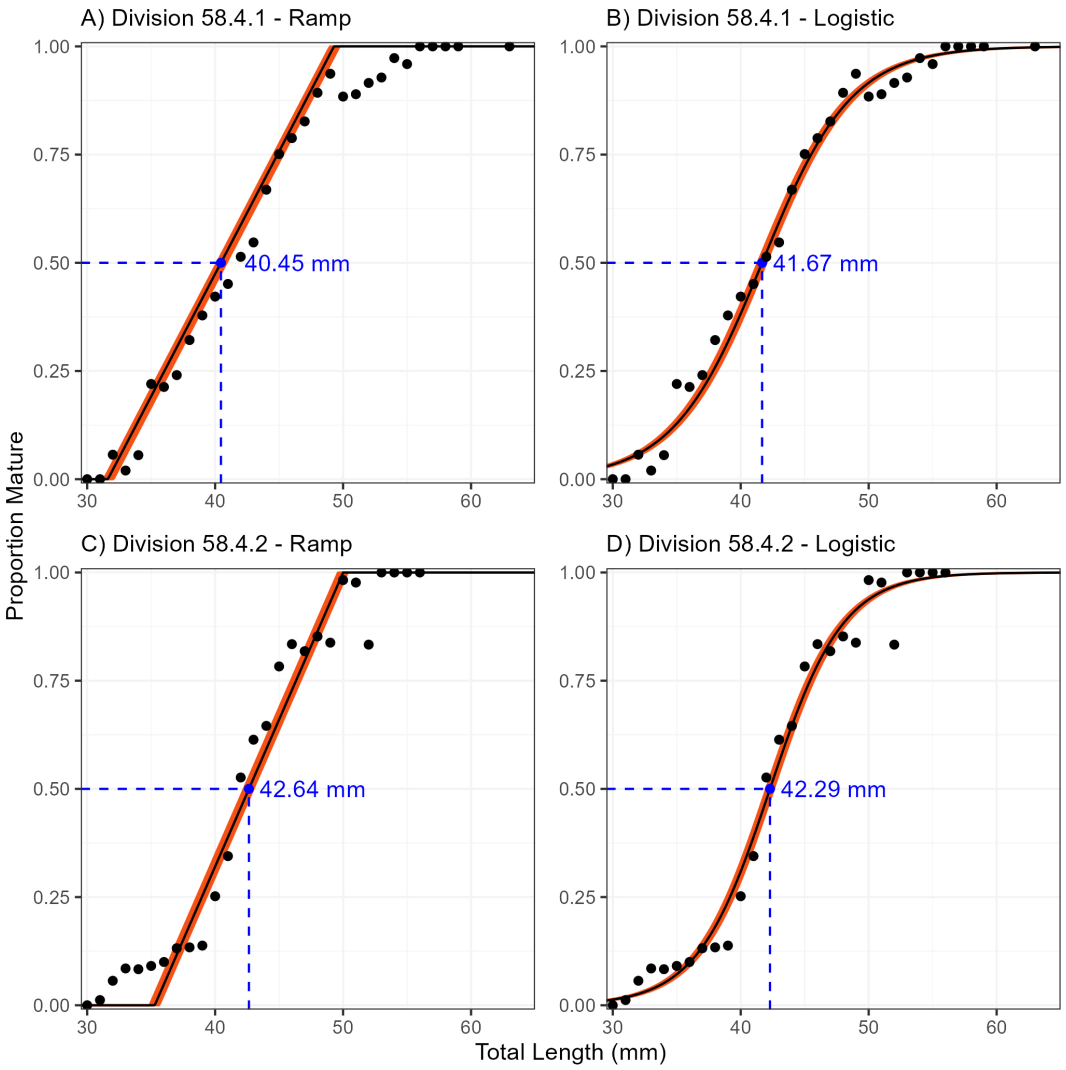


FIGURE 4
Euphausia superba maturity at length range (orange) fitted with ramp and logistic ogives to survey data in Divisions 58.4.1 **(A, B)** and 58.4.2 **(C, D)** with Bayesian nonlinear binomial random effects model.

(Tables 1, 3). The d_{95} for this region was estimated as 8.38 mm (Figure 4D).

Similar to the ramp o-gives, in both Division 58.4.1 and Division 58.4.2 female krill were estimated to reach L_{50} maturity at a smaller size (39.84 and 40.11 mm respectively) than male krill (44.99 and 45.01 mm respectively, Table 2 and Figure 5).

3.2 Stock assessments

3.2.1 Natural mortality and recruitment

The natural mortality (M_Y^{-1}) associated with the generated recruitment series using an inverse-beta distribution across runs ranged from 0.388 – 1.585, with a mean of 0.857 and showed a 98.2% overlap with the expected natural mortality range for this species (Figure 6; 0.5-1.1; Pakhomov, 1995b). The generated recruitment series across runs resulted in recruitment variances between 0.0008 and 0.1288, with associated mean recruitments ranging from 0.229 to 0.809 (Figure 7).

3.2.2 Precautionary harvest rates

The precautionary harvest rates (γ) estimated for Divisions 58.4.1 and 58.4.2 ranged from 0.0854 to 0.1298 (Table 4). Across all models, the 75% escapement criterion (γ_2) was lowest and therefore determined the precautionary harvest rate. Each model following the step-wise change in parameters value showed a decrease in γ from the previous model. The exception to this being the model with updated B0logSD values for Division 58.4.1 as the values for B0logSD were identical.

The final models were those with updated maturity values. Models using the ramp maturity function resulted in slightly lower precautionary harvest rates than models with the logistic maturity function. Projections of median spawning stock status across final models indicate a stable population under the no fishing scenario.

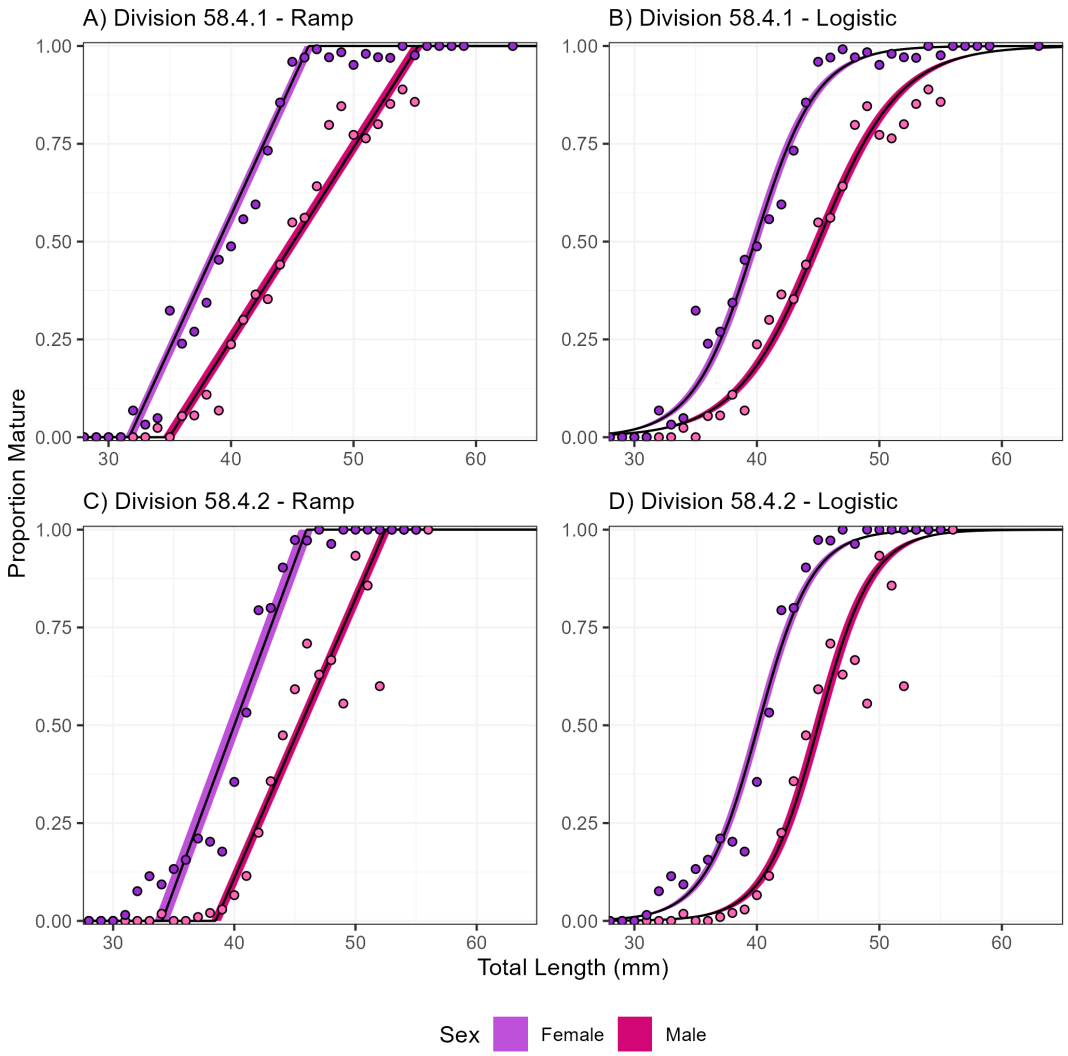


FIGURE 5
Euphausia superba maturity at length range for males and females fitted with ramp and logistic ogives to survey data in Divisions 58.4.1 **(A, B)** and 58.4.2 **(C, D)** with Bayesian nonlinear binomial random effects model.

For both γ_1 and γ_2 projections median spawning stock status declines towards 0.75 over approximately 5 years before stabilizing (Figures 8, 9).

3.2.3 Precautionary catch limits

The PCL for each Division and Subregions West, Middle and East in Division 58.4.1 and Division 58.4.2 East using the harvest rate resulting from the models using a logistic maturity curve ranged from 28,811 - 640,872 tonnes (Tables 5, 6).

4 Discussion

4.1 Maturity Estimation

As part of updated stock assessments for krill in CCAMLR Divisions 58.4.1 and Division 58.4.2, we provide new estimates for length at maturity for krill. These estimates display similar mean length at 50% maturity but much tighter confidence intervals than those calculated for Subarea 48.1. Data originating from single surveys could have contributed to the tighter confidence intervals, thus removing any inter-annual variability in length at maturity, which was included as a random effect in Maschette et al. (2021) for the estimates from Subarea 48.1. The sex specific estimates for maturity indicate that females in both Divisions (58.4.1 and 58.4.2) reach 50% maturity approximately 5 mm smaller than that of males. This is similar to the findings of Siegel and Loeb (1994) who found that females were reaching 50% maturity approximately 8 mm smaller than males in Subarea 48.1. For both sexes though the estimates in this study are larger than those of Siegel and Loeb (1994) by approximately 2 mm for males, and 5 mm for females. This may indicate differences in regional growth, however since the combined sex estimates in this study are similar to those presented by Maschette et al. (2021) and which are from the same region as Siegel and Loeb (1994) it may indicate environmental changes which have occurred across the Southern Ocean have resulted in

10.3389/fmars.2025.1448250

TABLE 3 Estimates of *Euphausia superba* length at maturity (mm) from Divisions 58.4.1 and 58.4.2 fitted with logistic o-gives.

Division	58.4.1			58.4.2		
Sex	All	Males	Females	All	Males	Females
Individuals	4191	2369 (1124)	2946 (1124)	2761	1746 (714)	1729 (714)
Length at 50% maturity (L_{50})	41.67	44.99	39.84	42.29	45.01	40.11
L_{50} 2.5% quantile	41.33	44.57	39.47	41.99	44.61	39.78
L_{50} 97.5% quantile	42.00	45.42	40.20	42.59	45.42	40.45
Distance to 95% maturity (d_{95})	10.27	9.88	7.45	8.33	6.49	6.50
d_{95} 2.5% quantile	9.65	8.99	6.87	7.78	5.78	5.92
d_{95} 97.5% quantile	10.92	10.84	8.05	9.01	7.29	7.11

O-gives are fitted for all sexes (male, females and juveniles), and males with juveniles, and females with juveniles. Number of juveniles shown in parenthesis.

a shift to a larger length at maturity of krill than was present in the 1980/90s. This could be confirmed by calculating sex specific estimates through time in Subarea 48.1 in future.

The comparison between different maturity models (ramp versus logistic) provided similar estimates of 50% maturity. The primary difference between the ogives comes in the differing shapes and width of each ogive. For example, when considering the two ogives from Division 58.4.1 (Figures 3, 5) the length at 50% maturity is approximately 0.6mm different, which is to be expected when fitting two models to the same data. Relative to the ramp model, the logistic model indicates that a larger proportion of the individuals in the population at lengths less than 42.43mm are mature. Conversely the ramp ogive indicates that a greater proportion of individuals at lengths greater than 42.43mm are mature.

When considering a population at equilibrium with no fishing, this would mean that overall, the logistic curve leads to a higher proportion of individual krill being mature (as there are more small krill than large ones). This effect however is often masked in stock assessments because numbers at age are converted to spawning stock biomass. By transforming each age class in the population to their relative biomass the differences between the two ogives are masked. That is, one large krill has the weight of many small krill so whilst a greater number of individual krill are considered mature using the logistic ogive, they have a similar weight of the larger krill included by the ramp ogive. A simplified example illustrating this is shown in Supplementary Material 3.

The use of the ramp ogive for krill was historically driven by limitations in the stock assessment software. Given that the limitation of modelling maturity has been overcome we recommend the use of logistic curves for maturity estimates for future krill assessments since they 1) are more representative of the biological process of maturity, and 2) are consistent with other fishery assessments in the Southern Ocean (such as Ziegler and Welsford, 2017).

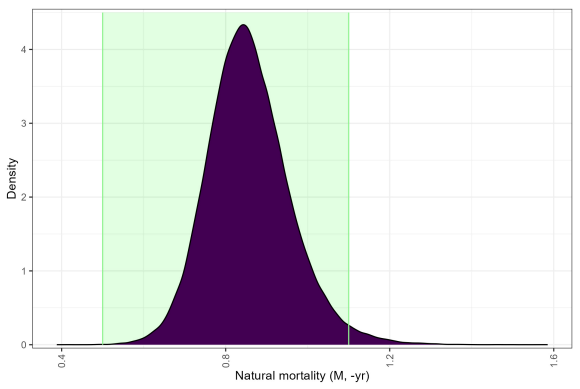


FIGURE 6
Overlap between Euphausia superba natural mortality (-yr, M) from proportional recruitment models using an inverse-beta distribution and the expected natural mortality range (0.5-1.1, green shaded region; WG-EMM-2021 Table 1).

4.2 Stock assessments

The currently accepted stock assessment model configuration for krill management in CCAMLR is based on the Grym using proportional recruitment (SC-CAMLR, 2019). This model structure has the advantage of providing harvest rates for stocks in which little is known, and fisheries data is absent, as is the case for Divisions 58.4.1 and 58.4.2. In future, should a fishery develop in these areas, the combination of fisheries collected data, with on-going research survey data collection may provide the opportunity to utilize integrated stock assessment software packages such as Casal2 (Doonan et al., 2016) or Stock Synthesis (Methot and Wetzel, 2013).

Unlike Divisions 58.4.1 and 58.4.2, in Subarea 48.1 a continual fishery has operated for over 50 years and had annual research surveys between 1992 - 2011 covering ~19% of the Subarea situated near the South Shetland Islands which have provided a multitude of data (Kinzey et al., 2015). Previous efforts to fit integrated assessments in this region using AD Model Builder highlighted issues in getting models to converge reliably (Kinzey et al., 2015; de Lestang, 2016; Thomson, 2016; Wang et al., 2021). Upon reviewing one of these models Thomson (2016), and SC-CAMLR (2016) highlighted that this may be due to over-parameterization of the

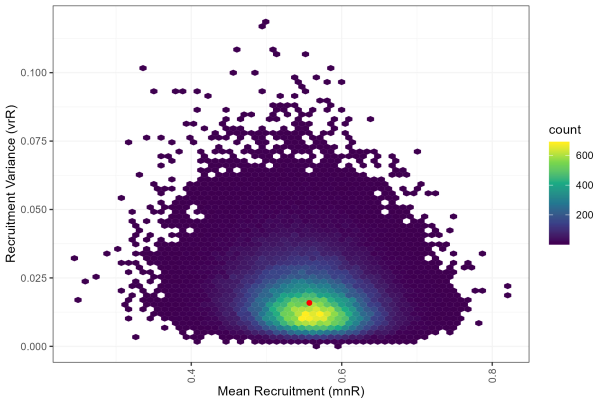


FIGURE 7
Comparison of *Euphausia superba* mean recruitment and recruitment variance with respect to the corresponding starting value combination in red (mean = 0.557, standard deviation = 0.126), fitted with proportional recruitment models using an inverse-beta distribution.

age-based models. Wang et al. (2021) developed a length-based model which estimated less parameters however still had issues fitting some of those estimated. They highlighted that this may be due to inconsistencies in the data collection in the surveys and fishery across the time series. More recently integrated model development in Casal2 (Kinzey and Watters, 2023) and Stock Synthesis (Mardones et al., 2024) have begun, however these will require overcoming similar challenges faced by previous models.

One option as a stepping-stone from the current stock assessment configuration in the Grym to an integrated assessment may be to explore fitting toothfish style assessments with the Grym (see Maschette et al., 2023). These incorporate previous survey biomass estimates, survey recruitments and fishery catch into the assessment to estimate catch limits. These were used within CCAMLR for toothfish until the fisheries had large quantities of data and developed integrated assessments. They have also been used for several bycatch species which often have less reliable data than target species (Dell et al., 2015; Maschette and Dell, 2015).

Regardless of the pathway taken to achieve an integrated assessment of krill in any area, focus needs to be given on the data collection required to enable models and parameters to be reliably fit. Arguably among the most important parameters for these assessments (and Grym assessments) are recruitment and annual growth (Punt, 2023). To estimate these reliably requires large amounts of survey data collected ideally on an annual basis.

With regards to growth, many studies have been conducted with either instantaneous or daily growth (such as Tarling et al., 2016; Melvin et al., 2018; Veytia et al., 2020; Sylvester et al., 2021) however few exist which attempt to estimate growth parameters used within stock assessments such as the von Bertalanffy growth curve with most assessments relying on estimates used by Constable and de la Mare (1996). Maschette and Wotherspoon (2023) recommended fitting growth curves by using the modal peaks of length classes fitted with a mixture distribution to survey time series data as has been done for other species. This has been conducted twice before for krill, the first by Siegel (1987) in the Atlantic sector and the second by Pakhomov (1995a) in the Indian sector. In both instances survey data was collected between 1983 and 1990. Despite multiple surveys being conducted for krill since, fitting mixture distributions to estimate growth has not been conducted. Modal lengths were calculated for two additional surveys by de la Mare (1994) who was using these to demonstrate the calculation of proportional recruitment.

When considering recruitment of krill into a fishery, some studies have reported large fluctuations of krill recruitment within Subarea 48.1 between years (Kinzey et al., 2013; Meyer et al., 2020; Maschette et al., 2021; Kinzey et al., 2023). Kinzey et al. (2013) examined the estimated proportional recruitments from the US-AMLR survey series and the Palmer LTER survey series using a length threshold as the cutoff for being a juvenile rather than the recommended mixture distribution method of de la Mare (1994). The two survey series have a small spatial overlap and between them cover most of the shelf zone of Subarea 48.1, unfortunately though there is only a three year period where both surveys were conducted. In all three of these years the Palmer LTER survey recruitment estimates were higher than the US-AMLR survey, particularly 2010 which was a 'low' recruitment year in the US-AMLR time series. Similar differences between surveys conducted in the same year were also seen by de la Mare (1994) which looked at 10 surveys (mostly from the Indian Sector) to estimate recruitment which was subsequently applied in all krill assessments until Maschette et al. (2021) where Subarea 48.1 specific values were estimated. Both studies highlight that in order to reliably estimate recruitment for a stock assessment the sampling needs to cover the entire region of the assessment (Siegel et al., 1997) either through multiple small-scale surveys, or large synoptic surveys (such as Krafft et al., 2021). This is particularly true for regions such as Subarea 48.1 which is

TABLE 4 Projected harvest rates (γ) following the CCAMLR decision rules for krill in Divisions 58.4.1 and 58.4.2 under two different maturity scenarios.

Parameter value change	Division 58.4.1			Division 58.4.1		
	γ_1	γ_2	γ to use	γ_1	γ_2	γ to use
Base Model	0.1298	**0.1125**	2	0.1297	**0.1128**	2
Updated B0logSD	0.1298	**0.1125**	2	0.1294	**0.1121**	2
Updated Length to weight relationship	0.1259	**0.1088**	2	0.1255	**0.1085**	2
Updated Maturity – Ramp ogive	0.1070	**0.0887**	2	0.1032	**0.0854**	2
Updated Maturity - Logistic ogive	0.1106	**0.0906**	2	0.1201	**0.0989**	2

γ_1 is the harvest rate where the probability of the spawning biomass dropping below 20% of its median pre-exploitation level over a 20-year harvesting period is 10%. γ_2 is the harvest rate where the median escapement at the end of a 20-year period is 75% of the median pre-exploitation level. Bold highlights value selected under CCAMLR decision rules.

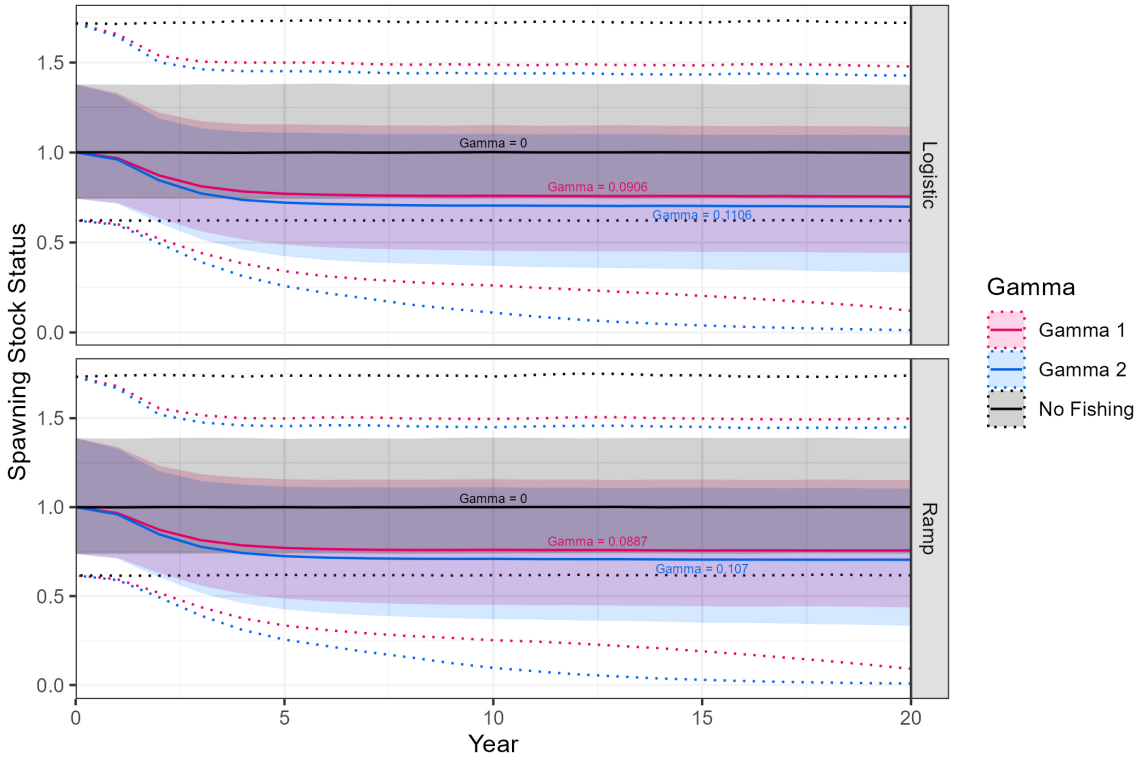


FIGURE 8
Euphausia superba spawning stock status projected over a 20-year period in Division 58.4.1 for three values of gamma using either ramp or logistic maturity o-gives. Stock status is shown as median (solid lines) with 90% (shaded) and 97.5% confidence intervals (dotted).

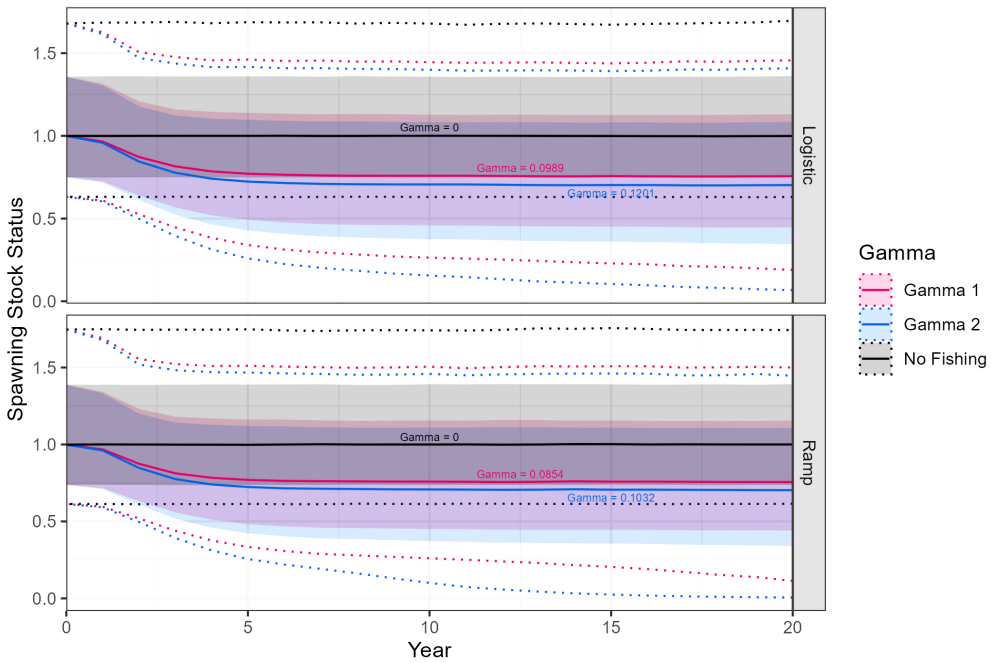


FIGURE 9
Euphausia superba spawning stock status projected over a 20-year period in Division 58.4.2 for three values of gamma using either ramp or logistic maturity o-gives. Stock status is shown as median (solid lines) with 90% (shaded) and 97.5% confidence intervals (dotted).

TABLE 5 Precautionary catch limits estimated for *Euphausia superba* in Division 58.4.1.

Division	Subregion	Longitude range	Biomass (Million tonnes)[1]	Precautionary Harvest Rate	Precautionary Catch limit (tonnes)
58.4.1	West	80°E - 103°E	1.567	0.0906	141,970
58.4.1	Middle	103°E - 123°E	0.643	0.0906	58,256
58.4.1	East	123°E - 150°E	2.114	0.0906	191,528
58.4.1	Total	80°E - 150°E			391,754

[1]Biomass estimates from Abe et al., 2023, Table 1).

subject to highly dynamic currents and region winds which may dictate whether juvenile krill are located inside or out of a static sampling region (Thompson and Youngs, 2013; Young et al., 2024).

Following the revised krill fishery management strategy recommended by the Scientific Committee and endorsed by CCAMLR in 2019 (CCAMLR, 2019, para. 5.17), we provide updated precautionary catch limits for krill in Divisions 58.4.1 and 58.4.2 East. These catch limits are based on recent biomass estimates from a 2018/19 survey conducted by Japan in Division 58.4.1 (Abe et al., 2023) and from a 2021 survey conducted by Australia in Division 58.4.2 East (Cox et al., 2022). These biomass estimates were combined with precautionary harvest rates for krill in Divisions 58.4.1 and 58.4.2-East estimated from stock assessments fitted with the Grym to derive precautionary catch limits.

4.2.1 Division 58.4.1

The 'BROKE' survey in 1996 found krill were more abundant and with a broader latitudinal distribution in the western survey area (80°-115°E) than the east (115°-150°E) where krill were confined to the narrow coastal band of cool water (Nicol et al., 2000; Pauly et al., 2000). Based on this information, CCAMLR agreed in 2000 to subdivide Division 58.4.1 into two management Subdivisions at the 115°E meridian and set individual precautionary catch limits for West and East Subdivisions (Nicol and Pauly, 2000).

The KY1804 krill biomass survey by Japan in Division 58.4.1 in 2018/19 was conducted in two separate legs, with leg 1 covering 80° E to 120°E, and leg 2 covering 120°E to 150°E (Murase et al., 2025). Krill biomass in the leg 1 survey area was estimated to be 2.210 million tonnes. More than 70% (1.567 million tonnes) of this biomass was distributed in the western stratum between 80°-103° E, and less than 30% (0.643 million tonnes) in the middle stratum between 103°-123°E (Abe et al., 2023). The areal biomass of krill in the leg 2 survey area in the eastern stratum between 123°-150°E was estimated at 2.114 million tonnes. The Scientific Committee considered this new estimate to be the best available estimate of krill biomass for this region (SC-CAMLR-2021, para. 2.6).

The total areal krill biomass of 4.325 million tonnes (CV 0.17) for the entire Division 58.4.1 in this survey was similar to the biomass estimated for the same area in the BROKE survey in 1996 (4.83 million tonnes, CV 0.17), and the Scientific Committee considered this new estimate to be the best available estimate of krill biomass for this region (SC-CAMLR-2021, para. 2.6). However, the biomass distribution across Division 58.4.1 was different between the 1996 and 2018/19 surveys, with relatively higher biomass in the east and west and low in the middle of the Division in 2018/19. This difference could be attributed to difference in the survey timings as well as difference in latitudinal coverage between the two surveys especially in the western part of the area.

Based on the three strata biomass estimates by Abe et al. (2023), and the low krill estimates for the middle stratum relative to the eastern and western strata, along with the CCAMLR Scientific Committee (SC-CAMLR, 2023) we recommend that catch limits for Division 58.4.1 are set by CCAMLR individually for three subdivisions following these strata boundaries, rather than the two subdivisions west and east of 115°E as currently defined in CM 51-02. If the middle stratum with low biomass was combined with either the eastern or western stratum with much higher krill biomass and managed as a single management unit, there could be a risk that the entire catch limit set for this management unit could come out of the middle stratum and disproportionately impact the ecosystem by exceeding the sustainable harvest rate through concentrated fishing effort. The proposed precautionary catch limits for the West, Middle, and East subdivisions are 141,970 tonnes, 58,256 tonnes and 191,528 tonnes, respectively.

Splitting the krill catch limits in Division 58.4.1 into three subdivisions would be also consistent with the result of the spatial overlap analysis by Kelly et al. (2018), which was based on data layers available at the time and indicated that krill predators across Division 58.4.1 could potentially be exposed to disproportionate effects of fishing if the harvest rate become close to the catch limit. The KY1804 survey (Murase et al., 2025) has also provided valuable data sets to update the data layers such as whales (Hamabe et al., 2024) and

TABLE 6 Precautionary catch limits estimated for *Euphausia superba* in Division 58.4.2.

Division	Subregion	Longitude range	Biomass (Million tonnes)[1]	Precautionary Harvest Rate	Precautionary Catch limit (tonnes)
58.4.2	West	30°E - 55°E			1,448,000*
58.4.2	East	55°E - 80°E	6.480	0.0989	640,872
58.4.2	Total	30°E - 80°E			2,088,872

*Catch limit from Conservation Measure 51-03 Paragraph 3. [1]Biomass estimate from Cox et al. (2022).

seabirds (Kokubun et al., 2024) in future implementations of spatial overlap analyses in this Division.

4.2.2 Division 58.4.2

Krill biomass across Division 58.4.2 was first estimated from a summer survey in 2006 (Jarvis et al., 2010) and later recalculated by Cox and Kawaguchi (2012), with revised estimates of 15.34 million tonnes (CV 0.21) in the western subdivision (30°-55°E), 11.47 million tonnes (CV 0.28) in the eastern subdivision (55°-80°E), and a total biomass of 28.43 million tonnes (CV 0.16) for the entire Division 58.4.2. The 2021 Australian survey estimated a krill biomass for Division 58.4.2 East of 6.48 million tonnes (CV 0.289; Cox et al., 2022) and this estimate was endorsed as the best available estimate by the Scientific Committee (SC-CAMLR, 2021, para. 2.6).

Based on the Grym assessment presented here, the precautionary catch limit for Division 58.4.2 East was calculated to be 640,872 tonnes. For Division 58.4.2 West, there is no updated biomass estimate available and we recommend that the current precautionary catch limit be retained. Together, the updated total precautionary catch limit for the entire Division 58.4.2 is 2,088,872 tonnes.

The areal size of Division 58.4.2 East of 775,732 km^2 (Cox et al., 2022) is larger than the entire Subarea 48.1 (595,490 km^2) in the Atlantic Sector, where management units at smaller scales are being discussed under the revised krill management strategy agreed in 2019. To follow consistent principles across different areas within the CAMLR Convention area, it would be important that the krill fishery in Division 58.4.2 is also managed using smaller spatial management units. The spatial overlap analysis conducted by Kelly et al. (2018) could be used for this purpose, however this analysis was preliminary in nature. Until an updated spatial overlap analysis can inform on a spatial allocation of catch within Division 58.4.2, we propose that the current trigger levels for both subdivisions in Division 58.4.2 (CM 51-03) remain in force.

4.3 Conclusion

Whist currently underutilized, the krill fisheries in East Antarctica show a substantial resource potential. Despite this, our work has shown that the current catch limits set in CCAMLR Conservation Measures are higher than those which should be set following the CCAMLR decision rule process. Specifically, based on the presented stock assessment for *Euphausia superba* in this paper, we recommend that CCAMLR consider the following:

- Given that historical limitations have been overcome, future assessments for krill should be based on the use of logistic ogives as they are more representative of krill biology.
- In Division 58.4.1, the total catch limit be set at 391,754 tonnes, with a subdivision of 141,970 tonnes west of 103°E, 58,256 tonnes between 103°E and 123°E, and 191,528 tonnes east of 123°E.
- In Division 58.4.2, the total catch limit be set at 2,088,872 tonnes, with a subdivision of 1.448 million tonnes west of 55°E and 640,872 tonnes east of 55°E.
- The current trigger levels in CM 51-03 for both subdivisions of Division 58.4.2 remain in force until such time that an updated spatial overlap analysis can inform on a spatial allocation of catch within this Division.

Data availability statement

The datasets presented in this study can be found in online repositories. The names of the repository/repositories and accession number(s) can be found below: https://data.aad.gov.au/metadata/AAS_4512_TEMPO_bioacoustics for TEMPO data. The KY1804 survey data will be shared on reasonable request to Hiroto Murase with permission from the funding institute and agencies.

Author contributions

DM: Conceptualization, Data curation, Formal analysis, Investigation, Methodology, Project administration, Resources, Software, Validation, Visualization, Writing – original draft, Writing – review & editing. SW: Formal analysis, Investigation, Methodology, Validation, Writing – original draft, Writing – review & editing. HM: Conceptualization, Funding acquisition, Investigation, Project administration, Resources, Writing – original draft, Writing – review & editing. NK: Methodology, Validation, Writing – original draft, Writing – review & editing. PZ: Resources, Supervision, Validation, Writing – original draft, Writing – review & editing. KS: Supervision, Writing – review & editing. SK: Conceptualization, Funding acquisition, Investigation, Project administration, Resources, Validation, Writing – original draft, Writing – review & editing.

Funding

The author(s) declare that financial support was received for the research and/or publication of this article. This project was supported and funded by Australian Antarctic Science Project 4512, 4578, and 4636 and received grant funding from the Australian Government as part of the Antarctic Science Collaboration Initiative program. This project also received financial support from Pew Charitable Trust and Antarctic Science Foundation. We acknowledge the use of the CSIRO Marine National Facility (https://ror.org/01mae9353) and grant of sea time on RV Investigator in undertaking this research. The KY1804 component was financially supported by the Institute of Cetacean Research, the Japan Fisheries Research and Education Agency and the Fisheries Agency of Japan.

Acknowledgments

The authors would like to thank the TEMPO krill team members: Rob King, Jessica Melvin, Alicia Burns, Christine Weldrick, Olivia Johnson, Abigail Smith and Maddie Brasier for collecting the length and maturity data during the TEMPO survey

that was analyzed in this study. We would additionally like to thank Hiroko Sasaki, Ryuichi Matsukura, Marin van Regteren, Sara Driscoll, Ryan Driscoll, Jianfeng Tong, Rikuto Sugioka, Hideya Ohshima, Kaiki Ohshima, Ishihara, Qingyuan Yang and Hanae Doiguchi from the KY1804 survey for collecting the length and maturity data analyzed here. The Authors would like to thank the reviewers which provided useful comments to the manuscript.

Conflict of interest

The authors declare that the research was conducted in the absence of any commercial or financial relationships that could be construed as a potential conflict of interest.

Publisher's note

All claims expressed in this article are solely those of the authors and do not necessarily represent those of their affiliated organizations, or those of the publisher, the editors and the reviewers. Any product that may be evaluated in this article, or claim that may be made by its manufacturer, is not guaranteed or endorsed by the publisher.

Supplementary material

The Supplementary Material for this article can be found online at: https://www.frontiersin.org/articles/10.3389/fmars.2025.1448250/full#supplementary-material

References

Abe, K., Matsukura, R., Yamamoto, N., Amakasu, K., Nagata, R., and Murase, H. (2023). Biomass of Antarctic krill (Euphausia superba) in the eastern Indian sector of the Southern Ocean (80–150°E) in the 2018–19 austral summer. *Prog. Oceanography* 218, 103107. doi: 10.1016/j.pocean.2023.103107

Bull, B., Francis, R. I. C. C., Dunn, A., McKenzie, A., Gilbert, D. J., Smith, M. H., et al. (2012). CASAL C++ Algorithmic Stock Assessment Laboratory): CASAL user manual v2.30-2012/03/21. *Technical Report 135*, National Institute of Water and Atmospheric Research Ltd (NIWA), Wellington, New Zealand.

Cavan, E. L., Belcher, A., Atkinson, A., Hill, S. L., Kawaguchi, S., McCormack, S., et al. (2019). The importance of Antarctic krill in biogeochemical cycles. *Nat. Commun.* 10, 4742. doi: 10.1038/s41467-019-12668-7

CCAMLR (2019). *Report of the thirty-eighth meeting of the commission for the conservation of antarctic marine living resources (CCAMLR-38)* (Hobart, Australia: CCAMLR).

CCAMLR (2022). *CCAMLR statistical bulletin* (Hobart, Tasmania: CCAMLR), Vol. 34.

Constable, A. J. (2004). "Modifications to the generalised yield model in 2004, version GYM501E.EXE," in *Document WG-FSA 04/91*(Hobart, Tasmania, Australia: CCAMLR).

Constable, A. J. (2011). Lessons from CCAMLR on the implementation of the ecosystem approach to managing fisheries: Lessons from CCAMLR on EBFM. *Fish. Fish.* 12 , 138–151. doi: 10.1111/j.1467-2979.2011.00410.x

Constable, A. J., and de la Mare, W. K. (1996). A generalised model for evaluating yield and the long-term status of fish stocks under conditions of uncertainty. *CCAMLR Sci.* 3, 31–54.

Constable, A. J., and Nicol, S. (2002). Defining smaller-scale management units to further develop the ecosystem approach in managing large-scale pelagic krill fisheries in Antarctica. *CCAMLR Sci.* 9, 117–131.

Cox, M., and Kawaguchi, S. (2012). "Recalculation of Antarctic krill (Euphausia superba) biomass off East Antarctica (30–80°E) in January–March 2006," in *Document WG-EMM-12/31* (Hobart, Tasmania, Australia: CCAMLR).

Cox, M. J., Macaulay, G., Brasier, M. J., Burns, A., Johnson, O. J., King, R., et al. (2022). Two scales of distribution and biomass of Antarctic krill (Euphausia superba) in the eastern sector of the CCAMLR Division 58.4.2 (55˚E to 80˚E). *PloS One* 17, e0271078. doi: 10.1371/journal.pone.0271078

de la Mare, W. (1994). Estimating krill recruitment and its variability. *CCAMLR Sci.* 1, 55–69.

Delegation of Australia (2007). "Biomass of krill in Division 58.4.2 and an estimation of precautionary yield, including a subdivision of the precautionary catch limit along the 55°E longitude," in *Document SC-CAMLR-XXVI/07* (CCAMLR, Hobart, Tasmania, Australia).

de Lestang (2016). *Center for Independent Experts (CIE) independent peer reviewer's report of an age-based, integrated stock assessment for Antarctic krill (*Euphausia superba*) with projected catches to 2035* (Center for Independent Experts NOAA). Available online at: https://www.st.nmfs.noaa.gov/science-quality-assurance/cie-peer-reviews/cie-review-2016.

Dell, J., Maschette, D., Woodcock, E., and Welsford, D. (2015). "Biology, population dynamics and preliminary assessment of the long-term yield of *Macrourus caml* by-caught by the Australian fishery at Heard Island and the McDonald Islands (CCAMLR Division 58.5.2)," in *Document WG-FSA-15/63* (Hobart, Tasmania, Australia: CCAMLR).

Doonan, I., Large, K., Dunn, A., Rasmussen, S., Marsh, C., and Mormede, S. (2016). Casal2: New Zealand's integrated population modelling tool. *Fisheries Res.* 183, 498–505. doi: 10.1016/j.fishres.2016.04.024

Everson, I. (2000). *Krill biology, ecology and fisheries* (Oxford: Blackwell Science), 372.

Hamabe, K., Miyashita, T., Nagata, R., Sasaki, H., and Murase, H. (2024). Abundance of humpback whales in the eastern Indian sector of the Southern Ocean in 2018/19 using opportunistic sighting survey data with a note on the occurrence of other cetaceans. *Prog. Oceanography* 226, 103296. doi: 10.1016/j.pocean.2024.103296

Hewitt, R. P., Watters, G., Trathan, P. N., Croxall, J. P., Goebel, M. E., Ramm, D., et al. (2004). Options for allocating the precautionary catch limit of krill among small-scale management units in the Scotia Sea. *CCAMLR Sci.* 11, 81–97.

Jarvis, T., Kelly, N., Kawaguchi, S., van Wijk, E., and Nicol, S. (2010). Acoustic characterisation of the broad-scale distribution and abundance of Antarctic krill (Euphausia superba) off East Antarctica (30-80 degrees E) in January-March 2006. *Deep-Sea Res. Part II-Topical Stud. Oceanography* 57, 916–933. doi: 10.1016/j.dsr2.2008.06.013

Kawaguchi, S., Atkinson, A., Bahlburg, D., Bernard, K. S., Cavan, E. L., Cox, M. J., et al. (2024). Climate change impacts on Antarctic krill behavior and population dynamics. *Nat. Rev. Earth Environ.* 5, 43–58. doi: 10.1038/s43017-023-00504-y

Kawaguchi, S., and Nicol, S. (2020). "Krill fishery," in *Fisheries and aquaculture*. Eds. G. Lovrich and M. Thiel (Oxford University Press). doi: 10.1093/oso/9780190865627.003.0006

Kelly, N., Emmerson, L., Kawaguchi, S., Southwell, D., and Welsford, D. (2018). "An ecological risk assessment of current conservation measures for krill fishing in East Antarctica (CCAMLR Divisions 58.4.1 and 58.4.2)," in *Document WG-EMM-18/37* (Hobart, Tasmania, Australia: CCAMLR).

Kinzey, D., and Watters, G. (2023). "Casal2 stock assessment for antarctic krill in CCAMLR subarea 48.1," in *Document WG-FSA-23/14* (Hobart, Tasmania, Australia: CCAMLR).

Kinzey, D., Hinke, J. T., Reiss, C. S., and Watters, G. M. (2023). ecruitment variability of Antarctic krill in Subarea 48.1 expressed as 'proportional recruitment': length threshold effects. *CCAMLR Sci.* 24, 1–18.

Kinzey, D., Watters, G., and Reiss, C. S. (2013). Effects of recruitment variability and natural mortality on generalised yield model projections and the CCAMLR decision rules for Antarctic krill. *CCAMLR Sci.* 20, 81–96.

Kinzey, D., Watters, G. M., and Reiss, C. S. (2015). Selectivity and two biomass measures in an age-based assessment of Antarctic krill (Euphausia superba). *Fisheries Res.* 168, 72–84. doi: 10.1016/j.fishres.2015.03.023

Kokubun, N., Hamabe, K., Yamada, N., Sasaki, H., Nishizawa, B., Watanuki, Y., et al. (2024). Abundance and estimated food consumption of seabirds in the pelagic ecosystem in the eastern Indian sector of the Southern Ocean. *Prog. Oceanography*, 231, 103385. doi: 10.1016/j.pocean.2024.103385

Krafft, B. A., Macaulay, G. J., Skaret, G., Knutsen, T., Bergstad, O. A., Lowther, A., et al. (2021). Standing stock of Antarctic krill (Euphausia superba Dana 1850) (Euphausiacea) in the Southwest Atlantic sector of the Southern Ocean 2018-19. *J. Crustacean Biol.* 41 (4), 1-17. doi: 10.1093/jcbiol/ruab046

Liu, J., Wotherspoon, S., and Maschette, D. (2023). Multi-fleet stock assessment modelling with the Grym. *CCAMLR Sci.* 24, 95–109.

Makarov, R. R., and Denys, C. J. (1980). Stages of sexual maturity of Euphausia superba. *Biomass Handb.* 11, 1–13.

Mardones, M., Krüger, L., Santa Cruz, F., Cárdenas, C., and Watters, G. (2024). "Integrated approach to modeling krill population dynamics in the Western Antarctic Peninsula: spatial and ecosystem considerations," in *Document WG-FSA-24/27* (Hobart, Tasmania, Australia: CCAMLR).

Maschette, D., and Dell, J. (2015). "An updated assessment of unicorn icefish (Channichthys rhinoceratus) in Division 58.5.2, based on results from the 2015 random stratified trawl survey," in *Document WG-FSA-15/50* (Hobart, Tasmania, Australia: CCAMLR).

Maschette, D., and Wotherspoon, S. (2023). Description and use of parameters within Antarctic krill (Euphausia superba) assessment models conducted with the Grym. *CCAMLR Sci.* 24, 58–68.

Maschette, D., Sumner, M., and Raymond, B. (2019). *SOmap: Southern Ocean maps*. Version 0.5.0. Available online at: https://github.com/AustralianAntarcticDivision/SOmap

Maschette, D., Wotherspoon, S., Kawaguchi, S., and Ziegler, P. (2021). "Grym assessment for Subarea 48.1 Euphausia superba populations," in *Document WG-FSA-2021/39* (CCAMLR, Hobart, Australia).

Maschette, D., Wotherspoon, S., Pavez, S., Ziegler, P., Thanassekos, S., Reid, K., et al. (2023). Grym: A new open-source implementation of the generalised yield model for flexible stock assessments. *CCAMLR Sci.* 24, 69–94.

Melvin, J. E., Kawaguchi, S., King, R., and Swadling, K. M. (2018). The carapace matters: refinement of the instantaneous growth rate method for Antarctic krill Euphausia superba Dana, 1850 (Euphausiacea). *J. Crustacean Biol.* 38, 689–696. doi: 10.1093/jcbiol/ruy069

Methot, R. D., and Wetzel, C. R. (2013). Stock Synthesis: A biological and statistical framework for fish stock assessment and fishery management. *Fisheries Res.* 142, 86–99. doi: 10.1016/j.fishres.2012.10.012

Meyer, B., Atkinson, A., Bernard, K. S., Brierley, A. S., Driscoll, R., Hill, S. L., et al. (2020). Successful ecosystem-based management of Antarctic krill should address uncertainties in krill recruitment, behaviour and ecological adaptation. *Commun. Earth Environ.* 1, 28. doi: 10.1038/s43247-020-00026-1

Morris, D. J., Watkins, J. L., Ricketts, C., Buchholz, F., and Priddle, J. (1988). An assessment of the metrics of length and weight measurements of Antarctic krill *Euphausia supeba*. *Br. Antarctic Survey Bull.* 79, 27–50. Available online at: https://nora.nerc.ac.uk/id/eprint/521694.

Murase, H., Abe, K., Schaafsma, F. L., and Katsumata, K. (2025). Overview of the multidisciplinary ecosystem survey in the eastern Indian sector of the Southern Ocean (80–150°E) by the Japanese research vessel Kaiyo-maru in the 2018–19 austral summer (KY1804 survey). *Prog. Oceanography* 103456. doi: 10.1016/j.pocean.2025.103456

Nicol, S. (2000). BROKE" A multidisciplinary survey of the waters off East Antarctica (80-150D). *Deep-Sea Res. II* 47, 2281–2613. doi: 10.1016/S0967-0645(00)00026-6

Nicol, S., Foster, J., and Kawaguchi, S. (2012). The fishery for Antarctic krill – recent developments. *Fish Fisheries* 13, 30–40. doi: 10.1111/j.1467-2979.2011.00406.x

Nicol, S., Meiners, K., and Raymond, B. (2010). BROKE-West, a large ecosystem survey of the South West Indian Ocean sector of the Southern Ocean, 30°E–80°E (CCAMLR Division 58.4.2). *Deep Sea Res. Part II: Topical Stud. Oceanography* 57, 693–700. doi: 10.1016/j.dsr2.2009.11.002

Nicol, S., and Pauly, T. (2000). "A proposal to subdivide CCAMLR Statistical Division 58.4.1 using environmental data," in *Document WG-EMM-00/30* (Hobart, Tasmania, Australia: CCAMLR).

Nicol, S., Pauly, T., Bindoff, N. L., Wright, S., Thiele, D., Hosie, G. W., et al. (2000). Ocean circulation off east Antarctica affects ecosystem structure and sea-ice extent. *Nature* 406, 504–507. doi: 10.1038/35020053

Pakhomov, E. A. (1995a). Demographic studies of Antarctic krill Euphausia superba in the Cooperation and Cosmonaut Seas (Indian sector of the Southern Ocean). *Mar. Ecol. Prog. Ser.* 119, 45–61. doi: 10.3354/meps119045

Pakhomov, E. A. (1995b). Natural age-dependent mortality rates of Antarctic krill Euphausia superba Dana in the Indian sector of the Southern Ocean. *Polar Biol.* 15, 69–71. doi: 10.1007/BF00236127

Pauly, T., Nicol, S., Higginbottom, I., Hosie, G., and Kitchener, J. (2000). Distribution and abundance of Antarctic krill (Euphausia superba) off East Antarctica (80-150 degrees E) during the Austral summer of 1995/1996. *Deep-Sea Res. Part Ii-Topical Stud. Oceanography* 47, 2465–2488. doi: 10.1016/S0967-0645(00)00032-1

Pavez, C., Wotherspoon, S., Maschette, D., Reid, K., and Swadling, K. (2023). Recruitment modelling for Euphausia superba stock assessments considering the recurrence of years with low recruitment. *CCAMLR Sci.* 24, 110–124.

Punt, A. E. (2023). Those who fail to learn from history are condemned to repeat it: A perspective on current stock assessment good practices and the consequences of not following them. *Fisheries Res.* 261, 106642. doi: 10.1016/j.fishres.2023.106642

SC-CAMLR (1994). *Report of the thirteenth meeting of the Scientific Committee* (Hobart, Australia: CCAMLR).

SC-CAMLR (2000). "Report of the working group on ecosystem monitoring and management, annex 4," in *Report of the nineteenth meeting of the Scientific Committee* (CCAMLR, Hobart, Tasmania, Australia).

SC-CAMLR (2016). "Report of the working group on statistics, assessments and modelling, annex 5," in *Report of the thirty-fifth meeting of the scientific committee* (CCAMLR, Hobart, Tasmania, Australia).

SC-CAMLR (2019). *Report of the thirty-eighth meeting of the Scientific Committee* (Hobart, Australia: CCAMLR).

SC-CAMLR (2021). *Report of the fortieth meeting of the scientific committee* (Hobart, Australia: CCAMLR).

SC-CAMLR (2023). *Report of the fourty-second meeting of the scientific committee* (Hobart, Australia: CCAMLR).

Schaafsma, F. L., Driscoll, R., Matsuno, K., Sugioka, R., Driscoll, S., van Regteren, M., et al. (2024). Demography of Antarctic krill (*Euphausia superba*) from the KY1804 austral summer survey in the eastern Indian sector of the Southern Ocean (80 to 150°E), including specific investigations of the upper surface waters. *Front. Mar. Sci.* 11. doi: 10.3389/fmars.2024.1411130

Siegel, V. (1987). Age and growth of Antarctic Euphausiacea (Crustacea) under natural conditions. *Mar. Biol.* 96, 483–495. doi: 10.1007/BF00397966

Siegel, V., de la Mare, W. K., and Loeb, V. (1997). Long-term monitoring of krill recruitment and abundance indices in the Elephant Island area (Antarctic Peninsula). *CCAMLR Sci.* 4, 19–35.

Siegel, V., and Loeb, V. (1994). Length and age at maturity of Antarctic krill. *Antarctic Sci.* 6, 479–482. doi: 10.1017/S0954102094000726

Sylvester, Z. T., Long, M. C., and Brooks, C. M. (2021). Detecting climate signals in southern ocean krill growth habitat. *Front. Mar. Sci.* 8. doi: 10.3389/fmars.2021.669508

Tarling, G. A., Hill, S., Peat, H., Fielding, S., Reiss, C., and Atkinson, A. (2016). Growth and shrinkage in Antarctic krill Euphausia superba is sex-dependent. *Mar. Ecol. Prog. Ser.* 547, 61–78. doi: 10.3354/meps11634

Thompson, A. F., and Youngs, M. K. (2013). Surface exchange between the weddell and scotia seas. *Geophysical Res. Lett.* 40, 5920–5925. doi: 10.1002/2013GL058114

Thomson, R. (2016). *Center for Independent Experts (CIE) independent peer reviewer's report of an age-based, integrated stock assessment for Antarctic krill (*Euphausia superba*) with projected catches to 2035* (Center for Independent Experts NOAA). Available online at: https://www.st.nmfs.noaa.gov/science-quality-assurance/cie-peer-reviews/cie-review-2016.

Veytia, D., Corney, S., Meiners, K. M., Kawaguchi, S., Murphy, E. J., and Bestley, S. (2020). Circumpolar projections of Antarctic krill growth potential. *Nat. Climate Change* 10, 568–575. doi: 10.1038/s41558-020-0758-4

Wang, R., Song, P., Li, Y., and Lin, L. (2021). An integrated, size-structured stock assessment of antarctic krill, *euphausia superba*. *Front. Mar. Sci.* 8. doi: 10.3389/fmars.2021.710544

Watters, G. M., Hinke, J. T., and Reiss, C. S. (2020). Long-term observations from Antarctica demonstrate that mismatched scales of fisheries management and predator-prey interaction lead to erroneous conclusions about precaution. *Sci. Rep.* 10, 2314. doi: 10.1038/s41598-020-59223-9

Wotherspoon, S., and Maschette, D. (2023). *Grym: R implementation of the Generalized Yield Model*. R package version 0.1.2. Available online at: https://github.com/AustralianAntarcticDivision/Grym.

Young, E. F., Thorpe, S. E., Renner, A. H. H., and Murphy, E. J. (2024). Environmental and behavioural drivers of Antarctic krill distribution at the South Orkney Islands: A regional perspective. *J. Mar. Syst.* 241, 103920. doi: 10.1016/j.jmarsys.2023.103920

Ziegler, P., and Welsford, D. C. (2017). "The Patagonian toothfish (*Dissostichus eleginoides*) fishery at Heard Island and McDonald Islands (HIMI) – population structure and history of the fishery stock assessment," in *The Kerguelen Plateau: marine ecosystem and fisheries. Proceedings of the Second Symposium*. Eds. D. ,. J.D. Welsford and G. Duhamel (Australian Antarctic Division, Kingston, Tasmania, Australia).

frontiers | Frontiers in Marine Science

TYPE Original Research
PUBLISHED 19 May 2025
DOI 10.3389/fmars.2025.1502498

Check for updates

OPEN ACCESS

EDITED BY
Luca Rindi,
University of Pisa, Italy

REVIEWED BY
Sara Verni,
University of Pisa, Italy
Erica Jarvis Mason,
National Oceanic and Atmospheric Administration, United States

*CORRESPONDENCE
Leonie Suter
leonie.suter@aad.gov.au

RECEIVED 26 September 2024
ACCEPTED 18 April 2025
PUBLISHED 19 May 2025

CITATION
Suter L, Burns A, Bestley S, Bird J, Brasier MJ, Cox M, Hamer D, Johnson OJ, Kawaguchi S, King R, Klocker A, Melvin J, Weldrick CK, Wotherspoon S and Raymond B (2025) Monitoring Antarctic krill (*Euphausia superba*) distribution in the Southern Ocean: environmental DNA (eDNA) adds to the toolbox.
Front. Mar. Sci. 12:1502498.
doi: 10.3389/fmars.2025.1502498

COPYRIGHT
© 2025 Suter, Burns, Bestley, Bird, Brasier, Cox, Hamer, Johnson, Kawaguchi, King, Klocker, Melvin, Weldrick, Wotherspoon and Raymond. This is an open-access article distributed under the terms of the Creative Commons Attribution License (CC BY). The use, distribution or reproduction in other forums is permitted, provided the original author(s) and the copyright owner(s) are credited and that the original publication in this journal is cited, in accordance with accepted academic practice. No use, distribution or reproduction is permitted which does not comply with these terms.

Monitoring Antarctic krill (*Euphausia superba*) distribution in the Southern Ocean: environmental DNA (eDNA) adds to the toolbox

Leonie Suter[1,2*], Alicia Burns[3,4,5], Sophie Bestley[2,6], Jez Bird[2], Madeleine J. Brasier[1,2], Martin Cox[1,6], Derek Hamer[7], Olivia J. Johnson[2], So Kawaguchi[1,2,6], Rob King[1,6], Andreas Klocker[8], Jessica Melvin[2], Christine K. Weldrick[2,6], Simon Wotherspoon[1] and Ben Raymond[1,6]

[1]Australian Antarctic Division, Department of Climate Change, Energy, the Environment and Water, Kingston, TAS, Australia, [2]Institute for Marine and Antarctic Studies, University of Tasmania, Hobart, TAS, Australia, [3]School of Life and Environmental Sciences, University of Sydney, Sydney, NSW, Australia, [4]Cluster of Excellence 'Science of Intelligence' Technical University of Berlin, Berlin, Germany, [5]Faculty of Life Science, Humboldt University, Berlin, Germany, [6]Australian Antarctic Program Partnership, Institute of Marine and Antarctic Studies, University of Tasmania, Hobart, TAS, Australia, [7]Forest Policy Branch, Renewables, Climate and Future Industries Tasmania, Department of State Growth, Hobart, TAS, Australia, [8]NORCE Norwegian Research Centre, Bjerknes Centre for Climate Research, Bergen, Norway

Antarctic krill (*Euphausia superba* Dana) is a key species of the Southern Ocean ecosystem, immensely abundant and targeted by the krill fishery. For their sustainable management, krill distribution and biomass estimates are required, typically achieved through acoustic-trawl surveys. We explore how krill environmental DNA (eDNA) can contribute to our understanding or Antarctic krill habitat and distribution. We collected eDNA samples by filtering five liters of seawater per sample in the East Antarctic Southern Ocean from the surface (5 m depth) and seafloor (381–4422 m depth, total n = 110). We used quantitative PCR to measure Antarctic krill eDNA abundance and age, and eDNA metabarcoding to detect any krill species. This eDNA data was compared to acoustic, visual and trawl detections of Antarctic krill. Antarctic krill eDNA was common in surface samples and largely overlapped with visual and trawl detections. Highest eDNA concentrations were detected above krill swarms, with concentrations declining with increasing distance from swarms. Near recent eDNA sampling locations, krill swarms were more likely acoustically detected than near old eDNA sampling locations. Antarctic krill detections were less common in seafloor locations, and detections were concentrated in the continental slope area to the south of the survey area, both for visual detections and for recent eDNA detections. Both methods detected Antarctic krill at great depths (recent eDNA: 4300 m; visual: 3080 m). In both eDNA and trawl data, Antarctic krill was the dominant krill species, followed by *Thysanoessa macrura* G.O. Sars, which was particularly

abundant in larval stages throughout the survey area, including at Antarctic krill swarm locations. We recommend the inclusion of eDNA data for Antarctic krill distribution estimates and understanding of habitat use, particularly in difficult-to-access areas, such as under ice or benthic habitats.

KEYWORDS

Antarctic krill, *Euphausia superba*, eDNA, fishery management, survey tools

1 Introduction

Antarctic krill (*Euphausia superba* Dana) is a key species of the Southern Ocean, feeding on primary producers (phytoplankton) and small zooplankton, and in turn being preyed upon by a vast array of Southern Ocean predators, including fish, seabirds, seals and whales (Trathan and Hill, 2016; Schmidt and Atkinson, 2016), thus forming a central node in the Southern Ocean food web (Siegel, 2016; Everson, 2008). Antarctic krill is enormously abundant, with an estimated biomass of 379 million tons (Atkinson et al., 2009) – possibly the most abundant wild animal species on earth (Tarling and Fielding, 2016). Antarctic krill can form dense swarms near the surface (epipelagic zone; upper 250 m), which can contain hundreds, sometimes thousands of individual krill per cubic meter (Tarling et al., 2009; Cox et al., 2011). Typical smaller swarms extend 50–100 m horizontally, but occasional densely packed superswarms can extend over many kilometers in length and over 100 m in depth, containing vast amounts of krill biomass (Tarling et al., 2009; Cox et al., 2011). Antarctic krill are good swimmers and may actively move large distances (Atkinson et al., 2008; Kils, 1982; Richerson et al., 2015). They can also perform seasonal and diel vertical migration, e.g. moving to the food-rich surface (epipelagic zone) at night to avoid visual predators, and retreating to the deeper, darker mesopelagic zone during the day (Bahlburg et al., 2023; Kalinowski and Witek, 1980). They have also been observed near the seafloor in the bathypelagic zone down to 3500 m, where they may actively feed on seabed detritus year-round (Clarke and Tyler, 2008; Schmidt et al., 2011), making the benthic environment a potentially important retreat habitat for Antarctic krill. The rapid sinking of their carbon-rich fecal pellets and molts and their vertical migrations contribute to the marine biological carbon pump and long-term carbon storage in seafloor sediments (Gleiber et al., 2012; Cavan et al., 2019; Smith et al., 2025). Krill also play an important role in nutrient cycling (e.g. iron, nitrogen), which is critical for phytoplankton growth in the Southern Ocean (Schmidt et al., 2011; Cavan et al., 2019). During the Antarctic winter, sea ice forms an important part of Antarctic krill's habitat, particularly for larval and juvenile krill (Meyer et al., 2017). Antarctic krill's distribution range may be contracting southwards (Atkinson et al., 2019; Kawaguchi et al., 2024), likely driven by climate change pressures such as increasing water temperatures, reduced sea ice extent and ocean acidification (Flores et al., 2012; Cavanagh et al., 2021), however, the overall status of Antarctic krill population changes remain unclear (Atkinson et al., 2004; Cox et al., 2018).

Antarctic krill are also targeted by the krill fishery due to their dense nutritional and specialized pharmaceutical values, with the main fishery products sold as meal and oil (Kawaguchi and Nicol, 2020; Hill, 2013). The krill fishery is expanding, particularly around the Antarctic Peninsula, South Orkneys and South Georgia Islands and may expand into East Antarctica again after a multi-decade hiatus in this region (Kawaguchi and Nicol, 2020; Trathan, 2023). The krill fishery is sustainably managed by the Commission for the Conservation of Antarctic Marine Living Resources (CCAMLR; ccamlr.org; Constable and Nicol (2002); Miller and Agnew (2000)), which takes a precautionary approach to the management of krill fishing. To set precautionary catch limits, the CCAMLR requires biomass estimates for each management zone, which are achieved through acoustic-trawl surveys (e.g. Krafft et al., 2021; Cox et al., 2022; Hewitt et al., 2004). Acoustic-trawl surveys are typically carried out from a ship equipped with scientific (i.e. calibrated) downward looking echosounders accompanied by scientific net sampling. Both net and acoustic data are required for Antarctic krill biomass estimation (Reiss et al., 2008; Watkins et al., 2016; Cox et al., 2011). The management zones of the Antarctic Peninsula, South Orkney Islands, and South Georgia are relatively small (CCAMLR management areas 48.1, 48.2 and 48.3, see https://gis.ccamlr.org/) and accessible, and surveys are conducted regularly (Skaret et al., 2023; Fielding et al., 2014; Cutter et al., 2022). In contrast, the management zones off East Antarctica cover larger areas (CCAMLR management areas 58.4.1 and 58.4.2, see https://gis.ccamlr.org/), and distances to commercial ports are greater, making this area harder to access and more difficult to survey comprehensively. As a result, East Antarctic management zones are less frequently surveyed, leading to sparser temporal and geographic coverage of distribution and biomass surveys in this region (Jarvis et al., 2010; Cox et al., 2022; Baldo et al., 2006), which makes accurate and up-to-date Antarctic krill biomass estimates in East Antarctica challenging.

Here we explore whether environmental DNA (eDNA) – genetic material shed into the environment by all organisms, including krill – can provide an additional data layer to determine Antarctic krill distribution and abundance. The use of eDNA-based surveys is rapidly expanding across a huge range of

habitats, including marine, freshwater and terrestrial (Ruppert et al., 2019; Taberlet et al., 2018). In the marine environment eDNA surveys are for example used to determine reef biodiversity (Dugal et al., 2023; Mathon et al., 2022), to assess species distributions (Yu et al., 2022; Gargan et al., 2017) or to detect marine invasive species (LeBlanc et al., 2020; Ellis et al., 2022), to name a few applications.

Typically, two methods can be employed when assessing eDNA samples for species presence and/or abundance: firstly, species-specific assays using quantitative PCR (qPCR) can be used to assess the presence and abundance of eDNA shed by a single species (Langlois et al., 2021). These markers need to be carefully designed and validated to ensure their species-specificity, as cross-amplification of eDNA of different species could lead to false positive detections (De Brauwer et al., 2023; Langlois et al., 2021). Species-specific assays are typically more sensitive at detecting the presence of a species than metabarcoding assays (see below; Yu et al., 2022; McColl-Gausden et al., 2023) and separate assays have been developed to detect the presence and distribution of many species, including marine invasive species (Clarke et al., 2023; Roux et al., 2020; Wood et al., 2017). eDNA abundance can correlate with species abundance (Rourke et al., 2022; Lacoursière-Roussel et al., 2016; Yates et al., 2019; Salter et al., 2019), but calibrations are difficult and many variables (e.g. volume of the body of water, currents, eDNA degradation properties) can affect eDNA abundance, persistence and detectability (Yates et al., 2021). As eDNA may persist in some environments for extended periods, several studies have attempted to determine eDNA fragmentation by developing sets of species-specific markers of different amplicon length (Jo et al., 2017; Bylemans et al., 2018; Suter et al., 2023). More fragmented eDNA could indicate longer time since eDNA shedding, and incorporating such temporal aspects to eDNA-based surveys could greatly aid the interpretation of eDNA abundance measurements.

Secondly, metabarcoding markers can be used to detect multiple taxa simultaneously, for example all animal species (Suter et al., 2021; Nester et al., 2024; Jeunen et al., 2019) or all fish species (Miya, 2022; Bessey et al., 2020). Metabarcoding markers amplify sections of genes or DNA that are shared between all targeted taxa and act as 'barcodes': these DNA sequences differ between taxa, and through comparisons to reference databases the taxonomic composition of mixed eDNA samples can be determined (Deiner et al., 2017). Metabarcoding data can provide presence/absence information of taxa, as well as an estimate of relative abundance of taxa within a sample. Through elaborate calibrations taxa abundance across samples can be estimated from metabarcoding data, but these methods are complex, and not typically employed (Deiner et al., 2017; Luo et al., 2022).

In this study, we assess how eDNA-based methods can contribute to Antarctic krill surveys, using eDNA samples collected in East Antarctica from seawater collected near the surface and the seafloor. We firstly use two Antarctic krill-specific qPCR markers of different lengths (Suter et al., 2023) to assess Antarctic krill eDNA abundance and eDNA age. We use the eDNA concentration of the short marker to estimate overall krill eDNA abundance. In addition, we estimate the age of Antarctic krill eDNA in each sample by comparing the relative abundance of the short and the long marker using a model fitted to experimental data of known age and the concept that if the short and long markers are similarly abundant, the eDNA is considered relatively intact and therefore recent. If the short marker is more abundant than the long marker, the eDNA is considered fragmented and therefore old. Secondly, we use a euphausiid-specific metabarcoding marker that can detect any Southern Ocean krill species (Suter et al., 2023), revealing overall krill distribution patterns in the Southern Ocean. To achieve a broad, semi-quantitative eDNA abundance estimate of all krill species, we use the species-specific assay to calibrate the metabarcoding data across samples.

We then compare this eDNA-data to other Antarctic krill survey methods, including acoustic, visual and trawl surveys, to get a holistic perspective on Antarctic krill distribution and abundance in the Southern Ocean. We explore how Antarctic krill eDNA spreads and decays through the Southern Ocean environment, assess whether krill eDNA abundance and age patterns are reflected in Antarctic krill assessments of other data streams and highlight strengths and challenges for each data stream. Lastly, we recommend how eDNA-methods should be used in conjunction with other data streams in future surveys to improve our understanding of Antarctic krill distribution and habitat use.

2 Methods

2.1 Survey area

Multidisciplinary data was collected on board the RV *Investigator* on a research expedition named "Trends in Euphausiids off Mawson, Predators and Oceanography (TEMPO)" (IN2021_V01) between 13 February and 12 March 2021 in the eastern sector of the CCAMLR Division 58.4.2. The survey area was divided into six longitudinal transects (transect 1: 55°E; transect 2: 60°E; transect 3: 65°E; transect 4: 70°E; transect 5: 75°E, transect 6: 80°E), south of 62°S for transects 1 – 4, and south of 63°S for transects 5 and 6, with the southern end of each transect limited by the sea ice edge, varying between approximately 65°S and 68°S (Figure 1). Multiple data streams were collected: eDNA, acoustic, visual and trawl data (Table 1). The research was conducted under the Antarctic Marine Living Resources Conservation Act 1981 (Australia) Permit AMLR 20-23-4512.

2.2 Data collection

2.2.1 eDNA samples

2.2.1.1 Sample collection

Seawater samples (5 L each) were collected at 50 CTD stations. At each station, a sample was collected from the surface (approximately 5 m depth) as well as from near the seafloor (seafloor depth at CTD stations ranged from 381 m to 4422 m depth), resulting in a total of 98 CTD samples (two seafloor eDNA

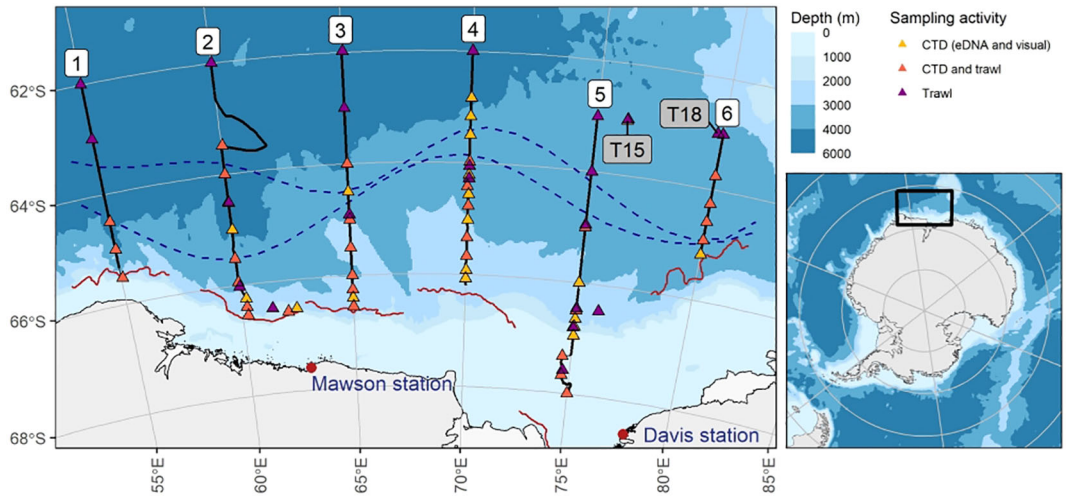


FIGURE 1
Overview of the survey area in relation to the broader Antarctic (map inset) and collected samples. Numbers 1 – 6 (white background) denote the six survey transects. Triangles denote sampling stations; black lines represent acoustic data collection along transects (1-6). T15 and T18 (grey background) indicate the location of two targeted krill swarms. Dotted lines indicate Southern Ocean oceanic fronts during the TEMPO voyage following Foppert et al. (2024): the northern line denotes the Southern Antarctic Circumpolar Current Front, at southern line the Southern Boundary of the Antarctic Circumpolar Current. The red wavy lines south of each transect indicate the sea ice edge at the time of each transect.

samples were unsuccessful). CTD operations were conducted using Sea-Bird SBE911 instrumentation and 31 x 12 L Niskin bottles on a rosette. In addition, two eDNA samples each were collected within two krill swarms (T15 and T18) from the ship's uncontaminated seawater line (5 L, depth approximately 5 m), and as the ship was moving away from the krill swarm, four further samples were collected at each krill swarm (n = 12). Seawater was transferred from the CTDs into a 5 L Cole-Parmer essentials wide mouth carboy (Cole-Palmer), or directly collected in these carboys if sampled from the uncontaminated seawater line. Samples were kept in a refrigerator at 4°C until filtering. Samples were filtered onto hydrophilic polyvinylidene fluoride membrane filter discs (5 µm pore size, 47 mm diameter; Merck) using a Masterflex L/S peristaltic pump (John Morris Scientific), either until all water was filtered (most samples), or until the filter got clogged, in which case the filtered volume was recorded. Every 10th sample was a field control consisting of 5 L Milli-Q water processed as described above. After each filtering round, all filtering equipment and laboratory desk surfaces were sterilized using 1% bleach followed by thorough rinsing with Milli-Q water. After filtering, every filter was halved, and both halves stored in separate 1.5 mL DNA LoBind Tubes (Eppendorf), which were stored at -80°C until DNA extraction.

2.2.1.2 DNA extraction

DNA was extracted from one half filter per sample, while the other half was kept for biobanking (Jarman et al., 2018) at -80°C for future studies. Samples were sent to eDNA frontiers (eDNA frontiers, Perth, Australia; http://www.ednafrontiers.com/) for DNA extraction using Qiagen DNeasy Blood & Tissue Kit (Qiagen) with the following minor modifications from the manufacturer's protocol: 540 µl of buffer ATL and 60 µl proteinase K were added to the filters and incubated at 56°C overnight, and samples were eluted in 100 µl elution buffer. Nine extraction blanks containing no filter material were extracted with the samples.

2.2.2 Species-specific *E. superba* assay

2.2.2.1 qPCR markers and conditions

To estimate Antarctic krill eDNA concentrations and eDNA age, two species-specific primer combinations developed by Suter et al. (2023) were used to amplify a short 16S rRNA gene fragment (henceforth called "short marker") and a long 16S rRNA gene fragment (henceforth called "long marker"). The short and long marker use the same forward primer (E_superba_16S_F3: 5'-TATTAAAGGATCATTCACACA-3') and fluorescent probe (E_superba_16S_Probe: 5'-/56-FAM/CGCCCCAAT/ZEN/AAAATAAATTCCACAAT/3IABkFQ/-3'), but different reverse primers, resulting in different lengths of amplicons: the short marker uses the E_superba_16S_R1 reverse primer (5'-AAGTGGAGTAGTTGATTAAAAC-3'), resulting in an amplicon length of 126 base pairs (bp), while the long marker uses the E_superba_16S_R3 reverse primer (5'-GTGCTAAGTAACTCGGCAAA-3'), resulting in an amplicon length of 412 bp. Quantitative PCR (qPCR) amplifications were conducted in 10 µL total reaction volume, including 2X PrimeTime gene expression master mix (integrated DNA Technologies), 0.5 µM of forward and reverse primer, 0.25 µM Probe and 2 µL of undiluted DNA template.

All qPCR amplifications were done in triplicates on a QuantStudio 6 Real Time PCR System (Thermo Fisher Scientific) using 384 well plates with the following cycling conditions: 95°C for 3 min, 45 cycles of 95°C for 15 sec, 60°C for 30 sec, 65°C for 45 sec, followed by a final extension of 72°C for 2 min. All qPCR plates

TABLE 1 Data streams collected in this study: what, where and how they measure presence or abundance of krill species, and a summary of their strengths and challenges.

	eDNA qPCR	eDNA metabarcoding	Acoustic	Visual	Trawl – RMT8	Trawl – RMT1
Target species	*E. superba*	Any euphausiid species	*E. superba*	*E. superba*	Any euphausiid species	*E. superba*, *T. macrura*, 'other' euphausiid (grouped)
Target developmental stage	Any, plus faeces, moults, etc	Any, plus faeces, moults, etc	Adult, juvenile	Adult, juvenile	Adult, juvenile	Larvae
Data type	Krill eDNA presence, abundance and age	Krill eDNA presence, estimate of eDNA abundance	Krill biomass, krill density	Krill abundance	Krill density	Krill density
Detection unit	DNA fragments	DNA fragment	Acoustic reflection of swarms	Video footage	Trawl catch	Trawl catch
Radius of detection	Unclear; potentially ~2.8 km for recent, further for old eDNA	Unclear – likely multiple km	250 m from ship	~5 m from camera	~200 m depth	~200 m depth
Sampling depth	Surface (5 m), Seafloor (down to 4422 m)	Surface (5 m), Seafloor (down to 4422 m)	Surface (within 250 m)	Surface (5 m), Seafloor (down to 4422 m)	Surface (within 200 m)	Surface (within 200 m)
Sampling location	At CTD stations (n = 50)	At CTD stations (n = 50)	Continuously	At CTD stations (n = 50)	At trawl stations (n = 53)	At trawl stations (n = 48)
Detection time	Potentially hours (short) for recent DNA Potentially days (long) for old DNA	Potentially days	Immediate	Immediate	Immediate	Immediate
Strengths	- Large temporal, geographic and depth coverage - eDNA abundance and age provide dynamic picture - Any developmental stage detectable	- Large temporal, geographic and depth coverage - Any Krill species can be detected - Any developmental stage detectable	- Precise estimate of biomass - Continuous survey - Fast data processing	- Any depth can be surveyed - Estimate of krill abundance - Fast data processing	- Developmental stage, sex, size of krill measurable - Any Krill species can be detected - Fast data processing	- Larval stages can be differentiated - Multiple krill species can be detected
Challenges	- Data processing, analysis and interpretation complex and slow - Origin of eDNA variable - Developmental stage, size etc not measurable - Relatively sparse data collection	- Data curation complex and slow - Abundance estimates imprecise - Origin of eDNA variable - developmental stage, size etc not measurable - Relatively sparse data collection	- Only adult/juvenile krill detectable - limited detection radius - only immediate presence of krill detectable	- Very limited detection radius - Only immediate presence of krill detectable - Only adult/juvenile krill detectable - Species ID uncertain - Relatively sparse data collection	- Limited depth - Only adult/juvenile krill detectable - Relatively sparse data collection - Krill swarms are often missed	- Adult/juvenile krill not representative - Limited depth - Relatively sparse data collection - Larvae of several krill species cannot be differentiated - Slow data processing

10.3389/fmars.2025.1502498

included triplicates of non-template negative controls (NTCs) and positive control (gblock fragment with 100 copies, see Suter et al. (2023)). Pre-PCR setups were prepared in a physically separate and PCR product free laboratory to minimize the risk of contamination.

2.2.2.2 Limits of detection and quantification

The copy number of gblock fragments per µL was calculated from the DNA concentration – measured using a Qubit DNA HS assay kit with a Qubit 2.0 Fluorometer (Life Technologies, Carlsbad, CA, USA) – and the molecular weight of the gblock fragment. To determine both the limit of detection (LOD) and limit of quantification (LOQ) for each marker, the gblock fragment was serially diluted to the following copy numbers per dilution standard: 100, 10, 2, 1, 0.5, 0.25, 0.125, 0.0625. qPCR amplifications were done in 12 replica per marker per standard with the PCR conditions as described above. The lowest standard with 95% of amplifications across all replicates determined the LOD, and the lowest standard with a coefficient of variation (CV) below 35% determined the LOQ (Klymus et al., 2020b). To derive the LODs, LOQs and primer efficiencies of the assay, the data was analyzed in RStudio (v 2022.02.2) following Klymus et al. (2020a) and Suter et al. (2023).

2.2.2.3 eDNA abundance calculations

qPCR results were quantified if at least two out of three technical replicas were within an acceptable quantification cycle (Cq) range, following Suter et al. (2023) and De Ronde et al. (2017). Acceptable ranges increased with increasing mean Cq value (range for mean Cq < 32 was 0.5, for > 32 it was 0.7, for > 33 it was 0.9, for Cq > 34 it was 1.3 and for > 35 it was 1.5). Outliers falling outside of these ranges were excluded if the other two technical replica fell within the acceptable range. Average Cq values of acceptable technical replicas were used. qPCR results that only had Cq values for one of three technical replicas were excluded. Copy number per qPCR sample were calculated separately for each qPCR plate using the intercept and slope calculated for each marker during the standard curve assessment, the Cq value of the samples and the Cq value of the standard gblock fragments (100 copies) on each qPCR plate. If copies detected in both markers per sample were below the limit of detection for three technical replicas, the data was removed. If only one of the two markers was below this threshold, copy numbers were retained, as the sample was considered to contain krill eDNA. The copy numbers per PCR amplification were then multiplied by 100 to calculate copy numbers per 5 L sample (DNA of half a filter eluted in 100 µl, 2 µl used per qPCR), and in samples were less than 5 L of seawater was filtered due to filter clogging, the copy number was divided by the proportion of 5 L that was filtered for those samples.

2.2.2.4 eDNA age classification

Antarctic krill eDNA detected in samples was estimated to "recent", "old" or "undetermined" based on the level of DNA fragmentation detected in each sample. The underlying concept to this approach assumes that eDNA recently shed into the environment is relatively intact and consists of long DNA fragments. A long and a short eDNA marker would therefore detect similar concentrations of eDNA. However, the longer the eDNA remains in the environment, the more fragmented it becomes. The proportion of short *vs* long fragments therefore increases, and a short marker would detect higher concentrations of eDNA than a long marker. To determine the likelihood of a sample of the current study being "recent" or "old", we applied a binomial generalized linear model developed by Suter et al. (2023) based on experimental Antarctic krill eDNA fragmentation data of known eDNA age. Samples associated with model probabilities close to zero (<0.1) were considered "recent", whereas samples associated with model probabilities close to one (>0.9) were considered "old". Samples that were not clearly "recent" or "old", i.e. with probabilities between 0.1 and 0.9, were classified as "undetermined". If krill eDNA was only detected with the short marker, the eDNA was considered fragmented and therefore "old". If eDNA was only detected with the long marker, eDNA was considered present at "undetermined" age, and the short marker read numbers were copied from the long marker read numbers.

2.2.3 Euphausiid metabarcoding

2.2.3.1 PCR and sequencing

A 16S euphausiid-specific metabarcoding marker [forward primer Euph_F: GTGACGATAAGACCCTATA (Suter et al., 2023); reverse primer Crust16S_R(short): ATTAC GCTGTTATCCCTAAAG (Berry et al., 2017)] was used to determine which krill species were present in each sample. PCR amplifications were conducted in two rounds: the first round was amplified on a QuantStudio 6 Real Time PCR System (Thermo Fisher Scientific), with the reaction mix containing 0.5 µM each of forward and reverse primer, 0.2 µl 100× Bovine Serum Albumin (NEB), 0.5 µl Evagreen (Biotium), 5 µl AmpliTaq Gold™ 360 Master Mix in 1 x reaction buffer (Life Technologies), and up to 5 ng eDNA in a total reaction volume of 10 µl. First round primers were composed of marker specific primers, a unique combination of 7 bp multiplex-identifier (MID) tags and Illumina sequencing primers. Thermal cycling conditions were 95°C for 10 min, followed by 40 cycles of 95°C for 30 s, 56°C for 30 s, and 72°C for45 s, with a final extension of 72°C for 5 min. The amplification product of the first round was diluted 1:20 for the second round PCR, where the reaction mix contained 0.1 µM each of forward and reverse primer, 5 µl AmpliTaq Gold™ 360 Master Mix in 1× reaction buffer (Life Technologies), 2 µl of diluted PCR product from round one, in a total reaction volume of 10 µl. PCR amplifications were conducted with the following thermal cycling conditions: 95°C for 10 min, followed by 10 cycles of 95°C for 30 s, 55°C for 20 s, and 72°C for 45 s, with a final extension of 72°C for 5 min. With the second-round primers, sequencing adapters and two additional 8 bp MIDs (unique i5/i7 combination for each sample) were added to the final amplicons. Second round PCR products were pooled and purified using Agencourt AMPure XP beads (Beckman Coulter). The pooled library amplicons were assessed on a 2100 Bioanalyzer (Agilent Technologies), quantified using the Qubit dsDNA HS assay on a QUBIT 2.0 fluorometer (Life Technologies), diluted to 2 nM and sent to the Ramaciotti Centre for Genomics (UNSW; https://www.ramaciotti.unsw.edu.au) for Illumina NextSeq 1000–150 bp paired-end sequencing.

2.2.3.2 Euphausiid species identification

Paired-end raw sequencing data was processed using the pipeline described in Suter et al. (2023) with the software usearch v11.0.667 (Edgar, 2010). In brief, paired-end reads were merged using the usearch command "fastq_mergepairs", first-round MID tags and primers were identified, filtered and trimmed using the R package "ShortRead" (Morgan et al., 2009) and reads were dereplicated using the usearch command "fastx_uniques". To maintain maximal read diversity, zero-radius OTUs (zOTUs) were identified using the usearch command "fastx_uniques" and the zOTU table was calculated using the usearch command "unoise3". zOTU sequences were searched against the NCBI nucleotide database using the command "blastn" (Madden, 2013), and taxonomy was assigned through lowest common ancestor assessment using MEGAN (Huson et al., 2016) and manual curation. In general, if the NCBI match contained at least 97% identical DNA bases, species-level taxonomic assignment was possible. Read numbers below 100 for any zOTU in any sample were set to zero.

2.2.3.3 Metabarcoding semi-quantitative copy number estimate

To estimate semi-quantitative metabarcoding krill copy numbers per CTD sample, primer standard curve intercept was estimated using a sample where only Antarctic krill was detected in the metabarcoding assay, the sample's first round metabarcoding qPCR Cq value, the Antarctic krill copy number determined from the species-specific qPCR assay, and primer standard curve slope that assumed PCR primer efficiency of 2 (100% efficient). This intercept was then used to calculate the overall amplicon copy numbers for all other samples, taking DNA dilutions and filtered volume into account as well as multiplying by 100 to extrapolate copy numbers from each qPCR mix to copy numbers per 5 L sample. Relative read abundance of any krill species detected in each sample was used to estimate the copy number for each krill species in each sample.

To estimate metabarcoding krill copy numbers for target trawl samples, Antarctic krill copy numbers from the species-specific qPCR assay were transferred to the Antarctic krill metabarcoding dataset. Relative read abundances of each krill species together with these Antarctic krill copy numbers were then used to estimate copy numbers for other krill species present in these samples. This approach was possible as all target trawl samples contained some Antarctic krill metabarcoding reads, whereas in the CTD samples, some samples only contained eDNA from other krill species, without any Antarctic krill eDNA present that would have allowed estimation of overall krill metabarcoding copy numbers in those samples.

2.2.4 Acoustic estimates of krill biomass

Krill were sampled as part of a line-transect survey carried out from RV *Investigator* using a calibrated scientific echosounder operating at 120 kHz. The echosounder transducer was drop keel-mounted and faced vertically downward. Acoustic echoes arising from krill were isolated using the swarms-based method described in Krafft et al. (2021) to a maximum depth of 250 m. Krill swarm metrics describing morphology (e.g. length), energy (e.g. mean volume backscattering strength (Sv, dB re 1 m-1; see MacLennan et al. (2002)) and position (e.g. mean depth of swarm) were extracted for each krill swarm using Echoview version 13.1 (Echoview, Hobart, Australia) using validated methods (e.g. Tarling et al., 2009; Cox et al., 2011). Krill echoes were then integrated along transect on a one nautical mile by 250 m grid. The integrated values, called Nautical Area Scattering Coefficient (NASC; MacLennan et al., 2002) with units (m^2/NM^2), are a linear measure of average acoustic energy scattered by krill and were converted to a real krill biomass density (g wetmass/m^2) following standard methods (Krafft et al., 2021; Cox et al., 2022).

2.2.5 Visual krill abundance

A Canon HFG10 camera in a waterproof housing was attached to the CTD rosette to enable filming at each CTD station. Once the CTD was approximately 30m from the sea floor and still descending, the camera and lights were switched on and filming commenced. Filming continued as the CTD reached approximately five m from the seafloor at which point it stopped descending and maintained this depth for a further five minutes. After five minutes at the seafloor the camera and lights were switched off and the CTD made its ascent to the surface. Once the CTD reached approximately five m from the surface, the process was repeated, so that 5 minutes of footage at both the bottom and the surface was obtained at each CTD station.

In total, surface and seafloor videos from 50 CTDs were used for analysis (255 minutes footage at both the bottom and surface). Abundance data was obtained first as a binary yes/no occurrence, whereby videos were watched in their entirety and then categorized as either containing at least a single krill ('yes') or no krill ('no'). 'Yes' videos were then re-watched twice to gain abundance data. To account for movement of the camera and currents, we used two measures of abundance to form the basis of a categorical abundance classification. First, we measured MaxN - the maximum number of individuals in a single frame, which is usually used for stationary baited underwater videos with a single maximum obtained over a set filming period (e.g. Gardner and Struthers, 2013; Campbell et al., 2015; Schobernd et al., 2014). Since MaxN measures are typically taken by cameras fixed to the substrate, this method alone underestimated the abundance when the camera was substantially moving. Therefore, we also used absolute abundance by counting all krill occurrences throughout the 5-minute videos, which is usually used when calculating abundance from moving transects (e.g. French et al., 2021; Pelletier et al., 2011). A combination of these methods meant that our data fell broadly into three abundance categories: "low", < 10 krill; "medium", 10–100 krill; and "high", > 100 krill.

2.2.6 Trawls

Trawls were conducted with a Rectangular Midwater Trawl (RMT 8 + 1). This incorporated two nets: a primary net which was optimized for adult and juvenile krill with an 8 m^2 mouth opening equipped with a flow meter, and a 4 mm mesh aperture (RMT 8)

and a smaller secondary net optimized for zooplankton and larval krill with a 1 m^2 mouth opening and a 300 µm mesh aperture (RMT 1). At some locations, only one of the two nets were successfully deployed. Trawls were either conducted as target trawls (n_{RMT8} = 15; n_{RMT1} = 13) which were acoustically targeted at krill swarms to capture a sample of the target (10 to 108 m deep), or routine trawls (n_{RMT8} = 38; n_{RMT1} = 35) at pre-determined stations to examine the distribution of zooplankton, which were performed as oblique trawls from 200 meters depth to 10 meters depth. RMT 8 samples were sorted into broad taxonomic groups, photographed, individuals counted and preserved. RMT 8 target trawls capturing *E. superba* were subsampled with a 1 liter jug and 200 individuals were randomly selected for measuring body length, sex and maturity stage. The number of individuals of other krill species caught in the net during routine trawls were counted. When the number of individual krill was likely to be more than ~1,000 individuals, approximate number of individuals were estimated by measuring total volume of the species in milliliters using a volumetric cylinder, and multiplied by conversion factors of 16.1, 29.7, 16.1 for *E. crystallorophias*, *Thysanoessa macrura*, and *E. triacantha* respectively (assuming wet weights of 62.2, 33.7, and 62.2 mg, with density of 1), to derive individual numbers. Numerical densities of these species were expressed in individuals per 1000 m^3. RMT 1 samples were preserved in 5% buffered formaldehyde and seawater solution for later analysis in the laboratory at the Institute for Marine and Antarctic Studies, Hobart, Australia (Weldrick et al., 2024). After rinsing in filtered seawater and splitting into subsamples (Motoda, 1985), individual euphausiids were enumerated and identified to species level for *E. superba* and *T. macrura*, or grouped into "other Euphausiids", using a Leica M165 C stereoscopic microscope. The counts were adjusted based on the splitting ratio and the calibration value from flowmeter readings. Numerical densities were calculated for each euphausiid group per sampling site and expressed as the number of individuals per 1000 m^3.

2.3 Data analysis

2.3.1 eDNA

Antarctic krill eDNA detection and abundance was explored using the short marker, as this marker was more sensitive than the long marker and detected Antarctic krill in more samples than the long marker. eDNA age was calculated using both species-specific qPCR markers (short and long), and both eDNA abundance and age were visualized separately for CTD surface and seafloor samples using R packages SOmap (Maschette et al., 2019) and "ggplot2" (Wickham, 2016). To assess whether sampling depth (surface *vs* seafloor) affected the likelihood of detecting Antarctic krill eDNA in CTD samples, we used a binomial generalized linear model with logit link and with krill eDNA detection (eDNA present/absent) as the dependent and sampling depth (surface/seafloor) as the explanatory variable. To assess whether eDNA amounts decreased with increasing distance from two separate krill swarms, a linear model with eDNA amounts as the dependent variable and distance from swarm and separate swarms as explanatory variables was fitted. Using this model, we extrapolated the distance from swarms at which the swarm's eDNA signal may still be detected, using the lowest value of a recent eDNA detection in CTD samples as the threshold of detectability (26 copies).

Using the euphausiid-specific metabarcoding marker, presence of different krill species, relative abundance within samples and total estimated euphausiid eDNA abundance was calculated and visualized separately for CTD surface and seafloor samples as well as for the two krill swarms where samples were taken at increasing distances.

To compare the two eDNA analysis methods (qPCR and metabarcoding), the co-occurrence of Antarctic krill eDNA detections was investigated and visualized, taking eDNA abundance and age into account. Specifically, the overlap of Antarctic krill eDNA detections was visualized with an Euler diagram (R package "eulerr", Larsson, 2020). The relationship of eDNA age, abundance and detection overlap between methods was further visualized using stacked barplots in R package "ggplot2", separately for overlapping and non-overlapping eDNA detections. The relationship of metabarcoding eDNA abundance with qPCR eDNA abundance was explored using a linear regression model, with sampling depth (surface or seafloor) included as an explanatory variable.

2.3.2 Acoustics

Surface eDNA samples collected from CTDs were compared to acoustic areal krill biomass estimates in the immediately surrounding waters. The acoustic data were converted to presence/absence by thresholding at the 25th percentile of the non-zero acoustic biomass values. For each surface eDNA sample, acoustic presence was collated up to 15km either side of the CTD station location. The relationship between acoustic presence and eDNA age class was examined by fitting a binomial generalized additive model with logit link using the *mgcv* R package (Wood, 2017), with a cyclic smooth term for normalized time of day and distance from station, and a factor term for eDNA age class. Models with combinations of those terms were compared using Akaike's information criterion (AIC) and comparisons between age classes were conducted using Tukey's multiple comparisons method and the *emmeans* R package (Lenth, 2024). These analyses were repeated with distances of 5 and 10 km, and thresholds of 0 and the 10^{th} percentile of the non-zero acoustic biomass values, with equivalent results (not presented here).

Krill are known to exhibit diurnal vertical migration as well as variations in swarming behavior (Tarling et al., 2018; Bahlburg et al., 2023). The normalized time of day term in the above model allows for acoustic detection probability to vary according to the solar cycle. The times of midnight, sunrise, noon, and sunset around each acoustic biomass estimate were calculated using the *suncalc* R package (Thieurmel and Elmarhraoui, 2022). The normalized time of day was calculated by linear interpolation of the acoustic sampling time to a value in the range of 0 to 2, where 0 corresponds to midnight, 0.5 to sunrise, 1.0 to noon, 1.5 to sunset, and 2 to midnight.

2.3.3 Visual

Visual detections and abundance estimates of Antarctic krill were plotted separately for surface and seafloor samples using R packages "SOmap" and "ggplot2". To assess whether sampling depth (surface *vs* seafloor) affected the likelihood of detecting Antarctic krill visually, we used a binomial generalized linear model with logit link, and with krill visual detection (krill present/absent) as the dependent and sampling depth (surface/seafloor) as the explanatory variable. The relationship of visual abundance, eDNA abundance and eDNA age was explored using samples of known age (recent or old, undetermined age was excluded). Recent or old eDNA samples were only associated with low or medium visual abundances at the surface, therefore a binomial generalized linear model with logit link and with visual abundance as the dependent and eDNA abundance and age (recent or old) as explanatory variables was used. This data was further visualized using stacked barplots (R package ggplot2). There was not enough overlap between visual and eDNA detections at the seafloor to conduct meaningful statistical comparisons of eDNA abundance and age with visual abundance.

2.3.4 Trawl

Trawl detections and abundance estimates of euphausiid species were visualized separately for adult or juvenile krill (data from RMT 8 catches) and larval krill (data from RMT 1 catches) using R packages "SOmap" and "ggplot2", separately for target and regular trawls. Differences of krill densities between target and regular trawls were explored separately for RMT 8 and RMT trawls by summarizing detections (number of detections; minimum, maximum and average densities detected) by trawl type and species detected. Trawl locations were matched to CTD locations if they were within 2,794 m of each other (see results – estimated distance of eDNA detectability from krill swarm), and trawl results were compared to eDNA results for trawls where both RMT 8 and RMT 1 data was successfully collected. Overlap of krill detections between trawls and eDNA were visualized using an Euler diagram (R package "eulerr"), and the relationship of krill densities determined by trawls with eDNA data was explored using a linear regression model with trawl krill density as the dependent variable and krill eDNA abundance, age and trawl type as the explanatory variables.

2.4 Data availability

Raw metabarcoding sequencing data, R markdown code for data processing and CTD videos are available from the Australian Antarctic Data Centre (Suter 2025). All other data, metadata and R markdown codes for data processing and analyses are available on GitHub: https://github.com/AustralianAntarcticDivision/tempo-krill-comparisons. Specifically, the R markdown file "TEMPO_qPCR_data.Rmd" provides the code for all data processing, including LOD/LOQ calculations, krill qPCR and metabarcoding data processing, and linking the genetic data to other data streams. The R markdown file "TEMPO_qPCR_analysis.Rmd" provides the code for all figures, tables, statistical analyses and additional Supplementary Material.

3 Results

3.1 Krill detections in eDNA samples

3.1.1 Species-specific *E. superba* assay

Limit of detection, limit of quantification, primer efficiency and standard curve intercept for the short and long marker are listed in Supplementary Table S1 and illustrated in Supplementary Figure S1.

Using the combination of the short and long marker, Antarctic krill was detected in most CTD surface samples (44 out of 50 samples), with short marker copy numbers varying from 26 to 2734 (median: 276) copies per sample (Figure 2A; Supplementary Figure S2). Based on eDNA fragmentation, 15 samples were classified as "recent", 21 as "old" and eight as "undetermined". Recent samples were largely found in transect 2 and further south, whereas many old samples were detected in transect 4 and further north (Figure 2A).

In CTD samples collected near the seafloor, substantially fewer samples contained Antarctic krill eDNA (29 out of 48, Figure 2B) than surface samples (44 out of 50, $z = 2.985$, $p = 0.003$, Figure 2A). eDNA abundance in seafloor samples was generally lower than in surface samples: apart from of one sample (3609 copies, recent), seafloor samples had less than 1000 copies (ranging from 20 to 955, median 158, Supplementary Figure S2). When compared to the surface, fewer samples were classified as recent, but a larger proportion of samples were classified as old in seafloor samples (seafloor: six recent, 15 old, eight undetermined, Figure 2B), however, due to small sample numbers, eDNA abundance and age patterns could not be formally assessed. Recent eDNA was generally detected further south near the continental slope, while older DNA was detected throughout the survey area. Antarctic krill eDNA was detected at great depth: nine detections were between 3000 m and 4000 m depth (one recent, six old, two undetermined age), four detections below 4000 m (one recent, one old, two undetermined age), with the deepest detection at 4327 m depth (undetermined age) and the deepest recent eDNA detection at 4300 m depth.

At two target trawl krill swarm locations (T15 and T18, Figure 1), eDNA was collected while the ship was positioned above the detected krill swarms (two samples each) and at several short intervals as the ship was moving away from/around the swarms. Preliminary analyses indicated that T15 likely falls into the 'superswarm' category, while T18 was of smaller, 'standard swarm' size (Tarling et al., 2009). While the ship was above these krill swarms, very high short marker copy numbers were detected (T15: 1,213,447 and 117,420 copies; T18: 49,360 and 4,428 copies) – higher than the highest copy numbers for any CTD samples at the surface (2,734 copies). The amount of eDNA significantly decreased with increasing distance from the swarms, and overall at T18 significantly lower eDNA concentrations were detected than at T15 (Figure 2E; Supplementary Table S2). At both swarm locations, the short marker copy numbers at the furthest distance measured from the swarm (T15: 837 m; T18: 739 m) was still greater than any surface detections from CTD samples (T15: 10,976 copies;

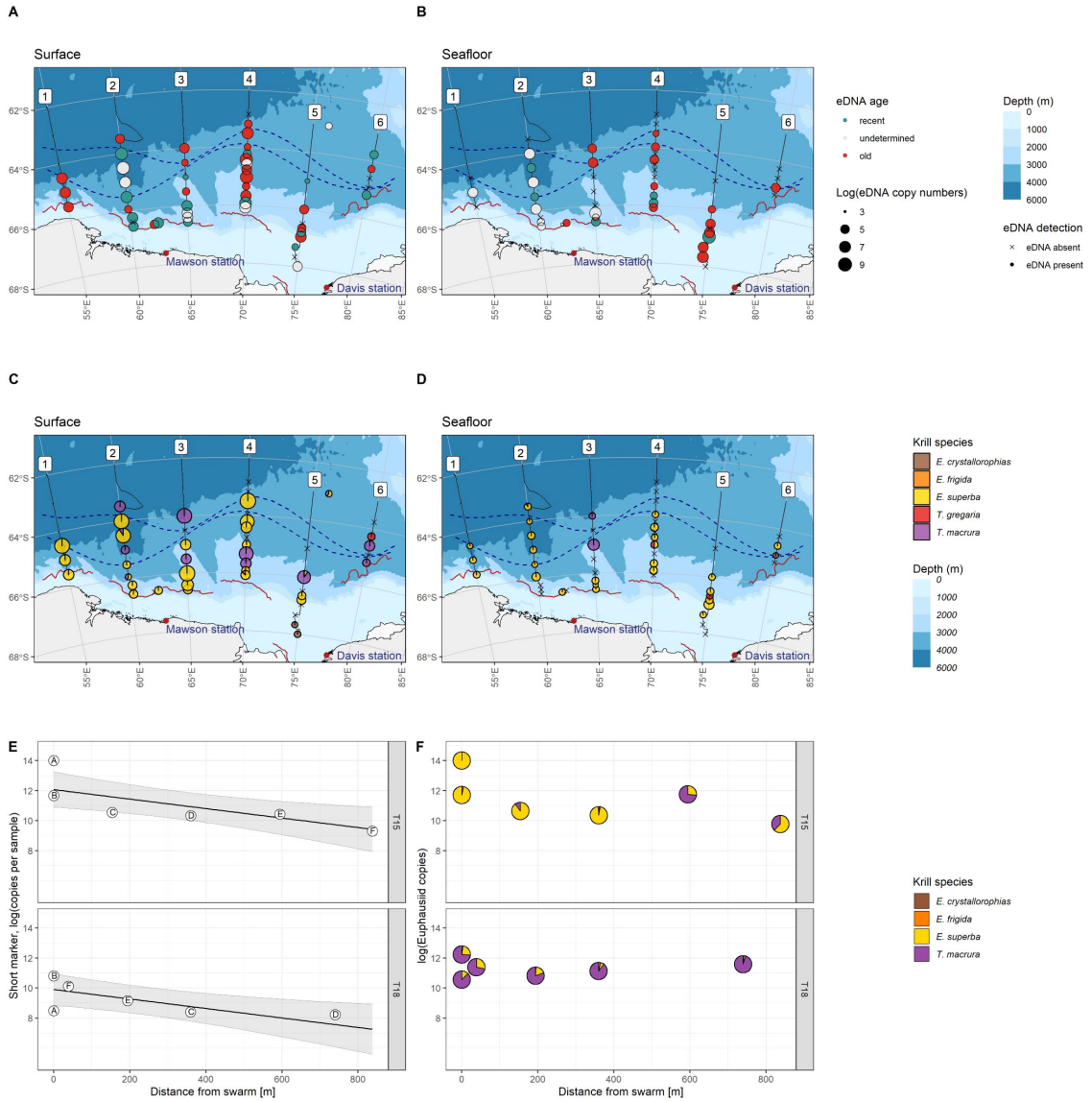


FIGURE 2
Top: Antarctic krill eDNA detected with the species-specific qPCR markers at CTD stations, in surface **(A)** and seafloor **(B)** samples. Colour denotes eDNA age estimated from DNA fragmentation, circle size corresponds to short marker copy numbers, dotted lines denote Southern Ocean oceanic fronts (see Figure 1) and red wavy lines indicate sea ice edge (see Figure 1). Middle: Krill species detected with the krill-specific metabarcoding marker at CTD stations, in surface **(C)** and seafloor **(D)** samples. Pie fractions correspond to metabarcoding read proportions within each sample, and circle size corresponds to estimates of overall krill eDNA abundance. Bottom: eDNA at two targeted krill swarms, T15 and T18. **(E)** Antarctic krill eDNA abundance measured with the species-specific markers significantly decreases with increasing distance from krill swarms, and overall at T18 significantly lower eDNA concentrations were detected than at T15. Letters within circles denote the order of sampling (at T18 the ship returned towards the swarm). **(F)** Krill species detected at increasing distance from krill swarms.

T18: 3,730 copies). When the linear model was extrapolated to the lowest short marker copy number of any recent Antarctic krill eDNA detection (26 copies), the estimated distance at which the recent eDNA signal may still be detectable from a krill swarm was 2,794 m (T15) and 2,107 m (T18).

None of the negative PCR controls (36 NTC qPCRs) or the negative DNA extraction controls (54 qPCRs) amplified with either species-specific marker. Of the 11 field controls (66 qPCR amplifications), one qPCR amplification was positive. As only one of three technical replicas amplified, this control sample was still considered to be krill negative.

3.1.2 Euphausiid metabarcoding

Across all samples, five euphausiid species were detected: *Euphausia superba*, *E. frigida* Hansen, *E. crystallorophias* Holt & Tattersall, *Thysanoessa macrura* G.O. Sars and *T. gregaria* G.O. Sars. In the 50 CTD surface samples, predominantly two species were detected: *E. superba* (in 24 samples) and *T. macrura* (in 13

samples, Figure 2C). Traces of eDNA of *E. frigida* were found in one sample and of *T. gregaria* in two samples. The two southernmost samples in transect five (near 68°S) contained eDNA of *E. crystallorophias*.

In seafloor samples, predominantly *E. superba* was detected (25 samples), with traces of three other species present (*T. macrura*: three samples; *T. gregaria*: two samples; *E. crystallorophias*: one sample; Figure 2D). When estimates of semi-quantitative copy numbers were considered, generally less eDNA was detected in seafloor samples when compared to surface samples.

At the krill swarm locations where eDNA was sampled as the ship was moving away from the swarm, *E. superba* was the dominant krill species detected at swarm T15, however, at increasing distances from the swarm, substantial amounts of *T. macrura* eDNA were detected (Figure 2F, top). At swarm T18, only small proportions of reads were assigned to *E. superba*, while *T. macrura* was the dominant species detected (Figure 2F, bottom). At swarm T15, eDNA traces of *E. crystallorophias* (1 sample) and *E. frigida* (3 samples) were detected, while at swarm T18 eDNA traces of *E. crystallorophias* (1 sample) and *E. frigida* (4 samples) were detected.

3.1.3 Species-specific qPCR *vs* metabarcoding performance

There was a large overlap of samples where the species-specific assay (qPCR) and the metabarcoding assay both detected Antarctic krill eDNA (57 samples). However, in 30 additional samples, only the species-specific assay detected Antarctic krill eDNA (Supplementary Figure S3). These detections contained relatively low eDNA concentrations, and eDNA was often fragmented (26–861 copies; 20 samples old, six undetermined, four recent, see also Supplementary Figure S4A). In six samples, Antarctic krill eDNA was only detected with the metabarcoding marker (Supplementary Figure S3). The semi-quantitative estimate of metabarcoding copy numbers indicated that the eDNA concentrations in these samples was low for Antarctic krill (9–67 copies, median across all samples: 343 copies, see also Supplementary Figure S4B).

Antarctic krill eDNA copy numbers measured with the short species-specific marker positively correlated with copy numbers estimated from the metabarcoding assay, however, there was also a strong effect of sampling depth (Supplementary Table S3; Supplementary Figure S5), indicating that metabarcoding tended to overestimate the amount of Antarctic krill eDNA in surface samples, but not in seafloor samples, when compared to the species-specific marker.

3.2 Comparison to other methods

3.2.1 Acoustic

Acoustic detections of Antarctic krill across the survey area were previously reported in Cox et al. (2022) and are shown in Figure 3. Detection of acoustic biomass was best explained by the binomial generalized linear model that included terms for time of day and eDNA age class (decrease in AIC of 74.6 relative to the intercept-only model, Supplementary Table S4). Krill swarms were most likely to be detected around noon (Supplementary Figure S6). There was little evidence to suggest that adding distance (within the 15km limit) to this model further improved the fit (decrease in AIC of 1.4). Pairwise contrasts indicated that the probability of detecting acoustic biomass within 15 km of a "recent" eDNA sample (probability 0.35, averaged over the diel cycle) was significantly higher than for an "old" eDNA sample (probability 0.18; difference $t(723) = 4.285$, $p < 0.001$). The probability of detecting acoustic biomass within 15 km of an eDNA sample in which krill was not detected was 0.23, and this was not found to be significantly different from either "recent" or "old" eDNA samples (recent: $t(723) = 2.303$, $p > 0.05$; old: $t(723) = 1.166$, $p > 0.05$), but we note the low number ($n = 6$) of "no krill" eDNA samples.

3.2.2 Visual

At surface CTD stations, Antarctic krill were visually detected at 18 out of 50 surveyed locations, largely south of the Polar Front, with some higher concentrations detected at the southern ends of transect two and three (Figure 4A). Antarctic krill eDNA was

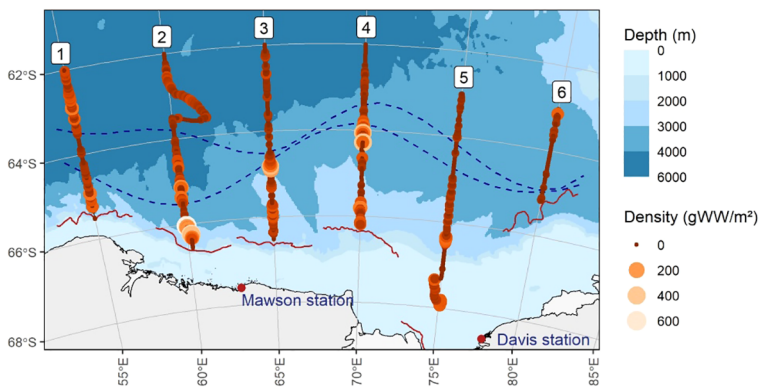


FIGURE 3
Acoustic measurement of Antarctic krill biomass. Circle size and colour denote areal density per nautical mile.

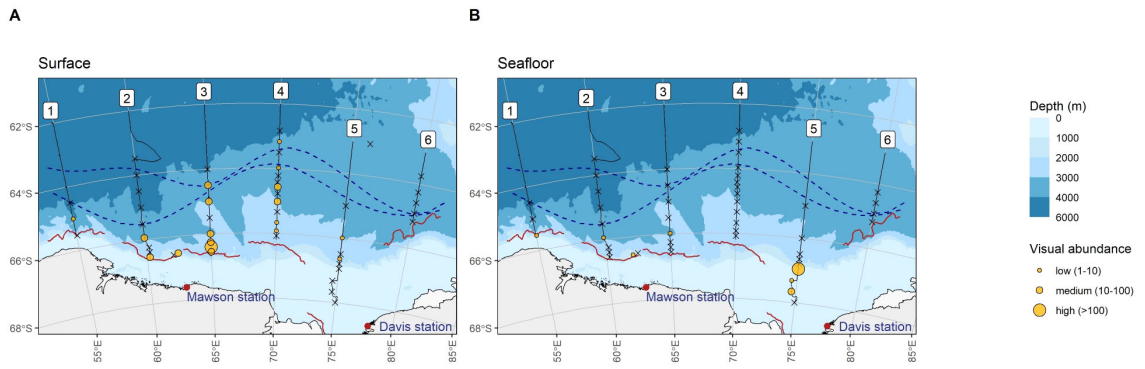


FIGURE 4
Top: Visual detection of Antarctic krill at the surface **(A)** and seafloor **(B)**.

detected at every surface CTD station where Antarctic krill was visually detected (18 stations). In addition, Antarctic krill eDNA was also detected at 26 additional CTD surface locations where Antarctic krill was visually absent. At surface stations, there was no evidence that Antarctic krill eDNA abundance was associated with low or medium visual Antarctic krill abundance (likelihood ratio test 0.505, df = 1, p = 0.477, see also Supplementary Table S5). However, eDNA age was associated with visual detections: the probability of visually detecting medium krill abundances at surface stations was higher when the eDNA age was "recent" (likelihood ratio test 4.253, df = 1, p = 0.039, Supplementary Figure 7A).

Similar to the pattern observed with eDNA, visual krill detections at the seafloor were less frequent (seven of 48 CTD station) than visual detections at the surface (18 out of 50 CTD stations, z = 2.365, p = 0.018, Figures 4A, B). The distribution of visual detections at depth was also similar to "recent" eDNA detections, i.e. concentrated at the southern end of the survey area (south of the Southern Boundary Front), near the continental slope (Figure 4B). Visual abundances at the seafloor were generally lower than at the surface, except for a krill swarm detected at the southern end of transect five at 381 m depth, where hundreds of Antarctic krill were caught on camera (Figure 4B; Supplementary Figure 7B) – the same location where exceptionally high concentrations of recent eDNA were detected (see above). Two visual detections were below 3000 m depth, with the deepest detection at 3080 m. At five of the seven visual detection locations, Antarctic krill eDNA was present. At one location (960 m depth, transect one), Antarctic krill eDNA was only detected with the metabarcoding assay, but not with the qPCR markers. At the deepest visual detection location (3080 m, transect three), eDNA was not detected with either method (qPCR or metabarcoding). At both those locations, visual krill abundance was low (1–10 krill, Supplementary Figure 7B). Antarctic krill eDNA was furthermore detected at 24 seafloor locations where visual detections were absent. There was not enough overlap between visual and eDNA detections at the seafloor to conduct meaningful statistical comparisons of eDNA abundance and age with visual abundance but see Supplementary Figure 7B for a visualization of the data.

3.2.3 Trawl

Krill densities (individuals per 1000 m^3) were estimated for juvenile and adult krill from RMT 8 trawls, and for larval krill from RMT 1 trawls, at routine locations (pre-determined survey design; $n_{RMT8} = 38$; $n_{RMT1} = 35$) and at target locations (after acoustic detection of krill swarms; $n_{RMT8} = 15$; $n_{RMT1} = 13$). Similar to eDNA metabarcoding results, the most commonly detected juvenile/adult krill species across all RMT 8 trawls was *E. superba* (35 of 53 trawls, mean density of 281.91 krill per 1000 m^3), followed by *T. macrura* (27 of 53 trawls, mean density 25.80 krill per 1000 m^3, Supplementary Table S6). Results from RMT 8 trawls differed substantially between target and routine locations: At target trawls, *E. superba* was the dominant krill species: detected densities were higher than at routine trawl locations (Target trawls: mean density of 1023.75 krill per 1000 m^3, Regular trawls: mean density of 28.99 per 1000 m^3), and krill were detected more frequently (Target trawls: 14/15 locations, regular trawls: 21/38 locations, see Figures 5A, B; Supplementary Table S6). At regular trawls, other krill species were more commonly detected than at target trawls: *T. macrura* was detected at 25 locations throughout the survey area, *E. crystallorophias* at four southern locations and *E. triacantha* at eight northern/eastern locations (Figure 5A; Supplementary Table S6).

Species detection patterns of RMT 1 trawl data (larval krill) differed both from RMT 8 (juvenile/adult) as well as eDNA metabarcoding data, however, there were no significant differences between routine and target trawl larval detections (Supplementary Table S7).*Thysanoessa macrura* was the most common euphausiid larval species, detected in 29 of 48 RMT 1 trawls throughout the survey area, both at routine and target locations, with an average density of 234.1 larvae per 1000 m^3 (Figures 5C, D; Supplementary Table S7). *Euphausia superba* larvae were detected in nine of 48 RMT 1 trawls (both routine and target), and all detections were at the southern end of the survey area near the continental shelf (Figure 5B; Supplementary Table S7).

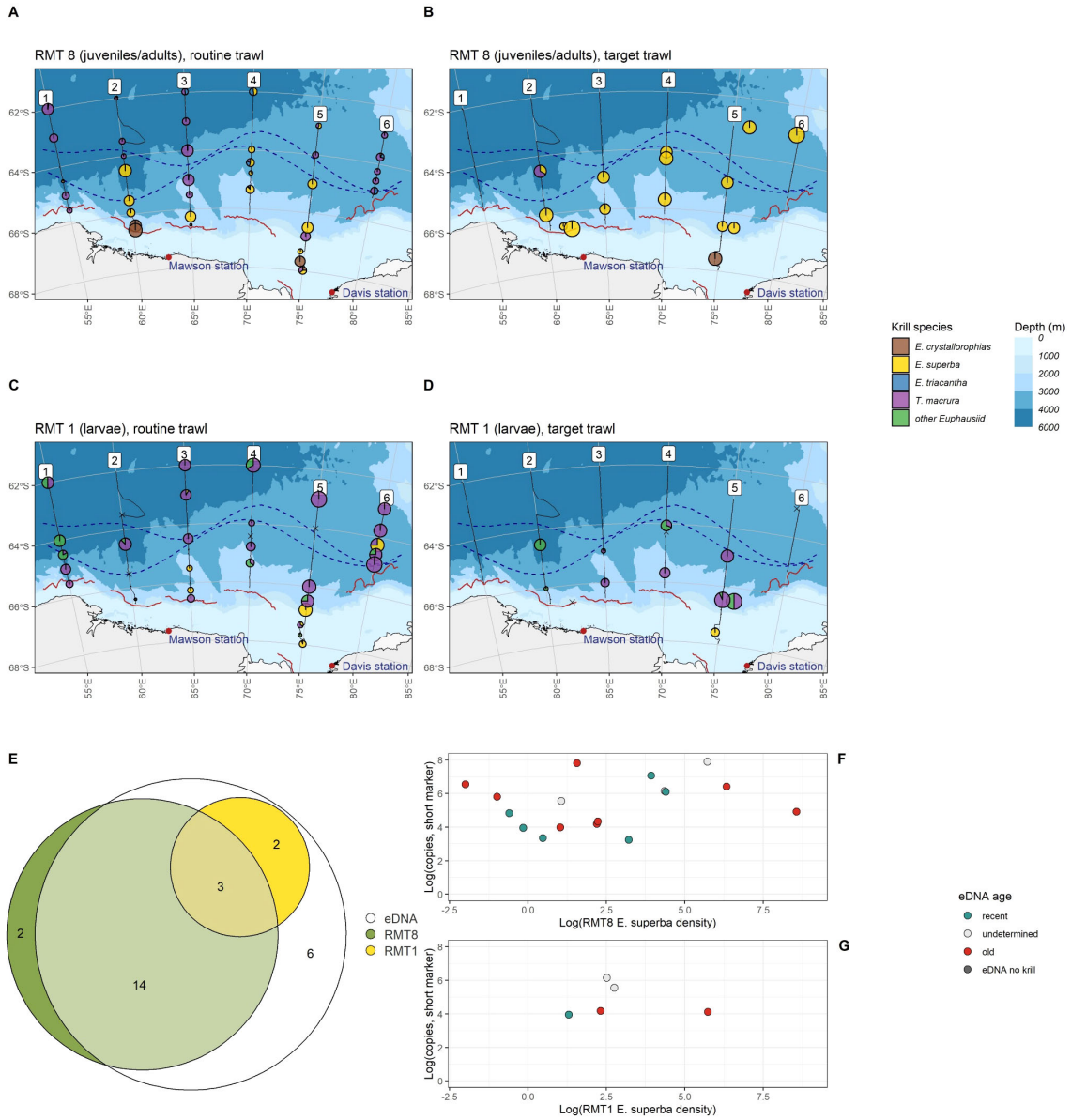


FIGURE 5
Top: Krill species (adults and juveniles) caught in RMT 8 trawls at routine **(A)** and target **(B)** trawl locations. Middle: Krill species (larvae) caught in RMT 1 trawls at routine **(C)** and target **(D)** trawl locations. Bottom: **(E)** overlap of Antarctic krill detections using species-specific eDNA amplification, RMT 8 trawls and RMT 1 trawls at locations where all three data types were collected. **(F)** eDNA age and abundance was not associated with juvenile/adult Antarctic krill density caught in RMT 8 trawls. **(G)** eDNA age and abundance did not correlate with Antarctic krill density of larval Antarctic krill caught in RMT 1 trawls.

Trawl results were further compared to eDNA results for trawls where both RMT 8 and RMT 1 data was successfully collected, and where a surface eDNA sample was collected from a CTD within 2,794 m distance. At most locations where juvenile/adult krill were present, and at all locations where larval krill were detected, Antarctic krill eDNA was also detected (19 of 21 and 5 of5, respectively, Figure 5E). In addition, Antarctic krill eDNA was also detected at six further locations where Antarctic krill was absent from trawls. Antarctic krill density from trawls did not correspond to eDNA abundance or eDNA age, neither for juvenile/adult krill (Figure 5F) nor for larval krill (Figure 5G).

4 Discussion

In this study we aimed to investigate whether eDNA-based methods can contribute to surveying Antarctic krill spatial and temporal distributions – crucial information for understanding Antarctic krill ecology and life history and the effects on and the krill-dependent ecosystem, but also important for the management of the Antarctic krill fishery. While eDNA methods have become more standardized and reliable over the last decade (Beng and Corlett, 2020; De Brauwer et al., 2023), understanding eDNA results, particularly in highly dynamic environments such as

the Southern Ocean and for newly developed eDNA markers, requires careful comparisons to other survey methods (Burian et al., 2021). Here we compared two species-specific assays that can estimate Antarctic krill eDNA abundance and age, and a euphausiid-specific metabarcoding marker that can detect any Southern Ocean krill species, to three other krill survey methods (acoustic, visual, trawl), to gain a better understanding of krill eDNA properties in the Southern Ocean.

4.1 Surface

4.1.1 Antarctic krill

Antarctic krill eDNA was detected using species-specific qPCR assays (short and long marker) in most surface samples throughout the survey area. These results reflect that although Antarctic krill distribution is patchy in the Southern Ocean, krill swarms move around actively and with currents, and continuously release high concentrations of eDNA, for example through their molts and faeces. This eDNA can persist in the environment long after krill swarms have passed, and can spread further with currents, resulting in a nearly ubiquitous Antarctic krill eDNA presence in Southern Ocean surface waters, particularly of short eDNA fragments.

However, when eDNA abundance and eDNA age (estimated from eDNA fragmentation) were considered, a more diversified picture emerged: when eDNA samples were collected within or immediately above krill swarms, Antarctic krill eDNA concentrations were much higher than at other locations, reflecting the high eDNA shedding rates of dense krill swarms. With increasing distance to the swarms, eDNA concentrations declined at similar rates for both swarms. We estimated the distance at which recent eDNA shed from a krill swarm could still be detected to be up to approximately 2,794 m, however, as we did not collect samples beyond 800 m from the krill swarms, this estimate will need further examination with greater sampling density at greater distances from krill swarms, ideally also taking swarm size, krill density as well as the direction and strength of currents into account (Tarling et al., 2009; Andruszkiewicz et al., 2019). At T15, likely a very large 'superswarm', Antarctic krill eDNA concentrations were much higher than at T18, likely a smaller 'standard swarm', indicating that swarm size may relate to eDNA concentrations within the swarm. It is not yet clear whether Antarctic krill eDNA concentrations can provide quantitative information that would contribute to Antarctic krill biomass estimates across a survey area. However, as a first step, more frequent eDNA sampling along survey transects and further measurements of Antarctic krill eDNA concentrations within more krill swarms of different sizes would assist in characterizing the relationship between local biomass and eDNA concentrations.

Several aspects of our results suggested that recent eDNA detections indicated the presence of krill swarms nearby: in the vicinity (within 15 km) of recent eDNA detections, the probability of detecting krill swarms with acoustic surveys was greater than in the vicinity of old eDNA detections. In addition, higher visual krill abundance on video footage was related to more recent eDNA detections. In the acoustic data, the likelihood of detecting krill swarms was significantly higher around noon than other times of the day. This pattern is consistent with previous results from the same voyage in which krill densities during daytime were found to be higher than at night (Cox et al., 2022), and with results from other krill surveys of East Antarctica: during the BROKE-West voyage in 2006, lower krill densities were detected at night and krill surface swarms were visually detected during the day (Jarvis et al., 2010), and during the ENRICH voyage in 2019, more krill swarms were encountered during daytime around solar noon than during the night (Miller et al., 2019).

Based on the comparisons to the trawl data, Antarctic krill eDNA detections at the surface largely originated from juvenile or adult krill, with only a small proportion of the detections originating from larval krill. Larval Antarctic krill detections in trawls were restricted to the southern end of the survey, corresponding to the continental slope area, matching findings from Kawaguchi et al. (2010), who found larval krill distributions restricted to the shelf break.

4.1.2 Other euphausiids

For Antarctic krill surveys, metabarcoding of all krill species provided less differentiated data on Antarctic krill than the species-specific approach: the detection sensitivity was lower, eDNA abundance estimates were less reliable and eDNA fragmentation could not be measured (see also section 4.3). However, euphausiid metabarcoding was very useful to gain an understanding of the distribution, relative abundance and interaction of other krill species. In both eDNA metabarcoding and trawl data, *E. superba* was the most common species, followed by *T. macrura*, both following distribution and abundance expectations (Cuzin-Roudy et al., 2014). In RMT 8 trawls, *E. superba* densities and detection frequencies were significantly higher at target trawl locations than at regular trawl locations, reflecting the nature of the trawls: target trawls were conducted at locations where krill swarms (juvenile/adult krill) were acoustically detected, whereas regular trawls were conducted at pre-determined locations independent of acoustic presence of krill. The trawl type had no influence on the presence or abundance of other krill species, highlighting the specificity of acoustic krill swarm detections. While *E. superba* eDNA detections likely largely originated from juvenile/adult krill, a large proportion of *T. macrura* detections may have originated from larval krill: *T. macrura* was the most abundant larval krill species in RMT 1 trawls, matching findings of previous surveys (Hosie, 1991). Larval *T. macrura* were more abundant than adult *T. macrura*, and often co-occurred with adult *E. superba*. *Thysanoessa macrura* eDNA was also common around the two *E. superba* target swarms, and while we did not have RMT 1 trawl data for those locations due to net-opening failure, no adult *T. macrura* were detected there, thus the *T. macrura* eDNA likely originated from larvae.

In addition to these two dominant krill species, *E. crystallorophias* was detected in southernmost samples near the ice edge, the expected habitat of this species (Pakhomov and Perissinotto, 1996), both in eDNA samples (n = 2) and in trawls (n = 4). Traces of *E. frigida* eDNA were detected in one CTD sample and at both target swarms within the expected habitat (Hosie, 1991), and *T. gregaria* traces were found in two samples, outside of

its expected more northerly range (Kirkwood, 1982). Neither *E. frigida* nor *T. gregaria* were detected in trawls, however, *E. triacantha* was detected in low densities in eight regular trawls, but not detected in eDNA samples. Mismatches between trawl and eDNA species detections could be related to the low densities/abundances of these species, or the mismatch of sampling depth (eDNA: surface; trawls: down to 200 m) or geographic location (CTD and trawl locations were up to 2.8 km apart). In addition, larval krill detections in trawls were only resolved to *E. superba T. macrura* and "other euphausiid", thus other species detected with eDNA but not in trawls could have been present in un-identifiable larval form (compare to e.g. Hosie, 1991). *Thysanoessa gregaria* was the only krill species found outside its expected distribution range. Whether some *T. gregaria* individuals were lost in the South, whether their eDNA was carried south, e.g. through consumption by southwards moving predators (Reidy et al., 2022; Kawamura, 1980), or whether *T. gregaria* mitochondrial DNA introgressed into the *T. macrura* genome via the overlapping ranges of these closely related species (Qi et al., 2014; Seixas et al., 2018) requires further investigation.

4.2 Seafloor

4.2.1 Antarctic krill

Similar to surface samples, determining eDNA age in seafloor samples was essential to understand the presence and distribution of Antarctic krill in the seafloor environment: while low concentrations of Antarctic krill eDNA were detected throughout the survey area, recent eDNA detections were concentrated in the south at the continental slope area, only extending further north in transect two. Visual detections of Antarctic krill at the seafloor were also confined to the continental slope area, suggesting that recent eDNA detections in seafloor samples indicated the presence of Antarctic krill at depth. Recent eDNA detections towards the north of transect two may be related to different water properties discovered along this transect: Foppert et al. (2024) discovered higher dissolved oxygen and lower salinity at the seafloor along transect two, potentially related to an export pathway of Antarctic bottom water from the Cape Darnley Polynya through the Daly Canyon (Foppert et al., 2024). The exact relationship of krill at depth with Antarctic bottom water chemistry will require further in-depth investigation. Both recent eDNA and visual detections were found down to great depths, at 3080 m for the deepest visual detections, and at 4300 m for the deepest recent eDNA detections – considerably deeper than the deepest recorded presence of Antarctic krill to date (3500 m, Clarke and Tyler, 2008). The distribution of Antarctic krill at depth in the continental shelf area may be related to the seabed in this area providing an attractive and attainable alternative feeding ground for Antarctic krill (Schmidt et al., 2011). For example, phytodetritus can accumulate and persist on the continental shelf, providing a long-lasting food source for benthic feeders (Mincks et al., 2005; Smith et al., 2008). In times of relatively high predator abundance and low or patchy concentrations of phytoplankton in surface waters the seabed may present a preferable feeding ground for krill (Clarke and Tyler, 2008; Schmidt et al., 2011). Both individual and cooperative feeding behaviors have been described from benthic camera observations, from including the individual krill "skimming" the surface of the sediment to collect organic material to "balls" of krill resuspending sediment (Kane et al., 2021), and krill have been observed to excrete at depth, contributing to carbon export at depth as well as releasing eDNA into the environment (Smith et al., 2025). At one location at the southern end of transect five, an exceptionally large number of Antarctic krill were captured on camera (> 1000 krill at 381 m depth). At this location, the Antarctic krill eDNA concentration was the highest of any CTD sample (3609 copies), including surface samples, suggesting that high eDNA concentrations at depth corresponded to the presence of high krill numbers. In all other seafloor samples, Antarctic eDNA concentrations and visual krill densities were generally lower than in surface samples, suggesting that fewer Antarctic krill were present in the seafloor habitat, and/or krill were more spread out (generally not forming dense swarms at depth), resulting in lower eDNA concentrations at depth. The formation of dense krill swarms in the epipelagic zone is thought to be a mechanism to avoid visual predators (Olson et al., 2013) – in the darkness of the bathypelagic or even abyssopelagic zones swarming may be less useful to Antarctic krill, and individuals may spread out more at these depths.

Antarctic krill eDNA detections classified as "old" were spread throughout the survey area, including further north than recent detections. While these detections indicate the presence of Antarctic krill eDNA at depth, they may not necessarily indicate the presence of Antarctic krill, particularly beyond the continental slope: fecal pellets and molts released in great quantities by krill swarms in the epipelagic zone are known to sink (Cavan et al., 2019). While during the sinking process, particles may break up or be absorbed by microorganisms (Cavan et al., 2021), considerable amounts of krill debris may still reach the seafloor (Belcher et al., 2017; Smith et al., 2025), contributing to carbon export, and importantly carrying Antarctic krill eDNA to these depths. The sinking rate of krill fecal pellets is estimated to be 27–1218 m d^{-1} (median 304 m d^{-1}) (Atkinson et al., 2012), and krill molts are estimated to sink at 52–1020 m d^{-1} (mean 674 m d^{-1}) (Nicol and Stolp, 1989). To reach 3000 m depth, it could take 2.5–111 days (median 9.9 days) for fecal pellets, and 2.9–58 days (mean 5.5 days) for molts. During this sinking period the eDNA contained in the krill debris would likely fragment and reach the seafloor as "old" eDNA (Suter et al., 2023). Detection and quantification of old Antarctic krill eDNA could therefore indicate the amount and location of krill debris reaching the seafloor, which could contribute to estimates of krill-derived high-particulate organic carbon fluxes to the deep ocean (Manno et al., 2020).

4.2.2 Other euphausiids

The dominant euphausiid species detected in seafloor samples with the euphausiid-specific metabarcoding marker was *E. superba*. This likely reflects that of the detected krill species, *E. superba* is the only one known to descend to and actively inhabit the deep-sea environment. In addition, *E. superba* discarded matter may be more

likely to reach the seafloor than the debris of other krill species: unlike other common Southern Ocean krill species (e.g. *T. macrura*), *E. superba* can form swarms of immense proportions. The generated localized large amounts of discarded krill matter may over-saturate scavenging communities, making it more likely for the discarded matter to reach the seafloor (Manno et al., 2020; Belcher et al., 2019). In addition, larger molts (such as adult *E. superba* molts) may sink faster than smaller molts (e.g. juvenile molts or molts of smaller euphausiid species such as *T. macrura*) (Nicol and Stolp, 1989), and molts can disintegrate within a few days, further reducing the likelihood of small molts reaching the seafloor (Nicol and Stolp, 1989).

4.3 Comparison of eDNA methods

When comparing Antarctic krill detections between eDNA methods (species-specific qPCR *vs* euphausiid-specific metabarcoding), the species-specific assay was more effective at detecting Antarctic krill eDNA, particularly at low eDNA concentrations and for old eDNA. This matches the findings of other studies (Yu et al., 2022; McColl-Gausden et al., 2023), where species-specific assays were also found to be more sensitive than metabarcoding assays. In the few instances where metabarcoding exclusively detected Antarctic krill eDNA, we estimated eDNA concentrations to be very low and potentially near or beyond the limit of detection for the species-specific markers. When we compared the eDNA amounts estimated for the metabarcoding data with species-specific qPCR eDNA amounts, the data matched very well, particularly for samples collected at the seafloor. However, metabarcoding tended to over-estimate the eDNA abundances for surface samples. For the semi-quantitative estimate of krill eDNA from metabarcoding data, Cq values from metabarcoding dye-based qPCRs were used (see methods). If surface samples contained non-euphausiid DNA that co-amplified in the krill metabarcoding assay, this could have contributed to lower Cq values and an over-estimation of total krill eDNA abundance. Resulting non-euphausiid sequences could subsequently have been removed during the library preparation or sequencing, or during the bioinformatic processing of the sequencing data, particularly if the off-target amplicon size differed from the krill amplicon size. If more reliable quantification of metabarcoding data were desired, this method would require further development, e.g. through addition of internal standards (Harrison et al., 2021), or through incorporation of euphausiid-specific fluorescent probes in the first-round metabarcoding qPCR instead of non-specific qPCR dye (Suter et al., 2023).

4.4 Comparison of different data types

Each eDNA survey method we attempted to integrate in this study had individual strengths and limitations (compare to Table 1). Data was collected at different intervals, with different geographic and temporal krill detection ranges (compare to Table 1) and targeting different developmental stages. For example, acoustic data was collected nearly continuously, with krill swarms (adult and juvenile) detectable to a depth of 250 m below the ship. In contrast, eDNA was only collected at CTD sampling stations from surface and seafloor waters, but eDNA could potentially detect the presence of krill (of any developmental stage) several kilometers away from the nearest krill swarm, and/or hours to days after a swarm had passed. Each data type provided a different angle on surveying Antarctic krill, and together the data provided a more holistic picture of Antarctic krill abundance and habitat use than either method could on its own.

Comparing the different data types not only helped interpret the eDNA data, but also expanded our geographic and temporal survey horizon. eDNA samples were comparatively simple to collect and could provide krill presence data beyond the immediate surroundings of the ship, including in areas that were otherwise hard to systematically sample by net or acoustics, such as the seafloor. Another area where eDNA but not many other data streams can be sampled is under sea ice, an important yet understudied habitat of Antarctic krill (Kawaguchi et al., 2024). In addition, eDNA metabarcoding data could also be used to optimize acoustic data interpretation in the future, for example by determining the species composition of krill swarms. Species compositions are traditionally assessed through trawls; however, krill swarms are often missed due to their high mobility and ability to avoid nets. eDNA on the other hand remains detectable for hours and could therefore be used more reliably to determine species compositions of swarms. Furthermore, eDNA samples also contain the DNA of any other organisms present in the sampled environment. Using a range of metabarcoding markers targeting taxonomic groups of interest could reveal the broader taxonomic community associated with krill swarms, ranging from diet species (phyto- and microzooplankton species) to krill predators (fish, marine mammals, seabirds), and could include any other species associated with krill swarms, including species commonly caught as bycatch by the krill fisheries (Stat et al., 2017; Krafft et al., 2023). Combining the eDNA-based krill survey method developed here with broader eDNA-based community assessments by using a suite of genetic markers on the same eDNA samples could therefore vastly improve our understanding of the entire trophic network connected to Antarctic krill.

5 Conclusions

This study is the first large-scale Southern Ocean survey that compared eDNA surveys of Antarctic krill and other euphausiids (species-specific qPCR assays to determine Antarctic krill eDNA abundance and age, and a euphausiid metabarcoding assay to detect all krill species) to other krill survey methods, including acoustic, visual and trawl surveys. Through these comparisons we gained new insights into Antarctic krill eDNA abundance, spread and decay in the dynamic Southern Ocean environment, interactions between krill species, and how eDNA based surveys could be used in the future to understand krill distributions and habitat use throughout the water column. We found that recent eDNA detections likely indicated the presence of Antarctic krill in the vicinity, both at the surface and at

the seafloor. Very high eDNA abundances corresponded to the presence of krill swarms, but further studies are needed to interpret eDNA abundances more comprehensively. We recommend that future krill surveys integrate eDNA sampling throughout the water column in the survey design to complement other krill-related data streams. eDNA data can also expand our survey range to areas where other data streams cannot easily collect information, e.g. under sea ice or in the deep sea. Furthermore, eDNA samples could not only be used to assess Antarctic krill eDNA abundance and age but could also be used to assess other krill species, or indeed any taxonomic group of interest using targeted metabarcoding markers to expand our understanding of krill diet, interactions with other species and predator movements.

Data availability statement

The original contributions presented in the study are included in the article/Supplementary Material. Raw data and processing code are deposited on GitHub (https://github.com/AustralianAntarcticDivision/tempo-krill-comparisons) and on the Australian Antarctic Data Centre (https://data.aad.gov.au/metadata/AAS_4556_TEMPO_Euphausiid_metabarcoding_data). Further inquiries can be directed to the corresponding author/s.

Ethics statement

The manuscript presents research on animals that do not require ethical approval for their study.

Author contributions

LS: Conceptualization, Data curation, Formal Analysis, Investigation, Methodology, Project administration, Software, Validation, Visualization, Writing – original draft, Writing – review & editing. AB: Conceptualization, Data curation, Formal Analysis, Investigation, Methodology, Writing – original draft, Writing – review & editing. SB: Investigation, Writing – review & editing. JB: Investigation, Writing – review & editing. MB: Investigation, Writing – review & editing. MC: Data curation, Formal Analysis, Investigation, Methodology, Writing – original draft, Writing – review & editing. DH: Investigation, Writing – review & editing. OJ: Investigation, Writing – review & editing. SK: Conceptualization, Data curation, Formal Analysis, Funding acquisition, Investigation, Methodology, Project administration, Writing – review & editing. RK: Conceptualization, Investigation, Supervision, Writing – original draft, Writing – review & editing. AK: Investigation, Writing – review & editing. JM: Investigation, Supervision, Writing – review & editing. CW: Data curation, Formal Analysis, Investigation, Methodology, Writing – original draft, Writing – review & editing. SW: Conceptualization, Formal Analysis, Investigation, Writing – review & editing. BR: Conceptualization, Data curation, Formal Analysis, Investigation, Methodology, Validation, Writing – original draft, Writing – review & editing.

Funding

The author(s) declare that financial support was received for the research and/or publication of this article. Data collection and processing was funded by the Australian Antarctic Science Program (AAS 4556, AAS 4512, and AAS 4636). This project received grant funding from the Australian Government as part of the Antarctic Science Collaboration Initiative program. This project also received financial support from Pew Charitable Trust and Antarctic Science Foundation. We acknowledge the use of the CSIRO Marine National Facility (https://ror.org/01mae9353) and grant of sea time on RV Investigator in undertaking this research. AB was funded by an ARC Discovery Grant DP190100660 and the University of Sydney, Australia.

Acknowledgments

We thank Nat Kelly for designing the TEMPO survey, Gavin Macaulay, Dale Maschette and Abigail Smith for acoustic data collection, and Anna MacDonald, Andrea Polanowski and Abigail Smith for fruitful discussions. Thanks are also extended to the crew of the RV *Investigator* for their support throughout the voyage.

Conflict of interest

The authors declare that the research was conducted in the absence of any commercial or financial relationships that could be construed as a potential conflict of interest.

Generative AI statement

The author(s) declare that no Generative AI was used in the creation of this manuscript.

Publisher's note

All claims expressed in this article are solely those of the authors and do not necessarily represent those of their affiliated organizations, or those of the publisher, the editors and the reviewers. Any product that may be evaluated in this article, or claim that may be made by its manufacturer, is not guaranteed or endorsed by the publisher.

Supplementary material

The Supplementary Material for this article can be found online at: https://www.frontiersin.org/articles/10.3389/fmars.2025.1502498/full#supplementary-material

References

Andruszkiewicz, E. A., Koseff, J. R., Fringer, O. B., Ouellette, N. T., Lowe, A. B., Edwards, C. A., et al. (2019). Modeling environmental DNA transport in the coastal ocean using Lagrangian particle tracking. *Front. Marine Sci.* 6, 477. doi: 10.3389/fmars.2019.00477

Atkinson, A., Hill, S. L., Pakhomov, E. A., Siegel, V., Reiss, C. S., Loeb, V. J., et al. (2019). Krill (Euphausia superba) distribution contracts southward during rapid regional warming. *Nat. Climate Change* 9, 142–147. doi: 10.1038/s41558-018-0370-z

Atkinson, A., Schmidt, K., Fielding, S., Kawaguchi, S., and Geissler, P. A. (2012). Variable food absorption by Antarctic krill: Relationships between diet, egestion rate and the composition and sinking rates of their fecal pellets. *Deep Sea Res. Part II: Topical Stud. Oceanogr.* 59-60, 147–158. doi: 10.1016/j.dsr2.2011.06.008

Atkinson, A., Siegel, V., Pakhomov, E. A., Jessopp, M. J., and Loeb, V. (2009). A re-appraisal of the total biomass and annual production of Antarctic krill. *Deep Sea Res. (Part I Oceanogr. Res. Pap.)* 56, 727–740. doi: 10.1016/j.dsr.2008.12.007

Atkinson, A., Siegel, V., Pakhomov, E., and Rothery, P. (2004). Long-term decline in krill stock and increase in salps within the Southern Ocean. *Nature* 432, 100–103. doi: 10.1038/nature02996

Atkinson, A., Siegel, V., Pakhomov, E. A., Rothery, P., Loeb, V., Ross, R. M., et al. (2008). Oceanic circumpolar habitats of Antarctic krill. *Marine Ecol. Prog. Ser.* 362, 1–23. doi: 10.3354/meps07498

Bahlburg, D., Hüppe, L., Böhrer, T., Thorpe, S. E., Murphy, E. J., Berger, U., et al. (2023). Plasticity and seasonality of the vertical migration behaviour of Antarctic krill using acoustic data from fishing vessels. *R. Soc. Open Sci.* 10, 230520. doi: 10.1098/rsos.230520

Baldo, L., Dunning Hotopp, J. C., Jolley, K. A., Bordenstein, S. R., Biber, S. A., Choudhury, R. R., et al. (2006). Multilocus sequence typing system for the endosymbiont Wolbachia pipientis. *Appl. Environ. Microbiol.* 72, 7098–7110. doi: 10.1128/AEM.00731-06

Belcher, A., Henson, S., Manno, C., Hill, S., Atkinson, A., Thorpe, S., et al. (2019). Krill faecal pellets drive hidden pulses of particulate organic carbon in the marginal ice zone. *Nat. Commun.* 10, 889. doi: 10.1038/s41467-019-08847-1

Belcher, A., Tarling, G., Manno, C., Atkinson, A., Ward, P., Skaret, G., et al. (2017). The potential role of Antarctic krill faecal pellets in efficient carbon export at the marginal ice zone of the South Orkney Islands in spring. *Polar Biol.* 40, 2001–2013. doi: 10.1007/s00300-017-2118-z

Beng, K. C., and Corlett, R. T. (2020). Applications of environmental DNA (eDNA) in ecology and conservation: opportunities, challenges and prospects. *Biodivers. Conserv.* 29, 2089–2121. doi: 10.1007/s10531-020-01980-0

Berry, T. E., Osterrieder, S. K., Murray, D. C., Coghlan, M. L., Richardson, A. J., Grealy, A. K., et al. (2017). DNA metabarcoding for diet analysis and biodiversity: A case study using the endangered Australian sea lion (Neophoca cinerea). *Ecol. Evol.* 7, 5435–5453. doi: 10.1002/ece3.2017.7.issue-14

Bessey, C., Jarman, S. N., Berry, O., Olsen, Y. S., Bunce, M., Simpson, T., et al. (2020). Maximizing fish detection with eDNA metabarcoding. *Environ. DNA* 2, 493–504. doi: 10.1002/edn3.v2.4

Burian, A., Mauvisseau, Q., Bulling, M., Domisch, S., Qian, S., and Sweet, M. (2021). Improving the reliability of eDNA data interpretation. *Mol. Ecol. Resour.* 21, 1422–1433. doi: 10.1111/1755-0998.13367

Bylemans, J., Furlan, E. M., Gleeson, D. M., Hardy, C. M., and Duncan, R. P. (2018). Does size matter? An experimental evaluation of the relative abundance and decay rates of aquatic environmental DNA. *Environ. Sci. Technol.* 52, 6408–6416. doi: 10.1021/acs.est.8b01071

Campbell, M. D., Pollack, A. G., Gledhill, C. T., Switzer, T. S., and Devries, D. A. (2015). Comparison of relative abundance indices calculated from two methods of generating video count data. *Fish. Res.* 170, 125–133. doi: 10.1016/j.fishres.2015.05.011

Cavan, E., Belcher, A., Atkinson, A., Hill, S., Kawaguchi, S., Mccormack, S., et al. (2019). The importance of Antarctic krill in biogeochemical cycles. *Nat. Commun.* 10, 4742. doi: 10.1038/s41467-019-12668-7

Cavan, E. L., Kawaguchi, S., and Boyd, P. W. (2021). Implications for the mesopelagic microbial gardening hypothesis as determined by experimental fragmentation of Antarctic krill fecal pellets. *Ecol. Evol.* 11, 1023–1036. doi: 10.1002/ece3.v11.2

Cavanagh, R. D., Melbourne-Thomas, J., Grant, S. M., Barnes, D. K., Hughes, K. A., Halfter, S., et al. (2021). Future risk for Southern Ocean ecosystem services under climate change. *Front. Marine Sci.* 7, 615214. doi: 10.3389/fmars.2020.615214

Clarke, L. J., Shaw, J. D., Suter, L., Atalah, J., Bergstrom, D. M., Biersma, E., et al. (2023). An expert-driven framework for applying eDNA tools to improve biosecurity in the Antarctic. *Manage. Biol. Invasions* 14, 379–402. doi: 10.3391/mbi.2023.14.3.01

Clarke, A., and Tyler, P. A. (2008). Adult antarctic krill feeding at abyssal depths. *Curr. Biol.* 18, 282–285. doi: 10.1016/j.cub.2008.01.059

Constable, A. J., and Nicol, S. (2002). Defining smaller-scale management units to further develop the ecosystem approach in managing large-scale pelagic krill fisheries in Antarctica. *Ccamlr Sci.* 9, 117–131.

Cox, M. J., Candy, S., de la Mare, W. K., Nicol, S., Kawaguchi, S., and Gales, N. (2018). No evidence for a decline in the density of Antarctic krill Euphausia superba Dana 1850, in the Southwest Atlantic sector between 1976 and 2016. *J. Crustacean Biol.* 38, 656–661. doi: 10.1093/jcbiol/ruy072

Cox, M. J., Macaulay, G., Brasier, M. J., Burns, A., Johnson, O. J., King, R., et al. (2022). Two scales of distribution and biomass of Antarctic krill (Euphausia superba) in the eastern sector of the CCAMLR Division 58.4. 2 (55 E to 80 E). *PloS One* 17, e0271078. doi: 10.1371/journal.pone.0271078

Cox, M. J., Watkins, J. L., Reid, K., and Brierley, A. S. (2011). Spatial and temporal variability in the structure of aggregations of Antarctic krill (Euphausia superba) around South Georgia 1997–1999. *ICES J. Marine Sci.* 68, 489–498. doi: 10.1093/icesjms/fsq202

Cutter, G. R. Jr., Reiss, C. S., Nylund, S., and Watters, G. M. (2022). Antarctic krill biomass and flux measured using wideband echosounders and acoustic Doppler current profilers on submerged moorings. *Front. Marine Sci.* 9, 784469. doi: 10.3389/fmars.2022.784469

Cuzin-Roudy, J., Irisson, J.-O., Penot, F., Kawaguchi, S., and Vallet, C. (2014). *6.9. Southern Ocean Euphausiids*. (Cambridge, United Kingdom: Scientific Committee on Antarctic Research).

De Brauwer, M., Clarke, L. J., Chariton, A., Cooper, M. K., De Bruyn, M., Furlan, E., et al. (2023). Best practice guidelines for environmental DNA biomonitoring in Australia and New Zealand. *Environ. DNA* 5, 417–423. doi: 10.1002/edn3.395

Deiner, K., Bik, H. M., Mächler, E., Seymour, M., Lacoursière-Roussel, A., Altermatt, F., et al. (2017). Environmental DNA metabarcoding: Transforming how we survey animal and plant communities. *Mol. Ecol.* 26, 5872–5895. doi: 10.1111/mec.2017.26.issue-21

De Ronde, M. W., Ruijter, J. M., Lanfear, D., Bayes-Genis, A., Kok, M. G., Creemers, E. E., et al. (2017). Practical data handling pipeline improves performance of qPCR-based circulating miRNA measurements. *Rna* 23, 811–821. doi: 10.1261/rna.059063.116

Dugal, L., Thomas, L., Meenakshisundaram, A., Simpson, T., Lines, R., Colquhoun, J., et al. (2023). Distinct coral reef habitat communities characterized by environmental DNA metabarcoding. *Coral Reefs* 42, 17–30. doi: 10.1007/s00338-022-02301-3

Edgar, R. C. (2010). Search and clustering orders of magnitude faster than BLAST. *Bioinformatics* 26, 2460–2461. doi: 10.1093/bioinformatics/btq461

Ellis, M. R., Clark, Z. S., Treml, E. A., Brown, M. S., Matthews, T. G., Pocklington, J. B., et al. (2022). Detecting marine pests using environmental DNA and biophysical models. *Sci. Total Environ.* 816, 151666. doi: 10.1016/j.scitotenv.2021.151666

Everson, I. (2008). *Krill: biology, ecology and fisheries* (John Wiley & Sons).

Fielding, S., Watkins, J. L., Trathan, P. N., Enderlein, P., Waluda, C. M., Stowasser, G., et al. (2014). Interannual variability in Antarctic krill (Euphausia superba) density at South Georgia, Southern Ocean: 1997-2013. *ICES J. Marine Sci.* 71, 2578–2588. doi: 10.1093/icesjms/fsu104

Flores, H., Atkinson, A., Kawaguchi, S., Krafft, B. A., Milinevsky, G., Nicol, S., et al. (2012). Impact of climate change on Antarctic krill. *Marine Ecol. Prog. Ser.* 458, 1–19. doi: 10.3354/meps09831

Foppert, A., Bestley, S., Shadwick, E. H., Klocker, A., Vives, C. R., Liniger, G., et al. (2024). Observed water-mass characteristics and circulation off Prydz Bay, East Antarctica. *Front. Marine Sci.* 11, 1456207. doi: 10.3389/fmars.2024.1456207

French, B., Wilson, S., Holmes, T., Kendrick, A., Rule, M., and Ryan, N. (2021). Comparing five methods for quantifying abundance and diversity of fish assemblages in seagrass habitat. *Ecol. Indic.* 124, 107415. doi: 10.1016/j.ecolind.2021.107415

Gardner, J., and Struthers, C. (2013). Comparisons among survey methodologies to test for abundance and size of a highly targeted fish species. *J. Fish Biol.* 82, 242–262. doi: 10.1111/j.1095-8649.2012.03478.x

Gargan, L. M., Morato, T., Pham, C. K., Finarelli, J. A., Carlsson, J. E., and Carlsson, J. (2017). Development of a sensitive detection method to survey pelagic biodiversity using eDNA and quantitative PCR: a case study of devil ray at seamounts. *Marine Biol.* 164, 1–9. doi: 10.1007/s00227-017-3141-x

Gleiber, M. R., Steinberg, D. K., and Ducklow, H. W. (2012). Time series of vertical flux of zooplankton fecal pellets on the continental shelf of the western Antarctic Peninsula. *Marine Ecol. Prog. Ser.* 471, 23–36. doi: 10.3354/meps10021

Harrison, J. G., John Calder, W., Shuman, B., and Alex Buerkle, C. (2021). The quest for absolute abundance: The use of internal standards for DNA-based community ecology. *Mol. Ecol. Resour.* 21, 30–43. doi: 10.1111/1755-0998.13247

Hewitt, R. P., Watkins, J., Naganobu, M., Sushin, V., Brierley, A. S., Demer, D., et al. (2004). Biomass of Antarctic krill in the Scotia Sea in January/February 2000 and its use in revising an estimate of precautionary yield. *Deep Sea Research Part II: Topical Studies in Oceanography*. 51 (12-13), 1215–36. doi: 10.1016/j.dsr2.2004.06.011

Hill, S. L. (2013). Prospects for a sustainable increase in the availability of long chain omega 3s: lessons from the Antarctic krill fishery. *Omega-6/3 Fatty Acids: Functions, Sustainability Strategies and Perspectives*. (Totowa, NJ: Humana Press), 267–296. doi: 10.1007/978-1-62703-215-5_14

Hosie, G. (1991). Distribution and abundance of euphausiid larvae in the Prydz Bay region, Antarctica. *Antarctic Sci.* 3, 167–180. doi: 10.1017/S0954102091000202

Huson, D. H., Beier, S., Flade, I., Górska, A., El-Hadidi, M., Mitra, S., et al. (2016). MEGAN community edition-interactive exploration and analysis of large-scale microbiome sequencing data. *PloS Comput. Biol.* 12, e1004957. doi: 10.1371/journal.pcbi.1004957

Jarman, S. N., Berry, O., and Bunce, M. (2018). The value of environmental DNA biobanking for long-term biomonitoring. *Nat. Ecol. Evol.* 2, 1192. doi: 10.1038/s41559-018-0614-3

Jarvis, T., Kelly, N., Kawaguchi, S., Van Wijk, E., and Nicol, S. (2010). Acoustic characterisation of the broad-scale distribution and abundance of Antarctic krill (Euphausia superba) off East Antarctica (30–80 E) in January-March 2006. *Deep Sea Res. Part II: Topical Stud. Oceanogr.* 57, 916–933. doi: 10.1016/j.dsr2.2008.06.013

Jeunen, G. J., Knapp, M., Spencer, H. G., Lamare, M. D., Taylor, H. R., Stat, M., et al. (2019). Environmental DNA (eDNA) metabarcoding reveals strong discrimination among diverse marine habitats connected by water movement. *Mol. Ecol. Resour.* 19, 426–438. doi: 10.1111/men.2019.19.issue-2

Jo, T., Murakami, H., Masuda, R., Sakata, M. K., Yamamoto, S., and Minamoto, T. (2017). Rapid degradation of longer DNA fragments enables the improved estimation of distribution and biomass using environmental DNA. *Mol. Ecol. Resour.* 17, e25–e33. doi: 10.1111/men.2017.17.issue-6

Kalinowski, J., and Witek, Z. (1980). Diurnal vertical distribution of krill aggregations in the Western Antarctic. *Polish Polar Res.* 1, 127–146.

Kane, M. K., Atkinson, A., and Menden-Deuer, S. (2021). Lowered cameras reveal hidden behaviors of Antarctic krill. *Curr. Biol.* 31, R237–R238. doi: 10.1016/j.cub.2021.01.091

Kawaguchi, S., Atkinson, A., Bahlburg, D., Bernard, K. S., Cavan, E. L., Cox, M. J., et al. (2024). Climate change impacts on Antarctic krill behaviour and population dynamics. *Nat. Rev. Earth Environ.* 5, 43–58. doi: 10.1038/s43017-023-00504-y

Kawaguchi, S., and Nicol, S. (2020). Krill fishery. *Fish. Aquac.* 9, 137–158. doi: 10.1093/oso/9780190865627.003.0006

Kawaguchi, S., Nicol, S., Virtue, P., Davenport, S. R., Casper, R., Swadling, K. M., et al. (2010). Krill demography and large-scale distribution in the Western Indian Ocean sector of the Southern Ocean (CCAMLR Division 58.4.2) in Austral summer of 2006. *Deep Sea Res. Part II: Topical Stud. Oceanogr.* 57, 934–947. doi: 10.1016/j.dsr2.2008.06.014

Kawamura, A. (1980). A review of food of balaenopterid whales. *Sci. Rep. Whales Res. Inst* 32, 155–197.

Kils, U. (1982). *The swimming behavior, swimming performance, and energy balance of Antarctic krill, Euphausia superba* (Cambridge: SCAR).

Kirkwood, J. M. (1982). "A guide to the Euphausiacea of the Southern Ocean," in *ANARE Research Notes* (Kingston, Tasmania, Australia: Australian Antarctic Division).

Klymus, K. E., Merkes, C. M., Allison, M. J., Goldberg, C. S., Helbing, C. C., Hunter, M. E., et al. (2020a). Reporting the limits of detection and quantification for environmental DNA assays. *Environ. DNA* 2, 271–282. doi: 10.1002/edn3.v2.3

Klymus, K. E., Ramos, D. V. R., Thompson, N. L., and Richter, C. A. (2020b). Development and testing of species-specific quantitative PCR assays for environmental DNA applications. *JoVE (Journal Visualized Experiments)* 165, e61825. doi: 10.3791/61825

Krafft, B. A., Lowther, A., and Krag, L. A. (2023). Bycatch in the Antarctic krill (Euphausia superba) trawl fishery. *Fish. Manage. Ecol.* 30, 154–160. doi: 10.1111/fme.12607

Krafft, B. A., Macaulay, G. J., Skaret, G., Knutsen, T., Bergstad, O. A., Lowther, A., et al. (2021). Standing stock of Antarctic krill (Euphausia superba Dana 1850) (Euphausiacea) in the Southwest Atlantic sector of the Southern Ocean 2018–19. *J. Crustacean Biol.* 41, 1–17. doi: 10.1093/jcbiol/ruab071

Lacoursière-Roussel, A., Côté, G., Leclerc, V., and Bernatchez, L. (2016). Quantifying relative fish abundance with eDNA: a promising tool for fisheries management. *J. Appl. Ecol.* 53, 1148–1157. doi: 10.1111/1365-2664.12598

Langlois, V. S., Allison, M. J., Bergman, L. C., To, T. A., and Helbing, C. C. (2021). The need for robust qPCR-based eDNA detection assays in environmental monitoring and species inventories. *Environ. DNA* 3, 519–527. doi: 10.1002/edn3.v3.3

Larsson, J. (2020). eulerr: Area-Proportional Euler and Venn Diagrams with Ellipses. *R package version 7.0.2.* Available online at: https://CRAN.R-project.org/package=eulerr.

LeBlanc, F., Belliveau, V., Watson, E., Coomber, C., Simard, N., Dibacco, C., et al. (2020). Environmental DNA (eDNA) detection of marine aquatic invasive species (AIS) in Eastern Canada using a targeted species-specific qPCR approach. *Manage. Biol. Invasions* 11, 201–217. doi: 10.3391/mbi.2020.11.2.03

Lenth, R. (2024). *emmeans: Estimated Marginal Means, aka Least-Squares Means. R package version 1.10.3.* Available online at: https://CRAN.R-project.org/package=emmeans.

Luo, M., Ji, Y., and Douglas, W. Y. (2022). Extracting abundance information from DNA-based data. *Molecular Ecology Resources*. 23 (1), 174–89. doi: 10.1111/1755-0998.13703

MacLennan, D. N., Fernandes, P. G., and Dalen, J. (2002). A consistent approach to definitions and symbols in fisheries acoustics. *ICES J. Marine Sci.* 59, 365–369. doi: 10.1006/jmsc.2001.1158

Madden, T. (2013). "The BLAST sequence analysis tool," in *The NCBI Handbook, 2nd edition* (National Center for Biotechnology Information (US, Bethesda (MD).

Manno, C., Fielding, S., Stowasser, G., Murphy, E., Thorpe, S., and Tarling, G. (2020). Continuous moulting by Antarctic krill drives major pulses of carbon export in the north Scotia Sea, Southern Ocean. *Nat. Commun.* 11, 6051. doi: 10.1038/s41467-020-19956-7

Maschette, D., Sumner, M., and Raymond, B. (2019). *SOmap: Southern Ocean maps*. Available online at: https://github.com/AustralianAntarcticDivision/SOmap.

Mathon, L., Marques, V., Mouillot, D., Albouy, C., Andrello, M., Baletaud, F., et al. (2022). Cross-ocean patterns and processes in fish biodiversity on coral reefs through the lens of eDNA metabarcoding. *Proc. R. Soc. B.* 289, 20220162. doi: 10.1098/rspb.2022.0162

McColl-Gausden, E. F., Weeks, A. R., Coleman, R., Song, S., and Tingley, R. (2023). Using hierarchical models to compare the sensitivity of metabarcoding and qPCR for eDNA detection. *Ecol. Inf.* 75, 102072. doi: 10.1016/j.ecoinf.2023.102072

Meyer, B., Freier, U., Grimm, V., Groeneveld, J., Hunt, B. P., Kerwath, S., et al. (2017). The winter pack-ice zone provides a sheltered but food-poor habitat for larval Antarctic krill. *Nat. Ecol. Evol.* 1, 1853–1861. doi: 10.1038/s41559-017-0368-3

Miller, D., and Agnew, D. (2000). Management of krill fisheries in the Southern Ocean. *Krill Biol. Ecol. Fish.*, 300–337. doi: 10.1002/9780470999493

Miller, E., Potts, J., Cox, M., Miller, B., Calderan, S., Leaper, R., et al. (2019). The characteristics of krill swarms in relation to aggregating Antarctic blue whales. *Sci. Rep.* 9, 16487. doi: 10.1038/s41598-019-52792-4

Mincks, S. L., Smith, C. R., and Demaster, D. J. (2005). Persistence of labile organic matter and microbial biomass in Antarctic shelf sediments: evidence of a sediment 'food bank'. *Marine Ecol. Prog. Ser.* 300, 3–19. doi: 10.3354/meps300003

Miya, M. (2022). Environmental DNA Metabarcoding: A novel method for biodiversity monitoring of marine fish communities. *Annu. Rev. Marine Sci.* 14, 161–185. doi: 10.1146/annurev-marine-041421-082251

Morgan, M., Anders, S., Lawrence, M., Aboyoun, P., Pages, H., and Gentleman, R. (2009). ShortRead: a bioconductor package for input, quality assessment and exploration of high-throughput sequence data. *Bioinformatics* 25, 2607–2608. doi: 10.1093/bioinformatics/btp450

Motoda, S. (1985). Devices of simple plankton apparatus VII. *Bull. Mar. Sci.* 37, 776–777.

Nester, G., Suter, L., Kitchener, J., Bunce, M., Polanowski, A., Wasserman, J., et al. (2024). Long-distance Southern Ocean environmental DNA (eDNA) transect provides insights into spatial marine biota and invasion pathways for non-native species. *Authorea Preprints.* 951, 175657. doi: 10.1016/j.scitotenv.2024.175657

Nicol, S., and Stolp, M. (1989). Sinking rates of cast exoskeletons of Antarctic krill (Euphausia superba Dana) and their role in the vertical flux of particulate matter and fluoride in the Southern Ocean. *Deep Sea Res. Part A. Oceanogr. Res. Pap.* 36, 1753–1762. doi: 10.1016/0198-0149(89)90070-8

Olson, R. S., Hintze, A., Dyer, F. C., Knoester, D. B., and Adami, C. (2013). Predator confusion is sufficient to evolve swarming behaviour. *J. R. Soc. Interface* 10, 20130305. doi: 10.1098/rsif.2013.0305

Pakhomov, E., and Perissinotto, R. (1996). Antarctic neritic krill Euphausia crystallorophias: spatio-temporal distribution, growth and grazing rates. *Deep Sea Res. Part I: Oceanogr. Res. Pap.* 43, 59–87. doi: 10.1016/0967-0637(95)00094-1

Pelletier, D., Leleu, K., Mou-Tham, G., Guillemot, N., and Chabanet, P. (2011). Comparison of visual census and high definition video transects for monitoring coral reef fish assemblages. *Fish. Res.* 107, 84–93. doi: 10.1016/j.fishres.2010.10.011

Qi, Y., Lu, B., Gao, H., Hu, P., and Fu, J. (2014). Hybridization and mitochondrial genome introgression between Rana chensinensis and R. kukunoris. *Mol. Ecol.* 23, 5575–5588. doi: 10.1111/mec.2014.23.issue-22

Reidy, R. D., Lemay, M. A., Innes, K. G., Clemente-Carvalho, R. B., Janusson, C., Dower, J. F., et al. (2022). Fine-scale diversity of prey detected in humpback whale feces. *Ecol. Evol.* 12, e9680. doi: 10.1002/ece3.v12.12

Reiss, C. S., Cossio, A. M., Loeb, V., and Demer, D. A. (2008). Variations in the biomass of Antarctic krill (Euphausia superba) around the South Shetland Islands 1996–2006. *ICES J. Marine Sci.* 65, 497–508. doi: 10.1093/icesjms/fsn033

Richerson, K., Watters, G. M., Santora, J. A., Schroeder, I. D., and Mangel, M. (2015). More than passive drifters: a stochastic dynamic model for the movement of Antarctic krill. *Marine Ecol. Prog. Ser.* 529, 35–48. doi: 10.3354/meps11324

Rourke, M. L., Fowler, A. M., Hughes, J. M., Broadhurst, M. K., Dibattista, J. D., Fielder, S., et al. (2022). Environmental DNA (eDNA) as a tool for assessing fish biomass: A review of approaches and future considerations for resource surveys. *Environ. DNA* 4, 9–33. doi: 10.1002/edn3.185

Roux, L. M. D., Giblot-Ducray, D., Bott, N. J., Wiltshire, K. H., Deveney, M. R., Westfall, K. M., et al. (2020). Analytical validation and field testing of a specific qPCR assay for environmental DNA detection of invasive European green crab (Carcinus maenas). *Environ. DNA* 2, 309–320. doi: 10.1002/edn3.v2.3

Ruppert, K. M., Kline, R. J., and Rahman, M. S. (2019). Past, present, and future perspectives of environmental DNA (eDNA) metabarcoding: A systematic review in methods, monitoring, and applications of global eDNA. *Global Ecol. Conserv.* 17, e00547. doi: 10.1016/j.gecco.2019.e00547

Salter, I., Joensen, M., Kristiansen, R., Steingrund, P., and Vestergaard, P. (2019). Environmental DNA concentrations are correlated with regional biomass of Atlantic cod in oceanic waters. *Commun. Biol.* 2, 461. doi: 10.1038/s42003-019-0696-8

Schmidt, K., and Atkinson, A. (2016). Feeding and food processing in Antarctic krill (Euphausia superba Dana). *Biol. Ecol. Antarctic krill*, 175–224. doi: 10.1007/978-3-319-29279-3_5

Schmidt, K., Atkinson, A., Steigenberger, S., Fielding, S., Lindsay, M. C., Pond, D. W., et al. (2011). Seabed foraging by Antarctic krill: Implications for stock assessment, bentho-pelagic coupling, and the vertical transfer of iron. *Limnol. Oceanogr.* 56, 1411–1428. doi: 10.4319/lo.2011.56.4.1411

Schobernd, Z. H., Bacheler, N. M., and Conn, P. B. (2014). Examining the utility of alternative video monitoring metrics for indexing reef fish abundance. *Can. J. Fish. Aquat. Sci.* 71, 464–471. doi: 10.1139/cjfas-2013-0086

Seixas, F. A., Boursot, P., and Melo-Ferreira, J. (2018). The genomic impact of historical hybridization with massive mitochondrial DNA introgression. *Genome Biol.* 19, 1–20. doi: 10.1186/s13059-018-1471-8

Siegel, V. (2016). "Introducing Antarctic krill Euphausia superba Dana 1850," in *Biology and Ecology of Antarctic Krill* (Switzerland: Springer).

Skaret, G., Macaulay, G., Pedersen, R., Wang, X., Klevjer, T. A., Krag, L., et al. (2023). Distribution and biomass estimation of Antarctic krill (Euphausia superba) off the South Orkney Islands during 2011–2020. *ICES J. Marine Sci.* 80, 1472–1486. doi: 10.1093/icesjms/fsad076

Smith, C. R., Mincks, S., and Demaster, D. J. (2008). The FOODBANCS project: introduction and sinking fluxes of organic carbon, chlorophyll-a and phytodetritus on the western Antarctic Peninsula continental shelf. *Deep Sea Res. Part II: Topical Stud. Oceanogr.* 55, 2404–2414. doi: 10.1016/j.dsr2.2008.06.001

Smith, A., Wotherspoon, S., Ratnarajah, L., Cutter, G., Macaulay, G., Hutton, B., et al. (2025). Antarctic krill vertical migrations modulate seasonal carbon export. *Science* 387, eadq5564. doi: 10.1126/science.adq5564

Stat, M., Huggett, M. J., Bernasconi, R., Dibattista, J. D., Berry, T. E., Newman, S. J., et al. (2017). Ecosystem biomonitoring with eDNA: metabarcoding across the tree of life in a tropical marine environment. *Sci. Rep.* 7, 1–11. doi: 10.1038/s41598-017-12501-5

Suter, L., Polanowski, A. M., Clarke, L. J., Kitchener, J. A., and Deagle, B. E. (2021). Capturing open ocean biodiversity: Comparing environmental DNA metabarcoding to the continuous plankton recorder. *Mol. Ecol.* 30, 3140–3157. doi: 10.1111/mec.v30.13

Suter, L., Wotherspoon, S., Kawaguchi, S., King, R., Macdonald, A. J., Nester, G. M., et al. (2023). Environmental DNA of Antarctic krill (Euphausia superba): Measuring DNA fragmentation adds a temporal aspect to quantitative surveys. *Environ. DNA* 5, 945–959. doi: 10.1002/edn3.v5.5

Suter, L. (2025). Euphausiid-specific metabarcoding data from eDNA samples and video footage collected on the TEMPO voyage, Ver. 1, Australian Antarctic Data Centre -. doi: 10.26179/hr9a-jv26

Taberlet, P., Bonin, A., Zinger, L., and Coissac, E. (2018). *Environmental DNA: For Biodiversity Research and Monitoring* (Oxford UK: Oxford University Press).

Tarling, G. A., and Fielding, S. (2016). "Swarming and behaviour in Antarctic krill," in *Biology and Ecology of Antarctic Krill* (Switzerland: Springer).

Tarling, G. A., Klevjer, T., Fielding, S., Watkins, J., Atkinson, A., Murphy, E., et al. (2009). Variability and predictability of Antarctic krill swarm structure. *Deep Sea Res. Part I: Oceanogr. Res. Pap.* 56, 1994–2012. doi: 10.1016/j.dsr2.2008.06.001

Tarling, G. A., Thorpe, S. E., Fielding, S., Klevjer, T., Ryabov, A., and Somerfield, P. J. (2018). Varying depth and swarm dimensions of open-ocean Antarctic krill Euphausia superba Dana 1850 (Euphausiacea) over diel cycles. *J. Crustacean Biol.* 38, 716–727. doi: 10.1093/jcbiol/ruy040

Thieurmel, B., and Elmarhraoui, A. (2022). *suncalc: Compute Sun Position, Sunlight Phases, Moon Position and Lunar Phase. R package version 0.5.1*. Available online at: https://CRAN.R-project.org/package=suncalc.

Trathan, P. N. (2023). What is needed to implement a sustainable expansion of the Antarctic krill fishery in the Southern Ocean? *Marine Policy* 155, 105770. doi: 10.1016/j.marpol.2023.105770

Trathan, P. N., and Hill, S. L. (2016). The importance of krill predation in the Southern Ocean. *Biol. Ecol. Antarctic krill*, 321–350. doi: 10.1007/978-3-319-29279-3_9

Watkins, J., Reid, K., Ramm, D., Zhao, X., Cox, M., Skaret, G., et al. (2016). The use of fishing vessels to provide acoustic data on the distribution and abundance of Antarctic krill and other pelagic species. *Fish. Res.* 178, 93–100. doi: 10.1016/j.fishres.2015.07.013

Weldrick, C. K., Brasier, M. J., Burns, A., Johnson, O. J., and Maschette, D. (2024). Zooplankton abundance and distribution along the Mawson coast, East Antarctica. *Front. Marine Sci.* 11, 1360541. doi: 10.3389/fmars.2024.1360541

Wickham, H. (2016). *ggplot2: Elegant graphics for data analysis* (New York, USA: Springer).

Wood, S. N. (2017). *Generalized additive models: an introduction with R* (New York: Chapman and Hall/CRC).

Wood, S. A., Zaiko, A., Richter, I., Inglis, G. J., and Pochon, X. (2017). Development of a real-time polymerase chain reaction assay for the detection of the invasive Mediterranean fanworm, Sabella spallanzanii, in environmental samples. *Environ. Sci. Pollut. Res.* 24, 17373–17382. doi: 10.1007/s11356-017-9357-y

Yates, M. C., Cristescu, M. E., and Derry, A. M. (2021). Integrating physiology and environmental dynamics to operationalize environmental DNA (eDNA) as a means to monitor freshwater macro-organism abundance. *Mol. Ecol.* 30, 6531–6550. doi: 10.1111/mec.v30.24

Yates, M. C., Fraser, D. J., and Derry, A. M. (2019). Meta-analysis supports further refinement of eDNA for monitoring aquatic species-specific abundance in nature. *Environ. DNA* 1, 5–13. doi: 10.1002/edn3.2019.1.issue-1

Yu, Z., Ito, S.-I., Wong, M. K.-S., Yoshizawa, S., Inoue, J., Itoh, S., et al. (2022). Comparison of species-specific qPCR and metabarcoding methods to detect small pelagic fish distribution from open ocean environmental DNA. *PloS One* 17, e0273670. doi: 10.1371/journal.pone.0273670

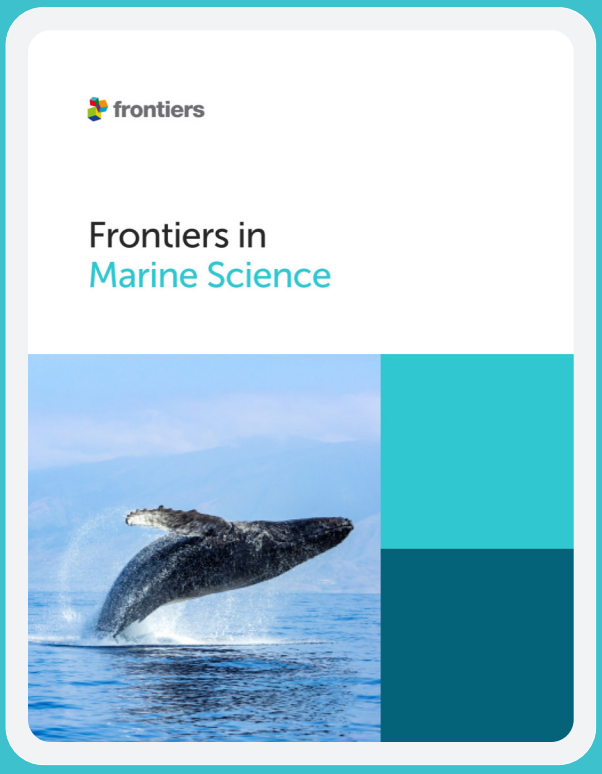
Frontiers in Marine Science

Explores ocean-based solutions for emerging global challenges

The third most-cited marine and freshwater biology journal, advancing our understanding of marine systems and addressing global challenges including overfishing, pollution, and climate change.

Discover the latest Research Topics

See more →



Frontiers

Avenue du Tribunal-Fédéral 34
1005 Lausanne, Switzerland
frontiersin.org

Contact us

+41 (0)21 510 17 00
frontiersin.org/about/contact